Transactions

of the

ASME

AUGUST, 1952

VOL. 74, NO. 6

Transactions

of The American Society of Mechanical Engineers

Published on the tenth of every month, except March, June, September, and December

---

Published monthly by The American Society of Mechanical Engineers. Publication office at 20th and Northampton Streets, Easton, Pa. The editorial department is located at the headquarters of the Society, 29 West Thirty-Ninth Street, New York 18, N. Y. Cable address, Dynamic, New York. Price $1.50 a copy, $12.00 a year for Transactions and the *Journal of Applied Mechanics* to members and editors, $1.00 a copy, $4.00 a year. Changes of address must be received at Society headquarters four weeks before they are to be effective on the mailing list. Please send old as well as new address. . . . By-Laws: The Society shall not be responsible for statements or opinions advanced in papers or . . . printed in its publications (B13, Par. 4). . . . Entered as second-class matter March 2, 1928, at the Post Office at Easton, Pa., under the Act of August 24, 1912. . . .

How to Obtain Instrument Accuracy With Proportioning Pumps

By J. N. SWARR,[1] CHICAGO, ILL.

Proportioning pumps can be used as flow-rate controllers to good advantage, if the stroke and speed are known and controllable, and if the volume discharged by the pump is equal to its displacement. The discharge may be greater or less than the displacement, depending upon the relationships between such parameters as rate of plunger displacement, friction losses in the suction-side and discharge-side piping, masses of liquor in both the suction and discharge lines which must be accelerated and decelerated at each stroke, elevations of supply and discharge tanks, and so forth. The relationships between these factors, as they affect pump volumetric performance, are eveloped on a theoretical basis, and simple tests are devised which will enable an engineer to predetermine whether or not a proposed installation will be satisfactory, and which indicate what changes must be made to correct an unsatisfactory design. The conclusion is drawn that the range of conditions under which a proportioning pump will give satisfactory performance as a meter is considerably restricted so that a careful and thorough analysis of each proposed installation is essential.

Nomenclature

The following nomenclature is used in the paper:

- A = cross-sectional area of inside of suction-side pipe, sq ft
- A_p = cross-sectional area of plunger, sq ft
- a_l = instantaneous acceleration which liquid in suction-side piping would attain if not restrained by plunger, fps per sec
- a_p = instantaneous acceleration of the plunger, fps per sec
- a_{pl} = instantaneous acceleration which is required of column of liquid in suction-side piping to satisfy rate of withdrawal of plunger, fps per sec
- D = inside diameter of suction-side piping, ft
- F_f = total force which must be applied to column of liquid in suction-side piping to overcome force of friction, lb
- F_a = total force which must be applied to column of liquid in suction-side piping to overcome inertia of mass, lb
- F_s = total force exerted at pump end of suction-side piping by static head of liquid in pipe and supply tank, lb
- f = friction factor in Darcy equation; it is a function of Reynolds number and condition of pipe
- h = elevation of supply above pump, ft
- h_f = head loss due to friction in suction-side piping, ft
- L = actual length of line in suction-side piping, ft
- L_e = equivalent length of line in suction-side piping; equivalent length of straight pipe which would have same friction loss as existing pipe and fittings, ft
- M = mass of liquid in suction-side piping, slugs
- N = speed of pump, strokes per sec
- P_1 = pressure applied to surface of liquid in supply tank, psia
- P_2 = vapor pressure of liquid at existing temperature, psia
- P_d = total pressure on downstream side of discharge valve; pressure tending to close valve, psia
- P_p = pressure within pump cylinder tending to open the discharge valve, psia
- P_f = pressure loss due to friction in suction-side piping, psi
- V = total volume displacement of plunger per stroke; product of cross section and stroke, cu ft
- v_l = instantaneous average velocity in suction-side piping, fps
- v_p = instantaneous velocity of plunger, fps
- v_{pl} = instantaneous velocity required of column of liquid in suction-side piping to satisfy rate of withdrawal of plunger, fps
- α = angular distance of crank from beginning of suction stroke, radians
- ρ = density of liquid being pumped, pcf

Primed (′) symbols apply to discharge side of pump.
Unprimed symbols apply to suction side of pump.

Introduction

In recent years the process-control engineer has become more and more aware that the controlled-volume pump is, in fact, an automatic control device and as such commands his interest to the same extent as instruments, valves, and other process-control mechanisms. It is therefore important that he understand the complete range of usefulness of these pumps and, what is more important, that he fully comprehend the laws governing their operation, in order to be fully cognizant of their limitations. It is important, too, that the manufacturer and his sales representatives realize that certain basic conditions must be satisfied in order that a metering pump actually can control liquid flow rate with acceptable accuracy.

Methods of combining these pumps with various types of other control devices and auxiliary apparatus to perform a wide variety of control functions is covered adequately in the technical as well as in manufacturer's literature. This paper, therefore, is concerned only with the limitations of these pumps as flow controllers, or perhaps more correctly stated, with the factors which must be determined and evaluated and the laws which must be observed in order to insure satisfactory performance from a given installation. Instrument-type flow-rate controllers measure and control some physical quantity which is directly associated with the phenomenon of fluid flow. The metering pump, on the other hand, controls plunger displacement and frequency of operation. It is assumed that the product of these two factors is equal to the volume of liquid discharged. It is the purpose of this paper to examine the range of conditions under which this assumption is valid.

How the Pump Functions

As in the case of instruments and other control devices, the limitations usually do not originate in the construction and de-

[1] Project Engineer, Corn Products Refining Company. Mem. ASME.

Contributed by the Industrial Instruments and Regulators Division and presented at the Annual Meeting, Atlantic City, N. J., November 25–30, 1951, of The American Society of Mechanical Engineers.

Note: Statements and opinions advanced in papers are to be understood as individual expressions of their authors and not those of the Society. Manuscript received at ASME Headquarters, July 27, 1951. Paper No. 51—A-53.

sign of the unit itself, but in the conditions associated with its installation. The problem can be illustrated by reference to Fig. 1. During the suction stroke, the plunger is withdrawn from the cylinder, thereby creating a change of volume within the system.

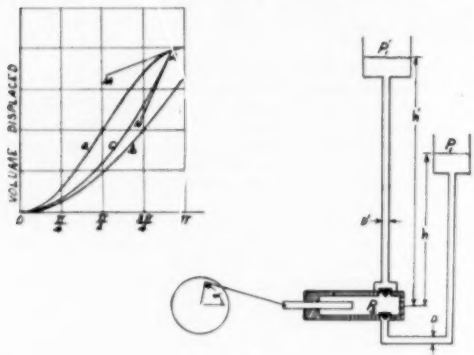

FIG. 1

This change of volume, as a function of time, is shown as curve (*a*). Satisfactory operation of the pump as a flow controller requires that liquid must flow into the cylinder from the suction side at a rate which, at every instant, will equal the plunger displacement. If this condition is met, the curve representing the volume of liquid flowing into the cylinder will exactly coincide with curve (*a*) and the pump will function satisfactorily. On the other hand, if at any time during the suction stroke the rate of flow of liquid through the suction-side piping is less than the rate of change of plunger displacement, a vapor pocket will be formed within the cylinder. In this case the volume flowing through the suction-side piping may be represented by curve (*b*) or by curve (*c*).

Curve (*b*) represents the condition wherein the cylinder is only partly filled at the end of the suction stroke. In this case the volume discharged during the discharge stroke will be less than the plunger displacement, thereby making an unsatisfactory installation.

Curve (*c*) represents the case in which the flow of liquid into the cylinder is at a slower rate than the rate of change of displacement during most of the suction stroke, but which catches up with the displacement as the plunger slows down toward the end of its stroke. Just prior to the instant when the two volumes become equal (*A* on the curve), the velocity of liquid in the suction-side piping is greater than the rate of change of displacement. Consequently, at instant *A* the liquid column is decelerated rapidly from an energy level proportional to the square of the slope *NA* to the lower level proportional to the square of the slope *MA*. The resultant release of energy will create a high pressure within the cylinder which may be greater than the pressure on the discharge valve, a condition which will cause liquid to be discharged even though the pump is still in its suction stroke. In this case the volume discharged by the pump will exceed its displacement.

The rate at which liquid is flowing through the suction-side piping, at any instant, is in no way related to, or determined by, the design of the pump, but is determined entirely by the various physical forces acting on the column of liquid itself. It is these forces which this paper will undertake to evaluate.

Conditions are somewhat different during the discharge stroke. Here the piston imparts energy to the column of liquid in the discharge line. This energy reaches its maximum value when the crank reaches its 270-deg position. Thereafter the piston decelerates to zero velocity at the end of the stroke. The rate at which the liquid column decelerates depends upon the rate at which its energy is dissipated within the discharge piping, and bears no relation to the design and operation of the pump. If at any time during this second half of the discharge stroke the rate of dissipation of energy is such that the deceleration of the liquid column is less than that of the plunger, the excess energy will cause liquid to flow into the cylinder from the suction side, even though the pump is still in its discharge stroke. In this case the volume discharged will be greater than the displacement.

From these observations it becomes evident that in order to determine whether, in a given installation, the volume discharged by the pump will be exactly equal to the displacement, it is necessary to study the relationships between various forces acting within the system, which relationships must be determined from the known physical parameters of the suction-side and discharge-side piping.

In the discussion which follows, the motion of the plunger is assumed to be sinusoidal. This, of course, is not strictly true, but since the actual equation of motion is different with every manufacturer, and since it was impractical to analyze them all, this simplifying assumption seemed permissible since the error is small. It is hoped that this paper will chart a course which can be followed by an exact analysis by each manufacturer as it applies to his own particular machine.

First Half Suction Stroke—0 to 90 Deg

During the first quarter-cycle, it is necessary that the column of liquid in the suction-side piping be accelerated at a rate sufficient to keep the cylinder completely filled with liquid as the plunger is being withdrawn. Consequently, it is necessary to compare the acceleration which the liquid column will experience due to the forces acting upon it, with the acceleration required to satisfy the rate of plunger withdrawal during every portion of this part of the cycle. The forces opposing the acceleration of the liquid column are (1) the force required to overcome friction losses, and (2) the force required to accelerate the mass. These forces are balanced by those resulting from the differential pressure applied to the column.

The pressure loss due to friction in the suction-side piping, in feet head of liquid, is given by the Darcy equation as

$$h_f = \frac{f L_e v_l^2}{2Dg} \quad [1]$$

or in pounds per square inch

$$P_f = \frac{f L_e v_l^2 \rho}{288gD} \quad [2]$$

The force which must be applied to the column to overcome this friction is

$$F_f = P_f A = \frac{P_f D^2 \pi 144}{4} \quad [3]$$

therefore

$$F_f = \frac{f L_e v_l^2 \rho \pi D}{8g} \quad [4]$$

The force on the column required to accelerate the mass of liquid in the column is

$$F_a = \frac{dv_l}{dt} M \quad [5]$$

The total mass M, of liquid in the column is given by

$$M = \frac{\pi D^2 L \rho}{4g} \quad [6]$$

Since the total force which must be overcome to produce acceleration is the sum of F_f and F_a, we have

$$F = \frac{f L_e v_l^2 \rho D \pi}{8g} + \frac{dv_l}{dt}\left(\frac{\pi D^2 \rho L}{4g}\right) \quad [7]$$

The actual total force applied to the liquid column is made up partly by the static head of the liquid and partly by the difference in absolute pressures applied to both ends of the column. With a given pressure applied to the tank end of the line, the maximum differential pressure is developed just as flashing occurs within the cylinder in which case the absolute pressure at the pump end of the line is the vapor pressure at the existing temperature of the liquid being pumped.

The force due to the static head of liquid is given by

$$F_s = \frac{\pi D^2 \rho h}{4} \quad [8]$$

The total force applied to the column then is

$$F = \frac{144 \pi D^2}{4}\left[\frac{\rho h}{144} + (P_1 - P_2)\right] \quad [9]$$

Equating [7] to [9]

$$\frac{144\pi D^2}{4}\left[\frac{\rho h}{144} + (P_1 - P_2)\right] = \frac{f L_e v_l^2 \rho D \pi}{8g} + \frac{dv_l}{dt}\left[\frac{\pi D^2 \rho L}{4g}\right] \quad [10]$$

From this expression the acceleration of the liquid column as a function of time can be derived. This would express the acceleration of the liquid column if it were permitted to flow freely. However, when connected to the suction of the pump, the acceleration is limited by the rate of withdrawal of the plunger. The acceleration of the liquid column can, therefore, be less than that due to plunger displacement, but it cannot be greater. Therefore, since the acceleration of the column is not determined by the combination of forces represented by Equation [10], it is not possible to write a general expression for the acceleration in the time domain.

However, if $(dv_l)/(dt)$ is replaced by a_l, we obtain

$$\frac{144 \pi D^2}{4}\left[\frac{\rho h}{144} + (P_1 - P_2)\right] - \frac{f L_e v_l^2 \rho D \pi}{8g} = a_l\left[\frac{\pi D^2 \rho L}{4g}\right] \quad [11]$$

from which

$$a_l = \frac{144\, g}{\rho L}\left[\frac{\rho h}{144} + (P_1 - P_2)\right] - \frac{f L_e v_l^2}{2DL} \quad [12]$$

Since time t does not appear as a factor in this equation, we find that the acceleration of the column, at any instant, is a function only of the velocity of the column at that instant, when the constant force represented by the left-hand side of Equation [10] is applied to it.

In order for the pump to meter accurately during this quarter-cycle, that is, in order that the cylinder be filled completely throughout this portion of the stroke, it is necessary that this acceleration of the liquid column be equal to, or greater than, the acceleration required to satisfy the rate of change of volume within the cylinder caused by the piston withdrawal. Therefore it is necessary to determine the acceleration of the liquid column which is required to satisfy the plunger motion, and in order that this required acceleration can be compared directly with the actual acceleration, as given by Equation [12], it must be expressed as a function of the velocity of the column.

The volume displacement of the plunger is given by

$$V = A_p \int v_p\, dt \quad [13]$$

$$v_p = c \sin \alpha \quad [14]$$

$$\alpha = 2\pi N t \quad [15]$$

Substituting Equations [14] and [15] into [13]

$$V = A_p c \int_0^{1/2N} \sin 2\pi N t\, dt \quad [16]$$

$$\frac{V}{A_p} = \frac{-c}{2\pi N}\left[\cos 2\pi N t\right]_0^{1/2N} = \frac{-c}{2\pi N}\left[(-1) - (1)\right] = \frac{c}{\pi N} \quad [17]$$

from which

$$c = \frac{\pi V N}{A_p} \quad [18]$$

Therefore the instantaneous velocity of the plunger is given by substituting Equation [18] into [14]

$$v_p = \frac{\pi V N}{A_p} \sin \alpha \quad [19]$$

The velocity of the plunger can be translated into the velocity of liquid in the line from the relation

$$v_{pl} A = v_p A_p \quad [20]$$

from which

$$v_p = \frac{v_{pl} A}{A_p} \quad [21]$$

Substituting Equation [21] into [19], we obtain an expression giving the velocity as a function of crank position, which the liquid column must attain to keep the cylinder filled

$$v_{pl} = \frac{\pi V N}{A} \sin 2\pi N t \quad [22]$$

The acceleration which must be imparted to the liquid column to keep the cylinder filled is given by

$$a_{pl} = \frac{dv_{pl}}{dt} \quad [23]$$

Thus from Equation [22]

$$a_{pl} = \frac{\pi V N}{A} 2\pi N \cos 2\pi N t = \frac{2\pi^2 N^2 V}{A} \cos 2\pi N t \quad [24]$$

To transfer this function to the velocity domain, $\cos \alpha$ must be replaced by an equivalent velocity term.

From Equation [22]

$$\sin \alpha = \frac{v_{pl} A}{\pi V N} \quad [25]$$

Also

$$\sin \alpha = \sqrt{1 - \cos^2 \alpha} \quad [26]$$

Combining Equations [25] and [26] and squaring

$$1 - \cos^2 \alpha = \left(\frac{v_{pl} A}{\pi V N}\right)^2 \quad [27]$$

from which

$$\cos^2\alpha = 1 - \left(\frac{v_{pl}A}{\pi V N}\right)^2 \quad \ldots\ldots [28]$$

Squaring Equation [24]

$$a_{pl}^2 = \frac{4\pi^4 N^4 V^2}{A^2}\cos^2\alpha \quad \ldots\ldots [29]$$

from which

$$\cos^2\alpha = \frac{a_{pl}^2 A^2}{4\pi^4 N^4 V^2} \quad \ldots\ldots [30]$$

Equating [30] to [28]

$$1 - \frac{v_{pl}^2 A^2}{\pi^2 V^2 N^2} = \frac{a_{pl}^2 A^2}{4\pi^4 N^4 V^2} \quad \ldots\ldots [31]$$

from which

$$a_{pl}^2 = \frac{4\pi^2 N^2}{A^2}(\pi^2 V^2 N^2 - v_{pl}^2 A^2) \quad \ldots\ldots [32]$$

or

$$a_{pl} = 8\pi N\sqrt{\frac{V^2 N^2}{D^4} - \frac{v_{pl}^2}{16}} \quad \ldots\ldots [33]$$

Since v_{pl} is exactly equal to the velocity in the line so long as the cylinder is filled, v_l may be substituted for v_{pl}, in which case

$$a_{pl} = 8\pi N\sqrt{\frac{V^2 N^2}{D^4} - \frac{v_l^2}{16}} \quad \ldots\ldots [34]$$

Curves of both a_l and a_{pl} are plotted as functions of the liquid velocity in Fig. 2. Curve I represents a_{pl}. Curve II represents a_l with constants so chosen that both functions have the same acceleration at the beginning and at the end of the first quarter-cycle. In this case the cylinder would not be filled with liquor during any portion of this period. In curve III the constants of a_l are chosen so that both systems have the same acceleration at the beginning of the stroke, but a_l is higher at the end of the stroke. This represents a condition in which the cylinder would be only partly filled until the 90-deg position is nearly reached. For curve IV the constants are so chosen that a_l has a higher value than a_{pl} at the beginning of the stroke, becomes lower than a_{pl} during the middle of the stroke, and then again becomes higher toward the end of the stroke. Curve V represents the only satisfactory combination in that a_l is greater than a_{pl} all the way from 0 to 90 deg.

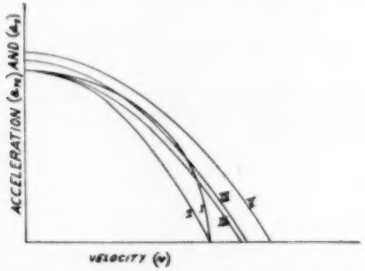

FIG. 2 ACCELERATION CURVES OF PLUNGER AND LIQUID

(Curve I, acceleration required of the liquid column in the suction-side piping to satisfy rate of plunger withdrawal. Curves II to V, acceleration of liquid in suction-side piping due to forces acting on the liquid column.)

The tedious task of plotting these two curves to obtain a solution can be avoided by analyzing Equations [12] and [34] directly. To determine whether $a_l \geqq a_{pl}$ for every value of v, proceed as follows:

1 Determine whether the two curves cross by setting a_l equal to a_{pl} and solving for v_l. If the roots are real, the curves do cross, and the cylinder will not be full during the entire quarter-cycle, making an unsatisfactory installation. If the roots are imaginary, the curves do not cross, in which case a_l may be greater or less than a_{pl}. In this case it remains to be determined whether the curve of a_l lies above or below a_{pl}. To do this, the following is necessary:

2 Set $v_l = 0$ and solve for both a_l and a_{pl}. If a_l is greater than a_{pl}, and if the curves do not cross, the cylinder will be full throughout the entire first quarter-cycle. If a_{pl} is greater, the cylinder will not be full during any portion of the first quarter-cycle.

Obviously, if these tests indicate that the proposed installation will be unsatisfactory, it will be necessary to change the constants of the suction-side piping or the speed of the pump.

SECOND HALF OF SUCTION STROKE—90 TO 180 DEG

During this portion of the stroke, the plunger, and, therefore, the suction-side liquid column, is being decelerated. If the resultant pressures developed within the cylinder exceed the static pressure in the discharge line, liquid will flow through the pump and out of the discharge valve even though the pump is still in its suction cycle. In this case, of course, the pump will discharge a volume exceeding its displacement.

The pressure seating the discharge valve is given by

$$P_d = \frac{\rho h'}{144} + P_1' \quad \ldots\ldots [35]$$

The pressure tending to unseat the discharge valve is

$$P_p = \frac{\rho h}{144} + P_1 - \frac{f L_s \rho v_l^2}{288 g D} - \frac{L\rho}{144 g}\frac{dv_l}{dt} \quad \ldots\ldots [36]$$

In order for the discharge valve to remain seated during the entire portion of this quarter-cycle, $P_d \geqq P_p$ or

$$\frac{\rho h}{144} + P_1 - \frac{f L_s \rho v_{pl}^2}{288 g D} - \frac{L\rho}{144 g}\frac{dv_{pl}}{dt} \leqq \frac{\rho h'}{144} + P_1' \quad \ldots\ldots [37]$$

From Equation [24]

$$\frac{dv_{pl}}{dt} = \frac{2\pi^2 N^2 V}{A}\cos\alpha \quad \ldots\ldots [38]$$

From Equation [22]

$$v_{pl} = \frac{\pi V N}{A}\sin\alpha \quad \ldots\ldots [39]$$

Substituting Equations [38] and [39] into [37]

$$\frac{\rho h}{144} + P_1 - \frac{f L_s \rho \pi^2 V^2 N^2 \sin^2\alpha}{288 g D A^2} - \frac{L\rho 2\pi^2 N^2 V}{144 g A}\cos\alpha \leqq \frac{\rho h'}{144} + P_1' \quad \ldots\ldots [40]$$

Since the right-hand member is constant, it is necessary only that it exceed the maximum value of the left-hand side. This maximum value will occur when $\alpha = \pi$ at which time the third term becomes zero, and the fourth term becomes

$$\frac{L\rho\ 2\pi^2 N^2 V}{144 g A}$$

Therefore it is only necessary to check the condition

$$\frac{\rho h}{144} + P_1 + \frac{2L\rho\pi^2 N^2 V}{144\, gA} \leq \frac{\rho h'}{144} + P_1' \ldots\ldots [41]$$

Obviously, if this check indicates an unsatisfactory combination, it can be corrected by changing conditions on either the suction or discharge sides. However, if the suction-side conditions are changed, it will, of course, be necessary to recheck these conditions on the basis of Equations [12] and [34].

Third Quarter-Cycle—180 to 270 Deg

During this portion of the cycle, the liquid within the cylinder is under pressure, and it has no choice but to flow into the discharge line. Consequently, the volume discharged is exactly equal to the plunger displacement.

Fourth Quarter-Cycle—270 to 360 Deg

During this portion of the cycle the plunger is being decelerated by the crank, and the column of liquid in the discharge piping is decelerating, owing to the dissipation of its own kinetic energy. If the plunger decelerates faster than the column of liquid, the pressure within the cylinder will fall below the pressure on the line side of the suction side check valve. This will cause fluid to pass through the cylinder from the suction side even though the pump is still in its discharge cycle. In this case the liquid discharged by the pump will exceed the displacement.

The development of the relations between the forces acting during this portion of the cycle follows that for the first quarter cycle. Here, however, the minimum pressure permitted within the cylinder is not the vapor pressure (P_2) but the pressure at which the suction side check valve will open or $\rho h/144 + P_1$.

The deceleration of the liquid column is therefore given by

$$a_l' = \frac{g}{L'}\left[(h' - h) + \frac{144}{\rho}(P_1' - P_1)\right] + \frac{f' L_s' v_l'^2}{2D' L'} \ldots [42]$$

Since the deceleration of the plunger between 270 and 360 deg is equal to the acceleration between 0 and 90 deg, from Equation [34]

$$-a_{pl}' = 8\pi N\sqrt{\frac{V^2 N^2}{D'^4} - \frac{v_l'^2}{16}} \ldots\ldots [43]$$

In order that no liquid flow past the intake valve during this portion of the cycle it is necessary that $a_l' \geq a_{pl}'$ throughout this entire quarter-cycle. In order to determine if this is the case:

1 Determine whether the two curves cross by setting a_l' equal to a_{pl}' and solving for v_l'. If the roots are real, the curves do cross, which indicates that during a portion of this quarter-cycle a_{pl}' exceeds a_l' a condition which will cause liquid to flow through the suction-side valve thereby making the installation unsatisfactory. If the roots are imaginary, the curves do not cross, but it remains to be proved that a_l' is greater than a_{pl}'. To do this:

2 Set v_l' equal to zero and solve for both a_{pl}' and a_p'. If a_l' is greater than a_{pl}', the installation will be satisfactory.

Destructive Effects of Cavitation

While this paper is primarily concerned with the use of reciprocating pumps as metering devices it should be noted that the phenomenon studied is a form of cavitation and, therefore, is destructive to the system with which it is associated.

The collapse of a vapor pocket which has been formed within the cylinder obviously will release a large block of energy which must be absorbed by the pump and piping. Therefore an installation which is unsatisfactory as a metering unit also can be expected to cause (1) leaking pipe joints and, in some cases, ruptured pipes; (2) packing-gland leakage and excessive gland maintenance; (3) excessive crank and crosshead-bearing wear; and (4) check-valve destruction. These destructive cavitation forces apply to any reciprocating-pump installation regardless of the requirements for volumetric efficiency.

Conclusion

This analysis indicates that the installation of a so-called "controlled-volume" pump provides no assurance that the volume of liquid discharged by the pump will be equal to its displacement. More accurate terminology might be "adjustable volume" pump. The pump can be used as a flow controller only if the engineer designing a given installation rigidly imposes the necessary restrictions on his design. If these limitations are not observed, the pump may discharge either more or less than the displacement.

Mention should also be made of the rather obvious restriction regarding suction-side and discharge-side heads. It is self-evident that ($\rho h'/144 + P_1'$) must always exceed ($\rho h/144 + P_1$).

Mention should also be made of the occasional use of spring-loaded discharge valves. These, of course, would alter the relations developed within this paper. This case can be included readily in this analysis, providing the pressure required to unseat the valve is known.

The analysis covered by this paper applies to the duplex pump also, either the type in which the two pistons are in phase or the type in which they are 180 deg out of phase. Triplex or quadruplex pumps are less common and are not covered by this paper.

Discussion

J. R. Hefler.[2] The objective set by the author is to predict the conditions limiting accurate performance of a proportioning pump in terms of basic variables for the system. The problem is complicated by the fact that no steady-state flow conditions are reached. For this reason it is necessary to solve a general expression for instantaneous conditions for successive points through a complete cycle. For convenience it is desirable to determine the fewest possible points that will define satisfactory conditions.

Possibly the lack of a steady-state equilibrium is the reason for very few formulas in engineering literature applying to reciprocating pumps in comparison with rotary pumps of various types.

A proportioning pump is a reciprocating pump required to deliver an accurately reproducible volume of liquid for a given displacement. It is particularly important, therefore, to be able to determine under what conditions an ideal reciprocating pump would be unable to deliver liquid exactly equivalent to its displacement.

An ideal pump would have no valve slip due to delay in seating when the plunger changes direction, as well as a perfect seal in the valves and stuffing box. An actual pump will approach closely the ideal under proper conditions. Some valve slip is unavoidable and will vary slightly from one liquid to another with changes in density and viscosity. Accordingly, the accuracy is taken as the reproducibility of performance with a given liquid in maintaining a constant volumetric efficiency.

The author arrives at three critical points where the volumetric efficiency of a pump is most likely to be upset. From a complete knowledge of operating conditions and basic pump data it is possible to predict whether or not a given installation can be expected to work or whether uniform volumetric efficiency is out of the question.

Many of the author's statements cannot be emphasized too strongly. Of particular importance is the fact that during the

[2] Engineering Department, Proportioneers, Inc. Providence, R. I.

suction cycle any pump is completely dependent on external forces driving fluid into it. This is true of every pump since a liquid supports no appreciable tensile stresses. Another point which frequently is overlooked is the importance of inertia. This is a severe limitation for reciprocating pumps generally and for proportioning pumps in particular. Owing to high capacity and steady flow, friction is the main limitation for rotary pumps and can be calculated by simple procedures. For the intermittent flow from a proportioning pump, inertia forces are considerable. Friction is generally secondary and is difficult to determine using conventional procedures.

Probably the importance of the external forces needed by a proportioning pump to maintain its volumetric efficiency is not fully realized because most engineers are more familiar with centrifugal or turbine pumps. As the author points out, these forces are required not only to produce flow into the pump but also to stop flow away from the pump. Therefore the discharge cycle must be considered as well as the suction cycle.

In Equations [1] through [12] the author sets up an expression for the maximum available external driving force. Since this always would be balanced by frictional resistance and inertia at its maximum instantaneous value a complete balance can be set up as in Equation [10]. This is a cavitation-force balance. Equation [12] rearranges this balance to express the maximum rate at which flow can change for any given velocity. Thus a_l is the instantaneous free acceleration of liquid moving with velocity v_l into a region maintained at the vapor pressure of the liquid instead of into the pump cylinder; or it also can be considered the value of acceleration of flow into the cylinder when the plunger is moving back faster than the liquid can follow.

Equations [13] through [34] derive a similar expression for flow equivalent to the motion of the plunger which, in Equation [14], is assumed pure harmonic motion. Assuming the cylinder remains full, the acceleration required by the pump can be expressed as a function of liquid velocity.

Equation [33] can be obtained directly from the basic expressions for harmonic pump flow. Using Equations [15], [22], and [24] and replacing A with $\pi D^2/4$ gives

$$v_{pl} = \frac{4VN}{D^2} \sin \alpha, \quad a_{pl} = \frac{8\pi VN^2}{D^2} \cos \alpha$$

since $\sin^2\alpha + \cos^2\alpha = 1$

$$\frac{v_{pl}^2}{\left(\frac{4VN}{D^2}\right)^2} + \frac{a_{pl}^2}{\left(\frac{8\pi VN^2}{D^2}\right)^2} = 1$$

This is in the general form for an ellipse $x^2/a^2 + y^2/b^2 = 1$, although proper choice of scales for unit values of v and a will give a circular plot as in Fig. 2 of the paper.

Solving for a_{pl}

$$a_{pl} = 2\pi N \sqrt{\left(\frac{4VN}{D^2}\right)^2 - v_{pl}^2}$$

$$a_{pl} = 8\pi N \sqrt{\frac{V^2N^2}{D^4} - \frac{v_{pl}^2}{16}}$$

The cavitation curves II through V in Fig. 2 are in a general parabolic form $y = a - bx^2$. It should be noted that both the pump-flow ellipse and the cavitation parabola are potential flow paths.

Real flow at any given velocity will follow the path of least resistance due to inertia. Acceleration will correspond to whichever value is smaller, a_l or a_{pl}.

To save unnecessary calculation it would be logical to perform step 2 first and perform step 1, determining if the roots are real or imaginary only after checking the condition

$$\frac{g}{L}\left[\frac{144}{\rho}(P_1 - P_2) + h\right] > \frac{8\pi VN^2}{D^2}(S)$$

where S is the correction for a_{pl} (max) due to the actual sinusoidal motion of the plunger.

Multiplying both sides of this expression by D^2 gives a form showing the pump factors on one side and the installation variables on the other.

Requirement at 0 deg

$$g\left(\frac{D^2}{L}\right)\left[\frac{144}{\rho}(P_1 - P_2) + h\right] > 8\pi VN^2(S)$$

The most significant installation factor in satisfactory initial operation will be having D large enough and L small enough for the existing pump, pressures, and head. In regard to pump design, since a given capacity VN is required, the right-hand side varies with N and not N^2. However, a large slow-speed pump will perform more accurately under conditions of limited driving force than a smaller high-speed pump. In comparing pumps of equal capacity for service on liquefied gases, for example, where $P_1 - P_2 = 0$, a pump operating at 30 strokes per min will require one half the driving force of one operating at 60. However, the proper location of the pump and size of line has even more to do with balancing low values of h.

In equating the expressions for pump and cavitation flow to see if they cross, the expression for v reduces to the general form $ax^4 + bx^2 + c = 0$, a, b, and c representing numerical quantities. The complex expression represented by a contains f^2, and b contains f. The assumption is implied that f remains constant with v_l or can be expressed as a function of v_l. In borderline cases the value of f may determine whether the final expression has a positive or negative quantity under the radical signs.

Some discussion of evaluating f is necessarily within the scope of the paper. For strongly turbulent flow in rough pipes f may be assumed constant and can be determined to one significant figure for a given velocity, liquid, and line from an empirical curve of f versus Reynolds number. An estimating value such as 0.04 would define a reasonably accurate curve only when v_{pl} has maximum values well above the lower critical velocity for the liquid and line size. If v_{pl} (max) is more than 5 times the critical velocity (Re = 10,000) the cavitation curve could be assumed virtually a pure parabola in the form $y = a - bx^2$.

The comparatively low flow rates for proportioning pumps and the frequency with which viscous liquids are handled do not give very large Reynolds numbers. Below critical velocity the cavitation curve is a straight line expressed by the Hagen-Poiseuille equation, and in the region just beyond critical velocity there is no reliable mathematical expression for friction as a simple function of velocity which would define the cavitation curve. A typical condition where v_{pl} (max) is about twice the lower critical velocity at which flow changes from streamline to turbulent is shown in Fig. 3 of this discussion.

During the second half-suction stroke the liquid must be decelerated without causing the discharge valve to open. Since at the start velocity is at maximum, friction forces can assist static forces in bringing the column of liquid to rest. This friction term declines as the velocity decreases and the minimum value of the decelerating force will be the static differential pressure

$$P_1' - P_1 + \frac{\rho}{144}(h' - h)$$

If this is greater than the inertia force at maximum the liquid will decelerate without opening the discharge valve and delivering more than pump displacement.

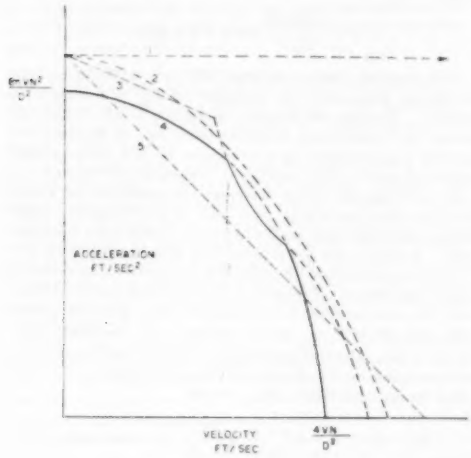

1 FRICTIONLESS FLOW a_l constant at a_l max $= \frac{g}{L}\left[\frac{144}{\rho}(P_s - P_v) + h\right]$

2 HYPERBOLIC CAVITATION CURVE $a_l = f_{1_2} v^2 / 2DL$ f constant

3 TYPICAL MIXED FLOW CAVITATION CURVE f variable

4 PUMP CURVE $a_l = 2\pi N\sqrt{(v \max)^2 - v^2}$

5 STREAMLINE FLOW CAVITATION CURVE $a_l = \frac{32\mu v}{\rho L D^2}$

FIG. 3

The limiting conditions at 180 deg can be written as follows:

Requirement at 180 deg (pressure)

$$P_1' - P_1 + \frac{\rho}{144}(h' - h) > \frac{\pi\rho VN^2L}{18gD^2} \quad (S)$$

The minimum decelerating potential, total available static differential, must be larger than inertia forces at maximum. This pressure expression resolves to the same general form as that from equating a_l and a_{pl} for $v_l = 0$, to check if the first quarter-cycle can start without cavitation.

Requirement at 180 deg (head)

$$g\frac{D^2}{L}\left[\frac{144}{\rho}(P_1' - P_1) + h' - h\right] > 8\pi VN^2 \quad (S)$$

The third quarter-cycle resembles the first quarter-cycle. However, the driving force required to overcome friction and inertia and produce flow from the pump is provided by the pump itself. This is in the form of increased pump pressure P over the static term $P_1' + \rho h'/144$. The result is a peak power load but it does not threaten volumetric efficiency.

The fourth quarter-cycle 270 to 360 deg resembles the second quarter-cycle 90 to 180 deg, and with the similar requirement that the cylinder pressure remain above $P_1 + \rho h/144$ so that liquid will not flow through from the suction side of the pump and cause overdelivery of liquid. The limiting condition becomes:

Requirement at 360 deg (pressure)

$$P_1' - P_1 + \rho/144(h' - h) > \frac{\pi\rho VN^2L'}{18g(D')^2} \quad (S)$$

The only difference between 180 deg and 360 deg is in the respective values for L and D for the suction and for the discharge lines in the factor D^2/L.

Requirement at 360 deg (head)

$$g\frac{(D')^2}{L'}\left[\frac{144}{\rho}(P_1' - P_1) + h' - h\right] > 8\pi VN^2 \quad (S)$$

For uniform volumetric efficiency the external discharge pressure and head must be sufficiently larger than suction-side static forces to decelerate the liquid even when there is no friction force to help and the deceleration is at maximum. In this case not only should step 2 be taken first, but step 1 does not appear to supply any additional information.

The grossly destructive effects of cavitation can be compared to water hammer caused by a quick-closing valve and a long column of liquid in motion. If a condition occurs as shown in curve *b*, Fig. 1 of the paper, where the cylinder is only partly filled with liquid at the end of the suction stroke, there will be no instantaneous change in pump pressure at zero velocity as when the cylinder is full of incompressible liquid.

The discharge valve will remain closed until an appreciable crank angle is passed through and the vapor is compressed to $P_1' + \rho h'/144$. At this time the entire mass of liquid in the discharge line must then accelerate from rest to the value v_{pl}'. This abrupt change in motion requires a high value of a_l, and a shock load will develop when the pump applies this acceleration to a considerable mass of fluid in the discharge line. Frequently, the load is far in excess of normal design loads and when repeated with each revolution of the pump leads to rapid breakdown. This is analogous to a quick-closing valve shutting off in the face of a moving liquid column. If the column is long enough the pipe will break. A pump with a short line can cavitate without immediate damage but with sufficient mass of liquid the condition approaches that of pumping against a closed valve.

The cure for this shock-load condition is obvious. A surge chamber, preferably a gas-loaded bladder type, in the discharge line will eliminate the need for a virtually instantaneous change in velocity of the entire column of liquid exactly as in the case of the quick-closing valve. However, the important thing is to prevent cavitation and maintain uniform volumetric efficiency which can be done by putting the surge chamber in the suction line. If the flow in the lines can be brought to a more nearly steady equilibrium, the maximum value of v_l will approach an average value v_{pl}/π as a limit for a simplex pump.

Thus, for a simplex pump, friction could be reduced to approximately $^1/_3$ to $^1/_{10}$ of its original value depending on whether flow is streamline or turbulent. As v_l approaches a uniform average value all the inertia loads approach zero and the pump will operate with the internal cylinder pressure P very nearly constant at $P_1 + \rho h/144$ during suction and at $P_1' + \rho h'/144$ during discharge.

As the chamber will not be effective in changing v_l in the length of line between itself and the pump, the chambers will give maximum effect in reducing inertia and friction when installed as close as possible to the pump.

To establish definitely that cavitation does not take place during the entire first quarter-cycle, it is necessary to determine the maximum value of friction and inertia in combination.

The general condition to be met for any angle between 0 and 90 deg is as follows:

0 to 90 deg general

$$P_1 - P_2 + \frac{\rho h}{144} > \frac{f\rho L_e V^2 N^2 \sin^2 \alpha}{18gD^5} + \frac{\pi\rho LVN^2 \cos \alpha}{18gD^2}$$

$$> \frac{\rho VN^2}{18gD^2}\left(\frac{fL_eV}{D^3} \sin^2 \alpha + \pi L \cos \alpha\right)$$

To determine f it is necessary to find the Reynolds number for maximum velocity. If this Reynolds number is less than 2000 the Darcy expression uses 64/Re for f and reverts to the Hagen-Poiseuille formula where friction is linear with velocity. If the Reynolds number for v_{pi}(max) is sufficiently far in the turbulent region for variation in f to be insignificant with respect to variations in v_{pi}^2, it is satisfactory to assume f constant. For Re greater than 10,000 this condition is approached as an ideal limit by large pumps. For normal pump capacities, line sizes, and liquid viscosities and densities, the Reynolds number corresponding to v_{pi} max will be in the region of streamline flow or not greatly beyond. The Reynolds number is given by Re = $Dv\rho/\mu$ where μ is absolute viscosity in lb-sec ft units consistent with ρ. The maximum Reynolds number, Re(max) = 4 $VN\rho/D\mu$. Since VN is so small, "ideal" turbulent flow is rare and may never be fully established.

The writer's procedure for finding the maximum combined value of friction and inertia is to determine the type of flow conditions from Re(max) and evaluate friction at maximum, sin α one, and assume this maximum friction loss is reached by increasing as sin α or sin^2 α according to the type of flow. Assuming the former gives a conservative working basis for any flow condition.

When Re(max) is below 2000, flow can be taken as viscous for the entire quarter-cycle. The general expression assumes the following:

0 to 90 deg general streamline flow

$$P_1 - P_2 + \frac{\rho h}{144} > \frac{VN}{9gD^2}\left(\frac{8L_e\mu}{D^2} \sin \alpha + \frac{\pi\rho NL}{2} \cos \alpha\right)$$

The right-hand side has the general form $c\,(a \sin \alpha + b \cos \alpha)$. For any values of a, b, c, and α the maximum value is $c\sqrt{a^2 + b^2}$. The condition for cavitation to be impossible becomes:

0 to 90 deg limit Re < 2000

$$P_1 - P_2 + \frac{\rho h}{144} > \frac{VN}{9gD^2}\sqrt{\left(\frac{8L_e\mu}{D^2}\right)^2 + \left(\frac{\pi\rho NL}{2}\right)^2 (S)^2}$$

This method has the advantage of determining directly the excess driving force in psi (equivalent to NPSH) and gives the safety factor in the system by taking the difference. Generally, the difference between the maximum available driving force and the combined load should, if possible, be equal to P_2 to allow for pump entrance and valve losses and unfavorable changes in ambient temperature. If not, temperature control and special valve design would be indicated to maintain a good safety factor. For Reynolds numbers over 10,000, ideal conditions may be assumed and f taken constant. This is the limiting case for increasing pump capacity. In this case f is taken from empirical handbook values allowing for pipe roughness at the average Reynolds number, $2/\pi$ Re(max), for the quarter-cycle. This appears the most reasonable value to use.

The right-hand side of the general expression for 0 to 90 deg is now in the form $c_1(a_1 \sin^2 \alpha + b_1 \cos \alpha)$ which has a maximum value c_1b_1 when $a_1 < b_1/2$. When $a_1 > b_1/2$ the maximum value will be $c_1(a_1 + b_1^2/4a_1)$.

The limiting condition for strongly turbulent flow becomes:

0 to 90 deg limit Re > 10,000

$$P_1 - P_2 + \frac{\rho h}{144} > \frac{\rho VN^2}{18gD^2}\left[\frac{fL_eV}{D^3} + \frac{\pi L^2D^3}{4fL_eV}(S^2)\right]$$

where

$$f > \frac{\pi LD^3(S)}{2L_eV} \text{ for } 2/\pi \text{ Re(max)}$$

With Reynolds numbers between 2000 and 10,000 for v_{pi}(max) the friction term cannot be evaluated reliably by a general expression. The most unfavorable assumption is that friction will increase to its calculated maximum based on f at Re(max) as a function of sin α rather than sin$^2\alpha$, since sin α is always greater between 0 and 1. The result is to compensate for increase in f at Reynolds numbers below maximum and agree with the known condition that flow always must start in the streamline region and increase faster than sin$^2\alpha$ when cos α is close to its maximum value. Actually, this assumption overcorrects for increase in f and gives a safe method for evaluating the combined maximum of friction and inertia. Taking f for Re(max) from empirical handbook data and assuming it constant with sin α, gives the general form $c_1(a_1 \sin \alpha + b_1 \cos \alpha)$, having as its maximum value $c_1\sqrt{a_1^2 + b_1^2}$. The final possibility for limiting conditions to prevent cavitation for 0 to 90 deg will then be as follows:

0 to 90 deg limit 2000 > Re < 10,000

$$P_1 - P_2 + \frac{\rho h}{144} > \frac{\rho VN^2}{18gD^2}\sqrt{\left(\frac{fL_eV}{D^3}\right)^2 + (\pi L)^2 (S^2)}$$

f taken at Re(max).

Assume pure harmonic motion is satisfactory in calculating v_{pi}(max) for Reynolds numbers and friction forces. For pumps of normal design the correction is only a few per cent above harmonic values at maximum. Since f and viscosity are not established to any greater degree of precision, correction of v_{pi}(max) for sinusoidal motion can be omitted. Although the amplitude of the velocity curve is not changed the slope is greatly altered by the swing of the connecting rod and values of a_{pi} should be corrected for sinusoidal values as shown by S, for proper maximum values of the inertia term. The correction for a_{pi}(max) can be obtained by substituting $(1 + s/2r)$ for cos $\alpha = 1$ at 0 and 360 deg and $(1\text{-}s/2r)$ for cos α at maximum at 180 deg, where s is the stroke length of the pump and r the connecting-rod length in consistent units. For 0 to 90 deg limiting conditions, S is squared in some cases as shown.

In conclusion, there are three simple basic inertia requirements easily determined at 0, 180, and 360 deg; if these are met there is the further requirement that combined friction and inertia during the first quarter cycle shall not cause cavitation by having a greater value than inertia at maximum. If friction at maximum is less than inertia at maximum the combined requirement cannot exceed $\sqrt{2}$ times the requirement at 0 deg. For small pumps and viscous liquids, friction may exceed inertia. In this case the combined requirement approaches $\sqrt{2}$ times the requirement at 90 deg as a limit by combination of two harmonic components 90 deg out of phase.

Assuming the cylinder remains full gives a means of determining the magnitude of the forces required for each at maximum and the type of flow a basis for estimating the probable peak with some assurance of success. For most proportioning pumps the assumption of linear increase of friction to maximum is the best way to determine the NPSH of the system in view of limited data for friction under conditions of continuously varying velocity.

The author is to be complimented for the general attitude of taking guesswork out of pump installations that are required to perform accurately. The nature of the limiting expressions

shows clearly how much detailed information on job conditions, properties of the liquid, and piping layout must be available for the manufacturer to evaluate an installation. The manufacturer is vitally interested in securing the most favorable conditions possible but must rely on the process-control engineer for data in order to co-operate effectively.

R. McFarland.[3] This paper is of exceptional merit and is an excellent presentation of a difficult subject. The mathematical analysis is clear, and is the first that we know of that has appeared in the literature.

We have done some similar work in connection with adjustable-volume pumps of our own design, and have obtained some interesting results on the subject of velocity waves or hydraulic shock and reversals during the pump cycle. We have found the instrumentation in this research work to be difficult, requiring techniques heretofore unknown, and have yet to solve numerous problems, in order to achieve the determination of data in the extreme high-velocity ranges of shock transmittal in typical pumping systems.

In the basic Darcy equation, an average f-value would have to be assumed, and a corresponding Reynolds-number value, as the friction factor varies with Reynolds number. Also there would have to be some theoretical instantaneous value in the pump quarter-cycle under examination. Further, the viscosity of the fluid in the system dictates the f-value and Reynolds number, so that some method of high-speed analysis of this phenomenon ultimately may yield a series of flow constants to apply to these equations and further modify them to give an even clearer picture of the hydraulics of the quarter pump cycle.

R. T. Sheen[4] and G. S. Paul[5] Our first comment concerns the conclusion reached by the author on the nomenclature employed. The senior writer introduced the term "controlled-volume" pump in a previous paper,[6] discussing the engineering and application of this type of equipment to controlled flows. The paper analyzes from theoretical considerations and standard hydrodynamic formulas, the limiting parameters in which a controlled-volume pump may operate and still not experience cavitation or a condition similar to water hammer, causing the pump to discharge a volume greater than its displacement. The author would seem to intimate that a large majority of these pumps are operating in such a manner as to have these two effects predominate. Actually, these limiting parameters are such that at least 95 per cent or more of the controlled-volume pumps installed in service are operating well within these limitations with resultant satisfactory operation and the full effect of controlled-volume flow. Furthermore, these parameters are well recognized and definite limitations are recommended by reputable manufacturers of this type of instrument on installation. When properly installed in accordance with these recommendations, a controlled reproducible volumetric efficiency is obtained so that, in effect, the controlled-volume pump acts as an instrument delivering well within 1 per cent of a reproducible volume. Therefore we reject any terminology of "adjustable-volume" pump and hold to the thesis that "controlled-volume" pump is more properly descriptive of the apparatus.

The author presents a mathematical analysis of the hydraulics of suction and discharge on this type of displacement pump. He is correct in stating that this type of unit is used as a flow-rate controller and the control of flow based on three variables, namely, the diameter of the plunger, which of course is fixed for any given pump, the speed of the pump, and the length of the stroke. Practically all manufacturers design this pump to have an adjustable-stroke length, in fact, adjustable from 0 to the full length of stroke. Various automatic positioners with motorized stroke adjusters through linkages are designed to function while the pump is in operation. Speed may be variable by means of a mechanically adjustable speed drive or varied by means of an electronic drive through Thymotrol to give a speed variation of as much as 20 to 1. The important point is, according to this paper, that any adjustment by either length of stroke or in speed of the pump, properly recognizes the hydraulics of suction and discharge that will give a metered displacement of liquid caused by plunger movement.

The first part of the author's analysis deals with the derivation of a formula relating the maximum acceleration of a liquid column in the suction side of the pump with the movement of the plunger.

The forces causing this acceleration in the liquid column are the atmospheric pressure pressing down on the surface of the liquid in the suction tank and the static head of liquid in the suction line. The pressure against the surface of the liquid and the static head are fixed by construction of the suction piping. In addition to these pressures must be added the partial vacuum inside the pump chamber created by the movement of the plunger. The limit of this vacuum is the vapor pressure of the fluid being pumped, since if at any time this pressure drops below the vapor pressure, cavitation or flashing will occur. The author predicts the maximum flow which can enter the pump chamber. Actually he has set up in Equations [1] to [4] an expression for the friction loss in the suction pipe line in terms of the force required to overcome it. The friction factor f in this expression is an experimental coefficient primarily dependent upon the Reynolds number of the system, the condition of the piping itself, that is, the smoothness of the walls inside the piping, the number of bends, fittings, orifices in the line, and so forth. Knowing this friction factor we can determine accurately the force required to accelerate the fluid in the line.

However, for many liquids and for many piping systems, this friction factor is difficult to determine in so far as it must include any frictional losses resulting from rise of the check valves in the pump, as well as those that occur in the suction piping or in the suction tanking. It is much simpler to set up a condition, in so far as the manufacturer of this type of equipment is concerned, that specifies to the customer that we must have certain minimum net positive suction head (NPSH), with a definite limitation on pump speed, knowing that this will avoid the cavitation which the author describes. The NPSH is determined at the suction of the pump itself so that this factor of safety is ample under all conditions to avoid cavitation in the pump with a speed limitation of approximately 50 strokes per min. With a higher NPSH, speeds as high as 100 strokes per min on stroke length as large as 4 in. and even 6 in. are practiced without cavitation.

For easier practical analysis to the problem, it is preferable to divide the available suction head into two parts, namely, that required to overcome all losses up to the suction of the pump and that required due to the pressure drop through the suction valves of the pump. The first portion is a function of piping and head losses and is usually more subject to accurate calculation by the design engineer. The second is a function of pump design and properly should be recognized by the pump manufacturer and specified to the customer for his individual installation. It is obvious that limits must be set on suction piping, the speeds at which the pumps operate, and the viscosity of

[3] Technical Director, Hills-McCanna Company, Chicago, Ill.
[4] President, Milton Roy Company, Philadelphia, Pa.
[5] Milton Roy Company. Jun. ASME.
[6] "Electronics in Automatic Chemical Feed Systems," by R. T. Sheen, Trans. AIChE, vol. 42, 1946, pp. 725–739.
"Controlled Volume Chemical Pumps; Design and Operation," by R. T. Sheen, *Chemical Engineering Progress*, vol. 44, 1948, pp. 327–332.

the fluids to be pumped, as it is found that cavitation will only take place under the extreme conditions of these variables. These are, however, all special cases, and the limitations normally set by the manufacturers of controlled-volume pumps are sufficient to guarantee that they will operate well within the parameters set up in this paper.

The author shows an interesting condition that is possible on the second half of the suction cycle, namely, the plunger has started deceleration. However, the mass of liquid in the suction line is at maximum velocity and must be decelerated to match the deceleration of the plunger so that it is theoretically possible to build up a pressure inside the displacement chamber that would be greater than that inside the discharge line in order that flow would pass out of the chamber while the pump is still on suction stroke. This would cause the pump to pump more liquid than its actual displacement. This condition could exist primarily when a high-speed pump is pumping a liquid of low viscosity through a lengthy suction line. If the viscosity or friction in the line is of any magnitude, this pressure surge will be damped considerably and trouble will be averted.

Reference to Fig. 4 of this discussion will illustrate readily the fact that there will be appreciable friction drop at the point of entrance of the liquid into the displacement chamber through the two check valves in the suction end of the pump. This will vary with variations in the design of the pump. The double check valve on the suction certainly will act to dampen the acceleration of the liquid on the suction stroke, and the specification on this style of pump of a pressure differential of at least 5 psi between suction and discharge is sufficient to eliminate this effect in an over-all operation. In certain installations, in fact, the pumps operate through pressure-reducing valves to obtain this necessary differential head and so eliminate this surge effect.

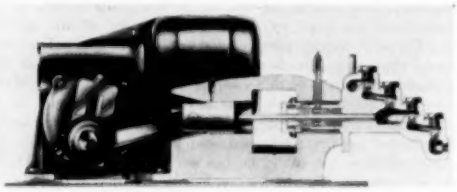

FIG. 4 TYPICAL CONTROLLED VOLUME PUMP

A controlled-volume pump will seldom operate at exactly 100 per cent volumetric efficiency, that is, it will seldom operate by discharging exactly the same amount as the plunger displacement. It is not necessary to do so. The important point is that it give repetitive accuracy so that, once a pump is calibrated properly with its attached system of suction and discharge piping and with a certain liquid, it will repeat and deliver exactly the same amount of liquid over a period of time. There is another variable in the design of the pump which is even more important in its effect on its repetitive accuracy and the variables discussed by the author, that is, the variable of valve design. Any slippage of liquid past the suction or discharge valve or valves obviously will cause inaccuracies. It will be noted in this design that a double check is used on suction and discharge. Should a slight imperfection in one valve occur, or should solids in suspension interfere with proper valve seating, the chances are that the second check will hold and give a positive check-valve action. Also it is necessary that any gas which might be drawn from solution by reduction of pressure be discharged properly and not present an opportunity for entrapment. The slope of the interior of this chamber will cause any gas introduced to be discharged automatically without the chance of alternate compression and expansion of a gas bubble leading to inaccuracies of displacement.

Mathematical derivation of the relationships involved, determining the effects of the second half of the suction stroke, are straightforward. Starting with Equation [35], the author says that the discharge pressure is given by the pressure against the surface of the liquid in the discharge tank plus the height of the liquid column in the discharge line. Now the pressure tending to unseat the valves is the pressure acting against the surface of the liquid in the suction tank plus the head of the suction line less any losses in the pressure due to the deceleration of liquid in the suction line. This is given by Equation [36]. The author then states that for the discharge balls to be unseated, the pressure inside the pump, which is given by Equation [36], must be greater than the discharge pressure, as given by Equation [35]. These two equations are equated together in Equation [37] which is actually the basic equation of this section. The author then states that, since the discharge pressure remains constant, it is only necessary to check the suction pressure plus the inertia pressure and find its maximum value. If the maximum value of this expression is less than the discharge pressure the balls will never be unseated and this effect will not occur. This is done in Equation [40]. It is found that in terms of the angle α, which is the crank angle of the pump, that the left-hand side of Equation [40] will become maximum when α is equal to π, or when the plunger is at the very end of the suction stroke. By making this substitution into Equation [40] we arrive at Equation [41] which is actually what the author says to check. If the left-hand side of that equation, which represents the maximum pressure inside the pump chamber, is less than the discharge pressure, the overpumping will not occur. However, if it is greater than the discharge pressure, some of the liquid in the suction line will be carried directly through the pump chamber into the discharge line during the suction stroke of the pump.

The author then discusses the third quarter of the pumping cycle. This is the first half of the discharge stroke where the plunger is accelerating forward, pushing water out through the discharge line. There are several factors which may act to decrease the amount of water pumped during this portion of the pumping cycle. At the moment of reversal of plunger throw from suction to discharge, there will be a slight flow back of liquid from the displacement chamber to the suction line to give the suction balls a chance to seat. The next factor is the compressibility of the liquid inside the pump chamber and also the expansion of the pump chamber when subjected to an internal pressure or any compressibility of packing used in the stuffing box.

These pumps are designed and in operation against pressures as high as 30,000 psi, so these other factors become quite important. Particularly with a number of organic liquids, compressibility at these higher pressures must be recognized. Hence we come into a study of the volume of displacement in the chamber relative to the total liquid volume of the chamber, as the discharge valves will not open until the pressure in the discharge chamber exceeds the pressure in the discharge line. During the first portion of the discharge stroke, the forward motion of the plunger is effecting compressibility.

The author points out the possibility of "overpumping" occurring in the second half of the discharge cycle due to the acceleration of the liquid from the pump to the discharge line and the deceleration not matching the acceleration of the plunger. Here again this could take place only in the event of a very low discharge pressure.

The author then speaks of the destructive effects of cavitation. He states that the collapse of a vapor pocket which has formed

within a cylinder obviously will release a large block of energy which must be absorbed by the pump. This is actually a misstatement of what occurs, for it is not a release of energy which causes the destructive effect of cavitation, but rather a momentum effect. It can be shown that when cavitation occurs there is a condition of lower energy rather than one of higher energy, as the author states. This destructive effect results from impact on the plunger when the cavitation pocket collapses and the plunger suddenly meets a solid body of liquid while traveling at fairly high velocity. No energy is liberated by the pocket. Actually, energy is consumed by the process. However, as the author states, cavitation is "quite destructive to the entire pumping system including the pump, suction line, discharge line, and possibly other equipment to which these lines are attached." Therefore it is most important in any plunger-type installation that the cavitation effect be avoided if at all possible.

Of the two limiting conditions described, which might cause inaccuracies in controlled-volume pumping, the conditions associated with the suction stroke obviously are the more serious, inasmuch as this piece of equipment, in the majority of installations, acts as a pump as well as a meter, effecting a considerable rise in the pressure state of the liquid flow. The author states that the analysis covered by this paper applies to the duplex pump also where the two pistons are in phase, or in the type where they are 180 deg out of phase. A novel design of controlled-volume pump known as the "Constametric pump" was placed on the market recently, Fig. 5.

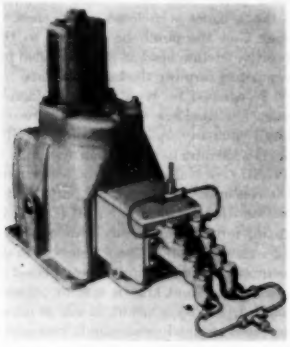

Fig. 5 Constametric Pump

This pump is a duplex unit with accentuated sinusoidal suction curve and an overlapping discharge curve so designed as to give a constant rate of discharge flow. Fig. 6 shows this characteristic curve. Operation of this pump is by means of face cams. One plunger accelerates to a constant speed and at the end of the stroke decelerates, while plunger No. 2 is on its acceleration curve. The acceleration of one plunger is matched with the deceleration of the second plunger and, with due allowance for slippage for the valve rise and fall, a straight-line flow characteristic is obtained on the discharge stroke. Any suction conditions causing cavitation would be accentuated on this design. The whole success of this unit in its application today is as an instrument to give a straight-line, nonpulsating flow. Tests made on this unit in a number of installations to date have shown it to do exactly this, without difficulty caused by either of the phenomena described by the author.

Fig. 7 shows how this type of discharge is obtained by means of

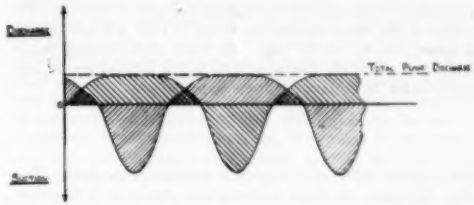

Fig. 6 Discharge Curves of Constametric Pump

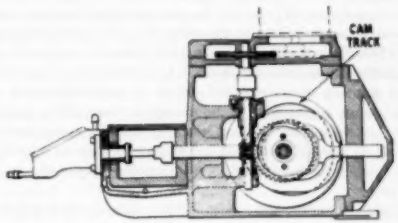

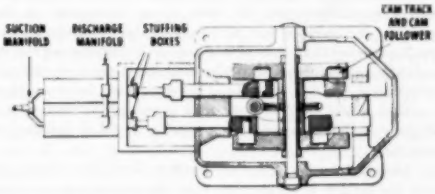

Fig. 7 Internal Details of Constametric Pump

a vertical drive to a central shaft on which are mounted two face cams. The rate of plunger travel is determined by the cutting of the cams, properly matching acceleration and deceleration.

In conclusion, the author's paper is an interesting mathematical analysis of the hydraulics flow and will aid in the understanding of the application of controlled-volume pumps as instruments—to control accurately flows of liquid to points of higher pressure in processes. The limitations described by the author are limitations that are avoided by following the recommendations of competent manufacturers in this field. When installed in accordance with these limitations, controlled-volume pumping will result with repetitive accuracies in most cases well within 1 per cent of the capacity of this instrument.

Author's Closure

The author is grateful for the contributions made to his paper by the discussers. It is particularly gratifying to note that they all represent manufacturers. If the paper has directed attention to this problem and has stimulated sufficient interest to promote further investigation, it will have served its intended purpose.

Mr. Hefler especially is to be congratulated not only for making a very thorough study of the paper but for having independently extended this study. In connection with his discussion the author feels called upon to add a few comments regarding the friction factor (f). It is assumed that any engineers who will use the relations developed in my paper understand the meaning, use, and derivation of this factor. They will, therefore, under-

stand that it is not constant throughout any quarter cycle but is a function of the Reynolds number which, in turn, is a function of the mean velocity in the pipe. In those proportioning pump applications where the flow is entirely in the laminar region, the friction factor f in Equation [12] can be replaced by

$$\frac{64\mu}{v_l D}$$

where μ is the coefficient of kinematic viscosity of the fluid. This makes Equation [12] linear in the laminar region as is shown by curve 5 of Mr. Hefler's Fig. 3.

However, in cases where the flow is above the laminar region during a portion of the stroke, a rigid solution will require that the curves of Equations [12] and [34] be plotted, using for each point the value of f corresponding to the value of (v_l) for that particular point. Then if the curve of a_l lies wholly above the curve for a_{pl} the installation under investigation will be satisfactory. However, this rigid solution is not required except in borderline cases, so that it is usually permissable to assume some reasonable constant value for f, such as 0.04, and perform steps 1 and 2 as outlined in the paper. If this indicates that conditions are close to a borderline, the more tedious method of plotting the curves should be resorted to.

Mr. Hefler suggests that in connection with the first quarter-cycle, some computation could be saved if step 2 were to be performed before step 1. Actually, the order in which these steps are performed is unimportant. If there is any advantage in the reverse order it would seem to stem from the fact that the algebra of step 2 is simpler than that of step 1 so if the installation can be proved to be unsatisfactory by performing step 2, the more difficult computation is avoided. It should be emphasized, however, that while either one of the two steps may prove an installation unsatisfactory, both steps must be employed to prove an installation is satisfactory.

Mr. Hefler points out that if the method of analysis which was used by the author in connection with the second quarter-cycle were to be applied to the fourth quarter-cycle, it would be shown that it is necessary to perform only step 2 in connection with the fourth quarter-cycle. This step 2 is merely a method of determining that a_l', as defined by Equation [42], is equal to or greater than a_{pl}', as defined by Equation [43], when v_l is zero.

Or

$$\frac{g}{l'}\left[(h' - h) + \frac{144}{\rho}(P_1' - P_1)\right] \geq \frac{8\pi N^2 V}{D'^2}$$

By applying the method of the second quarter-cycle to the fourth quarter-cycle this same relation is arrived at, thereby verifying Mr. Hefler's contention. The method proposed in the paper can, therefore, be simplified by eliminating step 1 in connection with the fourth quarter-cycle.

Mr Hefler introduces the correction for nonsinusoidal motion of the simple-crank and connecting-rod system. The use of this correction increases the accuracy with which a given system can be analyzed when dealing with a pump which uses this simple design. However, as stated in the paper, for a pump using any other than this simple design, this higher degree of accuracy can be attained only if the manufacturer will determine and supply this factor. It may be pointed out that there are designs in which the plunger moves at essentially constant velocity. The analysis of the paper fails completely in this case. It can readily be shown, however, that with this type of pump the volume discharged is never equal to the displacement.

Mr. McFarland points out the difficulties of measuring shock waves in hydraulic systems. These problems have been undertaken by a number of investigators within the past several years and improved methods and techniques are gradually emerging into the literature. His comments regarding the friction factor f are pertinent. Suggested methods for handling this are outlined in the foregoing.

This author is somewhat at a loss to account for the depreciatory tenor of the discussion by Messrs. Sheen and Paul. While much of this requires no further comment because of its irrelevancy to the problem, there are several points which must be clarified.

They state that the friction factor f is a function of "the number of bends, fittings, orifices in the line, and so forth." They further state, "However, for many liquids and for many piping systems this friction factor is difficult to determine in so far as it must include any frictional losses resulting from rise of the check valves in the pump, as well as those that occur in the suction piping or in the suction tanking." It will be recognized at once that this is completely in error. None of these items affect the friction factor f. It is these which, when added together, establish the value of L_e. Since L_e is the direct sum of all these items, including the pressure loss across the check valves, it would appear that the possibility exists for the manufacturer to determine and express this check-valve pressure loss directly in pipe-length equivalents. By publishing this value for each pump he would provide the process-control engineer with the data which would make it possible to include the pump friction factors as well as the external system factors in Equation [12] thereby increasing the accuracy with which results can be predicted by this method. It is hoped the pump manufacturers will take this important step in the near future.

These discussers imply that the method developed and proposed in the author's paper is useless and unnecessary, the only requirement being that the pump be installed so that it has a minimum net positive suction head as recommended by the manufacturer, the parameters forming the bases for these recommendations being well recognized by reputable manufacturers. However, an investigation discloses that the only recommendation which Mr. Sheen's company makes regarding NPSH is the following: "If there is a vacuum in the suction system, a net positive suction head (NPSH) equivalent to 8 ft of water must be maintained above the centerline of the suction port." It is not clear from this instruction whether this 8 ft NPSH is (1) that calculated by standard existing formulas for steady-state conditions, (2) that as measured under the cylic conditions which exist in the hydraulic system after the proportioning pump has been placed in operation, or (3) that as calculated from known system parameters before the pump is installed. If (1) is meant, it will at once be obvious that calculations based on steady-state conditions have no meaning when applied to cyclic conditions. If (2) is meant, it may be useful in helping to determine why an unsatisfactory installation is not performing properly, but it is of no use in the design stage where the proper conditions should be established to insure satisfactory performance before the installation is made. Naturally, no engineer can afford to be satisfied with a method which merely tells him that he did his job wrong. He must have analytical tools which permit him to do his job correctly the first time. If (3) is meant, this author would be interested in learning more about the methods used. The specific reason why the investigation presented in this paper was undertaken was because no method could be found in existing literature for calculating NPSH in this type of system. The method disclosed in this paper, and the extension presented in Mr. Hefler's discussion, are the only methods known by this author and if Messrs. Sheen and Paul have previously used either of these, or some other method, it is unfortunate that they did not disclose it as a part of their discussion because it would have made a valuable and creditable contribution to this subject.

These discussers imply that the conditions which may cause underpumping during the first quarter-cycle, or overpumping

during the second or fourth quarter-cycles, are so extreme as to be essentially nonexistent so that any analytical method for detecting these conditions is unnecessary. However, a number of everyday combinations immediately come to mind which would be unsatisfactory if only the recommendations of Mr. Sheen's company were followed. Assume, for example, a process which requires the use of a solvent for one reason or another. This solvent would normally be received and stored in a large yard storage tank from which it would be pumped to the process which often would be a considerable distance from the yard tank. In the process it is required that the solvent be proportioned to a variable-rate process stream. For maintenance and various other reasons, it would usually be desirable to locate the proportioning pump within the processing area rather than at the yard tank. If the solvent enters the process stream at atmospheric pressure on the first floor, there will be cavitation on the first quarter-cycle and overpumping on the second quarter-cycle unless the installation is very carefully designed. Yet this represents a common application problem. If the pump were located at the opposite end of the line, that is, at the yard tank, overpumping would be apt to occur on the fourth quarter-cycle. However, systems can be designed to assure satisfactory performance from this type of application using the methods developed in the paper. In many cases this can be done by merely juggling parameters in the equations developed in the paper. In other cases air-loaded surge chambers may be required. These discussers state that overpumping will not occur on the second-quarter cycle if a minimum of 5 psi is maintained between suction and discharge. It is the author's belief that any experienced process-control engineer, with the help of Equation [41], can readily visualize a number of common applications in process-control work which would overpump if no precautions were taken except to provide this minimum-pressure differential.

These discussers state that it is not necessary that a controlled-volume pump operate at 100 per cent volumetric efficiency. It is only necessary "that it give repetitive accuracy, so that once a pump is calibrated properly with its attached system of suction and discharge piping and with a certain liquid, it will repeat and deliver exactly the same amount of liquid over a period of time." This, of course, is true only if the proportioning pump is to be restricted to simple constant-flow rate service. It is unusual to find a manufacturer who advocates the observance of conditions which limit the use of his product to such a narrow field. It is probably this restriction which permits the statement that 95 per cent of existing installations are satisfactory despite the lack of analytical methods to predict their performance. This author feels that if all the parameters are known and properly evaluated, the field of usefulness of this device can be greatly extended. If proportioning pumps are to be used extensively as flow-rate controllers in process-control work, they must operate, not at constant-flow rates, but over a wide range of flow rates which usually are continuously variable. This type of service requires that they maintain constant ratios between rate of delivery and speed, and rate of delivery and stroke length, which is to say that volumetric efficiency must be maintained at 100 per cent throughout the entire operating range. This author believes that if these requirements are met, the proportioning pump is capable of handling certain classes of process-control problems more satisfactorily than any other control device now available.

These discussers attempt to offer an explanation of the nature of cavitation and state that its destructive effects are not due to a release of energy. Inasmuch as the destruction represents work, and inasmuch as work can be done only at the expense of energy, (in this case it is derived from the kinetic energy of the moving liquid column) it would appear that their comments can be readily evaluated.

Mr. Hefler as well as Messrs. Sheen and Paul mention factors which are inherent in reciprocating pump design which make it impossible to ever achieve exactly 100 per cent volumetric efficiency. These are principally (1) the slippage which occurs past the valves due to the delay in seating when the plunger changes direction, and (2) the compression of the gland packing and plunger and the expansion of the cylinder when pumping against high heads.

These errors must be recognized as must the errors in any measuring device. A well-designed instrument-type flow-rate control installation, with its inherent error detection, will have a maximum error within ± 2 per cent. Error detection is not inherent in the proportioning pump system. However, if a proposed installation satisfies the tests developed in this paper, the maximum error will be of the same order as that of an instrument system. This is usually satisfactory for most process-control work. Somewhat higher accuracies can be achieved in low-pressure applications with a pump operating at slow speeds.

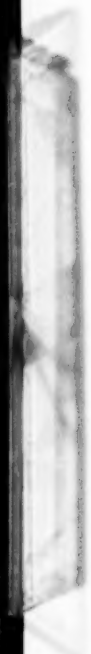

Discharge Coefficients of Herschel-Type Venturi Tubes

By A. L. JORISSEN,[1] ITHACA, N. Y.

An analysis has been made of a large number of calibration curves of Herschel-type Venturi tubes, in order to obtain average values of the coefficient of discharge, both in the range of constant coefficient and of coefficient varying with Reynolds number. The data furnished by American practice have been compared with foreign standards of flow measurement.

Introduction

THE description of the Venturi tube, as originally adopted by Clemens Herschel in 1887 (1),[2] is given in a Society research publication (2), as follows:

"Starting at the upstream flange, the first portion is a short cylindrical inlet which is a continuation of the upstream pipe line. This part is either machined inside or cast smooth so that its diameter can be accurately determined. A side hole, or several holes, drilled through its wall, lead into a piezometer ring, to which a pressure pipe-connection can be made for measuring the static pressure of the fluid at the inlet.

"Following the preliminary straight part is the entrance cone which has an included angle of about 21 deg. The straight and converging parts are joined by a curved surface. The entrance cone leads to the short cylindrical throat which is accurately machined and is provided with a side hole or holes for piezometer measurement of the static pressure in the throat. The transition from the entrance cone into the straight throat is rounded off by an easy tangential curve to avoid the resistance caused by a sharp corner and also to preclude the possibility that the fluid might break away from the wall at high speeds and not fill the throat completely.

"... The end of the throat leads, by another easy curve, into the exit or diffuser cone which has an included or total angle of between 5 and 7 deg. This terminates in the outlet flange, or other type of end, for connecting the Venturi to the pipe line..."

This type of Venturi tube has been used consistently in American practice. It is, moreover, very similar to the types used abroad, sometimes under the denomination of "classical Venturi" (3) and which are currently described in the British (4) and French (5) standards of flow measurement.

At the 1950 Annual Meeting of the Society, the author delivered a paper in which the state of development of the method of flow measurement by means of Venturi tubes was reviewed (6). This paper contained a brief historical sketch of the various steps taken toward an international standardization of Venturi tubes and presented information on the coefficients and data used in European countries, mostly England and France, codified in their national Standards (4, 5).

Since the Society is now participating actively in the work of the International Organization for Standardization: ISO/TC/30 Committee on Measurement of Fluid Flow,[3] it appears that the preparation of international standards will soon be undertaken.

Analysis of Calibration Curves of American Venturi Tubes

To help in the choice of average coefficients, the author made an analysis of calibration curves of American Venturi tubes, obtained from various sources. A total of more than 200 tubes was studied, calibrated between the years 1925 and 1951, for pipe diameters ranging between 2 and 32 in. and diameter ratios β between 0.270 and 0.755. The total angle of the converging cone was always approximately equal to 21 deg, the diffusers had various angles, varying between 5 and 28 deg.[4] Other construction details are the property of the manufacturers. Many of the tubes were of cast iron; others of cast steel; in many cases, the throat was made smooth by means of a bronze lining. Most of the tubes were new, when calibrated; a few of them, however, had been in use before the calibrations were made.

The results of the analysis are given in Table 1[5] and Figs. 1, 2, and 3. For each tube, the following data were obtained:

1 Pipe diameter, D, in.

2 Throat diameter, d, in.

3 Diameter ratio $\beta = d/D$.

4 Opening ratio, $m = (d/D)^2 = \beta^2$ (opening ratio is used in Europe in preference to diameter ratio).

5 Material.

6 Coefficient of discharge C in range where it is independent of Reynolds number; this is the coefficient of calibration, to be used in the formula

$$Q = \frac{CA_2}{\sqrt{1-\beta^4}} \sqrt{2g \frac{p_1 - p_2}{\gamma}}$$

in which

Q = rate of flow, cfs

A_2 = area of throat section = $\pi d^2/4$, sq ft

$\frac{p_1 - p_2}{\gamma}$ = differential pressure head, ft of flowing fluid

γ = specific weight of fluid, pcf

7 Coefficient C_β obtained, for the same value of β, from the ASME Research report (2).[6] This value may be considered as corresponding to standard American practice, although the formula from which it is obtained has been criticized as being complicated, and hope has been expressed that a more convenient

---

[1] Head of the Department of Hydraulics and Hydraulic Engineering, School of Civil Engineering, Cornell University. Mem. ASME.

[2] Numbers in parentheses refer to the Bibliography at the end of the paper.

Contributed by the Fluid Meters Research Committee, the Industrial Instruments and Regulators Division, and presented at the Annual Meeting, Atlantic City, N. J., November 25–30, 1951, of The American Society of Mechanical Engineers.

Note: Statements and opinions advanced in papers are to be understood as individual expressions of their authors and not those of the Society. Manuscript received at ASME Headquarters, September 12, 1951. Paper No. 51—A-56.

[3] Minutes of the December, 1949, meeting of ASME Power Test Codes Committee (3071).

[4] Diffuser angles used in practice are thus sometimes considerably larger than those of the Herschel Venturis. It appears, however, that within the limits considered, the angle of the diffuser is without influence on the coefficient of discharge.

[5] Copies of this table may be obtained from the Research Department, The American Society of Mechanical Engineers, 29 West 39th St., New York 18, N. Y.

[6] Formula 261, p. 99.

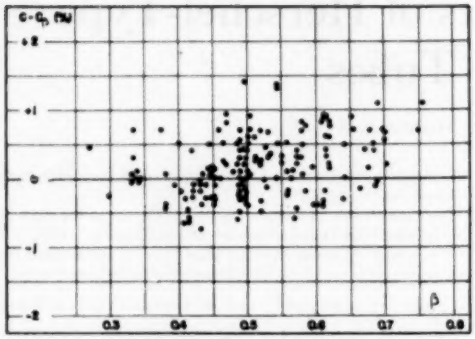

FIG. 1 $C - C_B$ (IN PER CENT OF C) IN FUNCTION OF β

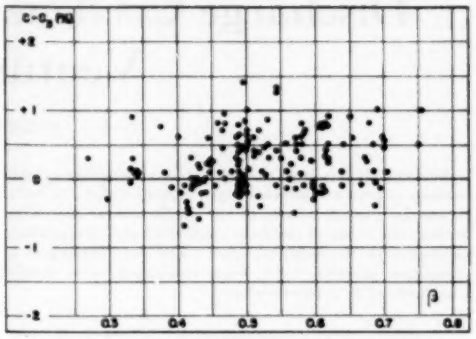

FIG. 2 $C - C_B$ (IN PER CENT OF C) IN FUNCTION OF β

form of determining the coefficient for diameter ratios other than 0.5 would be found.

8 Difference $C - C_\beta$, per cent of C.

9 Coefficient C_B obtained, for the same value of β (or m), from the British Standards (4).

10 Difference $C - C_B$, per cent of C.

11 Coefficient C_F obtained, for the same value of β (or m), from the French Standards (5).

12 Difference $C - C_F$, per cent of C.

13 Value $(N_R)_s$ of Reynolds number for which the coefficient C, having ceased to be constant, differs by 0.1 per cent of its constant value. Since practically all the experimental curves of discharge coefficient in function of Reynolds number indicate the same trend, the coefficient increasing with increasing Reynolds number until it levels off at some value of the latter number, the value of $(N_R)_s$ gives some indication concerning the value at which the limit of constancy is attained. All Reynolds numbers are expressed in function of the pipe diameter, according to what will be from now on standard practice.

Among the data collected, some had to be eliminated because they corresponded to tubes not conforming with the Herschel type described. Furthermore, it was found that Venturi tubes with a single pressure tap, either at the throat or at the entrance section, were liable to behave in a completely different manner, the difference between their coefficient of discharge and that of Venturi tubes with conventional piezometer connections reaching, in some cases, more than 2 per cent. For this reason, these tubes have not been included in this analysis.

Finally, all the calibrations have been conducted using water as the flowing fluid. Hence no information has been obtained on compressibility effects.

DISCUSSION OF RESULTS

Inspection of Figs. 1, 2, and 3 shows a good agreement, in most cases, between the experimental coefficient C and either C_β or C_B. Differences between C and C_F are usually larger. It must be observed, however, that the French Standards (5) do not apply to values of β smaller than 0.4 ($m = 0.16$) and that the coefficients C_F had to be obtained by extrapolation for low values of β.

Closer examination of Figs. 1 and 2 leads to the conclusion that a larger number of points lie above the line of abcissas than below it. A statistical analysis shows that this line should be raised by approximately 0.25 per cent in Fig. 2 to obtain a uniform distribution of the deviations. This amounts to adopting as average coefficients values 0.25 per cent higher than those

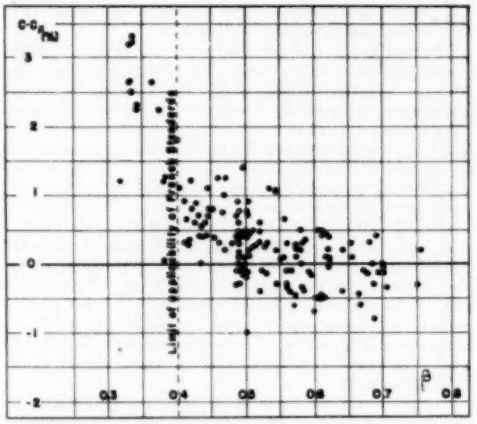

FIG. 3 $C - C_F$ (IN PER CENT OF C) IN FUNCTION OF β

given by the British standards (4). Since these standards afford an easy method of computing the coefficient of discharge, the same method has been used to establish an average coefficient C_S, which is, roughly, 0.25 per cent larger than C_B. Values of C_S in function of β are given, for pipe diameters between 2 and 32 in., in Fig. 4.

Table 1[8] and Fig. 5 provide a comparison between the experimental coefficient C and the average coefficient C_S. If the latter is taken as standard reference, the maximum deviation for the great majority of the tubes does not exceed 0.75 per cent, the root-mean-square error of an experimental coefficient being 0.4 per cent, and the probable error less than 0.3 per cent. Furthermore, a close examination of the data in Table 1 shows that it is not possible to assign different values of the deviation for various pipe diameters. The figure of 0.75 per cent seems to be valid for large as well as for small pipe diameters.

Of the 181 Venturis included in Table 1, only five have experimental coefficients C differing by more than 0.75 per cent from the average coefficient C_S. They are as follows:

Venturi No. 72. This is a tube of relatively small size (4.070 × 2.0182). The calibration curve is rather irregular. Straightening vanes were placed immediately upstream of the Venturi and may have affected the calibration.

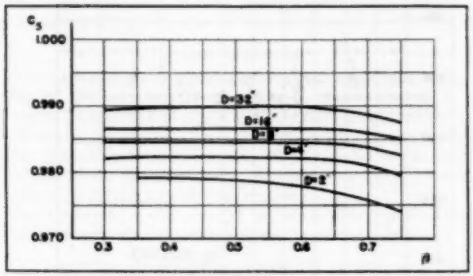

FIG. 4 AVERAGE COEFFICIENT C_S IN FUNCTION OF β FOR PIPE DIAMETERS BETWEEN 2 AND 32 IN.

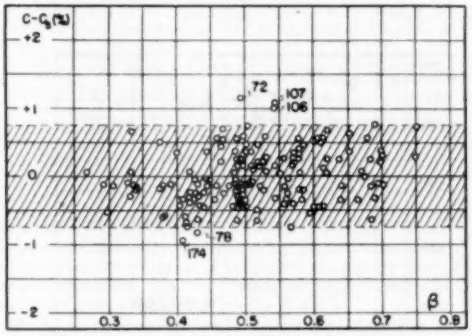

FIG. 5 $C - C_S$ (IN PER CENT OF C) IN FUNCTION OF β

Venturi No. 78. The diameter of the inlet pipe was not exactly equal to the Venturi tube inlet diameter. The throat vents were in poor condition.

Venturis Nos. 106 and 107. No explanation can be found for the large discrepancy. Both Venturis were rather small (4.000 × 2.178), and the calibration curves show only a small number of points.

Venturi No. 174. No explanation can be found for the large discrepancy. This is also a small Venturi (3.981 × 1.631). It is suspected that a recalibration may have given a higher coefficient.

CONCLUSION

It may be said that the diagram, Fig. 4, gives the value of the average coefficient with a maximum deviation of ±0.75 per cent for practically all tubes of pipe diameters between 2 and 32 in.

Inspection of the individual calibration curves shows that single measurements give deviations from the mean coefficient varying between 0 and ±0.5 per cent, the root-mean-square error of one measurement being between 0 and ±0.3 per cent, and the probable error between 0 and ± 0.2 per cent. It is evident that these figures will vary from laboratory to laboratory and depend upon the accuracy of the equipment used and the care with which measurements are analyzed.

The experimental curves have also been studied in the region of nonconstant coefficient. As explained previously, the trend is practically always a decreasing one with decreasing Reynolds number. For a limited number of tubes, as Reynolds number decreases, a slight increase in the coefficient is noticed before the characteristic decrease takes place. This trend has been observed already by Schlag (3), mostly with very smooth pipe lines.

For each tube, the value of the discharge coefficient has been measured from the curve at Reynolds numbers of 10,000; 20,000; 30,000; 50,000; 100,000; 200,000; and 300,000. No extrapolation was made, however, when the actual calibration curve did not cover all these values of Reynolds number. The ratios of these coefficients to the constant coefficient for each curve have been taken as coefficients of correction and are plotted in function of β, in Fig. 6. No effect of the diameter ratio β is apparent.

The mean values of the coefficients of correction for low Reynolds numbers are indicated in Table 2 and plotted in Fig. 7. They indicate values by which the average coefficient has to be multiplied to give the coefficient of discharge for Reynolds numbers below the limit of constancy.

An examination of Fig. 6, however, shows that the deviations may be extremely important in individual cases, particularly at low values of Reynolds number. Therefore the coefficients of correction are given only as an indication of possible values, in the hope that they will be refined by comparison with the results of further calibration tests, and that by drawing attention to unusual

TABLE 2 COEFFICIENTS OF CORRECTION FOR LOW REYNOLDS NUMBERS

Reynolds number	Coefficient of correction
10000	0.964
20000	0.975
30000	0.977
50000	0.9835
100000	0.9945
200000	0.9995
300000	1.000

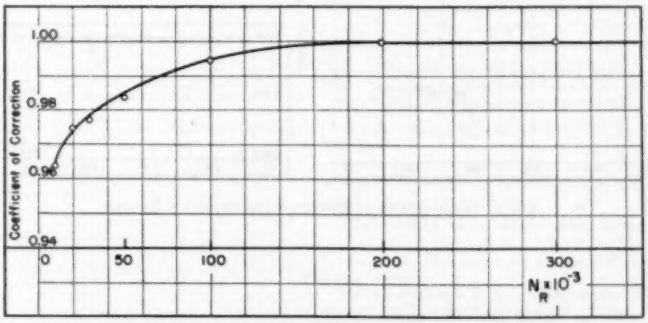

FIG. 7 COEFFICIENT OF CORRECTION IN FUNCTION OF REYNOLDS NUMBER

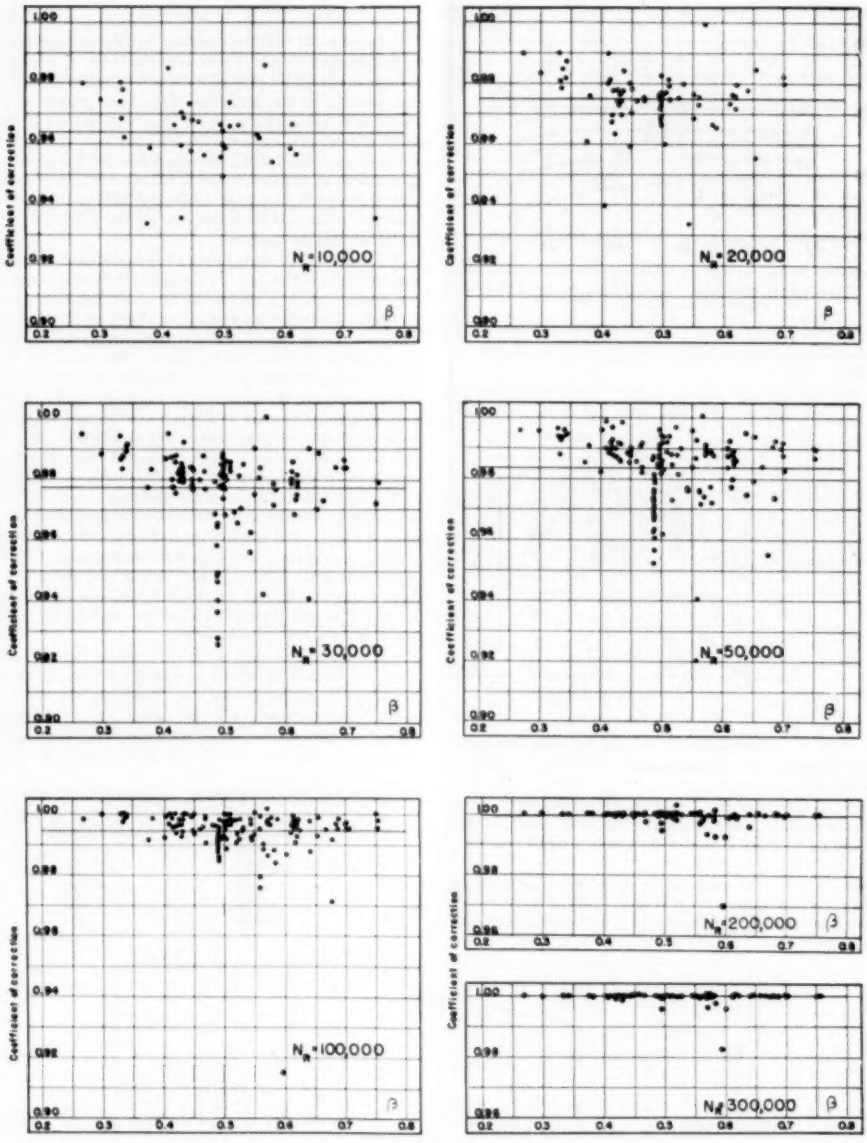

FIG. 6 COEFFICIENT OF CORRECTION FOR REYNOLDS NUMBER

results, they may justify a more thorough study of the various factors affecting the calibration of Venturi tubes.

ACKNOWLEDGMENTS

The author wishes to express his sincere gratitude to Prof. W. S. Pardoe of the University of Pennsylvania, and to Prof. S. R. Beitler of Ohio State University, for rendering assistance at various stages of this study. He is also indebted to Messrs. I. O. Miner of Builders-Providence, Inc., M. M. Borden of Simplex Valve and Meter Company, and R. E. Sprenkle of Bailey Meter Company for furnishing valuable information.

Miss Constance Wellen and M. R. B. Robinson performed many of the computations and checking.

BIBLIOGRAPHY

1 "The Venturi Meter," by Clemens Herschel, Trans. ASME, vol. 17, 1887, p. 228.
2 "Fluid Meters, Their Theory and Application," ASME Research Publication, fourth edition, 1937.
3 "Contribution à la normalisation des tubes de Venturi classiques," by René Rousselet and Alb. Schlag, *Revue Universelle des Mines*, series 9, vol. 6, 1950.
4 "Flow Measurement," British Standard Code 1042, 1943.
5 "Mesure des Débits instantanés des Fluides," Association Française de Normalisation, NF X10-101, 1949.
6 "Discharge Measurements by Means of Venturi Tubes," by A. L. Jorissen, Trans. ASME, vol. 73, 1951, pp. 403–411.

Discussion

I. O. MINER.[7] The author's recommended Venturi-tube discharge coefficients indicated by his Fig. 4, are amply accurate for use within the range of sizes covered. Undoubtedly the data will be extrapolated because of the lack of comparable data for larger Venturi tubes. Fig. 8 of this discussion shows the author's coefficients plotted against line size for $\beta = 0.5$.

The curve appears a little too straight to the right of 8-in. line size, because generally it is considered that the curve should be asymptotic to unity coefficient.

The writer recommends that the curve for 32-in. line size be dropped approximately 0.1 per cent for $\beta > 0.4$ and made constant for $\beta < 0.58$.

It is highly regrettable that the data from which the author plotted his results were not published. The author gave the writer a copy of his data in tabular form. There were three Venturi tubes larger than 16 in. in diam, being numbered 1, 2, and 121 by him. $C—C_s$ will be smaller for tubes Nos. 1 and 2 if the curve for the 32-in. tube is dropped as recommended. C_s for 24-in. tube No. 121, as given in the table, is 0.75 per cent below the actual coefficient. However, if C_s is interpolated by Fig. 8 of this discussion, it will be found to be slightly higher than the table indicates. Dropping the 32-in. curve 0.1 per cent will result in $C—C_s$ for tube No. 121 being —0.72 per cent, within the author's conclusions of 0.75 per cent maximum.

If the curve for 4-in. line size in Fig. 4 of the paper is dropped 0.03 per cent a smoother curve of coefficient versus line size will result. Such a slight change will have no other significance.

Fig. 11 of the discussion by Schlag indicates an unlikely trend if the data from the French Standard are extrapolated to larger sizes. Unity coefficient is rapidly exceeded when line size exceeds about 2000 mm.

[7] Vice-President and Chief Engineer, Builders-Providence, Inc., Providence, R. I. Mem. ASME.

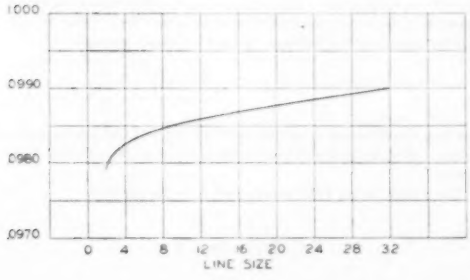

FIG. 8

ALB. SCHLAG.[8] In this discussion the author's conclusions are compared with the recommendations of the French standard NF X 10–101 (1949 edition) and of the British Standard Code B.S. 1042–1943 (Flow measurement). This comparison is also based on the writer's experience with Venturi tubes.

The discussion is limited to the region of large Reynolds numbers, such that the numerical value of this coefficient is without importance. This is the only region which is now of practical interest. Furthermore, it appears that, outside this zone, the experimental results are still too uncertain to allow for definite conclusions.

The French standard and the British standard code give:

A diagram $C = f(m)$ (Fig. 56 in the French standard; Fig. 20a in the British standard code).

A diagram of the coefficient J to take into account the effect of the diameter (Fig. 57 in the French standard; Fig. 20c in the British standard code).

However, neither the French nor the British standard offers a clear definition of the coefficient C. For other pressure-differential devices C is the coefficient to be used when no correction is necessary either for scale and roughness effects (D larger than 300 mm or 12 in. for nozzles) or for Reynolds-number effect.

In the French standard, Fig. 57 shows that the correction J equals unity when D is slightly larger than 1000 mm, but the exact value of this diameter is not indicated. For $D = 1500$ mm, J is larger than unity (approximately 1.004).

The same lack of precision exists in the British standard code; it appears from Fig. 20c that C could be the coefficient for very large values of D (above 32 in.) but this value is not indicated clearly.

To obviate this lack of precision, we suggest drawing the curve of the coefficient for a given diameter. A value of $D = 100$ mm was chosen arbitrarily (being the pipe diameter most frequently used in the writer's experiments), but there would be no difficulty in using another value. This coefficient has been conventionally called C (the notation CJ_{100} might have been preferable).

In Fig. 9 of this discussion are given the diagrams $C — m$, according to the French standard (NF), the British standard code (NB), and the author's paper (J). A curve SR, obtained from the writer's experiments,[9] has been added.

An important discrepancy exists at low values of m (smaller than 0.2 or 0.25) and, to a lesser degree, at values larger than 0.45–0.50.

We propose, until this discrepancy is lifted, to limit the standardization to values of m between 0.20 and 0.50 (or β approximately between 0.45 and 0.70).

There should be no serious disadvantage in this limitation,

[8] Professor, Director of the Hydraulic Laboratory, University of Liége, Belgium.

[9] "Contribution à la normalisation des tubes de Venturi classiques," by René Rousselet and Alb. Schlag, *Revue Universelle des Mines*, series 9, vol. 6, 1950, pp. 301–308.

since a Venturi tube is used when it is sought to reduce the nonrecoverable loss of pressure, which precludes the use of low values of m. Furthermore, at too high values of m, the differential-pressure readings are small and the precision is unsatisfactory.

A study of Fig. 9 discloses a satisfactory agreement between the French and the British standards at a value of $m = 0.25$. According to both standards, the coefficient C is equal to 0.98. This fact is not surprising, since Venturi tubes with a diameter

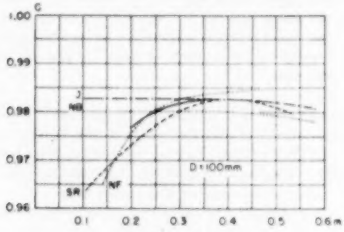

FIG. 9

ratio $\beta = d/D = 0.5$ have been more frequently built and thus more frequently calibrated than tubes of other proportions.[10]

Therefore we have plotted in Fig. 10 of this discussion, values of CJ in function of D for an opening ratio m equal to or approximately equal to 0.25. It is seen that an average curve may be drawn with good accuracy, particularly for values of D not over 1000 mm.

Therefore we propose the adoption of this curve of CJ in function of D for $m = 0.25$.

It is seen that for our diameter of reference (100 mm) one reads again distinctly $CJ = 0.98$. We shall adopt, for $m = 0.25$, $C =$

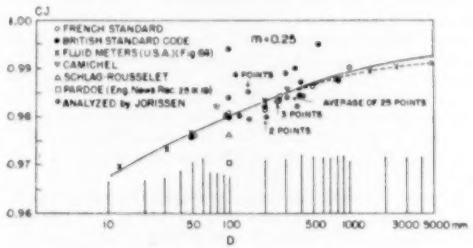

FIG. 10

0.98 (it must be recalled that the definition of C has been given for this diameter).

In brief, the result of the foregoing discussion is that, for $D = 100$ mm, the curve of C must fit the curves in Fig. 9 and give a value of $C = 0.98$ for $m = 0.25$.

We propose using the curve of C drawn as a solid line in Fig. 9. The use of this curve may be justified as follows:

It gives a value $C = 0.98$ for $m = 0.25$; between 0.20 and 0.25, it coincides practically with the curve of the French standard. Between 0.25 and 0.40, it is located between the curves of the French standard and of the author, on the one hand, the British curve and the curve of Rousselet and Schlag, on the other hand; the difference is always smaller than 0.25 per cent and often appreciably less. Furthermore, an examination of the results analyzed by the author (J), seems to indicate that instead of being constant at low values of m, C would decrease, as indicated by the French standard and by Rousselet and Schlag, but to a lesser extent.

Between 0.40 and 0.50, the suggested curve coincides with the author's curve and almost with the curve of Rousselet and Schlag; it is situated between the French and the British curves, with a deviation at most equal to 0.25 per cent.

Influence of Diameter (Coefficient of Correction J). We have plotted in Fig. 11 the diagrams of CJ according to the French standard and to the British standard code. (The author's diagram is identical to that of the British standard code, but raised by 0.25 per cent.)

For the British standard code, the values are independent of m; in the French standard, different curves are obtained for different values of m.

It appears, however, that all the diagrams are identical in trend, being simply shifted parallel to the vertical axis.

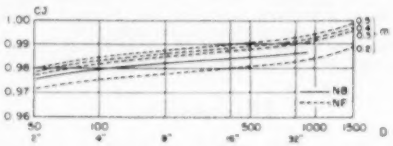

FIG. 11

Calling C the value corresponding to $D = 100$ mm, the coefficient J of transfer to another diameter does not depend on m but only on D.

Since we have proposed the adoption of $C = 0.98$ for $D = 100$ mm and $m = 0.25$, Fig. 10 of this discussion shows that for these values, $J = 1$. Therefore, for all values of m, the values of J are to be read on the CJ scale, Fig. 10, increased by 0.02.

In brief, we may suggest the following:

(*a*) To limit the standardization to values of m between 0.2 and 0.5.

(*b*) To adopt the curve $C = f(m)$ indicated by a solid line in Fig. 15 of this discussion.

(*c*) To adopt for the coefficient of correction J due to the diameter effect, the values of the ordinate scale of CJ in Fig. 10, increased by 0.02.

W. S. PARDOE.[11] One of the objects of a study such as this should be an extrapolation to coefficients of larger meters. Each test should be looked on as a model test of larger meters which cannot be calibrated. The author confines his entire effort to interpolation by dealing with the coefficient. The writer would call his attention to Professor Moody's step-up formula

$$(1 - e_p) = (1 - e_m)\left(\frac{d_m}{d_p}\right)^{1/4}$$

in which the difference between the efficiency and unity is stepped-down. Also, in fluid mechanics use is made of the velocity deficiency.

The writer, in his 1944 paper, uses K in the formula

$$C = \sqrt{\frac{1 - \beta^4}{1 - \beta^4 + K}}$$

[10] It must be observed that the formula for the coefficient of discharge given in "Fluid Meters" (1937 edition, p. 99) refers to the case where $m = 0.25$; the same is true of figs. 63 and 64 in this publication; on the latter figure, a value of $C = 0.98$ is read for $D = 4$ in.

[11] Merion Station, Pa.

in which K is the coefficient of loss in

$$_1h_2 = K \frac{V_2^2}{2g}$$

and finds that

$$K = \frac{0.0435}{(d_2{}'')^{1/4}}$$

see Fig. 12, herewith. It is evident from Fig. 13 of this discussion that the greatest part of the loss $_1h_2$ takes place in the throat and the upstream cone adjacent to the throat or at points of high velocity and hence K does not vary much with β.

This also can be shown mathematically as

$$K = 1.25\left[f_1 \frac{1}{d_1}\beta^4 + f\frac{M^2}{4d_2}\left(\frac{1}{M^4} - \frac{1}{(M+\ )^4}\right) + f_2\frac{l_2}{d_2}\right]$$

the 1.25 being an empirical correction as β decreases f_1 decreases and the first term decreases but l increases and hence the second term increases, thus keeping K nearly constant for a given throat diameter. Arithmetically the $12 \times 8^1/_4$ ($\beta = 0.687$) shown in Fig. 14, $K = 0.02840$, $C = 0.983$, and a $16^1/_2 \times 8^1/_4$ ($\beta = 0.5$) $K = 0.02711$, $C = 0.985$ or K varies little with β if d_2 is constant and C checks closely with the 1944 curves. These are the reasons which governed the writer in the indirect approach and the use of the throat diameter as being the most characteristic dimension of a Venturi meter.

The author, in Fig. 1 of the paper, neglects the variation of accuracy in terms of size shown in Fig. 14 of this discussion, derived from Fig. 1. Small Venturi meters are usually less accurate than large ones—hence the writer takes exception to the basis of this study and, therefore, to some of its conclusions.

Fig. 14 shows also a comparison of the author's coefficients with those of the 1944 paper for $\beta = 0.5$. If the author's curve be extrapolated it will run above unity, and this writer cannot abide coefficients above unity. He believes the maximum value of C is close to 0.993 which is the value for the very smooth General Electric flow nozzles. To increase this by 0.025 would give a value of 0.9955 which is much above any coefficient of Herschel Venturi meters ever obtained by the writer.

In Fig. 7 the author indicates that the coefficient curves become flat at Reynolds number 200,000. The writer calls his attention to the Moody friction-factor curve, Fig. 15 of this discussion, in which the values of f become flat at higher values of R_n for smooth pipes; that is, this value varies inversely with roughness.

Fig. 16, herewith, from the '1944 paper shows the same thing, that is, the point of tangency increases in terms of Reynolds number as the meters become larger and, consequently, proportionately smoother.

The writer showed in his paper on the "Ambient Effect" we could place no confidence in the curved part of the coefficient curves—hence any deductions from them must be wrong. Therefore he used the test of the 4×2 in. 1936 Oklahoma test on oil for lower Reynolds number.

The author's Fig. 4 is, in general, in agreement with the writer's formula. Also in Fig. 3 there is a surprising agreement on the coefficient of a 16×8 in. Venturi meter. In these results we may both be wrong.

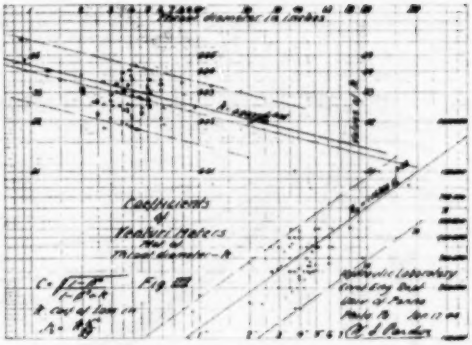

FIG. 12 COEFFICIENTS OF VENTURI METERS, PLOT OF THROAT DIAMETER, k

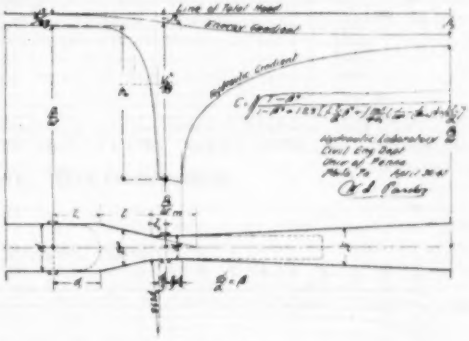

FIG. 13

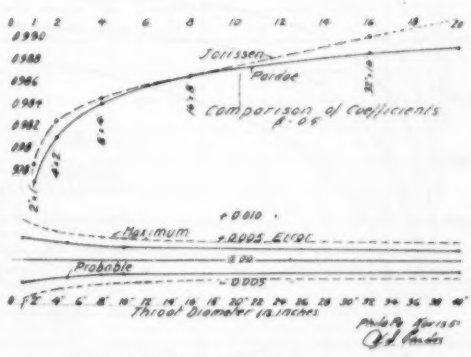

FIG. 14 COMPARISON OF COEFFICIENTS, $\beta = 0.5$

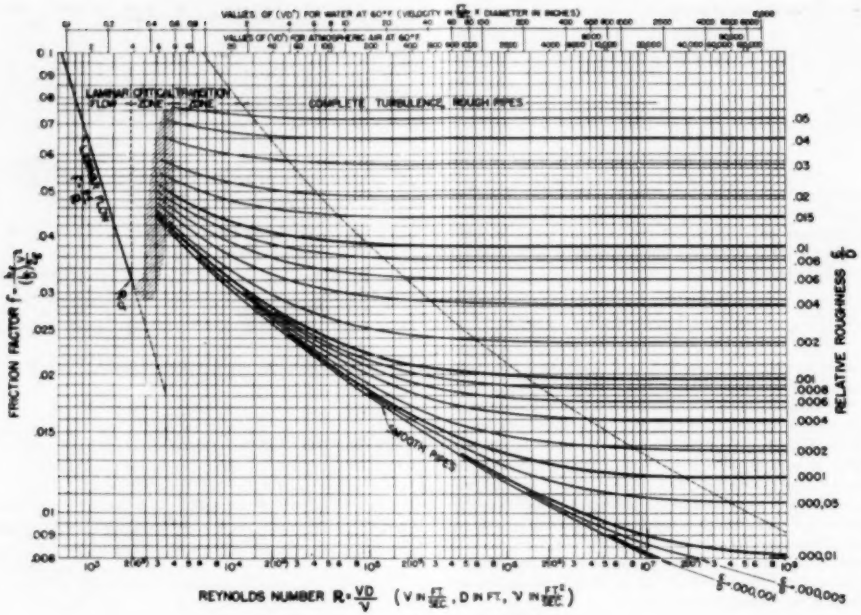
VALUES OF (VD) FOR WATER AT 60°F (VELOCITY IN FT/SEC × DIAMETER IN INCHES)
VALUES OF (VD) FOR ATMOSPHERIC AIR AT 60°F
LAMINAR CRITICAL TRANSITION FLOW ZONE
COMPLETE TURBULENCE, ROUGH PIPES
SMOOTH PIPES
FRICTION FACTOR $f = \frac{h}{(L/D)\frac{V^2}{2g}}$
RELATIVE ROUGHNESS $\frac{\epsilon}{D}$
REYNOLDS NUMBER $R = \frac{VD}{\nu}$ (V IN $\frac{FT}{SEC}$, D IN FT, ν IN $\frac{FT^2}{SEC}$)
$\frac{\epsilon}{D}$ = .000,001
$\frac{\epsilon}{D}$ = .000,005

FIG. 15

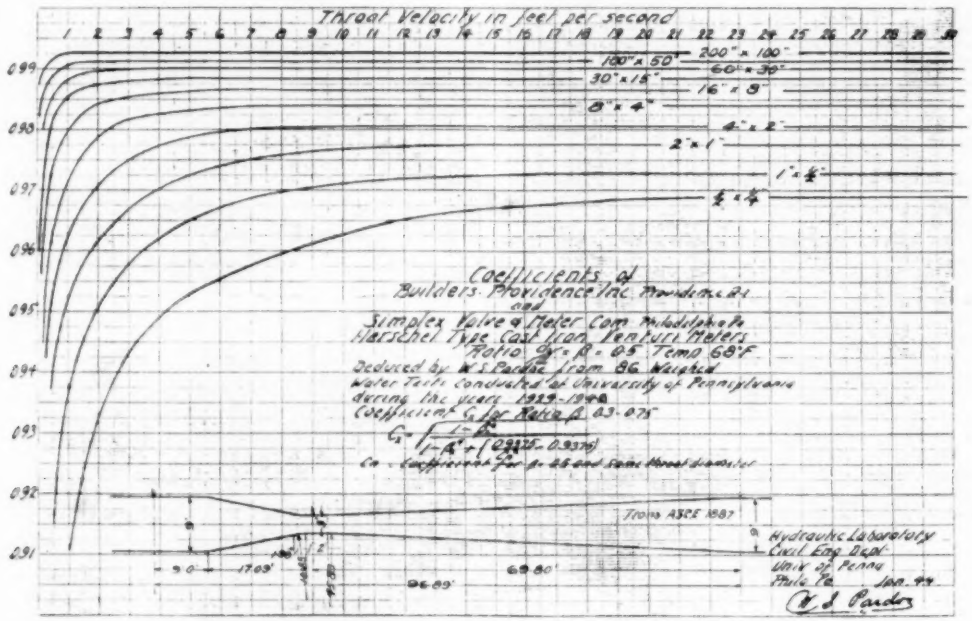
Throat Velocity in feet per second
200" x 100"
100" x 50"
60" x 30"
30" x 15"
16" x 8"
8" x 4"
4" x 2"
2" x 1"
1" x ½"
½" x ¼"
Coefficients of
Builders-Providence Inc. Providence RI
and
Simplex Valve & Meter Com Philadelphia Pa
Herschel Type Cast Iron Venturi Meters
Ratio $\frac{d}{D}$ = R = .09 Temp 68°F
Deduced by R S Parker from 86 Weighed
Water Tests Conducted at University of Pennsylvania
during the years 1929-1948
Coefficients C for Ratio R .03-.075"
$C_v = \frac{C}{\sqrt{1-R^4 \times (.9937 - 0.9376)}}$
Cv = Coefficients for R .25 and Same Throat Diameter
From ASME 1937
Hydraulic Laboratory
Civil Eng Dept
Univ of Penna
Phila Pa Jan 44
R S Parker

FIG. 16

Author's Closure

The author feels gratified that his analysis of Herschel-type Venturi-tube coefficients has been the occasion of a confrontation of the views of the specialists in this matter. It definitely seems that progress has thus been accomplished toward the international standardization of this type of flowmetering device.

In an attempt to bridge the gap indicated by Fig. 9 of Professor Schlag's discussion at low values of m, the author agrees that the values of C_s should be slightly reduced for values of β below 0.5. It is further suggested to limit the present discussion to values of β between 0.4 and 0.75. Direct contacts will have to be established before an agreement can be reached regarding coefficients at lower β. The author believes that the trend which would best fit American experimental results would be that indicated in Fig. 17, herewith. The curves for 4-in., 8-in., 16-in., and 32-in. line sizes of Fig. 4 of the paper have been dropped by 0.25 per cent at $\beta = 0.4$. Smooth connections have been drawn with the values of Fig. 4 at $\beta = 0.5$. The trend of the curve for 2-in. line size for β smaller than 0.5 may not be indicated at present. A discrepancy still exists between Fig. 17 and curves SR and NF of Fig. 9. A possible assumption is that this discrepancy would be due to differences in the radius curves of the inlet section but more information will be needed before definite conclusions can be drawn in this matter.

In plotting Fig. 17, attention has been paid to Mr. Miner's suggestion of dropping the curve for 32-in. line size of 0.1 per cent. For $\beta = 0.5$ the coefficient is thus $C_s = 0.989$. This value compares with Professor Pardoe's 0.9885. Also, the curve for 4-in. line size has been dropped by 0.03 per cent.

The author is well aware of the great need for more complete information on the coefficients of Venturi tubes of large sizes; he cannot help but feel that the utmost caution should be exercised in extrapolating experimental values. Extrapolation is at best an extremely dangerous procedure and the author hesitates to follow Professor Pardoe on these grounds. It is difficult to imagine that a Venturi tube is a model of another since the first requirement of dynamic similarity, namely, that of geometric

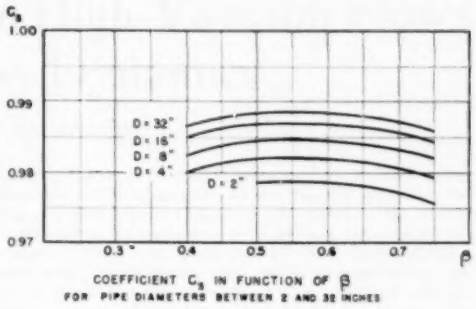

Fig. 17

similitude, is generally not fulfilled. Furthermore, the author has tried to analyze by Professor Pardoe's method the coefficients of Venturi tubes having a diameter ratio other than 0.5. For example, considering a ratio close to 0.4, there are 29 tubes with values of β between 0.35 and 0.45. For each of these, the value of K has been computed from

$$K = \frac{1 - \beta^4}{C^2} - (1 - \beta^4)$$

The values range from 0.0218 to 0.0441 (excluding tube No. 174 for which $K = 0.0548$). A plot of K in function of the diameter fails to disclose a trend similar to that which Professor Pardoe indicates in Fig. 12 of his discussion. If anything, it seems that a plot of K in function of D would give a horizontal line corresponding to $K = 0.0353$ (average value). This, in turn, would give an average C of 0.9825. It must be noted, however, that all the available data are for Venturi tubes with D smaller than 15 in. Thus the analysis points again toward the need for more experimental data on Venturi tubes of large sizes.

Nozzle Characteristics in High-Vacuum Flows —Rarefied Gas Dynamics

By R. G. FOLSOM,[1] BERKELEY, CALIF.

The growing importance of processes carried out under high-vacuum conditions increases the interest in the performance characteristics of flow-measuring devices for gases under low-Reynolds-number conditions. Published information on flow coefficients for liquids in throttling devices such as orifices, nozzles, and Venturi meters indicates that these coefficients change rapidly in the lower Reynolds-number regions. Similarly, coefficients in this region for compressible fluids, such as gases at subsonic velocities and normal pressures, are available in a limited number. A review of the literature fails to uncover any data on viscous compressible flow in nozzles. This paper presents a limited number of results of experiments on small ASME shaped nozzles at very low Reynolds numbers, achieved by operating at extremely low pressures over a wide range of pressure ratios.

Nomenclature

The following nomenclature is used in the paper:

A_y = nozzle throat area = $\pi D^2/4$
C = discharge coefficient
D = nozzle-throat diameter
k = ratio of specific heats
Kn = Knudsen number
p_1 = pressure at upstream tap
p_2 = pressure at downstream tap
r = p_2/p_1
R = gas constant
T_1 = upstream temperature
W = weight rate of flow
β = ratio upstream diameter to nozzle throat diameter
λ = molecular mean free path
μ = microns = 10^{-3} mm = 3.9×10^{-5} in.

Introduction

Since the absolute viscosity of a gas is a function of temperature alone, low Reynolds numbers exist in a flow system when the density or pressure of the gas is decreased to small magnitudes. For example, if the ambient temperature and velocity in the system are maintained constant, and the pressure reduced from 1 to 0.001 atm, then the density and Reynolds number are reduced in the same ratio. Thus a Reynolds number of 10^6 at normal pressures becomes 10^3 for this high-vacuum flow. Differential metering devices operating with liquids and gases at Reynolds numbers in the order of 100 have coefficients of about one half compared with the high Reynolds-number values.

For a continuum fluid, the drop in coefficient for a converging nozzle is due to the increase in boundary-layer thickness as the Reynolds number decreases and the viscosity effects become greater. With increased boundary-layer thickness, the velocity distribution at the upstream position and also at the throat will change. This, in turn, affects the coefficient. As the gases become more rarefied, the Reynolds number decreases further and a new phenomenon becomes of importance. This new phenomenon is associated with the molecular mean free path of the molecule, the relative magnitude being measured by the Knudsen number λ/D, the ratio of the molecular mean free path to the diameter of the nozzle throat. The condition for demarcation between the continuum and transition regimes is not definite but the experimental evidence available indicates that the normal continuum fluid mechanics begins to break down at a Knudsen number of about 0.01. In the transition regime, the interaction between the molecules and the surface becomes important and "slip flow" must be considered. As a first approximation, the fluid in contact with a surface possesses a motion with respect to the surface—hence slip occurs. As the pressure is decreased further and the molecular mean free path correspondingly increased, fully developed molecular flow is approached when the associated Knudsen number is greater than about 15.

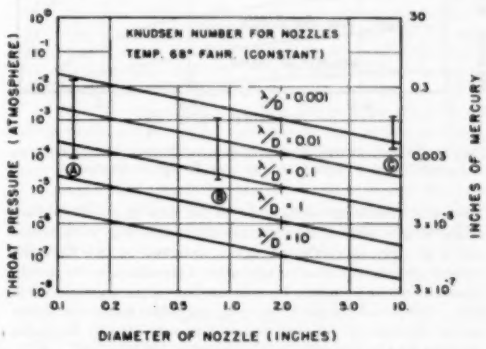

Fig. 1 Flow Regimes in Nozzle Throats for High-Vacuum Flows as Defined by Knudsen Number

(Test ranges shown by lines *A* for 0.125-in-diam throat ASME nozzle; *B* for 0.875-in-diam ASME nozzle; and *C* for 9.00-in-diam 18A nozzle.)

Fig. 1 illustrates the pressure conditions at normal atmospheric temperatures for nozzle-throat phenomena for the different flow regimes of continuum (Kn < 0.01), transition or slip (0.01 < Kn < 15), and fully developed molecular flow (Kn > 15). The vertical limited lines indicate the region of experimental data reported in this paper.

Nozzle Flow Characteristics

The standard flow equation (1)[2] for nozzles with a compressible fluid is expressed as

[1] Professor and Chairman of Division of Mechanical Engineering, University of California. Mem. ASME.

Contributed by the Fluid Meters Research Committee, the Industrial Instruments and Regulators Division and presented at the Annual Meeting, Atlantic City, N. J., November 25–28, 1951, of The American Society of Mechanical Engineers.

Note: Statements and opinions advanced in papers are to be understood as individual expressions of their authors and not those of the Society. Manuscript received at ASME Headquarters, February 13, 1952.

[2] Numbers in parentheses refer to Bibliography at end of paper.

$$W = CA_2 p_1 r^{1/k} \left[\frac{2g}{RT_1} \frac{k}{k-1} \left(1 - r^{\frac{k-1}{k}} \right) \right]^{1/2} \div \left[1 - \beta^4 r^{2/k} \right]^{1/2} \quad \ldots\ldots [1]$$

When tests are made with upstream conditions held constant, that is, temperature and pressure, and the downstream pressure is varied for pressure ratios of downstream to upstream of less than the critical ratio (0.528 for air), experiments at normal pressures have shown that the weight rate of discharge is a constant and independent of the downstream pressure. Preliminary experiments, made at low Reynolds numbers attained by operating with air at very low pressures, demonstrate that the weight rate of flow is not constant for pressure ratios below the critical value.

Typical dimensionless characteristic curves are presented in Fig. 2. The theory curve corresponds to Equation [1] with C taken as 1.00. At high values of Reynolds numbers, the difference between theory and actual flow rates is very small (C = 0.98) but as the upstream pressure is decreased the difference increases. The "normal low pressures" curve represents nozzle performance at about 1 in. of mercury absolute pressure and an average Reynolds number of about 1000. The "very low pressures" curves refer to average Reynolds numbers of 10 and 1. The "molecular flow" line corresponds to characteristic curves when the Knudsen number is greater than 15.

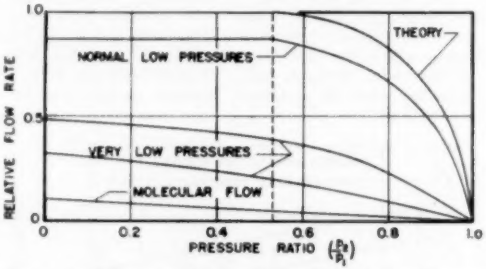

FIG. 2 CHARACTERISTIC RELATIVE WEIGHT RATE OF FLOW CURVES FOR NOZZLES WITH GASES IN LOW-PRESSURE OPERATION

Since the discharge coefficient C is the ratio of actual to theoretical weight rates of flow through the nozzle, Fig. 2 illustrates the large drop in coefficient values obtained as the Reynolds number decreases to small magnitudes, a phenomenon frequently reported in the literature for viscous flow of an incompressible fluid. Grace and Lapple (2) recently published nozzle-coefficient curves illustrating the nonconstant flow rate for low Reynolds numbers for pressure ratios below the critical value.

Available calibration results for nozzles with viscous liquids were investigated with the expectation that a reference curve for comparison with compressible-fluid characteristics could be developed. A study of the literature reveals that for the limited amount of data available, it is not possible to develop a satisfactory reference curve owing to the nongeometrical similarity of nozzle shapes, pressure-tap locations, and nozzle-to-pipe dimensions.

Velocity distributions at the nozzle throat for both compressible and incompressible fluids exhibit thick boundary layers at low Reynolds-number flows. Since the boundary layer is a region of reduced velocity and, in turn, reduced flow, the discharge coefficient decreases as the boundary-layer thickness increased. Shapiro and Smith (3) have computed discharge coefficients for nozzles based on viscous boundary-layer growth in a straight pipe having an effective length equivalent to the nozzle and compared their results with experiments by other authors. Reasonable correlation was obtained with the data of Buckland (4) and Smith and Steele (5), and excellent correlation with one of the curves of the latter authors.

The Smith and Steele (5) curve for a 0.125-in. nozzle in a $1^3/_8$-in. pipe has been selected arbitrarily as a comparison curve for this work. It should be noted that owing to nongeometrical similarity, the comparison curve is of relative value for trends only.

The Flow System

The special small low-pressure wind tunnel described by Kane and Folsom (6) was used for making the calibrations reported here. Air was drawn into the upstream or stagnation chamber through an air drier, filter, and gasometer. The test nozzle was located between the stagnation chamber and the downstream, or test chamber. The air passed through the nozzle, the test chamber, and a connecting pipe into the ballast tank. The high-vacuum pumps are connected to the ballast tank. The upstream temperature T_1, and pressure p_1, were measured at points $2^3/_4$ in. upstream from the nozzle plate in the cylindrical stagnation chamber of 8.5 in. diam and 12 in. long. The test chamber was rectangular in section with sides 10 and 11 in. and 12 in. in length along the flow direction. The downstream pressure p_2 was measured at a point 1 in. downstream from the nozzle and 8 in. from one edge of the chamber in the 10-in. side.

The 9.00-in. ISA nozzle was tested in a similar wind tunnel of larger dimensions. Geometrical similarity does not exist; however, due to the ratios involved, it is believed that the differences in arrangements are not important. The large tunnel system has been described by Schaaf, Horning, and Kane (7).

Pressure-Measuring Instruments

A mercury-in-glass barometer was used to determine barometric pressures. Absolute pressures were measured with a McLeod gage having the range of 0.001 mm mercury to 0.4 mm mercury. In addition, a precision manometer (essentially a U-tube with butyl phthalate as the fluid) was used for the pressure range 0.1 mm mercury to 25 mm mercury. Although the McLeod gage and the precision manometer were very slow in response, it was necessary to employ primary instruments of this type. Normally, high vacuum pressures are measured by Pirani gages or similar devices. These are secondary instruments and experience has shown that the reading taken at any one time on a Pirani, ionization, or similar gage, depends on the previous history of that gage. For example, a Pirani gage could be used to measure the vacuum in a system just after it is brought down from atmospheric conditions. Twenty-four hours later, although the absolute vacuum in the system was set to be exactly the same, the conditions on the hot wire for heat transmission will have changed and the pressure indicated by the Pirani gage will be different. As a result, convenient secondary gages were not used in making the measurements.

Temperature Measurement

Ambient-air conditions were measured by a mercury-in-glass thermometer. A thermocouple (copper-constantan) was installed in the stagnation chamber. No determination was made of downstream temperatures.

Volume-Rate Measurement

With the small wind tunnel, two gasometers were used for the measurement of volume of air flowing. The first gasometer was 8 in. in diam and had a bell travel of approximately 15 in. It was uncompensated for pressure differences due to variation in submergency of the bell because the change in absolute pressure be-

tween the positions of the bell at the top and the bottom was approximately 0.1 per cent. The liquid used was Lytton low vapor pressure oil (8). Calibration of the gasometer indicated variations in cross-sectional area of less than 0.2 per cent. The time of descent of the bell was measured with a stop watch and duplicate determinations were made in all cases. The length of travel varied from 0.2 to 14 in.

Owing to the difficulty of determining the travel of the 8-in. gasometer bell at the lower flow rates, a second gasometer of smaller capacity was constructed. This consisted of a $1^1/_2$-in-diam bell which had a test travel of about 13 in. Corresponding nozzle-calibration runs (1000 μ for p_1) showed the gasometers did not give the same results. Analysis indicated the discrepancy to be in the small gasometer, but all values have been presented in the graphs in order to establish trends.

In calibrating the subsonic nozzle in the large low-pressure wind-tunnel, weight rate of flow was determined with the aid of a calibrated dry-gas meter.

Nozzles Tested

Two nozzles having throat diameters of 0.125 and 0.875 in. were constructed according to ASME specifications (1). These nozzles were tested over a pressure-ratio range from approximately 0 to 0.95. One 9.00-in-diam ISA nozzle was constructed and tested over a limited range of subsonic pressure ratios. Fig. 1 shows the test range for these nozzles in terms of throat flow characteristics. Table 1 summarizes important nozzle features.

TABLE 1 FEATURES OF NOZZLES TESTED

Nozzle no.	Nozzle diam, in.	Type	β	m
1	0.125	ASME	0.0147	0.00022
2	0.875	ASME	0.103	0.0106
3	9.00	ISA	0.25	0.0625

Nozzles Nos. 2 and 3 had pressure taps in the throat. In nozzle No. 2 the tap was located with the center line $^1/_4$ in. upstream from the nozzle outlet and the pressure-tap hole was 0.060 in. diam. For nozzle No. 3, the throat tap was 0.060 in. diam with the center line $^1/_2$ in. upstream from the outlet face.

Experimental Results

Discharge coefficients for nozzles Nos. 1 and 2 are plotted in Fig. 3 against the pressure ratio. The experimental points show the general trend predicted from the characteristics illustrated in Fig. 2. Each curve is for a constant pressure and approximately constant temperature in the upstream chamber. The experimental points shown in Fig. 3 apply to a specific geometry of flow nozzle (ASME) and installation, including pressure-tap locations and β-ratios. The test nozzles were installed between two relatively large chambers so that the velocity of approach to the nozzle was too small to consider, and the kinetic energy of the jet issuing from the nozzle dissipates a good portion of its kinetic energy through mixing and introducing turbulence into the air in the downstream chamber. When the pressures are measured in the large chambers some variation of coefficients is to be expected between compressible and incompressible flow at a given Reynolds number, the difference decreasing as the pressure ratio for the compressible flow approaches unity.

In Fig. 4 the discharge coefficients are plotted against the throat Reynolds number. For pressure ratios below critical, throat conditions were calculated on the basis of isentropic expansion to the critical pressure. At larger pressure ratios, calculations were based on isentropic expansion to the pressure measured at the tap in the downstream chamber. The reference curve taken from Smith and Steele (5) was for a viscous liquid in a long throat nozzle with double radii of curvature for the long entrance portion, upstream pressure tap at 1 in. from the 0.125-in-diam nozzle (β = 0.091) and the downstream tap in the throat.

Referring to the test points in Fig. 4, it will be noted that each nozzle at each upstream pressure condition exhibits a coefficient characteristic departing from a generally continuous line, or narrow region, as the Reynolds number increases and the pressure ratio decreases. Efforts to predict or correlate these "breakaway" points has been fruitless. The trend shown apparently is a characteristic of viscous-compressible flow through ASME nozzles installed as for these experiments.

The test points for the No. 3 nozzle are included in Fig. 4. Since these tests were at high pressure ratios, compressibility has very little influence, but there is a loss in accuracy as the coefficient depends on a calculation based on the small difference in two relatively large numbers. The increased spread in experimental points is to be expected.

In order to investigate more fully the peculiar shape of the nozzle-coefficient curves for compressible flow shown in Fig. 4, a series of tests was made with the No. 2 nozzle to compare pressures measured at the throat and in the downstream chamber. The pressures at the throat tap proved to be higher than the corresponding values measured in the downstream chamber. Table 2 expresses the averaged results when given in terms of the pressure ratio.

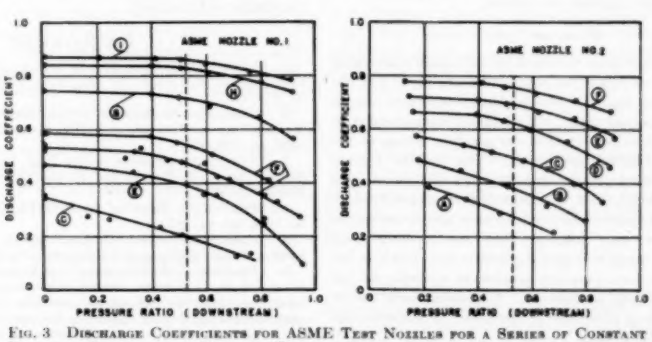

Fig. 3 Discharge Coefficients for ASME Test Nozzles for a Series of Constant Upstream Conditions at Variable Pressure Ratios Based on Downstream Chamber Pressures

(Curve letter designates upstream pressure in microns of mercury as A-25, B-50, C-100, D-250, E-500, F-1000, G-4000, H-15000, I-22800.)

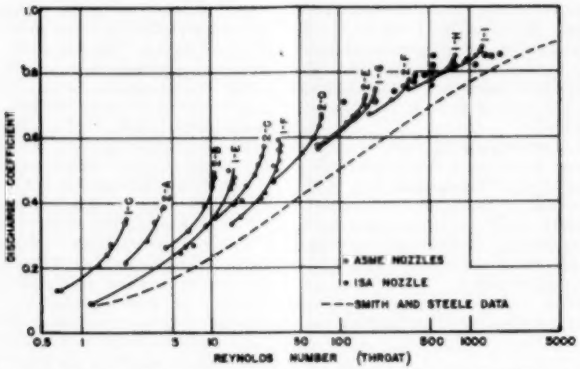

FIG. 4 DISCHARGE COEFFICIENT VERSUS REYNOLDS NUMBER FOR TEST NOZZLES
(Notation as 2-D indicates data for No. 2 nozzle with upstream pressure of 250 microns of mercury. See Fig. 3 for letter-designation table.)

TABLE 2 AVERAGE PRESSURE RATIOS

	(p_3/p_1)throat		
(p_3/p_1)test chamber	p_1 = 100	p_1 = 250, p_1 = 500	p_1 = 1000
0.20	0.56	0.56	0.54
0.30	0.585	0.565	0.54
0.40	0.61	0.565	0.56
0.50	0.66	0.625	0.60
0.60	0.715	0.69	0.655
0.70	0.785	0.765	0.73
0.80	0.855	0.835	0.815
0.90	0.925	0.915	0.905

It should be noted that the pressure ratios for throat conditions are always greater than the critical value of 0.528. If the measurement of the throat pressure is correct, it would appear that the pressure in the thick boundary layer does not correspond to the magnitude normally expected. Since it is possible to have pressures in the boundary layer different from those at corresponding positions in the core of the fluid, it is to be expected that the expansion ratios and velocity distributions will be different and this change will be manifested as a change in coefficient for otherwise similar flow conditions.

Fig. 5 gives the discharge coefficient versus Reynolds number characteristic curves for downstream pressures measured at the throat tap as well as the related curves from Fig. 4. The throat-tap curves possess the breakaway characteristics but to a smaller degree than the chamber-tap curves.

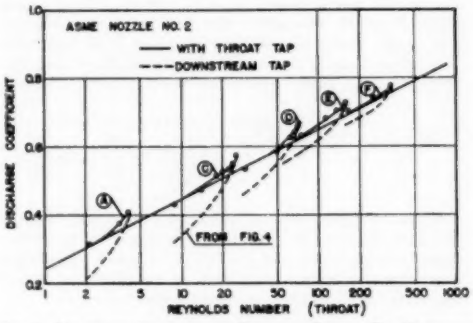

FIG. 5 DISCHARGE COEFFICIENTS BASED ON THROAT-TAP PRESSURE AS COMPARED WITH COEFFICIENTS BASED ON DOWNSTREAM-CHAMBER PRESSURES FOR NOZZLE NO. 2
(See Fig. 3 for letter-designation table.)

SUMMARY

Calibration data have been obtained for two small converging ASME nozzles and one large ISA nozzle with dry air in the viscous-compressible flow regime. The discharge-coefficient magnitudes were in the expected range, but no direct comparison with viscous (incompressible) flow regime was possible, owing to the lack of suitable published coefficients. The results demonstrate the importance of pressure-tap location and installation geometry on coefficients, and a distinctive breakaway characteristic which developed as the pressure ratio across the nozzle decreased. Slip flow may influence the results since tests were conducted in the region where slip effects are known to begin to be appreciable, but it was not possible to separate the low Reynolds number and slip phenomena. Additional work will be necessary to develop a complete presentation of viscous-compressible metering with nozzles.

ACKNOWLEDGMENT

This work was done at the Division of Mechanical Engineering of the University of California as part of a joint contract sponsored by the Office of Naval Research and the Air Research and Development Command.

BIBLIOGRAPHY

1 "Fluid Meters, Their Theory and Application," fourth edition, THE AMERICAN SOCIETY OF MECHANICAL ENGINEERS, New York, N. Y., 1937.

2 "Discharge Coefficients of Small-Diameter Orifices and Flow Nozzles," by H. P. Grace and C. E. Lapple, Trans. ASME, vol. 73, 1951, pp. 639–647.

3 "Friction Coefficients in the Inlet Length of Smooth Round Tubes," by A. H. Shapiro and R. Douglas Smith, NACA TN 1785 November, 1948.

4 "Fluid-Meter Nozzles," by B. O. Buckland, Trans. ASME, vol. 56, 1934, pp. 827–832.

5 "Rounded-Approach Orifices" by J. F. Downie Smith and Sydney Steele, *Mechanical Engineering*, vol. 51, 1935, pp. 760–780.

6 "Problems and Progress in Low Pressure Research," by E. D. Kane and R. G. Folsom, *Journal of the Institute of Aeronautical Sciences*, vol. 16, 1949, pp. 46–54. See also University of California, Institute of Engineering Research, HE-150-57, March, 1949.

7 "Design and Initial Operation of a Low Density Supersonic Wind Tunnel," by S. A. Schaaf, D. O. Horning, and E. D. Kane, Heat Transfer and Fluid Mechanics Institute, 1949, pp. 223–235.

8 "Scientific Foundations of Vacuum Technique," by S. Dushman, John Wiley & Sons, Inc., New York, N. Y., 1949.

Basic Difficulties in Pulsating-Flow Metering

By A. R. DESCHERE,[1] BOULDER, COLO.

Practically all research work in the field of flow metering has been devoted to a development of devices for obtaining an average of the square root of the pressure differential, and means for preventing distortion of the pressure transmission in the lines connecting the primary to the secondary part of the meter. The author shows that, in measurement of severely unsteady flow, these may not be the most important factors, but rather that the primary element itself does not give a response in this type of flow which can be interpreted correctly by the usual steady flow-metering methods.

Introduction

FOR more than 30 years the problem of accurate metering of pulsating flow of liquids and gases has occupied considerable time on the part of men in the flow-measurement field, and has developed a voluminous literature of its own. A sizable portion of the materials being transported in pipe lines is propelled by devices, such as reciprocating compressors, which make the flow unsteady or pulsating, while research and control work with internal-combustion engines is constantly faced with the measurement of this type of flow. For almost as long as "inferential" flow measurement (in which the flow rate is inferred from some other property, usually pressure, instead of being measured directly) has been used, it has been known that unsteadiness in the rate of flow is a troublemaker and may lead to extremely inaccurate measurements with those methods which do an excellent job with steady flow.

Practically all research work that has been done in this field to date has been based on some such assumption as the following: "Any inferential-head meter will measure correctly if the secondary device will measure accurately the differential pressure across the primary element, and if the average of the square roots of the instantaneous readings can be determined." Because of this belief, almost all time and energy devoted to this study has been channeled into two paths, namely, devices for obtaining an average of the square root of the pressure differential, and means for preventing distortion of the pressure transmission in the lines connecting the primary to the secondary part of the meter. It is the object of this paper to show that in measurement of severely unsteady flow, these may not be the most important factors, but rather that the primary element itself does not give a response in this type of flow which can be interpreted correctly by the usual steady flow-metering methods. However, to lead into this concept easily, it would be well to discuss the background of the earlier investigations.

The basis of inferential methods of metering lies in an equation whereby the velocity, quantity, or weight of flow can be calculated from measurement of areas, pressure differential between the entrance and throat of the meter or other related locations, and density of the material flowing. The basic equation is derived for a Venturi type of unit in which the flow is guided within fixed walls so that the true cross-sectional area of the flow is known at all times. In steady flow, the more common orifice plate provides a flow situation similar to a highly frictional Venturi and, through the use of experimentally determined "coefficients" for correction, fully satisfactory metering is done with this very simple and inexpensive device; later it will be shown that this orifice type of meter is probably unsuited to flow circumstances where variations are large and rapid.

Metering of Steady Flow

The basic flow equation for the steady-flow case is

$$w = A_2 K \phi \sqrt{2 g \rho_1 \Delta p} \qquad [1]$$

where

w = gravimetric rate of flow = $VA\rho$
K = flow coefficient (coefficient of discharge with approach factor included)
Δp = difference between upstream pressure p_1, and throat pressure p_2
g = acceleration due to gravity
ρ_1 = upstream density
A_2 = throat area

$$\phi = \left[\frac{k}{k-1}(p_2/p_1)^{2/k}\,\frac{1-(p_2/p_1)^{k-1/k}}{1-(p_2/p_1)}\right]^{1/2} \left[\frac{1-(D_2/D_1)^4}{1-(D_2/D_1)^4(p_2/p_1)^{2/k}}\right]^{1/2}$$

where k = ratio of specific heats
D_1, D_2 = upstream and throat diameters, respectively.

This is derived by combining three fundamental equations from the theory of fluid mechanics: the energy (Bernoulli) equation, the continuity equation, and equation of state. On the assumption of steady flow of perfect gases, of the flow being one-dimensional (no variation of velocity across any cross section of the conduit at a given instant), and of reversible adiabatic (frictionless and no heat added or removed from the outside of the conduit) these equations are as follows:

(*a*) The Bernoulli equation, which states that the sums of the mechanical and thermal energies are equal at any two points in a horizontal pipe, is

$$\frac{V_1^2}{2g} + \frac{k}{k-1} p_2 v_2 = \frac{V_1^2}{2g} + \frac{k}{k-1} p_1 v_1 \qquad [2]$$

where v_1 and v_2 = specific volumes at points 1 and 2, respectively.

(*b*) The continuity equation, which says that the weight of the material passing through one cross section of the conduit is the same as that passing through another cross section at the same instant, is

$$w = V_1 A_1 \rho_1 = V_2 A_2 \rho_2 \qquad [3]$$

(*c*) The state equation, which states that, because of the assumption of reversible adiabatic flow for perfect gas, the specific volume of the gas will vary in a definite relationship with the variation of the pressure as the gas proceeds through various parts of the meter, is

$$p_1 v_1^k = p_2 v_2^k \qquad [4]$$

---

[1] Associate Professor, Mechanical Engineering Department, University of Colorado. At present, Head, Rocket Development Section, Redstone Arsenal Research Division, Rohm and Haas Company, Huntsville, Ala.

Contributed by the Fluid Meters Research Committee and presented at the Annual Meeting, Atlantic City, N. J. November 25–30, 1951, of The American Society of Mechanical Engineers.

Note: Statements and opinions advanced in papers are to be understood as individual expressions of their authors and not those of the Society. Manuscript received at ASME Headquarters, November 21, 1951.

These equations, when combined to eliminate all variables except the pressures, one of the velocities, and the known areas, result in the basic equation given previously. Then, with the Venturi, to allow for such deviations from basic assumptions as the facts that the gas is not exactly perfect, is not truly frictionless, and is not truly one-dimensional (especially at the throat where work by Hooker shows the velocity to be different at the edges from that at the center of the conduit), flow coefficients must be incorporated, based on experimental work. The orifice meter uses different flow coefficients and substitutes an empirical equation

$$Y = 1 - [0.41 + 0.35(D_2/D_1)^4]\left[\frac{\Delta p}{p}\Big/k\right]$$

for ϕ, because the fluid is not guided by solid walls and so finds its narrowest cross section (vena contracta) beyond the hole in the orifice plate. Also, the orifice has far more friction loss due to turbulence than is found in the Venturi. All of these empirical matters have been studied thoroughly and tabulated carefully in many publications, but for the steady-flow case only.

Now it is possible to see why the emphasis has been so strong on the square-root error: Equation [1] shows that the flow velocity is roughly proportional, except for variations of the density and the pressure ratio, to the square root of the differential pressure across the meter taps. An averaging manometer would average the pressure differential, but the square root of this average would not be equal to the average of the velocities or instantaneous square roots of the differentials, and so would introduce an error. Speaking in calculus terms, this means

$$\left[\frac{1}{t}\int \Delta p\,dt\right]^{1/2} \neq \frac{1}{t}\int (\Delta p)^{1/2}dt \quad \ldots\ldots\ldots [5]$$

Lindahl has calculated equations for the error which is involved in this factor for sinusoidal, rectangular, and triangular wave shapes. Witte presents curves for rectangular waves of various amplitudes and time relationships, while G. Sauer and others have made similar computations, assuming simple wave forms.

Special devices and linkages have been developed, and in some cases patented, by Bailey, G. Sauer, and many others, which would handle this difficulty. Schultz-Grünow also proposes an ingenious method which involves two sets of measurements, one of the regular flow and a second with a known amount added or removed to this flow, for which situation equations may be derived which eliminate the calculation error discussed in the foregoing. An important fact which should be noted here is that despite the need for metering of unsteady flow, none of these methods has been widely adopted. Except for special instances, they do not appear to solve the problem completely.

The second source of error which has received attention is that of distortion of the pressure pulses, occurring in the metering of unsteady flow, as they pass from the primary part of the meter to the secondary part. Since the material in the tubes between the meter taps and the recording device is usually a compressible gas and since, in the case of manometers at least, there is usually some movement on the part of the pickup device, there is almost bound to be some flow in these tubes. Throttling of the tubes, unequal flow which is almost bound to occur because of the different pressures at the two taps, and similar phenomena will distort the pressure pulse so that the pressure reaching the secondary part is not the same as that leaving the primary part. It is also quite possible for waves to be set up within these lines themselves, causing further trouble.

This, of course, further complicates the problem. Witte has presented curves calculated for a particular case. Another study of this same problem by Taback is based on electrical-analog methods, which have a certain usefulness in this field, and has been checked by experiment.

If this were the only other serious source of error it could be mainly eliminated, also, by using connections as short as possible and with maximum bore, by introducing linear throttling in the connecting tubes, and by using taps as symmetrical as possible. Or, better still, electronic devices can be used which are attached directly to the conduit and thus transmit, electrically, to the amplifiers or other intermediate devices, the exact impression of the pressure within the conduit.

Effects of Unsteady Flow on Primary Unit

When methods are employed to overcome the errors just discussed it is found that incorrect results are still obtained in fairly severe cases of unsteadiness. This led to the development, by Beitler, Lindahl, et al., of the "pulsameter" which is intended to indicate those situations in which pulsating flow will give erroneous readings on meters, although it does not attempt to estimate the error nor does it supply any correction factor which may be applied. Investigators are agreed, in general, that there is no correction factor which has been determined experimentally which can correct observed values to correct values in most cases of pulsating flow.

A closer analysis of the problem indicates the likelihood that the source of error is more fundamental than has been indicated up to now. It seems probable that the usual steady-flow equations are inapplicable in the most general case and that the true equations lead to results which show that it is impossible for the usual measuring methods, even if the errors discussed earlier are eliminated, to give correct results in the presence of severe pulsations. That is to say, the principal error arises in the primary device and the pressure responses at that device do not have the same inferential connection to velocity of flow in the unsteady case as is found in the steady case.

A basic assumption in these studies in the past has been that the unsteady case may be treated as a modified case of steady flow, using the steady-flow methods with what seemed to be appropriate modifications, instead of recognizing that steady flow is actually a special case of unsteady flow and that the fundamental equations for unsteady flow have additional, time-dependent terms as compared with those of Equations [2] and [3].

The energy equation for the more general case is

$$\frac{V_2^2}{2g} - \frac{V_1^2}{2g} + \frac{k}{k-1}(p_2v_2 - p_1v_1) = -\frac{1}{g}\int_1^2 \frac{\partial V}{\partial t}\,dx \quad \ldots [6]$$

while the continuity equation is

$$\rho_2 V_2 A_2 - \rho_1 V_1 A_1 = \int_1^2 A\,\frac{\partial \rho}{\partial t}\,dx \quad \ldots\ldots\ldots [7]$$

The state equation, which has to do only with conditions at any particular point and not with the instantaneous difference between two points, is not affected by the flow condition and remains the same. Notice that if the flow is steady, the right-hand terms of the energy and continuity equations become zero because the derivatives with respect to time disappear if there is no variation with time, and the equations reduce to the special cases which are Equations [2] and [3].

If these equations are now combined in a manner similar to that used for Equation [1], the result is a mess. It can be handled more readily in the differential form, but then the result is what is known as a nonlinear partial-differential equation which is capable of solution only in particular cases and then by step-by-step approximation methods which are hardly "practical." It may be that a special computing device could be designed into which

the pressure readings and time rate of change of pressure readings could be fed electrically, but such a possibility has not been explored as yet. Even if it could be designed, the equations are of such a nature that the apparatus would have to be quite complex. Unfortunately, the electrical analogies which work so well for acoustic problems do not work here because the pulsating flow ("waves of finite amplitude" as Lamb calls them) involves nonlinear partial-differential equations while acoustic problems, with their "infinitesimal perturbances," employ linear equations.

The question now arises as to whether these extra time-dependent terms are really significant or whether they are of negligible magnitude. It was suggested in the discussion of an earlier paper that such terms could be neglected because "what goes up must come down," so that any positive rate of change would be balanced by the corresponding decrease that must follow and, on the average, the terms could be omitted. However, the fact that the resulting equation is nonlinear indicates that this is not so because the various positive and negative values will be multiplied by different quantities and so will not balance out.

But this is not really convincing evidence since a long, complicated, mathematical development is necessary before it can be proved. It is better to look at the experimental evidence which has been gathered so that one may see qualitatively, at least, that these time-dependent terms are really significant and therefore cannot be ignored in their nonlinear equation.

Perhaps the most convincing argument that they are significant is found in the experimentally determined negative pressure differentials. When pressure differentials across orifices and other metering devices have been studied with sensitive instruments, it has often been noticed that the pressure differentials will often actually reverse; that is, the entry pressure will be lower than the throat pressure. This phenomenon has been observed in Venturis and flow nozzles with both compressible and incompressible flows. Generally this has been interpreted as meaning a reversal of flow, but this is difficult to visualize, as there is little, if any, reason why flow which is going in one direction should suddenly turn around and go in the other. Also, if the steady-flow equations were to hold for such stream-guiding units as Venturis, it can be proved readily, for the usual case of steady subsonic flow, that the pressure will always be lower at the narrower section, regardless of the direction in which the stream is flowing.

The correct answer seems to lie in the fact that force is proportional to acceleration, not to velocity. In the usual meter, the fluid accelerates from the entry to the throat of the meter and, if the entry velocity and the acceleration between the two points are steady, this fixes the throat velocity and, in turn, the pressure differential. A negative pressure differential, then, does not mean a reversal of flow but greater decrease in velocity at the throat than is occurring at the entry; neither of these velocities needs, nor probably does, reverse. Since the time-rate-of-change of velocity is the acceleration, and since this is tied to the relative pressures and their changes, it is clear that the time-dependent terms should not be negligible, at least in the presence of severe pulsations.

Another phenomenon points to the same conclusion: Experiments have shown that for the same cyclical rate and the same maximum-to-minimum pressure variation across a primary device the error is considerably greater for a pulsation wave of complex shape, with several harmonics present, as compared with a simple wave. These wave shapes were determined by use of fast-acting, electronic equipment. The presence of ripples on a basic wave should have little effect on the average value of the pressure differential since the difference between the average of the square roots and the square root of the average root of the average is negligible when the magnitude of the variation is small. However, these complex waves have, as the steeper slopes of their sides indicate, far higher time-rate-of-change values than do the simple waves. Clearly, then, there is significance to the time-dependent terms in Equations [6] and [7].

The same factors explain the situation where considerable errors are found in cases in which the pressure changes are small but rapid, such as those caused by the blades of a centrifugal blower. Since the pressure surges are minute, the average square root should be only infinitesimally different from the square root of the average, but the time-rate-of-change of pressure can be very large, leading to importance for the time-dependent terms of the unsteady-flow equations. Experiments by the author were conducted on a 250-rpm air compressor with a Cox Type 3 quartz pressure element, an amplifier, and a Hathaway oscillograph using an OA-2 galvanometer of natural frequency of 2000 cps. Irregular pressure fluctuations were shown superposed on the larger cycles corresponding to the main motion of the compressor, and these smaller variations appeared to be of highly irregular frequency but averaging about 500 cps. Under these circumstances, the length of the propagating pressure waves is seen to be approaching in general magnitude the dimensions of the usual metering instruments; the usual assumption in studies of this kind is that the waves are very long compared with the meter dimensions.

Finally, the other chief phenomena concerning error in unsteady flow which were observed by Judd and Pheley, Beitler, and the Fluor Corporation, are all readily explained by the unsteady-flow analysis as discussed in this paper. These phenomena are as follows:

1 Increasing the pressure differential by decreasing the area ratio with constant flow will cause the error in the flow reading to increase.

2 As the flow rate is decreased with constant area ratio, the relative error in the flow reading will increase.

3 For constant pressure differential, the error in w is increased as the area ratio decreases.

Unsuitability of Orifice for Unsteady Flow

In the earlier portion of this discussion it was pointed out that the fundamental equations for flow through an orifice arise from the theoretical analysis of the Venturi with empirical correction factors included to take care of the vena contracta cross-sectional area as compared with the orifice area, and the high turbulence in the downstream section. As conventionally pictured in the steady-flow case, flow through an orifice does indeed resemble that through a Venturi except that the "walls" are of turbulent gas or liquid instead of metal.

However, as flow through an orifice varies from one steady condition to another, the vena contracta and the coefficient will change also. This variation is quite pronounced when compared with that for the Venturi's coefficient, as might be expected because of the absence of fixed walls to guide the flow. The difficulty in determining the proper coefficient is therefore great in the case of pulsating orifice flow, and is magnified by the fact that the up and downstream pressures do not vary at exactly the same time, since it takes an instant for a pressure pulse to propagate along the flow, thus distorting the Venturi-like pattern even more.

Another complicating factor is the reflection of pressure waves from the face of the orifice plate. In steady flow there is, of course, no phenomenon of wave reflection since there are no waves, but the pressure surges of unsteady flow will reflect off the fixed plate surface on the upstream side of the orifice, complicating the pressure conditions above the orifice. This may be seen occurring in a ripple tank, in which wave phenomena of compressible fluids may be visualized through surface ripples on

shallow water. A similar reflection situation with a somewhat simplified analysis of its effects is analyzed by DeJuhasz.

It would appear, therefore, that if progress is to be made in the actual metering of unsteady flow, it has a better chance with the Venturi than with the customary orifice. It is perhaps pertinent here to mention study of the unsteady flow of liquids through a flow nozzle by Estel in which he shows that the variation of the coefficient of discharge for this Venturi-like device is very small in the presence of different cyclical rates of pressure variation.

Conclusion

In a sense, this is a pessimistic paper in that it demonstrates that the problem of metering pulsating flow is considerably more complex than seems to have been realized heretofore. The basic difficulties in the metering of unsteady flow lie not only in the difficulties in obtaining proper response in the secondary unit and its connections, but even more in the nature of the relationships between pressure and velocity in the primary unit. Since the equations involved are far less simple than those in the steady case, it cannot be expected that the usual metering equipment could give satisfactory values for highly pulsating flow. Nor can a correction factor be used because it would depend on the infinite possibilities of frequencies and wave shape in addition to the usual variables.

It is quite conceivable, however, that there is a "twilight" zone between the region in which the usual metering methods are satisfactory and the region in which the discussion of this paper applies. Hardway of the Beta Corporation, has been working on an electronic method designed for use in this range, and the results will be of much interest.

For the severe cases, there appear to be only two possible courses:

1 Eliminate the pulsations. This is the method usually used today and involves such means as throttling of the flow, surge tanks, or specially designed pulsation dampers. Unfortunately, these methods are either wasteful or else they will operate only under particular flow conditions and so are not applicable in the many situations where the flow rate is highly variable.

2 Develop a metering device which will be based on the proper equations as developed in this paper. If this device is to be actuated by pressures, it would have to be quite elaborate and, perhaps, could not be developed except through the use of approximations which would still lead to inaccuracies in many cases. There is also the possibility that a metering device could be built on some other basis than pressure, but what this would be is not immediately apparent.

REFERENCES

Literature Concerned With Pulsating-Flow Measurement

1 "Measurement of Steam Flow," by E. G. Bailey, *Power*, vol. 43, 1916, pp. 854–858.

2 "Pulsating Air Flow," by N. P. Bailey, Trans. ASME, vol. 56, 1934, pp. 781–786.

3 "Pulsating Air Velocity Measurement," by N. P. Bailey, Trans. ASME, vol. 61, 1939, pp. 301–308.

4 "Survey of Metering of Pulsating Flows of Gas," by H. S. Bean, *Western Gas*, vol. 11, 1935, pp. 46–50.

5 "The Effect of Pulsations on Orifice Meters," by S. R. Beitler, Trans. ASME, vol. 61, 1939, pp. 309–314.

6 "Research on Flow Nozzles by the ASME Special Research Committee on Fluid Meters," by S. R. Beitler and H. S. Bean, Ohio State University Engineering Experiment Station, Bulletin 131, 1939.

7 "The Effect of Pulsating Flow on Gas Measurement," by S. R. Beitler, West Virginia University Engineering Experiment Station, Technical Bulletin 16, 1940.

8 "Pulsating Flow in Orifice Meters—Its Causes and Possible Remedy," by S. R. Beitler and H. B. McNichols, West Virginia University Engineering Experiment Station, Technical Bulletin 19, 1941.

9 "Development in the Measuring of Pulsating Flows With Inferential Head Meters," by S. R. Beitler, E. J. Lindahl, and H. B. McNichols, Trans. ASME, vol. 65, 1943, pp. 353–356.

10 "Three Gas Line Problems Discussed," by J. C. Diehle, *Oil and Gas Journal*, 1929.

11 "An Investigation of Pulsating Flow and Pulsation Elimination by Orifice Meters," by J. H. Eagle and W. A. Dabenko, Master's thesis, Ohio State University, 1937.

12 "Flow and Measurement of Air and Gases," by A. B. Eason, second edition, Griffin and Company, Ltd., London, England, 1930.

13 "Experimental Untersuchung des Einflusses von Pulsationen auf den Strömungswiderstand von Kreisrohren und die Durchflussahl von Normdüsen," by E. Estel, Doctor's Dissertation, University of Leipzig, 1936. ("Experimental Investigation of the Influence of Pulsation on the Flow Resistance of Round Pipes and the Flow Coefficient of Flow Nozzles.")

14 "Durchflussahl von Normdüsen und Druckabfall in Rohren bei pulsierender Strömung," by E. Estel ("Flow Coefficient of Standard Flow Nozzles and Pressure Drop in Pipes Having Pulsating Flow"), *Physikalische Zeitschrift*, vol. 38, 1937, p. 748.

15 "Establishing a Standard of Measurement for Natural Gas in Large Quantities," by F. P. Fisher, Trans. ASME, vol. 38, 1916, pp. 241–284.

16 "Flow Measurement," Power Test Codes, part 5, The American Society of Mechanical Engineers, chapter 4, 1940.

17 "Abnormal Coefficients of the Venturi Meter," by A. H. Gibson, Proceedings of The Institution of Civil Engineers, vol. 196, 1914, pp. 391–408.

18 "Integration of Pulsation Errors in Measurement of Quantities of Gas Flowing Through an Orifice," by D. Gilmour, *Journal of the Institution of Petroleum Technology*, vol. 19, 1933, pp. 25–68.

19 "Pulsation of Air Flow From Fans and Its Effect on Test Procedures," by H. F. Hagen, Trans. ASME, vol. 55, 1933, pp. 105–115.

20 "Theory of Operation of a Proposed New Instrument for Measuring Pulsation Error in Differential Pressure Type Flow Meters," by E. V. Hardway, Jr., Southwestern Industrial Electronics Company, Houston, Texas, 1950.

21 "A Method for Correcting Orifice-Meter Measurements for Flow Pulsations," by E. V. Hardway, Jr., *Instruments*, vol. 24, 1951.

22 "Venturi Meters Inaccurate on Lively Lines," by Allen Hazen, *Power*, vol. 46, 1916, p. 354.

23 "Durchflussmessung bei pulsierender Strömung," by H. Herning and Chr. Schmid ("Metering With Pulsating Flow"), *Zeitschrift des Vereines deutscher Ingenieure*, vol. 82, 1938, pp. 1107–1114.

24 "Commercial Metering of Air Gas and Steam," by J. L. Hodgson, Proceedings of The Institution of Civil Engineers, vol. 204, 1916–1917, pp. 108–193.

25 "The Laws of Similarity for Orifice and Nozzle Flows," by J. L. Hodgson, Trans. ASME, vol. 51, 1929, pp. 303–332.

26 "Effect of Pulsations on Flow of Gases," by H. Judd and D. B. Pheley, Trans. ASME, vol. 44, 1922, pp. 853–918.

27 "Effects of Pulsations on Flow of Gases," by H. Judd and D. B. Pheley, Ohio State University Engineering Experiment Station, Bulletin 24, 1923.

28 "Pulsations and Its Effect on Flowmeters," by E. J. Lindahl, Trans. ASME, vol. 68, 1946, pp. 883–894.

29 "Flowmeters Measure Rapidly Fuctuating Flow," by J. B. McMahon, Republic Flow Meter Company, Unit No. 44-4.

30 "Metering Pulsating Flow," by William Melas, *Power Plant Engineering*, vol. 45, 1941, p. 64. Similar articles by the same author in *Instruments*, *Steel*, and *Water Works and Sewerage*, all about the same time.

31 "Staudruckmessung bei pulsierenden Stoffströmen," by G. Sauer ("Static Pressure Measurement With Pulsating Flow of Material"), Doctor's Dissertation, Technischen Hochschule Darmstadt, 1930. Also published in Heft 4 of *Messen und Prüfen*, L. Litinsky, editor, Halle (Saale), 1930.

32 "Durchflussmessverfahren für pulsierende Strömungen," by F. Schults-Grünow, *Forschung auf dem Gebiete des Ingenieurwesens*, vol. 12, 1941. ("A Flow Measurement Procedure for Pulsating Flow.")

33 "Eliminating Pulsating Errors in Orifice Meter Measurement," by T. K. M. Smith, *Western Gas*, vol. 8, 1932, pp. 38–42.

34 "The Detection and Mitigation of Pulsation in Orifice Meters," by T. K. M. Smith and R. E. Moster, *Gas*, vol. 14, 1938, pp. 55–68.

35 "Compressor Pulsations—Their Effect on Orifice Meter Accuracy," by Edward Sockett, *Gas*, vol. 16, 1940, pp. 20–22.

36 "Principles and Practice of Flow Meter Engineering," by L. K. Spink, The Foxboro Company, Foxboro, Mass., 1950.

37 "Flow Measurement With Orifice Meters," by R. F. Stearns.

R. M. Jackson, R. R. Johnson, and C. A. Larson, D. Van Nostrand Company, Inc., New York, N. Y., 1951.

38 "The Effect of Pulsation on Gas Measurement," by F. M. Stephans, West Virginia University Engineering Experiment Station, Technical Bulletin 26, 1947.

39 "Operational Factors in Orifice Flow," by H. W. Swift, *London, Edinburgh and Dublin Philosophical Magazine and Journal of Science*, vol. 5, Series 7, 1928, pp. 1–18.

40 "Methods of Measuring Discharge and Head," by W. M. Venable, Trans. ASCE, vol. 54D, 1905, pp. 502–504.

41 "Measurement of Gas and Liquid by Orifice Meter," by H. P. Westcott, Metric Metal Works, Erie, Pa., 1922.

42 "Mengenmessungen im Betriebe" ("Quantity Measurement in Industry"), by R. Witte and E. Padelt, *Der Chemie-Ingenieur*, Akad. Verlags, Leipzig, vol. 2, 1933, pp. 237–245.

43 "Effect of Pulsation on Gas Measurement," by C. Yates, *Gas Age*, 1949.

44 "Über Gasmengenmessung bei Kolbenmaschinen mittels Düsen und Blenden" ("On Gas Metering for Reciprocating Machines by Means of Nozzles and Orifices"), *Ingenieur Archiv.*, vol. 3, 1932, pp. 138–148.

ARTICLES ON PULSATING FLOW NOT SPECIFICALLY RELATED TO METERING

45 "Gasträgheit und Liefergrad bei Kolbenmaschinen" ("Gas Friction and Delivery-Degree in Piston Machines"), by J. Asberbronner, *Forschung auf dem Gebiete des Ingenieurwesens*, vol. 8, 1937, pp. 118–150, 285–294.

46 "Wave Action Following Sudden Release of Compressed Gas From a Cylinder," by F. K. Bannister and G. F. Mucklow, Proceedings of The Institution of Mechanical Engineers, vol. 159, 1948, pp. 269–300.

47 "Ebene Wellen in Idealen Gasen mit Reibung und Wärmeleitung" ("Plane Waves in Ideal Gases With Friction and Heat Conduction"), by K. Bechert, *Annalen der Physik*, vol. 40, 1941, pp. 207–248.

48 "Über die Ausbreitung von Zylinder—und Kugelwellen in reibungsfreien Gasen und Flussigkeiten" ("On the Propagation of Cylindrical and Spherical Waves in Frictionless Gases and Liquids"), by K. Bechert, *Annalen der Physik*, vol. 39, 1941, pp. 169–202.

49 "Über die Differentialgleichung der Wellenausbreitung in Gasen" ("On the Differential Equation of Wave Propagation in Gases"), by K. Bechert, *Annalen der Physik*, vol. 39, 1941, pp. 357–372.

50 "Pulsation Phenomena in Gas Compression Systems," by I. Bechtold, *Engineering and Science Monthly*, October, 1947.

51 "Thermodynamic Analysis of the Inlet Process of a Four-Stroke Internal Combustion Engine," by Chung-hua Wu, Doctoral Dissertation, M.I.T., 1947.

52 "Supersonic Flow and Shock Waves," by R. Courant and Friedrichs, Interscience Publishers, Inc., New York, N. Y., 1949.

53 "Graphical Analysis of Transient Phenomena in Linear Flow," by K. J. De Juhasz, *Journal of The Franklin Institute*, vol. 223, 1937, p. 463.

54 "The Occurrence and Elimination of Surge or Oscillating Pressures in Discharge Lines From Reciprocating Pumps," by H. Diederichs and W. D. Pomeroy, Bulletin of the Engineering Experiment Station, Cornell University.

55 "Memoire sur la propagation du mouvement dans un Fluide indefini" ("Report on the Propagation of Disturbances in an Unconfined Fluid"), by H. Hugoniot, *Journal of Mathematics*, vol. 3, 1887, p. 477; vol. 4, 1888, p. 153.

56 "Sur la propagation du mouvement dans les corps et specialement dans les gaz parfaits" ("On the Propagation of Disturbances in Bodies and Particularly in Perfect Gases"), by H. Hugoniot, *Journal, Ecole Polytech*, vol. 58, 1889, p. 80.

57 "Druckschwankungen in den Dampfleitungen schnellaufender Kolbenmaschinen" ("Pressure Losses in the Steam Lines of High-Speed Reciprocating Engines"), by H. Küttner, *Forschung auf dem Gebiete des Ingenieurwesens*, vol. 10, 1929, pp. 109–122.

58 "Dynamic Effects on the Gas Exchange Process in Two-Stroke Cycle Engines," by P. Kyropoulous, Doctoral Dissertation, California Institute of Technology, 1948.

59 "Strömungsvorgänge und Bewegungsverhältnisse bei Druckventilen schnellaufender Kompressoren" ("Flow Processes and Motion Relationships in Pressure Valves of High-Speed Compressors"), by E. Lansendörfer, Doctoral Dissertation, Technische Hochschule Darmstadt, 1931.

60 "Die Strömung in Saugrohren von Verbrennungskraftmaschinen" ("Flow in the Intake Pipes of Internal Combustion Engines"), by H. List, *Zeitschrift des Vereines deutscher Ingenieure*, vol 85, 1941, pp. 301–305.

61 "Study of the Dynamics of Induction and Exhaust Systems of a Four-Stroke Engine by Hydraulic Analogy," by W. H. Loh, Doctoral Dissertation, M.I.T., 1947.

62 "Resonanzschwingungen in der Rohrleitungen von Kolbenmaschinen" ("Resonant Vibrations in the Exhaust Pipes of Reciprocating Machines"), by O. Luts, Ber. Lab. Verbrenn, vol. 3, 1934.

63 "Resonanzerscheinungen in der Rohrleitungen von Verbrennungskraftsmaschinen" ("Resonance Phenomena in the Exhaust Pipes of Internal Combustion Engines"), by W. Maier and O. Luts, Ber. Lab. Verbrenn, vol. 3, 1934.

64 "Natural Frequencies of Piping Systems as Determined by Electrical Analogy," by E. F. Murphy, Doctoral Dissertation, Illinois Institute of Technology, 1948.

65 "Die ebene, ungedämpfte Druckwelle grosser Schwingungsweite" ("The Plane, Undamped Pressure Wave of Large Amplitude"), by H. Pfriem, *Forschung auf dem Gebiete des Ingenieurwesens*, vol. 12, 1941, pp. 51–64.

66 "Reflexionsgesetze für ebene Druckwellen grosser Schwingungsweite" ("Laws of Reflection for Plane Pressure Waves of Large Amplitude"), by H. Pfriem, *Forschung auf dem Gebiete des Ingenieurwesens*, vol. 12, 1941, pp. 244–256.

67 "A New Method of Producing Ripples for Optical Analogies," by A. H. Pfund, *Physical Review*, vol. 32 (old series), 1911, p. 324.

68 "Bewegungsvorgänge in Gassäulen insbesondere beim Auspuff- und Spülvergang von Zweitaktmaschinen" ("Motion Phenomena in Gas Columns, Especially During Exhaust and Scavenging Processes on Two-Cycle Engines"), by A. Pischinger, *Forschung auf dem Gebiete des Ingenieurwesens*, vol. 6, 1935, pp. 245–257.

69 "Resonanzschwingungen in Rohrleitung" ("Resonant Vibrations in Exhaust Pipes"), *Deutsh. Kraftf. Forsch.*, vol. 39, 1939, pp. 1–17.

70 "Über die Fortpflanzung ebener Luftwellen von endlicher Schwingungsweite" ("On the Propagation of Plane Air Waves of Finite Amplitude"), by B. Riemann, *Nachr. Ges. Wiss.* Göttingen, vol. 8, 1860.

71 "Zur Einfuhrung in die Strömungslehre zusammendruckbaren Flussigkeiten" ("Introduction into the Theory of Compressible Fluid Dynamics"), by R. Sauer, *Zeitschrift des Vereines deutscher Ingenieure*, vol. 88, 1944, pp. 301–307. Translated, in part, in *Engineering Digest*, London, England, vol. 3, 1946, p. 297.

72 "Pulsation as Encountered in Flowing Gases," by L. F. Scheel, *Western Gas*, vol. 6, 1930, pp. 46–48.

73 "Das Differenzenverfahren zur Lösung von Differentialgleichungen der Nichtstationären Wärmeleitung, Diffusion und Impulsausbreitung" ("The Method of Finite Differences for the Solution of the Differential Equations of Unsteady Heat Flow, Diffusion and Impulse Propagation"), by E. Schmidt, *Forschung auf dem Gebiete des Ingenieurwesens*, vol. 13, 1942.

74 "Schwingungen grosser Amplituden in Rohrleitungen" ("Pulsations of Large Amplitude in Pipes"), by E. Schmidt, *Zeitschrift des Vereines deutscher Ingenieure*, vol. 79, 1935, pp. 671–673.

75 "Schwingungen in Auspuffleitungen von Verbrennungsmotoren" ("Pulsations in the Exhaust Pipe of Combustion Engines"), by Th. Schmidt, *Forschung auf dem Gebiete des Ingenieurwesens*, vol. 5, 1934, pp. 226–236.

76 "Nichtstationäre eindimensionale Gasbewegung" ("Unsteady, One-Dimensional Gas Motion"), by F. Schultz-Grünow, *Forschung auf dem Gebiete des Ingenieurwesens*, vol. 13, 1942, pp. 125–134.

77 "Nichtstationäre, kugelsymmetrische Gasbewegung und nichtstationäre Gasströmung in Düsen und Diffusoren" ("Unsteady Spherically Symmetrical Gas Motion and Unsteady Gas Flow in Nozzles and Diffusors"), by F. Schultz-Grünow, *Ingenieur Archiv*, vol. 14, 1943, pp. 21–29.

78 "Pulsierende Durchfluss durch Rohre" ("Pulsating Flow Through Pipe"), by F. Schultz-Grünow, *Forschung auf dem Gebiete des Ingenieurwesens*, vol. 11, 1940, pp. 170–188.

79 "Study of Exhaust Valve Design from Gas Flow Standpoint," by Seng-chui Hu, Doctoral Dissertation, M.I.T., 1942.

80 "Mobile Laboratory for Testing Performance of Pulsation Dampeners in Compressor Stations," by R. C. Sollars, *Gas*, February, 1950.

81 "Notes on Wave Motion," by C. W. Tricks, General Electric Company, Electrical Course, eighth semester, 1930.

82 "Sound Waves in a Moving Mechanism," by J. D. Trimmer, *Journal of the Acoustical Sciences*, vol. 9, 1937.

83 "Polar Diagram for Tuning of Exhaust Pipes," by T. Warming, Trans. ASME, vol. 68, 1946, p. 31.

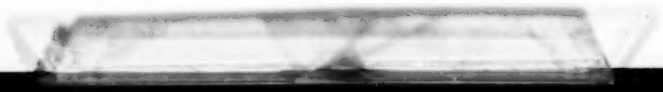

Orifice and Flow Coefficients in Pulsating Flow

By N. A. HALL,[1] MINNEAPOLIS, MINN.

The flow equations pertaining to the behavior of a fluid passing through an orifice are set forth so as to relate the flow coefficient to the orifice configuration and to flow losses. The general nature of the flow coefficient is developed both for the case of instantaneous flow and pressure differences and for mean flow and pressure difference.

Nomenclature

The following nomenclature is used in the paper:

A = flow cross-section area
A_t = minimum fluid-meter cross-section area
C_p = fluid-meter pressure coefficient
C_v = fluid-meter energy-loss coefficient
C_c = coefficient of contraction
D = local hydraulic diameter
f_m = local generalized momentum friction factor
f_s = local generalized loss factor
g_c = gravitational conversion factor
J = mechanical equivalent of heat
K = instantaneous flow coefficient
K_m = mean flow coefficient
p = pressure
s_i = internal entropy
t = time
T = temperature
V = velocity
w = mass-flow rate
x = linear distance along flow path
β = flowmeter diameter ratio
ρ = density

Subscripts:

1 = upstream pressure-measuring position
2 = downstream pressure-measuring position
m = mean value across fluid meter

Introduction

The universal success and acceptance of differential head meters as satisfactory and simple measuring devices for steady-flow systems is due largely to the fairly basic physical principles on which they operate and their use of a single differential manometer as a measuring instrument. This situation has produced a popularity which has led to a natural desire to use the same equipment for all types of flow. It was recognized early that significant errors occurred if the same technique and formulation were used for pulsating as for steady flow. The difficulty involved has been discussed clearly and capably by a number of individuals (1–8, 10, 11, 15, 17).[2]

Most of these discussions have either endeavored to establish limits of operation to insure that specified errors were not exceeded or have been concerned with modifications of the basic instrument in order to accommodate the pulsating flow. These efforts have been very successful and by accepting the principles set forth the measurement of flow where nonsteady effects occur can be accomplished accurately and without excessive complexity in instrumentation. There remains still, however, some uncertainty as to just what goes wrong with the conventional meter installation in nonsteady flow and what kind of analytical correlation can be given for the behavior.

The errors and discrepancies are due to improper application of the auxiliary pressure-measuring equipment as well as of formulas and coefficients. It is common knowledge to careful experimenters that a conventional static-pressure tap and lead which give very accurate readings on a differential manometer for steady pressures may indicate a reading for nonsteady situations having no apparent relation to true mean or even instantaneous pressures. This difficulty has been investigated briefly (12, 13) and some efforts have been made to provide means of obtaining consistent results. No standard recommended procedures are available as yet, however.

The basic equation for flow measurement[3] is

$$w = A_t K \sqrt{2 g_c \rho_1 \Delta p} \quad \text{[1]}$$

where the flow coefficient K is primarily a function of the meter configuration and only slightly dependent on flow as expressed by the throat Reynolds number. Assuming that it is possible to obtain true values for either instantaneous or mean pressure differentials for nonsteady flow, there remains the question as to whether the established flow coefficient will give true values of the flow rate. This question has been considered experimentally and some working rules developed (11).

The flow coefficient can be shown as suggested previously[4] to be dependent in all cases only upon the meter configuration and a loss factor determined by friction and flow separation. The extent of its applicability to nonsteady flow is then dependent on the modifications implied by acceleration terms in the basic flow equations and transient effects on the loss factor.

The flow process in the neighborhood of a differential head meter such as an orifice or a flow nozzle is of sufficient complexity so that it is quite impractical to write down the flow equations in their most complete generality. The immediate concern is the effect of time dependence of properties in a linear direction along the flow system across the meter. Furthermore, the time dependence need include only large-scale fluctuations and not random turbulence. It is convenient to assume that the flow is one-dimensional. In so doing the various properties are averaged across the flow system. This is analogous to the averaging which is tacitly admitted in eliminating random turbulent fluctuations. A slight error is introduced in that different mean velocities actually arise in determining flow rate, momentum, and energy. This error, however, can be incorporated fully in the over-all coefficients ultimately introduced. It is recognized that

[1] Professor of Mechanical Engineering, University of Minnesota. Mem. ASME.

[2] Numbers in parentheses refer to the references at the end of the paper.

Contributed by the Fluid Meters Research Committee and presented at the Annual Meeting, Atlantic City, N. J., November 25–30, 1951, of The American Society of Mechanical Engineers.

Note: Statements and opinions advanced in papers are to be understood as individual expressions of their authors and not those of the Society. Manuscript received at ASME Headquarters, November 7, 1951. Paper No. 51—A-149.

[3] Reference (16), p. 146.

[4] Ibid., chapter 10.

the corrections for deviations from one-dimensional flow may be quite as large as some of those for nonsteady flow. The former are not included in the analysis to follow in order to bring out more clearly the nonsteady-flow effects.

Flow Equations

The flow equations may be set up initially allowing for a continuous change of state and configuration along the direction of flow through the meter. The over-all effect can then be obtained by integration. On this basis and accepting the several assumptions stated, the flow equations are as follows

Continuity

$$A\frac{\partial \rho}{\partial t} + \frac{\partial}{\partial x}(AV\rho) = 0 \quad [2]$$

Momentum

$$\frac{1}{g_c}\rho\left(\frac{\partial V}{\partial t} + V\frac{\partial V}{\partial x}\right) + \frac{\partial p}{\partial x} + \frac{1}{2g_c}\rho V^2\frac{f_m}{D}\frac{V}{|V|} = 0 \quad [3]$$

Energy

$$J\rho T\left(\frac{\partial s_i}{\partial t} + V\frac{\partial s_i}{\partial x}\right) = \frac{1}{2g_c}\rho V^3 M\frac{f_s}{D} \quad [4]$$

These correspond under the restricted condition to more general and more fundamental equations (14, 15). The first term in the momentum equation represents the change in momentum of a moving fluid element, the second the pressure gradient, and the third an effective measure of external force distribution, such as wall friction and pressure discontinuities resulting from separation. The term f_m is, accordingly, a generalized momentum friction factor, D is any suitable reference diameter, and the term $V/|V|$ is introduced solely to provide proper sign in case of reversal of flow direction. The energy equation equates the energy dissipated by a fluid element in motion as expressed by an internal entropy change[5] to a term involving a generalized local loss coefficient (14), f_s. The two coefficients f_m and f_s are nearly equivalent and would be exactly so except for losses involved in the dissipation of random turbulent fluctuations in addition to that due to wall friction.

These equations describing the local behavior must be integrated across the flowmeter as the local friction and loss coefficients would be determined only with difficulty and are only of secondary interest in themselves. The integration is from a position 1, upstream of the meter, to a downstream position 2, in the neighborhood of the meter throat. These correspond to the positions at which static-pressure measurements would be made.

The continuity equation becomes

$$A_2V_2\rho_2 - A_1V_1\rho_1 + \int_{x_1}^{x_2} A\frac{\partial \rho}{\partial t}\,dx = 0 \quad [5]$$

or

$$w_2 - w_1 + \Delta w_t = 0 \quad [6]$$

where

$$w = AV\rho, \quad \Delta w_t = \int_{x_1}^{x_2} A\frac{\partial \rho}{\partial t}\,dx \quad [7]$$

The correction Δw_t is zero for steady or constant-density flow and is small in almost all cases likely to occur.

In integrating the momentum and energy equation an arithmetic-mean value for density and temperature may be used since the total change in these properties across the meter will be small. On this basis the momentum equation becomes

$$\frac{1}{\rho_m}(p_2 - p_1) + \frac{1}{2g_c}(V_2^2 - V_1^2) + \frac{1}{g_c}\int_{x_1}^{x_2}\frac{\partial v}{\partial t}\,dx + \frac{1}{2g_c}\int_{x_1}^{x_2} V^2\frac{f_m}{D}\frac{V}{|V|}\,dx = 0 \quad [8]$$

or

$$\frac{1}{\rho_m}(p_2 - p_1) + \frac{1}{2g_c}(V_2^2 - V_1^2) + \frac{1}{\rho_m}\Delta p_t + \frac{1}{2g_c}V_2^2\,C_p = 0 \quad [9]$$

where

$$\Delta p_t = \frac{1}{g_c}\rho_m\int_{x_1}^{x_2}\frac{\partial v}{\partial t}\,dx \quad [10]$$

and

$$C_p = \frac{1}{V_2^2}\int_{x_1}^{x_2} V^2\frac{f_m}{D}\frac{V}{|V|}\,dx \quad [11]$$

The correction Δp_t is zero for steady and constant-density flow. However, in pulsating flow with any degree of compressibility it may be very significant in accounting for phase differences in pressure waves across the fluid meter.

For steady flow the term[3] corresponding to C_p is also a measure of energy loss corresponding to the internal entropy increase. Basically, however, the dissipation of energy is an action of individual fluid elements and should be derived from the energy equation. In integrating the energy equation across the meter the change in both time and position according to the motion of the fluid element must be included. The dissipation as a line integral applying (4) is then

$$\begin{aligned}\rho_m T_m \Delta s_i &= \int_1^2 \rho\, T\, ds_i = \int_1^2 \rho\, T\left(\frac{ds_i}{dt}\Big/\frac{dx}{dt}\right)dx \\ &= \int_1^2 \rho\, T\left(\frac{\partial s_i}{\partial t} + V\frac{\partial s_i}{\partial x}\right)\frac{dx}{V} \\ &= \frac{1}{2g_c J}\int_1^2 \rho\, V^2\frac{f_s}{D}\frac{|V|}{V}\,dx \\ &= \frac{1}{2g_c J}\rho_m V_2^2\, C_s\end{aligned} \quad [12]$$

where

$$C_s = \frac{1}{V_2^3}\int_1^2 V^2\frac{f_s}{D}\frac{|V|}{V}\,dx \quad [13]$$

The loss coefficient C_s, and the pressure coefficient C_p, will differ not only because of the small difference in the local coefficients but more so because of the difference in the integration path. This distinction indicates that in nonsteady flow the determination of energy loss may require an independent approach from the evaluation of pressure differences and that the corresponding coefficients in instantaneous flow may be very different. Thus the conventional procedure of computing energy loss directly from pressure drop as in steady flow may be in error (9).

Applying Basic Flow Equation

The basic flow Equation [1] may be applied formally to the

[5] See Reference (16), p. 51.

determination of flow from instantaneous-flow conditions. In such a case the flow coefficient will depend not only on meter configuration but also on the pulsation pattern as well. From the flow Equation [1], continuity Equation [6], and momentum Equation [9], the flow coefficient may be expressed as

$$K^2 = \frac{(\rho_1/\rho_m)(A_2^2/A_1^2)}{\rho_1^2/\rho_2^2\left(1 + C_p + \frac{2g_c}{\rho_m}\frac{\Delta p_t}{V_2^2}\right) - \frac{A_2^2}{A_1^2}\left(1 + \frac{\Delta w_t}{w_1}\right)^2} = \frac{C_c^2\,\rho_1/\rho_m}{\rho_1^2/\rho_2^2\left(1 + C_p + \frac{2g_c}{\rho_m}\frac{\Delta p_t}{V_2^2}\right) - \beta^4 C_c^2\left(1 + \frac{\Delta w_t}{w_1}\right)^2} \quad [14]$$

where C_c is the area ratio relating the downstream pressure-point flow area to the meter throat area and β is the meter diameter ratio. This is identical in form to the corresponding equation for steady flow[6] aside from the correction terms Δp_t and Δw_t. Since these are equal to zero for constant density flow, in this case

$$K^2 = \frac{C_c^2}{1 + C_p - \beta^4 C_c^2} \quad [15]$$

As an initial approximation the value of C_p can be assumed constant and equal to the steady-flow value.[7] This is equivalent to assuming an instantaneous-flow coefficient equal to that for steady flow. This appears to be reasonably satisfactory in many cases. In ordinary fluids where a small amount of compressibility may occur it will be necessary to account not only for nonsteady effects on C_p but also to include the term

$$\frac{2g_c}{\rho_m}\frac{\Delta p_t}{V_2^2}$$

Usually the instantaneous flow rate and instantaneous pressure difference are not of as great interest or convenience in pulsating flow as the mean values. If the nonsteady flow is pulsating so that any time variation may be averaged to a fixed mean value, the several flow equations may be transformed to corresponding mean value equations by applying an averaging time integral operator

$$\lim_{t\to\infty}\frac{1}{t}\int_0^t (\quad)\,dt \quad [16]$$

This implies pulsations of rather high frequency with respect to the time interval of observing mean values. Indicating the result of the averaging operator by a bar over the quantities concerned the following equations result

Continuity, from Equation [2]

$$\overline{w} = A_1\,\overline{\rho_1 V_1} = A_2\,\overline{\rho_2 V_2} \quad [17]$$

Momentum, from Equation [9]

$$\overline{\Delta p/\rho_m} = \frac{1}{2g_c}\left(\overline{V_2^2} - \overline{V_1^2}\right) + \frac{1}{2g_c}\,\overline{V_2^2 C_p} \quad [18]$$

The corresponding flow equation is

$$\overline{w} = A_1 K_m \sqrt{2g_c\,\overline{\rho_1}\,\overline{\Delta p}} \quad [19]$$

where K_m is the effective flow coefficient for the mean condition. As before, from the foregoing equations this may be expressed in terms of the flow condition and the pressure coefficient; in this case by

$$K_m^2 = \frac{\overline{\rho_1 V_2^2}}{\overline{\rho_1}\,\overline{\rho_m}\,\overline{V_2^2}}\,\frac{\overline{\Delta p/\rho_m}}{\overline{\Delta p}/\overline{\rho_m}}\,\frac{C_c^2}{1 + \overline{C_p} - \overline{V_1^2}/\overline{V_2^2}} \quad [20]$$

where $\overline{C_p}$ is the mean pressure coefficient defined by

$$\overline{C_p} = \overline{V_2^2 C_p}/\overline{V_2^2} \quad [21]$$

For constant-density flow this simplifies somewhat to the form

$$K_m^2 = \frac{\overline{V_2^2}}{\overline{V_2}^2}\,\frac{C_c^2}{1 + C_p - \beta^4 C_c^2} \quad [22]$$

The initial term, $\overline{V_2^2}/\overline{V_2}^2$, is the most significant since even if C_p is constant and equal to the steady-flow value, this ratio, always less than 1, may be very small for pulsations of any significant amplitude or for intermittent flow. If the pulsating velocity is expressed in terms of harmonic components such that the ratio of each harmonic amplitude to the mean velocity is a_n, then

$$\frac{\overline{V_2^2}}{\overline{V_2}^2} = 1 + \frac{1}{2}(a_1^2 + a_2^2 + a_3^2 + \ldots + a_n^2 + \ldots) \quad [23]$$

If the flow is constant density and if $C_p = \overline{C_p}$, then

$$K_m^2 = \frac{\overline{V_2^2}}{\overline{V_2}^2}\,K^2 \quad [24]$$

or by Equations [1] and [19]

$$\frac{\overline{w}^2}{\overline{\Delta p}} = \frac{\overline{V_2^2}}{\overline{V_2}^2}\,\frac{w^2}{\Delta p} \quad [25]$$

and

$$\frac{w}{\overline{w}} = \sqrt{\frac{\Delta p}{\overline{\Delta p}}\,\frac{\overline{V_2^2}}{\overline{V_2}^2}} \quad [26]$$

Taking the mean value of this relation it follows in this case that

$$\frac{K_m^2}{K^2} = \frac{\overline{V_2^2}}{\overline{V_2}^2} = \frac{\overline{\sqrt{\Delta p}}^2}{\overline{\Delta p}} \quad [27]$$

For constant-density flow the values of the flow coefficients K and K_m consequently depend on a knowledge of the effect of pulsation on the pressure coefficients C_p and $\overline{C_p}$ and the ratio $V_2^2/\overline{V_2}^2$. If the local loss is sufficiently localized as in an orifice and if the pulsations do not interact too strongly with the local flow separation, both C_p and $\overline{C_p}$ will nearly equal the steady-flow value. There appears to be almost a total lack of experimental data on this point. As indicated previously, the velocity ratio, $\overline{V_2^2}/\overline{V_2}^2$ depends strongly on the pulsation wave pattern. However, in most applications this can be predicted or determined from test runs so that sufficiently accurate values can be obtained for routine use.

Experimental Problem

The primary experimental problem in nonsteady-flow measurement is that of pressure measurement. This will involve either instantaneous pressure differentials for transient flow or mean pressure differentials for mean flow. The conventional differential pressure-gage installation is recognized as deficient, in general. However, there is no basic reason why modifications cannot be made to provide satisfactory readings. Recent studies (12, 13) have indicated in part some of the characteristics which must be considered. It is sufficient to realize that the pressure-measuring system when applied to nonsteady flow is no longer a static equilibrium system. Consequently the dynamic actions

[6] See Reference (16), p. 147.
[7] See Reference (16), p. 150.

within the pressure tap, leads, connections, and gage itself must be sufficiently well understood in order to make predictions and set up installation specifications. This information is essential for the usual liquid manometer obtaining mean pressures and also for any of the several types of electrical or electronic instantaneous pressure pickups. In general, it is not practical to obtain a direct local pressure reading on any type of gage or pickup. The effect of the local pressure must be transmitted in some manner and the behavior of this transmission system remains a problem.

REFERENCES

1 "Effect of Pulsations on Flow of Gases," by Horace Judd and D. B. Pheley, Trans. ASME, vol. 44, 1922, pp. 853–918.

2 "The Laws of Similarity for Orifice and Nozzle Flows," by J. L. Hodgson, Trans. ASME, vol. 51, 1929, paper FSP-51-42.

3 "Pulsating Air Flow," by N. P. Bailey, Trans. ASME, vol. 56, 1934, pp. 781–786; vol. 57, 1935, p. 188.

4 "Durchflusszahl non Normdusen und Druchahfall in Rohren bei Pulsierender Strömung," by E. Estel, *Physikalische Zeitschrift*, vol. 38, 1937, p. 748.

5 "Durchflussmessung bei pulsierender Strömung," by F. Herning and C. Schmid, *Zeitschrift des Vereines deutscher Ingenieure*, vol. 82, 1938, pp. 1107–1114.

6 "Pulsating Air Velocity Measurement," by N. P. Bailey, Trans. ASME, vol. 61, 1939, pp. 301–308.

7 "The Effect of Pulsations on Orifice Meters," by S. R. Beitler, Trans. ASME, vol. 61, 1939, pp. 309–314.

8 "Messfehler bei Durchflussmessung pulsiender Gasstrome," by C. Schmidt, *Zeitschrift des Vereines deutscher Ingenieure*, vol. 84, 1940, pp. 596–598.

9 "Pulsierder Durchfluss durch Rohre," by F. Schultz-Grünow, *Forschung auf dem Gebiete des Ingenieurwesens*, vol. 11, 1940, pp. 170–187.

10 "Durchflussmessverfahren für pulsierende Strömungen," by F. Schultz-Grünow, *Forschung auf dem Gebiete des Ingenieurwesens*, vol. 12, 1941, pp. 17.

11 "Developments in the Measuring of Pulsating Flows With Inferential Head Meters," by S. R. Beitler, E. J. Lindahl, and H. B. McNichols, Trans. ASME, vol. 65, 1943, pp. 353–356.

12 "The Response of Pressure Measuring Systems to Oscillating Pressures," by I. Taback, NACA TN 1819, 1949.

13 "Attenuation of Oscillatory Pressures in Instrument Lines," by A. S. Iberall, Trans. ASME, vol. 72, 1950, pp. 689–695.

14 "The Action of Friction in Non-Steady Flow of Fluids," by Newman A. Hall, Proceedings of the First Midwestern Conference on Fluid Mechanics, 1950.

15 "One-Dimensional, Transient Flow With Consideration of Friction, Heat Transfer, and Change of Section," by E. Jenny, *Brown Boveri Review*, vol. 37, 1950, pp. 447–461.

16 "Thermodynamics of Fluid Flow," by Newman A. Hall, Prentice-Hall, Inc., New York, N. Y.

17 "Flow Measurement With Orifice Meters," by R. F. Stearns, R. M. Jackson, R. R. Johnson, and C. A. Larson, D. Van Nostrand Company, Inc., New York, N. Y., 1951.

Discussion

V. P. Head.[8] Many of us have been schooled by experience to regard the dimensional-analysis approach coupled with rigorous experiment as superior to a mathematical approach in getting at the laws of nature. As the author points out, experiment is sooner or later necessary to confirm the findings of any mathematical investigation. We suggest that before such experiments can be conducted properly, our ideas of the types of quantities to be investigated must be clarified carefully. In the interests of economy and ultimate usefulness these quantities may differ from those in which the theoretical physicist may express himself. The author offers three concepts which may be very useful in an experimental study of pulsation: (*a*) The dominant expression in mathematical analysis, the ratio of average velocity to rms velocity. (*b*) He also points out that to talk about flow-rate pulsation in terms of the magnitude of fluctuation of pressures or pressure differentials can only be regarded as valid in incompressible flow. (*c*) Another point that should be highlighted is the importance of higher frequencies, of the type radio hams call "hash," sometimes superimposed upon certain fundamentals.

When the last two points are considered carefully, we are forced to conclude that in pulsation problems, incompressible flow does not exist. All pulsations are sound waves and depend on the compressibility of the gas or liquid for their very existence.

Those who are concerned with the strength of ducts and containers undoubtedly will find it convenient to talk about pressure pulsation. However, those of us who are concerned with the measurement of rate of flow will find it convenient and almost imperative, if we are to keep our thinking straight, to define pulsation as the variation from instant to instant in the "rate of flow" itself. A sound wave traveling in still air may be regarded in any of several lights. It may be regarded as a wave of instantaneous velocity variation, a wave of density variation, or a wave of pressure variation. Pulsation in a closed conduit carrying a liquid similarly may be regarded as a sound wave characterized by any of these three aspects. That aspect in which we are interested is superimposed on a steady value of the same type of quantity.

The simplest possible equation for rate of flow in any variable-head meter is

$$Q = KD^2\sqrt{gh}$$

where K is a pure number that presupposes nothing. We leave out $\sqrt{2}$ because it presupposes much. This equation is equally valid for instantaneous rate of flow under steady-flow conditions, for instantaneous rate of flow under pulsating conditions, and for average rate of flow under pulsating conditions. In general, it is the latter that is of importance. We must expect to find the experimental coefficient to be a function of several dimensionless parameters which are made up of the variables encountered in the experimental situation. These variables, as is well known, include the viscosity of the flowing fluid, the elasticity of the flowing fluid, and the many geometric influences which define the flowmeter and its installation, and one more, the pulsation intensity.

There is a marked need, then, for a quantitative idea of pulsation intensity and of an experimental means of determining it. We suggest that for fluid-flow measurement the quantitative notion of pulsation intensity should be simply the ratio of average rate of flow to rms rate of flow. This concept may be modified to yield a "point" quantity in the same way that temperature or static pressure or velocity are "local" quantities, to be measured at a designated point in a flow conduit, by using average velocity/rms velocity. For purposes of geometric similarity, a specified design and location of a "pulsation intensity probe" could be identified with a curve or table of pulsation factors, just as a specified location for an absolute static-pressure tap is identified with a tabulation for expansion factors for inferential variable-head or variable-area fluid-flow meters.

We hope that this line of thinking may inject a note of optimism into the discussion of this subject. Specifically, we need the following:

(*a*) A device to determine whether "flow-rate" pulsation is significant at any meter installation—let us call it a "rate-pulse-intensity" probe, and let us not confuse it with a pressure probe.

(*b*) The experimental evaluation of various types of rate-pulse-intensity "regulators and controllers." (Such regulators and controllers may be devices to reduce rate-pulse-intensity or devices to hold constant the rate-pulse-intensity.)

(*c*) Experiments to provide tables of corrections for various types of inferential flowmeters when employed with rate-pulse-intensity probes, indicators, recorders, regulators, and controllers.

(*d*) The fact of inherent decay of rate-pulse-intensity over the

[8] Director of Hydraulic Research, Fischer and Porter Co., Hatboro, Pa. Jun. ASME.

length of a long conduit should not be overlooked, and our rate-pulse-intensity probe may be used at two stations properly selected in a straight pipe run to provide experimental data as a function of average Reynolds and Mach numbers.

Under the category of devices to reduce intensity we may include conventional flow controllers when rate-pulse frequencies are in the order of 1 cycle per min to 1 cycle per day; capacity bells when pulse frequencies are in the order of 100 cycles per sec to 10 cycles per hr; mufflers for rate-pulse frequencies of 10,000 cycles per sec to perhaps 10 cycles per sec; "reflectors" which are opaque to sound but not to flow, such as partially closed "venetian blinds" or ball-lattice structures which have "optical" effects in transmitting or reflecting very high-frequency sound (rather similar to the optical effects of such structures in the television broadcast band of electromagnetic waves) from about 5000 cycles per sec up. The desirability or possibility of controlling pulsation intensity at a constant level in spite of variations in inherent pulsation in a line, as by high-frequency sound input controlled at a rate-pulse-intensity higher than the highest expected inherent intensity in any particular installation, so that the "pulsation factor" would remain constant, is perhaps too Buck Rogersish for the moment.

It is manifest that pressure fluctuation, whether measured by the swing of a pressure-gage needle or an oscillograph of a crystal pressure-probe output, has failed to qualify. It has been observed experimentally at our company's laboratory and at least one aircraft-engine test laboratory, that in the process of satisfactorily eliminating rate-pulse-intensity, particularly by reflection methods, pressure-pulse-intensity is often increased rather than decreased.

We are therefore eminently grateful to the author for his analysis which points up the prime importance of the ratio V (average)/V (rms), and seek his opinion as to the feasibility of lumping all the other complex but second-order effects disclosed by his analysis into "geometric similarity criteria," so that our experimental approach may apply equally well to nozzles, orifices, Venturis, and variable-area meters employing float shapes whose annular flow passages may resemble in a way the concentric flow passage of nozzles, orifices, and Venturis, with no concern whatever for "velocity-of-approach factor," "coefficient of contraction," and similar notions derived from purely "geometric" considerations. We commend to all interested persons the first serious problem, the development of a satisfactory rate-pulse probe.

Author's Closure

The comments of Mr. Head confirm the fact that certain parameters determined by averages related to the pulsation wave pattern are sufficient to provide corrections to the basic steady-flow equations. The most important of these is the ratio of average velocity to rms velocity. Whether this parameter would be sufficient to determine others adequately is uncertain. This question among others can only be answered by an extensive testing program involving various types of flow-measuring elements in pulsating flow. It would be expected that some simplification of the most general formulation by reducing the number of descriptive parameters would be possible. However, although various semi-theoretical estimates could be made, experimental confirmation and correlation should be regarded as essential.

In steady flow, Reynolds number is the primary parameter. Perhaps pulsation intensity as measured by the velocity ratio would play a similar role for pulsating flow as a characterizing parameter for the effects of pulsation. However, the possibility of local resonance and selective distortion by the flow-system configuration may limit the adequacy of any single general parameter in describing the average effects of pulsations.

Pulsations in Gas-Compressor Systems

By E. G. CHILTON[1] and L. R. HANDLEY,[2] EMERYVILLE, CALIF.

This paper presents the causes of pulsation, their effects on the piping and the compressor, and the methods by which pulsations can be reduced. By means of an analogy to electrical networks,[3] the interaction between the compressor and the piping can be visualized more easily, and the action of the system can be expressed in mathematical form. The resultant equations are not readily solvable but can be simplified and solved for the special cases which have a tank or filter close to the compressor. The results of the computations are compared with experiments on a laboratory compressor and a few large-size installations. They are expressed in the form of graphs which make it possible to select an appropriately sized surge tank or filter for any compressor and any allowable pulse magnitude.

Summary of Recommendations for Design of Compressor Installations

It has been established that pressure pulsations are harmful and undesirable in suction or discharge lines of compressors, means should be provided, therefore, to eliminate pulsations.

1 In general, a single tank is the simplest and most satisfactory pulse eliminator, and its proper size can be computed from the enclosed curves if compressor data are available and if the allowable pulse amplitude is known.

2 Allowable pulse amplitudes should be determined from experience, but an upper limit of 2 per cent seems safe for the average installation. This figure should be decreased somewhat for high-pressure lines and may be increased for low-pressure suction lines.

3 Filter-type dampeners will prove efficient only if it is more important to remove pulses from the line than from the compressor. Comparing, for instance, a single-tank dampener with a π-type filter whose two tanks combined have the same volume as the single tank, it is found that pulsations at the compressor are over twice as large with the filter as with the single tank, while those going into the piping are about one half as large.

4 The only filter considered here is the π-type filter since it appears to be as efficient as any. It is shown diagrammatically in Fig. 2(*a*), and the curves pertaining to it are calculated for a cutoff frequency[4] equal to 0.9 times the minimum piston frequency, so that the relation between the tank volume and the line connecting the tanks can be expressed by (see nomenclature in Appendix for terms)

$$\frac{l}{A} = 450.3\,\frac{a^2}{V_c N^2}$$

5 It is essential that any dampener, whether a filter or a single tank, be connected as closely to the compressor cylinder as possible, and that any pipe connecting it with the cylinder be of large diameter and have no sharp corners. This is to reduce vibrations in the pipe and to minimize inertance between cylinder and dampener, for any inertance will increase compressor pulses appreciably. Therefore it is suggested that, wherever possible, the dampener be attached directly to the compressor cylinders. This method also avoids beat-frequency effects in the manifolds connecting several compressors, as the pulses of each compressor already will be reduced to a minimum.

6 Should resonant pulsations occur in any section of the line and should it be undesirable to change the length of that line or introduce a dampener, experience indicates that the use of an orifice of one half the pipe diameter placed in the resonant section will result in a material improvement.

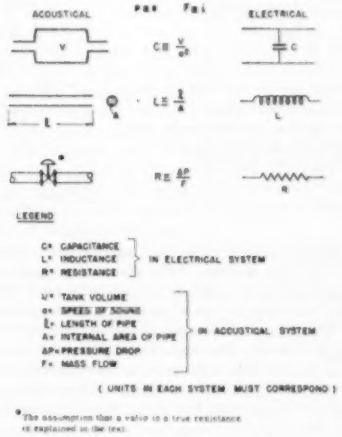

Fig. 1 Terms in Electrical-Acoustical Analogy

Pipes can be resonant at a great number of multiples and submultiples of the fundamental wave length; moreover, resonance generally will occur over a wide range so that it is difficult to predict whether or not resonance will occur. It is much safer to remove pulsations first so that no dangerous pulses remain to create resonance conditions. For the same reason the dampener should be placed as close to the compressor as possible, as already outlined.

7 Elbows and bends in a pipe do not form reflection points for pressure pulses for they do not form acoustical impedances. This has been proved conclusively in laboratory tests. However, if pulses are present in the flow, vibrating stresses will be introduced into the pipe at these bends, as shown by Baird and Bechtold (28),[5] such corners form the focal points of pipe vibration if pulses have not been previously removed from the fluid.

---

[1] Research Engineer, Shell Development Company. Jun. ASME.

[2] Junior Engineer, Shell Development Company. Jun. ASME.

[3] Terms in electrical-acoustical analogy are given in Fig. 1.

[4] Cutoff frequency is the frequency beyond which a low-pass filter stops conducting pulsations.

Contributed by the Fluid Meters Research Committee and presented at the Annual Meeting, Atlantic City, N. J., November 25–30, 1951, of The American Society of Mechanical Engineers.

Note: Statements and opinions advanced in papers are to be understood as individual expressions of their authors and not those of the Society. Manuscript received at ASME Headquarters, September 18, 1951. Paper No. 51—A-90.

[5] Numbers in parentheses refer to the Bibliography at the end of the paper.

8 Double-acting compressors can be treated like single-acting pistons of twice the crankshaft rpm if the assumption can be made that each side of the double-acting piston discharges approximately one half the total amount of gas.

9 It has been suggested by Moore (15) that the design of tanks preferably should be such that all of their internal dimensions be less than $^1/_{12}$ the wave length ($60\,a/N$) of the pulses.

Causes of Pulsation

It is well known that pressure and flow in a pneumatic system are related to each other; flow will not take place unless a pressure is present to cause it, or, in turn, varying flow will be accompanied by varying pressure. The alternating motion of a reciprocating-compressor piston inherently will cause alternating flow in, say, the discharge pipe, even if no discharge valve were present. The action of the valve which prevents flow in one direction aggravates the flow variations by permitting the entire gas mass to flow in what is generally a very short portion of the cycle, so that very high rates of change of flow may result. In fact, the actual shape of the flow versus time curve depends upon the piping attached to the compressor. Thus a large surge tank can accommodate rapid flow changes without appreciable changes in pressure—similar to a soft mechanical spring absorbing accelerations at one of its ends, or an electric capacitor absorbing changes in electric current in the line without appreciable voltage changes.

A fairly long, small-diameter pipe, on the other hand, behaves like a large inertia mass with respect to accelerations or a large electrical inductance with respect to current changes. It will not tolerate flow-rate changes without large increases in pressure. Such a pipe connected to the discharge of a compressor will cause a large pressure rise at the moment the piston forces gas through it, and thus may alter the compressor characteristics appreciably. Hence there is a continuous interaction between compressor and pipe line, one affecting the other; and accurate formulas can be established only if the two are considered jointly. Just as the voltage fluctuations in an electrical system cannot be computed without considering the generator, one must consider the characteristics of the compressor in calculations for a compressor system.

It is worth mentioning here that pressure pulses in gases (or, for that matter, in liquids and solids) travel through the fluid with the speed of sound: consequently, the phenomena discussed here fall into the realm of acoustics, and, under certain assumptions to be outlined, can be treated by the well-established laws of that science.

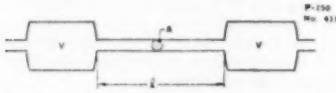

Fig. 2(*a*) Schematic Diagram of π-Type Filter

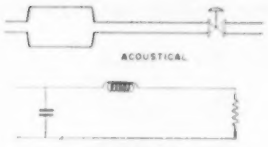

Fig. 2(*b*) Schematic Diagram of Analogous Acoustical and Electrical Circuits

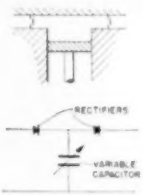

Fig. 2(*c*) Electrical Analog of Piston and Valves

Effects of Pulsations

Before analyzing in detail the mathematical aspects of the pulsating system, let us review the various ways in which pulsations can be detrimental to compressor operations. For purposes of convenience these may be divided into effects on the piping and effects on the compressor.

1 Effects on the piping system:

(*a*) In general, the most serious piping troubles, at least the ones most easily observed, come from vibration of the pipe lines. Pressure pulsations cause oscillating forces at bends of the pipe and if any section of the pipe is resonant to any of the numerous harmonics of the pulse, large vibrations are likely to occur, and in turn may cause pipe failures. Arnold (17) has described this phenomenon and, moreover, gives valuable data for computation of the natural frequencies of various types and lengths of pipe. Baird and Bechtold (28) also describe the physical causes of pipe vibration and the effects of frequency on stress.

(*b*) It is important, but not generally known, that pulsations also can increase pipe friction. Binder (14) has shown that actual damping (friction) factors for pulsating flow can be computed with fair accuracy by the use of an eddy-viscosity term added to the actual viscosity of the fluid. This eddy viscosity is an empirical term originally proposed by Boussinesq (1), and used by Murphree (5) and others, to account for differences in friction between turbulent and laminar flow. It is a function of many variables, including the magnitude and frequency of pulsations, but little experimental information is available.

(*c*) In the inferential measurement of flow, the existence of pulsations causes serious errors which have been particularly troublesome in the natural-gas industry for many years. Judd and Pheley (2) have extensively covered the subject experimentally and are also probably the first to have shown the acoustical nature of pulsations. Eagle and Daberko (6) discuss various means for eliminating these measurement errors showing particularly the futility of using dampeners in the manometer lines. Mathematical analyses by Herning and Schmid (8) and Lindahl (21) indicate the difficulty of predicting flowmeter errors, even if the pulse amplitude is known.

(*d*) The effect of pulsation on the process served by the compressor has not received too much attention, partly perhaps because this effect is rarely obvious; yet it is known that many chemical processes are affected severely by such pulsations.

2 Effects on compressor performance:

(*a*) The literature shows but few considerations of the effects of pulsations on the compressor performance. For internal-combustion engines, however, such effects are described in the papers by Morse, et al. (9), and Lutz (11, 12). Under circumstances very similar to those in compressor systems, the pulsations in the intake and exhaust manifolds of those engines are shown to affect volumetric efficiency and power output to a marked degree.

(*b*) Pulsations at the compressor in some instances will cause valve flutter, valve hammer, and repeated valve failures. While the reason for this occurrence is obvious, it is a phenomenon difficult to analyze for it depends on many variables and design details of the compressor, some of which are analyzed by Costagliola (31). The authors know of a number of installations where consistent valve breakage has been stopped by alleviating the pulsations at the compressor.

Methods for Reducing Pulsation

Since the troubles of pressure pulsations have been known, means for reducing or eliminating them have appeared in ever-increasing numbers, some of them of amazing complexity.[6]

The oldest, the simplest, and perhaps the most widely used pulsation dampener is merely a large vessel placed in the line—a capacity, if we wish to use the acoustical (or electrical) terminology. The authors believe that, due to its simplicity and other reasons to be discussed later, this dampener is also the most satisfactory for the average installation. Computation of the required size of these tanks thus far has been confined largely to empirical or semiempirical methods, as is evidenced by the in-

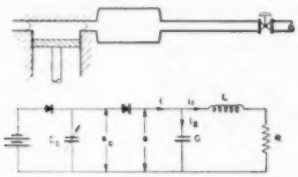

Fig. 3(*a*) Schematic Diagram of Simple Compressor System and Its Analog

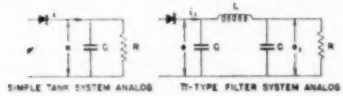

Fig. 3(*b*) Schematic Diagrams for Analogs of Simple Tank and π-Filter Systems

stallation manuals of compressor manufacturers. These are not adequate to permit reliable calculation of pulse amplitudes.

To connect a tank to the line by a pipe T so that it acts as a surge bottle is generally not as effective as to have it on the line, unless the leg of the T is short and of large diameter, in which case the unit approaches the in-line tank. Under certain circumstances, however, the combination of surge tank and neck can act as a resonator and will eliminate pulsations of a definite frequency only. Such a system is described by Heath and Elliott (20) and Stephens (30), but it is rarely of interest for compressor installations.

Another simple device that has found frequent use in pulse elimination is a restriction in the form of an orifice, a valve, or the like. It suffers from the primary drawback that it creates a pressure drop and absorbs power. Judd and Pheley (2), having experimented with orifices, found them occasionally effective when used in combination with volume tanks.[7] In certain cases it can even be shown that the friction loss in a pipe with an orifice can be less than the loss in the same pipe without the orifice but under resonant conditions. For this reason they are very useful to break up resonances in individual pipes of existing installations.

Combinations of acoustical elements designed to operate as a unit in eliminating pulsations may be grouped under the name of filters. These range from acoustically correct designs such as a so-called π-filter[8] to weird combinations of resistances, capacities, and acoustical inertances as, for instance, in the patent of Rudolph (18).

Analysis of Pulsating Flow by Analogy Methods

Some of the assumptions made in the following analysis are those customarily made in treatises of this kind, and include:

Constant Velocity of Sound in Piping System. Speed of sound in a gas varies very nearly as the square root of the absolute temperature. Its dependence on pressure is generally negligible. Since a workable analysis has to assume constant speed of sound, and since the absolute temperature in compressor piping does not usually vary a great deal between compressor and plant, calculations are always based on an average velocity of sound in the system.

Gas-Pressure Pulses Are Propagated With Speed of Sound. Sound waves travel downstream with a velocity equal to the sum of the stationary sound velocity and the stream velocity, while they are propagated upstream with the difference of these two velocities. The phenomenon is related closely to the familiar Doppler effect and has been well described by Trimmer (7). In general, however, flow velocities are very small compared to the velocity of sound, and it was deemed justifiable to neglect the flow velocity entirely.

Friction Pressure Drops Are Linear Functions of Flow. The resistance to flow through pipes, valves, orifices, and so forth, usually increases with increasing flow velocity so that the pressure drop across such a resistance is not proportional to flow but to some power of flow higher than unity. If, however, we are dealing with relatively small pulsations superimposed upon a steady flow, it is reasonable to approximate the actual pressure-flow curve by a straight line about the steady-flow point, or, in other words, to take the resistance as constant. This assumption is made throughout the paper.

The analogy used in the analysis is that commonly employed by acoustical engineers and most adequately described by Olson (16). It is briefly summarized in Fig. 1 and applied to a simple tank-line-valve system in Fig. 2(*b*). The neglect of distributed capacity and resistance in the pipe is justified in most practical cases, but, if necessary, can be taken into account by analogy to electrical transmission lines, as is well demonstrated by Murphy (25, 29). Inertance of the valve is also neglected.

In addition to Murphy, others who have worked in this field are Morse, et al. (9), Lutz (11, 12), Moore (15), and Binder and Hall (24). Some of these authors actually built electrical analogs to solve a variety of problems, most of them connected with the intake and exhaust pipes of internal-combustion engines.

In order to be able to predict pulse amplitudes as well as resonant frequencies, it is essential to find a close analog for the compressor (or engine) piston-cylinder-valve combination. The assumption of a voltage generator with some fixed voltage versus time characteristic, which has been used extensively, appears unreal. We have preferred a method, already suggested by Binder and Hall (24), of replacing the piston and cylinder by a time-variable capacity, and the pressure-operated valves of a compressor by idealized rectifiers with negligible impedance in the direction of flow [see Fig. 2(*c*)].

All parts of the analogous system are thus defined and, in theory at least, the pulsations of any real compressor piping system can be found from the analogous electrical system by either mathematical analysis or construction of the electrical model. Unfortunately, both approaches present serious difficulties. The mathematical one (see Appendix, second section, for detailed development) leads to linear differential equations with nonconstant coefficients. Construction of the analog, on the other hand, requires electrical equipment of unusual design, the

[6] See, for instance, Rudolph (18).

[7] Similar results are reported by Scheel (4).

[8] See Stephens (22), also Olson (16), page 94, and other works on acoustics. The name is derived from the appearance of the schematic diagram of the analogous electrical system as shown in Fig. 3(*b*).

construction of which was not deemed justifiable in this investigation.

Under certain conditions, notably those at which a relatively large capacity is situated directly adjacent to the compressor, the assumption can be made that, while the valve is open, the gas flow is directly proportional to the piston velocity.[9] Since this velocity usually is quite nearly sinusoidal, the current follows a pattern shown in Fig. 4(*a*). Experiments have demonstrated that this assumption is quite good as long as the tank is very near the compressor and its volume is larger than about 10 times the volume of gas discharged per stroke.

From considerations of the compression of the gas in the cylinder, the clearance volume, and the average suction and discharge pressures, the points at which the suction and discharge valves open can be computed readily. Graphs which simplify this procedure are shown in this paper.

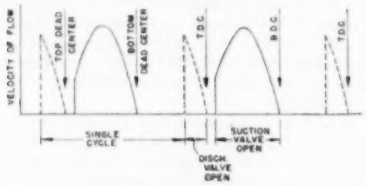

FIG. 4(*a*) TYPICAL FLOW VELOCITY SHAPES AS ASSUMED

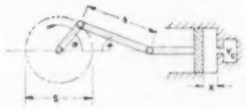

FIG. 4(*b*) PISTON-CRANK DIAGRAM

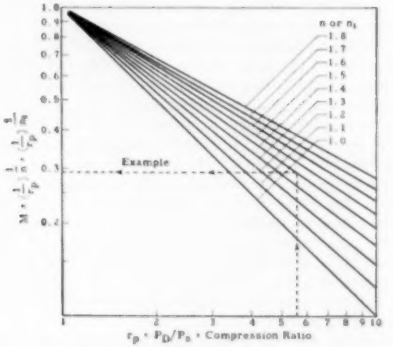

P_D = Absolute Discharge Pressure
P_S = Absolute Suction Pressure
n = Polytropic Constant During Compression
n_1 = Polytropic Constant During Expansion of Clearance Gas

FIG. 5 FIRST GRAPH FOR DETERMINATION OF VALVE-OPEN-TIME
(Suction or discharge valve.)

[9] See Binder and Hall (24).

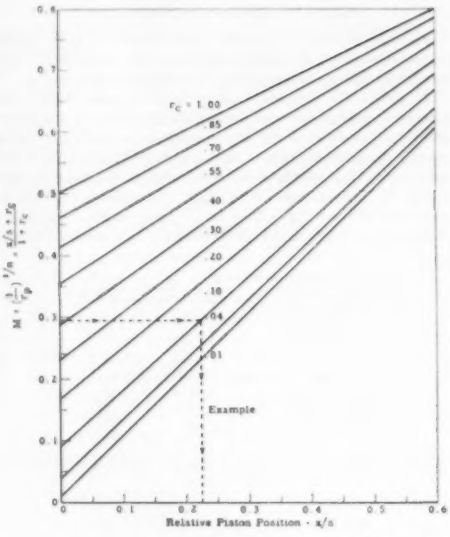

M-(Obtain from Fig. 5)
$r_c = V_c/V_D$ = Clearance Ratio
V_c = Clearance Volume
V_D = Piston Displacement

FIG. 6(*a*) SECOND GRAPH FOR DETERMINATION OF VALVE-OPEN-TIME
(Discharge valve only.)

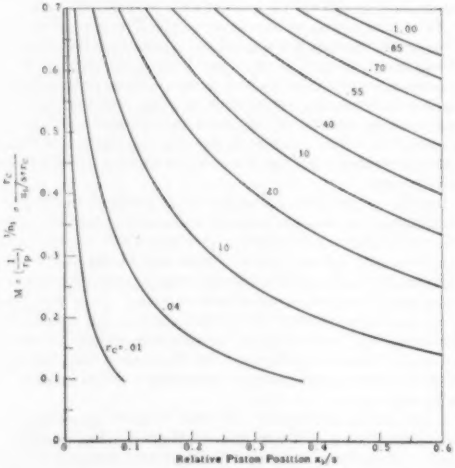

M-(Obtain from Fig. 5)
$r_c = V_c/V_D$ = Clearance Ratio
V_c = Clearance Volume
V_D = Piston Displacement

FIG. 6(*b*) SECOND GRAPH FOR DETERMINATION OF VALVE-OPEN-TIME
(Suction valve only.)

Present Solutions

Calculations have been made for the case of a single tank and for a π-type filter under the assumptions stated, and the results are given in graph form in Figs. 8 and 9. If the tank or filter reduces the pulsation to a desirable minimum, it is unlikely that conditions further along the line are of any influence on the pulse amplitude; and for that reason the remainder of the circuit can be considered as a pure dissipative element, that is, a plain resistance.[19] Hence the load circuits considered are represented by Fig. 3(*b*). They are equally suitable for suction and discharge lines, and the following procedure should be employed in finding pulsation magnitudes:

1 Find the ratio r_t, that is, the percentage of the cycle over which the valve is open, from Figs. 5 [6(*a*), 6(*b*) for suction], and 7.

2 For simple tank-type dampeners next use Fig. 8 (for π-type filter, Fig. 9) to determine the per cent pressure pulse.

Note that the effect of small changes in valve-open-time r_t is not large and an estimate of its value may suffice.

Specific heat ratios in gas mixtures generally can be estimated closely. A discussion of these is given by Edmister (32).

All pressures are absolute pressures.

Accurate knowledge of suction and discharge temperatures and pressures is essential for calculation of V_s.

Experiments

Description of Equipment. A small two-stage Rix air compressor (3¹/₄ in. × 1¹/₈ in. × 3 in., capacity 7 cfm) was used for the laboratory tests. The compressor was belt-driven by an electric motor through a variable-speed pulley. This type of drive offered a compressor working range from 350 rpm to 800 rpm; speed was measured by a tachometer generator attached directly to the compressor crankshaft and checked by a hand tachometer (see Fig. 10).

Three different sizes of tanks were used for capacity, offering a range in volume from 0.017 cu ft to 1.89 cu ft. These tanks permitted the use of pressures up to 1000 psi.

Gas-flow rates were determined by a "metric ironcase" gas

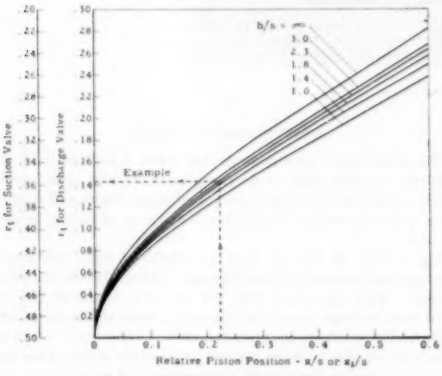

Fig. 7 Third Graph for Determination of Valve-Open-Time (Suction or discharge valve.)

[19] For this reason the accuracy of the data is greater if the pulse amplitude is small.

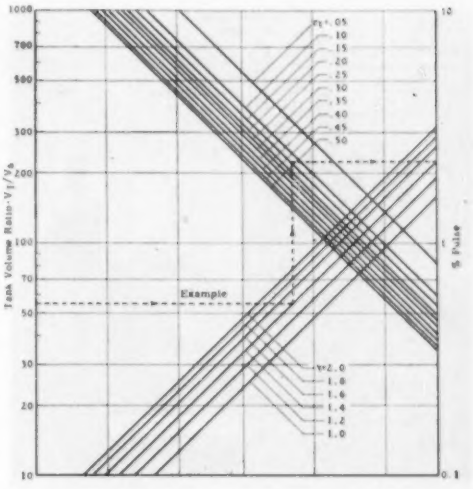

Fig. 8 Tank Volume Versus Pulse Amplitude for Single Tank Dampener

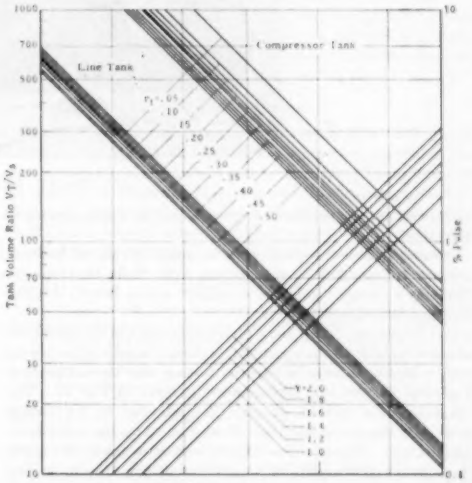

Fig. 9 Tank Volume Versus Pulse Amplitude for π-Type Filter

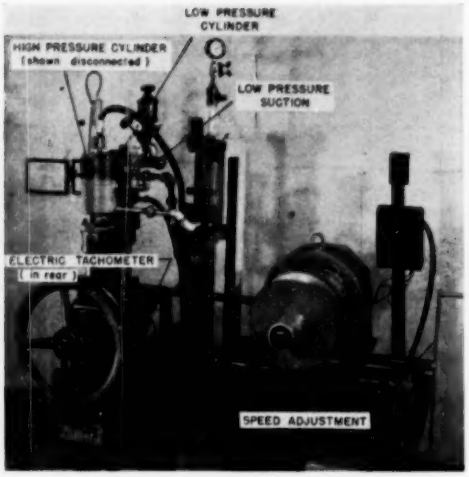

FIG. 10 RIX LABORATORY COMPRESSOR AND VARIABLE-SPEED DRIVE

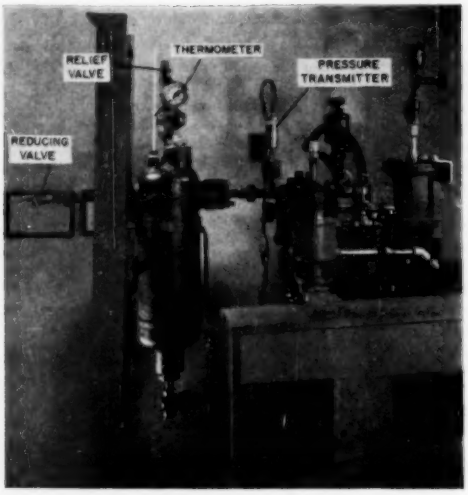

FIG. 12 SINGLE TANK TEST INSTALLATION; 0.27-CU-FT TANK

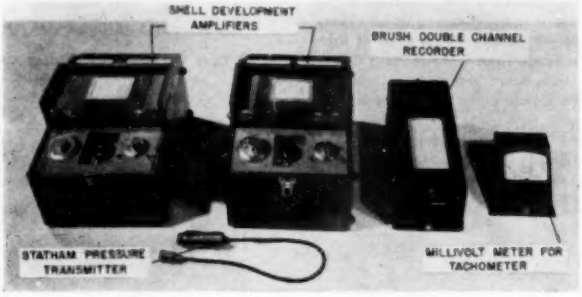

FIG. 11 INSTRUMENTATION

meter, and gas temperatures were measured at various points in the system.

Pressure-pulsation records were obtained by use of Statham pressure transmitters in conjunction with Shell Development Company's dynamic pressure amplifiers and a Brush, BL-202, recording oscillograph (see Fig. 11).

Test Procedure. After some preliminary tests to determine the extent of validity of the approximate theory, a series of tests were made with single tanks of variable volume near the compressor. A general view of this arrangement is shown in Fig. 12. The compressor was started, pressure was adjusted to the desired value, and the gas in the tank allowed to warm up to a steady temperature. Pressure-time records were then taken at various places in the system and for various compressor speeds, making sure that temperatures remained steady during each run. Similar tests were made at the suction side of the cylinder.

Tests with π-type filters (see Fig. 15) were necessarily fewer in number, inasmuch as for each speed and volume the connecting inertance had to be changed to a value corresponding to a cutoff frequency of 90 per cent of operating frequency. However, in general, these tests were similar to those just described.

RESULTS AND DISCUSSION

The preliminary tests showed that when a sufficiently large tank was installed close to the compressor cylinder, good agreement between measured and computed wave shapes and magnitudes could be obtained, regardless of the type of piping beyond the tank.

Figs. 13, 14, 16, and 17 show the results of tests with single tanks and π-type filters in suction and discharge lines of the compressors. Fair agreement with the theory is found except for small tank volumes where the approximations of the theory do not hold, but where its use gives conservative answers. Effect of friction in the pipe between the two tanks of the π-type filter becomes very noticeable at suction pressures and accounts for the deviations of the line-tank values in Fig. 17.

A few test results from large scale (1000-hp) compressors are also shown in Figs. 13 and 14.

It is hoped that the work here presented, which, admittedly, is only the beginning of a design theory for compressor systems, may be extended to give more generally applicable solutions. This can be done either by numerical solution of the differential

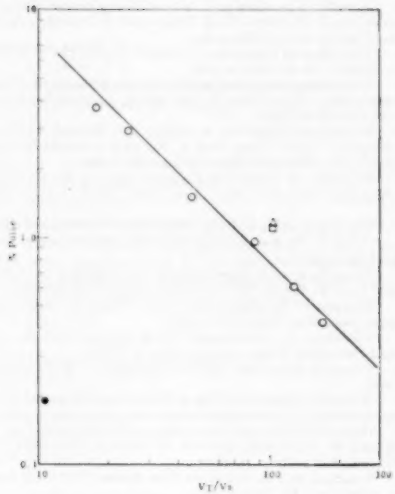

VT = Tank Volume
Vs = Gas Vol. Flowing per stroke
% Pulse = $\frac{\text{Peak to Peak Pulse}}{\text{Av. Absolute Press.}} \times 100$

Lab. Compr. — Theoretical Values; ○ Test Values (600 RPM)
Full scale Comprs. □ Theoretical Values; △ Test Value

FIG. 13 RESULTS OF TESTS ON SINGLE TANK DAMPENER IN SUCTION LINE

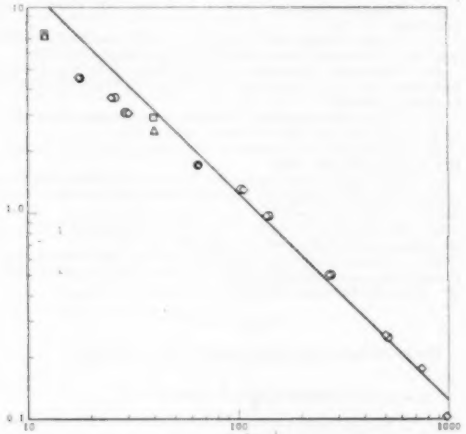

VT = Tank Volume
Vs = Gas Vol. Flowing per stroke
% Pulse = $\frac{\text{Peak to Peak Pulse}}{\text{Av. Absolute Press.}} \times 100$

Lab. Compr. — Theoretical Values; ○ Test Values (600 RPM); ◇ " " (450 RPM)
Full Scale Comprs. □ Theoretical Values; △ Test Value

FIG. 14 RESULTS OF TESTS ON SINGLE TANK DAMPENER IN DISCHARGE LINE

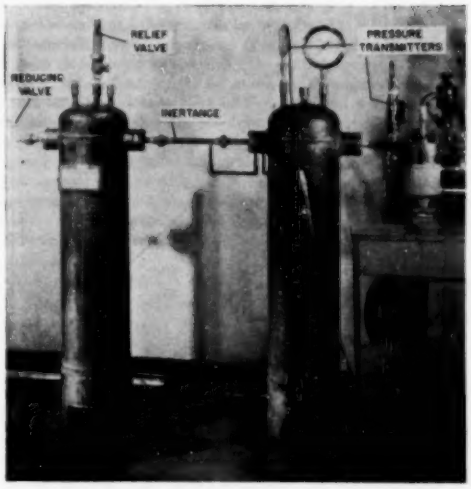

FIG. 15 π-TYPE FILTER TEST INSTALLATION; 1.9-CU-FT TANKS

equations for more general cases where some of the simplifying assumptions made here do not hold, or by construction of an actual analog which can solve a great variety of systems.

A practical evaluation of allowable pressure pulses also would be of value to give the designer the limits to which he must design his system. The arbitrary value of 2 per cent maximum pulse indicated previously is a safe limit based on a few—far too few—practical observations of the authors, and should not be considered as a fixed limit. The pressure level, the type of process, and many other considerations materially influence the safe limit to which pressure pulsations should be held.

ACKNOWLEDGMENT

The authors wish to acknowledge the ready assistance and information obtained from many of the compressor manufacturers with regard to their practices and experiences. Thanks are due particularly to Messrs. J. G. Wilson and H. M. Karr of Shell Oil Company, for encouraging advice, to many of the engineers of Shell Development Company for their assistance, and to its management for the permission to publish this work.

BIBLIOGRAPHY

1 "Essai Sur la Théorie des Eaux Courantes," by J. Boussinesq, Mémoires de l'Academie des Sciences, Paris, France, vol. 23, 1877.

2 "Effect of Pulsation on Flow of Gases," by H. Judd and D. B. Pheley, Ohio State University Engineering Experiment Station, Bulletin No. 24, 1923; see also Trans. ASME, vol. 44, 1921, p. 853.

3 "The Occurrence and Elimination of Surge or Oscillating Pressures, etc.," by H. Diederichs and W. D. Posneroy, Trans. ASME, vol. 51, 1929, Paper Pet—51-2.

4 "Pulsations as Encountered in Flowing Gases," by L. F. Scheel, *Western Gas*, vol. 6, 1930, p. 46.

5 "Relation Between Heat Transfer and Fluid Friction," by E. V. Murphree, *Industrial and Engineering Chemistry*, vol. 24, 1932, p. 726.

6 "An Investigation of Pulsating Flow and Pulsation Eliminators for Orifice Meters," by J. H. Eagle and W. A. Daberko, BS thesis, Ohio State University, 1937.

7 "Sound Waves in a Moving Medium," by J. D. Trimmer, *Journal of the Acoustical Society of America*, vol. 9, 1937, p. 102.

8 "Durchflussmessung bei pulsierender Stroemung," by F. Herning and C. Schmid, *Zeitschrift des Vereines deutscher Ingenieure*, vol. 82, 1938, p. 1107.

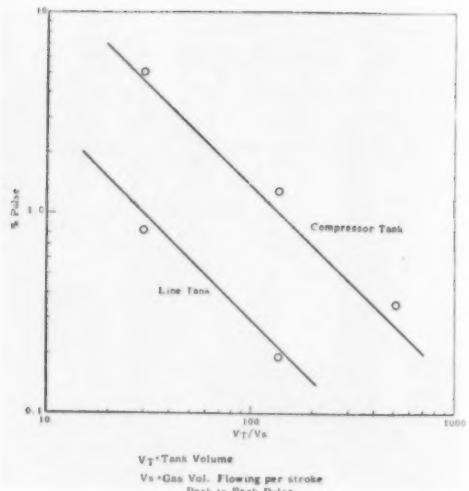

FIG. 16 RESULTS OF TESTS WITH π-FILTER IN DISCHARGE LINE

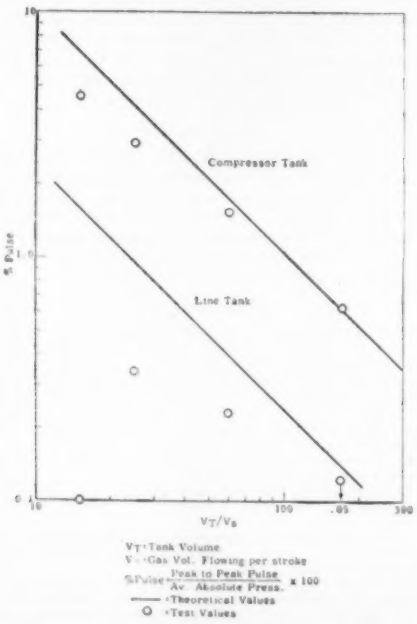

FIG. 17 RESULTS OF TESTS WITH π-FILTER IN SUCTION LINE

9 "Acoustic Vibrations and Internal Combustion Engine Performance," by P. M. Morse, R. H. Boden, and H. Schecter, *Journal of Applied Physics*, vol. 9, 1938, p. 16.

10 "The Effect of Pulsations on Orifice Meters," by S. R. Beitler, Trans. ASME, vol. 61, 1939, p. 309.

11 "Ueber Resonanzschwingungen in den Ansaug- und Auspuff-Leitungen, etc.," by O. Lutz, Parts 1 and 2, *Luftfahrtforschung*, vol. 16, 1939, pp. 139 and 384.

12 "Resonance Vibrations in Intake and Exhaust Pipes of In-Line Engines," by O. Lutz, Part 3, National Advisory Committee for Aeronautics, Technical Memorandum 957, 1940.

13 "Elements of Acoustical Engineering," by H. F. Olson, D. Van Nostrand Company, Inc., New York, N. Y., second edition, 1947.

14 "The Dampening of Large Amplitude Vibrations of a Fluid in a Pipe," by R. C. Binder, *Journal of the Acoustical Society of America*, vol. 15, 1943, p. 41.

15 "Theoretical and Experimental Investigation of Acoustical Filters," by J. E. Moore, MS thesis, University of California, 1943.

16 "Dynamical Analogies," by H. F. Olson, D. Van Nostrand Company, Inc., New York, N. Y., 1943.

17 "Vibration in Compressor Plant Piping," M. L. Arnold, *National Petroleum News*, vol. 37, 1945, p. R138.

18 "Vibration Absorber," by H. J. Rudolph, U. S. Patent 2,429,-297, 1945.

19 "A Study of Surging in Fan or Compressor Systems," by R. C. Binder, *Journal of The Franklin Institute*, vol. 241, 1946, p. 125.

20 "Control of Pulsation Frequency in a Duct System," by W. R. Heath and W. R. Elliott, *Journal of Applied Mechanics*, Trans. ASME, vol. 68, 1946, p. A-291.

21 "Pulsation and Its Effect on Flow Meters," by E. J. Lindahl, Trans. ASME, vol. 68, 1946, p. 883.

22 "Pulsation Elimination in Gas Lines, Etc.," by F. M. Stephens, U. S. Patents, 2,405,100, 1946; 2,437,446, 1948, and 2,474,555, 1949.

23 "Pulsation Phenomena in Gas Compression Systems," by I. C. Bechtold, *Engineering and Science Monthly*, October, 1947, p. 6.

24 "An Introduction to an Analysis of Gas Vibrations in Engine Manifolds," by R. C. Binder and A. S. Hall, Jr., *Journal of Applied Mechanics*, Trans. ASME, vol. 69, 1947, p. A-183.

25 "Determination of Natural Frequencies of Piping Systems by an Electrical Analog," by E. F. Murphy, PhD thesis, Illinois Institute of Technology, Chicago, Ill., June 1948.

26 "Pulsation Absorber," by J. A. Pellettere, U.S. Patent 2,448,-118, 1948.

27 "Pressure Surges and Vibration in Reciprocating-Pump Piping," by J. W. Squire, Trans. ASME, vol. 71, 1949, pp. 317–324.

28 "Mechanical Vibration of Piping Induced by Gas-Pressure Pulsations," by R. C. Baird and I. C. Bechtold, Trans. ASME, vol. 71, 1949, pp. 989–995.

29 "Natural Frequencies of Compressor and Engine Manifolds," by E. F. Murphy, *Gas*, vol. 25, March, 1949, p. 50.

30 "Elimination of Pulsation in Gas Lines," by F. M. Stephens, U.S. Patent 2,474,553, 1949.

31 "The Theory of Spring-Loaded Valves for Reciprocating Compressors," by M. Costagliola, *Journal of Applied Mechanics*, Trans. ASME, vol. 72, 1950, p. 415.

32 "Specific Heat Ratio in Compression Calculations," by W. C. Edmister, *Petroleum Engineer*, vol. 22, 1950, p. C-13.

33 "A Direct Recording Technique for Pressure Cycles in High-Pressure Reciprocating Equipment," by R. A. Strub, ASME Paper 50—IIRD-2, 1950 (not published).

NOMENCLATURE

The following nomenclature is used in the Appendix:

a = speed of sound = $\sqrt{\gamma \frac{p}{\rho}}$ fps

a_m = Fourier coefficient

$a_m' = 2\pi a_m / I$

b_m = Fourier coefficient

$b_m' = 2\pi b_m / I$

e = voltage (= pressure)

e_{avg} = average voltage

= compressor frequency = $\frac{\omega}{2\pi} = 1/T$, cycles per sec (cps)

h = connecting-rod length, ft

i = current (= mean flow rate)

i_{avg} = average current
$j = \sqrt{-1}$
l = pipe length, ft
m = harmonic of ω
n = polytropic exponent of gas during compression
n_1 = polytropic exponent of gas in V_e during expansion
$r_e = V_e/V_d$
$r_p = P_d/P_s$
r_t = ratio of valve-open-time to period T
s = length of piston stroke, ft
t = time variable
t_0 = time at which discharge valve closes
t_1 = time at which discharge valve opens
x = piston position from TDC when discharge valve opens
x_1 = piston position from TDC when suction valve opens
A = inside cross-sectional area of pipe, sq ft
B = a function
C = electrical capacity
C_e = variable-condenser capacity
C_m = complex coefficient
D = a function
F = mass flow rate
I = maximum value of i
$K_a = 4(\omega/\omega_c)^2$
$K_c = (2\pi/\gamma)(V_T/V_s)$
L = electrical inductance
= length variable
N = crank rpm for single-acting piston; 2 × crank rpm for double-acting piston
P = absolute pressure, psf
P_d = discharge pressure, psf
P_s = suction pressure, psf
Q = mass of gas delivered per stroke
R = resistance
S = piston area, sq ft
T = period of compressor cycle = $1/f = 2\pi/\omega$, sec
V = volume, cu ft
V_c = clearance volume, cu ft
V_d = piston displacement, cu ft
V_s = volume of gas discharged per stroke, cu ft
V_t = volume of each tank of π-type filter, cu ft
V_T = tank volume, cu ft
W = force variable
Z = impedance
γ = ratio of specific heats
ϵ = base of natural logarithms
θ = crank angle
ρ = gas density, (lb sec²/ft⁴)
Φ = angle of connecting rod with piston rod
ω = angular compressor frequency = $2\pi f = 2\pi/T$
ω_c = filter cutoff frequency

Appendix

Theoretical Computations

Relations Between Analogous Electrical and Acoustical Terms.[11] The analogy is based upon the assumption that both systems, the electrical as well as the acoustical, can be described by linear differential equations between, on the one hand, voltage and current, and, on the other hand, pressure and mass flow.[12] The coefficients of these differential equations are derived from the physical characteristics of the components of the electric circuit or piping system. Fig. 1 shows corresponding electrical and acoustical units and the relations between them.

General Differential Equations of a Typical Simple System. In order to demonstrate the difficulties encountered in a rigorous solution, we shall set up the equations for a combination of the simple tank-line-valve system in Fig. 2(*b*), and a single-acting compressor Fig. 2(*c*). The resultant system is again shown in Fig. 3(*a*).

It will be apparent that each cycle can be divided into two distinct periods, i.e., the time that the discharge valve is open and that time during which it is closed, assuming, of course, that pulsations are not so violent that valve flutter occurs.

Then by simple use of Kirchhoff's law, for $t_0 \leqslant t \leqslant t_1$

$$LC\frac{d^2e}{dt^2} + RC\frac{de}{dt} + e = 0 \quad \ldots\ldots\ldots\ldots [1]$$

while for $t_1 \leqslant t \leqslant (t_0 + T)$

$$e = e_s = \frac{1}{C_e}\int_{t_1}^{t} i dt \quad \ldots\ldots\ldots\ldots\ldots [2]$$

and

$$LC\frac{d^2e}{dt^2} + RC\frac{de}{dt} + e = L\frac{di}{dt} + Ri \quad \ldots\ldots [3]$$

It will be noted that C_e is not constant but varies directly as the cylinder volume so that it approaches a sine function. Thus by differentiating Equation [2] and substituting into Equation [3] we obtain a somewhat cumbersome linear differential equation containing the variable coefficient C_e, and its first two time derivatives. It is somewhat similar to the well-known Mathieu equation.

The boundary conditions for these equations result from the fact that Equations [1] and [3] are equivalent at $t = t_0$, t_1, and $t_0 + T$, and that at $t = t_1$, $e/C_e = Q$.

It is apparent that a general solution for such a set of equations is, at best, difficult. Approximate solutions have the disadvantage of having to be repeated for each change in any of the circuit constants. Further work may be undertaken to study such analytical methods more thoroughly, but this paper is confined to the approximation to be described.

Fourier Analysis of Assumed Flow Rate at Valves. To simplify the foregoing analysis it is assumed that as long as a sufficiently large tank (capacity) is placed close to the compressor, the current flow through the valve will be nearly proportional to the piston velocity, which, in turn, is assumed to be sinusoidal for this analysis.[13]

Fig. 4(*a*) shows typical shapes of this assumed flow for both suction and discharge valve. If we let the time $t = 0$ at the beginning of one full sine wave, i.e., at BDC for the discharge side, or TDC for the suction side, these curves can be defined by the following equations

$$0 \leqslant t \leqslant t_1 \qquad i = 0$$
$$t_1 \leqslant t \leqslant T/2 \qquad i = I \sin\frac{2\pi}{T}t$$
$$T/2 \leqslant t \leqslant T \qquad i = 0$$

It is assumed here, as well as in Fig. 4, that the discharge valve closes at TDC while the suction valve closes at BDC. Now let

$$i = \sum_{m=1}^{\infty} a_m \sin 2\pi m\frac{t}{T} + \sum_{m=0}^{\infty} b_m \cos 2\pi m\frac{t}{T}$$

[11] Refer to Olson (13) and (16).
[12] Some authors prefer volume flow.
[13] It can be shown that for this purpose the assumption is good, while for calculation of valve-open-time (r_t), the deviation from a true sine curve must be taken into account (see section, "Determination of Valve-Open-Time," of this Appendix).

Methods for finding the coefficients a_m and b_m are well known[14] and, after substitution and integration, and letting

$$\frac{\frac{T}{2} - t_1}{T} = r_t$$

we find, for the first six harmonics

m	$a_m' = 2\pi a_m/I$	$b_m' = 2\pi b_m/I$
0		$1 + \cos 2\pi r_t$
1	$\pi - 2\pi r_t + 1/2 \sin 4\pi r_t$	$(\cos 4\pi r_t - 1)/2$
2	$(\sin 6\pi r_t - 3 \sin 2\pi r_t)/3$	$(\cos 6\pi r_t - 3 \cos 2\pi r_t - 2)/3$
3	$(2 \sin 8\pi r_t - 4 \sin 4\pi r_t)/8$	$(2 \cos 8\pi r_t - 4 \cos 4\pi r_t + 2)/8$
4	$(3 \sin 10\pi r_t - 5 \sin 6\pi r_t)/15$	$(3 \cos 10\pi r_t - 5 \cos 6\pi r_t - 2)/15$
5	$(4 \sin 12\pi r_t - 6 \sin 8\pi r_t)/24$	$(4 \cos 12\pi r_t - 6 \cos 8\pi r_t + 2)/24$
6	$(5 \sin 14\pi r_t - 7 \sin 10\pi r_t)/35$	$(5 \cos 14\pi r_t - 7 \cos 10\pi r_t - 2)/35$

These coefficients can be computed readily for any value of r_t.

It is advantageous to convert the Fourier series into a vector (or complex) series of the form

$$i = \sum_{m=-\infty}^{\infty} C_m e^{jm\omega t}$$

The coefficients C_m become[15]

$$C_m = 1/2(b_m - ja_m)$$
$$C_0 = b_0$$
$$C_{-m} = 1/2(b_m + ja_m)$$

Application to Single-Tank System, see Fig. 3(b). It is assumed that the tank volume V_T is large compared to the volume of gas discharged per stroke V_s so that as a first approximation any pipe (inertance) or tank (capacitance) beyond the first tank has no effect on the pulsation in that tank, and we can represent the entire remainder of the piping system by a resistance alone.

It will be useful to define the dimensionless factor

$$K_V = \omega CR = \omega \frac{V_T}{a^2} \frac{e_{avg}}{i_{avg}} = \omega \frac{V_T \rho}{\gamma e_{avg}} \frac{2\pi e_{avg}}{\omega \rho V_s} = \frac{2\pi}{\gamma} \frac{V_T}{V_s}$$

since

$$V_s = \frac{i_{avg}}{\rho} T = \frac{i_{avg}}{\rho} \frac{2\pi}{\omega} \quad \text{and} \quad a^2 = \frac{e_{avg}\gamma}{\rho}$$

Thus K_V is determined primarily by the relative tank size.

As seen from the compressor, the impedance of the circuit is

$$Z = \frac{1}{jm\omega C + 1/R} = R \frac{1}{jm\omega CR + 1} = R \frac{1}{jmK_V + 1}$$
$$= R \frac{1 - jmK_V}{1 + m^2K_V^2}$$

and the voltage (or pressure)

$$e = iZ = R \sum_{m=-\infty}^{\infty} \frac{1 - jmK_V}{1 + m^2K_V^2} C_m e^{-jm\omega t}$$

By substitution and expansion, this becomes

$$\frac{e}{e_{avg}} - 1 = \frac{1}{1 + \cos 2\pi r_t} \sum_{m=1}^{\infty} \frac{1}{1 + m^2K_V^2}$$
$$[(b_m' - mK_V a_m') \cos m\omega t + (a_m' + mK_V b_m') \sin m\omega t]$$

It was assumed that $K_V \gg 1$, so that we can approximate

$$\frac{e}{e_{avg}} - 1 \approx \frac{1}{K_V(1 + \cos 2\pi r_t)} \sum_{m=1}^{\infty} (b_m'' \sin m\omega t - a_m'' \cos m\omega t)/m$$

This equation gives the complete curve for the pressure pulse. Since only peak-to-peak amplitudes are of interest, these were found for various values of r_t and K_V, and are shown plotted in Fig. 8.

Application to π-Filter System, see Fig. 3(b). The development of the equations for this system is very similar to that for the single tank, except that the impedance Z is more complicated and in that we are interested in two pulses, namely, that in the tank nearest to the compressor e, and that in the tank near the piping system e_1. The assumptions made are the same as in the foregoing.

In addition to the nondimensional K_V, which was defined previously and refers here to the volume V_t of one of the tanks, we also define

$$K_c = \omega^2 CL = 4\left(\frac{\omega}{\omega_c}\right)^2$$

where ω_c = cutoff frequency of the π-filter, i.e., the frequency beyond which the filter does not conduct. This frequency always should be taken somewhat below the minimum frequency of the compressor. For that reason, all of the present computations have been based upon the fixed ratio

$$\omega/\omega_c = 1/0.9$$

or

$$K_c = 4.94$$

The impedance

$$Z = R \frac{1 + jB}{D}$$

where

$$B = m\left[\frac{K_c}{K_V}(1 - m^2K_c) - K_V(1 - m^2K_c)(2 - m^2K_c)\right]$$
$$D = (1 - m^2K_c)^2 + m^2K_V^2(2 - m^2K_c)^2$$

By substituting this into the equation $e = iZ$, rearranging, and again letting $K_V \gg 1$ we obtain the approximate solution

$$\frac{e}{e_{avg}} - 1 \approx \frac{1}{K_V(1 + \cos 2\pi r_t)} \sum_{m=1}^{\infty} \frac{1 - m^2K_c}{m(2 - m^2K_c)}$$
$$(b_m' \sin m\omega t - a_m' \cos m\omega t)$$

as well as

$$\frac{e_1}{e_{avg}} - 1 \approx \left(\frac{e}{e_{avg}} - 1\right) \frac{1}{1 - m^2K_c}$$

A numerical analysis, similar to the one for the single tank, then produces the graphs in Fig. 9.

[14] See, for instance, "Mathematical Methods in Engineering," by T. von Kármán and M. A. Biot, McGraw Hill Book Company, New York, N. Y., p. 326 ff.

[15] Ibid, p. 384.

Determination of Valve-Open-Time. If it is assumed that the gas in the cylinder during compression follows the perfect-gas laws, and that the valve-open-times are not affected by pulsations:

for discharge 3 $P_d(V_d + V_c)^n = P_d(xS + V_c)^n$

and for suction $P_s V_c^{n_1} = P_s(x_1 S + V_c)^{n_1}$

These equations become

$$\left(\frac{1}{r_p}\right)^{1/n} = \frac{x/s + r_c}{1 + r_c} \quad \text{for discharge}$$

and

$$\left(\frac{1}{r_p}\right)^{1/n_1} = \frac{r_c}{x_1/s + r_c} \quad \text{for suction}$$

The solution of these equations for x/s and x_1/s is presented graphically in Figs. 5, 6(*a*), and 6(*b*). Note that x and x_1 are both measured from top dead-center position.

Considering now the geometry of the piston and crank arrangement, Fig. 4(*b*), one can readily convert the piston position x into crank angle θ; thus

$$x = \left(\frac{s}{2} + h\right) - \frac{s}{2}\cos\theta - h\cos\Phi$$

or

$$x/s = 1/2(1 - \cos\theta) + \frac{h}{s}(1 - \cos\Phi)$$

where

$$\sin\Phi = \frac{s}{2h}\sin\theta$$

Also note that the relative valve-open-times are

$$r_t = \frac{\theta}{2\pi}$$

for the discharge valve, and

$$r_t = 0.5 - \frac{\theta}{2\pi}$$

for the suction valve.

For convenience the equation connecting x/s and x_1/s with r_t and $(0.5 - r_t)$, respectively, is plotted in Fig. 7.

Hence, between Figs. 5, 6(*a*), 6(*b*), and 7, the valve-open-times can be computed readily. Notes on the accuracy with which certain of the characteristics have to be known appear in the section of the paper, Present Solutions.

Discussion

M. L. Arnold.[16] The bad effects of pulsative flow on compressor piping are readily discernible and command attention. Most previous authors have discussed this phase of the problem.[17] The effects upon the compressor itself are less apparent, particularly in the absence of suitable indicating devices. The authors are to be commended upon directing our attention to this phase of the problem and upon the original method they have developed for determining pulse amplitude.

It may be of interest to compare the results obtained by Chilton and Handley's method with those obtained by Thornton.[18] In his development Thornton considered a crank-driven plunger operating in one end of a closed pipe. A surge tank of volume V was installed at the plunger end. The distance from the tank to the closed end was L. His equation describing the behavior of this system is somewhat complex. However, he presents a simple equation for the special case where the length L is a multiple of the length of the wave generated by the action of the plunger. For this system, the capacity of the surge chamber V_t required to prevent the pressure rising above a specified value P, is given by the following equation

$$V = \frac{Kv}{2P}$$

where K is bulk modulus of elasticity of the medium; v is displacement of plunger.

For any particular problem a plunger could be selected such that Thornton's v would be equal to Chilton and Handley's V_s. The following equivalences can also be stated:

$V = V_t$
P = peak to peak pulse = ΔP
$K = \gamma P$ for an adiabatic process (γ = ratio of specific heats)

If it is assumed, that in the expression for K, P is equal to the average absolute pressure, P_{avg}, Thornton's equation can be rewritten as follows

$$V_t = \frac{\gamma P_{avg} V_s}{2\Delta P}$$

By definition

$$\text{per cent pulse} = \frac{\Delta P}{P_{avg}} \times 100$$

hence,

$$\frac{P_{avg}}{\Delta P} = \frac{100}{\text{per cent pulse}}$$

Making this substitution and rearranging

$$\frac{V_t}{V_s} = \frac{\gamma}{2} \times \frac{100}{\text{per cent pulse}}$$

If it is assumed that the authors' laboratory compressor was operating on air, this equation fits the test results of Fig. 13 nicely. It is in fair agreement with the high per cent pulse data in Fig. 14, but fails to conform with the data in the low per cent pulse region.

Now a couple of questions for the authors:

1 In comparing Figs. 13 and 14 with Figs. 16 and 17, it appears that the compressor tank of the pi-filter is just as effective as a single tank in limiting the per cent pulse in the discharge line. However, the figures indicate that to maintain a given per cent pulse in the suction line, the compressor tank of the pi-filter must have a considerably larger V_t/V_s ratio than would be required for a single tank. Would the authors care to comment on this?

2 Few of us, probably, have had the opportunity of correlating compressor operating and maintenance problems against per cent pulse in compressor piping. Therefore it would be of interest to learn the nature of the observations which led to the suggestion that 2 per cent pulse is on the average a satisfactory value.

[16] Chief Engineer, Gas Operations, Richfield Oil Corporation, Los Angeles, Calif. Mem. ASME.

[17] "Experiences in Dampening Pulsations in Compressor Piping Systems," by M. L. Arnold, *The Petroleum Engineer*, vol. 23, No. 9, August, 1951, pp. D-14–D-24.

[18] "Mechanics Applied to Vibrations and Balancing," by D. L. Thornton, John Wiley & Sons, Inc., New York, N. Y., first edition, 1940, article 82, p. 282.

R. C. Baird.[19] The corporation represented by the writer has pioneered the use of filter-type pulsation dampeners in industry from the particular standpoint of reducing pipe breakage due to pulsative flow in high-pressure lines associated with reciprocating compressors. The application of pulsation dampeners to the pipe-vibration problem has been eminently successful, especially so in view of the fact that compressor horsepower losses resulting from the extremely small per centwise pressure drop of filter-type pulsation dampeners are far outweighed by insurance afforded from costly pipe and vessel breakage.[20]

In view of the experience gained from actual field testing of filter-type pulsation-dampener installations throughout the gamut of operating conditions, coupled with practical knowledge regarding the effects on pulsative flow caused by suction and discharge bottles or tanks, it is believed that a certain amount of clarification of the recommendations contained in the paper might be in order. Specifically, it is felt that recommendation 3 needs some modification. Experimental field data obtained before and after the installation of properly designed filter-type dampeners show that such dampeners invariably will reduce pulses in compressor nozzles. Therefore it is believed that the recommendation as stated in the paper is somewhat misleading in that it gives the impression that filter-type dampeners will not themselves cause an appreciable reduction in pulsation at the compressor. This is, of course, not true, and the writer is sure that such inference was not the intent of the authors. In addition, it is believed that the comparison of the pulse-removing efficiencies, in so far as the compressor is concerned, between a tank having a volume double that of the inlet volume of a corresponding pi-type filter is not scientifically legitimate.

If orifice metering runs can be construed to be parts of gas-compressor systems, it might be in order to mention the fact that filter-type pulsation dampeners are of considerable utility in reducing orifice metering errors by virtue of the high efficiency (particularly in comparison with a tank) with which they can be used to remove pulses from a line. The exact way in which pulsative flow affects the differential reading in an orifice meter has not been determined completely as yet, but it has been found in the majority of cases that the reduction in pulsative flow will result in more reliable metering, the increased accuracy being somewhat in proportion to the degree of pulse removal.

Issue is taken with recommendation 7 wherein it is stated that elbows and bends in a pipe do not form reflection points for pressure pulses. This may well be in a practical sense; however, it can be demonstrated that some reflection of acoustical energy will occur whenever the change of direction in propagation of the acoustical wave is produced. This results from the fact that the energy contained in acoustical pressure waves is vectorial in nature and any forced alteration of the flow vector amounts to an impedance mismatch with attendant standing-wave resonance and so forth, even though the cross-sectional areas of the conduit through which the pulse energy is flowing remain constant. However, it would appear from the authors' experimental work that this effect is of negligible importance in typical piping elbows and bends and in most cases can be ignored.

In the design of filter-type pulsation dampeners we have long been aware that in addition to acoustical relationships between inertance and capacitance, the manner in which these acoustical elements are oriented with respect to each other is of considerable importance. Furthermore, the "pureness" of capacity and inertance is of importance in determining the acoustical efficiency with which pressure waves are filtered out. In some respects an acoustical filter reacts similarly to its mechanical counterpart and, since a mechanical filter requires that its components be related vectorially to each other, so also is a similar relationship required of the elements in the acoustical filter. It has been found that even though the capacitance-inertance relationship of two physically dissimilar pulsation dampeners is the same, thus giving the same theoretical attenuation curve, experimental results often disclose considerable variance in this respect. In another regard, extreme care must be used in comparing filter and/or tank attenuation efficiencies. This is of fundamental nature and concerns the relationship of source and load impedances to the impedances at inlet and outlet of the filter or tank. To compare attenuation efficiencies, therefore, the degree of impedance match between the filters (or tanks) with the inlet (source) and outlet (load) piping must be known. The experimental work of the authors involved a filter-type pulsation dampener having apparently an arbitrary physical relationship between the chambers and interconnecting tube. It is believed that accordingly the data obtained are not necessarily representative of the "average" filter-type dampener which would be used in practice for many different kinds of reciprocating compressors.

With reference to the section, Effects on Compressor Performance, it is hoped that the authors' research program will be continued to the extent of correlating compressor-horsepower cards with pulsative flow in suction and discharge nozzles. Such correlation, especially if it can be made quantitative, would be of great use. It is believed that electronic devices are now available which will allow very accurate information to be obtained for such a study.

E. F. Murphy.[21, 22] The following discussion is based on previous experience in the compressor field and on a doctoral thesis pertaining to natural frequencies of manifolds and piping systems and thus to pulsations in such systems. It has no relation to the writer's present position, and the views presented are solely his own.

The relative importance of pulsations varies with circumstances. The authors' limit of 2 per cent of the mean pressure seems safe and practical, even though it is obviously far beyond the usual assumption of small pressure variation used in deriving the usual equations in acoustics. The writer's experience supports the statement by the authors that the pulsation phenomena discussed can be treated by the laws of acoustics. Close to the compressor there are undoubtedly sharp pulses, but their effects can be calculated fairly satisfactorily by summation of sinusoidal waves. The relative importance of removing pulsations from the line or at the compressor will depend on whether difficulties have developed due to piping vibration, noise, and metering errors, or due to overloading or "hunting" of the compressor, deviation from design performance, and valve breakage. Similarly, the choice between adding a commercial or a pi-shaped filter, adding or enlarging a single tank or header, or carefully designing the entire piping system to avoid resonance with predictable natural frequencies, will depend upon whether trouble occurs in an existing plant with specified space limitations or whether the analyst can participate in the original design. Addition of an orifice, known to be effective in many existing installations, will reduce pulsations, typically not only because it wastes energy but to some extent because it adds inductive impedance to the line, changes the ratio of inductance to capacitance, hence somewhat changes the natural frequency and introduces a discontinuity into the line.

[19] Principal Research Engineer, The Fluor Corporation, Ltd., Los Angeles, Calif. Mem. ASME.

[20] "Experiences in Dampening Pulsations in Compressor Piping Systems," by M. L. Arnold, *Pipeline News*, September, 1951, p. 35.

[21] Assistant Director for Research, Prosthetic and Sensory Aids Service, Veterans Administration, New York, N. Y. Jun. ASME.

[22] Reviewed in the Veterans Administration and published with the approval of the Chief Medical Director.

A single-cylinder compressor with simple piping is likely to cause resonance with the fundamental of the pipe, yet a complex multicylinder compressor with header and long piping may exhibit resonance between the vector sum of a high harmonic of the wave from the individual cylinders operating in parallel and a complex mode of vibration of the entire piping system. The possible solutions for a compressor driven by an electric motor also may differ from those adequate for a compressor driven by a variable-speed gas engine.

As in torsional vibration, the first effort was to predict natural frequency of the system. An electrical analog, constructed in the laboratory or perhaps set up on a rented network calculator, may be suitable for more complicated systems than can be solved easily by mathematical or graphical methods. Several texts on torsional vibration explain the vector addition of harmonics of the exciting waves from the several cylinders. These vector additions indicate, at least qualitatively, whether several cylinders will reinforce. In torsional vibration it has long been possible to compare the energy absorbed by hysteresis of the crankshaft and by other damping with the energy added by a given harmonic of the energy waves applied to the crankshaft. Thus the amplitude of vibration at each point of resonance, between the various harmonics and each of the several modes, could be predicted. Now an analogous process could be applied to pulsations in compressor and engine manifolds, taking advantage of the contributions by the authors and by their predecessors listed in their bibliography. A co-operative effort by compressor manufacturers, oil and gas companies, designers of plants, trade associations, and interested universities and research foundations would cost very little for each participant, yet insure against substantial expenses in correcting the serious difficulties which the authors describe.

Authors' Closure

The authors have appreciated the interest expressed in both written and verbal form and particularly wish to thank the discussers for their comments.

The answer to Mr. Arnold's first question may be found in the wave-shape difference between suction and discharge side and their relative effect on single tanks and π-type dampeners. The discharge wave which contains a large portion of the higher harmonics is essentially damped by the first tank of the π-type filter as if this were a single-tank system, while this is not true for the simpler suction wave. This can be seen also from the equations describing the two systems in the Appendix.

As pointed out in the paper, the figure of 2 per cent for a safe pulse amplitude is based on a few actual measurements on installations judged "satisfactory" or "unsatisfactory" by their operating personnel, and is a figure which, it is felt, should be substantiated by industry-wide surveys. Such a survey would surely show a dependence of the allowable pulse amplitude on the average pressure as indicated in recommendation 2.

Mr. Baird's objections to the authors' preference of the single tank over the π-type filter for the average compressor installations appear to be based on his experience with the firm that pioneered the latter type of dampener in industry. As the authors have pointed out, it is, in their opinion, one of the few filters designed on an acoustically correct basis, and in cases where line pulsations are more critical than pulsations at the compressor, it is often preferable even to the simple tank.

The comparison in recommendation 3 is based on the economic consideration that the total volume of a dampener installation will essentially determine its cost. Due to the simplicity of construction of a single tank compared to a filter, such a comparison is more than fair to the filter, and a more exact economic evaluation will doubtlessly favor the single tank more than the remark in recommendation 3.

Mr. Baird questions some of the authors' experiments on filters because of neglect of "impedance matching" between filter and compressor on the one hand, and load on the other. The purpose of impedance matching is to transmit a maximum of power in the circuit. Both the single tank and the π-type filter in the sizes in which they are of practical interest have small resistive impedance, and thus do not seriously interfere with the transmission of the steady pressure (d-c component) of flow. Since it is the purpose of the tank or filter to disrupt the transmission of the pulsation (a-c) component, a mismatch of impedance due to reactance is not only desirable, but is the function of such a filter. The close agreement between theory and experiments makes it clear that the experiments are in fact representative and the theory applicable within the stated limits.

Dr. E. F. Murphy's comment on the inertance of orifices and valves is well taken, and the interested reader may be referred to an article by Ingard and Labate.[13]

The authors had hoped to extend Dr. Murphy's excellent work with the electrical analog by incorporation of the compressor analog. However, technical difficulties described in the paper have made such an attempt prohibitive to date.

---

[13] "Acoustic Circulation Effects and the Nonlinear Impedance of Orifices," by U. Ingard and S. Labate, *Journal of the Acoustical Society of America*, vol. 22, 1950, p. 211.

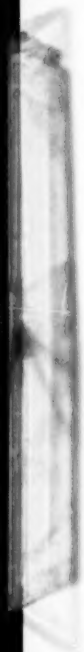

Progress Report on the Study of Supercompressibility Factors for Natural Gases

By R. H. ZIMMERMAN[1] and S. R. BEITLER,[2] COLUMBUS, OHIO

A report is given on the present status of an evaluation of supercompressibility factors of natural gases. The aim of the research work is an attempt to establish an accurate method for the prediction of these factors within the pressure range 0 to 4000 psi and in terms of gas properties generally known or conveniently determined. The working method used to predict supercompressibility factors is based on the method proposed by Dunkle in 1944. Results of the method are compared with supercompressibility factors experimentally determined on the Burnett deviation apparatus.

Nomenclature

The following nomenclature is used in the paper:

F_{pv} = supercompressibility factor of gas mixture, based on reference pressure of 14.4 psia

G = specific gravity of gas mixture, referred to molecular weight of 28.97

G_h = specific gravity of hydrocarbon fractions, referred to molecular weight of 28.97

G_c = specific gravity of carbon dioxide, 1.519 when referred to molecular weight of 28.97

G_n = specific gravity of nitrogen, 0.967 when referred to molecular weight of 28.97

H = gross heating value of gas mixture, dry basis, Btu per cubic foot at 60 F and 14.73 psia

H_h = gross heating value of hydrocarbon fractions, dry basis, Btu per cubic foot at 60 F and 14.73 psia

P = gage pressure of gas mixture, pounds per square inch

P_R = reduced gage pressure of gas mixture, P/π

T = absolute temperature of gas mixture, degrees Rankine.

T_R = reduced absolute temperature of gas mixture, T/θ.

X_h, X_c, X_n = mol per cent hydrocarbon fractions, mol per cent carbon dioxide, and mol per cent nitrogen, respectively, divided by 100

Z = compressibility factor of gas mixture, based on reference pressure of 14.4 psia

θ = pseudo-critical absolute temperature of gas mixture, degrees Rankine

θ_h, θ_c, θ_n = pseudocritical absolute temperatures of hydrocarbon fractions, carbon dioxide, and nitrogen, respectively, degrees Rankine

π = pseudocritical absolute pressure of gas mixture, pounds per square inch

π_h, π_c, π_n = pseudocritical absolute pressure of hydrocarbon fractions, carbon dioxide, and nitrogen, respectively, pounds per square inch

a, b, d, e
g, k, α, β = constants

Introduction

The quantity of natural gas which is produced, transported, or sold is usually measured in terms of cubic feet at some standard pressure and temperature known as the base pressure and temperature. In many cases the measurement of the gas is made at conditions which differ from the base conditions. The value of the volume at measured conditions is normally converted to the volume at base conditions by means of the perfect-gas laws.

It has long been realized that natural gas is not a perfect gas, and as a result, factors must be introduced to correct the volumetric calculations for this deviation. These factors have been called "compressibility factors." Present practice as recommended in Report Number (2) of The Orifice Meter Committee of the American Gas Association is to apply a factor determined by test from the gas being measured. This method is unsatisfactory unless the gas being measured has approximately the same composition at all times, since otherwise, it is necessary to take samples of the gas at various times and then test these samples on the apparatus available for measuring the factor. This test is time-consuming and expensive if frequently required and is not commercially practical especially for relatively small measurements. Realizing these problems, measurement engineers have been working in an attempt to correlate this factor with commonly measured and generally known properties of the gas, e.g., specific gravity and heating value, so that the factor can be determined continuously without too great cost.

Several methods are in use at present for predicting these factors. The methods are considered satisfactory for natural-gas mixtures when the pressure is less than 500 psig, and are fairly accurate for pressures slightly higher than this. However, for high pressures often met in present practice, tests have indicated that available methods do not give results which check actual tests within the range of allowable measurement accuracy.

A research program was established to determine the possibility of developing a method giving good agreement between predicted and measured values over the entire range of conditions encountered in normal gas measurements. The study is to cover the pressure range—zero to 4000 psi.

The program of research was to determine from available data a method of predicting the factors, and then check these factors computed by this method against measured values of the factors for the same gas.

This paper reports on the progress made to date on this program. Deviation factors are presented as the reciprocal of the square root of the compressibility factor and are referred to as the "supercompressibility factor, F_{pv}"

$$F_{pv} = \sqrt{1/Z}$$

[1] Assistant Professor of Mechanical Engineering, The Ohio State University. Jun. ASME.

[2] Professor of Hydraulic Engineering, The Ohio State University. Fellow ASME.

Contributed by the Fluid Meters Research Committee and presented at the Annual Meeting, Atlantic City, N. J., November 25–30, 1951, of The American Society of Mechanical Engineers.

Note: Statements and opinions advanced in papers are to be understood as individual expressions of their authors and not those of the Society. Manuscript received at ASME Headquarters, November 26, 1951. Paper No. 51—A-153.

where

$$Z = pv/RT$$

Numerical values of F_p, are evaluated on the basis of being equal to unity at a base pressure of 14.4 psia.

Test Program

The complete test program will determine the supercompressibility factors for pressures varying from zero to approximately 4000 psig for natural-gas mixtures having various specific gravities, fractional analyses, and temperatures. Supercompressibility factors are being determined by use of the Burnett-type apparatus, following standard procedure (1, 2).[2] In addition, specific gravity, heating value, and the fractional analysis are being determined for each gas sample.

Three hundred and ninety-three tests have been reported to date. Most of the samples on which these tests were run were taken from fields in Texas; a few samples were taken from fields in other states. The pressure and temperature ranges covered during these tests are shown in Table 1. The maximum test pressure was below 1100 psig for roughly 95 per cent of all tests. Test temperatures cover a fairly wide range, but over 90 per cent of the tests were made in the range 50 F to 120 F. Many test runs were duplicated to insure against possible error in experimental technique.

TABLE 1 BREAKDOWN OF TEST PRESSURES AND TEMPERATURES

Max test pressure, psi, in range	No. tests at indicated press. range	Test temp, deg F	No. tests at ind. temp	Test temp, deg F	No. tests at ind. temp
below 600	9	20	1	80	76
600–700	41	25	22	100	83
700–800	116	30	2	100	34
800–900	104	34	2	110	28
900–1000	58	40	11	120	30
1000–1100	42	45	2	160	1
1100–1200	2	50	20	180	2
2500–2600	2	60	46	200	2
2700–2900	3	70	52		
3000–3100	16				

Character of Gas Samples

The principal constituents to be considered in a study of supercompressibility factors for natural-gas mixtures are the hydrocarbon fractions, carbon dioxide, and nitrogen. Traces of other gases such as hydrogen, oxygen, hydrogen sulphide, and so on, are sometimes found to occur, but generally are absent and for this reason are not given consideration in the development of a working method for predicting supercompressibility factors. Carbon dioxide, nitrogen, and hydrocarbon fractions were the only gases found present in the gas samples used to date in the test program, with the exception of three samples which were found to contain negligible traces of hydrogen sulphide.

The predominant gas existing in all mixtures is, of course, methane, and, although present in varying degrees, it almost entirely suffices to denote singular character to the typical natural-gas mixture. The average methane content of a large number of gas samples was found to be 92.9 per cent on a mol fractional basis. Low methane content almost invariably results from high nitrogen and/or carbon-dioxide content. A breakdown of the average fractional analysis of the samples is shown in Table 2. Although the average carbon-dioxide plus nitrogen content is less than 1 per cent, this is not intended to infer that it is permissible to neglect these constituents when developing a method to define supercompressibility factors of natural-gas mixtures, for with some mixtures the carbon-dioxide and/or nitrogen content may be appreciable. For the majority of natural gases, however, carbon dioxide and nitrogen are of negligible importance in defining the character of the mixtures. Twenty-nine per cent of the samples contain hydrocarbon fractions only. Of the remaining samples, 55 per cent contain carbon dioxide with the hydrocarbon fractions, 2 per cent nitrogen with the hydrocarbon fractions, and 14 per cent carbon dioxide and nitrogen with the hydrocarbon fractions.

TABLE 2 BREAKDOWN OF AVERAGE FRACTIONAL ANALYSIS OF GAS SAMPLES

Hydrocarbon fractions — 99.2 mol per cent		Carbon dioxide plus nitrogen — 0.8 mol per cent	
92.9 mol per cent methane	6.3 mol per cent ethane plus higher fractions	0.4 mol per cent carbon dioxide	0.4 mol per cent nitrogen

Table 3 gives a breakdown of the carbon-dioxide contents for all samples. Nearly 60 per cent of the samples have less than 0.25 mol per cent and 87 per cent less than 1 per cent. The average carbon-dioxide content is 0.4 mol per cent and the maximum 3.2 mol per cent. The breakdown of the nitrogen contents is shown in Table 4. Well over 80 per cent of the samples have no detectable amount of nitrogen, and nearly 95 per cent have less than 1.0 mol per cent. The nitrogen content in several samples is, however, quite high.

TABLE 3 BREAKDOWN OF CARBON-DIOXIDE CONTENTS

Range carbon-dioxide content, mol per cent	Per cent of samples
Nil to 0.25	58
0.25 to 1.0	29
1.0 to 2.0	7
2.0 to 3.0	4
3.0 to 4.0	2

Considering the hydrocarbon fractions only, the average analysis on a mol per cent basis is 93.80 methane, 3.70 ethane, 1.45 propane, and 1.05 butanes and higher. The breakdowns of the various contents of these gases are given in Tables 5 and 6.

TABLE 4 BREAKDOWN OF NITROGEN CONTENTS

Nitrogen content mol per cent	Per cent samples
Nil	84
Nil to 1.0	10
1.0 to 3.0	4
12.57	1
18.27	1

TABLE 5 BREAKDOWN OF METHANE CONTENTS IN HYDROCARBON FRACTIONS OF SAMPLES

(Per cent methane on basis of hydrocarbon fractions only. Average mol per cent methane, 93.80)

Methane content mol per cent	Per cent samples
99 to 100	7
95 to 99	34
90 to 95	46
85 to 90	13
below 85	0

TABLE 6 BREAKDOWN OF ETHANE, PROPANE, AND BUTANES AND HIGHER CONTENTS IN HYDROCARBON FRACTIONS OF SAMPLES

(Mol per cent of basis of hydrocarbon fractions only)

Constituent content, mol per cent	Ethane, per cent samples	Propane, per cent samples	Butanes and higher, per cent samples
0 to 1.0	8	40	52
1.0 to 2.0	8	35	36
2.0 to 3.0	12	14	9
3.0 to 4.0	31	7	3
4.0 to 5.0	19	4	100
5.0 to 6.0	16	100	
6.0 to 7.0	4		
7.0 to 8.0	2		
	100		

Avg mol per cent ethane, 3.70
Avg mol per cent propane, 1.45
Avg mol per cent butanes and higher, 1.05

[2] Numbers in parentheses refer to the Bibliography at the end of the paper.

The hydrocarbon fraction consists of over 90 mol per cent methane in 87 per cent of the samples, has less than 5 mol per cent ethane in 78 per cent of the samples, and less than 3 mol per cent propane in 89 per cent of the samples. The butanes and higher fractions represent less than 2 mol per cent of the hydrocarbon fractions in 88 per cent of the samples. Although not shown in the tables, the butanes have an average content of about 0.64 mol per cent, the pentanes about 0.21, hexanes 0.15, and 0.07 heptanes plus.

The specific gravities as determined by test varied from 0.559 to 0.711. The average measured specific gravity for all samples is 0.616. Gross heating values on a dry basis averaged to 1082 Btu per cu ft at 60 F and 14.73 psia.

Correlation Method

Various methods for predicting supercompressibility factors of natural-gas mixtures are available (3, 4, 5, 6). All methods specifically designed for predicting values at high pressure utilize the "law of corresponding states," the concept of pseudocritical temperature and pressure and the generally accepted rule that critical temperature and pressure of a paraffin hydrocarbon mixture may be defined by its specific gravity. With consideration given to overlapping of the various methods, the method proposed by Dunkle (6) appeared most promising, not only because of apparent agreement between predicted results and test data, but primarily because of its make-up on the basis of methane as the only hydrocarbon and its representation in terms of convenient properties of natural-gas mixtures.

The framework of the method proposed by Dunkle consists of using supercompressibility factors of methane expressed in terms of reduced temperature T_R and reduced gage pressure P_R as the basis for evaluation of supercompressibility factors of mixtures of hydrocarbon fractions, carbon dioxide, and nitrogen. This assumes the "law of corresponding states" valid for any mixture, meaning that for the same reduced temperature and pressure the supercompressibility factor of a mixture equals that for methane alone. This assumption may be justified only because the principal constituent of a natural-gas mixture is methane, and hence any errors introduced because of deviations from this law should have negligible effect on the accuracy of the predicted value for the mixture.

The reduced temperature of a mixture is defined as the ratio of the absolute temperature T to its pseudocritical temperature θ, where

$$\theta = X_h\theta_h + X_c\theta_c + X_n\theta_n \quad [1]$$

The reduced gage pressure of a mixture is defined as the ratio of the gage pressure P to its pseudocritical pressure π, where

$$\pi = X_h\pi_h + X_c\pi_c + X_n\pi_n \quad [2]$$

Equations [1] and [2] require knowledge of the fractional analysis of a gas mixture to define the reduced temperature and pressure. Since in normal practice this analysis is not readily available, the generally accepted rules that pseudocritical temperature, pseudocritical pressure, and heating value of the hydrocarbon fractions vary linearly with the specific gravity of the hydrocarbon fractions will be employed. These may be stated in equation form as

$$H_h = g + kG_h \quad [3]$$

$$\theta_h = a + bG_h \quad [4]$$

$$\pi_h = d + eG_h \quad [5]$$

The specific gravity of the mixture of hydrocarbon fractions, carbon dioxide, and nitrogen is related to the fractional analysis by the equation

$$G = X_hG_h + X_cG_c + X_nG_n \quad [6]$$

Also, since nitrogen and carbon dioxide are diluents, the heating value of the mixture is

$$H = X_hH_h \quad [7]$$

Lastly

$$X_h + X_c + X_n = 1.0 \quad [8]$$

These Equations [1] through [8] may be solved simultaneously to yield

$$\theta = a + bG - (a + bG_c - \theta_c)\,X_c - (a + bG_n - \theta_n)\left[\frac{g + kG - (g + kG_c)\,X_c - H}{g + kG_n}\right] \quad [9]$$

$$\pi = d + eG - (d + eG_c - \pi_c)\,X_c - (d + eG_n - \pi_n)\left[\frac{g + kG - (g + kG_c)\,X_c - H}{g + kG_n}\right] \quad [10]$$

Inasmuch as a, b, d, e, g, k, θ_c, θ_n, G_c, and G_n are constants, Equations [9] and [10] may be reduced to

$$\theta = \alpha_0 + \alpha_1G + \alpha_2H + \alpha_3X_c \quad [11]$$

$$\pi = \beta_0 + \beta_1G + \beta_2H + \beta_3X_c \quad [12]$$

where the coefficients on the variables G, H, and X_c are constants. In this form the pseudocritical temperature and pressure are defined in terms of the conveniently determined properties of a gas mixture—the specific gravity, the heating value, and the carbon-dioxide content. Additional measurement of mixture temperature and pressure allows direct calculation of reduced temperature and reduced gage pressure, from which the supercompressibility factor of the gas mixture is defined.

Supercompressibility Factors for Methane

Existing data on the compressibility factors of methane (7, 8, 9, 10) were used to prepare the basic working chart of supercompressibility factor F_{pv} as a function of reduced temperature T_R and reduced gage pressure P_R. All data were converted to yield a supercompressibility factor of unity at a base pressure of 14.4 psia. A problem encountered in the preparation of these working data resulted from the fact that relatively low reduced temperatures must be included in order to make the data applicable to natural-gas mixtures having high percentages higher hydrocarbons. Compressibility factors in the temperature range —60 F to 200 F are necessary for preparation of working data. A thorough study of the available data in the low-temperature range shows appreciable inconsistency among various sources, and, in consequence, the values chosen represent what appeared as a best average. Considerable weight was attached to values calculated from the Benedict equation of state (10). Within the high-temperature range, 40 F to 200 F, data from the various sources are in fairly good agreement; the data of Sage and Lacey (7) were used exclusively in the final definition of the supercompressibility factors in this temperature range.

Table 7 lists the supercompressibility factors F_{pv} of methane for reduced gage pressures up to 3.0. Values for higher pressure are not presented because of lack of test data for confirmation of results. Linear interpolation of these data will introduce a deviation no greater than 0.01 per cent from a plotted curve of the listed data.

TABLE 7 SUPERCOMPRESSIBILITY FACTORS F_{PT} FOR PURE METHANE

Reduced gage pressure, P_R	Reduced temperature, T_R													
	1.16	1.18	1.20	1.22	1.24	1.26	1.28	1.30	1.32	1.34	1.36	1.38	1.40	1.42
0.2	1.0254	1.0237	1.0223	1.0210	1.0198	1.0186	1.0176	1.0167	1.0158	1.0150	1.0142	1.0134	1.0125	1.0119
0.4	1.0512	1.0481	1.0452	1.0425	1.0400	1.0375	1.0354	1.0334	1.0315	1.0298	1.0282	1.0267	1.0253	1.0240
0.6	1.0795	1.0743	1.0696	1.0652	1.0612	1.0574	1.0540	1.0509	1.0480	1.0453	1.0429	1.0405	1.0384	1.0362
0.8	1.1122	1.1037	1.0964	1.0896	1.0839	1.0786	1.0737	1.0693	1.0651	1.0613	1.0577	1.0545	1.0513	1.0484
1.0	1.1525	1.1393	1.1277	1.1176	1.1092	1.1017	1.0948	1.0888	1.0831	1.0780	1.0734	1.0690	1.0650	1.0612
1.2	1.2006	1.1802	1.1631	1.1489	1.1317	1.1265	1.1172	1.1093	1.1021	1.0957	1.0896	1.0840	1.0788	1.0740
1.4				1.1835	1.1667	1.1527	1.1411	1.1310	1.1219	1.1139	1.1063	1.0994	1.0930	1.0870
1.6					1.1972	1.1804	1.1657	1.1532	1.1418	1.1317	1.1226	1.1142	1.1067	1.0997
1.8							1.1926	1.1766	1.1622	1.1496	1.1385	1.1286	1.1199	1.1119
2.0								1.1970	1.1807	1.1662	1.1533	1.1423	1.1323	1.1234
2.2									1.1961	1.1811	1.1675	1.1552	1.1438	1.1340
2.4										1.1944	1.1798	1.1665	1.1545	1.1438
2.6											1.1907	1.1765	1.1636	1.1517
2.8											1.1993	1.1847	1.1712	1.1588
3.0												1.1905	1.1765	1.1639

P_R	Reduced temperature, T_R													
	1.44	1.46	1.48	1.50	1.52	1.54	1.56	1.58	1.60	1.62	1.64	1.66	1.68	1.70
0.2	1.0112	1.0106	1.0100	1.0095	1.0090	1.0085	1.0082	1.0078	1.0074	1.0070	1.0065	1.0063	1.0060	1.0056
0.4	1.0226	1.0214	1.0202	1.0191	1.0181	1.0171	1.0163	1.0155	1.0148	1.0140	1.0133	1.0125	1.0119	1.0114
0.6	1.0342	1.0324	1.0306	1.0289	1.0275	1.0260	1.0245	1.0233	1.0221	1.0210	1.0200	1.0190	1.0180	1.0171
0.8	1.0458	1.0433	1.0410	1.0388	1.0367	1.0348	1.0330	1.0312	1.0295	1.0280	1.0266	1.0253	1.0240	1.0227
1.0	1.0573	1.0544	1.0515	1.0487	1.0461	1.0437	1.0414	1.0392	1.0371	1.0351	1.0333	1.0315	1.0299	1.0284
1.2	1.0686	1.0656	1.0618	1.0583	1.0550	1.0520	1.0492	1.0465	1.0441	1.0419	1.0396	1.0375	1.0355	1.0335
1.4	1.0816	1.0768	1.0723	1.0680	1.0640	1.0605	1.0570	1.0539	1.0510	1.0482	1.0456	1.0432	1.0409	1.0386
1.6	1.0932	1.0874	1.0820	1.0771	1.0725	1.0684	1.0644	1.0607	1.0574	1.0543	1.0514	1.0486	1.0459	1.0434
1.8	1.1045	1.0977	1.0915	1.0859	1.0808	1.0761	1.0716	1.0674	1.0635	1.0600	1.0569	1.0537	1.0508	1.0481
2.0	1.1153	1.1078	1.1010	1.0947	1.0890	1.0836	1.0786	1.0740	1.0695	1.0655	1.0618	1.0583	1.0551	1.0521
2.2	1.1250	1.1168	1.1094	1.1025	1.0960	1.0901	1.0846	1.0795	1.0748	1.0705	1.0665	1.0626	1.0591	1.0558
2.4	1.1340	1.1250	1.1172	1.1099	1.1032	1.0969	1.0908	1.0850	1.0798	1.0750	1.0705	1.0664	1.0625	1.0589
2.6	1.1414	1.1321	1.1236	1.1158	1.1088	1.1020	1.0957	1.0898	1.0842	1.0791	1.0742	1.0699	1.0657	1.0618
2.8	1.1475	1.1376	1.1288	1.1206	1.1132	1.1061	1.0996	1.0935	1.0877	1.0825	1.0773	1.0727	1.0684	1.0643
3.0	1.1521	1.1412	1.1322	1.1238	1.1164	1.1092	1.1024	1.0961	1.0901	1.0844	1.0795	1.0750	1.0705	1.0663

P_R	Reduced temperature, T_R				
	1.72	1.74	1.76	1.78	1.80
0.2	1.0054	1.0050	1.0049	1.0046	1.0044
0.4	1.0108	1.0102	1.0098	1.0093	1.0089
0.6	1.0163	1.0154	1.0146	1.0138	1.0130
0.8	1.0210	1.0205	1.0194	1.0185	1.0174
1.0	1.0269	1.0255	1.0241	1.0229	1.0216
1.2	1.0318	1.0301	1.0285	1.0270	1.0254
1.4	1.0365	1.0346	1.0327	1.0310	1.0291
1.6	1.0411	1.0388	1.0365	1.0345	1.0324
1.8	1.0455	1.0429	1.0404	1.0380	1.0356
2.0	1.0492	1.0465	1.0439	1.0413	1.0387
2.2	1.0526	1.0496	1.0469	1.0440	1.0412
2.4	1.0556	1.0524	1.0494	1.0465	1.0435
2.6	1.0581	1.0547	1.0515	1.0484	1.0451
2.8	1.0605	1.0568	1.0534	1.0500	1.0466
3.0	1.0625	1.0586	1.0549	1.0513	1.0478

Determination of General Equations for Calculation of Pseudocritical Temperature and Pressure

Three basic relationships involved in the general equations for critical temperature and pressure of gas mixtures are the assumed linear variation of heating value, pseudocritical temperature, and pseudocritical pressure with specific gravity, when all variables are expressed on a pure hydrocarbon basis. The validity of the general Equations [9] and [10] depends directly on the accuracy of these straight-line equations.

Fig. 1 shows a plot of the gross heating value on a dry basis as a function of the specific gravity, both co-ordinates expressed on a pure hydrocarbon basis. The test points shown in Fig. 1 cover all gas samples employed to date in the deviation tests. A best straight line passing through the heating value for pure methane and the other points is given by the solid line. The constants g and k in Equation [3] are defined by this line and are

$$g = 186.0 \text{ and } k = 1485$$

so that the linear relationship between the pure hydrocarbon heating value and pure hydrocarbon specific gravity is

$$H_h = 186.0 + 1489\,G_h \quad \ldots\ldots\ldots\ldots\ldots\ldots\ldots [3a]$$

Fig. 2 shows the pseudocritical temperature of the gas samples plotted in terms of the specific gravity, with both co-ordinates expressed on a pure hydrocarbon basis. The pseudocritical temperatures were calculated directly from the fractional analyses of the gas samples, using values of the critical temperatures of the various hydrocarbon fractions as shown in Table 8. The critical

TABLE 8 CRITICAL TEMPERATURES AND PRESSURES OF HYDROCARBON COMPONENTS USED IN CALCULATING PSEUDOCRITICAL TEMPERATURES AND PRESSURES OF NATURAL-GAS MIXTURES

Component	Mol weight	Critical temperature, deg R	Critical pressure, psia
Methane	16.04	344	673
Ethane	30.07	595	712
Propane	44.09	666	617
Iso-butane	58.12	734	529
n-butane	58.12	766	551
Iso-pentane	72.15	830	483
n-pentane	72.15	846	485
Hexanes	86.17	911	440
Heptanes plus	110.0	1100	400

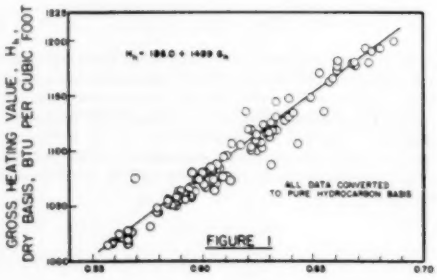

Fig. 1

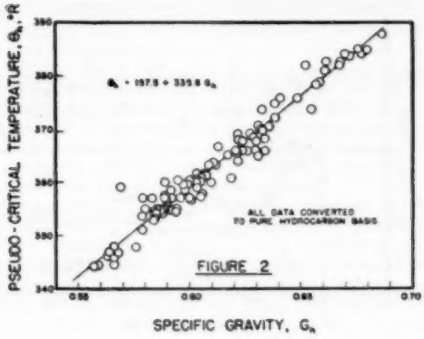

FIG. 2

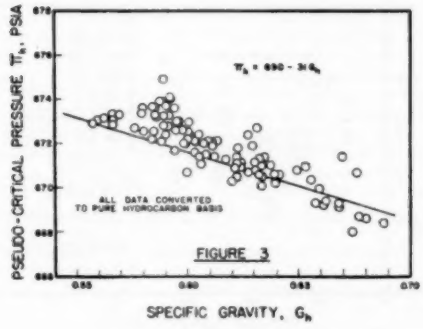

FIG. 3

temperature of ethane has been adjusted from the standard value of 550 R to 595 R. This adjusted value of the critical temperature of ethane was arrived at by comparison of the experimental data on the supercompressibility factor with those for methane given in Table 8. The straight line shown in Fig. 2 is given by

$$\theta_h = 157.5 + 336.6\, G_h \quad \ldots\ldots\ldots\ldots\ldots [4a]$$

Hence the constants of Equation [4] are a equal to 157.5 and b equal to 336.6.

A plot of the calculated hydrocarbon critical pressures versus hydrocarbon specific gravity is shown in Fig. 3. The critical pressures of the hydrocarbon components used in calculating the pseudocritical pressures of the mixtures of hydrocarbons are the standard values listed in Table 8. The straight line used to represent the variation of pseudocritical pressure with specific gravity is

$$\pi_h = 690 - 31\, G_h \quad \ldots\ldots\ldots\ldots\ldots [5a]$$

so that the constants d and e are equal to 690 and 31.

In making the data of methane, expressed in terms of reduced co-ordinates, apply to mixtures containing carbon dioxide and nitrogen, it is necessary to use adjusted values of their critical temperatures. The experimental data obtained to date in the test program containing appreciable quantities of these diluents are too few in number to allow direct evaluation of the adjusted values. For this reason the adjusted values as given by Dunkle (6) are employed. They are

$$\theta_c = 510 \text{ R and } \theta_n = 216 \text{ R}$$

The critical pressures of carbon dioxide and nitrogen are taken equal to their standard values of 1072 psia and 492 psia, respectively.

The general Equations [11] and [12] for calculation of pseudocritical temperature and pressure are obtained by direct substitution of these constants into Equations [9] and [10]. The resulting relationships are

$$\theta = 127.0 + 92.10\, G + 243.2\, X_c + 0.1642\, H \ldots [11a]$$

$$\pi = 670.8 - 184.8\, G + 681.9\, X_n + 0.1033\, H \ldots [12a]$$

Reduced temperature and pressure associated with the data of Table 7 are calculated from these equations.

Comparison of Predicted F_{pv} Factors With Experimentally Determined Data

Since specific gravity, carbon dioxide, and nitrogen content were determined for each test sample, an evaluation of the accuracy of the working method may be made by comparing the F_{pv} factors determined by test with those derived from the basic methane data.

The results obtained from this comparison are given in Figs. 4 through 10. Fig. 4 shows the supercompressibility factor F_{pv} as a function of reduced pressure for one temperature. The lines A, B, and C define the values of F_{pv} derived from existing methods for predicting supercompressibility factors. The solid line marked "working method" defines the values derived from use of Equations [11a] and [12a] and the basic methane data of Table 7. Agreement of working-method data with experimental data is within 0.10 per cent over the entire pressure range.

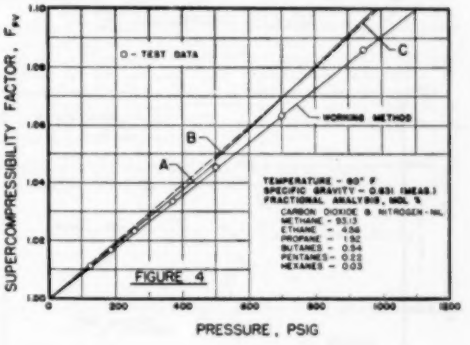

FIG. 4

Figs. 5, 6, and 7 summarize the difference between measured values of F_{pv} and the corresponding values derived from the working method. Differences are plotted as a function of the reduced temperature T_R. The reduced pressure P_R is constant for each plot, being equal to 0.40, 0.80, and 1.20 for Figs. 5, 6, and 7, respectively. A study of the three plots shows no detectable difference between the pure hydrocarbon mixtures and those containing less than 1 mol per cent carbon dioxide plus nitrogen. Hence for comparison purposes the mixtures containing slight amounts of diluents may be included with the pure hydrocarbons. For the reduced pressure of 0.40 the algebraic mean deviation is

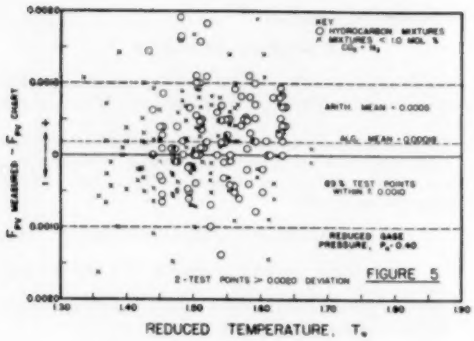

Fig. 5

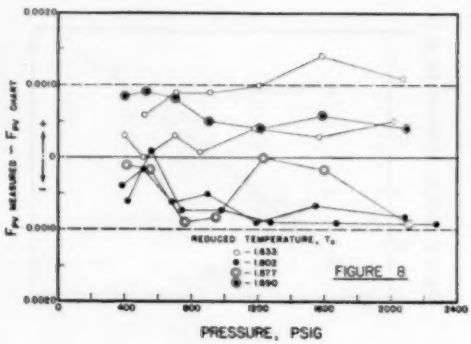

Fig. 8

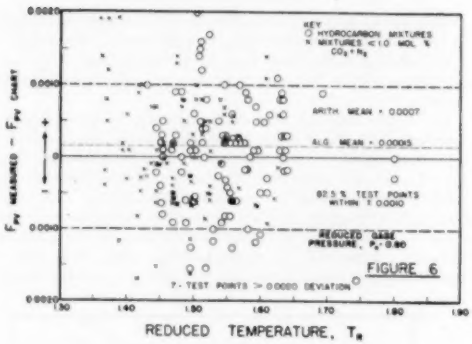

Fig. 6

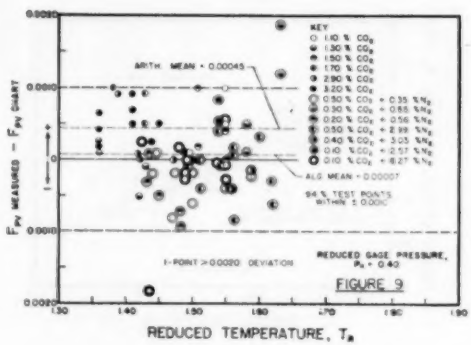

Fig. 9

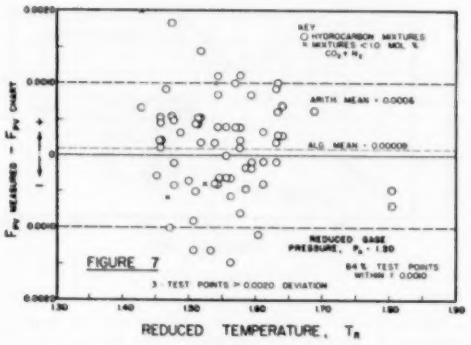

Fig. 7

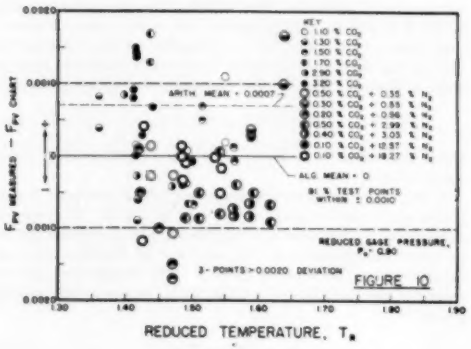

Fig. 10

roughly +0.0002, the arithmetic mean deviation 0.0005, and 89 per cent of all test points have differences less than 0.0010 from the values obtained by the working method. At a reduced pressure of 0.80, Fig. 6, the algebraic mean deviation is about +0.00015, the arithmetic mean 0.0007, and 82 per cent of all test points differ less than 0.0010 from the values obtained by the working method. Similar results are obtained for the reduced gage pressure of 1.20, Fig. 7; here, the algebraic mean deviation is +0.0001, the arithmetic mean 0.0006, and 84 per cent of all the points fall within the plus or minus 0.0010 range.

No apparent trend of deviation between predicted and test values exists for the presently covered range of temperature and pressure. Considerable study was given to the deviations in an effort to find if the differences might correlate in terms of some secondary variable, such as mol per cent propane or butane, specific gravity, test temperature, and so on. The results showed that the differences are independent of all variables. It is anticipated that minor modification of constituent critical pressures will be necessary when forthcoming very high-pressure data are analyzed.

Fig. 8 gives the differences between the predicted values of F_{pv} and corresponding test data for five high-pressure tests. The number of high-pressure tests is too few to check conclusively the accuracy of the working method at very high pressures, but, as may be seen from this plot, the trends of the difference curves do not suggest any fundamental inaccuracies in the working method.

A check on the validity of the working method when applied to mixtures containing the diluents carbon dioxide and nitrogen was made and the results for reduced gage pressures of 0.40 and 0.80 are presented in Figs. 9 and 10, respectively. The maximum carbon-dioxide content is 3.2 mol per cent and the maximum nitrogen content is 18.27 mol per cent. A study of the differences over this range of percentage of diluents indicates no particular trend with any variable, and it may be concluded that the differences can mostly be ascribed to experimental variations. Furthermore, it appears fairly conclusive that for the ranges of pressure and temperature studied, the adjusted values of the critical temperature for carbon dioxide and nitrogen as given by Dunkle are satisfactory.

In summary, it is believed that for the pressure range, zero to roughly 1100 psia, the temperature range, 40 F to 200 F, the specific-gravity range, 0.55 to roughly 0.75, and percentage diluents up to about 15 to 20, the working method quite accurately predicts the magnitude of the supercompressibility factor F_{pv}; the average error is found to be less than 0.10 per cent.

Future Work

A continuing test program is intended to furnish many high-pressure data from which the validity of the present working method may be checked. In addition, it is intended to study the deviations over wider ranges of specific gravity, diluents, temperature, and so on.

Acknowledgment

The research program herein reported is sponsored by the Tennessee Gas Transmission Company and the Columbia Gas System Service Corporation, acting as a joint sponsoring agency. The authors wish to extend appreciation to Mr. E. S. Plank of the Tennessee Gas Transmission Company, and to Messrs. J. E. Overbeck and H. B. McNichols of the Columbia Gas System Service Corporation, for their co-operation in providing test data and help in carrying out this program.

BIBLIOGRAPHY

1 "Compressibility Determinations Without Volume Measurements," by E. S. Burnett, *Journal of Applied Mechanics*, Trans. ASME, vol. 58, 1936, p. A-136.

2 "A Comparison of the Bean and Burnett Apparatus for Measuring Gas Law Deviation Factors," by O. T. Bloomer, American Gas Association, New York, N. Y., P C-51-14, May, 1951.

3 "Tentative Standard Method for Calculation of High Pressure Gas Measurement," Natural Gasoline Association of America, Tulsa, Okla., Standard 4142, December, 1942.

4 "Tentative Standard Procedure for the Determination of Superexpansibility and Manometer Factors Used in Measurement of Natural Gas by Orifice Meter at Pressures in Excess of 500 Psig," California Natural Gasoline Association, Los Angeles, Calif., Bulletin No. TS-461, 1947.

5 "Tentative Standards for the Determination of Superexpansibility Factors in High Pressure Gas Measurement," California Natural Gasoline Association, Los Angeles, Calif., Bulletin No. TS-354, 1936.

6 "The Pseudo-Critical Method for Evaluating Deviation of Natural Gas From Boyle's Law," by R. V. Dunkle, *Gas*, vol. 20, October, 1944, p. 41.

7 "Thermodynamic Properties of the Lighter Paraffin Hydrocarbons and Nitrogen," by B. H. Sage and W. N. Lacey, American Petroleum Institute, New York, N. Y., 1950.

8 "Thermodynamic Properties of Methane at Low Temperature," by W. H. Corcoran, R. R. Bowles, B. H. Sage, and W. N. Lacey, *Industrial and Engineering Chemistry*, vol. 37, 1945, p. 825.

9 "Volumetric Behavior of Methane," by R. H. Olds, H. H. Reamer, B. H. Sage, and W. N. Lacey, *Industrial and Engineering Chemistry*, vol. 35, 1943, p. 922.

10 "Theoretical Study of Thermodynamic Properties of Light Hydrocarbons and Their Mixtures," by M. W. Kellogg Co., Petroleum Research Division, Third Progress Report, December 8, 1938.

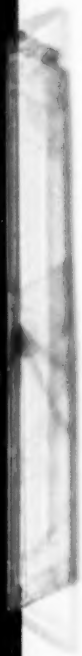

Heat Transfer and Fluid Friction During Flow Across Banks of Tubes—IV

A Study of the Transition Zone Between Viscous and Turbulent Flow

By O. P. BERGELIN,[1] G. A. BROWN,[2] AND S. C. DOBERSTEIN,[3] NEWARK, DEL.

The experimental results of a long-term research program on flow across tube banks have been extended from the zone of viscous flow through the transition zone and well into the zone of turbulent flow. Pressure drop and rate of heat transfer are reported for the flow of a light oil across five rectangular banks of ⅜-in-diam tubes. Equilateral triangle, staggered square, and in-line square arrangements on a 1.25 pitch ratio, and equilateral triangle and in-line square arrangements on a 1.50 pitch ratio are discussed. The flow rate of the oil covers a Reynolds number range of from 25 to 10,000. Heating, cooling, and isothermal tests are reported.

Nomenclature

The following nomenclature is used in the paper:

A_F = shell-side friction area, sq ft
A_H = outside surface area of tubes, sq ft
c = heat capacity, Btu/(lb)(deg F)
D_c = minimum clearance between tubes, ft
D_i = inside diameter of tube, in.
D_o = outside diameter of tube, ft
D_e = volumetric hydraulic diameter $= \dfrac{4 \times \text{free volume}}{\text{exposed area of tubes}}$, ft
d = tube core diameter, in.
E = pumping power loss per unit heat-transfer area, (ft)(lb force)/(hr)(sq ft)
f_{Cs} = friction factor defined by $f_{Cs} = \dfrac{2\Delta p g_c \rho}{4G_m^2 N}\left(\dfrac{\mu}{\mu_s}\right)^{0.14}$ dimensionless
G_m = mass velocity through minimum cross section, lb/(hr)(sq ft)
g_c = conversion factor, 4.18×10^8 (mass lb)(ft)/(force lb)(hr)^2
h = surface coefficient of heat transfer based on outside surface area of tubes, Btu/(hr)(sq ft)(deg F)
j = heat-transfer factor, $j = \left(\dfrac{h}{cG_m}\right)\left(\dfrac{c\mu}{k}\right)^{2/3}\left(\dfrac{\mu_s}{\mu}\right)^{0.14}$
k = thermal conductivity, Btu/(hr)(ft)(deg F)
L = length of tube bank, $L = nS_L$, ft
m = exponent on (μ/μ_s) ratio, dimensionless
N = number of major restrictions encountered in flow through the bank (equivalent to n where S_m occurs in transverse openings; equivalent to $n - 1$ where S_m occurs in diagonal openings), dimensionless
$N_{Re(i)}$ = Reynolds number D_iG_m/μ, dimensionless
$N_{Re(o)}$ = Reynolds number D_oG_m/μ, dimensionless
n = number of tube rows in direction of flow, dimensionless
P = pitch, defined as minimum center-to-center distance between adjacent tubes. (In case of staggered square arrangements pitch is measured along a line 45 deg from direction of flow), ft
p = pressure, psf
S_L = longitudinal pitch, distance between center lines of adjacent transverse rows, ft
S_L' = longitudinal pitch, center-to-center distance from a tube in transverse row to the nearest tube outside of that row, ft
S_m = shell-side minimum flow area, sq ft
S_T = transverse pitch, center-to-center distance between tubes in a transverse row, ft
V_m = velocity through shell-side minimum flow area, fps
S_W = total annulus area, sq ft
W = mass rate of flow, lb per hr
μ = absolute viscosity at average bulk temperature, lb/(hr)(ft)
μ_s = absolute viscosity at tube surface temperature, lb/(hr)(ft)
ρ = density at average bulk temperature, pcf

Introduction

Although flow rates in the zone of transition between viscous and turbulent flow are often utilized in the operation of heat-exchange equipment, there is no established equation to describe the variation in fluid friction and rate of heat transfer with flow rate in this range. For the case of flow inside tubes Colebrook (1)[4] has made a beginning in the analytical approach to pressure drop, but no similar presentation has been made for heat transfer. For flow across tube banks practically no data are available for either pressure drop or heat transfer, and the usual graphical correlations of tube-bank data either do not extend over this zone or show a smooth curve through the zone without adequate experimental verification.

In this paper experimental data for the transition zone are presented and are compared with the previous rough correlations. At the upper limit of the transition zone the data are compared with Grimison's correlation for turbulent flow, and at the lower limit with the data which have been reported previously for viscous flow as a part of the current research program.

Equipment and Procedure

The basic equipment and procedures have been described in detail previously (2, 3, 7) and, therefore, will be discussed only briefly at this time. Table 1 gives the physical dimensions of all

[1] Associate Professor, Department of Chemical Engineering, University of Delaware.
[2] Research Fellow in Chemical Engineering, University of Delaware. Now, Merck & Company, Inc., Rahway, N. J.
[3] Research Fellow in Chemical Engineering, University of Delaware. Now, E. I. du Pont de Nemours and Co., Wilmington, Del.

Contributed by the Heat Transfer Division and presented at the Annual Meeting, Atlantic City, N. J., November 25–30, 1951, of The American Society of Mechanical Engineers.

 Manuscript received at ASME Headquarters, August 29, 1951. Paper No. 51—A-109.

[4] Numbers in parentheses refer to the Bibliography at the end of the paper.

TABLE 1 HEAT-EXCHANGER DIMENSIONS AND CONSTANTS

Model number	1	2	3	4	5
Tube arrangement	Triangular	In-line square	Staggered square	Triangular	In-line square
Outside tube diameter, D_t, in.	0.375	0.375	0.375	0.375	0.375
Minimum tube clearance, D_c, in.	0.094	0.094	0.094	0.188	0.188
Exposed tube length, in.	6.0	6.0	6.0	6.0	6.0
Number of copper tubes	70	70	70	70	70
Equivalent exposed tubes	65	60	63	65	60
Volumetric hydraulic diam, D_e, ft	0.0225	0.0309	0.0309	0.0463	0.0582
Minimum flow area, S_m, sq ft	0.0254	0.0234	0.0352	0.0508	0.0469
Number of tube rows, n	10	10	14	10	10
Number of contractions, N	10	10	13	10	10
Heat-transfer area, Aft, sq ft	3.19	2.94	3.09	3.19	2.94
Friction area, Af, sq ft	3.44	3.10	3.36	3.57	3.24
Pitch ratio, P/D_t	1.25	1.25	1.25	1.50	1.50
S_L/D_t	1.08	1.25	0.883	1.30	1.50
S_L'/D_t	1.25	1.25	1.25	1.50	1.50
S_T/D_t	1.25	1.25	1.77	1.50	1.50
Length of tube bank, L, ft	0.338	0.391	0.387	0.406	0.469
Inside tube diameter, D_i, in.	0.277	0.277	0.277	0.277	0.277
Tube core diameter, d, in.	0.188	0.188	0.188	0.188	0.188
Annulus ratio, D_i/d	1.48	1.48	1.48	1.48	1.48
Total annulus area, Sw, sq ft	0.0158	0.0158	0.0158	0.0158	0.0158

TABLE 2 PHYSICAL PROPERTIES OF GULF 896 OIL

t, deg F	C_p* Btu / (lb) (deg F)	k** Btu / (hr) (ft) (deg F)	μ† lb / (hr) (ft)	$\frac{C_p}{k}$	$\left(\frac{C_p}{k}\right)^{1/3}$	ρ† lb / (cu ft)
80	0.468	0.0814	10.1	60.4	15.4	50.6
110	0.504	0.0807	6.82	42.5	12.2	49.9
140	0.521	0.0799	4.91	31.9	10.1	49.2
170	0.538	0.0792	3.72	25.3	8.61	48.5
200	0.558	0.0784	2.91	20.6	7.52	47.8

* Calculated using equation of Watson and Nelson, *Industrial Engineering Chemistry*, vol. 25, 1933, p 880: $C_p = 0.6811 - 0.308\,s + t(0.000815 - 0.000306\,s)\,(0.055K + 0.35)$
where
s = specific gravity at 60 F
t = temperature, deg F
K = characterization factor
† Experimentally determined values.
** Calculated using equation of C. S. Cragoe, Bureau of Standards Misc. Publication No. 97:
$k = \frac{1}{12}\frac{0.813}{s}[1 - 0.0003(t - 32)]$
s = specific gravity at 60 F
t = temperature, deg F.

the exchangers tested. Water at 100 or 200 deg F is passed upward through the vertical tubes of the models and a light oil, Gulf 896, whose properties are given in Table 2, is passed horizontally across the tube banks. Cores are used in the tubes to obtain high water velocities and high waterside film coefficients of heat transfer. Standardized test runs, made at the beginning and end of the testing of each model, show that there was no appreciable fouling during the tests. Heat balances with less than ±5 per cent deviation were obtained for all runs.

The pressure drop across each tube bank is taken between taps located along the horizontal center line of the model at points 1/4 in. upstream and downstream from the ends of the tube bank. The pressure drop is measured with inclined air-over-water manometers for the low rates of flow and oil-over-mercury manometers for the high rates. Temperature differences across the exchanger are measured with five-junction, series-connected, copper-constantan thermocouples which are inserted in an aluminum block in the flow stream. A single couple also is present in each block to measure the point temperature of each stream for evaluation of physical properties. These mixing blocks were installed during the tests on a heavier oil and have been retained because of the good heat balances which are obtained. This method of temperature measurement does not show a rapid response to temperature change, but it appears to be quite satisfactory for the steady-state conditions used during these tests.

Results

This paper presents the experimental results for one oil flowing across five tube banks and with various tube arrangements. Isothermal flow with the oil at 150 deg F, oil heating with water at 200 F, and oil-cooling runs with water at 100 deg F are reported. The maximum linear velocity of the oil ranges from 0.015 to 6.0 fps, and the Reynolds number from 25 to 10,000. Over-all coefficients of heat transfer vary from 632 to 28.4 Btu/(hr) (sq ft) (deg F) while the calculated water-film coefficients are 1540 at 100 F, and 2630 at 200 F. The oil-film coefficients are calculated by subtracting the resistances of the water film and the metal wall from the over-all values.

Discussion of Results

Pressure Drop. The variation of isothermal pressure drop with linear velocity in the tube banks is shown in Fig. 1. For the staggered tube banks having a 1.25 pitch ratio, models 1 and 3, the experimental results can be represented by straight lines with slope of about 1.75. The in-line arrangement with a 1.25 pitch ratio, model 2, yields a line with slope of about 2.15. The in-line arrangement has a lower pressure drop than the staggered arrangement at low flow rates, but because of its greater rate of change of pressure drop with velocity, the pressure drop for the in-line bank becomes greater than that for the staggered banks at a velocity between 1 and 2 fps. The arrangements with the 1.50 pitch ratios, models 4 and 5, show a similar reversal in relative pressure drop but the pressure drop is less for these models because of the wider tube spacing.

The pressure-drop results are shown in Figs. 3 to 7 as the friction factor recommended by Chilton and Genereaux (4) for turbulent flow, plotted versus the Reynolds number based on the tube diameter. While the present experiments do not extend very far into the turbulent zone, the curves established by previous investigators (5) are indicated in the figures. The considerable variation in the results for pressure drop during heating and cooling at low flow rates is probably due to the difficulty in measuring, under nonisothermal conditions, pressure differentials in the order of 0.02 in. of water. Previous results (6), which were obtained in this region with a heavier oil, are considered more reliable and are used to determine the position of the line in the zone of viscous flow.

In Figs. 3 to 7 the friction factors for cooling, in general, are somewhat greater than for isothermal flow, and during heating they are somewhat lower. Therefore a compensating viscosity correction $(\mu/\mu_s)^{0.14}$, has been applied. This has brought the data closer together but is not fully adequate. It appears that the variation due to heating or cooling is not a function of the bulk temperature and the tube-wall temperature only, nor does it change with the Reynolds number in a simple manner. The correct function may be $(\mu/\mu_s)^m$, where m is different for heating and cooling and is a function of the Reynolds number.

By using Figs. 3 to 7, a region of transitional flow through tube banks can be defined roughly as that zone, extending over a Reyn-

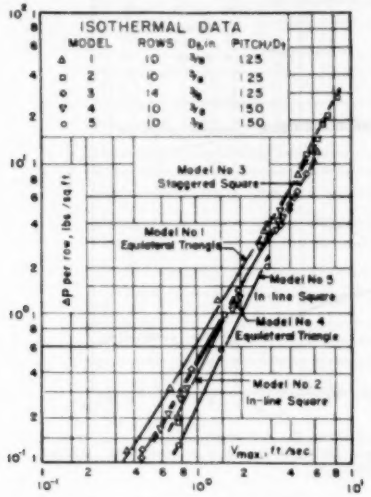

FIG. 1 PRESSURE DROP PER ROW DURING ISOTHERMAL FLOW OF OIL AT 150 DEG F FOR FIVE TUBE BANKS
(Flow normal to vertical tubes. Gulf 896 oil, viscosity 1.85 centipoises at 150 deg F.)

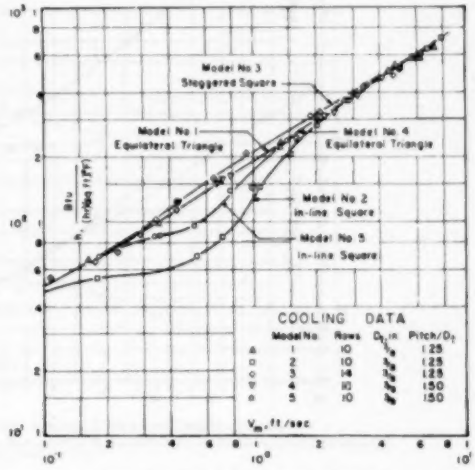

FIG. 2 OIL-FILM COEFFICIENTS OF HEAT TRANSFER FOR FIVE TUBE BANKS DURING COOLING
(Flow normal to vertical tubes. Gulf 896 oil at average bulk temperature of 150 deg F, viscosity 1.85 centipoises. Tube-surface temperature range 101–120 deg F.)

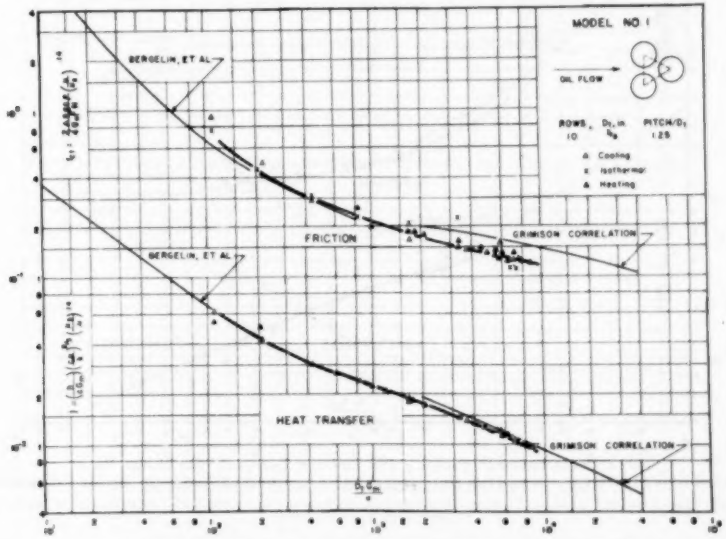

FIG. 3 HEAT-TRANSFER FACTOR j AND FRICTION FACTOR f_{ft}' FOR MODEL NO. 1
(Flow normal to vertical tubes. Gulf 896 oil at average bulk temperature of 150 deg F, viscosity 1.85 centipoises. Heating, cooling, and isothermal runs.)

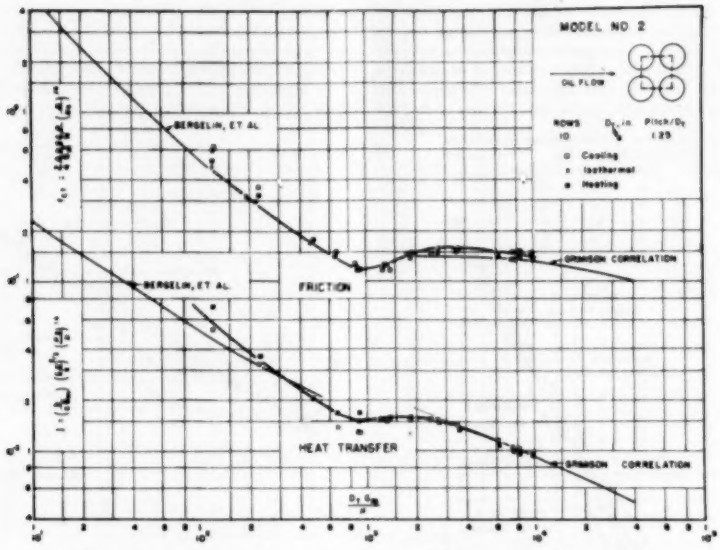

FIG. 4 HEAT-TRANSFER FACTOR j AND FRICTION FACTOR f_{ct}' FOR MODEL NO. 2
(Flow normal to vertical tubes. Gulf 896 oil at average bulk temperature of 150 deg F, viscosity 1.85 centipoises. Heating, cooling, and isothermal runs.)

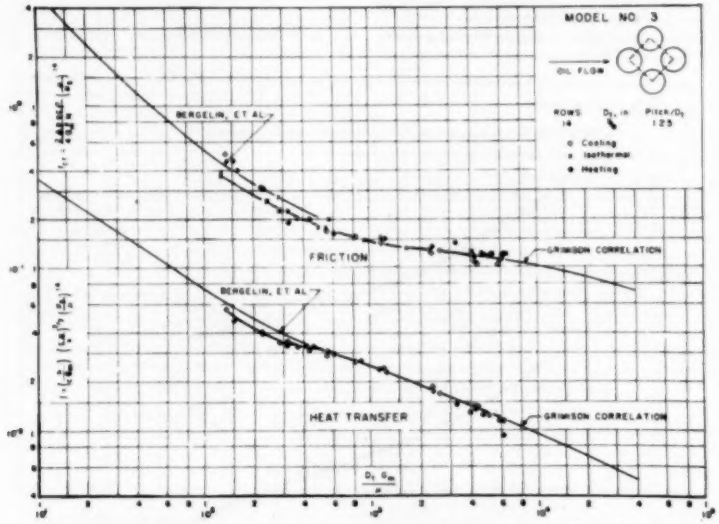

FIG. 5 HEAT-TRANSFER FACTOR j AND FRICTION FACTOR f_{ct}' FOR MODEL NO. 3
(Flow normal to vertical tubes. Gulf 896 oil at average bulk temperature of 150 deg F, viscosity 1.85 centipoises. Heating, cooling, and isothermal runs.)

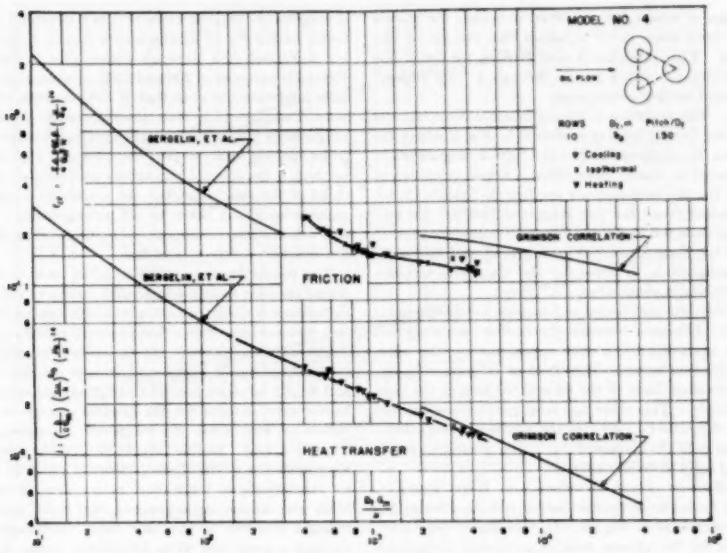

FIG. 6 HEAT-TRANSFER FACTOR j AND FRICTION FACTOR fa' FOR MODEL NO. 4
(Flow normal to vertical tubes. Gulf 896 oil at average bulk temperature of 150 deg F, viscosity 1.85 centipoises. Heating, cooling, and isothermal runs.)

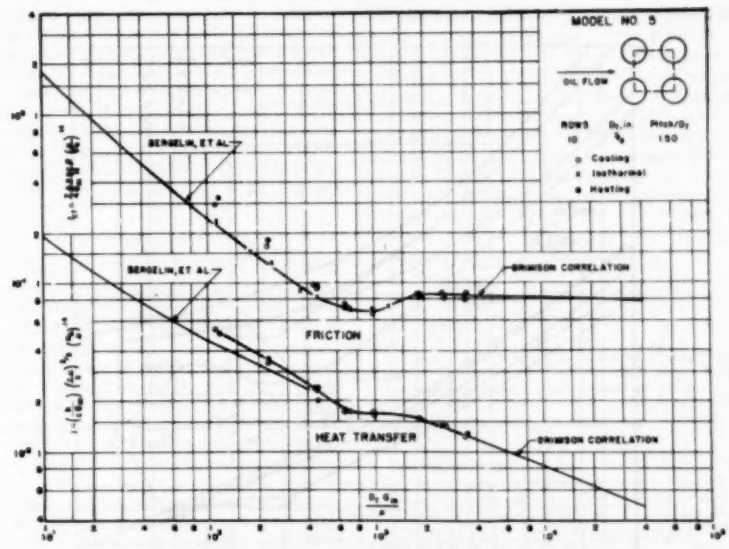

FIG. 7 HEAT-TRANSFER FACTOR j AND FRICTION FACTOR fa' FOR MODEL NO. 5
(Flow normal to vertical tubes. Gulf 896 oil at average bulk temperature of 150 deg F, viscosity 1.85 centipoises. Heating, cooling, and isothermal runs.)

olds-number range of about 200 to 5000, in which the curves are different in form from those in either the viscous or the turbulent regions. This difference is most striking for the in-line arrangements, where the curve passes through a "dip region" similar to that found for flow inside pipes.

Heat Transfer. The variation of the coefficient of heat transfer with linear velocity during cooling is shown in Fig. 2 where the difference between the staggered and in-line tube arrangements in the transition range is clearly discernible. From velocities of about 0.1 to 0.6 fps the heat-transfer coefficients for the in-line banks fall far below those for the staggered banks. At flow rates in the range from 0.6 to 2.0 fps the relative performance of the in-line banks improves compared to staggered, and the coefficients become comparable to those for the staggered arrangements above a velocity of about 4 fps.

In Figs. 3 to 7 the data are plotted as j-factors versus Reynolds numbers, and the difference between the in-line and staggered arrangements is again apparent over approximately the same range as for the friction factor. The effect of differences in viscosity between the main body of the oil and the film at the tube surface is also visible. This effect has been partly compensated for by including the ratio $(\mu_s/\mu)^{0.14}$ in the j-factor. The correction works well for both the staggered and in-line arrangements in the transition and early turbulent zones.

Comparisons Between Fluid Friction and Heat Transfer. Smoothed curves for both the friction factor and the j-factor are presented for comparison in Fig. 8. In this figure the upper Reynolds number for the viscous zone is arbitrarily designated as 200, which appears to be the average value at which the experimental results begin to deviate markedly from the straight lines which represent the data in the viscous zone. The lower Reynolds number for the turbulent zone is assumed to be 5000. At this value the heat-transfer curves for in-line and staggered arrangements become more or less coincident, and the friction-factor curves for all arrangements assume forms similar to those for turbulent flow through rough pipe. The range between Reynolds numbers of 200 and 5000 is taken as the transition zone. It is interesting to note that if flow through tube banks is considered analogous to flow through rough pipes, the in-line arrangements appear to have the greatest relative roughness. The wider spacing seems to give turbulence at a lower Reynolds number but, if the Reynolds numbers are based on the equivalent instead of the tube diameter, the transition occurs at a Reynolds number of about 6000 for all arrangements. Here again the equivalent diameter appears to be better than the tube diameter as a criterion for the type of flow.

The reason for the variation in the form of the curves in the transition zone as just defined may be due to the manner in which turbulence is initiated and spread throughout tube banks. Motion pictures have shown that in simple crossflow tube banks with staggered arrangements, the turbulence usually begins near the exit end, gradually works upstream as the flow rate is increased, and finally becomes general throughout the tube bank. This behavior may account for the gradual change in the slope of the curves in Fig. 8 for the staggered arrangements through the transition zone. In-line tube banks, on the other hand, seem to have more nearly the characteristics of pipes, in which the transition to turbulence takes place at one time throughout the fluid. With the in-line arrangements the fluid passes through the straight channels in the tube bank as though it were flowing through a duct, and when turbulence begins it occurs throughout the tube bank. In confirmation of these observations, Fig. 8 shows that there is a rapid change in pressure drop and rate of heat transfer for in-line arrangements in the transition zone, with the form of the curves being quite similar to the case for flow inside tubes.

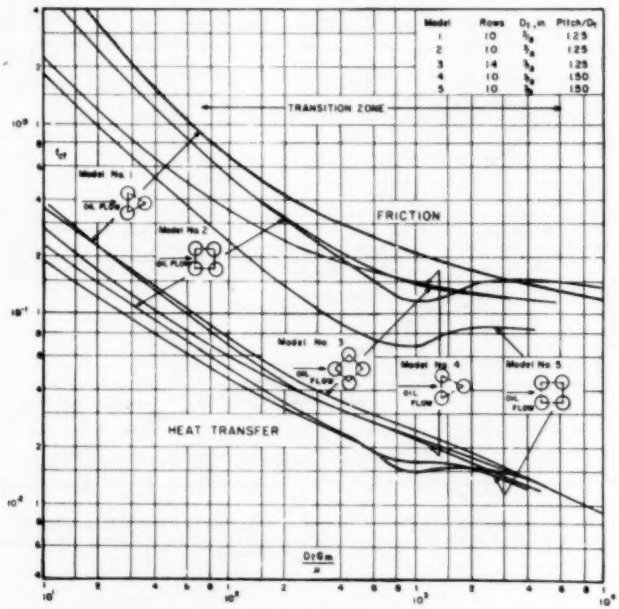

FIG. 8 SMOOTHED CURVES OF FRICTION AND HEAT-TRANSFER FACTORS FOR FIVE TUBE BANKS

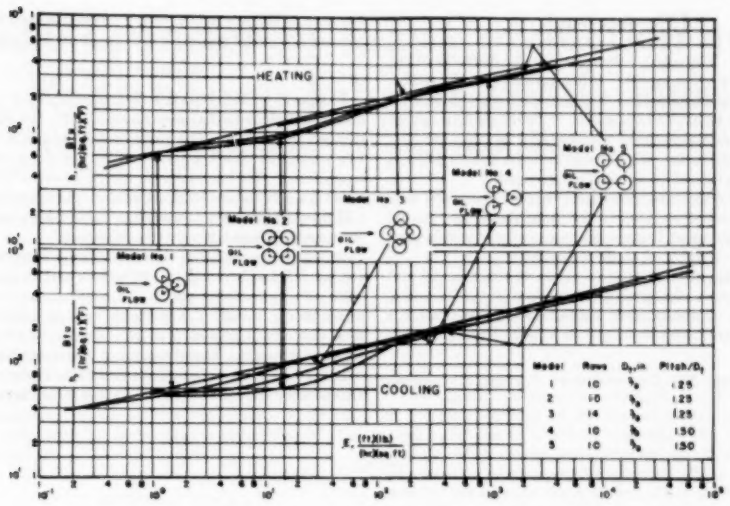

FIG. 9 COMPARISON OF HEAT-TRANSFER AND POWER REQUIREMENTS FOR FIVE TUBE BANKS
(Flow normal to vertical tubes. Gulf 806 oil at average bulk temperature of 150 deg F, viscosity 1.85 centipoises.)

The relationships between the heat-transfer coefficient and the power requirement for flow through the tube banks are shown in Fig. 9. The closely spaced tubes in staggered arrangements appear to be the most effective in the transition zone. Wider spacing in staggered arrangements appears to have an ill effect over the entire range of flow rates. In-line tube banks fall well below the staggered arrangements in the transition zone, but at higher flow rates the two types of arrangements with the same spacing appear to be about equal on this basis of comparison. An interesting difference between the two types of arrangements is that for the in-line tube banks an increase in tube spacing appears to improve the operation in the transition zone rather than to harm it. This improvement is not enough to bring the performance of widely spaced in-line arrangements up to that of the staggered arrangements.

CONCLUSIONS

1 Data not previously available are presented for pressure drop and heat transfer in the transition and turbulent-flow regions, and indicate the necessity of having experimental results, especially in the transition zone where tube arrangement plays an important and hitherto unpredicted role.

2 For staggered tube arrangements the change in pressure drop and heat transfer across the transition zone can be represented by curves which are without irregularities. On the other hand, in-line arrangements provide curves that have dips similar to those known for flow inside pipes. This difference in behavior is believed due to a difference in the mechanism of turbulence formation.

3 When the tube banks are compared on the basis of the heat-transfer coefficient for a given power loss, the staggered arrangements appear definitely superior in the transition zone. This superiority seems to disappear as full turbulence is reached throughout the tube bank.

It should be pointed out that these conclusions are based only upon crossflow experiments and may not be true for commercial baffled exchangers where the effects of varying cross section, leakages, nonuniform flow, and so on, may lead to far different results.

ACKNOWLEDGMENT

The authors acknowledge the many valuable suggestions by the Special Advisory Committee of the Heat Transfer Division, which is sponsoring this co-operative research project. The committee at the time of the work was composed of W. H. McAdams, Chairman, A. P. Colburn, S. Kopp, A. C. Mueller, B. E. Short, W. H. Thompson, T. Tinker, and P. R. Trumpler. The help of A. Wurster in the design and construction of the test unit was invaluable. Assistance in the experimental work was given by Research Fellows M. D. Marder and D. J. Newman. Funds and equipment were kindly furnished by the American Petroleum Institute, the Tubular Exchanger Manufacturers' Association, Andale Company, du Pont Company. The oil was provided by the Gulf Oil Corporation.

BIBLIOGRAPHY

1 "Friction Factors for Pipe Flow," by L. F. Moody, Trans. ASME, vol. 66, 1944, pp. 671–684.

2 "Heat Transfer and Fluid Friction During Viscous Flow Across Banks of Tubes," by G. A. Omohundro, O. P. Bergelin, and A. P. Colburn, Trans. ASME, vol. 71, 1949, pp. 27–34.

3 "A Study of Three Tube Arrangements in Unbaffled Tubular Heat Exchangers," by O. P. Bergelin, E. S. Davis, and H. L. Hull, Trans. ASME, vol. 71, 1949, pp. 369–374.

4 "Pressure Drop Across Tube Banks," by T. H. Chilton and R. P. Genereaux, Trans. AIChE, vol. 29, 1933, pp. 161–173.

5 "Correlation and Utilization of New Data on Flow Resistance and Heat Transfer for Cross Flow of Gases Over Tube Banks," by E. D. Grimison, Trans. ASME, vol. 59, 1937, pp. 583–594.

6 "Heat Transfer and Fluid Friction During Viscous Flow Across Banks of Tubes," by O. P. Bergelin, A. P. Colburn, and H. L. Hull, University of Delaware, Engineering Experiment Station Bulletin No. 2, 1950.

7 "Heat Transfer and Fluid Friction During Viscous Flow Across Banks of Tubes—III A Study of Tube Spacing and Tube Size," by O. P. Bergelin, G. A. Brown, H. L. Hull, and F. W. Sullivan, Trans. ASME, vol. 72, 1950, pp. 881–888.

Discussion

C. J. Wilson.[5] The tube pitches used for the diameter of the tube were excessive in the model. It is suggested that the recommendations of Standards of The Tubular Exchanger Manufacturers Association be used which states: "Tubes shall be spaced with a minimum center-to-center distance of 1.25 times the outside diameter of the tube. When tubes are on a square pitch, a minimum clearing lane of $^1/_4$ in. shall be provided."

In the test model the tubes are rigidly supported at both ends whereas in commercial exchangers the tube sheets are spaced from 10 to 20 ft apart with intermediate support plates that have clearance of from $^1/_{64}$ to $^1/_{32}$ in. on the diameter.

It is believed that the difference between the test model and commercial-size heat exchangers, as pointed out in the foregoing, are such that the combined effect would be to induce turbulent flow in the commercial-size exchanger at a lower Reynolds number than in the test model, owing to the less rigid structure of the commercial model and the relatively closer spacing of the tubes.

[5] Project Engineer, The Griscom-Russell Company, Massillon, Ohio.

Authors' Closure

In answer to Mr. Wilson's discussion, three of the five models tested had pitch-to-diameter ratios of 1.25, the minimum recommended by TEMA. The value of 1.50 was chosen for the other two models so that the effects of tube spacing could be greatly emphasized. Had a minimum clearing lane of $^1/_4$ in. been provided for the square-pitch models, a pitch-to-diameter ratio of 1.67 would have been necessary, a value more excessive than the values of 1.25 and 1.50 actually employed.

It is quite possible that the differences in structure between the test models and commercial equipment could lead to different results. It was pointed out in the conclusions of the paper that other effects in baffled exchangers, such as leakage and nonuniform flow, could invalidate to some extent the results from cross-flow experiments. Experiments are being continued at the University of Delaware laboratories to determine the relationship between "once-flow-through" and baffled exchangers.

Heat Transfer by Gas Conduction and Radiation in Fibrous Insulations

By J. D. VERSCHOOR[1] and PAUL GREEBLER,[2] MANVILLE, N. J.

Thermal conductivity measurements were made on samples of an experimental glass fibrous insulation ranging in density from 0.5 to 8.4 pcf. Tests were carried out at atmospheric pressure with four different gases in the insulation samples, and the thermal conductivity with air was studied over a pressure range of 1 micron to 760 mm of Hg. Gas conduction is the most important mechanism of heat transfer. A theory of gas conduction in fibrous insulations was developed, and agrees well with experimental results. Theoretical considerations of heat transfer by radiation were confirmed by the experimental thermal conductivity values at low pressures. Methods are discussed of producing considerable reduction in the thermal conductivity of fibrous insulations.

Nomenclature

The following nomenclature is used in the paper:

A = collision cross section, dimensionless
D = fiber diameter, micron
d = sample thickness, in.
f = fractional volume of insulation occupied by fibers, dimensionless
G_x = probability of an intermolecular collision in distance x, dimensionless
k = over-all thermal conductivity of fibrous insulation, Btu in./hr sq ft deg F
k_{cd} = thermal conductivity of gas within insulation, Btu in./hr sq ft deg F
k_{cv} = apparent thermal conductivity due to convection, Btu in./hr sq ft deg F
k_{rd} = apparent thermal conductivity due to radiation, Btu in./hr sq ft deg F
k_g = thermal conductivity of free gas, Btu in./hr sq ft deg F
k_s = thermal conductivity of solid conduction due to fiber contacts, Btu in./hr sq ft deg F
L_g = mean free path of gas molecules in a free gas, micron
L_f = mean free path at very low pressures for "molecule-fiber" collisions, micron
L = mean free path of gas molecules within a fibrous insulation, micron
n = summation index, dimensionless
P = pressure, mm Hg
Q_m = radiation power received by mean plane of insulation, Btu/hr sq ft
T_m = absolute mean temperature, deg R
t = temperature, deg F
Δt = temperature drop across insulation, deg F
x = random distance, micron
α = fraction of incident radiant energy absorbed by a fiber, dimensionless
Ψ_g = probability of intermolecular collision in distance x for a free gas, dimensionless
Ψ_f = probability of molecule-fiber collision in distance x at very low pressures, dimensionless
σ = Stefan-Boltzmann radiation constant, Btu/hr sq ft deg F^4

Introduction

The apparent thermal conductivity k, of a fibrous material can be expressed in terms of the apparent conductivities of a gas, usually air, and of the solid material. The term "apparent" is employed to denote that radiation and convection are being considered in addition to true conduction. If the gas separates the fibers so that they are not in direct contact, the heat transfer may be treated as though the volume fraction of fiber f was in series with the volume fraction of gas, $1 - f$; and the apparent thermal conductivity is calculated in a similar manner as the electrical counterpart of two conductances in series. When the volume fraction of fiber is small and the thermal conductivity of the fibers is large, compared with that of the enclosed gas, the following expression is obtained for the apparent thermal conductivity of the fibrous insulation

$$k = \frac{(k_{cd} + k_{cv} + k_{rd})}{1 - f} + k_s \quad \ldots\ldots\ldots\ldots [1]$$

where the term k_s has been added to take into consideration the small amount of heat transfer due to the irregular contacts between the fibers.

Air conduction and convection in a fibrous insulation become negligible at extremely low pressures. Measurements of thermal conductivity over a pressure range of 1 micron to 760 mm were made to separate these two mechanisms of heat transfer from radiation.

Experimental Apparatus and Techniques

The thermal conductivity apparatus used in the experimental portion of this investigation was a horizontal guarded hot plate (1)[3] contained in a vacuum chamber. The test assembly consisted of two identical insulation samples between two cold plates with the guarded hot plate between the samples. The chamber had the necessary pumps and controls to maintain pressures ranging from 1 micron mercury to atmospheric pressure. Fig. 1 gives an over-all view of the test apparatus.

The vacuum chamber used was a steel tank 3 ft diam × 2 ft high. The two halves of the tank were made vacuumtight by a rubber gasket. The chamber was evacuated by an oil-diffusion pump backed by two mechanical pumps. A solenoid-operated butterfly valve was placed in the vacuum line between the chamber and the pumps, to provide a positive means of regulating the pressure in the chamber.

Pressures below 1 mm mercury abs were measured with a McLeod gage equipped with a dry-ice and alcohol cold trap. Pressure control in this range was by a thermocouple vacuum gage.

[1] Physicist, Johns-Manville Research Center. Jun. ASME.
[2] Physicist, Johns-Manville Research Center.
Contributed by the Heat Transfer Division and presented at the Annual Meeting, Atlantic City, N. J., November 25–30, 1951, of The American Society of Mechanical Engineers.
Note: Statements and opinions advanced in papers are to be understood as individual expressions of their authors and not those of the Society. Manuscript received at ASME Headquarters, August 2, 1951. Paper 51—A-54.

[3] Numbers in parentheses refer to the Bibliography at the end of the paper.

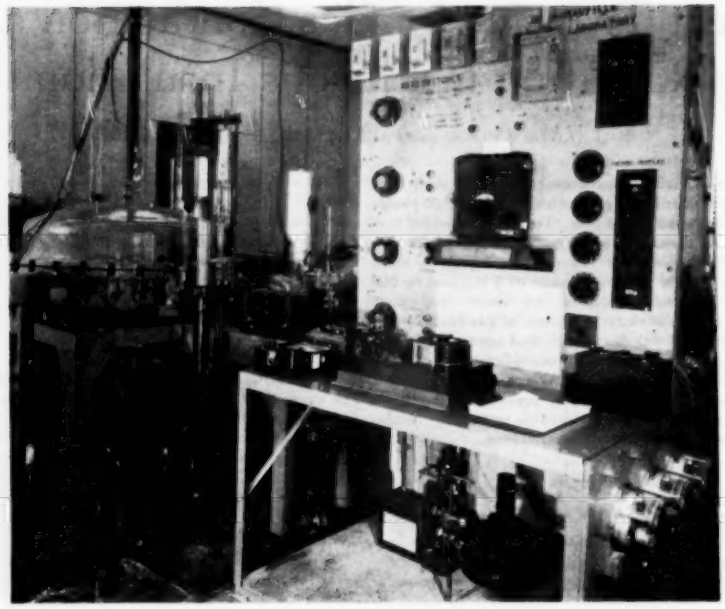

FIG. 1 VIEW OF LOW-PRESSURE THERMAL-CONDUCTIVITY APPARATUS SHOWING VACUUM CHAMBER AT LEFT, AND CONTROL PANEL AT RIGHT

The output voltage of the gage was fed into a conventional temperature controller which operated the solenoid vacuum valve. Above 1 mm a closed-tube mercury manometer was used to measure pressure. In this region very sensitive pressure control was achieved by a special contactor type of manometer filled with triethylene glycol. The glycol has a low vapor pressure and sufficient electrical conductance to operate a vacuum-tube relay.

The heater used in the guarded hot-plate assembly was circular, 10 in. diam with a 5-in-diam test section. A sample thickness of 1 in. was used in these tests. The faces of the heater were $^1/_8$-in-thick copper, with the test and guard sections separated by a $^1/_8$-in. air space. In addition to the test-section heater windings, the heater contained two sets of guard windings. The inner guard was in series electrically with the test-section heater. The outer guard was controlled separately by a temperature regulator which sensed the center-to-guard temperature difference by means of eight pairs of series-differential thermocouples. The cold plates were 12 in. diam and of brass. Water circulating through the cold plates was fed from a constant-head device through a thermostated water bath. Fig. 2 shows the inside of the vacuum chamber with the edge insulation removed from the hot plate.

The surface temperatures of the insulation samples were measured by copper-constantan thermocouples fastened to asbestos-paper thermocouple sheets with Scotch tape. Five symmetrically arranged couples connected in parallel were used to obtain a true average temperature of each face. The thermocouple voltages were measured with a precision potentiometer. Power for the heaters was obtained from a regulated a-c voltage source held to less than $^1/_4$ per cent fluctuation. Both power and thermocouple leads were brought into the vacuum chamber by Kovar seals.

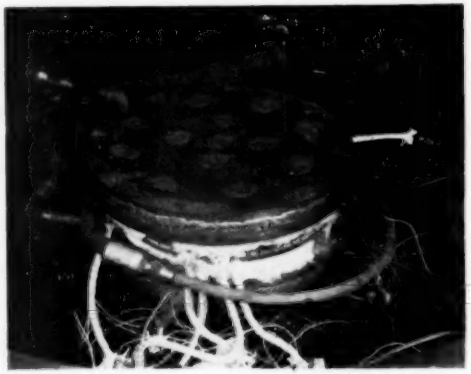

FIG. 2 GUARDED HOT-PLATE CONDUCTIVITY ASSEMBLY WITH EDGE INSULATION REMOVED

Most of the tests were conducted with the mean temperature at 150 F. The insulations of higher density were also tested at 300 F mean. During the tests the temperature of the cooling-water bath was adjusted to give an average temperature of 90 or 150 F at the two cold surfaces of the insulation samples. After the pressure control had been set to maintain the desired pressure, the power to the test-section heater was adjusted by a variable transformer so that the average hot-surface temperature was 210

or 450 F, and the mean temperature 150 or 300 F. During the tests the average deviation of the mean temperature was about $^1/_2$ F. Steady-state heat flow was deemed to have been reached when computed thermal-conductivity values over a 3-hr period varied less than 0.001 Btu in./sq ft hr deg F.

Thermal-conductivity determinations were also made at atmospheric pressure with gases other than air in the insulation. For these tests the chamber was first evacuated to a pressure of about 25 microns, and then refilled with the desired gas. Three determinations at mean temperatures of approximately 125, 150 and 175 F (90 F cold surface at all times) were made for each gas. A curve of conductivity versus mean temperature was drawn (a straight line in each case over the small temperature range investigated), and the conductivity at 150 F mean read off. A similar procedure was followed in the tests at 300 F mean.

The insulations tested were special glass fiber felts without binder. These insulations were selected because of their very low nonfibrous content. Most of the tests were run on an experimental glass fibrous insulation designated here as A, with additional measurements carried out on an insulation, designated as B, possessing fibers with somewhat different physical properties. Table 1 lists the fiber diameter and specific gravity of these fibers, and the insulation densities used in these experiments.

TABLE 1 INSULATION DATA

Insulation	Specific gravity of fiber	Average fiber diam D, microns	Insulation density, pcf	Volume fraction of fiber, f	Effective pore size L_f, microns
A.....	2.01	2.58	0.546	0.00436	465
A.....	2.01	2.58	1.50	0.0120	169
A.....	2.01	2.58	4.63	0.0369	54.8
A.....	2.01	2.58	8.35	0.0665	30.4
B.....	2.5	1.51	7.40	0.0474	25.0

Heat Conduction by a Gas in a Fibrous Insulation

Kinetic theory shows that the thermal conductivity of a gas is proportional to the mean free path of its constituent molecules, and to the gas density. A gas is defined as a free gas if the mean free path of its molecules is very small compared with the dimensions of the enclosure. As the gas pressure is lowered, the density decreases directly with pressure and the mean free path increases inversely with pressure. Since the thermal conductivity varies as the product of gas density and mean free path, this property is independent of pressure for a free gas.

Most fibrous insulations contain air as a free gas at atmospheric pressure, since the mean free path is small compared with the average fiber spacings. At very low pressures the mean free path of a free gas is much larger than the average fiber spacings. At such low pressures virtually all molecular paths are terminated by collisions with fibers, and so the fiber structure imposes an upper limit on the mean free path within the insulation. At intermediate pressures both intermolecular and molecule-fiber collision processes are taking place, and it will be shown that the latter collision mechanism reduces the mean free path of the gas molecules, thus reducing the thermal conductivity. Smoluchowski (2) suggested how this phenomenon might be used in fine powders to produce good insulators at moderately low pressures.

It is assumed here that the fibers lie in planes parallel to the mat which they form, but that they are otherwise randomly oriented. It is further assumed that the direction of heat flow is perpendicular to the planes in which the fibers lie, this assumption being consistent with many practical applications of fibrous insulations. Also it is assumed that the fibers are uniform in diameter, and that the insulation is free from nonfibrous solid particles.

Consider a thin volume element of the insulation of unit cross-sectional area and of thickness Δx, the x-direction being parallel to the temperature gradient and, therefore, perpendicular to the axes of the fibers. The volume of fiber in such an element is $f\,\Delta x$. Dividing this fiber volume by the cross-sectional area of a single fiber yields the total length of all fibers in the volume element, and this length multiplied by the diameter of a single fiber, D, gives as the total projected fiber area

$$A = \frac{4f\,\Delta x}{\pi D} \qquad [2]$$

Equation [2] expresses the fiber-collision cross section as viewed by a gas molecule moving in the direction of heat flow through a distance Δx. Since the volume element is of unit cross-sectional area, A is just the probability that a gas molecule will suffer a collision with a fiber in the path interval Δx. This collision probability, employed in the formal representation of collision probability developed from kinetic theory, yields the mean free path for molecule-fiber collisions at very low pressures. Kinetic theory of gases gives the following expression for the probability that a gas molecule, in a free gas, will collide with another molecule before moving a distance x

$$\Psi_g = 1 - e^{-x/L_g} \qquad [3]$$

where the mean free path L_g for a given gas is dependent on temperature and pressure. For air L_g is in microns (3)

$$L_g = \frac{81}{P} \text{ at } 150 \text{ F} \qquad [4]$$

$$L_g = \frac{101}{P} \text{ at } 300 \text{ F} \qquad [4a]$$

Entirely analogous with Equation [3] for a free gas, the following expression yields the probability that in a fibrous insulation at very low pressure a gas molecule will collide with a fiber before moving a distance x

$$\Psi_f = 1 - e^{-x/L_f} \qquad [5]$$

where L_f is the mean free path for such molecule-fiber collisions.

Equations [2] and [5] give the same collision probability if we set x equal to Δx in Equation [5]. Equating these expressions, and expanding the exponential in Equation [5], and retaining only first-power terms in Δx, yields as the mean free path at very low pressures for molecule-fiber collisions

$$L_f = 0.785\,\frac{D}{f} \qquad [6]$$

This quantity is of considerable importance in the theory of both air conduction and radiation in a fibrous insulation. L_f may be considered as an equivalent pore size of a fibrous insulation. It is readily computed from the fiber diameter, the density of the insulation, and the specific gravity of the fibers. Table 1 shows values of f and L_f computed for each of the insulation densities used in this investigation.

The probability that a random gas molecule will travel a distance x and then strike another molecule is obtained from Equations [3] and [5] as

$$G_x = (e^{-x/L_f})\,(e^{-x/L_g})\,(1 - e^{-dx/L_g}) = \left[e^{-x\left(\frac{1}{L_f} + \frac{1}{L_g}\right)}\right]\frac{dx}{L_g} \qquad [7]$$

where the first two terms in parentheses yield the probability that a collision does not occur with either a fiber or another molecule in the interval of length x, and the third term gives the probability that a collision does occur with another molecule in the subsequent infinitesimal distance dx. If we consider the

probability of an intermolecular collision for all values of x, we obtain as the mean free path for such collisions

$$L = \frac{\int_0^\infty \left[e^{-x\left(\frac{1}{L_f}+\frac{1}{L_g}\right)}\right]\frac{x\,dx}{L_g}}{\int_0^\infty \left[e^{-x\left(\frac{1}{L_f}+\frac{1}{L_g}\right)}\right]\frac{dx}{L_g}} = \frac{L_g L_f}{L_g + L_f} \quad [8]$$

Kistler (4) obtained this expression with a different mathematical approach for the mean free path of air molecules in silica aerogel, a material in which L_f is of the order of magnitude of L_g even at atmospheric pressure. Kistler employed experimental values of thermal conductivity of silica aerogel at low pressures to evaluate L_f as an effective pore size for this material.

To evaluate the mean free path for molecule-fiber collisions, the kinetic-theory formalism requires merely an interchange of L_f and L_g in Equations [7] and [8], and we get the identical expression L, for this mean free path. Thus L is the mean free path for all the gas molecules within a fibrous insulation. It is interesting to note from Equation [8] that L approaches L_g at higher pressures, where L_f is much larger than L_g, and L approaches L_f at low pressures, where L_f is much smaller than L_g.

Assuming that the random molecule-fiber collisions do not appreciably affect the molecular-velocity distribution (Maxwellian), then the thermal conductivity of the gas within the insulation k_{cd} is evaluated in the same manner as that of the free gas k_g except that we employ L as the mean free path in place of L_g. Thus we obtain

$$k_{cd} = k_g \frac{L_f}{L_f + L_g} \quad [9]$$

which for air in a fibrous insulation reduces to the following function of pressure, fiber diameter, and volume fraction of fiber, from Equations [4] and [6], at a mean temperature of 150 F

$$k_{cd} = 0.20 \frac{L_f}{L_f + \frac{81}{P}} = \frac{0.157\frac{DP}{f}}{81 + 0.785\frac{DP}{f}} \quad [10]$$

The solid curve in Fig. 3 shows experimental values of thermal conductivity k versus pressure for the type A insulation at 4.63 pcf density. As the pressure is lowered to a few microns, k approaches an asymptotic value of 0.016. This value represents the contribution to the thermal conductivity by radiation and solid conduction due to fiber contacts, these mechanisms remaining essentially invariant with respect to pressure changes. Adding 0.016 to the theoretical value of k_{cd} from Equation [10], and dividing the latter by the factor $(1 - f)$ in Equation [1] gives the dashed curve in Fig. 3. In the pressure range, where L_f and L_g are of comparable magnitude, k rises with increasing pressure. At still higher pressures, where L_g is very small compared with L_f, k again becomes independent of pressure since the air enclosed in the insulation is essentially free air. It is seen that the k-value of the experimental curve exceeds that of the theoretical curve throughout the pressure range where air conduction is important, and this difference in k is 0.02 at atmospheric pressure (the difference increases appreciably as fiber density decreases, as is shown by the k_{cv} values for air in Table 2). Since convection is the only mechanism of heat transfer omitted in the theoretical curve, the difference in k as between experimental and theoretical values, omitting convection considerations in the latter, was employed for several gases to measure convection in fibrous insulations.

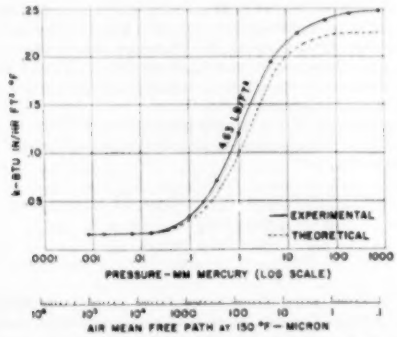

FIG. 3 THERMAL CONDUCTIVITY VERSUS AIR PRESSURE FOR 4.63-PCF TYPE A INSULATION AT 150 F MEAN TEMPERATURE
(Theoretical curve neglects contribution by air convection.)

Table 2 shows measured thermal conductivity values for the various densities of type A fiber insulation with the four gases, helium, air, carbon dioxide, and Freon-12. These measurements were made mostly at atmospheric pressure, with one set of experiments on the 1.5-pcf insulation being carried out also at 76 mm pressure. Comparison of these measured k-values with the corresponding k_{cd}-value for each of the gases, given in Table 2, shows that at atmospheric pressure gas conduction is by far the most important mechanism of heat transfer in fibrous insulations, even in the lowest of the insulation densities employed in these experiments. The contribution to the over-all thermal conductivity by radiation and solid conduction due to fiber contacts is given for each insulation density as the low-pressure asymptote of the k versus P curve in Fig. 4. Computed values of k_{cv} for each gas with the three lower insulation densities are also given in Table 2. It is seen that k_{cv} is dependent upon the insulation density and the gas enclosed by the insulation.

TABLE 2 THERMAL CONDUCTIVITY OF TYPE A FIBER INSULATION WITH DIFFERENT GASES

(150 F Mean Temperature, 120 F per Inch Temperature Gradient)

Gas	Insulation density, pcf	Pressure, mm of Hg	Thermal conductivity,[a] —Btu in./hr sq ft deg F— k	k_{cd} (5, 6, 9)	k_{cv}
Helium	0.546	760	1.415	1.124	0.158
Helium	1.50	760	1.336	1.123	0.144
Helium	1.50	76	1.310	1.102[b]	0.139
Helium	4.63	760	1.259	1.119	0.081
Air	0.546	760	0.395	0.203	0.063
Air	1.50	760	0.295	0.203	0.035
Air	1.50	76	0.293	0.202	0.034
Air	4.63	760	0.247	0.203	0.021
Carbon dioxide	0.546	760	0.326	0.136	0.061
Carbon dioxide	1.50	760	0.226	0.136	0.034
Carbon dioxide	1.50	76	0.226	0.136	0.034
Carbon dioxide	4.63	760	0.177	0.136	0.019
Freon-12	0.546	760	0.261	0.083	0.049
Freon-12	1.50	760	0.162	0.083	0.024
Freon-12	1.50	76	0.162	0.083	0.024
Freon-12	4.63	760	0.116	0.083	0.014

[a] The difference between the k-values listed and the sum of k_{cd} and k_{cv} is the contribution by radiation and solid conduction.

[b] For helium there is a noticeable difference, between k_{cd} and k_g at 76 mm pressure, and even some difference at atmospheric pressure, since the mean free path and the thermal conductivity of this gas are large.

HEAT TRANSFER BY RADIATION IN A FIBROUS INSULATION

The low-pressure asymptotes of the curves in Fig. 4 show that heat transfer by radiation is very small for the 4.6-pcf insulation density, but it becomes appreciable as the density is reduced to 0.5 pcf. Heat transfer by radiation can be treated by considering the fibrous insulation as successive plates of fiber perpendicular to the direction of heat flow. The average spacing between the plates is L_f, since this is the average distance that a photon of the

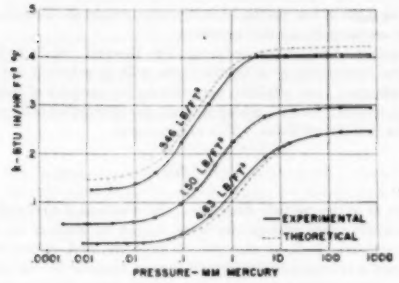

FIG. 4 THERMAL CONDUCTIVITY VERSUS AIR PRESSURE FOR THREE DENSITIES OF TYPE A INSULATION AT 150 F MEAN TEMPERATURE

radiation field can move in the direction of heat flow before encountering a fiber. The heat energy received by the mean plane, at an absolute temperature T_m, from all other planes closer to the hot-plate surface can be evaluated from the Stefan-Boltzmann radiation law. If α is the fraction of incident radiant energy absorbed by a single fiber plane (actually, by a single fiber), this heat energy is given in consistent units by the following series expression

$$Q_m = \sum_{n=1}^{\frac{d}{2L_f}} \sigma[(T_m + \frac{nL_f}{d}\Delta t)^4 - T_m^4](1-\alpha)^{n-1} \ldots [11]$$

Since $d/2L_f$, measured in consistent units, is very large, we may extend the upper limit of the series to infinity. If $L_f/d\ (\Delta t)$ is very small compared with T_m, which is the case for most practical applications of fibrous insulations, the solution of Equation [11] yields as a good approximation with L_f and d in consistent units

$$Q_m = \frac{4\sigma T_m^3 L_f \Delta t}{d\alpha^2} \ldots [12]$$

Division of Q_m by the temperature gradient, $\Delta t/d$, and conversion to our practical units, yields as the apparent thermal conductivity contributed by radiation

$$k_{r_m} = 2.74 \times 10^{-13} \frac{T_m^3 L_f}{\alpha^2} \ldots [13]$$

Transmission of infrared radiation in the 5-to-10 micron wavelength region by very thin samples of the fibrous insulations used in these tests was measured with a Perkin-Elmer infrared spectrometer. The opacity factor, $1/\alpha^2$, was integrated over the spectral distribution of radiant energy (Planck law); and the average value of $1/\alpha^2$ was thus obtained as a function of the mean temperature. (The details of this analysis are somewhat complex, and it is intended to give a complete description in a forthcoming paper.) For the type A insulation, $1/\alpha^2$ was found to be 5.1 at 150 F and 6.4 at 300 F; and for the B insulation, the corresponding values of $1/\alpha^2$ are 1.9 and 2.5, respectively.

CORRELATION OF THEORY WITH EXPERIMENT

In Fig. 4 experimental and theoretical curves of therma conductivity k are plotted against air pressure P at 150 F for three densities of type A insulation. Empirical values for k_{ce} at atmospheric pressure were taken from Table 2, and it was assumed in the theoretical curves that k_{cv} within the insulation varies with pressure in the same manner as k_{cd}, since free gas convection and gas conduction are closely related. Equations [10] and [13] were used to yield theoretical values for k_{cd} and k_{r_m}, and the $(1-f)$ factor in Equation [1] takes into consideration the contribution by series solid conduction. Solid conduction due to fiber contacts was neglected in plotting the theoretical curves. It is seen from Fig. 4 that good correlation exists between experimental k-values and the theoretical considerations of air conduction, radiation, and series solid conduction.

Fig. 5 shows theoretical curves of thermal conductivity versus air pressure for the type A insulation at 8.35 pcf, and B at 7.40 pcf density, and at 300 F mean. As in Fig. 4, the difference in

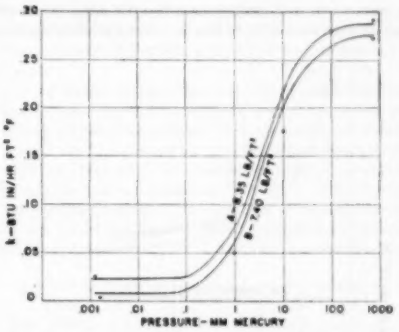

FIG. 5 THEORETICAL CURVES OF THERMAL CONDUCTIVITY VERSUS AIR PRESSURE FOR 8.35-PCF TYPE A INSULATION AND 7.40-PCF TYPE B INSULATION AT 300 F MEAN TEMPERATURE
(Heavy dots indicate experimental thermal-conductivity values.)

experimental k-values between very low pressure and atmospheric pressure, compared with the theoretical k_{cd}-value for air, was used to yield the correction factor for air convection. This factor is very small at these higher insulation densities. Two experimental thermal-conductivity values on the type B insulation, at 1 and 10 mm pressure, are seen in Fig. 5 to be in reasonably good agreement with the predicted values from the theoretical curve. Experimental data at these densities are given in Table 3.

TABLE 3 EXPERIMENTAL THERMAL CONDUCTIVITY AT HIGH DENSITIES

Insulation	Density, pcf	Pressure, mm of Hg	Mean temperature, deg F	Thermal conductivity, Btu in./sq ft hr deg F
A	8.35	760	150	0.236
A	8.35	0.00025	150	0.007
A	8.35	760	300	0.292
A	8.35	0.0012	300	0.024
B	7.40	760	150	0.222
B	7.40	760	300	0.272
B	7.40	10	300	0.176
B	7.40	1	300	0.049
B	7.40	0.002	300	0.004

At 150 F mean, the thermal conductivity of the 8.35-pcf type A insulation at very low pressure agrees well with Equation [13], the calculated k_{r_m}-value being 0.009 compared with the experimental value of 0.007. Since Equation [13] gives only the heat transfer by radiation, this close agreement indicates that, even at this higher density, conduction due to contact between fibers is negligible. At 150 F mean and atmospheric pressure, type B insulation possesses a slightly lower thermal conductivity than type A, owing to its finer pore size (smaller fiber diameter) and a greater opacity to infrared radiation. The effect of the latter factor is given greater emphasis in the thermal-conductivity values at 300 F mean at very low pressures. These values, listed in Table 3, show heat transfer by radiation in the type A insulation to be

about 6 times greater than that through type B at 300 F mean. However, k_{r_e} is only a small fraction of the total k at atmospheric pressure for both insulations.

Discussion

At the present time thermal conductivity of fibrous insulations with air at atmospheric pressure is of maximum practical interest. Fig. 6 is a plot of thermal conductivity at 150 F versus density of type A insulation over the density range studied. The contributions to the over-all thermal conductivity by air conduction, free convection, radiation, and series solid conduction are shown as separate curves in Fig. 6. Series solid conduction contributes a percentage of the total thermal conductivity equal to the volume fraction of fiber present, and this is rather small over the range of densities investigated. Solid conduction due to fiber contacts was found to contribute very little to the heat transfer in the fibrous insulations studied. It should be noted that these insulations did not contain a binder. In an insulation containing a binder, the contribution by fiber contacts to the heat transfer might be of significant magnitude. The presence of a binder might reduce heat transfer by radiation if it serves as an opacifying agent.

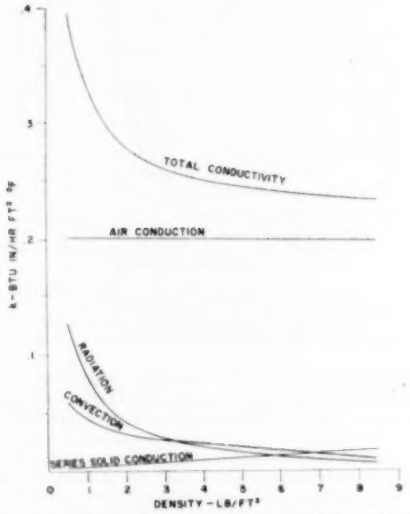

Fig. 6 Contribution by Each of Mechanisms of Heat Transfer in Type A Insulation at Atmospheric Pressure Versus Insulation Density at 150 F Mean Temperature

Fig. 4 shows that when L_g approaches the magnitude of L_f, thermal conductivity begins to drop, owing to the decrease in air conduction. If L_f, the effective pore size, is made sufficiently small, thermal conductivity will be reduced even at atmospheric pressure. L_f can be reduced by decreasing the fiber diameter, and by increasing insulation density (to the point where further increase of density gives diminishing returns due to increased solid conduction). For fibrous insulations used at present, L_f is much larger than L_g at atmospheric pressure. A very considerable reduction in thermal conductivity could be achieved by using a 0.01 micron fiber in a 10-pcf insulation (the k-value of the 8.35-pcf insulation used in this investigation could be reduced more than 50 per cent). Thermal conductivity also can be reduced by sealing a gas of low thermal conductivity within the insulation, or by evacuating the insulation system.

Another method for reducing the thermal conductivity of fibrous insulations is to fill the pores with powders of very fine particle size. An effective pore size L_f for particles of spherical shape is easily derived analogous with the derivation of Equation [6] for cylindrical fibers. This expression is

$$L_f = 0.667 \frac{D}{f} \quad \ldots\ldots [14]$$

where D is the particle diameter. By choosing a material with sufficiently small particle diameter, L_f can be made of the order of magnitude of L_g at atmospheric pressure, and, consequently, produce a considerable reduction in heat transfer by air conduction. Since such a powder will produce some increase in solid conduction, there is an optimum value of f for any given powder.

Thermal conductivity measurements were made on very fine carbon-black powders. A carbon black with an ultimate particle size of 0.010 micron, tested at a density of 4.5 pcf, gave a k-value of 0.17 at 300 F mean. The thermal conductivity of still air (5) at this temperature is 0.25. Another carbon black with an ultimate particle size of 0.018 micron showed a k-value of 0.20 at 8.1 pcf density. These values are in good qualitative agreement with Equation [6] or [14]. A quantitative correlation of the experimental results with these equations would require low-pressure thermal-conductivity measurements to determine the effects of solid conduction and radiation. Such measurements have not yet been carried out. Smith and Wilkes (8) measured the thermal conductivity of several carbon blacks at lower temperatures, and also obtained k-values less than that of still air.

Several investigators have measured thermal conductivity of powders as a function of pressure (4, 7). It has been known for quite some time that the reduction in gas conduction depends upon the effective pore size of the insulation. The effective pore size L_f has been derived in this paper in terms of the insulation density and the diameter of the fibers or particles of the insulation, and it has been correlated with experimental thermal-conductivity measurements. The possibility of using fine powders to fill the pore spaces and reduce the thermal conductivity of insulating materials below that of still air has been considered previously; but it has received little more than academic interest because of the effect of agglomeration and the difficulty in filling the pore spaces of a practical insulation homogenously (7). However, the results of measurements on carbon blacks and other materials show that these difficulties are not insurmountable.

Equation [13] shows the importance of α, the opacity of the fiber to infrared radiation, in determining the amount of heat transfer by radiation. This factor becomes particularly important at higher temperatures (300 F and above), where radiation is an appreciable factor in the over-all heat transfer for practical insulation densities. In fact, it is the radiation component of heat transfer that accounts almost entirely for the difference in k as between the type A and B insulations. Most common glasses undergo a sharp transition from almost total transparency to total opacity in the 5 to 10-micron infrared region, depending upon the chemical composition and glass film thickness. Since this is the important region of the radiation spectrum for the temperature range we are considering, the glass fibers may be opacified by variations in chemical composition that will shift to a lower wave length the transition from transparency to opacity.

Further experimental and theoretical work is needed to complete a study of free convection and radiation in fibrous insulations over a wide temperature range. The use of the infrared spectrometer in radiation studies is very promising. A more re-

fined theory of gas conduction within a fibrous insulation can be developed, taking into detailed consideration the contribution by nonviscous gas flow at low pressures and integrating over the fiber diameter distribution. However, the theory of gas conduction developed here is sufficiently accurate for practical considerations. Further work along these lines is now being carried out for fibrous, as well as nonfibrous, thermal insulations.

ACKNOWLEDGMENTS

The authors are indebted to the following and other members of the Johns-Manville Research Center for advice and technical assistance given to this investigation: Messrs. C. B. Bradley, H. T. Coss, B. S. Miller, W. F. Gulick, and J. Russo.

BIBLIOGRAPHY

1 "Thermal Conductivity—Guarded Hot Plate Method," ASTM, C-177-45.

2 "Euber den wärme leitwert des pulverförmigen Körper," by M. Smoluchowski, *Krakauer Anzeiger* (A), 1910, pp. 129–153; and Report About the Second International Congress on Heat, vol. 2, 1910, p. 166.

3 "Handbook of Chemistry and Physics," Chemical Rubber Publishing Company, Cleveland, Ohio, thirtieth edition, 1947, p. 2627; Molecular Constants, Mean Free Path (Boltzmann).

4 "The Relation Between Heat Conductivity and Structure in Silica Aerogel," by S. S. Kistler, *Journal of Physical Chemistry*, vol. 39, 1935, p. 79.

5 "A Summary of Viscosity and Heat-Conduction Data for He, A, H_2, O_2, N_2, CO, CO_2, H_2O, and Air," by F. G. Keyes, Trans. ASME, vol. 73, 1951, p. 589.

6 "Chemical Engineers' Handbook," by J. H. Perry, editor-in-chief, McGraw-Hill Book Company, Inc., New York, N. Y., third edition, 1950, p. 461.

7 "Heat Transfer," by Max Jakob, John Wiley & Sons, Inc., New York, N. Y., 1949, p. 91.

8 "Thermal Conductivity of Carbon Blacks," by W. R. Smith and G. B. Wilkes, *Industrial and Engineering Chemistry*, vol. 36, 1944, p. 1111.

9 "The NBS-NACA Tables of Thermal Properties of Gases," compiled by R. L. Nuttall at National Bureau of Standards, December, 1950.

Discussion

E. A. ALLCUT.[4] The relative importances of conduction, convection, and radiation and of the structure of insulating materials on the "conductivity" k finally obtained, has intrigued the writer for many years. The first serious approach to the subject was made by him in 1941,[5] but on account of war conditions the problem had to be shelved for several years. Another paper was read on the subject[6] recently, and the comparison between the various results obtained on glass wool may be of some interest.

The glass wool used by the authors had an average fiber diameter of 2.58 microns, while that used in the earlier Toronto experiments (1941) had the following dimensions: mode 5.5 microns; median 7.8 microns. The density of packing in each case was approximately 1.5 pcf, and the values of k were, in the authors' experiments, 0.29 and in the Toronto experiments, 0.27. It would appear, therefore, that the difference in average fiber diameter did not affect the results unduly. It should be noted, also, that the limits of fiber diameter in the Toronto experiments were from 4.2 to 17.2 microns, but no similar analysis is given by the authors for the material tested by them. With such a wide variation it would appear that the term "average fiber size" does not mean very much. It is interesting also to note that in the 1941 Toronto experiments the solid matter occupied 1 per cent of the total volume, as compared with 1.2 per cent in the authors' experiments. These figures, therefore, would seem to be fairly representative for the material in question.

A comparison between the Toronto tests (1950) and those described by the authors in connection with radiation is also of interest. The authors state that "heat transfer by radiation is very small for the 4.6 pcf insulation density but becomes appreciable as the density is reduced to 0.5 pcf." This may be compared with the statement made in the Toronto paper,[6] "Also, in the case of blankets of glass wool exceeding 2.0 lb per cu ft in density, the radiation effect appears to be negligible. . . . At 1.25 lb density the loss is about 11 per cent and at 1.75 lb it is approximately 2 per cent."

The agreement between the two sets of results on the loss of of heat by convection is also rather remarkable, particularly when it is realized that the authors' tests were made on circular specimens 10 in. in diam, placed horizontally, with a mean temperature of 150 F, and that the Toronto tests were made on specimens 8 in. square with a mean temperature of 90 F, with the specimen in the vertical position. The thickness of the specimens in both cases was 1 in., but different methods were used for estimating the influence of convection. Fig. 7, herewith, is a reproduction of Fig.

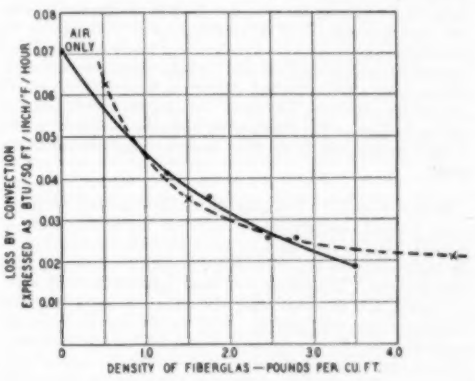

FIG. 7

8 of the Toronto paper[6] and, superimposed on the original curve, are points taken from the authors' Table 2. These are indicated by crosses and are connected by a dotted curve. The difference between them is practically negligible. In both sets of results, with an atmospheric pressure of 760 mm Hg and a material density of 1.5 pcf, convection accounted for 11 to 12 per cent of the total heat transmitted.

The influence on the results, of using different gases in place of air, to fill the voids in the material (Table 2 of the paper) is very interesting. This technique could be carried further advantageously. It must be realized, however, that in both sets of experiments the results obtained apply only to small and comparatively thin specimens. The next step evidently is to find out what happens when large and thick specimens are employed. The difficulties of applying similar techniques in these circumstances are obvious. It is somewhat surprising that the authors were able to maintain a vacuum of 1 micron of mercury in this apparatus. The writer was unable to approach this figure in his own experiments on account of the difficulty of maintaining tight joints at

[4] Professor and Head of the Department of Mechanical Engineering, University of Toronto, Toronto, Canada. Mem. ASME.

[5] "Properties of Heat Insulating Materials," by E. A. Allcut, *Engineering Journal*, vol. 24, 1941, pp. 514–520.

[6] "An Analysis of Heat Transfer Through Thermal Insulating Materials," General Discussion on Heat Transfer, London, England, September, 1951.

the points where the liquid and wiring connections passed through the walls of the vacuum chamber.

C. B. Bradley.[7] This paper is the culmination of a great deal of intensive work by the two authors. Also it is the realization of plans made by the Research Center more than 10 years ago. As long ago as 1947, in discussing a paper on low-temperature thermal-conductivity tests before the American Society of Refrigeration Engineers, the writer mentioned our plans for studying the influence of the various modes of heat transfer on the apparent conductivity of insulating materials. Pressure of other duties and the difficulty of finding qualified men to do the work delayed the project until we were able to permit the authors to devote a considerable amount of their time to it. We of Johns-Manville are proud of the job they have done.

The authors have not discussed to any great extent the identity of the glass-wool samples used in the investigation. It should be pointed out that these were not commercial insulations, but experimental wools, prepared by our Mineral Wool Development Section and having the physical characteristics which made them suitable for this use.

In the writer's opinion the result of this research, which will be of greatest interest to the practical insulation man, is the predominant influence of gas conduction on the conductivity of fibrous and porous insulations. The reduction of thermal conductivity by making the mean free path of the gas molecules of the order of magnitude of the confining spaces is not new as the authors have indicated;[8] nevertheless, most people concerned with thermal insulations have assumed that gas conduction was negligible and that solid conduction, convection, and radiation were the predominant modes of heat flow. Bringing the true function of gas conduction to the attention of insulation people is, in the writer's opinion, one of the most useful accomplishments of this paper.

Hyman Marcus.[9] The guarded hot-plate method for measuring over-all conductance or apparent conductivity of insulating felts has been used for some time—never, however, to distinguish between the effects of gas pressure, bulk density, and fiber diameter. The influence of these variables on conduction, convection, and radiation while also known for some time, has been known only qualitatively. Now the quantitative treatment by the authors affords a means of varying intelligently such properties as bulk density and fiber diameter to achieve a given heat-transfer coefficient with greater expectation for success. This should be of prime interest to insulation manufacturers.

It has been demonstrated that reduction of the over-all conductance can be achieved by reducing L_f, the mean free path for molecule-fiber collision and that this, in turn, can be effected by decreasing simultaneously the fiber diameter and increasing the the insulation density. It might be pointed out that L_f can be reduced by decreasing the fiber diameter without increasing the insulation density. Reduction of the fiber diameter and increasing the number of fibers will lower L_f without necessarily raising the bulk density. Of course, increasing the number of fibers to the point where the density is increased, substantially cuts down the value of L_f.

The pore size or volume of voids is particularly important at elevated temperatures where radiation streaming becomes a significant factor. For a given opacity the apparent conductivity contributed by radiation is directly proportional to L_f. It becomes important, then, to a manufacturer of high-temperature insulation, to determine just what the optimum pore size is from the standpoint of radiation versus conduction and convection, and the relation of all these to weight, density, and economy.

The authors are to be commended for their fine work, but one statement in their paper might well bear further emphasis. They mention the need for additional study. Operating temperatures for various types and pieces of equipment are being pushed upward continually. This has been made possible by the development of new, refractory, lightweight felts embodying glass and other ceramic fibers. The imposition of 1000 deg F temperature differentials across $^1/_2$-in. layers of insulation is becoming commonplace; however, the choice of insulation densities and weights is still almost altogether arbitrary. This endangers the choice of safety factors to the point where they can become entirely meaningless and cause a designer to wonder whether he is being ridiculously cautious or designing for dangerously marginal conditions. The authors have explained how real insulation behaves at conventional temperatures. It is urgent that this same type of approach be applied to the more extreme temperatures encountered today.

Authors' Closure

Professor Allcut has presented an interesting comparison between the tests made at Toronto and our experiments. The observed excellent agreement, in so far as convection is concerned, is likely fortuitous. In our experiments heat loss by air convection was taken as the difference between the observed total heat loss and the calculated heat loss due to the other mechanisms of heat transfer. This quantity was generally quite small, so that a slight error in the observed total conductivity would greatly affect the computed air convection. The average fiber diameter used was an arithmetic mean based on 100 microscopic measurements. As Professor Allcut has pointed out, "average fiber size" is not a very significant term for an insulation possessing a very wide dispersion of fiber diameters. For such insulations the effective fiber diameter D is the ratio of the mean square diameter to the mean diameter. This effective diameter is always larger than the arithmetic mean diameter and gives a truer value of the effective pore size L_f.

Mr. Marcus has emphasized the need for further work in analyzing the mechanisms of heat transfer at high temperature, particularly radiation. We are currently carrying on the infrared transmission measurements on various materials at shorter wave lengths, which correspond with higher temperatures.

[7] Research Physicist, Physics Section, Johns-Manville Research Center, Manville, N. J. Mem. ASME.
[8] Authors' Bibliography (2, 4).
[9] Dayton, Ohio.

A Method of Correlating Heat-Transfer Data for Surface Boiling of Liquids

By W. M. ROHSENOW,[1] CAMBRIDGE, MASS.

A method based on a logical explanation of the mechanism of heat transfer associated with the boiling process is presented for correlating heat-transfer data for nucleate boiling of liquids for the case of pool boiling. The suggested relation is

$$\frac{c_l T_x}{h_{lg}} = C_{sf}\left(\frac{q/A}{\mu_l h_{lg}}\sqrt{\frac{(q/A)\sigma}{g(\rho_l-\rho_v)}}\right)^{0.33}\left(\frac{c_l\mu_l}{k_l}\right)^{1.7}$$

where the various fluid properties are evaluated at the saturation temperature corresponding to the local pressure and C_{sf} is a function of the particular heating surface-fluid combination.

Nomenclature

The following nomenclature is used in the paper:

C_s, C_{ls}, C_w, C_g = coefficients in Equations [3], [4], [5], [9], [7], respectively
C_{sf} = coefficient of Equation [14], which depends upon nature of heating surface-fluid combination
D_b = diameter of bubble as it leaves heating surface, ft
G_b = mass velocity of bubbles at their departure from heating surface, $lb_m/hr\ ft^2$
$N_{Nu,b}$ = bubble Nusselt number, defined by Equations [8] and [9]
N_{Pr} = Prandtl number $= c_l\mu_l/k_l$
$N_{Re,b}$ = bubble Reynolds number, defined by Equations [1] and [7]
T_x = heating surface temperature minus saturation temperature, deg F
c_l = specific heat of saturated liquid, $Btu/lb_m F$
f = frequency of bubble formation, 1/hr
g = acceleration of gravity
g_c = conversion factor, 4.17×10^8 (lb mass) (ft)/(hr²) (pounds force)
h_{lg} = latent heat of evaporation, Btu/lb_m
$h_x = q/A \div T_x$, film coefficient of heat transfer, $Btu/hr\ ft^2\ deg\ F$
k_l = thermal conductivity of saturated liquid, Btu/hr ft deg F
n = number of points of origin of bubble columns per sq ft of heating surface
$(q/A)_b$ = heat-transfer rate to bubble per unit heating surface area while bubble remains attached to surface, $Btu/hr\ ft^2$
q/A = heat-transfer rate per unit heating surface area, $Btu/hr\ ft^2$
β = bubble contact angle, defined in Fig. 3
σ, σ_{lv} = surface tension of liquid-vapor interface, lb/ft
σ_{vs} = surface tension of vapor-solid interface, lb/ft
σ_{sl} = surface tension of solid-liquid interface, lb/ft
ρ_l = density of saturated liquid lb_m/ft^3
ρ_v = density of saturated vapor lb_m/ft^3
μ_l = viscosity of saturated liquid, $lb_m/ft\ hr$

Introduction

Heat-transfer data for forced-convection flow without boiling are correlated by the normal Nusselt number, Reynolds number based on pipe diameter, and Prandtl number. For pool boiling with essentially saturated liquids, Jakob (1)[2] shows that the heat transfer from the surface is for the most part transferred directly to the liquid, the increased heat-transfer rate associated with boiling being accounted for by the resulting agitation of the fluid by motion of the liquid flowing behind the wake of the bubble departing from the surface. Rohsenow and Clark (2) showed a similar result in studying motion pictures by McAdams (3) for subcooled liquids flowing in forced convection with surface boiling but no net generation of vapor. Gunther and Kreith (4) and Gunther (5) presented photographic evidence that in highly subcooled liquids in pool boiling and in forced convection with surface boiling, the bubbles could form at the surface, grow, and then collapse while remaining attached to the surface. Nevertheless, the increased heat transfer in boiling was attributed to the agitation of the liquid by the bubble motion.

As the rate of heat transfer is increased and bubble agitation becomes more vigorous, the effect of forced-convection fluid velocity and hence Reynolds number based on pipe diameter becomes less and less. This effect is shown by the data of Rohsenow and Clark (6) reproduced here in Figs. 1 and 2. These data are representative of data of others for surface boiling with forced convection. In these figures the curves for various fluid velocities are seen to merge into one curve, showing that as the boiling becomes more vigorous, the effect of fluid velocity disappears. It seems reasonable then to seek a correlation of the heat-transfer data by means of a bubble Reynolds number based on bubble diameter and velocity.

For purposes of analysis one can visualize a number of streams of bubbles receding from the heating surface and a bubble Reynolds number defined by

$$N_{Re,b} \equiv \frac{G_b D_b}{\mu_l} \qquad [1]$$

based on the mass velocity of the bubbles and their diameter as they leave the surface. This quantity is a measure of the local agitation of the fluid at the heating surface and hence is analogous to the ordinary pipe Reynolds number which is a measure of the turbulence in the stream.

To evaluate the bubble Reynolds number, characteristics of bubbles in pool boiling will be employed since there is more detailed visual evidence available for this case than there is for

---

[1] Associate Professor of Mechanical Engineering, Massachusetts Institute of Technology. Jun. ASME.

Contributed by the Heat Transfer Division and presented at the Annual Meeting, Atlantic City, N. J., November 25–30, 1951, of The American Society of Mechanical Engineers.

Note: Statements and opinions advanced in papers are to be understood as individual expressions of their authors and not those of the Society. Manuscript received at ASME Headquarters, August 29, 1951. Paper No. 51—A-110.

[2] Numbers in parentheses refer to the Bibliography at the end of the paper.

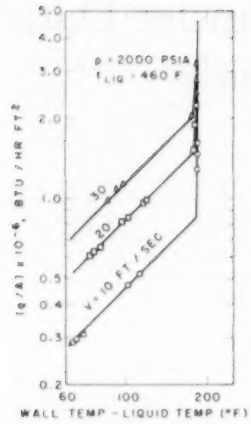

FIG. 1 EFFECT OF FLUID VELOCITY ON HEAT-TRANSFER RATE IN NUCLEATE BOILING
(Data of Rohsenow an reference 6.

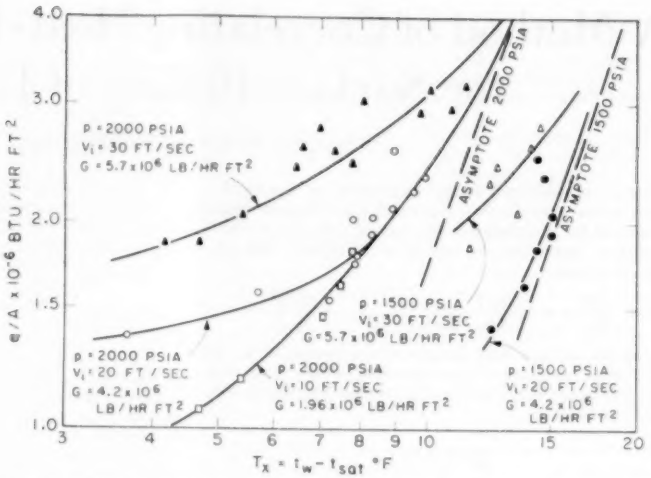

FIG. 2 EFFECT OF FLUID VELOCITY ON HEAT-TRANSFER RATE IN NUCLEATE BOILING
(Data of Rohsenow and Clark, reference 6.)

forced-convection surface boiling. Results of these bubble characteristics are compiled by Jakob (1). The heat transfer to the bubbles while attached to the surface can be written with good approximation (2) as

$$\left(\frac{q}{A}\right)_b = h_{lg}\rho_v n \frac{\pi}{6} D_b^3 f \quad \ldots\ldots [2]$$

Fritz (8) presents a relation for the diameter of the bubble as it leaves the surface, which may be written in the form

$$D_b = C_d \beta \sqrt{\frac{2g_c\sigma}{g(\rho_l - \rho_v)}} \quad \ldots\ldots [3]$$

where β is the angle of contact of the bubble as shown in Fig. 3. Jakob (9) has shown for vapor bubbles of water and of carbon tetrachloride a relation exists between the frequency of bubble formation at a favored point on the surface and the diameter of the bubble when it leaves the surface. This relation can be approximated by the equation

$$f D_b = C_{fd}, \text{ const} \quad \ldots\ldots [4]$$

without serious error.

Inspection of the terms of Equation [2] in the light of Equations [3] and [4] shows that $(q/A)_b$ is proportional to n for a given operating pressure, since all other quantities are functions of saturation pressure alone or are constant. Experiments have shown that bubbles form at selective points on a surface, forming swaying columns of bubbles. Jakob (7) found that the number of columns or points of origin of bubbles was very nearly directly proportional to the rate of heat transfer from the heating surface for a given operating pressure. Therefore $q/A \sim (q/A)_b$ and can be written as

$$\frac{q}{A} = C_q h_{lg}\rho_v n \frac{\pi}{6} D_b^3 f \quad \ldots\ldots [5]$$

where C_q may be a function of pressure.

The mass velocity of the vapor bubbles leaving the surface may be written as

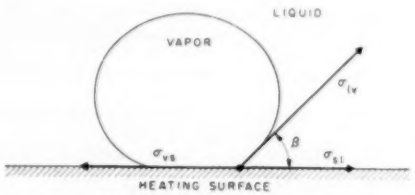

FIG. 3 SURFACE-TENSION FORCES ACTING AT POINT OF BUBBLE CONTACT

$$G_b = \frac{\pi}{6} D_b^3 f \rho_v n \quad \ldots\ldots [6]$$

Equations [3], [5], and [6] may be substituted into Equation [1] to obtain an expression for the bubble Reynolds number as

$$N_{Re,b} = C_R \beta \frac{q/A}{\mu_l h_{lg}} \sqrt{\frac{g_c\sigma}{g(\rho_l - \rho_v)}} \quad \ldots\ldots [7]$$

where D_b, G_b, and n have been eliminated, and $C_R = \sqrt{2}\, C_d/C_q$. The term $[(q/A)/\mu_l h_{lg}]\ [g_c\sigma/g(\rho_l - \rho_v)]^{1/2}$ is dimensionless and β has as units radians of angle, which are dimensionless.

In applying this reasoning to attempt to correlate heat-transfer data in the boiling regime it would seem that a bubble Nusselt number would be useful, defined as

$$N_{Nu,b} = \frac{hD_b}{k_l} \quad \ldots\ldots [8]$$

This quantity has been defined and utilized by Jakob (1, 16). Substituting Equation [3] into Equation [8] results in

$$N_{Nu,b} = C_n \beta \frac{h}{k_l} \sqrt{\frac{g_c\sigma}{g(\rho_l - \rho_v)}} \quad \ldots\ldots [9]$$

where $C_n = \sqrt{2}\, C_d$. Here, too, the term $(h/k_l)\ [g_c\sigma/g(\rho_l - \rho_v)]^{1/2}$ is dimensionless.

Since the postulated mechanism of heat transfer indicates that most of the heat transfer goes directly from the wall to the liquid, and since the Prandtl number is significant in relations for heat transfer to a nonboiling fluid, it probably should be included in the correlation for heat transfer to a boiling fluid. Then the correlation suggested is

$$N_{Re,b} = \phi_1(N_{Re,b}, N_{Pr}) \quad [10]$$

where c_l, μ_l, k_l, σ, ρ_l, ρ_v are all evaluated at the saturation temperature corresponding to the local pressure. The foregoing relation applies to the region of vigorous boiling where the fluid velocity or pipe Reynolds number does not influence the heat-transfer rate. It would also apply to the case of pool boiling. In the case of surface boiling with forced convection and not very vigorous boiling where the fluid velocity does influence the heat-transfer rate, some form of a pipe Reynolds number might be added to the right side of Equation [10]. There is some doubt that the ordinary pipe Reynolds number would be significant because the motion of the bubbles might tend to destroy the normal relationship between viscous and inertia forces.

Contact Angle β. The bubble contact angle β, shown in Fig. 3, is determined by the values of σ_{sl}, σ_{lv}, and σ_{vs}; hence it is determined both by the kind of fluid and the kind of heating surface. All of the other properties in the expressions for bubble Reynolds number and bubble Nusselt numbers are functions of the fluid alone. The angle β from Fig. 3 is seen to be related to the various surface tensions by the relation

$$\cos\beta = \frac{\sigma_{sl} - \sigma_{vs}}{\sigma_{lv}} \quad [11]$$

For lack of available information the effect of pressure on β was disregarded in applying Equation [10] to existing data. This assumption is equivalent to assuming that the effect of pressure on the values of σ_{lv}, σ_{sl}, and σ_{vs} of Fig. 3 is such that the angle β remains independent of pressure. In applying Equation [10] to the correlation of experimental data the terms C_{sl}, C_s, and β will be omitted.

Effect of Liquid Subcooling. In pool boiling the primary region of interest is the case in which the liquid temperature is essentially at the saturation temperature. However, in forced convection with surface boiling the liquid temperature may be greatly subcooled. It has been shown by many experimenters that the effect of subcooling of the liquid may be eliminated if the data are plotted as q/A versus T_x as shown in Figs. 1 and 2. Hence, defining the film coefficient in the bubble Nusselt number as $h_x = (q/A) \div T_x$ eliminates the necessity of including liquid subcooling as a variable in a correlation.

Other Forms of Proposed Correlation Equation

Since both the bubble Reynolds number and the bubble Nusselt number embody a (q/A)-term, it will be desirable to employ the term

$$\frac{N_{Re,b}\, N_{Pr}}{N_{Nu,b}} = \frac{c_l T_x}{h_{lg}} \quad [12]$$

This dimensionless group is the ratio of liquid superheat enthalpy at the surface temperature to the latent enthalpy of evaporation.

Equation [10] may be replaced by

$$N_{Re,b} = \phi_2\left(\frac{c_l T_x}{h_{lg}}, N_{Pr}\right) \quad [13]$$

Correlation of Experimental Data

Pool Boiling. The proposed correlation Equation [13] has been applied to the data of various experimenters. It will be of interest to observe in some detail its application to the data of Addoms (10) for pool boiling of water because of the wide range of pressures covered—14.7 psia to 2465 psia. In these experiments, degassed distilled water was boiled by an electrically

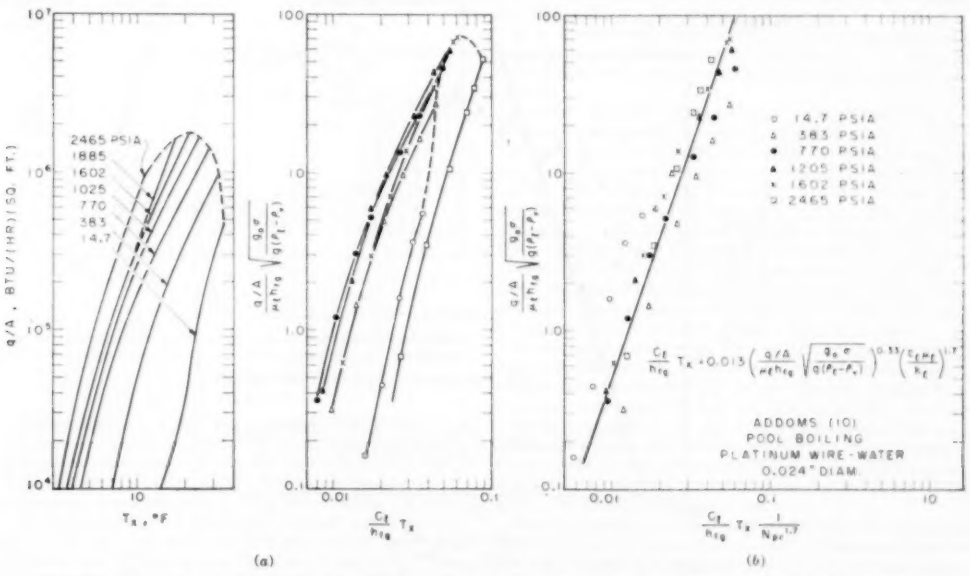

Fig. 4 Correlation of Data of Addoms, Reference 10, for Platinum-Water Interface for Pool Boiling

heated horizontal platinum wire. Data for a wire diameter of 0.024 in. are shown in Fig. 4(*a*). A plot of

$$[(q/A)/\mu_l h_{fg}]\ [g_c\sigma/g(\rho_l - \rho_v)]^{1/2} \text{ versus } c_l T_x/h_{fg}$$

is shown in Fig. 4(*b*). On this plot the position of the lines rises to a maximum with pressure and then falls again. At the pressure corresponding to the highest line on this plot, the Prandtl number is very nearly at its minimum value according to the data tabulated by Wellman (11). Values of surface tension for water were obtained from the International Critical Tables and were found at the higher temperatures by interpolating linearly between the value at 100 C and a value of zero at the critical temperature. Hence this effect appears to be a Prandtl-number effect, which was anticipated in the analysis. A cross-plot of $c_l T_x/h_{fg}$ versus N_{Pr} for constant values of bubble Reynolds number shows the slope of the line on a log-log plot to be approximately 1.7; hence the final correlation as shown in Fig. 4(*c*) results in an equation of the form

$$\frac{c_l T_x}{h_{fg}} = C_{sf}\left(\frac{q/A}{\mu_l h_{fg}}\sqrt{\frac{g_c\sigma}{g(\rho_l - \rho_v)}}\right)^{0.33}\left(\frac{c_l\mu_l}{k_l}\right)^{1.7} \quad \ldots\ldots [14]$$

where the value of C_{sf} is 0.013 with a spread of data of approximately ±20 per cent.

This process was repeated for some of the data of Cichelli and Bonilla (12) who boiled various fluids on a polished chromium-plated, horizontal plate which was electrically heated. The results of the proposed correlation are shown in Figs. 5 through 7. In each case the resulting equations are of the form of Equation [14]. Only the data for single component fluids on clean surfaces were correlated.

The data of Cryder and Finalborgo (15) are shown correlated in Fig. 8. In every case the correlation Equation [14] was applied and the resulting values of C_{sf} are listed in Table 1.

Forced Convection With Surface Boiling. In order to show the effect of forced-convection flow on the boiling process, plots of

$$N_{Re,b} \text{ versus } (C_l T_x/h_{fg})N_{Pr}^{1.7}$$

were made for the surface-boiling data of Rohsenow and Clark (6, 13) for degassed distilled water flowing in a vertical nickel tube 0.180 in. diam 9.4 in. long, and for the data of Kreith and Summerfield (14) for degassed distilled water flowing in a stainless-steel tube 0.587 in. diam 17.5 in. long. Superimposed on these plots, Figs. 9 and 10, is the correlation line for the pooling boiling data for water from Fig. 4(*c*).

Lines of constant forced-convection velocity and pressure are seen to merge toward a single line which probably would be parallel to this line for pool boiling from Fig. 4(*c*). When the boiling becomes more vigorous at the higher values of T_x, the effect of forced-convection fluid velocity apparently disappears. In this region the motion of the bubbles seems to control the mechanism of heat transfer due to fluid agitation.

TABLE 1 VALUES OF C_{sf}

Reference	Fluid-heating surface	C_{sf}
Addoms (10)	Water—platinum	0.013
Cichelli-Bonilla (12)	Benzene—chromium	0.010
Cichelli-Bonilla (12)	Ethyl alcohol—chromium	0.0027
Cichelli-Bonilla (12)	n-pentane-chromium	0.015
Cryder-Finalborgo (15)	Water-brass	0.0060

Evaluation of Fluid Properties

In these correlations the fluid properties have been evaluated as properties of liquid at the saturation temperature. This was done both for the case of pool boiling with saturated liquid and for the case of surface boiling in forced convection of a subcooled liquid. In each case the liquid near the heating surface is very nearly at saturation temperature or possibly even at a metastable superheated temperature. Properties of the liquid were used for the c, μ, and k-values in the bubble Nusselt number, the Prandtl number, and the new term $c_l T_x/h_{fg}$ because the heat transfer was found to occur primarily by transfer of heat directly from the heating surface to the liquid. The value of μ of the bubble Reynolds number was evaluated as a property of liquid because viscous forces acting to retard the motion of the bubble are those of the liquid.

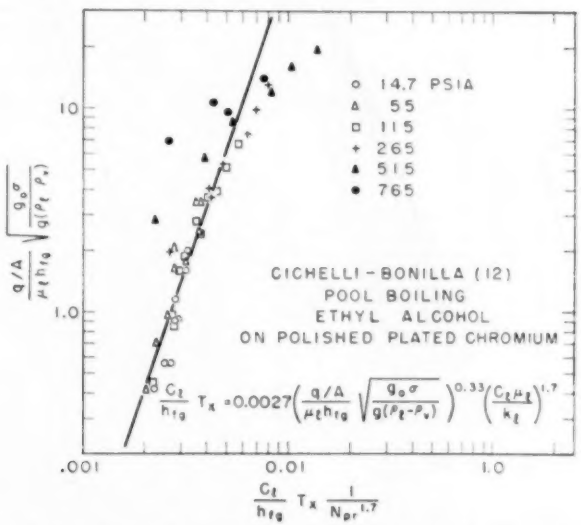

FIG. 5 CORRELATION OF DATA OF CICHELLI-BONILLA, REFERENCE 12, FOR CHROMIUM-BENZENE INTERFACE FOR POOL BOILING

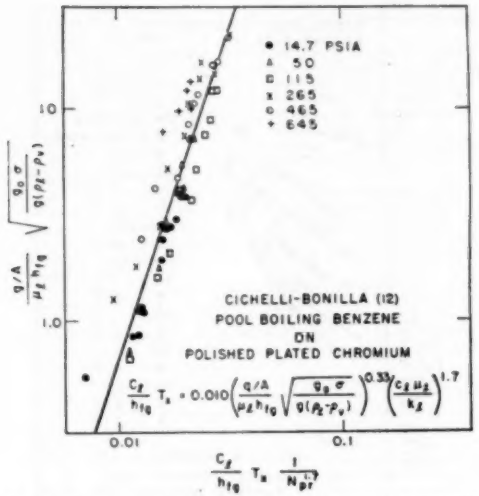

FIG. 6 CORRELATION OF DATA OF CICHELLI-BONILLA, REFERENCE 12, FOR CHROMIUM-ETHYL ALCOHOL INTERFACE FOR POOL BOILING

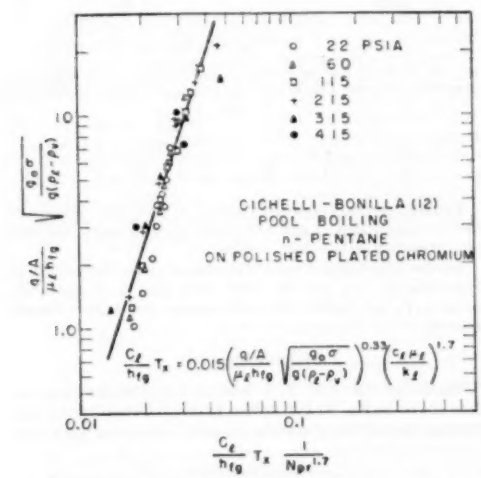

FIG. 7 CORRELATION OF DATA OF CICHELLI-BONILLA, REFERENCE 12, FOR CHROMIUM-*n*-PENTANE INTERFACE FOR POOL BOILING

DISCUSSION OF RESULTS

The results shown in Figs. 4 through 10 are essentially plots of q/A versus T_x each multiplied by a judicious combination of fluid properties thus effecting the correlation. It is readily observed that q/A rises rapidly with small changes in T_x. Further, the magnitude of T_x is rather small, being of the order of 50 deg F for water at atmospheric pressure and of the order of 5 or 10 deg F for water at 2000 psia. In all of the data correlated here the energy was supplied by electricity; hence T_x became the dependent variable in each case. It is difficult to measure the heating-surface temperature directly when electric heating is employed. It must be calculated from other measured values such as outer-tube surface temperature or resistance of the heating wire. The value of T_x is obtained by subtracting the saturation temperature from this determined heating-surface temperature. Since the magnitude of T_x is small, any errors in the determined value of heating-surface temperature will be greatly magnified in the resulting value of T_x. This can possibly account for some of the difference in the value of C_{sf} of Equation [14] as obtained by various experimenters.

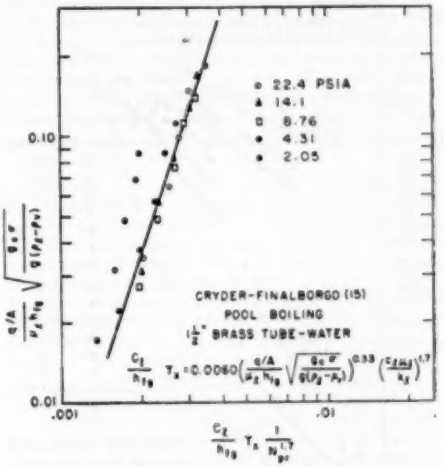

FIG. 8 CORRELATION OF DATA OF CRYDER-FINALBORGO, REFERENCE 15, FOR BRASS-WATER INTERFACE FOR POOL BOILING

It is, of course, essential in obtaining a correlation of data that the properties of the fluid employed be correct. Any error in the values for these properties is directly reflected in the data correlation.

Probably the most significant cause of the difference in the values of C_{sf} is the result of omitting, for lack of currently available information, the term β from the bubble Reynolds number and the bubble Nusselt number in arriving at the correlation as applied. The effect of this is to cause C_{sf} to be a function of β which is determined by the character of and the kind of heating surface and by the properties of the fluid as shown by Equation [11]. There is then good reason to expect a different value of C to result for every combination of kind of surface and kind of fluid. Additional information regarding the values of β for various combinations of surfaces and fluids should clarify this matter and produce a valid correlation for all such combinations.

In arriving at Equation [5], and hence Equations [7] and [9], the expressions for bubble Reynolds number and bubble Nusselt number, it was assumed that β did not vary with pressure for a particular combination of fluid and heating surface. This assumption may account for some of the small spread of the final correlation for each surface-fluid combination. The assumption appears to be fairly good, nevertheless, since the data for a particular fluid-heating surface combination are correlated within about ±20 per cent by Equation [14].

It is not suggested that the exponents 0.33 and 1.7 of Equation [14] are the true values nor that the form of Equation [14] is the best one. Rather it is suggested that the dimensionless groups of Equation [14] are significant in correlation boiling heat-trans-

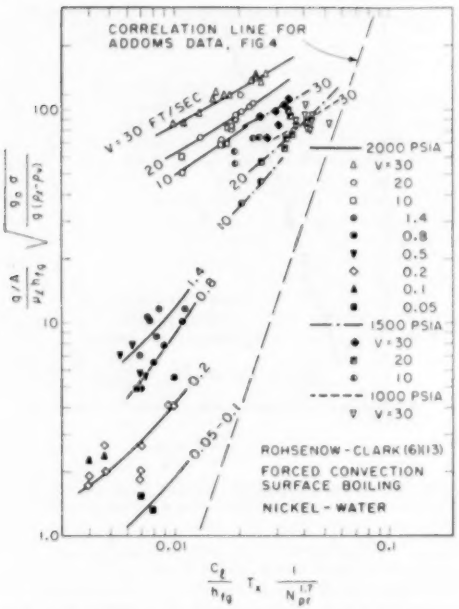

FIG. 9 DATA OF ROHSENOW-CLARK, REFERENCES 6, 13, FOR NICKEL-WATER INTERFACE FOR FORCED-CONVECTION SURFACE BOILING

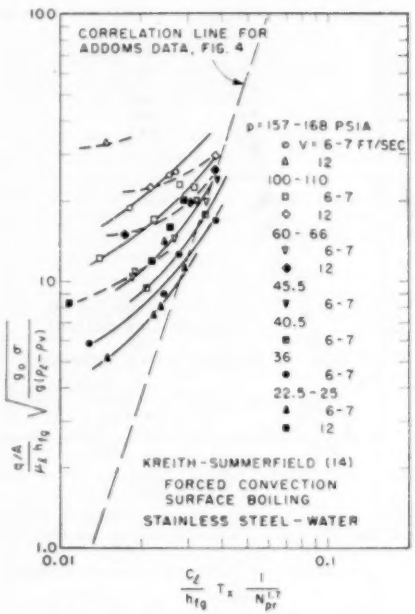

FIG. 10 DATA OF KREITH-SUMMERFIELD, REFERENCE 14, FOR STAINLESS-STEEL WATER INTERFACE FOR FORCED-CONVECTION SURFACE BOILING

fer data. Much more data were correlated than are presented here. Only the data for single component fluids on clean surfaces are presented here. They seemed to be correlated quite adequately by Equation [14] with the exponents of 0.33 and 1.7. The 0.33 exponent of the bubble Reynolds number appeared to be adequate for most of the data whether the heating surface was clean or not, but the 1.7 exponent appeared to be valid only for clean surfaces. With dirty surfaces the value of this exponent was quite erratic, varying between 0.8 and 2.0.

For purposes of comparison, the correlation Equation [14] may be rewritten in the form

$$\frac{q/A}{T_x k_l}\sqrt{\frac{g_c\sigma}{g(\rho_l-\rho_v)}} = \frac{1}{C_{sf}}\left(\frac{q/A}{\mu_l h_{lg}}\right)\sqrt{\frac{g_c\sigma}{g(\rho_l-\rho_v)}}^{0.667}\left(\frac{c_l\mu_l}{k_l}\right)^{-0.7} \quad [15]$$

or

$$N_{Nu,b} = \frac{1}{C_{sf}} N_{Re,b}^{0.667} N_{Pr}^{-0.7}$$

which may be compared with the nonboiling forced-convection expression

$$N_{Nu} = C_2 N_{Re}^{m} N_{Pr}^{1/3} \quad [16]$$

where m is in the range of 0.5 to 0.7 when the flow area varies along the direction of flow, e.g., for flow across tubes, around spheres or cylinders, or across interrupted fins.

CONCLUSIONS

Data for pool boiling of a liquid on a clean surface can be correlated by an equation of the form

$$\frac{c_l T_x}{h_{lg}} = C_{sf}\left(\frac{q/A}{\mu_l h_{lg}}\sqrt{\frac{g_c\sigma}{g(\rho_l-\rho_v)}}\right)^{0.33}\left(\frac{c_l\mu_l}{k_l}\right)^{1.7}$$

Further experimental work is needed to study the variation of bubble contact angle β and coefficient C_{sf} with pressure and with type of heating surface-fluid combination.

Further experimental work is needed to study the validity of Equations [3], [4], and [5] which were used in obtaining the terms ($c_l T_x/h_{lg}$), bubble Reynolds number and bubble Nusselt number.

ACKNOWLEDGMENT

Thanks are due to Dr. J. N. Addoms for permission to use his data shown in Fig. 4, and to Mr. Fakhri Rahmatallah for performing most of the calculations required in preparing this report.

BIBLIOGRAPHY

1 "Heat Transfer," by M. Jakob, John Wiley & Sons, Inc., New York, N. Y., 1949, chapt. 29.

2 "A Study of the Mechanism of Boiling Heat Transfer," by W. M. Rohsenow and J. A. Clark, Trans. ASME, vol. 73, 1951, pp. 609–620.

3 "Heat Transfer at High Rates to Water With Surface Boiling," by W. H. McAdams, *Industrial and Engineering Chemistry*, vol. 37, 1945, pp. 1010–1016.

4 "Photographic Study of Bubble Formation in Heat Transfer to Subcooled Water," by F. C. Gunther and F. Kreith, Heat Transfer and Fluid Mechanics Institute, Berkeley, Calif., 1949, pp. 113–126.

5 "Photographic Study of Surface-Boiling Heat Transfer to Water With Forced Convection," by F. C. Gunther, Trans. ASME, vol. 73, 1951, p. 115.

6 "Heat Transfer and Pressure Drop Data for High Heat Flux Densities to Water at High Sub-Critical Pressures," by W. M. Rohse-

now and J. A. Clark, Heat Transfer and Fluid Mechanics Institute, Stanford, Calif., 1951.

7 "Local Temperature Differences Occurring in Evaporation, Condensation, and Catalytic Reaction," in "Temperature, Its Measurement and Control in Science and Industry," by M. Jakob, Reinhold Publishing Corporation, New York, N. Y., 1941, p. 834.

8 "Berechnung des Maximalvolumens von Dampfblasen," by W. Fritz, *Physikalische Zeitschrift*, vol. 36, 1935, p. 379.

9 "Kondensation und Verdampfung: Neuere Anschauungen und Versuche," by M. Jakob, *Zeitschrift des Vereines deutscher Ingenieure*, vol. 76, 1932, pp. 1161–1170.

10 "Heat Transfer at High Rates to Water Boiling Outside Cylinders," by J. N. Addoms, DSc thesis, Chemical Engineering Department, Massachusetts Institute of Technology, June, 1948.

11 "Survey of Thermodynamic and Physical Properties of Water," by E. J. Wellman, MS thesis, Purdue University, Lafayette, Ind., January, 1950.

12 "Heat Transfer to Liquids Boiling Under Pressure," by M. T. Cichelli and C. F. Bonilla, Trans. AIChE, vol. 41, 1945, pp. 755–787.

13 "Heat Transfer Data for Low Velocity Forced Convection Flow of Water With Surface Boiling," by J. A. Clark, P. Malherbe, F. Mullin, and W. M. Rohsenow, Technical Report No. 4, DIC Project 6627, M.I.T., July 1, 1951.

14 "Heat Transfer to Water at High Flux Densities," by F. Kreith and M. J. Summerfield, Trans. ASME, vol. 71, 1949, 805–815.

15 "Heat Transmission From Metal Surfaces to Boiling Liquids: Effect of Temperature of the Liquid on Film Coefficient," by D. S. Cryder and A. C. Finalborgo, AIChE, vol. 33, 1937, p. 346.

16 "The Influence of Pressure on Heat Transfer in Evaporation," by M. Jakob, Proceedings of the 5th International Congress for Applied Mechanics, 1938, p. 561.

Discussion

W. Daskin.[3] The writer is interested in the effect of various surface-active agents on the contact angle, β. Has the author attempted to correlate data on boiling in the presence of such agents?

M. Jakob.[4] In 1935 the writer, in co-operation with W. Linke,[5] introduced a Nusselt number $(N_{Nu})_b$ for the heat transfer from a heating surface to boiling liquid with the diameter of the bubble, when breaking from the surface in approximately spherical shape, as characteristic length. We represented the results of our experiments on vigorous pool boiling by an equation which the writer recently converted to the form

$$(N_{Nu})_b = \Psi\,(v_f/v_b) = C(v_f/v_b)^n$$

where

Ψ = is a function, C and n are empirical constants ($C = 30$, $n = 0.8$)

v_f = velocity of vapor leaving free pool surface

v_b = velocity of gravitational center of bubble in formation at, and just above, heating surface[6]

The author adds a power function of the Prandtl number as a factor on the right side of the equation, as Bonilla and Perry[7] had done before. He further replaces our ratio,[8] v_f/v_b, by a Reynolds number which is also based on the bubble diameter as characteristic length. No doubt this is a novel and promising step, which takes care of the fact that vehement liquid motion occurs around the bubble in the formation and break-off process. The writer is gratified to see that in this new concept the coefficient of heat transfer retains approximately the relationship to σ which we had found. (It is now proportional to $1/\sqrt[3]{\sigma}$ compared to our $1/\sqrt{\sigma}$.)

While Figs. 4 to 10, inclusive, of the paper seem to indicate that the author is on the correct path, he is well aware of the fact that much remains to be done before a perfectly satisfactory semitheoretical representation of the process of vigorous boiling is obtained. He mentions different items missing or questionable; a few more may be added.

It is surprising that in Equation [15] the —0.7th power of the Prandtl number occurs instead of about the +0.3th power. Since the variation of c_l/k_l with temperature is small compared to that of the viscosity, a change to $(N_{Pr})^{0.3}$ might be compensated by changing the constant factor to $k_l/c_l\mu_s C_{sf}$ by using an average fixed value of $k_l/c_l\mu_s$ and by further adding a factor μ_a/μ_l, where μ_a is a reference dynamic viscosity, for instance, that of saturated liquid at atmospheric pressure, and μ_l is the dynamic viscosity of the liquid under the conditions of operation. This would correspond to the modification of the writer's original equation by adding the kinematic-viscosity ratio ν_a/ν_l as a factor which was suggested[9] in order to take care to some extent of the influence of pressure.[10] It may be mentioned that Bonilla and Perry[7] accepted this suggestion.

Another item which seems to need further experimentation is the assumed proportionality of q/A and $(q/A)_b$. The author used as basis for this assumption some data which the writer published in 1941 and which go back to earlier experiments of Jakob and Linke.[11] We found indeed almost proportionality in the investigated range from about 3000 to 18,500 Btu hr^{-1} ft^{-2}, but we did not claim that this holds up to the order of 100,000 Btu hr^{-1} ft^{-2} and more. While in our experiments at least about 1.5 sq in. of cross-sectional area were available for each bubble column as an average, less than 0.3 sq in. would be available at 100,000 Btu hr^{-1} ft^{-2}. The influence of convection under such crowded conditions and, therefore, the heat transfer on the bubbles rising in the column, are difficult to predict. It may be found necessary to introduce a parameter which takes care of this part of the heat transfer, as Jakob and Linke found necessary in their analysis.

For boiling in subcooled liquid the proportionality may be more closely approached, because here the heat transfer just above the heating surface is the essential thing while the bubbles vanish in rising above this zone. It remains to be seen whether in such vehement boiling the equations derived for the bubble in formation are still valid. The author's plots for forced-convection surface boiling are promising in this respect.

R. H. Sabersky.[12] Correlations by the use of judiciously selected Reynolds and Prandtl numbers also have been considered at this laboratory. The correlation that the author proposes is one relating the heat-transfer rate to the tempera-

[3] Instructor in Mechanical Engineering, The Johns Hopkins University, Baltimore, Md. Jun. ASME.

[4] Research Professor of Mechanical Engineering, Illinois Institute of Technology, Chicago, Ill. Mem. ASME.

[5] "Der Wärmeübergang beim Verdampfen von Flüssigkeiten an senkrechten und waagerechten Flächen," by M. Jakob and W. Linke, *Physikalische Zeitschrift*, vol. 36, 1935, pp. 267–280.

[6] Considering that the frequency f of bubble formation included relaxation intervals almost equal to the formation time, it was as though the bubble centers were rising by a height equal to the breaking-off diameter in the time $1/f$.

[7] "Heat Transmission to Boiling Binary Liquid Mixtures," by C. F. Bonilla and C. W. Perry, Trans. AIChE, vol. 37, 1941, pp. 685–705.

[8] This ratio was not introduced from reasons of dimensional analysis; it was rather obtained by some physical considerations.

[9] "The Influence of Pressure on Heat Transfer in Evaporation," by M. Jakob, Proceedings of the 5th International Congress for Applied Mechanics, 1938, p. 561.

[10] If the liquid densities were exactly the same at the reference pressure and at the pressure under consideration, then the relation $\nu_a/\nu_l = \mu_a/\mu_l$ would hold exactly.

[11] "Der Wärmeübergang von einer waagerechten Platte an siedendes Wasser," by M. Jakob and W. Linke, *Forschung auf dem Gebiete des Ingenieurwesens*, vol. 4, 1933, pp. 75–81.

[12] Assistant Professor of Mechanical Engineering, California Institute of Technology, Pasadena, Calif. Jun ASME.

ture difference T_s, in a region between incipient boiling and the so-called "burnout" point (transition to film boiling). The burnout point as such is not indicated by the correlation. In that region, however, the heat transfer changes extremely rapidly with changes in T_s, or in other words, the wall temperature never exceeds the boiling temperature of the fluid by a large margin. The curve relating heat transfer to the temperature difference T_s is therefore very steep (see e.g., author's Figs. 1 and 4). This fact makes it difficult to prove the validity of the correlation by experimental results because even if the correlation were in error the experimental points must be expected to cluster reasonably well about the theoretical curve. Nevertheless, there is some lack of correlation among the various liquids considered, which the author ascribes to differences in bubble contact angle, and there is also some scatter for each individual liquid. Some doubt seems to remain, therefore, as to whether the theory has been substantiated adequately or not.

From an engineering point of view there is also the following to be considered: In the usual convection problem a correlation between heat transfer and temperature difference is all that is required. In the case of boiling heat transfer, however, it was already pointed out that the wall temperature will always remain close to the boiling point of the fluid. For design purposes it is often not necessary to predict the wall temperature any closer than that. A knowledge of the burnout point is, however, essential because it determines the design limits. The writer believes, therefore, that a correlation for the burnout points would be of particular importance.

Author's Closure

We have no information on the effect of additives on the bubble contact angle, as requested by Mr. Daskin. This phase of investigation is planned for the future.

The discussion presented by Dr. Jakob is most welcome since it co-ordinates the present paper and much of the past work with which he has been associated so intimately. The present correlation indeed hinges upon Equations [3] and [4] of the paper and the statement that q/A is proportional to $(q/A)_b$. Each of these relations, as well as the concept of a bubble Nusselt number, is taken directly from some of Dr. Jakob's earlier work.

The purpose in the present work is not to arrive at a correlation of heat-transfer data as such. The author has attempted to describe the mechanism of boiling and logically has arrived at dimensionless groups to be included. Because of this he has attempted to avoid the use of ratios of the values of properties at the operating condition to values at some reference condition as suggested by Dr. Jakob. Such quantities introduced into the analysis often can force a correlation but add little to the explanation of the processes.

In order for the exponent of the Prandtl number in Equation [15] to be $^1/_3$ instead of —0.7, the exponent of the Prandtl number in the abscissa in Figs. 4 through 8 of the paper would have to be 0.667. Recently the detailed plots required to construct Figs. 4 through 8 have been reviewed and magnitude of this 1.7 exponent has been found actually to cover a range of about 1.3 to 1.8 with most of the data resulting in an exponent in the range of 1.6 to 1.8.

Professor Sabersky raises some questions regarding the degree of correlation obtainable in this range of boiling where the temperature differences are low. If one compares the first graph with the third graph in Fig. 4, the author believes he will conclude that the effect of pressure on boiling in a particular apparatus is fairly well correlated. This is shown also in Figs. 5 through 8, each figure being for a particular surface-fluid combination and a particular apparatus. It seems reasonable to conclude that any errors in temperature in any particular apparatus would be consistent and each individual correlation would be valid except that the magnitude of C_{sf} would directly reflect any error in the temperature measurement. The difference in the magnitudes of C_{sf} found for each of the surface-fluid combinations in Figs. 4 through 8, possibly can be interpreted, as suggested, as being the effect of the magnitude of the bubble contact angle or as the effect of errors in the surface temperature measurement. On the other hand, Figs. 5, 6, and 7 represent different fluids on the same surface in the same apparatus. Therefore it seems reasonable to conclude that any temperature measuring errors would be consistent within these three figures and the variation in the magnitude of C_{sf} probably can be attributed to the effect of bubble contact angle. Unfortunately, at this time we do not have the magnitudes of the bubble contact angles present in any of these boiling data.

The burnout points require a separate correlation. We are currently obtaining data on burnout points in the high-pressure region. This information is indeed very important but cannot be included in a correlation as presented in this paper. A number of burnout correlations have been presented, two of which are by Addoms,[13] and by Buchberg, et al.[14]

[13] "Heat Transfer at High Rates to Water Boiling Outside of Cylinders," by J. N. Addoms, ScD thesis 1948, M.I.T., Cambridge, Mass.

[14] "Heat Transfer, Pressure Drop, and Burnout Studies With and Without Surface Boiling for De-Aerated and Gassed Water at Elevated Pressures in a Forced Flow System," by H. Buchberg, R. Lipkis, and M. Greenfield, presented at the 1951 Heat Transfer and Fluid Mechanics Institute, Stanford University, June, 1951.

Heat Transfer and Pressure Drop for Turbulent Flow of Air-Water Mixtures in a Horizontal Pipe

By H. A. JOHNSON[1] and A. H. ABOU-SARE[2]

The static pressure drop and heat transfer for two-phase, two-component flow of air and water were measured for flow in a horizontal 15-ft length of 1-in. 16-gage brass tubing. Flow rates include the range of 1000 to 15,000 lb per hr for the water and 0 to 200 lb per hr for the air. Tentative correlations are presented from which prediction of pressure drop and heat transfer may be made under restricted flow conditions.

Nomenclature

The following nomenclature is used in the paper:

A = cross-sectional area of pipe, sq ft
A_g = effective gas flow area, $\beta\pi D_g^2/4$, sq ft
A_l = effective liquid flow area, $\alpha\pi D_l^2/4$, sq ft
c_p = specific heat of fluid, Btu per lb
D_g = effective hydraulic diameter of gas, ft
D_l = effective hydraulic diameter of liquid, ft
D_p = inside pipe diameter, ft
G = weight rate of flow per unit area, W/A, lb/sec ft^2
g = gravitational force per unit mass, 32.2 ft/sec^2
h_G = calculated single-phase heat-transfer coefficient for gas based on A_g and D_g, Btu/hr ft^2 deg F
h_L = calculated single-phase heat-transfer coefficient for liquid based on A_l and D_l, Btu/hr ft^2 deg F
h_l = calculated single-phase heat-transfer coefficient for liquid based on A and D_p, Btu/hr ft^2 deg F
h_{TP} = two-phase heat-transfer coefficient, Btu/hr ft^2 deg F
k = thermal conductivity of fluid, Btu/ft^2 hr (deg F/ft)
P_m = mean static pressure of test section, psig
ΔP_g = calculated single-phase pressure drop for gas based on A and D_p, psf
ΔP_l = calculated single-phase pressure drop for liquid based on A and D_p, psf
ΔP_{TP} = two-phase pressure drop, psf
q = heat-transfer rate, Btu per hr
R_g = gas-volume fraction, fraction of tube filled with gas
R_e = liquid-volume fraction, fraction of tube filled with liquid
t_M = mean mixed fluid temperature for test section at which all properties are evaluated, deg F
t_1 = mixed mean temperature at entrance, deg F
t_2 = mixed mean temperature at exit, deg F
t_{wi} = mean temperature of inside tube-wall surface, deg F
V_g = velocity of the gas, $W_g/A_g\rho_g$, fps
V_l = velocity of liquid, $W_l/A_l\rho_l$, fps
W_g = gas flow rate, lb per sec
W_l = liquid flow rate, lb per sec
X = two-phase flow parameter = $(\Delta P_l/\Delta P_g)^{1/2}$
Z = two-phase heat-transfer coefficient functions defined by relation:

$$h_{TP} = h_L Z_g + h_G Z_l$$

α = flow-pattern modulus for liquid
β = flow-pattern modulus for gas
μ = absolute viscosity, lb/sec ft
ρ = specific weight, pcf
ϕ_l = two-phase pressure-drop modulus = $(\Delta P_{TP}/\Delta P_l)^{1/2}$

Subscripts:

G, g = gas
L, l = liquid
p = pipe
sp = single-phase
TP = two-phase

Flow-Pattern Symbols:

St B = stratified-bubble
B = bubble
PB = pulsating-bubble
St W = stratified-wavy
StSl = stratified-sluggish
Sl = sluggish
SlA = sluggish-annular
SA = semiannular
A = annular

Introduction

Pipe-flow systems with mixtures of vapor and liquid are common in many industrial equipments. More often these systems are for single-component fluids attended by condensation or vaporization due to heat transfer or large pressure drop, i.e., "flashing." Less common are two-phase two-component systems under flow conditions of limited pressure drop and heat transfer such that compressibility, momentum, and phase-change effects along the pipe length are negligible. This investigation (1)[3] and the related literature[3] are limited to the latter simplified case.

Approximate correlations of isothermal pressure drop for several such systems have been developed and are summarized in their latest form by Lockhart and Martinelli (2). Interpretation of the results presented here is made in terms proposed by Lockhart and Martinelli who characterize the essential features of the flow with the following parameters:

[1] Associate Professor of Mechanical Engineering, University of California, Berkeley, Calif. Mem. ASME.

[2] Agricultural Engineering Department, College of Agriculture, Chatby, Alexandria, Egypt; formerly, Graduate Student in Mechanical Engineering, University of California. Jun. ASME.

Contributed by the Heat Transfer Division and presented at the Annual Meeting, Atlantic City, N. J., November 25-30, 1951, of The American Society of Mechanical Engineers.

Note: Statements and opinions advanced in papers are to be understood as individual expressions of their authors and not those of the Society. Manuscript received at ASME Headquarters, October 2, 1951. Paper No. 51—A-111.

[3] Numbers in parentheses refer to the Bibliography at the end of the paper. Additional references to the literature than are mentioned in the text are included.

ϕ, two-phase pressure drop ratio defined as $(\Delta P_{TP}/\Delta P_{sg})^{1/2}$
X, single-phase pressure-drop ratio defined as $(\Delta P_l/\Delta P_g)^{1/2}$
R, "volume fraction" which is fraction of the conduit volume containing one phase

Proceeding from concepts related to single-phase pipe flow, functional relations between ϕ and X, and R and X were established. These relations were indicated to be different for four modes of flow grouped according to either viscous or turbulent for the liquid and the gas. For each mode there are also several flow patterns arbitrarily characterized by descriptive terms such as stratified, sluggish, annular, and others (3, 4). Of the four possible modes, all data presented in this paper are in the turbulent-turbulent regime and include several flow patterns.

The heat transfer to such flow is also of interest and is the subject of the present investigation. While experimental results for heat transfer to single-component systems (boiling) are available, no previous experiments appear to have been made with a two-component system in which heat is transferred without change of phase. To obtain such data the system was so constructed as to yield measurements of the heat transfer, pressure drop, liquid-volume fraction, and flow pattern for air-water mixtures.

Apparatus

All results are for flow through a horizontal 1-in. 16-gage drawn-brass tube in two sections of equal length, closely connected at the center to provide for pressure measurement at that point. The over-all length between end pressure taps is 15.7 ft and by means of the central tap the pressure drops in the two halves can be compared. A steam jacket, also divided at the mid-point of the tube, provides a heating section 15.5 ft long with condensate from both sections being united before measurement in the present experiments. Internal baffling was arranged so that the condensate formed by external heat loss was withdrawn separately. Tube-wall temperatures were observed by means of 24 thermocouples located spirally along the length of the exterior wall of the test tube. This arrangement, since abandoned, produced circumferential variation of the tube-wall temperature which is considered inconsistent with that expected for a uniform condensate film. It is inferred that the thermocouple lead wires caused irregular condensate flow and so produced the variation observed. Maximum deviations from the mean temperature were as much as ± 10 deg F and, while unsatisfactory, did not introduce too great an error because the wall-to-fluid temperature differences are large for the experiments reported here. The water and air are mixed in a standard pipe tee 70 diam upstream of the test section. This method of mixing was selected from previous investigations reported by Martinelli, et al. (3) and Bergelin and Gazley (4).

Fig. 1 shows the principal features of the test system although all instrumentation is not shown in detail. A traversing thermocouple, for measurements across the stream, is provided at the outlet of the heating section as a check on the mixed mean temperature measurements in the mixing pot. Special disk-type valves, of uniform tube-diameter bore when open, are placed at each end of the test section and are spring-loaded to enable rapid simultaneous closing. In this way the air-liquid content of the test section could be determined, under operating conditions, with the aid of a graduated water tank from which the test section could be filled with liquid by venting at a pressure tap. Residual air was measured by pressurizing this system and measuring the additional displacement in the graduated tank.

Single-Phase Tests

A series of single-phase flow tests for both air and water were made to establish the validity of the system and testing technique. The pressure-drop results, both isothermal and nonisothermal, agreed with accepted smooth-pipe values with deviations of $\pm$ 3 per cent. For heat transfer, the agreement when compared with McAdams (5) was satisfactory for water, i.e., 5 to 10 per cent low for Reynolds number above 40,000. However, the results for air were not satisfactory. The fault for the air is attributed to the combined effect of low heat-flux rates, a long high effectiveness heating section, and poor precision in the measurement of the outlet mixed mean temperature. This difficulty was not considered serious, however, since the heat rates at the minimum water rate are substantially greater than for air alone and those results did agree with predicted performance.

Two-Phase Flow Test Procedure

Thirty-five isothermal and 116 nonisothermal two-phase runs were made which included the following range of variables:

Water rate, lb per hr	1000 to 15000
Air rate, lb per hr	4.5 to 200
Pressure drop, lb/ft² per ft	4 to 250
Heat rate, Btu/ft² hr	35000 to 175000
Mean pressure, psig	1 to 50
Mean temperature of flow, deg F	70 to 140
Wall temperature, deg F	175 to 210

The two-phase test series was conducted at constant liquid rates of 2, 4, 10, 18, and 30 gpm. For each liquid rate, the air rates were about 0, 1, 2, 4, 7, 13, 25, and 45 scfm. At the end of each series of runs for one liquid rate, every third air rate was repeated as a check. Also, a reference 14 gpm single-phase water run was made at regular intervals to detect any changes in the system such as leakage, fouling, and instrumentation faults.

For the nonisothermal runs steady state obtained when the tube-wall temperatures, taken at 15-min intervals, showed fluctuations of less than ± 0.5 deg F. Heat balances for all runs were within 10 per cent and the majority better than 5 per cent.

Results

All two-phase experimental results for the present investigation are shown in graphical form in Figs. 2 to 5. Tables 1 and 2 present the data for the last consecutive group of runs made, excluding only duplicate check runs. The estimated maximum errors are 5 per cent for the pressure drop and liquid-volume fraction and 25 per cent for the heat-transfer coefficient.

Results of pressure-drop measurements for both isothermal and nonisothermal flow are revealed in Fig. 2 with the points for nonisothermal indicated to demonstrate the experimental scatter. Similar scatter obtains for the isothermal flow points which are not shown. It should be noted that the curves in Fig. 2 are not directly related because the system pressure level varies with changes in flow rate. The differences that exist between the isothermal and nonisothermal may be rationalized in terms of the variation in viscosity and by accounting for small variations in stream momentum along the test length.

Visual observations of the flow patterns are indicated in Fig. 3. These are arbitrary and subject to the interpretation of the observer but appear to be the best possible means for the present. Stroboscopic and photographic techniques, while employed, yielded no better indication for flow-pattern characterization. The demarcation between patterns is so vague that no attempt was made to fix them.

Liquid-volume-fraction data are shown in Fig. 4 and indicate large reduction with only slight additions of air followed by little diminution for large increases in air rate. The points shown are for nonisothermal flow and include all observations made for these experiments.

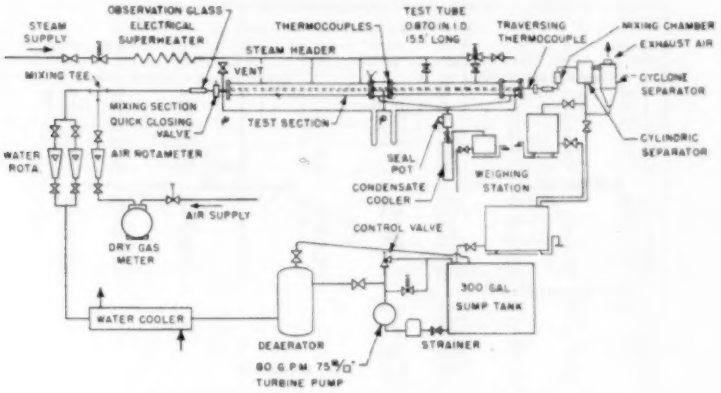

FIG. 1 SCHEMATIC DIAGRAM OF EXPERIMENTAL EQUIPMENT

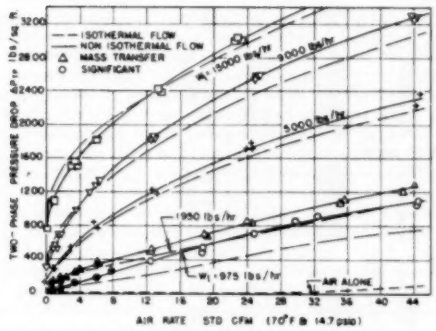

FIG. 2 TOTAL PRESSURE-DROP DATA FOR TWO-PHASE AIR-WATER FLOW IN A 0.870-IN-ID HORIZONTAL TUBE 15.7 FT LONG

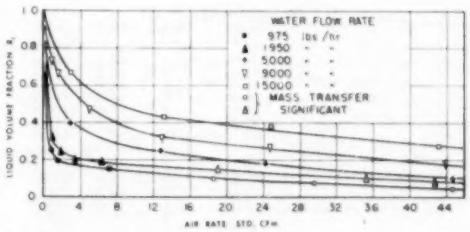

FIG. 4 LIQUID-VOLUME FRACTION FOR NONISOTHERMAL TWO-PHASE AIR-WATER FLOW IN 0.870-IN-ID HORIZONTAL TUBE

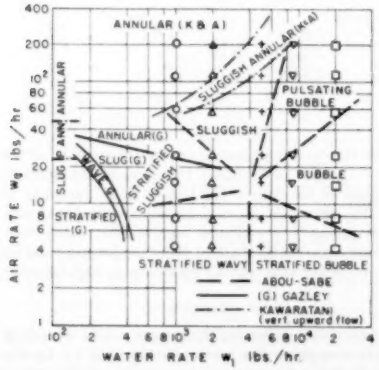

FIG. 3 AREAS OF FLOW PATTERNS FOR TWO-PHASE AIR-WATER FLOW IN 0.870-IN-ID HORIZONTAL TUBE

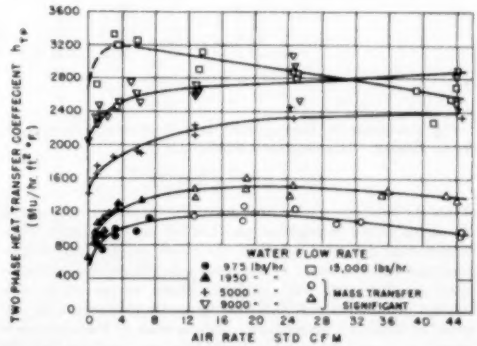

FIG. 5 HEAT-TRANSFER COEFFICIENTS FOR TWO-PHASE AIR-WATER FLOW IN 0.870-IN-ID HORIZONTAL TUBE

TABLE 1 SUMMARY OF ISOTHERMAL TWO-PHASE DATA

(Atmospheric pressure 14.6 ± 0.1 psia)

Air rate, scfm[a]	P_m, psig	t_m, deg F	ΔP_{TP}, psf	Flow type	Air rate, scfm	P_m, psig	t_m, deg F	ΔP_{TP}, psf	Flow type
Water flow rate = 975 lb per hr					Water flow rate = 1950 lb per hr				
1.02	1	85	38	St W	1.02	2	76	76	St W
1.54	1	80	65	St W	1.6	3	76	135	St W
3.2	2	79	88	St SI	3.2	3	75	235	St SI
5.7	4	78	118	St SI	5.6	4	74	310	St SI
12.7	7	77	212	S A	12.8	7	74	440	SI
24.8	8	77	465	A	24.9	11	83	733	S A
44.7	12	77	780	A	43.8	16	83	1060	A
Water flow rate = 5000 lb per hr					Water flow rate = 9000 lb per hr				
0.98	3	92	260	St B	0.97	6	84	598	St B
1.45	3	91	330	St B	1.6	7	83	827	St B
3.2	4	90	500	B	3.2	9	82	951	B
5.8	7	89	740	P B	5.4	12	80	1260	B
12.8	9	87	1130	SI	12.7	16	78	1690	B
24.9	14	86	1480	SI A	24.7	23	76	2380	P B
43.6	21	84	2520	SI A	42.2	33	74	2660	P B
Water flow rate = 15000 lb per hr									
9	11	69	1295	St B					
1.7	12	69	1440	B					
3.3	16	67	1660	B					
6.0	21	64	2015	B					
15.0	27	73	2520	P B					
23.4	34	79	2950	P B					
39.4	47	84	3740	P B					

[a] Standard conditions for air rate are 70 deg F and 14.7 psia.

TABLE 2 SUMMARY OF NONISOTHERMAL TWO-PHASE FLOW DATA

(Atmospheric pressure 14.6 + 0.1 psia)

Air rate, scfm	P_m, psig	t_1, deg F	t_2, deg F	ΔP_{TP}, psf	t_{wi}, deg F	Q/A_i, Btu/hr ft²	R_1	Flow type
Water flow rate = 975 lb per hr								
1.03	1	66.0	196.5	78	208	38600	0.25	St W
1.68	1	65.5	192.3	71	203	37500	0.19	St W
3.30	2	65.0	194.8	108	204	42600	0.18	St SI
7.30	4	65.8	191.3	243	200	51400	0.15	SI A
18.6*	6	65.0	184.8	495	197	55600	0.09	S A
29.7*	9	64.5	179.6	860	196	60000	0.08	A
44.7*	12	65	171.3	1110	194	59300	0.04	A
Water flow rate = 1950 lb per hr								
0.97	2	72.5	176.7	121	201	58600	0.32	St W
1.84	2	73.5	179.2	170	202	60300	0.24	St W
3.40	3	74.4	188.0	233	204	67800	0.19	St SI
6.30	4	73.5	182.0	330	195	66400	0.19	St SI
19.0*	8	76.5	181.2	700	194	75800	0.15	S A
25.8*	15	73.0	175.0	1120	195	83900	0.10	S A
42.7*	16	71.6	171.0	1220	193	83500	0.09	A
Water flow rate = 300 lb per hr								
0.96	3	92.8	165.0	282	197	105000	...	St B
2.9	6	91.5	168	534	197	110000	0.40	...
12.8	11	76.5	161.7	1190	186	126000	0.25	SI ...
24.2	17	89.2	170.0	1720	192	128000	0.18	SI A
44.7	22	88.8	164.0	2380	189	128000	0.10	SI A
Water flow rate = 9000 lb per hr								
1.0	6	99.2	154.5	368	188	141000	0.73	St B
1.64	7	92.4	145.7	602	181	136000	0.67	St B
5.1	12	97.8	154.8	1200	184	146000	0.47	St B
13.0	16	98.8	151.2	1850	181	137000	0.32	P B
24.8	26	99.2	155.6	2580	185	155000	0.27	P B
44.0	37	94.5	152.0	3310	185	159000	0.18	...
Water flow rate = 15000 lb per hr								
1.06	11	108.4	143.7	1090	182	149000	...	ST B
3.0	17	110.0	151.6	1500	186	176000	0.66	...
13.2	29	102.8	141.0	2430	181	164000	0.43	...
24.0	38	98.2	133.5	3020	176	152000	0.38	P B
43.2	51	97.2	134.0	3890	180	161000	0.27	P B

[a] Mass transfer significant.

Fig. 5 presents the heat-transfer data in terms of a heat-transfer coefficient. This coefficient is defined by

$$h_{TP} = (q/A) \div \text{LMTD}$$

where the heat rate q is the heat gained by the mixture, assuming the air saturated throughout, and LMTD the logarithmic mean temperature difference based on the mixed mean terminal temperatures and the mean of the tube-wall temperatures extrapolated to the inner wall surface. These curves show substantial increases in the coefficient for small additions of air followed by tendency for maxima. The increase at low air rates is explained in part by reduced liquid-flow area and resulting increases in liquid velocity and heat-transfer coefficient. At high air rates the decreasing values are not necessarily attributed to the effect of lower heat-transfer performance characteristic of air. The scatter of the data at the highest liquid rate may not fully justify the curve as drawn. At the lowest liquid rate, mass transfer probably contributes significantly, since this would tend to decrease the final mixed mean temperature and cause the depression of the heat-transfer coefficient at high air rates.

Discussion

A primary comparison for the present results consists in evaluating the two-phase flow parameters defined by Lockhart and Martinelli (2) and to compare the results of the other investigators on this basis. Fig. 6 reveals this comparison for isothermal

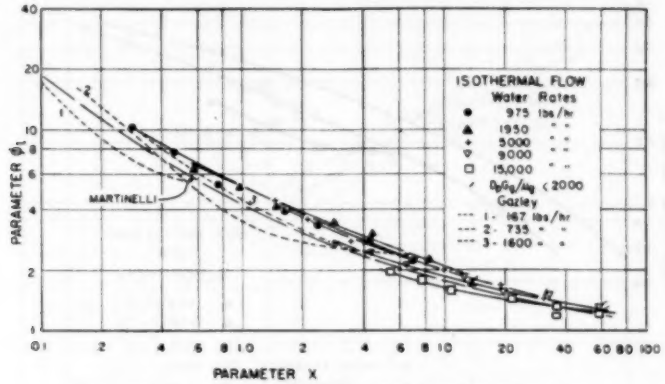

FIG. 6 TWO-PHASE PRESSURE-DROP CORRELATION FOR ISOTHERMAL FLOW

flow and includes the data of Gazley and Bergelin (6). The present results and those of Gazley show a trend with water rate; however, the order with increasing water rate for the two sets of data is reversed indicating secondary effects. All results are generally within ±30 per cent of the line presented by Martinelli which is the average of a large volume of previous data. Apparently significant secondary effects, which may be dependent on flow pattern, Fig. 7, are not accounted for in the simple rationalization leading to the correlation method of Fig. 6. It is believed that the effect of mechanical energy dissipation at the liquid-gas interface exerts a significant influence and has not yet been idealized in such a way as to permit an accounting for it in the generalized representation for Fig. 6. This has been shown by studies considering ideal annular viscous-viscous flow (7) and an extension of the Martinelli analysis (1).

Fig. 8 represents the nonisothermal results in the same manner, and trends shown for the isothermal case are somewhat exaggerated in this case with a mean line through the data lying about 25 per cent above the Martinelli line.

In Fig. 9 experimental values of the nonisothermal liquid-

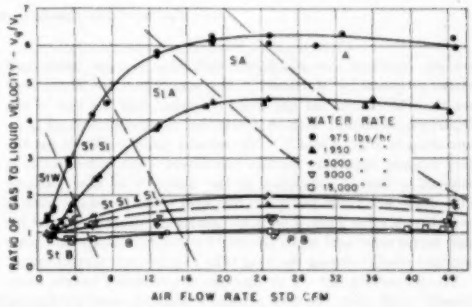

FIG. 7 CORRELATION OF FLOW PATTERN AND GAS-TO-LIQUID VELOCITY RATIO
(Nonisothermal flow)

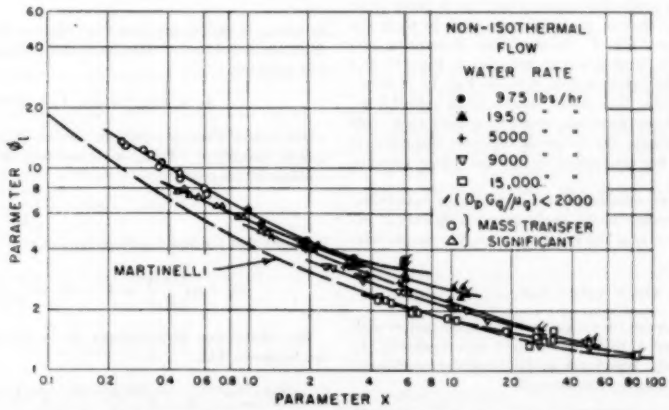

FIG. 8 TWO-PHASE PRESSURE-DROP CORRELATION FOR NONISOTHERMAL FLOW

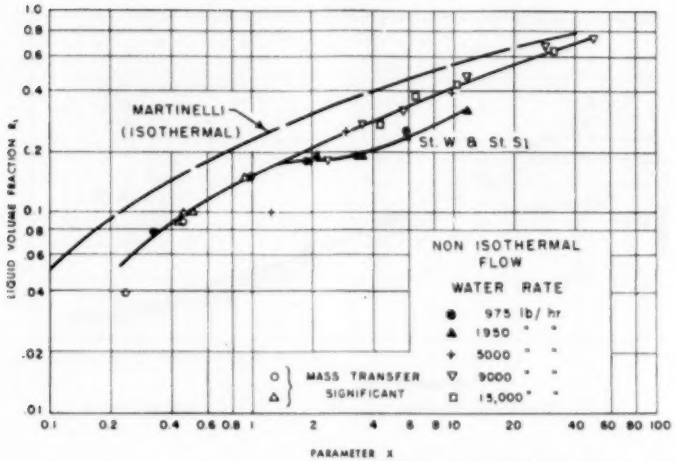

FIG. 9 CORRELATION OF LIQUID-VOLUME FRACTION R_l

volume fractions are compared with the average isothermal values proposed by Martinelli. The magnitudes are 50 per cent less than Martinelli but the trend is similar, and the sign of the departure consistent with that revealed for nonisothermal pressure drop in Figs. 2 and 7. No rational cause is offered for the very evident departure for the two lowest water rates but it is believed a further indication of the influence of flow pattern. The single low-value point for the 5000 lb per hr water rate is probably in error since it is at the minimum value measured for high liquid rates and much affected by system leakage and temperature change during the long time required for measurement.

No comparable data or predictions are available for the heat-transfer coefficient. Several arbitrary methods were tried using the ratio of the two-phase heat-transfer coefficient to that for the single-phase liquid, h_{TP}/h_l, with several independent variables including X. All were similar to Fig. 10 which only serves to show the data to be consistent. In this figure the values at the maximum liquid rate are less than unity because single-phase tests showed that the prediction equation used for h_l tends to be high for this system: that is, small amounts of air increase the heat-transfer coefficient, Fig. 4. Some success at securing correlation, ±20 per cent, is obtained as revealed in Figs. 11 and 12. The heat-transfer pressure-drop ratio in Fig. 11 is determined from experimental data alone. Had a mean value for ϕ_l from Fig. 7 been used the dispersion would be greater than ±20 per cent. For this reason the following tentative procedure is preferred since it is less dependent on the two-phase pressure drop:

Considering that any relationship for a two-phase heat-transfer coefficient would reduce to the single-phase coefficients at extreme values for the ratio of the two fluid rates, the simple relation is postulated

$$h_{TP} = h_L Z_g + h_G Z_l \quad \ldots\ldots [1]$$

where Z_g and Z_l are, respectively, gas and liquid rate factors with values between 0 and 1 to be determined experimentally, h_L and h_G are, respectively, liquid and gas heat-transfer coefficients assumed to be represented by reference (5)

$$hD/k = 0.023(DG/\mu)^{0.8}(c_p\mu/k)^{0.4} \quad \ldots\ldots [2]$$

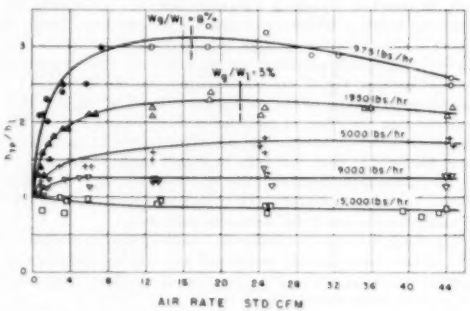

FIG. 10 RATIO OF TWO-PHASE TO SINGLE-PHASE LIQUID HEAT-TRANSFER COEFFICIENT

in which D and G are based on effective hydraulic diameters. With the definitions of Martinelli and Lockhart (3) the effective flow areas are

$$A_l = \alpha\pi D_l^2/4 \text{ and } A_g = \beta\pi D_g^2/4 \quad \ldots\ldots [3]$$

where α and β are flow-pattern factors, D_l and D_g effective hydraulic diameters. Then, since the sum of the gas and liquid volumes fill the pipe

$$\alpha D_l^2 + \beta D_g^2 = D_p^2 \quad \ldots\ldots [4]$$

it follows that the liquid-volume fraction is

$$R_l = \alpha\left(\frac{D_l}{D_p}\right)^2 = 1 - R_g = 1 - \beta\left(\frac{D_g}{D_p}\right)^2 \quad \ldots\ldots [5]$$

By substitution of Equations [2] to [5] into Equation [1] it can be shown that

$$\frac{h_{TP}}{h_l} = \frac{\alpha^{0.1}}{R_l^{0.9}} Z_g + \left(\frac{W_g}{W_l}\right)^{0.8} \frac{\beta^{0.1}}{R_g^{0.9}} \left(\frac{k_g}{k_l}\right)^{0.6} \left(\frac{c_{pg}\mu_l}{c_{pl}\mu_g}\right)^{0.4} Z_l \quad \ldots [6]$$

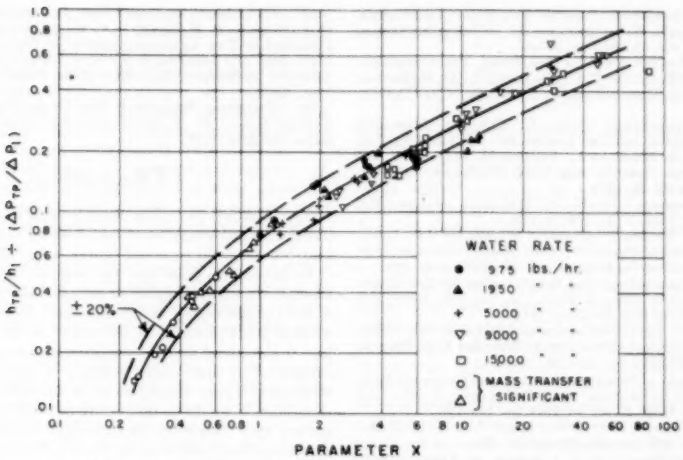

FIG. 11 CORRELATION OF HEAT TRANSFER BASED ON PRESSURE DROP

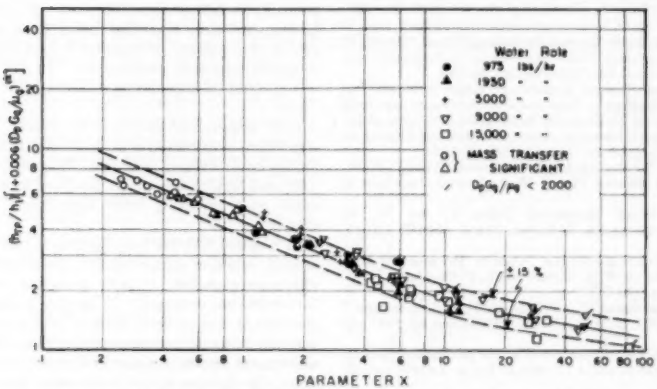

FIG. 12 CORRELATION PROCEDURE FOR TWO-PHASE FLOW HEAT TRANSFER

where h_l is defined by Equation [2] based on the pipe diameter D_p.

For the data presented here it can also be shown, with the aid of the relations[4] for α and β that the multiplier of Z_l in Equation [6] is less than 2 per cent of that for Z_g and since Z_l and Z_g should not exceed unity, the second term is dropped, that is, if the gas rate is not controlling

$$\frac{h_{TP}}{h_l} = \frac{\alpha^{0.1}}{R_l^{0.9}} Z_g \quad \ldots\ldots [7]$$

Again using the relations for α the data where plotted to obtain the empirical relation

$$Z_g = \frac{1}{1 + 0.006(D_p G_g \mu_g)^{3/5}} \quad \ldots\ldots [8]$$

[4] For turbulent-turbulent flow from Martinelli and Lockhart (2).
$\alpha = R_l^{4}\phi_l^{2.22}$ α function of X.
$\beta = R_g^{4}(X\phi_l)^{2.22}$ α function of X.

The use of the gas-phase Reynolds modulus for this relation was arbitrary and for convenience since it is evaluated as a criterion for the mode of flow.

This development is admittedly crude and the correlation obtained with it as shown in Fig. 12 may not be any better than that based on the two-phase pressure drop. Considerable additional data for other systems and fluids will be necessary to answer these questions.

ACKNOWLEDGMENT

The authors are deeply grateful for the technical assistance of C. D. King and F. Rossi, the very helpful suggestions of Dr. R. A. Seban, and for the aid in construction of the equipment to H. L. Eagles and F. W. Moore.

BIBLIOGRAPHY

1 "Heat Transfer and Pressure Drop During Two-Phase, Two-Component Flow in a Horizontal Tube," by A. H. Abou-Sabe PhD thesis, University of California, Berkeley, 1951.

2 "Proposed Correlation of Data for Two-Phase, Two-Component Flow in Pipes," by R.W. Lockhart and R.C. Martinelli, *Chemical Engineering Progress*, vol. 45, 1949, pp. 39–48.

3 "Isothermal Pressure Drop for Two-Phase, Two-Component Flow in a Horizontal Pipe," by R. C. Martinelli, L. M. K. Boelter, T. H. M. Taylor, E. G. Thomsen, and E. H. Morrin, Trans. ASME, vol. 66, 1944, p. 139.

4 "Co-Current Gas-Liquid Flow. I. Flow in Horizontal Tubes," by O. P. Bergelin and Carl Gazley, Jr. Published by THE AMERICAN SOCIETY OF MECHANICAL ENGINEERS, May, 1949, and presented at the Heat Transfer and Fluid Mechanics Institute, Berkeley, Calif., June 22–24, 1949.

5 "Heat Transmission," by W. H. McAdams, McGraw-Hill Book Company, New York, N. Y., 1942, p. 168.

6 Discussion of "Proposed Correlation of Data for Two-Phase, Two-Component Flow in Pipes," by Carl Gazley, Jr., and O. P. Bergelin, *Chemical Engineering Progress*, vol. 45, 1949, pp. 45–48.

7 "Theory of Pressure Drop and Heat Transfer for Two-Phase, Two-Component Annular Flow in Pipes," by Salomon Levy, MS thesis, University of California, Berkeley, 1951.

8 "Flow of Steam and Condensation as Affected by High Pressures, Horizontal Offsets and Valves," by L. Ebin and R. L. Lincoln, Trans. ASHVE, vol. 30, 1924, pp. 323–338.

9 "Critical Velocity of Steam and Condensate Mixtures in Horizontal, Vertical, and Inclined Pipes," by F. C. Houghten, L. Ebin, and R. L. Lincoln, Trans. ASHVE, vol. 30, 1924, pp. 139–156.

10 "Supersaturation and Flow of Wet Steam," by G. A. Goodenough, *Power*, vol. 66, 1927, pp. 466–469 and 511–514.

11 "Supersaturated Steam," by J. I. Yellott, Jr., Trans. ASME, vol. 56, 1934, paper FSP—56-7, pp. 411–430.

12 "Fluid Flow Through Two Orifices in Series," by M. C. Stuart and P. R. Yarnall, *Mechanical Engineering*, vol. 58, 1936, pp. 481–484.

13 "Flow of Boiling Water Through Orifices and Pipes," by W. T. Bottomley, Trans. Northeast Coast Institution of Engineers and Shipbuilders, (England), vol. 53, 1936–1937, pp. 65–100.

14 "The Co-Current Flow of Liquids and Gases in Pipes," by R. L. Hershey of E. L. du Pont de Nemours and Co.; paper presented before the Fifth Chemical Engineering Symposium, Division of Industrial and Engineering Chemistry, American Chemical Society at Carnegie Institute of Technology, December 27–28, 1938.

15 "Heat Transfer for Boiling Inside Horizontal Tubes," by W. K. Woods, Doctor of Science thesis, Massachusetts Institute of Technology, 1940.

16 "Vaporization Inside Horizontal Tubes I," by W. H. McAdams, W. K. Woods, and R. L. Bryan, Trans. ASME, vol. 63, 1941, pp. 542–552.

17 "Vaporization Inside Horizontal Tubes II. Benzene Oil Mixtures," by W. H. McAdams, W. K. Woods, and L. C. Heroman, Trans. ASME, vol. 64, 1942, pp. 193–200.

18 "The Flow of Saturated Water Through Throttling Orifices," by M. W. Benjamin and J. G. Miller, Trans. ASME, vol. 63, 1941, pp. 419–426.

19 "The Flow of a Flashing Mixture of Water and Steam Through Pipes," by M. W. Benjamin and J. G. Miller, Trans. ASME, vol. 64, 1942, pp. 657–669.

20 "Studies of Heat Transmission Through Boiler Tubing at Pressures From 500 to 3000 Pounds," by W. F. Davidson, P. H. Hardie, C. G. R. Humphreys, A. A. Markson, A. R. Mumford, and T. Ravese, Trans. ASME, vol. 65, 1943, pp. 553–591.

21 "Prediction of Pressure Drop During Forced-Circulation Boiling of Water," by R. C. Martinelli and D. B. Nelson, Trans. ASME, vol. 70, 1948, pp. 695–702.

22 "Flow of a Flashing Mixture of Water and Steam Through Pipes and Valves," by W. F. Allen, Jr., Trans. ASME, vol. 73, 1951, pp. 257–265.

23 "Simultaneous Flow of Water and Air in Pipes," by L. S. O'Bannon, Trans. ASHVE, vol. 30, 1924, pp. 157–166.

24 "Flow Resistance of Gas-Oil Mixtures," by L. C. Uren, P. P. Gregory, R. A. Hancock, and G. V. Feskov, *Oil and Gas Journal*, vol. 28, October, 1929, pp. 148 and 152.

25 "Hydraulics in Flowing Wells," by J. Versluys, Trans. AIME, Petroleum Division, vol. 86, 1930, pp. 192–204.

26 "Pressure Drop Accompanying Two-Component Flow Through Pipes," by L. M. K. Boelter and R. H. Kepner, *Industrial and Engineering Chemistry*, vol. 31, 1939, pp. 426–434.

27 "A Method of Determining the Pressure Drop for Oil-Vapor Mixtures Flowing Through Furnace Coils," by F. W. Dittus and A. Hildebrand, Trans. ASME, vol. 64, 1942, pp. 185–192.

28 "Two-Phase, Two Component Flow in the Viscous Region," R. C. Martinelli, J. A. Putnam, and R. W. Lockhart, Trans. AIChE, vol. 42, 1946, p. 681.

29 "Co-Current Gas-Liquid Flow, II Flow in Vertical Tubes," by O. P. Bergelin, P. K. Kegel, F. C. Carpenter, and Carl Gazley, Jr. Published by THE AMERICAN SOCIETY OF MECHANICAL ENGINEERS, May, 1949, and presented at the Heat Transfer and Fluid Mechanics Institute, Berkeley, Calif., June 22–24, 1949. ASME Publication, May, 1949.

30 "Transition Behavior of Two-Phase, Two-Component Fluid Flow in Tubes," by T. Kawaratani, MS thesis, University of California, Berkeley, 1951.

Discussion

CARL GAZLEY, JR.[5] This paper provides much interesting and useful data and should serve as a basis for determination of local heat-transfer rates occurring during forced-circulation boiling.

As the authors point out, the effects of the type of flow (e.g., whether stratified, sluggish, or annular) are probably important in both pressure-drop and heat-transfer considerations. In our work at the University of Delaware[6] on the stratified types of flow it was found that the initiation of waves and slugs was accompanied by appreciable increases in both pressure drop and mechanical energy dissipation at the air-water interface. In this connection it would be interesting to know whether the authors utilized their traversing thermocouple to evaluate the relative amounts of heat picked up by the two fluids and hence the interfacial heat-transfer rate.

Establishment of the limits of the various types of flow is probably as difficult as establishment of an exact criterion for the laminar-turbulent transition point in single-phase flow. The effects of a variety of external factors, e.g., mixing device or vibration, probably predominate. In our work we found that waves could be initiated by small external vibrations.

C. V. STERNLING[7] AND C. E. SANBORN.[7] This paper makes a significant contribution in an important field where little, even of an empirical nature, is known. The data should be useful in analyzing similar situations; however, as stated by the authors, much work involving other vapor-liquid systems is certainly needed.

It is stated that the investigation is limited to two-phase-flow conditions where compressibility, momentum, and phase-change effects are negligible. It is by no means certain that this is true for all the data presented. In the runs at high air and water rates the ratio of inlet to outlet pressure is large so that the flow should properly be treated as compressible. Also, the addition of heat to a saturated air-water mixture inherently involves the transfer of mass. In the runs at low water rates, the outlet temperature is generally high so that the partial pressure of water vapor can become a major fraction of the total pressure. Consequently, the volumetric ratio of gas to liquid may change many fold from the inlet to outlet. Though perhaps not directly significant in relation to the heat transferred, the quantities of mass transferred do greatly affect the volume fraction liquid R_L, and the liquid velocity, and hence the pressure drop and local heat-transfer coefficient.

The authors should be congratulated for developing an accurate experimental technique for measuring the volume fraction liquid. However, in the nonisothermal case the method may not give results corresponding to the actual experimental conditions. During a run a considerable temperature gradient exists along the length of the tube so that the temperature of the air-water mixture may be greatly different from the temperature of the water used to displace vapor from the tube. During this determination, some condensation or evaporation undoubtedly occurs; perhaps

[5] General Engineering Laboratory, General Electric Company, Schenectady, N. Y. Jun. ASME.

[6] Authors' bibliography, reference (4).

[7] Shell Development Company, Emeryville, Calif.

the water temperature is such that these counteract or nearly so. In any event it is not apparent that the length average fraction liquid thus determined is a significant parameter. It is the fraction liquid at a given cross section, which varies greatly from inlet to outlet, that determines the heat transfer and pressure-drop characteristic at that point. The functional variation of these quantities with fraction liquid is unknown, but does exhibit maxima, at least in the case of the heat-transfer coefficient in a vertical tube as recently shown by Verschoor and Stemerding.[5] It is improbable that a simple average would correctly reflect this complex relation. In particular, the occurrence of maxima or of any rapid changes in the dependent variables are obscured by the use of an average value.

It is mentioned that the apparatus used was provided with a pressure tap at its mid-point. Perhaps the authors have data on the differences in pressure drop, and so forth, between the two halves of the tube which might throw some light on these questions.

It is suggested that the deviations between volume fraction liquid for the runs at low water rate which appear to deviate from the curve defined by the other data might be explained in part by the change in volumetric-phase ratio along the tube.

The applicability of the log mean temperature difference is somewhat questionable. Its validity is contingent upon, among other conditions, the constancy of the local over-all heat-transfer coefficient. This condition is certainly not met in those runs where the vapor-liquid ratio changes appreciably.

The attempt to describe the limits of various regimes of flow in detail is admirable and of great importance. Many questions in fluid flow cannot be answered now simply because we do not know what type of flow exists. In addition, a final correlation eventually must be described in terms of actual flow regimes rather than by such arbitrary descriptions as turbulent-turbulent, viscous-turbulent, and so on. It is known that quite considerable changes in heat-transfer rate occur at the transition between types of flow. For example, Verschoor and Stemerding[5] recently have found that changes in the curve relating heat-transfer coefficient with the gas rate coincide in certain cases with transitions between bubble flow and slug flow and between slug flow and annular flow in a vertical tube.

Authors' Closure

The several pertinent questions submitted by Messrs. Sternling and Sanborn concern the effect of the change in momentum rate on the evaluation of the two-phase friction pressure drop and secondary effects of vaporization on the heat-transfer coefficients.

The momentum change which can occur in the test system is due to the acceleration produced by the change in density of the gas or vapor phase and this is influenced by the change in local pressure and temperature and also by such vaporization of the liquid phase as occurs. For these conditions, accounting for the vapor in the gas, the liquid-volume fraction can be expressed as

$$R_l = \frac{W_l/\rho_l}{(W_l/\rho_l) + (W_v + W_g)/(\rho_v + \rho_g)}$$

where

W_v = vapor flow rate as required for air saturation
ρ_v = specific weight of vapor at saturation pressure
ρ_g = specific weight of dry air at corresponding partial pressure

Incorporation of this expression into that for the portion of the measured two-phase pressure drop which is due to the change in momentum yields for that quantity the expression

$$\Delta P_M = \frac{G_1^2}{\rho_{g2}}\left(\frac{1}{R_{l2}} - \frac{1}{R_{l1}}\right) + \frac{G^2_{vg2}}{\rho_{vg2}\, gR_{vg2}} - \frac{G^2_{g1}}{\rho_{g1}\, gR_{g1}}$$

where G = weight rate of flow per unit cross-sectional area, lb/ft²-hr.

Table 3 of this closure contains values of this quantity, and values of the parameter $^1\phi_l$ corrected by subtraction of this momentum contribution from the observed two-phase pressure drop. Magnitudes are given for the extreme values of the flow rates and the correction is revealed to be significant in the cases of large ratios of air to water rates.

These evaluations show that momentum-effect corrections should have been applied for the pressure-drop parameter ϕ_l for all high air rates and for all low liquid rates. Had this been done the agreement with the Martinelli curve in Fig. 8 of the paper would be improved. The heat-transfer coefficients, however, do include the heat-of-vaporization contribution as indicated by the heat balances shown in Table 3 and inferred in the text of the paper.

The mean liquid-volume fraction R_l is not considered directly significant in the correlation of pressure drop but its measurement is of interest as a possible equivalent for identifying the flow patterns and for further development of analysis.

Fig. 13 of this closure compares the heat-transfer performance for this system with that reported by Verschoor and Stemerding. Agreement is not expected, however, since the reference system is

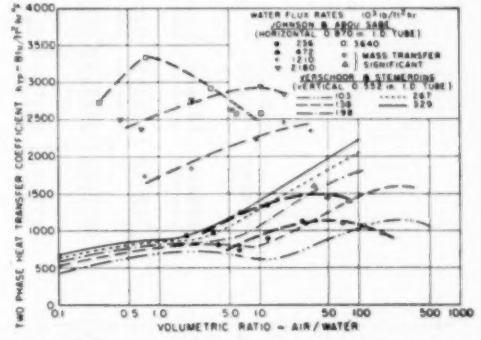

Fig. 13 Comparison With Results Reported by Verschoor and Stemerding

vertical (i.e., a more favorable arrangement for definitive slug and annular flow patterns) and limited to lower liquid-flow rates. It is believed that these two differences contribute to the development of maxima which probably included significant mass-transfer effects. It also should be noted that the volumetric flow-rate ratio is not suited for comparison since the density of the gas phase may have been different in the two test systems.

The mid-point pressure tap was used throughout the test program; however, the pressure drops were equal in the two half-sections indicating that the variation of R_l in each section is substantially the same.

Unfortunately, the condensate collection in the two sections was not measured separately as originally planned so that no comparison can be made of the relative heat-transfer performance of two half-sections.

The logarithmic mean temperature difference is strictly appro-

[5] "Heat Transfer in Two Phase Flow," by H. Verschoor and S. Stemerding, The Institution of Mechanical Engineers, General Discussion on Heat Transfer, London, England, Sept. 11–13, 1951, sect. 2, p. 27.

TABLE 3 SUPPLEMENTAL ESTIMATES FROM NONISOTHERMAL DATA OF TABLE 2

Air rate, scfm	W_{eo}, lb per hr	R_{ti}	R_{to}	ΔP_M, psf	X, Fig. 8	ϕ_{lo}, Fig. 8	ϕ_{lo}, Cor	Q_B/A_i, Btu/hr ft²	$\frac{Q\Delta h}{Q_{cond}}$
				Water rate = 975 lb per hr					
1 03	7 72	0 214	0 056	29 5	5 9	3 57	2 80	2120	1 03
44 7	92 3	0 012	0 004	469	0 24	13 4	10 2	25300	1 04
				Water Rate = 1950 lb per hr					
0 97	2 02	0 372	0 224	16	11 8	2 40	2 20	560	1 06
42 7	37	0 028	0 014	356	0 44	7 65	6 4	10200	0 8
				Water Rate = 5000 lb per hr					
0 96	1 28	0 632	0 472	31	27 8	1 56	1 49	357	1 03
44 7	29	0 072	0 038	823	1 24	4 68	3 80	8000	0 94
				Water Rate = 9000 lb per hr					
1 0	0 80	0 776	0 668	30	50	1 36	1 31	220	1 03
44 0	13 5	0 181	0 108	820	2 4	3 28	2 84	3740	0 96
				Water Rate = 15000 lb per hr					
1 06	0 52	0 874	0 802	56	84	1 20	1 17	136	1 01
43 2	6 2	0 317	0 215	771	4 4	2 27	2 04	1700	1 01

Note: W_{eo} = vapor rate at exit based on assumption of saturated vapor.
Q_B/A_i = heat flux due to the vaporization assuming saturated vapor.
$Q\Delta h$ = heat transfer based on increase of enthalpy which includes vaporization contribution. Note that this is the quantity used in evaluating the two-phase heat-transfer coefficient.
Q_{cond} = Heat transfer deduced from steam condensate measurements.

TABLE 4 SUMMARY OF NONISOTHERMAL TWO-PHASE FLOW DATA FOR 0.736-in.-ID COPPER TUBE

(Atmospheric pressure 14.5 ± 0.1 psia)

Air rate, scfm	P_{in}, psig	t_{fi}, deg F	t_{fo}, deg F	ΔP_{TP}, psf	t_{wo}, deg F	Q/A_i, Btu/hr ft²	R_t	Flow type inlet	Flow type outlet
				Water flow rate = 1375 lb per hr					
0 82	1 8	76 6	204	215	211	61000	0 35	STW	SA
1 21	1 4	77 3	202	285	210	60700	0 31	STW	A
2 32	3 2	75 7	201	390	208	62500	0 30	STW	SA
3 72	4 4	77 0	199	464	208	63400	0 25	STW	SA
5 15	5 2	77 6	198	531	205	63500	...	AW	A
5 18	5 7	77 1	201	537	204	66100	0 25	AW	A
11 9	9 5	76 5	193	984	204	65300	0 18	AW	A
24 6	15 0	75 8	186	1569	204	65000	0 14	AW	A
42 5	21 2	75 8	178	2264	202	63000	0 12	AW	A
				Water flow rate = 3570 lb per hr					
1 30	5 0	97 4	191	578	206	113500	0 48	A	A
3 95	6 7	98 8	186	952	195	108100	0 36	A	A
5 28	8 4	96 4	186 2	1132	198	115700	0 33	A	A
13 92	15 8	93 3	188	1936	196	121600	0 26	AB	AB
24 0	22 1	94 2	185	2576	194	120000	0 20	AB	AB
43 7	32 1	93 0	178	3283	192	116100	0 16	AB	AB
				Water flow rate = 6410 lb per hr					
1 02	5 6	103	175	692	194	156000	0 75	B	SIA
3 80	11 2	104	180	1510	191	163200	0 45	B	SIA
5 38	14 0	103	179	1670	192	167100	0 40	AB	SIA
11 82	20 1	103	177	2580	189	166000	0 34	AB	SIA
24 0	30 8	102	170	3530	184	151800	0 22	AB	SIA
38 8	40 5	103	169	4460	185	149000	0 24	AB	SIA

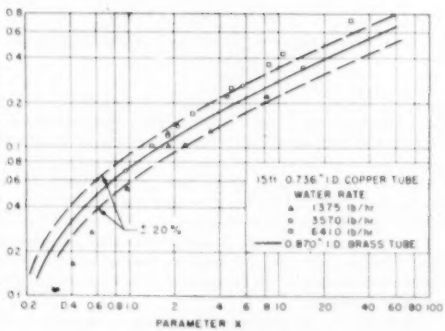

FIG. 14 COMPARISON OF HEAT-TRANSFER RESULTS FOR THE 0.736-IN AND 0.870-IN-ID TUBES

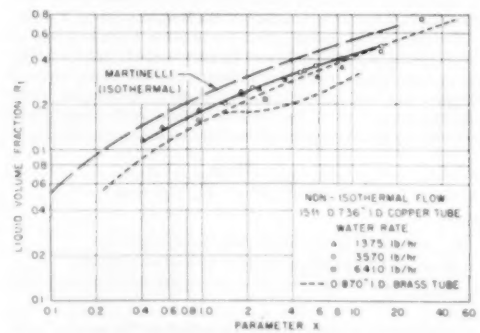

FIG. 15 COMPARISON OF LIQUID-VOLUME-FRACTION RESULTS FOR 0.736-IN. AND 0.870-IN-ID TUBES

priate only when the thermal resistance between fluids or reference surface and fluid is invariable with length. An appropriate mean or equivalent heat-transfer coefficient does satisfy this requirement if the tube-wall temperature is constant. If, however, the actual local heat-transfer coefficients are subject to large variations along the tube length, subsequent data will show the heated length to be a significant parameter. Separate condensate collection from the two test sections is planned for this purpose. There may remain some further question as to the validity of these mean heat-transfer coefficients since the observed wall-temperature variation (±10 deg F) was greater than anticipated. But the single-phase water-flow tests, cited in the paper, are believed satisfactory evidence that this variation is admissible.

Mr. Gazely has inquired as to response of the traversing thermocouple at the air-water interface. These data were obtained for the majority of the tests but the observed flow patterns, including annular flow, always indicated substantial liquid mist in the air stream and the thermocouple is believed to have measured only liquid temperatures. In fact, when averaged across the stream the value agreed with the mixing-pot temperature or was too low, indicating significant mass-transfer effects.

Since the original data were submitted for the paper the test system has been rebuilt and fitted with an extra heavy wall copper pipe (0.736 in. ID) in which the 24 wall thermocouples are imbedded and made flush with the outside tube surface. The data for this pipe as obtained by Mr. C. D. G. King[9] are presented in Table 4, herewith, and a comparison with the original data is shown in Figs. 14 and 15. In Fig. 15 it is noted that the departure in R_l for low liquid rates which is not evident in these more recent data may be due to differences in testing techniques, i.e., elapsed time in the measurement of R_l as was suggested by the discussers.

The authors wish to thank the discussers for their interest and helpful suggestions and to acknowledge the additional data supplied by Mr. King. It is also hoped that others interested in this problem will find these data of value in their efforts to extend the analyses of two-phase flow systems.

---

[9] Instructor in Mechanical Engineering, Washington University, St. Louis, Mo.

Runaway Speed of Kaplan Turbines

By G. H. VOADEN,[1] YORK, PA.

The object of this paper is to illustrate the type of laboratory test data which a turbine manufacturer must have to predict intelligently the runaway speed of a Kaplan turbine. The significant differences between the "on-cam" and "off-cam" runaway speeds are explained and data on actual runaway-speed tests conducted on a large Kaplan turbine installation are given. Attention is called to the possibility of reducing the runaway speed by restricting the minimum angle to which the runner blades can be pitched, and information is presented that will aid the purchaser of a Kaplan turbine to decide what runaway speed should be provided for in the generator.

THE runaway speed of Kaplan turbines is, in general, 2.5 to 3 times normal speed whereas with Francis turbines it is rarely over twice normal. This high runaway speed requires greater understanding and consideration in design by the manufacturers of Kaplan turbines, by the purchaser and operators, and by the generator manufacturer. In both types the runaway speed of a prototype can be predicted from the laboratory test of an homologous runner by proportioning inversely as the runner diameter and as the $\sqrt{H}$. It has also been found by laboratory test that the runaway speed is affected by the cavitation characteristic "sigma," i.e.

$$\frac{H_B - H_V - H_S}{H}$$

where

H_B = barometric pressure, ft of water
H_V = vapor pressure, ft of water
H_S = distance of runner above tailwater, ft
H = net head on turbine, ft

The effect of the cavitation characteristic on runaway speed is much more pronounced in a Kaplan turbine than in a Francis turbine as will be seen by comparing Figs. 1 and 2. For all practical purposes this effect can be neglected with a Francis turbine, but with a Kaplan turbine it is very significant.

Runaway speed of both Kaplan and Francis turbines also varies with gate opening, and it will be seen from Figs. 1 and 2 that the maximum runaway speed is not necessarily at full gate opening, for a given sigma value.

In a Kaplan turbine there is an additional variable—the blade angle—providing an infinite number of possible combinations of blade angle and gate opening if the blades and gates either accidentally or intentionally are out of their proper controlled relationship as determined by a cam, i.e., off-cam. In a Kaplan turbine there is, from the standpoint of turbine efficiency, an optimum relationship between runner blade angle and wicket-gate opening, this relationship being determined by laboratory tests

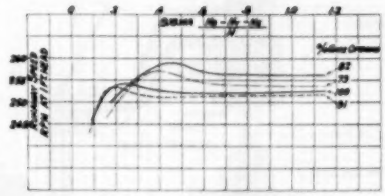

FIG. 1 RUNAWAY-SPEED TEST OF MODEL FRANCIS TURBINE SHOWING VARIATION WITH SIGMA AND GATE OPENING

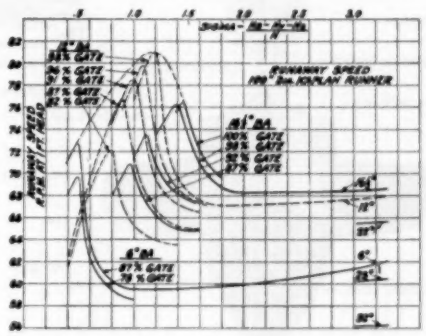

FIG. 2 RUNAWAY-SPEED TEST OF MODEL KAPLAN TURBINE SHOWING VARIATION WITH SIGMA, BLADE ANGLE, AND GATE OPENING

and usually checked in the field by means of an index test.[2] Fig. 3 shows a typical blade-pitching mechanism. Starting with the mechanical connection from the gate-operating mechanism to the blade cam, the functional operation may be traced readily through to the pitching of the runner blades.

In order to make an intelligent prediction of the maximum possible runaway speed for a Kaplan turbine, a manufacturer must have laboratory test data of the type illustrated in Fig. 2. To avoid confusion this figure omits the data of 9, 22, 28, and 32 deg at the lower sigma values. This curve applies only to one particular design of runner blade. Other designs of this same manufacturer will have different runaway-speed characteristics and certainly those of other manufacturers will also.

At the time these particular model tests were made, i.e., in 1935, prior to the first two Bonneville units, no thought was given to designing the generators for any lower runaway speed than the maximum off-cam blade-gate relation could produce. Hence model tests for runaway speed were not made at the low gate openings or on-cam relationship and cannot be shown in Fig. 2.

RUNAWAY-SPEED TESTS AT BONNEVILLE

Fig. 4 shows actual runaway speed attained under tests on the Bonneville main units, supplemented where necessary by tests

---

[1] Assistant Chief Hydraulic Engineer, S. Morgan Smith Company. Mem. ASME.

Contributed by the Hydraulic Division and presented at the Annual Meeting, Atlantic City, N. J., November 25–30, 1951, of THE AMERICAN SOCIETY OF MECHANICAL ENGINEERS.

NOTE: Statements and opinions advanced in papers are to be understood as individual expressions of their authors and not those of the Society. Manuscript received at ASME Headquarters, October 9, 1951. Paper No. 51—A-100.

[2] "Index Testing of Hydraulic Turbines," by G. H. Voaden, Trans. ASME, vol. 73, 1951, p. 481.

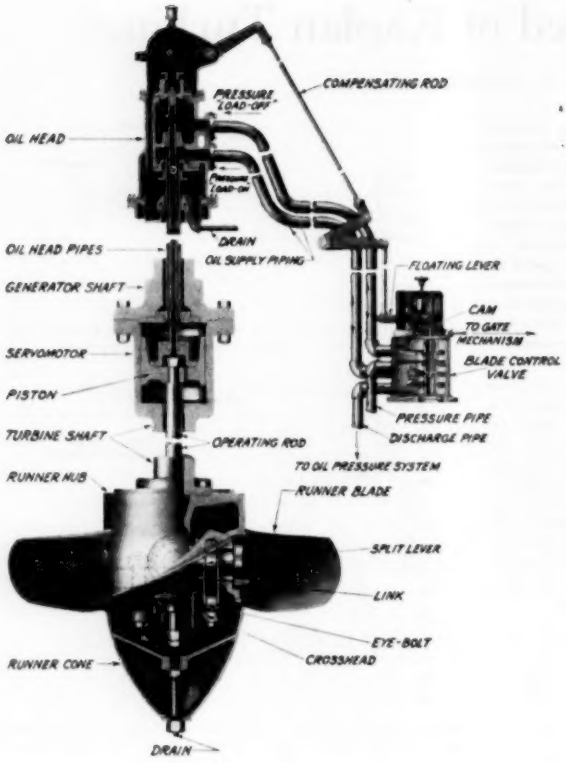

FIG. 3 SCHEMATIC ARRANGEMENT OF TYPICAL BLADE-OPERATING MECHANISM FOR A KAPLAN TURBINE

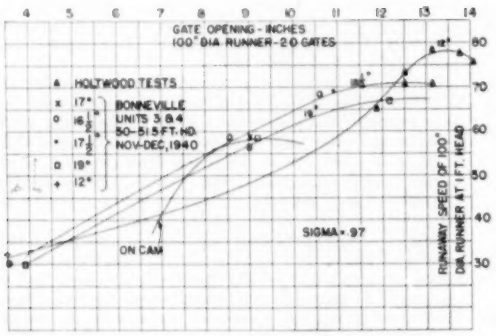

FIG. 4 ON-CAM VERSUS OFF-CAM RUNAWAY SPEED BASED ON BONNEVILLE FIELD AND HOLTWOOD MODEL TESTS

made at Holtwood on a 16-in-diam runner at 1 ft head for comparison. The method of obtaining the on-cam runaway-speed curve is illustrated by the following example: At $16^1/_2$ deg BA it was found from an index test of the unit that the correct on-cam gate opening was 8.25 in. In Fig. 4 at 8.25 in. and $16^1/_2$ deg BA the runaway speed is 56 rpm which, therefore, is one point on the on-cam runaway-speed curve. It will be seen from Fig. 4 that the maximum on-cam runaway speed is 58.5 rpm. This figure is only 75 per cent of 78 rpm, the maximum off-cam runaway speed.

Substantiated by these field[7] results and by subsequent model tests, it is safe to say that the on-cam runaway speed will not exceed 85 per cent of the maximum possible off-cam speed.

WHICH RUNAWAY SPEED?

Should the turbine and generator be designed for the maximum off-cam runaway speed or the on-cam or normal runaway?

It is not difficult or expensive to design and construct the turbine for the maximum runaway speed, and it is standard practice of the turbine manufacturers to do so. The generator is a more difficult and expensive problem. It is clearly the turbine manufacturer's responsibility to tell the purchaser or his consulting engineer what the estimated maximum off-cam and also the on-cam runaway speeds are and to provide any other data to assist in making the decision as to which runaway speed should be provided for in the generator.

As an aid to the purchaser and his consultants in making this decision the following data and discussion should be useful:

1 What are the probabilities of the maximum off-cam runaway speed being attained?

2 What are the probable effects of maximum runaway speed on the unit?

Referring to (1), it will be seen from Fig. 2 that there is an infinite number of off-cam blade-gate relationships which would not produce the maximum runaway speed. However, it is always possible to obtain the worst possible relationship deliberately by voiding the cam, locking the blades by governor oil pressure or some mechanical means, and operating the gates by hand—or vice versa. The chances of obtaining this combination accidentally will now be discussed.

Fig. 5 shows typical blade-operating curves of work required to pitch the blades in each direction. It will be noticed that as the rpm increase above normal, it requires less and less force to open them, and above a speed of about 40 per cent above normal, the blades will open by themselves. Thus if the oil pressure to the blades were lost or the mechanical linkage were to break so that the blades were out of control, they would not remain at a low pitch where maximum runaway is attained but would drift rapidly to a high pitch where the runaway speed is low (see Fig. 2).

Fig. 6 shows a typical chart of differential gate-operating pressures. It will be seen that the hydraulic forces on the gates are balanced at a very low gate opening—about 15 per cent. Therefore, on loss of control of the gates, they would drift rapidly to a position far below the opening required for maximum runaway speed.

If the blades were to stick because of increased friction at the worst pitch for runaway speed, and the gates were still under governor control, and the unit were isolated, and the load increased sufficiently, the governor would keep on opening the gates to the maximum opening. Then if the load were suddenly lost, the governor would close the gates fully and would pass through the gate position for maximum overspeed, but only momentarily as the total closing time would be a matter of only 2 to 8 sec.

Fig. 7(a) shows a typical speed-time chart obtained during a

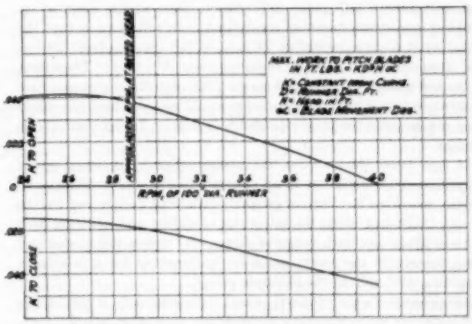

FIG. 5 TYPICAL KAPLAN BLADE-OPERATING FORCES SHOWING VARIATION WITH SPEED

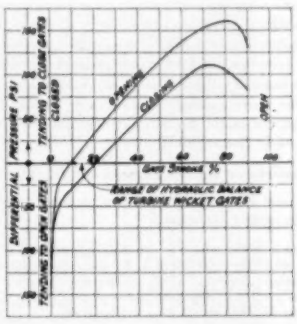

FIG. 6 TYPICAL WICKET GATE DIFFERENTIAL OPERATING PRESSURES

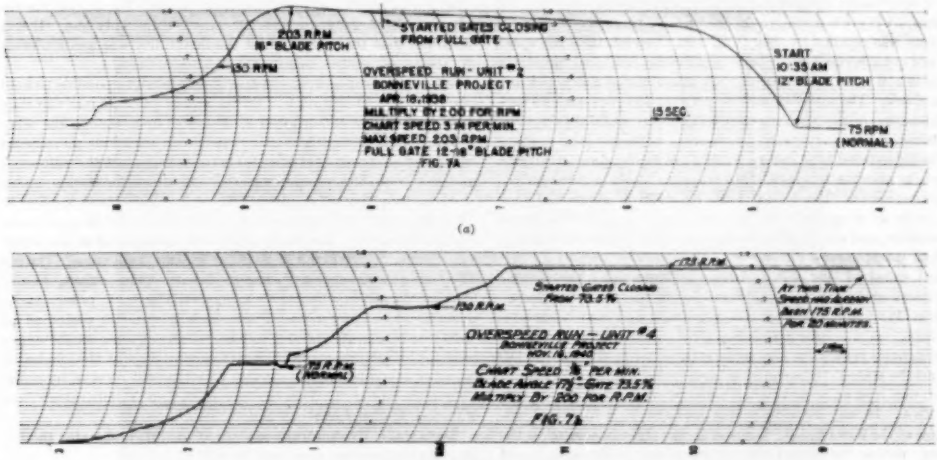

FIG. 7 TYPICAL SPEED-TIME CHARTS OF KAPLAN TURBINE WITH NO LOAD AND DISCONNECTED FROM EXTERNAL LOAD
(a, Bonneville unit No. 2 at full gate and with blades "fixed" at angle for maximum runaway. b, Bonneville unit No. 4, gates and blades controlled to test at 175 rpm, 133 per cent above normal for 30 min.)

test with blades and gates deliberately fixed at the start at estimated maximum runaway conditions. It will be seen that the speed went from a normal of 75 rpm to 170 rpm in about 38 sec, and from normal to 203 rpm required about 3¾ min. Therefore, in the foregoing example, just passing through the maximum runaway-speed condition momentarily would not produce anywhere near maximum overspeed—probably not even 10 per cent above normal.

It has been shown that maximum off-cam runaway speed cannot occur (*a*) with loss of oil pressure to either or both gates or blades, provided they are of properly balanced design and free to move; (*b*) except when the tail-water elevation and head are such as to produce a certain range of sigma; (*c*) unless the blades and gates remain in the worst possible combination for a relatively long time (3¾ min in the example given).

Maximum off-cam runaway speed can occur only if the blades and gates are deliberately or accidentally locked or "stuck" for a relatively long time in certain definite positions and at the same time sigma must be at the worst possible value.

To the author's knowledge, maximum off-cam runaway speed has never to date occurred accidentally on a Kaplan turbine. It is possible to produce it deliberately and it is, therefore, physically possible to produce it accidentally, operators and test engineers being human; however, the probability is decidedly remote.

Referring to item (2), there is only one example of maximum off-cam runaway speed actually having been obtained on automatically adjustable-blade Kaplan turbines and that was deliberately, on the early Bonneville units.

Case History of Runaway Speed at Bonneville

Briefly, the case history in respect to runaway speed on the Bonneville main units is as follows:

Units Nos. 1 and 2 (280-in-diam Smith-Kaplan runners)
Turbine rating, 60 ft head, 60,000 hp, 75 rpm, shaft diameter 39 in.
Estimated runaway speed, at 60-ft head with full gate and with blade angle for maximum runaway speed of 216 rpm
Generator rating, 48,000 kva, 13.8 kv, 3 phase, 60 cycle, designed for runaway speed of 216 rpm

On March 28, 1938, runaway-speed tests were made on unit No. 1 with blades blocked at a 12-deg angle, full gate opening for 2.1 min, 51 ft gross head, plant sigma 0.935. A runaway speed of 189 rpm was reached in about 2.37 min at which time the speed had not quite leveled off. Correcting this for head and sigma, the figure is 210 rpm, as compared with an estimated 216 which is a close check. The unit ran satisfactorily at 189 rpm with no serious vibration of the head cover or whip of the shaft, although the cavitation noise was terrific. However, while the gate opening was being reduced toward zero, at a rate corresponding to full gate closure in about 2½ min, a shaft whip and also a vertical pulsating movement of the rotating parts occurred at about 130 rpm. The order of magnitude of the whip was ¼ in. (at the blade servomotor) and the vertical movement ⅛ in. This was frightening but no apparent damage was done. The transverse first critical speed of the unit had been calculated by the turbine manufacturer to be 437.5 rpm and by the generator manufacturer at 425 rpm. The calculated torsional first critical speed is 390 rpm.

No definite reason for the unusual behavior of the unit at 130 rpm can be stated. A reasonable explanation is that the primary factor was hydraulic unbalance aggravated by the abnormally high flow. It may have been due partially to a hydraulic unbalance of the flow from the semispiral case and distributor to the runner; that is, the runner may not have been in the exact center of the natural vortex. If the resulting force normal to the shaft were constantly in one direction the effect would be a deflection, not a whip. Therefore, if this were the sole cause the lateral force must have been shifting in direction. A contributing factor may have been hydraulic unbalance of the runner itself due to differences between the five blades. However, the blades of unit No. 1 were machine-finished, and such unbalance could only have been minor and due to exceedingly small differences in pitch.

There is another possibility in the fact that at runaway speed the downward hydraulic thrust of the runner is reduced appreciably. The axial force, being a resultant of the hydraulic forces and the weight of the rotating parts, may not have been stable. The rate of gate closure also may have had an effect, because on rotational deceleration there is a tendency for the blades to act as a pump forcing the water downward. The rate of gate closure would affect the rate of deceleration, hence the degree of pumping effect, and hence the axial forces of hydraulic origin. All of these items, and possibly others, combined with the degree of rigidity and fixation of the turbine and generator shafts undoubtedly were involved in the instability.

On April 18, 1938, runaway-speed tests were made on unit No. 2 with blades blocked at a 12-deg angle, 50.8 ft gross head, plant sigma 0.94, gates full open for 3.25 min, then closed back to the normal on-cam position. A runaway speed of 203 rpm was reached in about 3.75 min, ½ min after the gates had started to close. Note that the gates were held at full gate for 53 per cent longer time than on the March 28 test, no doubt accounting for the higher speed. Correcting the 203 rpm for head and sigma, the speed would be 225.5 rpm, as compared with the estimated 216. The accuracy of the many measurements considered, both laboratory and field, this also is a reasonable check.

With the hope of eliminating the shaft whips that had occurred on unit No. 1, air was admitted above the runner during the run. The full capacity of two 600-cu-ft compressors was admitted to the head cover at 80 psi. After the gates had started to close, the air valves were opened (to the runner) and, by the time the gates were 10 per cent open, all the air in the tanks had been used as well as the compressor capacity, the pressure being down to zero.

No trouble was experienced except the instability of the rotating elements on closing the gates. The blades of units Nos. 2 to 10 were not machined, so any tendency to runner unbalance between blades was greater on this unit than on unit No. 1; yet the instability of the rotating elements was considerably less. It was assumed that this reduction of the instability was accomplished by the air admission described.

During the runaway-speed test it was found impossible to hold the blades at 12 deg angle. By the end of the 3.75 min run they had drifted from the original 12 to 16 deg even though the relay valve spool controlling the oil pressure to the blade servomotor was blocked closed. This was due to leakage past the valve and possibly past the servomotor piston. In normal operation, under governor control, pressure from the accumulator tank applied to the top of the blade servomotor through the outer oil pipe inside the shaft increases the blade angle, and pressure oil to the under side through the inner oil pipe decreases the blade angle. During the runaway-speed tests, with the Kaplan valve closed, disconnecting the servomotor from the accumulator tank, pressures developed on the under side of the blade servomotor piston at all values of blade pitch above 12 deg in excess of those on the upper side. This demonstrated the strong tendency of the blades to open, thus reducing the runaway speed as will be seen by referring again to Fig. 2. These data also confirm the laboratory data in blade balance shown in Fig. 5.

During the 3¾-min runaway-speed test, the generator thrust-bearing temperature rose from 60 to 85 C.

As a result of these tests it was decided by the purchaser that the generators for the next units would be procured for the maximum runaway speed that could be obtained with gates and blades

in proper relationship, i.e., on cam. A safe estimate of this speed, according to the manufacturer's tests, was 175 rpm. The principal factor in this decision was the extremely difficult design conditions encountered when attempting to design a generator with 25 per cent greater capacity than those of units Nos. 1 and 2 and with stresses within the limits set by the purchaser.

Ratings of Units Changed

On units Nos. 3 to 10 the rating was increased with the same-size runners and water passages because it had been found that without serious cavitation units, Nos. 1 and 2 could be operated far beyond the guaranteed power.

The new ratings were as follows:

Turbine, 60 ft head, 74,000 hp, 75 rpm; shaft diameter increased from 39 to 42 in.
Generator, 60,000 kva, designed for runaway speed of 175 rpm.

Runaway-speed tests were run on November 16, 1940, on unit No. 4, not to determine what the maximum runaway speed would be, but to gain greater knowledge of the functioning of the unit under runaway-speed conditions and particularly in respect to the generator and thrust bearing. The unit was run at 175 rpm for 30 min. With only 55.9 ft head it was necessary to produce an off-cam blade-gate relationship, namely, 17½ deg BA and 73 per cent gate.

This is what happened: The temperature of the thrust bearing plate flattened out in 23 min after rising from 60 to 91 C. The maximum oil temperature was 56.5 C. The turbine bearing temperature did not exceed 55 C. The Kaplan oil-head gland temperature did not exceed 38 C.

There was slight vertical vibration of the head cover—about 0.020 in. at 6-ft radius.

The vibration and noise at the draft-tube mandoor, from cavitation was terrific. Cavitation "implosions" occurred intermittently, sometimes 15 sec apart, sometimes only 5 or 6 sec, but the greater the interval the heavier the implosion. Each implosion was accompanied by a "sheet-lightning" effect in the tailrace—visible even in daytime. Building joints in the substructure opened up and let out a sheet of water with each implosion. Welding on the draft-tube mandoor cracked. Mud

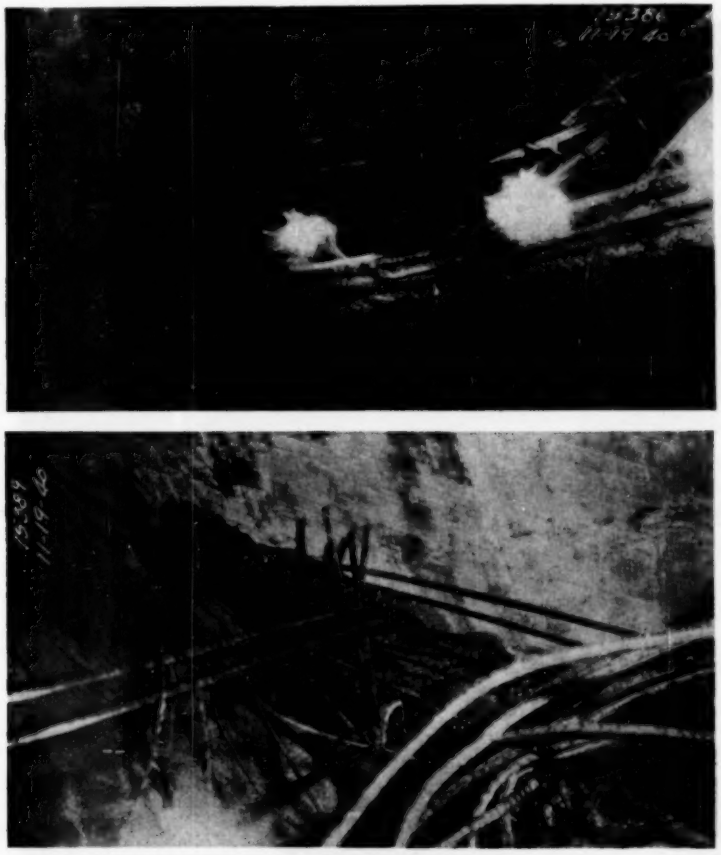

Fig. 8(a) Views of Bonneville Unit No. 4 Draft-Tube Splitter Damaged During Runaway-Speed Test of November 16, 1940

came to the surface in front of the forebay intake and the head gates were "banged around." There was no shaft whip, but a transverse deflection occurred amounting to 0.013 in. at the turbine-generator coupling as compared with 0.008 in. at normal speed. The vertically upward deflection of the rotating elements was 0.035 in. at 175 rpm, as compared with 0.006 in. at normal speed of 75 rpm.

Note that in Fig. 7(*b*), which shows the deceleration subsequent to this run, the closing rate of the gates was much slower than on the test of unit No. 2 shown in Fig. 7(*a*), closure from 73.5 per cent opening to speed-no-load position being performed in approximately 8 min. This may or may not have had some effect on instability of the rotating elements. However, attention is called to (*a*) the greater stability of the 42-in. shaft as compared with 39 in. on units Nos. 1 and 2, and (*b*) the greater weights of shafting and generator rotor. It is the author's opinion that there was very little difference between the hydraulic forces on the first two units and those installed later and that the greatly increased stability at higher than normal speeds on units Nos. 3 to 10 was due to (*a*) and (*b*).

The immediate report of the turbine manufacturer's representative to his home office after this test was "thirty-minute overspeed test completed successfully." Complete inspection of the unit occupied the next day or two. There was no damage to the turbine except that over considerable areas paint was removed from the runner and in certain localized areas the metal was roughened slightly.

Inspection Shows Draft Tube Damage

On November 19, however, when the draft tube was pumped out, it was found that the horizontal splitter was broken out for about 4 ft from the upstream nose. The heavy reinforcing steel was bent almost straight upward by reaction effects from the bottom of the tube. Cracks extended back several feet along the side walls [see Figs. 8(*a*) and 8(*b*), views of damaged splitter, and Fig. 9, over-all dimensions of draft tube]. The damaged splitter was repaired by cutting it back about 6 ft from, and parallel to, the original leading end. The nose was then rounded about as before but somewhat thicker. The unit has been operating satisfactorily since that time.

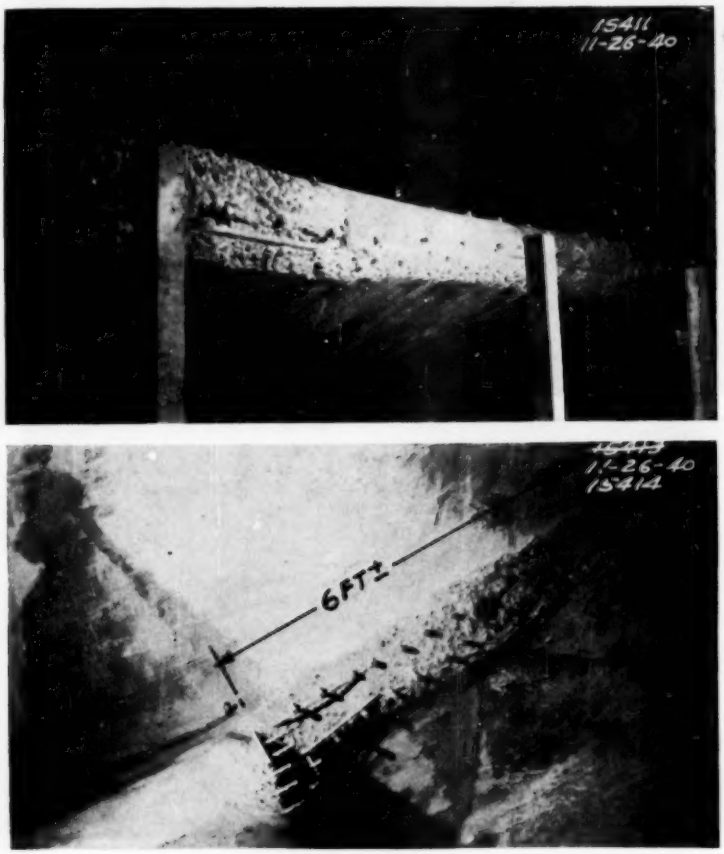

Fig. 8(*b*) Same Splitter, Cut Back Preparatory to Resurfacing of Broken Sections

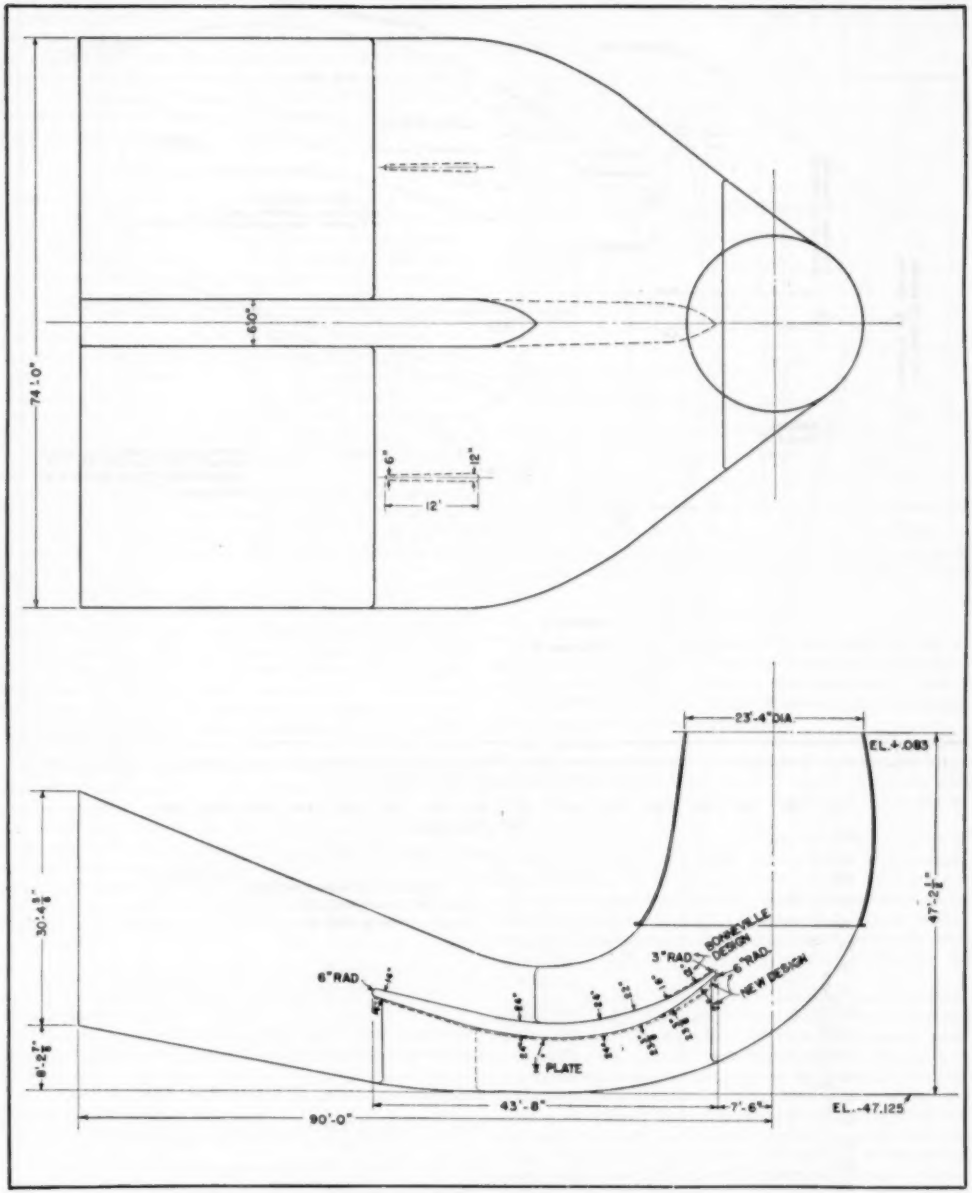

FIG. 9 BONNEVILLE DRAFT TUBE SHOWING OVER-ALL DIMENSIONS AND THICKNESS OF HORIZONTAL SPLITTER WHICH WAS DAMAGED DURING A 30-MIN RUNAWAY-SPEED TEST

(Dotted lines, comparable thickness used for more recent tubes.)

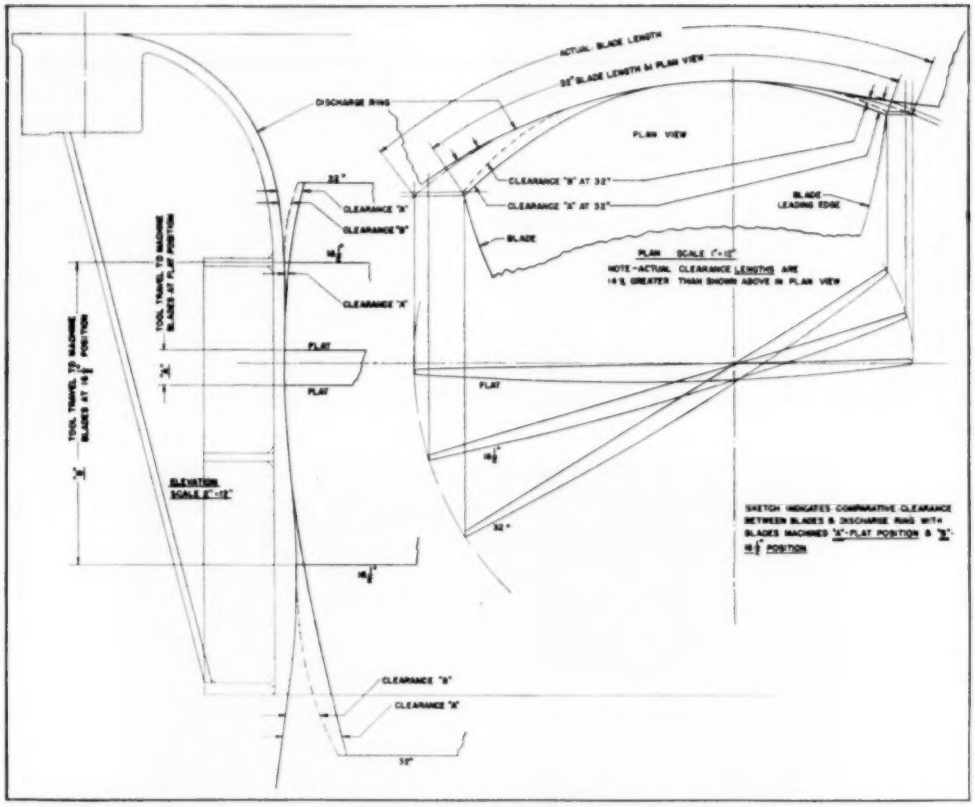

Fig. 10 Illustrating Difference in Blade Clearance With Discharge Ring Between Runners Machined on Periphery at Flat and 16½-Deg Blade Positions

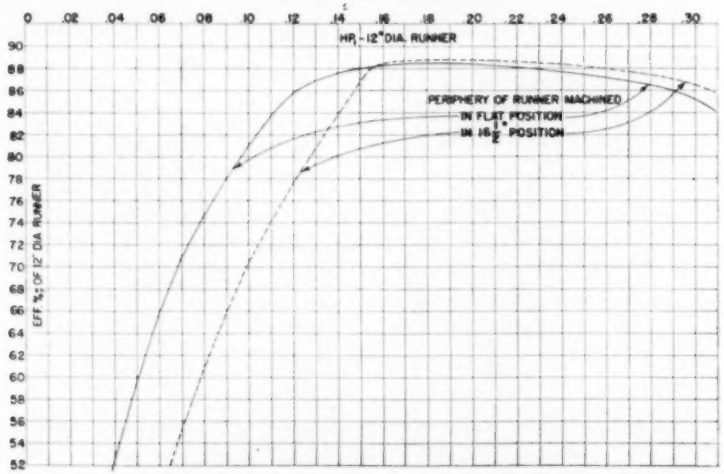

Fig. 11 Illustrating Difference in Performance Between Runners Machined on Periphery at Flat and 16½-Deg Blade Positions

The upstream end of this splitter had been designed structurally for a load of 300 psf. This has proved satisfactory for normal conditions but inadequate for the prolonged incalculable shock loads produced by severe cavitation during the thirty-minute runaway speed test. To permit additional reinforcing, the manufacturer has, on subsequent jobs, increased the thickness of the nose of the horizontal splitter and furnished a rolled surface plate for a considerable portion of the splitter as illustrated in Fig. 9.

Reducing Runaway Speed

Runaway speed of a Kaplan turbine may be reduced by designing the blade mechanism to limit the movement of the blades to some minimum pitch—say, $16^1/_2$ deg, rather than allowing them to go on down to 6 deg (see Fig. 2). In other words, at loads below that requiring $16^1/_2$ deg pitch and best gate opening, the turbine would be a fixed-blade propeller turbine. There is an additional advantage in this. Standard practice is to machine the periphery of the blades when in the flat or 0-deg blade-angle position. As the pitch increases, the clearance and leakage at the periphery increase. By machining at $16^1/_2$ deg to the contour of the discharge ring, the clearance at the higher blade angles is reduced, thus increasing the efficiency appreciably. The disadvantage of this limitation is, of course, loss of efficiency at low loads. However, this is sometimes of little importance, particularly in a plant containing a large number of units.

Fig. 10 indicates the difference in the peripheral clearance at the maximum blade angle when the runner is machined with blades in the flat position (clearance A) and in the $16^1/_2$-deg position (clearance B). Fig. 11 shows the difference in efficiency on a 12-in-diam model runner.

This entire runaway-speed situation was considered very thoroughly by the Corps of Engineers, U. S. Army, in connection with the McNary Project on the Columbia River in the Walla Walla, Washington, District, and also, of course, by the turbine manufacturer. There are presently on order for this development fourteen units with 280-in-diam runners rated at 80-ft head, 111,300 hp at 85.7 rpm. Heads ranging from 62 to 92 ft will be encountered and, therefore, wide variations in sigma and runaway speed.

Fig. 12 shows the expected runaway speeds of the prototype at heads of 92, 85, and 80 ft at the several critical blade angles, based on laboratory tests of a 12-in-diam model. It will be noted that at the 6-deg blade angle, the maximum off-cam runaway speed would be at 252 rpm and on-cam 186 rpm, whereas, if the minimum blade angle is limited to $16^1/_2$ deg, the corresponding figures would be 217 and 178 rpm, respectively.

After due consideration to all factors, it was decided to limit the blade pitch to a minimum to $16^1/_2$ deg. This decision results in the following:

1 Improved efficiency in the range of loads to be carried (but a sacrifice in efficiency if low loads were to be carried as might be the case in other plants).

2 Greatly reduced off-cam runaway speed. The generators have been designed for 190 rpm, 87.5 per cent of the maximum off-cam speed.

3 Reduced capacity requirements for governor oil pumps, pressure and sump tanks.

4 Probably less ultimate maintenance of the discharge ring.

Acknowledgment

The co-operation of Mr. W. K. Cave, Chief, Electrical and Mechanical Branch, Office of Chief of Engineers, Washington, D. C., and of the Corps of Engineers in charge of the Bonneville Plant, in the preparation of this paper is highly appreciated by the author.

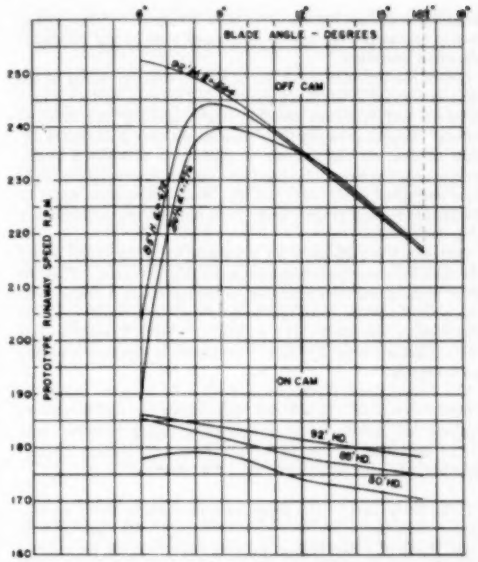

Fig. 12 Study of Runaway Speed Versus Minimum Blade Angle Made for McNary Project From Model Laboratory Tests

Discussion

R. A. Baudry.[2] The tests made on the Bonneville units are of particular interest in that they show the existence of violent shaft and supporting-structure vibrations, which undoubtedly reduce the calculated factor of safety of the turbine and generator structures when operating at maximum speed.

Any move made to alleviate such conditions will be welcomed by the electric manufacturers. The blocking of the blades to an angle of 16 deg is desirable, providing it is made in such a way that under any circumstance the blades cannot move to a smaller angle.

On Kaplan turbines the hydraulic thrusts are much larger than on other types of turbines thus introducing a more difficult starting condition for the generator thrust bearing. On one of the early Kaplan installations the blade angles were limited so as to reduce the thrust load during the starting period. Consequently, if this effect also applies to the modern Kaplan design, the limitation in blade angle to a minimum will benefit further the over-all performance.

It is of interest to note that the runaway speed of a Kaplan turbine usually will be less than the maximum possible under off-cam position, and that the "probability of reaching the maximum overspeed is very remote." Since the probability of running at such speed exists even if very remote, the generator certainly should be designed for this maximum speed.

Under the severe vibrations which occur at runaway speed, the possibility of damage to the blade control mechanism certainly exists. In addition, there is always the possibility of the guiding vanes being jammed by logs or other foreign materials; a blade also could be bent and locked in any position. That the possibility of such an incident exists is shown by the requirement of

[2] Manager, Mechanical Development Section, AC Engineering Department, Westinghouse Electric Corporation, East Pittsburgh, Pa. Mem. ASME.

designing machines for the maximum overspeed. Some hydroelectric operators even specify prolonged tests at the maximum overspeed condition.

Before recommending the use of the on-cam overspeed as the maximum speed to which a generator will operate, turbine manufacturers and operators should weigh carefully the different factors. Recent investigations have shown that it always is difficult to find out the number of overspeeds to which a hydroelectric unit has been submitted and also to determine the maximum overspeed which was reached. Such information could be obtained only from graphic speed indicators always maintained in perfect condition.

Hydroelectric units are built to operate for many years; many machines have now been operating more than 40 years. That the policy of designing these machines for the maximum overspeed was wise is shown by the very few cases of accidents which could be attributed to overspeed. It is certainly advisable to continue this policy if the same good record of operation is expected from the new machines.

The development of positive methods of limiting the overspeed is highly desirable. It is hoped that the author will be able to continue his investigations of operation during runaway conditions and thus be able to further the art of limiting this undesirable operating condition.

D. E. Brainard.[4] The propeller-type turbine was a revolutionary contribution to the hydroelectric field. Its high "specific speed" resulted in the highest possible rotative speed for a given set of hydraulic conditions. This, in turn, reduced size of generator and spacing of units and thus permitted the development of low-head sites that otherwise might not have been economical. The Kaplan turbine, maintaining high efficiency at part load and under variable heads, gave an even greater impetus. On the other hand, the high runaway speed and hydraulic thrust of this type of turbine multiplied the problems of generator design.

The request for a hydrogenerator must specify the runaway speed of the turbine. It is standard practice to provide for this runaway speed in the mechanical design of the generator. The generator supplier is responsible for maintaining proper factors of safety at that runaway speed. The generator supplier is not responsible for damage that may result from operation above the specified runaway speed.

With older types of turbines there has seemed little possibility of exceeding the runaway speed for which the generator was designed unless some obvious and major change was made, such as an increase of operating head or the substitution of a different runner. When the turbine is of the Kaplan type, there is the possibility, as the author states, that a generator designed for the on-cam (or lower) runaway speed might attain the off-cam (or higher) runaway speed. The decision as to the probability of exceeding an assumed reduced value of runaway speed must lie with the prospective owner. He alone must balance the saving in initial cost against the risk of very serious damage that might result from exceeding the design value of runaway speed.

The author has given a valuable exposition of the factors on which this decision may be based. He has indicated that, for his company's designs, the blades tend to open and the gates to close so as to avoid maximum runaway. We hope the discussion will show whether the same tendency is inherent in turbines designed by other companies. It appears inconsistent to propose using the on-cam value for generator design while basing the design of the turbine parts on the higher value.

In the early days of the Kaplan turbine in this country, the off-cam or maximum runaway speed was used generally for generator design. The prevalence of this type of installation led, to the development of special steels for rotor rims, having the desired mechanical properties without sacrifice of magnetic properties. In the majority of cases we have known, a design for the maximum runaway was feasible.

The author implies that units Nos. 3 to 10 at Bonneville are an exception to this statement. Because of a difference in the basis of temperature guarantee, the 60,000 kva generators are actually more than 25 per cent larger than the 48,000 kva units Nos. 1 and 2. Even so, the larger units could have been designed for the 216-rpm runaway speed used for the original and smaller units, but at the expense of an increase of about 250,000 lb in rotor weight as compared with units Nos. 1 and 2. Based on the runaway speed of 175 rpm, which the purchaser specified, the rotor weight increased only 70,000 lb and it was found possible to employ duplicate thrust bearings, with obvious benefits to the purchaser in the way of spare parts.

The Rione project in Uruguay is one of the few cases where it seemed impossible to meet the full off-cam runaway with normal construction and factors of safety. These units are rated 32,000 kva at 125 rpm. The off-cam runaway is 365 rpm, the on-cam value 310 rpm. When American industry was brought in, pit liners already had been installed for three of the four units, thus establishing a greater than normal diameter for the generator. With this handicap, the generator stresses at 365 rpm exceeded good practice and the customer's engineers finally specified a runaway speed of 330 rpm for design.

Difficulty in designing the generator for maximum overspeed should be experienced only in units of exceptional size or unusually high speed, such as those at McNary. In such extreme cases, design for the off-cam value of runaway might require the use of smaller units and a correspondingly larger number of units.

The McNary generators are rated 73,684 kva at 85.7 rpm. Because of a low value of guaranteed transient reactance, these units have the physical size of 90,000 kva generators of standard characteristics, making them among the heaviest and largest-diameter hydrogenerators yet designed. As the author has stated, the generator is being designed for the runaway speed of 190 rpm specified by the purchaser. The generator could have been designed to meet a runaway speed of 217 rpm, but the value of 252 rpm would have been difficult if not impossible to meet with usual construction. Since the thrust bearing load is already 4,000,000 lb as compared with 3,000,000 lb at Bonneville, hitherto the largest known, any reasonable factor which avoids increasing that load seems desirable.

With further reference to the McNary units, it would be instructive to know the method used to prevent the blades from closing below 16 1/2 deg. We understand that, in some cases, this has been accomplished through a fixed stop while in others the blade limit was adjusted by the operator. The latter procedure appears to increase the risk that the maximum runaway may occur. We would appreciate a more specific explanation of the basis for selecting 190 rpm runaway speed rather than 178 (maximum on-cam) or 217 (maximum off-cam) with blades blocked at 16 1/2 deg.

W. K. Cave.[5] Prior to the award of a contract for the first two Bonneville units by the Corps of Engineers, to S. Morgan Smith in May, 1935, a careful investigation was made of all information available concerning the maximum runaway speeds of Kaplan units. The large range in operating heads, 40 to 69 ft, and the selection of the very conservative speed of 75 rpm for the

[4] Large Motor and Generator Engineering, General Electric Company, Schenectady, N. Y.

[5] Chief, Electrical and Mechanical Branch, Engineering Division, Civil Works Office of the Chief of Engineers, Washington, D. C.

normal speed of the turbines, were responsible for the fact that the indicated runaway speeds for the Bonneville units were considerably higher than those which would obtain at other installations.

After due consideration of such factors as increase in generator cost resulting from the higher than normal overspeed design, the lack of prototype information, the installation of protective devices to afford the necessary safety rather than to rely alone on the strength of the revolving elements, and the effect on overspeed of limiting gate opening and blade angle, it was decided to specify that the generators and turbines would be designed for the estimated maximum turbine runaway speed, namely, 216 rpm.

As a result of model tests and prototype tests made on units Nos. 1 and 2 it was decided that the ratings of units Nos. 3 to 10 would be increased to 54,000 kw, and that 175 rpm would be a safe overspeed to use in designing the generators. The estimated weight of rotating parts and hydraulic thrust required that the generator thrust bearing be designed for a load of approximately 2,750,000 lb.

Overspeed tests on unit No. 4 were made to obtain greater knowledge of the functioning of the unit under overspeed conditions and were run to approximate the conditions that actually might exist on governor failure. The time of 30 min was picked with due consideration of the time that would be required to close the intake service gates using the intake gantry crane, and the time required to investigate the temperature rise of the thrust bearing.

The McNary Dam project of the Corps of Engineers located on the Columbia River will have an initial installation of fourteen 70,000-kw units at 85.7 rpm and an ultimate installation of twenty 70,000-kw units, the range in net head being from 62 to 92 ft, the minimum head occurring under high river flow conditions. The first units are scheduled to go into operation in December, 1953.

Prior to advertising for bids for the McNary generators, the generator manufacturers expressed reluctance to design generators of this size and speed, which would be physically the largest generators ever to be designed, to withstand, without exceeding the allowable working stresses, an overspeed greater than 200 rpm.

As a result of model runaway-speed tests and after investigating the operating characteristics of several Kaplan units operating at various blade angles and heads up to 86 ft, it was decided to restrict the blade angle of the prototype to a minimum of 16 $^1/_2$ deg. At this blade angle the maximum speed for any head is less than 217 rpm off-cam and less than 178 rpm on-cam. The runner is being machined with the blades in the 16 $^1/_2$ deg position, as shown in Fig. 10 of the paper. The generators being furnished by the General Electric Company are being designed to withstand a maximum speed of 190 rpm, without exceeding the allowable working stresses. The thrust bearings are being designed for a load of approximately 4,000,000 lb.

In view of the high operating head at McNary, the service gates for the units will be operated hydraulically with provisions for remote control. Three gates, approximately 20 ft × 50 ft, are required per unit and are designed for closing in approximately 4 min. In addition, a motor-operated adjustable stop, automatically controlled by a net head device, is being furnished on one gate servomotor of each turbine with which the motion of the turbine gates in the opening direction is positively limited in order to prevent overloading the generator during periods of high head. This also will limit the runaway speed to a predetermined value in case of full-load rejection and failure of governor oil pressure.

In order to make additional prototype tests which could not be made at Bonneville, one unit at McNary is being equipped with means for the emergency closing of the wicket gates. These provisions consist of a motor-operated pump and the necessary valves and piping connections, so that the pump and its connections can be isolated from the governor oil-pressure system, and so that, when so isolated, the pump can be operated to close the gates in less than 5 min.

While at Bonneville it has been demonstrated that the units can operate safely at speeds which would result from full-load rejection and loss of governor oil pressure, the secondary results are such that it has been considered desirable to provide for a faster method of shutting the unit down under such emergency conditions other than by closure of the head gates by use of the gantry crane.

The system selected for installation consists of a valving arrangement whereby the governor oil-pressure system is isolated near the gate servomotors, and the gate servomotors connected through a four-way valve to an oil-pressure tank connected through a pressure-reducing valve to a standard nitrogen cylinder charged to 2200 psi at room temperature and which had adequate gas to furnish the oil displacement volume at 300 psi to effect seven wicket-gate closures. This system was selected because of its compactness, self-contained power, and low cost of installation and upkeep.

J. J. HART.[6] In the case of a Kaplan turbine the overspeed is most important in the design of a generator since other considerations such as WR^2 are usually obtained automatically if the mechanical requirements are met for the higher overspeed of the turbine.

The suggestion that the overspeed be reduced by restricting the minimum angle to which the runner blades can be pitched seems to be an excellent one. The usual hydroelectric installation would not require the turbine to operate at this light load and even if it was required to do so, it is probable that the loss of efficiency at this load would not be very important. However, this would have to be determined by the ultimate customer in each case.

Before a generator is purchased to the on-cam instead of the off-cam runaway speed the purchaser should consider carefully all possibilities and particularly the following:

1 The design limits or so-called factor of safety of the generator design.

2 The possibility of the turbine ever reaching the off-cam runaway speed.

3 The possible damage in case of failure.

The following is a brief discussion of these points:

1 It has become standard practice in the United States to limit stresses in rotor parts to $^2/_3$ of the yield point at the runaway speed, and in some cases this is required by customer's contracts, although it is adhered to in any case. As an example of the variation in stresses involved, consider a generator with an on-cam runaway speed of 175 rpm and an off-cam runaway speed of 216 rpm. Such a generator would have rotor stresses increased by 52 per cent by going from the on-cam to the off-cam runaway speed. This would increase the calculated stresses to a point just beyond the yield point.

It is important to recognize that the purpose of a factor of safety is to take care of unknown quantities either in method of calculation of complex problems or in unknown variations in the strength of the materials. Although every effort is made to eliminate these unknowns by exhaustive tests of materials going into a generator rotor, it is doubtful that any generator manufacturer would consider reducing the factor of safety of the rotor. This would mean, in effect, that the generator manufacturer would only guarantee the generator for the maximum overspeed

[6] Mechanical Design Engineer, AC Engineering Department, Westinghouse Electric Corporation, East Pittsburgh, Pa. Mem. ASME.

specified in the contract and would be unwilling to stress rotor parts above $^{2}/_{3}$ yield point.

2 It appears improbable that a Kaplan turbine would ever accidently reach the off-cam runaway speed, although not entirely impossible. One method of accidentally obtaining maximum off-cam runaway speed would be for the blade control valve to jam so that it does not follow the cam, and then for a log or other foreign matter to lock the gates. If these two conditions occurred so that blades and gates were locked at the worst possible position, then maximum off-cam speed would be obtained whereas if they locked in some intermediate position the runaway speed would be intermediate between off-cam and on-cam. Perhaps there are other cases where maximum speed could be obtained due to carelessness or improper maintenance on the part of the operating personnel. While it seems improbable that the maximum off-cam speed would ever be obtained, it must be remembered that where a large number of units are operated over a long period of time, it is not entirely impossible.

3 The damage in case of a failure of the generator rotor would be catastrophic. Each field pole often weighs 2000 lb or more and would be traveling at a speed in excess of 200 mph. Many such field poles could lay down a fairly effective artillery barrage in addition to the damage possible from the heavy rotor rim. This would wreck not only the generator involved, but probably adjacent generators in the same power station in addition to possible damage to personnel.

The customer should consider the foregoing three points in determining the magnitude of the overspeed to incorporate in the specification.

In conclusion, it would seem that the customer should take full responsibility for any damage caused by operation of the generator at a speed in excess of that required by the contract specification. It also would appear that a safer method of reducing overspeed in Kaplan units would be the more positive reduction of the minimum angle to which the blades can be pitched, especially since in most installations this would not affect the efficiency of operation materially.

W. B. Hess.[7] The remarkable agreement of field-test data with the model tests and the additional quantitative information presented in the paper permits a more intelligent analysis of the factors effecting maximum speed most probably attainable. From this should evolve a standard practice procedure or specification that will be mutually beneficial to turbine manufacturer, generator manufacturer, and purchaser.

The combination of factors necessary to obtain even the on-cam runaway speed appears a rather remote probability on a turbine designed for balanced wicket-gate opening near the normal speed-no-load position and with the blade center of pressure toward the opening direction. The two most probable failures leading to runaway are believed to be (1) pressure failure in the control system, and (2) fracture of the servo linkages.

In either of these cases the generator would have to be tripped from the load and this most likely would occur only in an isolated system. Furthermore, in the event of such failures the blades would attain maximum opening and the wicket gates approximately 20 per cent of full opening with a resulting speed near normal. Since the Kaplan-type turbine is used at low heads, the gate-closure time can be rather fast, thus minimizing the transient-speed rise. Considering all factors, it appears that on-cam runaway would be more than ample. The probability of obtaining maximum off-cam runaway speeds is believed more remote than the failure of safety devices protecting equally valuable equipment with potentially greater danger to operating personnel.

Modern design and construction of generator rotors provides an additional safety factor from failure due to overspeed. The utilization of steel plate in fabricated construction, the knowledge of structures gained from dynamic stress testing, and the added assurance of flawless materials obtained from the several nondestructive tests available today, provide rotor structures far superior to those of 25 or more years ago.

Information from several rotor failures indicates that most of them occurred in integrally cast rotors containing cracks or other flaws which created serious stress raisers. Although accurate data on speed attained before failure are not available, in most incidents it has not been as high as the design maximum.

The seven Safe Harbor Kaplan units are designed for a maximum off-cam runaway speed of 252 rpm. This speed is 2.52 times normal speed on the 25-cycle units and 2.31 times normal on the 60-cycle units. There has been no case of excessive overspeed in 126 unit-years of operation. Records of differential pressures in the wicket gate and blade servomotors show the gates are hydraulically balanced very close to the normal speed-no-load position and that the center of pressure on the blades is toward the opening direction.

Machining the McNary runners to design diameter at the higher blade position suggests an idea to investigate the possibility of increasing the blade area on presently installed runners that may be removed from the setting for repairs. Acknowledging the qualifications of units available, load schedules, and so forth, pointed out in the paper, it would appear that a slight increase in efficiency and an apparent appreciable gain in power could be realized. It does not appear a difficult task to weld the additional metal to the blades and install a suitable stop in the blade servomotor to limit the minimum travel.

F. M. Lewis.[8] The runaway of a generating unit is a subject the operator often thinks of but hopes will never happen. What would cause a runaway, the speed the unit would attain, the method for again gaining control and the resulting damage, are the thoughts that are his concern. This paper should be of comfort to those associated with Kaplan turbines in that the runaway might not be as serious as imagination has indicated.

The off-cam runaway-speed tests, which are of great interest and furnish valuable data, are not the prime concern of the operator. Runaways which might occur under normal or on-cam operating conditions are his major concern. With this in mind, it is thought that on-cam overspeed tests should be included in the test procedure. Suggested tests would be a series of overspeed tests, starting at speed-no-load and increasing the load by steps to full load. Each test would be performed by relieving the oil pressure on the governor system and then rejecting the load on the generator. In this way the speed and the movement of the gates and blades from normal speed and load to the expected overspeed could be determined. The blades and gates would tend to move toward the hydraulic balance position. They would not reach this position because of any back pressure on the opening side of the servomotor pistons, mechanical friction and friction of the blade packing. Such a test would simulate the overspeed that might develop during operation and probably do much toward relieving the operator's mental hazard.

Two overspeed tests conducted at Bonneville might be of further interest. The overspeed test on unit No. 3 was an on-cam run. The 53–58-ft cam was used and the gross head was 50 ft. The maximum speed obtainable was 142 rpm at 58 per cent gate

[7] Senior Test Engineer, Safe Harbor Water Power Corporation, Conestoga, Pa. Mem. ASME.

[8] Resident Engineer, Corps of Engineers, U. S. Army, Portland District, Bonneville Dam, Bonneville, Ore.

and 22-deg blade angle. The overspeed test on unit No. 7 was an on-cam test. Due to temporary difficulties during erection, the blade angle was limited to between 20 and 32 deg instead of the normal 6 to 32 deg. With the abnormal minimum blade angle of 20 deg, it was impossible to open the gates beyond 44 per cent with full 300 lb oil pressure. The maximum speed was 125 rpm at 20-deg blade 44 per cent gate.

The limitation of the blade angle for the McNary turbines to 16 deg has merit. Operators' experience at Bonneville has shown that blade angles of less than 16 deg are seldom used and of little value. A blade angle of 16 deg is normally used for starting the Bonneville units.

W. R. MacNamee.[9] While the stresses in the generator rotor, induced by centrifugal force during overspeed, are by far the most dangerous and important, another element that is called upon for extra duty is the thrust bearing.

If the thrust load were to remain unchanged as the unit overspeeds, it is obvious that the bearing temperature would rise considerably, due to the increase in speed.

The largest single factor in determining the actual thrust load existing during overspeed is found to be the same as that determining the degree of overspeed itself, namely, the angle of the runner blades.

Three curves are shown in Fig. 13, each indicating how the turbine hydraulic thrust varies from normal to ultimate over-

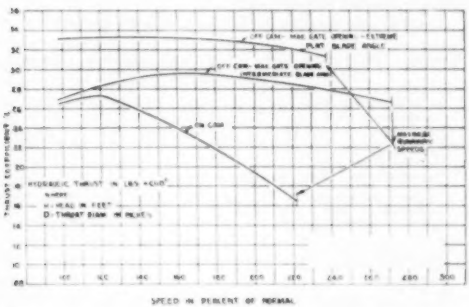

FIG. 13 HYDRAULIC THRUST VERSUS SPEED FOR TYPICAL KAPLAN RUNNERS

speed. The lowest curve, labeled on-cam, shows that the thrust drops off rapidly as the unit speeds up. This curve is approximately correct for overspeed occurring at any gate opening over the normal operating range, providing the on-cam relation is maintained. It also represents the maximum thrust obtainable if it is assumed that the blades rotate to the wide-open position.

The second curve shows the thrust when the turbine gates are assumed to be wide open, but the blades blocked in the position producing maximum overspeed.

For the third, and highest, curve it is assumed that the gates are wide open and the blades blocked in the extreme flat position. It may be noted that the abnormally high thrust occurs at normal speed, as well as at overspeed. Overspeed with this combination undoubtedly represents the worst possible overload on the thrust bearing.

Referring to the Bonneville tests, unit No. 4 was operated at 234 per cent normal speed, corresponding to the on-cam curve. In this case the thrust-bearing temperature leveled off with a rise to 91 deg C.

Unit No. 2 was operated at the maximum speed combination of gates and blades, but for a relatively short period. During 3¾ min the thrust-bearing temperature rose rapidly from 60 C to 85 C. What the final temperature would have been is impossible to say, but it seems probable that it would have been dangerously high.

The author has discussed limitation of the minimum blade angle as shown in his Fig 10. This limitation also has the advantage of reducing possible hazard to the thrust bearing during prolonged runaway speed, not only by reducing the speed but also by reducing the thrust load.

D. J. McCormack.[10] Throughout the years several bad runaways of hydroelectric units have occurred, the most publicized being the following:

The vertical units at Niagara Falls on the American side.

Cazadero Plant of the Portland Railway Light & Power Company, where 5 horizontal units were torn out one after another.

Ontario Power Plant, Niagara Falls: A twin horizontal turbine and generator went up through the roof during World War I.

Alabama Power Company Lock 12 Plant: A large vertical unit was put out of commission by the generator rotor blowing up.

Tennessee Valley Authority: The generator of a 15,000-hp horizontal unit went up through the roof and tore out part of the side of the building.

The resulting damage of each of these occurrences was very costly. To prevent such cases happening with Kaplan units is an important subject because of the relatively high cost of such units and the large ratio of runaway to normal speed as outlined in the paper.

After the Cazadero accident, the Portland Company insisted upon a runaway-speed device mounted on the base plate of its horizontal generators in all plants having such units, consisting of a set of flyballs driven from the generator shaft and actuating a 4-way valve to admit high oil pressure to the closing side of the governor cylinder in case the overspeed exceeded, say, 25 per cent above normal. Other plants on the West Coast were designed for and specified that the overspeed device should shoot penstock water into the closing side of the governor cylinder. Any such means is corrective and would not start to act until the speed had exceeded the normal amount for full load thrown off.

Other means to anticipate the speed rise by starting to act quicker upon failure of governor pressure, failure of any part of the governor, gate mechanism, or blade mechanism should be left to the power system to decide on what they want, because of the many protective devices that could be worked out.

Restricting the minimum blade angle to limit the magnitude of the runaway speed, as indicated in the paper, reduces the part gate of the Kaplan turbine—one of its main advantages. At the other end of the efficiency curve at full load the flat part of the curve is reduced in length at the high heads by the sigma value of the turbine for its setting with respect to tail water and at the same time meet the required generator capacity.

W. J. Rheingans.[11] The author states that there are two runaway speeds to be considered, the off-cam runaway speed and the on-cam runaway speed. The difference between these two speeds is apparently 20 to 25 per cent. The author also describes the conditions that have to be fulfilled to obtain the off-cam runaway speed and expresses the opinion that the probability of an

[9] Assistant manager, Hydraulic Turbine Engineering Division, Baldwin-Lima-Hamilton Corporation, Eddystone Division, Philadelphia, Pa. Mem. ASME.

[10] York, Pa. Mem. ASME.

[11] Manager, Hydraulics Section, Power Department, Allis-Chalmers Manufacturing Company, Milwaukee, Wis. Mem. ASME.

occurrence of the combination of conditions necessary to produce maximum off-cam runaway speed while quite remote, is however, possible.

The problem resolves itself to two main questions:

1 What saving in cost can be achieved by designing the turbine and generator for the lower runaway speeds?

2 Will this saving in cost warrant taking the chance of a failure and break-up of the unit?

The author states that it is not difficult or expensive to design and construct the turbine for maximum runaway speed. The writer concurs in this. Therefore the only major additional cost is with reference to the generators.

The generator manufacturers usually increase the selling price of the generator about 1 per cent for each 5 per cent increase of runaway speed above a normal runaway speed, which latter is 100 per cent above rated speed for generators below 50,000 kva and 85 per cent for generators above 50,000 kva.

Thus the difference in cost to the purchaser between a generator designed for maximum off-cam runaway speed and one designed for the lower on-cam runaway speed is 4 to 5 per cent of the cost of the generator.

The question then becomes one of whether the purchaser of the unit wants to take the risk of a generator break-up for this 4 to 5 per cent additional cost. A generator failure can be very costly, because not only will it do tremendous damage to the particular unit but it may damage adjacent units, auxiliary equipment, and even the power-plant structure. There have been few hydraulic unit failures resulting from runaway speed in the past 50 years. This is due to the fact that both the turbines and generators were designed for maximum runaway. However, whenever a failure did occur the damage was extensive and out of all proportion to any savings that might have been attained by a design for lower maximum speed.

The question of whether to design the generator for the high off-cam runaway speed or whether to design it for the on-cam runaway speed is a question which must be decided by the purchaser. The turbine manufacturer's duty ends when he gives the estimated runaway speed for the two conditions, although he might be asked to give an opinion as to the possibility of the unit attaining off-cam conditions and thus maximum runaway. The generator manufacturers cannot be expected to decide the runaway speed for which to design the generator, because they are willing and able to design for the higher speed at an appropriate increase in cost.

Hence the purchaser must determine whether the saving in the cost of the generator designed for the lower speed is sufficient to warrant the risk of a possible failure. It is really a question of insurance and the cost of such insurance.

Another factor to be taken into account is that for the lower-speed generators—say, below about 150 rpm—there is about a $1^1/_2$ per cent increase in WR^2 for each 5 per cent increase in maximum runaway-speed design of the generator. Since additional WR^2 adds to the stability and general performance of a unit, it is a welcome addition, especially for propeller-type turbines. Thus the increased cost for the higher-speed design not only reduces the possibility of a generator failure but adds to the over-all performance of the unit.

If the purchaser decides to use a generator designed for the lower on-cam runaway speed, there is an immediate problem as to what maximum speed is attained by the unit during a runaway. If a failure should occur, there is the question as to whether the unit failed at speeds below the designed runaway speed, or whether failure was caused by speeds above the design speed. Therefore it would seem necessary to have a recording tachometer attached to each unit, at least during the first year of operation, because this is the usual period for the guarantee of the equipment against failure.

The author calls attention to the reduction of maximum runaway speed for both the off-cam and on-cam conditions when the minimum blade pitch is limited to $16^1/_2$ deg. Since the limitation of the minimum blade pitch partly defeats one of the main reasons for use of an adjustable-blade propeller turbine, namely, the highest efficiency at part loads, it becomes questionable whether this is a satisfactory solution of the runaway-speed problem.

A fixed-blade propeller would have even a lower runaway speed, increased maximum efficiency (due to less peripheral clearance) and would eliminate entirely the blade servomotor, thus reducing still further the capacity requirements for governor oil pumps, pressure and sump tanks. This might then become a good argument for the use of fixed-blade propeller turbines with their lower runaway speeds, lower initial costs, and lower maintenance costs.

However, here again it seems to be a question for the purchaser to decide, whether the sacrifice of efficiency at part loads is compensated for by the reduced cost of a generator for lower runaway speeds.

R. A. Sutherland[12] and E. A. Woodhead.[13] The writers have been concerned with two Kaplan installations in recent years, namely, the Lower Salmon Hydroelectric Development and the Bliss Hydroelectric Development, both of the Idaho Power Company. Each of these plants has one Kaplan unit, the remainder being fixed-blade propeller units.

Physical data are given in Table 1 of this discussion.

TABLE 1 PHYSICAL DATA OF LOWER SALMON AND BLISS HYDROELECTRIC DEVELOPMENTS

Lower Salmon:	
No. of fixed-blade units	3
No. of Kaplan units	1
Rated head, ft	55.5
Rated kw	15000
Rated speed, rpm	120
Max. design head, ft	62
On-cam runaway, rpm	270
Overspeed, per cent	125[a]
Off-cam runaway, rpm	317
Overspeed, per cent	164[a]
Generator designed for rpm	317
Bliss:	
No. of fixed blade units	2[b]
No. of Kaplan units	1
Rated head, ft	70
Rated kw	23000
Rated speed, rpm	128.6
Max. design head, ft	75
On-cam runaway, rpm	300
Overspeed, per cent	133
Off-cam runaway, rpm	350
Overspeed, per cent	172
Generator designed for rpm	350

[a] Overspeed as given here is in accordance with generator manufacturer's usage.

[b] Provision for 3 units.

In each of these plants the fixed-blade units are normally operated at or near best efficiency while the Kaplan turbine takes care of load variations over its full range of output. Each plant supplies peak-load requirements by drawing on its pondage, particularly during fall and winter months when river flow is normally less than maximum requirements. In the design, the possibility of limiting runaway speed by fixing a minimum blade angle much greater than normal was not considered seriously, but if it had been, the detrimental effects on part-load efficiency, with consequent waste of water, undoubtedly would have been a factor in deciding against this course. We did consider limiting the maximum gate opening at increased head by means of an automatically variable gate stop but this was considered an undesirable

[12] Hydraulic Engineer, Ebasco Services, Incorporated, New York, N. Y. Mem. ASME.

[13] Superintendent of Power Plants, Idaho Power Company.

complication, liable also to be rendered inoperative deliberately at times of emergency.

We are inclined toward off-cam runaway provision where generator manufacturers experience no difficulty in meeting runaway requirements.

When first placing the Lower Salmon and Bliss units in service the blade angle was 6 deg at the zero position of gates. This flat position of blades made it necessary to open the wickets a considerable distance in starting the machine. It would then accelerate faster, and, being on the governor the gates would then return to closed position and remain so until the unit "drifted" down to normal where speed regulation took over and it was closed to the line.

No loss of time in returning a generator to service was experienced but on the part of the operators some alarm was felt since it was not considered altogether safe to open the gates so wide at initial starting after a unit has been out of service a considerable period of time.

The minimum blade angle was changed from 6 to 9½ deg. We felt no compunction in doing this because the variation in operation head from designed head was relatively small and no change in efficiencies was noticed.

For conditions other than those obtaining in the installations discussed, particularly where the maximum head is large compared to the normal head, the writers believe that the limiting of runaway speed may be worth considering.

R. B. WILLI.[14] While the author has avoided any specific conclusions in his paper, means are presented which justify the trend toward the selection of lower runaway speeds in the purchase of generators for adjustable-blade propeller turbines. In certain instances an additional advantage may be gained by the use of control devices outlined in the following.

It is usually the case that Kaplan turbines are required to operate over relatively wide ranges of head. The maximum head may be considerably above the normal head for which the generator capacity has been established. A twofold purpose is accomplished by a control device now being installed on some turbines. This unit limits the wicket-gate opening in inverse proportion to the net head of the turbine. As the head increases, gate opening is controlled to prevent overload of the generator. The protective device consists of a positive mechanical stop for the gates, automatically positioned to suit the net head available. If the gates approach the mechanical stop, a limit switch actuates the governor load-limit-adjusting motor to hold the gates just short of actual contact. In the event of any failure in the governor equipment, the mechanical stop provides positive back-up protection. Except for the secondary effect of sigma on runaway speed with respect to gate opening, as illustrated in the author's Fig. 2, it is a general rule that runaway speed increases as gate opening is increased. Therefore the control described serves to reduce the possible overspeed in many applications if the off-cam runaway is being considered.

Another safety feature which has been suggested is an overspeed operated solenoid in the governor, designed to position the main Kaplan relay valve so as to effect opening of the runner blades in the event of an abnormal rise in speed. Even in the event of simultaneous loss of governor oil pressure, such positioning of the main Kaplan valve would remove the possibility of locking the blade hydraulically in a dangerous position, such as would be the case were the Kaplan valve to remain in its midposition. Since the hydraulic torque on the runner blades, tending to open them, increases with an increase in speed, and, at the same time, the downward hydraulic thrust on the blades, and consequently the bearing-friction load, tends to decrease, the blades cannot but assume their steepest position if free to move. This is illustrated by the author's Fig. 5, as well as his experience in the Bonneville test of unit No. 2. Other turbine manufacturers also have confirmed this tendency.

The use of such controls, together with those presently in use, such as shutdown controls for overspeed and low oil pressure, would minimize the risk in using an overspeed approaching the on-cam value, as a basis for generator design. It must be considered, however, that the cam controlling the position of the runner blades is manually adjustable to suit the varying head on a turbine. If this is set for a low head and is not readjusted as the head increases to its maximum value, it may be possible to develop an overspeed somewhat higher than the on-cam runaway speed. If this factor is considered in determining the maximum attainable speed, a practically impossible sequence of failures would be required for such a speed to be exceeded. Certainly the risk so incurred would be far less than that encountered in the steam-turbine field, where an unfortunate sequence of failures would result in a runaway speed very much above that considered in the generator design.

The writer had an opportunity to participate in a series of tests recently, which may assist in explaining the behavior of the Bonneville unit No. 1 when operating at an overspeed of 130 rpm. Those tests were made because of a number of ship-propeller tail-shaft failures which, in appearance and performance, suggested the possibility of a resonant vibration at normal operating speed, although the critical speed was calculated to be much higher. It is well known that the thrust on each propeller blade varies during every revolution because of interference of the hull. In the laboratory, a model assembly of the shaft and propeller was run at varying speeds, each vane having to pass through an air jet to simulate an unbalanced thrust. Not one, but two critical speeds were found to exist, occurring at speeds much lower than the true first critical, namely, that value determined when the propeller was not subjected to the air jet. For different propellers having the same conventional first critical, the extra criticals occurred at lower speeds as the number of vanes was increased. In the case of a turbine, the radial or axial thrust on the runner blades might vary as they pass from the small to the large side of the scroll case, or as they pass an off-center vortex in the draft tube.

T. ZOWSKI.[15] Turbine runaway speed is usually an important factor requiring careful consideration in specifying and designing equipment for installations involving Kaplan turbines. In the case of a number of Kaplan installation projects for which the engineering services were performed by the consulting organization with which the writer is associated, our studies and subsequent review of all relevant factors with the purchaser resulted in the purchase of generators for the maximum off-cam runaway speed. It has been our experience that generator manufacturers are reluctant to design their machines for an overspeed lower than the maximum off-cam and to guarantee them on that basis, because in the event of damage resulting from runaway it may not be possible to determine exactly how much overspeed actually was attained.

An exception to our practice of specifying maximum off-cam runaway speed is the Rio Negro Project where the maximum head of 105 ft is substantially higher than the turbine design head of 69.2 ft, resulting in a maximum calculated off-cam runaway speed of 2.92 times normal synchronous speed. It was not considered economical to design the generators for this high overspeed; therefore a gate servomotor stop-nut mechanism was provided which

[14] Manager, Hydraulic Turbine Engineering Department, Baldwin-Lima-Hamilton Corporation, Philadelphia, Pa.

[15] Chief Mechanical Engineer, Harza Engineering Company, Chicago, Ill. Mem. ASME.

automatically limits the gate opening under high heads so the maximum runaway speed will never exceed 2.60 times normal. It can be argued that this protective mechanism is not absolutely immune from malfunctioning or failure, and its reliability has limits, as do most other protective devices, including the anti-runaway blade mechanism ("antiracing hydrobrake") featured by a turbine manufacturer in England. However, the probability of its failure occurring simultaneously with the existence of all the other factors pointed out by the author as necessary for attaining the maximum runaway speed, may be considered sufficiently remote. The saving in cost of the Rio Negro generators due to the limitation of maximum runaway speed was approximately 7 per cent.

The positive limitation of runaway speed by restricting the minimum blade angle appears to constitute a very practical solution. The resultant loss of efficiency in the range of small loads may be insignificant in multiple-unit plants where the turbines can be operated primarily in the range of larger gate openings. The loss may then be outweighed by the remarkable increase in efficiency made possible by the reduced blade-tip clearances. It is worth noting that the efficiency loss at small loads is relatively smaller on lower-head Kaplan turbines owing to their characteristic lower part-load efficiencies.

Author's Closure

The importance of the subject with which the paper is concerned is evidenced by the large number of excellent discussions by engineers who are among the best qualified in their respective phases of the hydroelectric business. It will be noted that of those who discuss the paper, three are employees of generator manufacturers, four are or have recently been employees of turbine manufacturers, two are in consulting engineering, and three represent the viewpoint of turbine owners and operators. Let us try to summarize and get the opinion of each group on the question: Should the generator be designed for the maximum off-cam or for the on-cam runaway speed? In doing this let us keep in mind three things:

(1) The discussions are by individuals, and are not necessarily the "official" opinions of the companies they represent.

(2) The discussions represent the thinking of the individuals at the time they were written and as time goes on there may be other considerations which might cause them to change their minds.

(3) The following is only the author's interpretation of the opinions of the individuals on this question.

Those employed by generator manufacturers think that, if possible, the generator should be designed for the maximum runaway speed that can occur but are willing to build it for something less than this if for good reason the purchaser so directs. Reading between the lines the author gathers that they would like to have the purchaser specify one and only one overspeed figure and that is it with no "ifs," "ands," or "buts," about "on-cam" or "off-cam" or any other qualifications which the peculiarities of the turbine introduce. To sum up briefly, they say design the generator for the maximum overspeed but do everything you can to hold it as low as possible.

Those representing turbine manufacturers have all contributed valuable and greatly appreciated data to the paper. Mr. Willi says "means are presented which justify the trend toward the selection of lower runaway speeds in the purchase of generators for adjustable-blade propeller turbines" and offers suggestions regarding the use of preventive devices. Mr. Rheingans leans toward designing for maximum off-cam—the decision resting with the purchaser on the basis of cost versus the degree of improbability of destructive overspeed occurring. Mr. McCormack advocates protection against the maximum runaway speed. Mr. MacNamee has dealt principally with thrust considerations. The specific question we are considering in the closure is not answered one way or the other with unanimity by this group.

The two hydroelectric consultants concur in the opinion that unless it is impracticable, the generator should be designed for the maximum possible overspeed.

In considering the discussions of these three groups, it must be realized that they feel a great responsibility to the purchasers of their equipment and services.

The three discussions from those representing owners of hydroelectric equipment collectively, are probably the most forthright of all. The men of this group represent those who, after weighing all the data, have to make the final decision. Therefore, as compared to the first three groups, they can be relatively more outspoken.

Mr. Hess, who for over 20 years has been in close contact with the first large Kaplan turbines on this continent, says "Considering all factors, it appears that on-cam runaway should be more than ample."

Mr. Cave and Mr. Lewis as evidenced by what has actually been done at Bonneville and McNary, think that the generator need not be designed for the maximum off-cam runaway, however, in both cases they have gone slightly higher than the on-cam runaway.

A very interesting item of Mr. Lewis's discussion is that on Bonneville Unit No. 7, a test showed that with 20-deg blade angle and 125 rpm (67 per cent overspeed) it was found impossible to open the wicket gates beyond 44 per cent. No doubt, at this speed, the force of the whirling water acting upon the tips of the gates created much higher than normal forces in the closing direction. The overlapping of the gates in this position minimized the effect of the force on the portion of the gates outside of the gate stem circle so that almost the entire effect was on the inner tips of the gates thus resisting the effort of the servomotors trying to open them. This is another factor tending toward runaway speed lower than the maximum off-cam.

In conclusion, the data in the paper, in the author's opinion, fully support the decisions of the Corps of Engineers in respect to runaway speed at Bonneville and McNary. In the case of McNary, the author approves of the limiting of the minimum blade angle because it results in higher efficiency at the loads where these particular units will operate—the lower off-cam runaway speed being of secondary benefit. The author also concurs with Mr. Hess.

Assuming that the turbine manufacturers in their Kaplan turbine bids continue to give both the maximum off-cam and the on-cam runaway speed figures, the author, if representing a purchaser would proceed somewhat as follows:

(1) Obtain generator prices for at least the two runaway speeds and, if over-all considerations warrant it, for one or more intermediate overspeeds.

(2) Obtain assurance from the turbine manufacturer that, even at normal speed, his blades are in reasonably good hydraulic balance, preferably with some unbalance tending toward the opening direction so that, if free to move, they would drift open from any position below mid-position. In case of runaway, as the speed increases above normal, the forces tending to open the blades will greatly increase.

(3) Consider the cost and degree of reliability of all possible safety devices to limit runaway speed to that on-cam or below.

In the author's opinion, by following this process and applying it to the particular units under consideration, the purchaser's engineers will, in many cases, find adequate justification for purchasing the generator for the on-cam runaway speed.

Contributions to Hydraulic Control

1 Steady-State Axial Forces on Control-Valve Pistons

By SHIH-YING LEE[1] AND J. F. BLACKBURN,[2] CAMBRIDGE, MASS.

A theory is given of the origin of the steady-state force exerted upon a piston by fluid flowing past its corner, brief reference is made to a considerable body of experimental evidence in support of that theory, and a practical valve construction is described which very nearly eliminates that force.

Foreword

VERY early in the work of the Dynamic Analysis and Control Laboratory of the Massachusetts Institute of Technology it became apparent that the satisfactory performance of many of its assigned tasks would require the development of servomechanisms of considerably greater accuracy and speed of response than any that were then available. The acceleration requirements were so severe that no existing electric motors could be used, and the chance of developing satisfactory motors seemed rather remote. Accordingly, the laboratory started a program of research and development of flow-valve-controlled hydraulic servos. This program has resulted both in the development of a number of high-performance servos and in the accumulation of a store of information on hydraulic control, much of which has not been easily available and some of which is believed to be new. This paper is the first of a series which will summarize certain parts of this store of information in a form convenient for the designer.

Many members of the laboratory have contributed to the work which is to be reported, but the principal contributors have been the following: The fundamental research on flow phenomena has been carried out by Dr. Shih-Ying Lee. The mechanical design of the several types of flow valves developed by the laboratory has been done successively by Messrs. G. F. Kelly, John Bankas, and R. D. Atchley. Mr. Atchley has also been responsible for the development of the high-performance torque motors used with the valves, with assistance in the earlier phases of the work from Mr. Stanford D. Blitzer. Mr. Irving Kotlier has made a number of contributions to the theory and has been in charge of the test work, assisted by Mr. J. E. Drinkwine. The servo work has been done by Messrs. R. W. Bond and H. E. Blanton and, in its earlier stages, also by Mr. S. B. Williams. The hydraulic and mechanical work was supervised by Dr. J. F. Blackburn, and the over-all direction of the laboratory was until recently in the hands of Prof. A. C. Hall, who is also responsible for much of the basic theory of the flow valve as a servo element.

The work to be reported in this series was supported by the Bureau of Ordnance, United States Navy, Contract NOrd 9661 with the Division of Industrial Cooperation, Massachusetts Institute of Technology.

[1] Research Engineer, Dynamic Analysis and Control Laboratory, Massachusetts Institute of Technology.

[2] Research Engineer, Dynamic Analysis and Control Laboratory, Massachusetts Institute of Technology.

Contributed by the Machine Design Division and presented at the Annual Meeting, Atlantic City, N. J., November 25-30, 1951, of The American Society of Mechanical Engineers.

Note: Statements and opinions advanced in papers are to be understood as individual expressions of their authors and not those of the Society. Manuscript received at ASME Headquarters, August 7, 1951. Paper No. 51—A-52.

Introduction

In designing a hydraulic control valve for servo systems or similar applications, it is important to know the axial force necessary to operate the piston. This force has three principal components: namely, inertial force, which is easily calculable; friction, which can be estimated approximately; and a third and usually far larger force which is produced by the flow of the hydraulic fluid through the metering orifices of the valve. Since there appears to be practically no information available on the origin of this last force or on methods for its reduction, it seems desirable to present the results of work performed in this field by the Hydraulic Section of the Dynamic Analysis and Control Laboratory.

Origin of Steady-State Flow Force

A typical control system using a 4-way valve is shown schematically in Fig. 1. When the piston is displaced to the right of its neutral position, as shown in the figure, fluid will flow from the

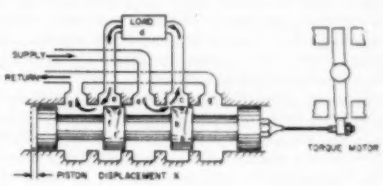

Fig. 1 Conventional Four-Way Valve With Square Lands

inlet line to the inlet chamber a, then through the upstream orifice b, motor line c, load (hydraulic motor or ram) d, motor line e, and downstream orifice f to the exit chamber and line g. If the piston is displaced to the left, the sequence is a-f'-e-d-c-b'-g', which reverses the flow through the load. If the valve is overlapped or zero-lapped, only the two orifices, b and f, or the two orifices, f' and b', will be passing fluid at any one time. For the sake of simplicity, only this type of valve will be discussed for the remainder of this paper. The theory can be extended easily to other types of valves except for those in which projections from the sleeve extend into the spaces between the piston lands, thus destroying the static axial balance of the piston.

The following theory is based upon three main assumptions: (1) The fluid is assumed to be essentially nonviscous and incompressible; this is approximately true in most practical cases. (2) The peripheral width of the orifice is assumed to be large compared with its axial length so that the flow can be considered to be two-dimensional. This is also true for small piston displacements in all valves and is approximately true for other cases. (3) The flow is assumed to be quasi-irrotational in a region immediately upstream from the orifice. This last assumption is far from the truth throughout most of the hydraulic circuit. However, it is fairly well satisfied in the region of interest where the strong convergence of the flow lines as they approach the orifice assures that only a negligibly small fraction of the energy in the

fluid exists in the form of kinetic energy of rotation, and that practically all of it is either potential energy of the static head or kinetic energy of irrotational flow. In any event, all the assumptions are adequately justified by the excellent agreement between the theory and the experimental results.

With the assumptions that the flow is two-dimensional, irrotational, nonviscous, and incompressible, the solution of the flow pattern in the region upstream from the orifice becomes a solution of Laplace's equation for the configuration shown in Fig. 2.

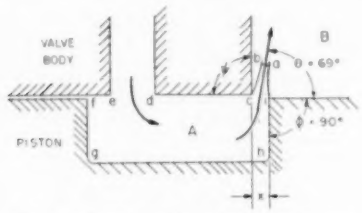

FIG. 2 SQUARE-LAND CHAMBER CONFIGURATION

This solution has been obtained by von Mises,[1] and it is found that for a square-land valve when the valve opening x is small compared with the other dimensions of the upstream chamber, the angle θ which the axis of the stream makes with the piston axis is $\cos^{-1} 0.36$, or 69 deg. This value has been verified experimentally both on actual valves and on a two-dimensional valve model with glass sides. For lands with angles other than 90 deg the value of θ also can be found either experimentally or theoretically. When θ is known, the axial force on the piston can be derived in the following manner:

The axial force on the piston equals the axial component of the net rate of efflux of momentum through the boundary *a-b-c-d-e-f-g-h-i-a* in Fig. 2 where *a-b* is the vena contracta of the jet. In an actual valve the area of *a-b* is much smaller than that of *d-e* where the fluid enters the upstream chamber A. Since the velocities are inversely proportional to the areas, the influx of momentum through *d-e* is negligibly small compared with the efflux at *a-b*, which is equal to $Qu\rho$ where

Q = total rate of flow
u = velocity of jet at vena contracta
ρ = density of fluid

By Bernoulli's equation

$$u = \sqrt{\frac{2\Delta p}{\rho}}$$

and the net axial force

$$F_{AB} = F_{fg} - F_{hi} = Q\,u\rho\cos\theta \quad \ldots\ldots\ldots [1]$$

Equation [1] can be transformed into the more useful form

$$F_{AB} = 2\,C_q\,wx\,\Delta p\cos\theta \quad \ldots\ldots\ldots [2]$$

where

C_q = coefficient of discharge

$$= \frac{Q}{wx\sqrt{\frac{2\Delta p}{\rho}}}$$

[1] "Berechnung von Ausfluss- und Überfallzahlen" ("Calculation of Discharge and Weir Coefficients"), by R. von Mises, *Zeitschrift des Vereines deutscher Ingenieure*, vol. 61, May-June, 1917, pp. 447–452, 469–474, 493–498 (especially pp. 494 and 495).

w = peripheral width of orifice
x = axial length of orifice
Δp = pressure difference between chamber A and chamber B

Since θ is always less than 90 deg for valves of the type under discussion, F_{AB} of Equation [1] is always positive and tends to close the valve. If the direction of flow is reversed so that the jet flows into chamber A instead of out of it, the equation is still valid, and if the jet angle θ is the same for both cases, the force will be the same. It should be noted that for Fig. 2 the jet angle depends upon the angle ϕ but is independent of ψ; for the reversed flow, the opposite is true. In either case it is the configuration of the *upstream* chamber that determines the force.

Equations [1] and [2] apply only to an ideal valve with perfectly sharp corners and zero radial clearance. Since such an ideal valve cannot be built, it is important to investigate the effects of these imperfections. For an orifice with radial clearance C_r as shown in Fig. 3, Equation [2] becomes

$$F_{AB} = 2\,C_q w\Delta p\,\sqrt{x^2 + C_r^2}\cos\theta \quad \ldots\ldots\ldots [3]$$

Here $\cos\theta$ is no longer a constant but varies with the quantity x/C_r, as shown by the curve.

If the net force on the piston is plotted against the displacement for a constant value of pressure drop, a curve similar to those in Fig. 4 is obtained. Here the curve for an ideal valve is shown dashed. It can be seen that the effect of radial clearance is to make the curve rise abnormally rapidly for small openings,

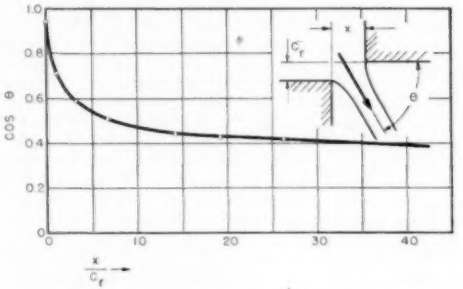

FIG. 3 EFFECT OF RADIAL CLEARANCE ON COS θ

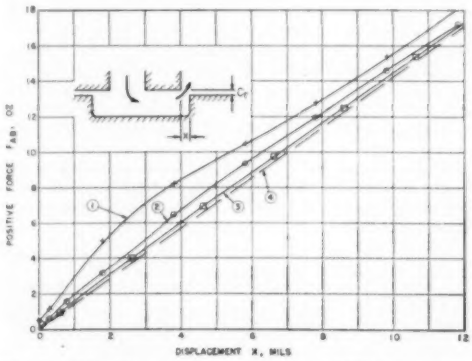

(1) C_r = 0.0003 in., r = 0
(2) C_r = 0.00005 in., r = 0.0003
(3) C_r = 0.0001 in., r = 0
(4) Ideal case: C_r = 0, r = 0

FIG. 4 EXPERIMENTAL POSITIVE-FORCE CURVES

after which it sags downward and approaches the ideal curve asymptotically.

The effect of finite radius of the land edges is difficult to calculate theoretically but is very similar to that of radial clearance. Qualitatively, the variation of θ can be visualized with reference to Fig. 5. In Fig. 5(*a*) the ideal case of zero radial clearance and sharp land edges is represented. The figure is skew-symmetrical about the center of the opening; it is the skewness of the symmetry that causes the axis of the jet to deviate from the vertical, and it is this deviation and the resulting x-component of momentum that give rise to the axial force on the piston.

(*a*)	(*b*)	(*c*)
$C_r = 0$	$C_r = x$	$C_r = 0$
$r = 0$	$\theta = 45$ deg	$r > 0$
$x =$ any value	$r =$ any value	$\theta < 69$ deg
$\theta = 69$ deg		

FIG. 5 LAND CONFIGURATIONS

Fig. 5(*b*) represents a valve with the axial displacement x set equal to the radial clearance C_r. The figure is symmetrical about the two 45-deg lines, and the jet angle θ is 45 deg because of this symmetry. This is true also for any value of radius r of the land edges so long as the r are the same for both edges. If the valve opening x is varied, however, the symmetry will be destroyed, and θ will no longer equal 45 deg. For large values of x the behavior will approach that of an ideal valve, and θ will approach 69 deg; for small values of x the jet will approach parallelism with the axis, and the force will be greater than that for an ideal valve.

For a valve with zero radial clearance but finite curvature of the land edges, as in Fig. 5(*c*), the symmetry is skewed as for the ideal valve but not to such a great extent; the angle θ is less than 69 deg; the piston force is greater than for an ideal valve; and θ varies with x. For large values of x, θ approaches 69 deg; for negative values of x, θ approaches 0 deg as x approaches $-r$. For an actual valve in which neither C_r nor r is zero, θ approaches zero at small or negative values of x, and the slope of the curve of force versus x increases at most by a factor of $1/0.36 = 2.78$. This is not particularly serious, of course, since in most cases the curve drops off and approaches that for an ideal valve before the actual value of the force is very large, i.e., the phenomenon occurs essentially only for small values of x.

In an actual 4-way valve there are two identical orifices in series and, therefore, twice the force on the piston. Equation [1] then becomes

$$F_T = 2\,F_{AB} = 2\,Q\,\sqrt{\rho P_v}\cos\theta \quad \ldots\ldots [4]$$

or for a particular fluid

$$F_T = K_1\,Q\,\sqrt{P_v} \quad \ldots\ldots [5]$$

where F_T is the total flow force on the piston and the total pressure drop across the valve for the two orifices in series $P_v = 2\,\Delta p$. For petroleum-base fluids with specific gravities of about 0.85, $K_1 = 0.0064$ when Q is given in cubic inches per second and P_v in pounds per square inch.

Two useful variants of Equation [5] may be obtained by combining it with the flow equation. For the same units and fluid

$$Q = 67\,A\,\sqrt{P_v} \quad \ldots\ldots [6]$$

where A is the area of each orifice in square inches. Eliminating P_v from Equation [5] gives

$$F_T = 9.6 \times 10^{-4}\,\frac{Q^2}{A} \quad \ldots\ldots [7]$$

and eliminating Q gives

$$F_T = 0.43\,A\,P_v \quad \ldots\ldots [8]$$

To illustrate the order of magnitude of the forces ordinarily encountered, computation of the magnitude for a typical case may be useful. The maximum horsepower which a valve with a given orifice area can deliver to a load is $3.9 \times 10^{-3}\,A\,P_s^{3/2}$, and this power is delivered when two thirds of the supply pressure P_s appears as drop across the load, and one third across the valve. For this condition of maximum output and the common supply pressure of 3000 psi, the force on the piston is 0.67 lb per hp.

So far, nothing has been said about the radial component of the force on the piston. It could be calculated by substituting $\sin\theta$ for $\cos\theta$ in Equation [2] but it is not usually of interest since it can be canceled easily by the simple scheme of dividing the port peripherally into two or more equal parts equally spaced around the sleeve.

COMPENSATION OF STEADY-STATE FORCE

Flow-control valves used in high-performance systems such as fast hydraulic servos are usually stroked by electromagnetic torque motors driven by vacuum tubes. The use of tubes makes it highly desirable to keep the power input to the torque motor down to a few watts or less, and this restriction plus the inherent design limitations of electromagnetic devices and the large force required to stroke a square-land piston have in the past limited the outputs of single-stage valves to perhaps 1 hp; higher outputs were controlled by using two or more valves in cascade. In an effort to eliminate the additional stages, several attempts have been made to reduce or eliminate the flow force discussed in the previous section, but so far as is known these attempts either were unworkable or at best gave adequate compensation only over a narrow range of flows and pressure drops. The Hydraulics Group of the Dynamic Analysis and Control Laboratory has developed a valve design which gives perfect cancellation of the flow forces within the limits imposed by manufacturing imperfections and which at the same time is little more difficult to build than a conventional valve.

In the valve construction to be described, the axial component of efflux of momentum from the downstream chamber is made greater than the influx so that a negative (opening) force is developed which is proportional to x for a given pressure drop, and this negative force is balanced by the positive force generated at a conventional square-land orifice. It has been found experimentally that, except for very small openings, the two forces can be balanced perfectly for all pressures and flows. Here the effects of radial clearance and of rounding the land edges operate to give a positive force which at its maximum is only a very small fraction of the maximum for a conventional valve.

Perhaps it should be noted that this method can be used to give a zero-force port, but since the special port construction is somewhat more difficult to manufacture than a conventional square port, and since it may lead to the transient instability discussed later, the balancing scheme is preferable.

The construction of the negative-force port is shown schematically in Fig. 6. It differs from a conventional port in two ways; the chamber in the piston is shaped somewhat like a turbine bucket, and the sleeve is cut out to form an extension of the downstream chamber. Here the jet through the orifice enters the piston chamber at an angle θ_i, is reflected from the chamber

wall near d, and leaves at an angle θ_2. If the cross section of the flow were constant and the frictional force negligible, the resulting force on the piston would be

$$F_{CD} = Q\, u\, \rho\, (\cos \theta_1 - \cos \theta_2) \quad \ldots\ldots\ldots\ldots [9]$$

Thus the positive force of Equation [1] easily may become a negative force, since $\cos \theta_2$ is ordinarily considerably larger than $\cos \theta_1$.

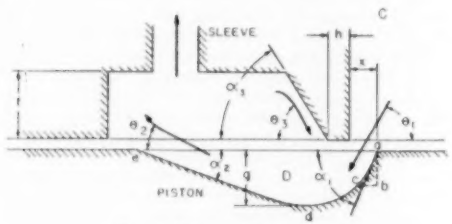

FIG. 6 NEGATIVE-FORCE PORT

Furthermore, an eddy is produced which moves clockwise (in the case shown), and an additional flow enters the piston chamber at an angle θ_3, which increases the negative force still more.

The total resultant force on the piston is thus rather complicated. It depends upon numerous variables such as α_1, α_2, α_3, ρ, μ, w, and d where ρ is the density and μ the viscosity of the fluid, w the peripheral width of the port, and d the piston diameter. A theoretical derivation of the force would be practically impossible.

The port width w occupies only a portion of the circumference of the piston in many valves. Although it is usually large compared with x so that the flow can be treated as two-dimensional at the orifice, it is small compared with the dimensions of the chambers. When the incoming jet of fluid hits the piston near the point d and is reflected upward, it tends to spread out normal to the plane of the figure, and the condition of constancy of cross section assumed in Equation [9] no longer holds. The actual exit angle θ_2 thus tends to be greater than α_2, and the jet tends to separate from the piston surface. Experiment shows that the spreading tendency is greatly dependent on the angle of incidence of the jet on the piston surface. If $\alpha_1 = \theta_1$, the angle of incidence is zero, and the negative force is a maximum; α_1 should normally be made equal to 69 deg, the influx angle for a square land. It is found, however, that a square step such as a-b-c in Fig. 6 has little effect on the force if it is not too deep, and it is desirable for manufacturing reasons that such a step be provided. In the case for which $w = 360$ deg, there would be no lateral spreading.

Although the actual force for a given case is too complicated to calculate, it is found that for a given valve profile the force varies with x and with the pressure drop Δp across the orifice as follows:

1 For a constant pressure drop, F_{CD} varies with x, according to the curves in Fig. 7. For very small values of x the force is positive, going through a maximum and returning to zero when $x = a$. The distance a is directly proportional to the unavoidable errors of manufacture, i.e., to C_r and r. It is also somewhat affected by the shape of the piston profile. The explanation of the positive force is analogous to that given previously; when x is small, θ_1 is small, and the x-component of momentum is a maximum for a given flow. Furthermore, the angle of incidence on the piston and the resultant spreading of the jet increase, θ_2 increases, and the negative force is reduced. The additional spreading decreases the velocity of the return flow θ_3 and its contribution to the negative force. If C_r and r could be made zero, θ_1 would be independent of x, and the positive hump would vanish; the curve of F_{CD} plotted against x would be as shown by the dashed curve in Fig. 7. The effects of changing C_r and r are shown in the experimental curves in Fig. 7.

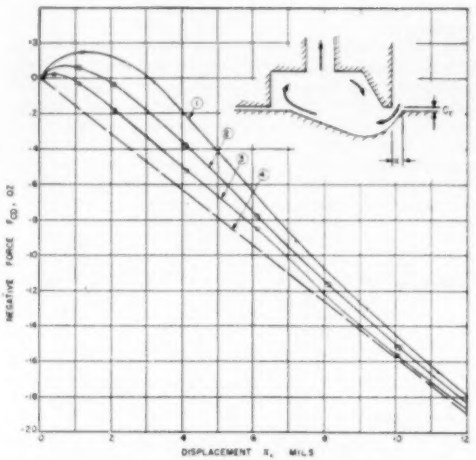

(1) $C_r = 0.0006$ in., $r = 0.0003$ in. (3) $C_r = 0.0004$ in., $r = 0$
(2) $C_r = 0.0006$ in., $r = 0$ (4) Ideal case: $C_r = 0$, $r = 0$

FIG. 7 EXPERIMENTAL NEGATIVE-FORCE CURVES

2 When x is large compared to C_r and r, F_{CD} is directly proportional to Δp for a given value of x. This indicates that for an ideal valve it would be proportional for all values of x. These two experimental results can thus be combined into the equation

$$F_{CD} = -Kx\, \Delta p \quad \ldots\ldots\ldots\ldots [10]$$

where K is a constant for an ideal port of a given geometrical design but is a function of x/C_r and of x/r for an actual valve. As previously stated, the modified piston profile a-b-c-d-e in Fig. 6 gives results almost identical with those of the profile a-c-d-e as long as the angle e-a-c is equal to or a little greater than 69 deg.

The coefficient K depends upon both α_2 and α_3 in Fig. 6. For manufacturing reasons, α_3 is somewhat less easy to vary than α_2, but K can be controlled easily by varying the latter. The value of K also depends to some extent upon the dimensions f, g, and h. For maximum compensation, f should be as large and h as small as possible.

Since in an ideal 4-way valve such as that in Fig. 1, there are always two identical orifices in series and, since C_q, w, x, Q, and Δp are the same for both, the positive force of the square-land port will be equal to the negative force of the modified port if F_{AB} of Equation [1] is equal to F_{CD} of Equation [10]. This will be the case if

$$K = 2\, C_q\, w \cos \theta \quad \ldots\ldots\ldots\ldots [11]$$

or if

$$K = 0.72\, C_q\, w \quad \ldots\ldots\ldots\ldots [12]$$

since $\cos \theta = 0.36$ for an ideal valve. Since K depends upon a number of controllable dimensional parameters, it is a simple if somewhat laborious matter to satisfy Equation [12] in practice. As already pointed out, however, it is impossible to build an ideal valve, and the compensation will be imperfect to an extent depending upon the errors of manufacture; specifically,

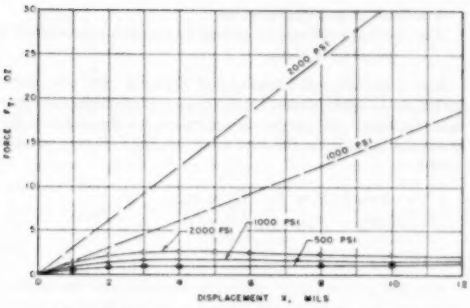

FIG. 8 PERFORMANCE OF FIRST COMPENSATED PISTON

upon the magnitudes of the radial clearance C_r and the radius of curvature r of the port and land edges. Actual experimental results obtained with a valve of the construction just described are given in Fig. 8 where curves are also sketched for an ideal uncompensated valve of the same dimensions.

It can be seen from the figure that the force for a given pressure drop is everywhere less than for an uncompensated valve and that, instead of rising linearly with valve opening, the force reaches a low maximum (at least for the higher pressures) and then decreases slowly.

One possible measure of the effect of the modified construction would be the ratio of the maximum forces on the pistons of a conventional and a modified valve. For the example given, this ratio reaches a value of about 18 at 2000 psi and 15-mil displacement. Since it is almost directly proportional to displacement, however, the ratio has little meaning except as a measure of maximum displacement. If the valve had been tested at 50-mil displacement, for example, which is about average for the DACL power pistons used, the improvement ratio would have been about 50; for a displacement of 5 mils such as is used in the pilot valves the ratio would have been only 6. The quantity of greatest importance is the maximum force required. The curves show that this maximum force is greatly decreased by the use of the modified construction. Further substantial reductions can be made by minor adjustments of the dimensional parameters and by improved workmanship. A sketch of a 4-way valve of the proposed construction is given in Fig. 9. The results illustrated are by no means the best that can be attained; optimum design and improved workmanship would reduce the remaining stroking force considerably.

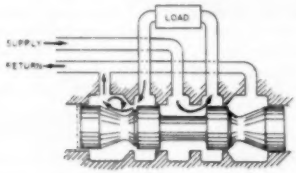

FIG. 9 FOUR-WAY VALVE WITH FORCE COMPENSATION

Discussion

F. C. PADDISON.[4] The existence of reaction forces within hydraulic control valves has been realized by designers for many years, although apparently they were not of great concern until the advent of high-speed aircraft, guided missiles, and aircraft and missile simulators.

The high-speed large power servomechanisms normally required by missiles and high-speed aircraft, require simplicity, low internal delays with the servo loop, physically small components, and low electrical power consumption. A combination of electrical, mechanical, and hydraulic systems is one of the common solutions. The severe requirements necessitate a thorough understanding of components and their operational characteristics. The most critical component of such a servo system has been the hydraulic transfer valve both from a manufacturing and analysis standpoint and is, surprisingly, seldom discussed in the available literature.

One approach to the transfer-valve design in servo-system applications has been to develop an actuating device whose force levels were greater than the reaction forces within the valve. Direct-current torque motors are in existence, or can be designed to actuate transfer valves transmitting up to 4 hp. For higher-power servo systems, internal compensation, such as discussed in the paper, or force amplifiers preceding the valve are necessary if the requirements of low internal delays, small components, and low electrical power consumption are to be met.

Force amplifiers preceding the hydraulic transfer valve and two-stage transfer valves have been developed by the Cornell Aeronautical Laboratory, the Department of Electrical Engineering of Yale University, the Dynamics and Control Laboratories of the Massachusetts Institute of Technology, and there are undoubtedly others. The force amplifiers are normally rather complicated and, consequently, less reliable than a valve incorporating the force compensation as discussed by the authors.

There are applications where "complete" compensation of reaction forces in the transfer valve may not be desirable. Assume a servo system designed to actuate an aerodynamic surface as part of a control system; the transfer-valve flow rate is selected by the geometry of the power actuator, the available pressure drop across the power actuator (or piston), the maximum aerodynamic load and a maximum available velocity of the surface under maximum aerodynamic load. The present procedure is to allow two thirds of the supply pressure (assumed constant) across the power actuator while overcoming the maximum load, while the remaining one third of the supply pressure is taken across the transfer valve. Knowing the required flow rate and the available pressure, the transfer-valve orifice area may be selected.

In missile and aircraft applications the aerodynamic load normally will be a function of Mach number, altitude, and center of pressure location and conceivably can approach zero under some conditions, or even change sign. At this time, nearly the full system pressure will appear across the transfer valve. The volumetric rate of the transfer valve and the servo-loop gain, therefore, will increase by approximately 70 per cent. If, however, the selection of the transfer-valve orifice area is predicated on a pressure drop across the transfer valve of less than one third the supply pressure, at full load, the change in gain of the hydraulic valve and the servo-loop gain under no-load conditions can become appreciable. The change in servo-loop gain between full load and no load, if of concern, can be minimized by tailoring the force characteristics of the torque motor to the valve reaction forces such that the transfer-valve flow rate is nearly independent of changes in load on the power actuator. For the case considered, the change in gain between the two load conditions can be decreased from 70 per cent to approximately 5 per cent.

To be more specific about this type of gain compensation, if the motor actuating a four-way transfer valve without force

[4] Applied Physics Laboratory, Johns Hopkins University, Silver Spring, Md.

compensation could be built with the following force versus displacement characteristics, the gain of the motor and transfer valve would be independent of changes in load

$$F_m = \frac{2 \cos \theta F_L \sqrt{P_{\min}}\, \dot{x}_0}{K_V (P_S - P_{\min}) x_{e_{\max}}} x_{e_{\max}} \quad \ldots\ldots\ldots\ldots [13]$$

where

θ = has same meaning as in Lee and Blackburn's paper
F_L = maximum design load of servomechanism
$\dot{x}_0$ = maximum design power piston-output velocity under full load, F_L
$K_V = \sqrt{1/\rho}$ where ρ = mass density of hydraulic fluid. For hydrocarbon hydraulic oil Mil-0-5606 approx $\rho = 7.8 \times 10^{-5}$ lb sec^2/in.^{4}
P_S = supply pressure; assumed constant
$P_{\min}$ = hydraulic pressure drop across transfer valve (total drop across both series orifices) while providing maximum velocity $\dot{x}_0$, at maximum load F_L
x_e = transfer valve-spool displacement
$x_{e_{\max}}$ = maximum valve-spool displacement used when selecting transfer valve orifice area

A motor of the force characteristics required by Equation [13] of this discussion would be rather difficult to build, although motors having a force characteristic similar to that given in the following equation are in common use

$$F = -Kx_e + bI \quad \ldots\ldots\ldots\ldots [14]$$

where

K = slope of force curve
b = force at zero displacement
I = normally differential current or function proportional to servo-error signal

Now if the slope and intercept of Equation [14] are selected such that the available force from the motor intercepts the hyperbola, Equation [13] at the displacements for the required flow at the no-load and the full-load condition, the following equation results

$$F_M = \frac{2 \cos \theta \dot{x}_0 F_L \sqrt{P_S}}{K_V (P_S - P_{\min}) x_{e_{\max}}} \left[\left(\frac{\sqrt{P_{\min}}}{\sqrt{P_S}} + 1 \right) x_{e_{\max}} I - x_e \right] \quad \ldots\ldots [15]$$

Now if Equation [13] is equated to Equation [15] the resulting Equation [16] describes the output velocity ($\dot{x}$) of the servo's power actuator as a function of valve-spool displacement x_e. Owing to the gain compensation, the valve-spool position is now a function of load as well as servo error I; therefore Equation [16] describes the output velocity $\dot{x}$, under various load conditions for a constant servo error. The servo error I is a parameter and simply shifts the curves

$$\dot{x} = \dot{x}_0 \left\{ \frac{\sqrt{P_S}}{\sqrt{P_{\min}}} \left[\left(\frac{\sqrt{P_{\min}}}{\sqrt{P_S}} + 1 \right) \frac{I x_e}{x_{e_{\max}}} - \frac{x_e^3}{x_{e_{\max}}^3} \right] \right\}^{1/2} \quad [16]$$

Fig. 10 of this discussion is a solution of Equations [13] and [15] for three servo systems, designed for the same output velocity $\dot{x}_0$, and load F_L, and using the same supply pressure P_S, although with transfer-valve coefficients selected for the following different pressure distributions within the system while overcoming maximum load:

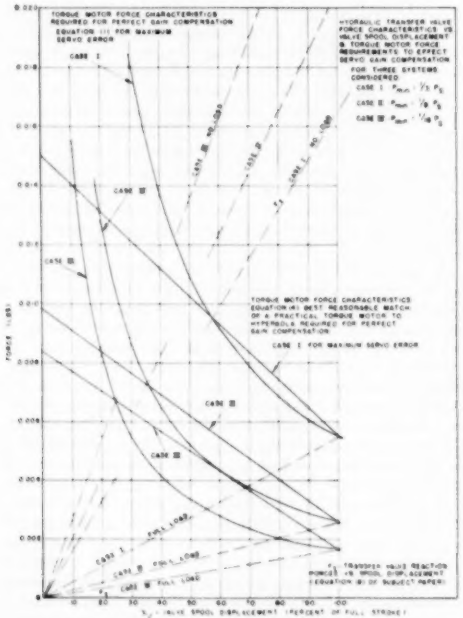

Fig. 10

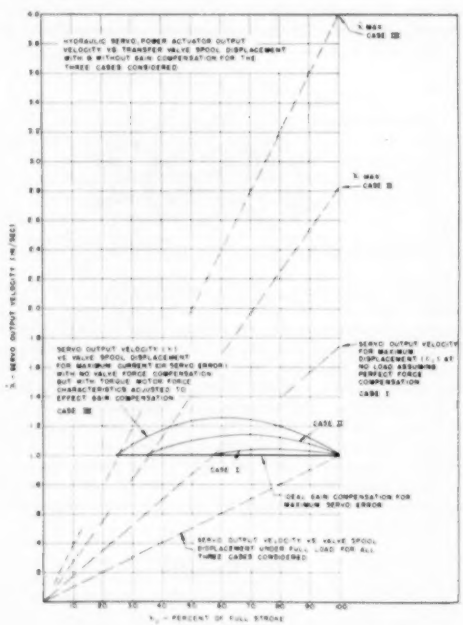

Fig. 11

Case I	$-P_{min} = 1/2\ P_S$	for $F_L = 1$ lb
II	$P_{min} = 1/4\ P_S$	$P_S = 1$ psi
		$\dot{x}_0 = 1$ in/sec
III	$P_{min} = 1/16\ P_S$	$x_{max} = 1$ in

Fig. 11, herewith, is a solution of Equation [16] for the three cases considered. The maximum change in gain for the three systems considered at maximum servo error, compared to identical systems where valve-spool position is directly a function of servo error and independent of load, is as follows:

	No gain compensation, per cent	With gain compensation, per cent
Case I	70	5
II	283	16
III	400	25

Note that the previous discussion should in no way be construed as a recommendation to design systems utilizing a pressure distribution P_{min}, of less than $1/2\ P_S$, at maximum load.

It is suggested that the authors comment on the following questions:

1 Is there a minimum or maximum power limit for this valve configuration?

2 Have any experimental studies been made where this type of valve has been used in a servo system driving a large inertia load, to investigate the effects of oil compressibility and finite-pressure propagation velocities on the compensated-valve or servo-loop characteristics?

The authors are to be commended for their significant contributions to the hydraulic-control field—specifically for the derivation of the equations of the valve-reaction forces and the development of a valve that has no apparent power limitations.

Authors' Closure

Mr. Paddison has raised, by implication at least, so many important points that an adequate discussion would require an inordinate amount of space even if we were competent to write it. If we may grossly condense and simplify his principal argument, however, the pertinent points seem to be the following:

1 Important classes of loads may be very nonlinear.

2 This nonlinearity results in a change of gain which may be fairly large and which is a function of the ratio of valve pressure drop at full load to supply pressure.

3 This change of gain can be considerably reduced by working with valve drops much larger than normal.

4 It can also be reduced by tailoring the torque-motor characteristics in the proper way and not compensating the flow forces in the valve.

One reasonable, or at least plausible, way of thinking about the problem of nonlinear loads is to consider that the load is linear but that it has superposed upon the "normal" linear-load reactions various extraneous disturbances, such as wind loading on a radar antenna, tool reactions on a milling-machine table drive when taking an intermittent cut, or the aerodynamic phenomena referred to by Mr. Paddison. The effect of these disturbances on the servo output is a measure of the "stiffness" of the servo, and this stiffness may be of two types. In any position servo there is a tendency for the output to assume the position called for by the input signal, and the servo is stiffer the greater the loop gain; thus a position servo with a high loop gain is very stiff, and if properly designed, using reasonably linear components, it is nearly immune to disturbances. In addition, some types of drive are mechanically stiff; thus a hydraulic motor or ram with the flow valve closed is exceedingly stiff because of the low compressibility of the oil. An extreme case would be an irreversible worm drive, though this is often unsuitable for servo applications. In the case of a rate servo, which is what a flow valve wants to be, the second type of stiffness is not present, but the first is, and if the loop gain is high the servo will pay little attention to the disturbance, within the force and velocity limits imposed by the design of the driver.

It is true that the effect of change of gain can be minimized by wasting a large part of the available supply pressure in the valve but this seems an excessive price to pay for a not very serious variation in gain. It is also true that the torque-motor characteristic can be modified to help in attaining the same goal, but we have preferred not to do so. This is, first, because such a modified motor would be useful only under a very restricted range of conditions as to supply pressure, performance, and character of load; second, because we do not like to try to compensate for a nonlinearity in one component by deliberately making another one worse than it needs to be; and third, because as Mr. Paddison points out, it is highly desirable to have as strong a torque motor as possible. This last point is true even in the absence of flow forces; a comfortable margin of force is necessary to prevent sticking of the piston, which is a condition that has plagued every user of hydraulic equipment. He also points out that a two-stage valve can be used, and in the past has been used universally for powers over a certain level. In this case, however, there is the added complication of an extra complete valve plus an extra integration that must be removed somehow, and in addition, the change of gain which he refers to would still be present, and could not be removed by modifying the torque motor.

Finally, we must give at least partial answers to the two explicit questions in Mr. Paddison's comments:

1 There do not seem to be any minimum or maximum power limits as such to the application of Dr. Lee's method of force compensation. As pointed out in the paper, it is of comparatively little benefit in valves with very short strokes, but should be valuable in large long-stroke valves. The practical minimum size would be essentially the same for any hydraulic valve, whether compensated or not.

2 We have not observed any phenomena due to oil compressibility or to the finite velocity of propagation in the oil with this valve that would not occur with an uncompensated valve, whether working into a high-inertia load or not. In fact, we have never observed an effect of any kind which we thought was due to the finite velocity, and since the velocity of sound in oil is such that it would traverse the dimensions of most hydraulic control systems in a fraction of a millisecond, we would not expect to observe any such effects. There is an effect of compressibility that may be serious for high-inertia loads, however; in some cases the natural frequency of the heavy load working against the compliance of the oil becomes so low that the speed of response of the servo system is greatly reduced. In most cases, however, the compliance of the oil is small compared to that of the mechanical structure and this compressibility effect is negligible.

Contributions to Hydraulic Control

2 Transient-Flow Forces and Valve Instability

By SHIH-YING LEE[1] AND J. F. BLACKBURN,[2] CAMBRIDGE, MASS.

An outline is presented of a theory of a transient force which is one likely cause of oscillation of control valves, with supporting experimental evidence and methods of eliminating it.

ONE annoying characteristic of many hydraulic flow-control valves and similar devices is a tendency to instability. This may result only in acoustical noise or "singing," or it may cause nonlinear, unstable operation, or even violent oscillation of the whole system in which the valve is used. There are several causes of instability, but the following paper will be concerned with one type of transient instability which apparently has not been reported previously.

Mathematical Derivation of General Force Equation

The somewhat involved mathematical derivation of the theory given in the Appendix results in the equation

$$F_x' = \rho Q u_2 + \rho L \frac{dQ}{dt} \quad \ldots\ldots [1]$$

where

F_x' = axial component of force on valve piston due to flow through one piston chamber
ρ = density of fluid
u_2 = axial component of velocity of fluid through valve orifice
Q = rate of flow through orifice
$\frac{dQ}{dt}$ = rate of change of flow
L = axial distance between centers of incoming and outgoing flows, as shown in Fig. 3.

Since flow-valve-controlled hydraulic systems are normally operated from constant-pressure supplies it is desirable to state the valve force in terms of pressure instead of flow. A further simplification is obtained at a small cost of generality by assuming that the pressure drop across the orifice is constant and equal to ΔP, so that the flow Q depends only upon the axial valve opening x. For this case the basic equation for flow through an orifice gives

$$u_2 = -C_v \sqrt{\frac{2\Delta P}{\rho}} \cos\theta \quad \ldots\ldots [2a]$$

$$Q = C_q w x \sqrt{\frac{2\Delta P}{\rho}} \quad \ldots\ldots [2b]$$

and

$$\frac{dQ}{dt} = C_q w \sqrt{\frac{2\Delta P}{\rho}} \frac{dx}{dt} \quad \ldots\ldots [2c]$$

where

C_v = velocity coefficient
C_q = discharge coefficient
θ = angle between axis of jet and axis of valve
w = peripheral width of port

Substituting in Equation [1], therefore

$$F_x' = -(2 C_q C_v \Delta P w \cos\theta) x + (C_q w \sqrt{2 \Delta P \rho}\, L) \frac{dx}{dt} \quad \ldots [3]$$

This equation is of the form

$$F_x' = -K_1 x - K_2 \frac{dx}{dt} \quad \ldots\ldots [4]$$

in which

$$K_1 = 2 C_q C_v \Delta P w \cos\theta \quad \ldots\ldots [4a]$$

and

$$K_2 = -C_q w \sqrt{2 \Delta P \rho}\, L \quad \ldots\ldots [4b]$$

Inspection of Equation [4] shows that the effect of the oil flowing past the piston land can be represented as a linear spring which tends to restore the piston to its center position at $x = 0$, plus a linear damping term. The spring term is the steady-state piston force discussed in part 1 of this series;[3] it will not be further discussed here.

The coefficient K_2 of the damping term depends upon only two dimensions of the valve, the peripheral port width w and the damping length L; it is independent of the other dimensions or the shape of the piston cavity.[4] The sign of K_2 depends upon the sign of L, since all other quantities involved are positive. If L is positive, then K_2 is negative, an increasing flow tends to increase x, the damping will be negative, and the valve will oscillate unless sufficient positive damping is available from some other source. The damping length L will be positive when the flow through the metering orifice is inward toward the piston axis; reversing the flow reverses the signs of L and of the damping.

In a conventional 4-way valve there will be two orifices in series, for which all quantities are the same except the L. Accordingly, an effective damping length for the whole valve can be defined, which will be the algebraic sum of the L for the two chambers. Again, if this effective L is negative, the valve will be stable; if positive, it is likely to oscillate. This prediction has been verified by the experiments to be reported.

Experimental Valve for Stability Tests

The valve used for the stability tests was an experimental

---

[1] Research Engineer, Dynamic Analysis and Control Laboratory, Massachusetts Institute of Technology.
[2] Research Engineer, Dynamic Analysis and Control Laboratory, Massachusetts Institute of Technology.
Contributed by the Machine Design Division and presented at the Annual Meeting, Atlantic City, N. J., November 25–30, 1951, of The American Society of Mechanical Engineers.
Note: Statements and opinions advanced in papers are to be understood as individual expressions of their authors and not those of the Society. Manuscript received at ASME Headquarters, August 7, 1951. Paper 51—A-60.

[3] "Steady-State Axial Forces on Control-Valve Pistons," by Shih-Ying Lee and J. F. Blackburn, Paper No. 51—A-52, to be presented at the Annual Meeting, Atlantic City, N. J., November 25–30, 1951, of The American Society of Mechanical Engineers.
[4] These results do not apply strictly to the special port construction described in reference 3, since the assumption that $u_1 = 0$ of Equation [1] in the Appendix is not justified, in that case. Qualitatively, however, they are still valid.

model which contained certain features, such as the provision for independent control of the directions of flow through the several orifices, which would not normally be included in a production design. In function it was a conventional 4-way flow-control valve with steady-state-force compensation, but its actual design included the following features:

1 The twin-piston design is shorter than a single-piston valve, saving space for the complete assembly of valve plus torque motor.

2 The moving parts are inherently balanced, eliminating the counterweight required in many applications of the single-piston design and permitting a higher natural frequency.

3 One critical axial dimension is eliminated on both piston and sleeve.

4 With the ports faced as shown and with no underlap, fluid never passes both pistons at the same time. This eliminates the requirement of transmitting either steady-state or transient flow forces from one piston to the other through the relatively compliant torque-motor armature and linkage; this is very desirable for a device requiring precise positioning.

5 The damping coefficient of the valve can be controlled easily by suitable choice of the lengths L_1 and L_2.

The principal dimensions of interest are as follows:

Piston diameter, in.	0.250
Maximum stroke, in.	0.007
Port width (360-deg ports), in.	0.785
Maximum area per orifice, sq in.	0.0055
Maximum output at 3000 psi, hp	3.5
Damping lengths:	
Negative-force ports, in.	0.08
Positive-force ports, in.	0.33

During the stability tests the valve was connected to a standard torque motor with the valve output shortcircuited (no load). For each of the four flow conditions shown in Fig. 1 the supply pressure was increased gradually to 3000 psi or until oscillations occurred. It was found that for the oscillatory configurations the onset of oscillations was fairly consistent, the critical pressure varying over a range of perhaps 5 to 10 per cent. The test results showed the following:

Test Results

1 Configuration *a* had a small negative damping in the downstream port and a larger positive damping upstream, since L_1 was purposely made larger than L_2. This was the normal configuration for this valve; the steady-state force was compensated and the valve was stable at all pressures up to 3000 psi.

2 For configuration *b* the supply and return lines were interchanged, reversing all flows through the valve and load. The negative-force port now acted as an ordinary square-land port, and there was no steady-state force compensation. The small positive damping only partly compensated the larger negative damping of L_1; the net negative damping overcame the viscous damping, and the valve oscillated violently for all pressures above 1100 psi.

3 Configuration *c* was similar to *a* except for the reversal of flow through the left-hand port. The steady-state force was compensated but both damping terms were negative, and the valve oscillated for all pressures above 500 psi.

4 The supply and return lines were again interchanged, giving configuration *d*. This was the most stable of the four, since both damping terms were positive, but the steady-state compensation was destroyed by reversing the flow through the upstream port.

Since the viscous-damping forces were not known, it was impossible to predict the value of the critical pressures above which the valve would oscillate, but at least the experiments agree qualitatively with the predictions of the theory.

Appendix

Derivation of General Force Equation

Consider first a container of arbitrary shape filled with an incompressible fluid and without fluid sources or sinks within its volume. Assume initially that flow may take place at any point either within the container or across its boundary, and let flow outward across the boundary be considered positive. At any instant the total momentum of all fluid particles within the container is

$$\bar{M} = \rho \int_V \bar{q}\, dV \qquad [5]$$

where ρ is the density of the fluid, dV an elementary volume, and $\bar{q}$ its instantaneous velocity; the integration is taken over the whole volume of the container.

The three components of the momentum will be

$$\left.\begin{aligned} M_x &= \rho \int_V u\, dV \\ M_y &= \rho \int_V v\, dV \\ M_z &= \rho \int_V w\, dV \end{aligned}\right\} \qquad [6]$$

where u, v, and w are the x, y, and z-components of the velocity $\bar{q}$.

The volume integration of Equations [5] and [6] may be replaced by a surface integration with the use of Green's theorem. Let dS be an element of the surface of the container. Let the direction of the outward normal to this surface be denoted by $\bar{n}$, whose directional components are α, β, and γ. Let q_n denote the normal component of fluid velocity across the boundary at dS.

By Green's theorem

$$\begin{aligned} \int_S x\, q_n\, dS &= \int_S x\,(u\cos\alpha + v\cos\beta + w\cos\gamma)\, dS \\ &= \int_V \left[\frac{\partial}{\partial x}(xu) + \frac{\partial}{\partial y}(xv) + \frac{\partial}{\partial z}(xw)\right] dV \\ &= \int_V \left(\frac{\partial u}{\partial x} + \frac{\partial v}{\partial y} + \frac{\partial w}{\partial z}\right) x\, dV + \int_V u\, dV \qquad [7] \end{aligned}$$

But if the fluid is incompressible and there are no sources or sinks within the container, the equation of continuity gives

$$\frac{\partial u}{\partial x} + \frac{\partial v}{\partial y} + \frac{\partial w}{\partial z} = 0$$

the first term on the right side of Equation [7] vanishes, and there results

$$M_x = \rho \int_V u\, dV = \rho \int_S x\, q_n\, dS = \rho \int_S x\, dQ$$

and the two analogous expressions

$$\left.\begin{aligned} M_y &= \int_S y\, dQ \\ M_z &= \int_S z\, dQ \end{aligned}\right\} \qquad [8]$$

where dQ denotes the total flow across the elementary surface dS

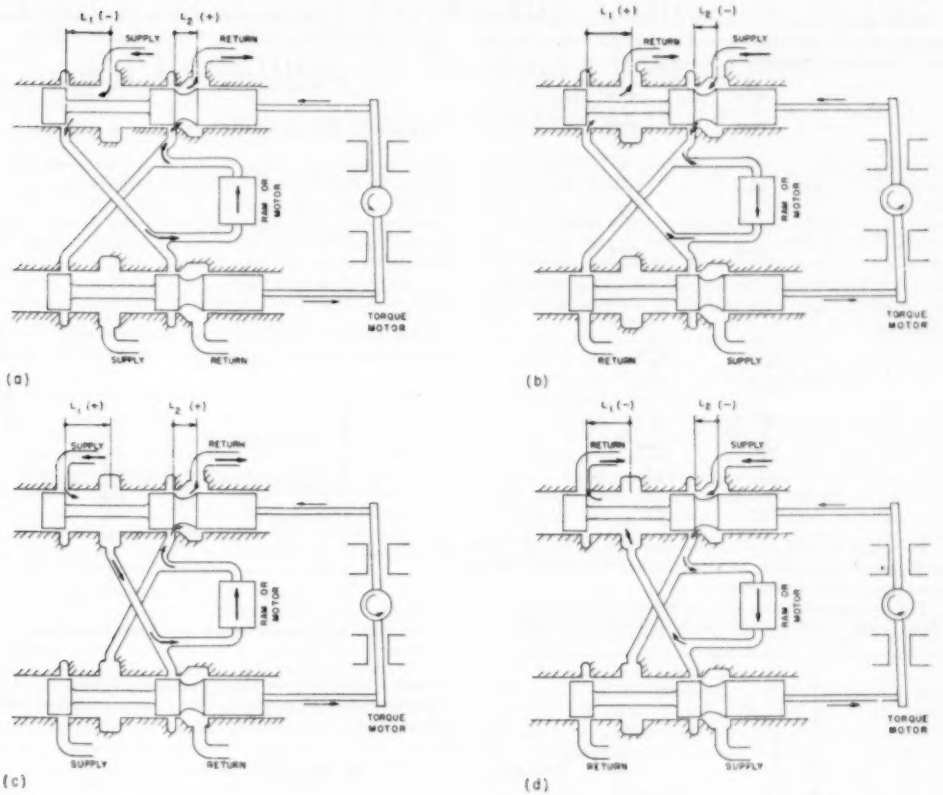

Config.	L_1, in.	L_2, in.	Net L, in.	Stability	Critical pressure psi	Steady-state balance
(a)	−0.33	+0.08	−0.25	Stable	—	Yes
(b)	+0.33	−0.08	+0.25	Unstable	1100	No
(c)	+0.33	+0.08	+0.41	Unstable	500	Yes
(d)	−0.33	−0.08	−0.41	Stable	—	No

FIG. 1 STABILITY TESTS OF SINGLE-STAGE VALVE

Thus the total momentum of the fluid within the container can be determined from the flow conditions at the boundary.

The only assumption inherent in the use of Green's theorem is that the velocities u, v, w, and their derivatives with respect to x, y, and z are continuous. For viscous fluids this must be true; for an ideal fluid a surface of discontinuity could exist, but Green's theorem could still be used by considering the container to be divided into more than one volume by the surfaces of discontinuity and integrating separately over each of the volumes. Thus Equation [8] will apply *for any type of flow whatever* as long as there are no fluid sources or sinks within the volume considered.

Next, consider the same container but with a boundary impermeable except for ... small holes through which fluid can flow. Assume the holes to be small enough so that the velocity can be considered uniform and parallel across each hole. Then the integral

$$\int_S x\, dQ = \sum_{k=1}^{N} x_k Q_k \qquad [9]$$

where x_k is the x-co-ordinate of the kth hole and Q_k is the total flow through it. Equation [8] then becomes

$$\left.\begin{aligned} M_x &= \rho \sum_{k=1}^{N} x_k Q_k \\ M_y &= \rho \sum_{k=1}^{N} y_k Q_k \\ M_z &= \rho \sum_{k=1}^{N} z_k Q_k \end{aligned}\right\} \qquad [10]$$

Knowing the total momentum of the fluid within the vessel we can calculate the total force exerted on it by the walls of the vessel. The three components of this force will be

$$\left.\begin{aligned} F_x &= \frac{\partial M_x}{\partial t} = \rho \sum_{k=1}^{N} Q_k \frac{\partial x_k}{\partial t} + \rho \sum_{k=1}^{N} x_k \frac{\partial Q_k}{\partial t} \\ F_y &= \frac{\partial M_y}{\partial t} = \rho \sum_{k=1}^{N} Q_k \frac{\partial y_k}{\partial t} + \rho \sum_{k=1}^{N} y_k \frac{\partial Q_k}{\partial t} \\ F_z &= \frac{\partial M_z}{\partial t} = \rho \sum_{k=1}^{N} Q_k \frac{\partial z_k}{\partial t} + \rho \sum_{k=1}^{N} z_k \frac{\partial Q_k}{\partial t} \end{aligned}\right\} \quad [11]$$

In these expressions $\partial x_k/\partial t = u_k$, the x-component of the velocity of the fluid at the kth hole, $\partial y_k/\partial t = v_k$, and $\partial z_k/\partial t = w_k$; therefore

$$\left.\begin{aligned} F_x &= \rho \sum_{k=1}^{N} Q_k u_k + \rho \sum_{k=1}^{N} x_k \frac{\partial Q_k}{\partial t} \\ F_y &= \rho \sum_{k=1}^{N} Q_k v_k + \rho \sum_{k=1}^{N} y_k \frac{\partial Q_k}{\partial t} \\ F_z &= \rho \sum_{k=1}^{N} Q_k w_k + \rho \sum_{k=1}^{N} z_k \frac{\partial Q_k}{\partial t} \end{aligned}\right\} \quad [12]$$

For steady flow $\partial Q_k/\partial t = 0$, the second terms on the right sides of Equations [12] vanish, and the equations become the familiar force equations for steady flow.

For the particular case of a container with only two holes shown in Fig. 2, the equations can be simplified still further. Let the subscript 1 apply to the hole with the fluid flowing outward, and 2, to that with inward flow. Then $Q_1 = Q = -Q_2$ and

$$F_x = \rho Q (u_1 - u_2) + \rho(x_1 - x_2) \frac{dQ}{dt} \quad [13]$$

When F' is the force exerted by fluid on the container

$$\left.\begin{aligned} F_x' &= -F_x = \rho Q (u_2 - u_1) + \rho(x_2 - x_1) \frac{dQ}{dt} \\ F_y' &= \rho Q (v_2 - v_1) + \rho(y_2 - y_1) \frac{dQ}{dt} \\ F_z' &= \rho Q (w_2 - w_1) + \rho(z_2 - z_1) \frac{dQ}{dt} \end{aligned}\right\} \quad [14]$$

These general formulas now may be applied to the case of a conventional square-land valve. Let Fig. 3 represent one port

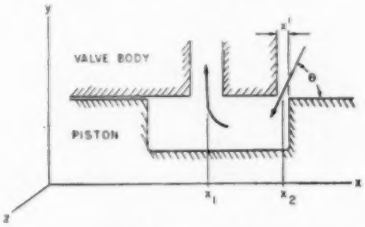

FIG. 3 DAMPING LENGTH OF A VALVE CHAMBER

of such a valve, with the piston displaced a distance x'. As the valve has cylindrical symmetry, both F_y and F_z cancel out around the axis, but

$$F_x' = \rho Q (u_2 - u_1) + \rho(x_2 - x_1) \frac{dQ}{dt} \quad [15]$$

or, assuming that $u_1 = 0$ (since the exit port is large compared to the orifice)

$$F_x' = \rho Q u_2 + \rho L \frac{dQ}{dt} \quad [16]$$

where $L = x_2 - x_1$.

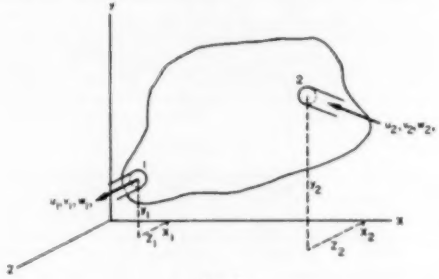

FIG. 2

Tool Forces and Tool-Chip Adhesion in the Machining of Nodular Cast Iron

By K. J. TRIGGER,[1] L. B. ZYLSTRA,[2] AND B. T. CHAO[3]

This paper presents the results of an investigation on the machining characteristics of nodular cast iron in both the as-cast and the annealed conditions. Tool forces, cutting temperatures, and tool-chip contact areas are compared for different grades of cemented-carbide tools. An adhesion phenomenon observed with this material provides evidence in support of the oxide-film theory and provides an explanation for some of the differences in wearing qualities of cemented-carbide tools.

Introduction

THE industrial potentialities of nodular cast iron have been the subject of much discussion ever since its discovery. It was first reported by H. Morrogh (1)[4] in 1948.[5] He termed the new material "nodular cast iron," which he defined as "...gray, or substantially gray, iron in which all or part of the graphitic carbon content is in the form of nodules or spherulites prior to heat-treatment." This metal was produced by inoculating molten iron with ladle additions of cerium followed by a post inoculation of silicon if more complete graphitization were desired.

Subsequent literature (2, 3, 4) reported that nodular iron also could be made by using magnesium, lithium, calcium, barium, and strontium as inoculants. At the present time, magnesium or magnesium alloys are preferred for inoculation. Experiments to be described in this report were all conducted on nodular iron produced by magnesium additions.

Proponents of this new engineering material have forecast a brilliant future for it in applications demanding a combination of the advantages of both steel and gray iron. Industry still has need of information concerning the characteristics of nodular cast iron. In addition to casting and control aspects from the production standpoint there is need for information concerning such application properties as wear resistance, fatigue strength, weldability, damping capacity, and machining characteristics.

A significant amount of information concerning some of the foregoing factors has been obtained during the past 2 years. Certain of this information is summarized in a recent article by Gagnebin (5). Excellent work has been reported by Rehder (6, 7, 8) regarding composition, control of melt, inoculation, and heat-treatment. Of particular interest in connection with the present paper is "The U. S. Air Force Machinability Report, 1950" (9), which presents the results of tool-life comparisons made by Metcut Research Associates, Cincinnati, Ohio. These tests indicate that as-cast nodular iron, having a tensile strength of 93,000 psi, has the same machinability as gray iron of 45,000 psi tensile strength (and substantially equal hardness). According to the same report, the weakest nodular iron (70,000 psi, 170 Bhn) can be machined over 6 times as fast, for the same tool life, as the strongest gray iron in the series tested. It is also stated that nodular iron and cast steel of essentially the same hardness give substantially the same tool life when appropriate grades of carbide are used on each material.

The purpose of this investigation was to study the machining of nodular iron with particular reference to the performance of cemented-carbide tools on this material. The results are based primarily upon short-time, single-point turning tests. The study includes tests on cutting temperatures and cutting forces acting upon the tool at various cutting speeds, observation and measurement of tool-chip contact areas, and the tool-chip adhesion characteristics.

Test Equipment

The test equipment and general procedure for the determination of interface temperatures, tool forces, and tool-chip contact areas were the same as those used in similar tests previously reported for steel cutting (10, 12, 13).

The test stock was obtained in the form of as-cast logs, 30 in. long × 3¼ in. diam. Two separate heats of iron were tested, partially because of the limited supply in the first lot but also to study possible effects due to minor changes in composition. All test logs in each heat were poured from the same ladle of metal. The first lot is designated A-1 and A-2, denoting as-cast and annealed condition, respectively. The second lot is similarly denoted B-1 and B-2. Compositions and mechanical properties of the two heats in the as-cast condition are shown in Table 1.

TABLE 1 COMPOSITION AND PROPERTIES OF NODULAR-IRON TEST STOCK AS REPORTED BY THE INTERNATIONAL NICKEL COMPANY, INC.

	Lot A	Lot B
Composition, per cent		
Silicon	2.93	3.09
Manganese	0.54	0.32
Phosphorus	0.08	0.05
Sulphur	0.016	0.012
Nickel	0.97	0.88
Magnesium	0.085	0.064
Copper		0.33
Total carbon	3.55	3.38
Mechanical properties[a]		
Tensile strength, psi	95000	107000
Elongation, per cent in 2 in.	4.0	3.5
Brinell hardness[b]	242-262	246-267

[a] As-cast properties except hardness are taken from a 0.505-in. specimen machined from a 1-in. keel block poured with the test stock.
[b] Disks cut from the bottom of the logs gave the higher Bhn in both cases.

Stock A-2 was annealed to a hardness of 186 Bhn and stock B-2 to 180 Bhn. Micrographs of the as-cast and the annealed stock are shown in Figs. 1 and 2, respectively. It may be noted that in the as-cast stock with a Bhn of 242, the matrix is composed of

[1] Professor, Department of Mechanical Engineering, University of Illinois, Urbana, Ill. Mem. ASME.
[2] Instructor, Department of Mechanical Engineering, University of Washington, Seattle, Wash. Jun. ASME.
[3] Assistant Professor, Department of Mechanical Engineering, University of Illinois.
[4] Numbers in parentheses refer to Bibliography at end of paper.
[5] The International Nickel Company announced the magnesium process for producing spheroidal-graphite cast iron as a part of the discussion of Morrogh's paper.

Contributed by the Production Engineering Division and the Cutting Fluids and Metal Cutting Data and Bibliography Research Committees and presented at the Annual Meeting, Atlantic City, N. J., November 25-30, 1951, of THE AMERICAN SOCIETY OF MECHANICAL ENGINEERS.
NOTE: Statements and opinions advanced in papers are to be understood as individual expressions of their authors and not those of the Society. Manuscript received at ASME Headquarters, August 8, 1951. Paper No. 51—A-39.

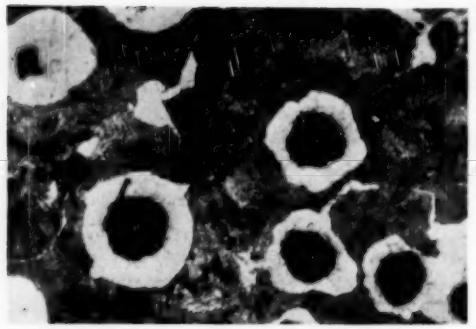

FIG. 1 AS-CAST NODULAR IRON STOCK A-1, 242 BHN; ×300

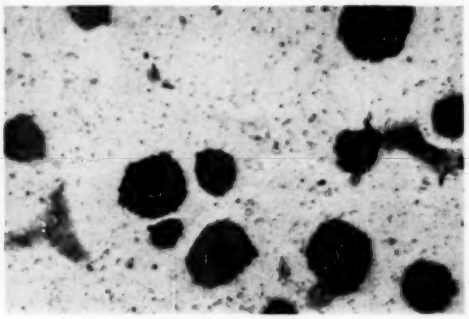

FIG. 2 ANNEALED NODULAR IRON STOCK A-2, 186 BHN; ×300

pearlite with the exception of an envelope of ferrite surrounding each nodule of graphite. In the annealed stock (186 Bhn) the matrix is almost entirely ferrite with some small, scattered areas of persistent pearlite.

The difference in hardness between the top and bottom (vertical cast position) of the test logs gave rise to some speculation regarding the distribution of hardness throughout the length and the possible effect of this factor upon the results of the cutting tests. A hardness survey was conducted on each lot as cast. Readings were taken at 1-in. intervals along the length of an as-cast log. The results of the test on stock A-1 indicated that the hardness dropped rapidly from 262 Bhn at the bottom to a nominal value of 242 Bhn within a distance of 4 in. from the bottom. This value remained fairly constant throughout the remaining length of the log, indicating that the initial chill of the first metal into the mold affected the extreme lower section only. The bottom section was gripped in the chuck and was not used in subsequent cutting tests of the as-cast iron. Stock B-1 showed a similar hardness distribution. The annealed stock from both lots showed uniform hardness along the length of the log.

A representative group of standard-grade cemented-carbide cutting tools was selected to be used in the investigation. This group included both steel-cutting and cast-iron-cutting grades. Tool preparation was done on 120 and 320-grit diamond wheels and finishing was done with a 400-grit diamond hone. Except as otherwise noted, all tools were carefully shaped to the following specifications:

	Degrees		Degrees
Back rake angle	0	Side relief angle	7
Side rake angle	4	End cutting-edge angle	8
End relief angle	7	Side cutting-edge angle	0
Nose radius		1/64 in.	

Tool angles and radii were carefully checked by means of a vernier protractor and a radius gage. A feed of 0.0098 ipr, nominal depth of cut of 0.100 in., and a setting angle of 90 deg were used in all tests. In each case the tool was carefully adjusted to the center-line height of the workpiece. No cutting fluid was used.

The grade, nominal composition, and hardness of each tool is shown in Table 2 without trade-name identification. The tool number is that assigned by the authors and used in this paper. The tool numbers which are prefixed by the letter "S" designate steel-cutting grades while those with the letter "C" denote tools intended primarily for the cutting of cast iron. The group shown does not include all the tools tested, but it is representative of those used with regard to composition, grade, and performance.

In the investigation of cutting temperatures, the nodular-iron member of the tool-work calibration thermocouple was prepared from a portion of the workpiece upon which the cutting-temperature tests later were run. Thus it has the same microstructure and heat-treatment history. In each grade of cemented-carbide, the calibration bar, contact rod, and tool insert were all made from the same lot of mix and were all sintered under identical conditions.

TABLE 2 NOMINAL COMPOSITION AND HARDNESS OF TEST TOOLS

		—Nominal composition, per cent—				
No.	Recommended use	WC	Co	TiC	Others (TaC, CbC)	Hardness RA
	STEEL CUTTING					
S-1	General purpose	82	10	8	..	90.5
S-2	Precision finishing	61	7	32	..	92.5
S-3	Finishing	76	8	12	4	92.0
S-4	General purpose	78	10	7	5	91.0
S-5	General purpose	74	4	0	22	92.0
S-6	Roughing	57	12	11	20	91.0
S-7	Finishing	78	8	8	6	92.0
S-8	Roughing	78	12	..	10	89.5
	CAST-IRON CUTTING					
C-1	Roughing	89	11	..	..	89.3
C-2	Finishing	94	6	..	..	92.0
C-3	Finishing	93	3	Trace	4	92.1
C-4	General purpose	94	6	..	..	91.0
C-5	General purpose	94	6	..	..	92.0
C-6	Roughing	94	6	..	..	91.0

TOOL-FORCE TESTS

Procedure. Each test proceeded from the lowest speed to the maximum in each case so that any temperature or wear effects could be noted.

During each test, readings of surface speed, vertical and horizontal forces were taken simultaneously and recorded. The dynamometer readings reached steady-state conditions in a few revolutions of the spindle, but the cuts were timed at 0.10 min, this interval being selected as sufficient to take all readings easily and not long enough to introduce heating effects into the dynamometer due to changes in the temperature of the cantilever arm.

Test Results. As-cast, stock A-1: Inasmuch as similar tools of comparable grades performed in nearly the same manner in these short-time tests, it was considered advisable to report only on typical tools of each general grade. Tools S-1 and S-2 represent general-purpose and finishing types, respectively, in the steel-cutting grade, while C-1 and C-2 represent the same respective types in cast-iron cutting grades.

The results of the tool-force tests conducted on stock A-1 (242

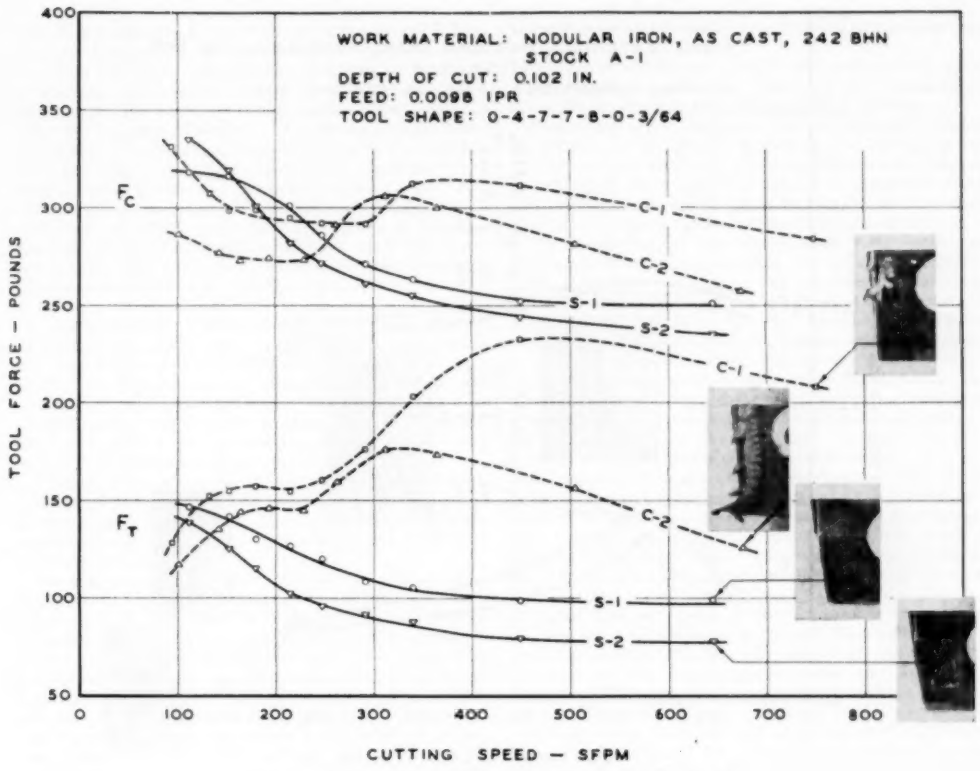

FIG. 3 CUTTING SPEED - TOOL FORCE RELATIONSHIPS FOR STOCK A-1

Bhn) are shown by the curves in Fig. 3. These curves show the variation in tool forces with change in speed for typical tools. The F_c-curves indicate the vertical or cutting forces, and the F_t-curves the horizontal or thrust forces. Examination of Fig. 3 reveals that the curves for some tools show irregularities which were caused by an adhesion phenomenon on the flank of the tool just below the cutting edge. This adhesion consisted of a build-up (or welding) of small particles of the workpiece to the tool flank. This material built up on the flank in such a manner as to reduce the 7-deg side-clearance angle to approximately the helix angle of the feed, and the end clearance to approximately zero.

The flank build-up was of rather gradual occurrence when cutting the as-cast stock. The incidence of flank build-up is best shown by changes in the thrust force, although an increase in the cutting force is also evident. In the test of tool C-1 shown in Fig. 3, the first evidence of flank build-up occurred at a cutting speed of about 250 sfpm. This is shown by an increase in the thrust force and a corresponding, though smaller, rise in the cutting force. Tests at successively higher speeds resulted in a further rise in force at each speed increment until the maximum was reached at 450 sfpm. The thrust force increased about 50 per cent from 247 to 450 sfpm. Visual observation of the tool showed that the flank build-up extended farther and farther down the tool flank with each successive cut. Above cutting speeds of 450 sfpm the chips began to leave the tool at a "visible red temperature" and an extension or "tail" on the flank build-up began to grow down the flank of the tool. The tool forces for the higher speeds decreased somewhat with further increase in cutting speed. This is partially due to the more plastic nature of the adhering flank build-up.

Tool C-2 containing more WC reveals a similar force pattern although the forces are, in general, somewhat lower than those for C-1 and the peak occurs at a lower speed, approximately 312 sfpm. In the speed range of 500 to 600 sfpm, the thrust force for tool C-1 is from 50 to 60 per cent higher than that for tool C-2. The respective cutting forces are about 12 per cent higher. Evidently the higher WC content of tool C-2 has an influence on the cutting forces above the flank build-up speed.

Tools S-1 and S-2 exhibited a gradual decrease in both tool forces with an increase in cutting speed. While measurements of chip thickness were difficult, owing to their fragmentary nature, there was a general trend toward a slightly thinner chip and clearer separating surface with increase in cutting speed. Neither tool S-1 nor S-2 exhibited evidence of significant flank build-up. The thrust force was some 20 per cent lower for tool S-2 while there was little difference in the cutting force over the speed range used.

Macrographs of each tool were made at a magnification of

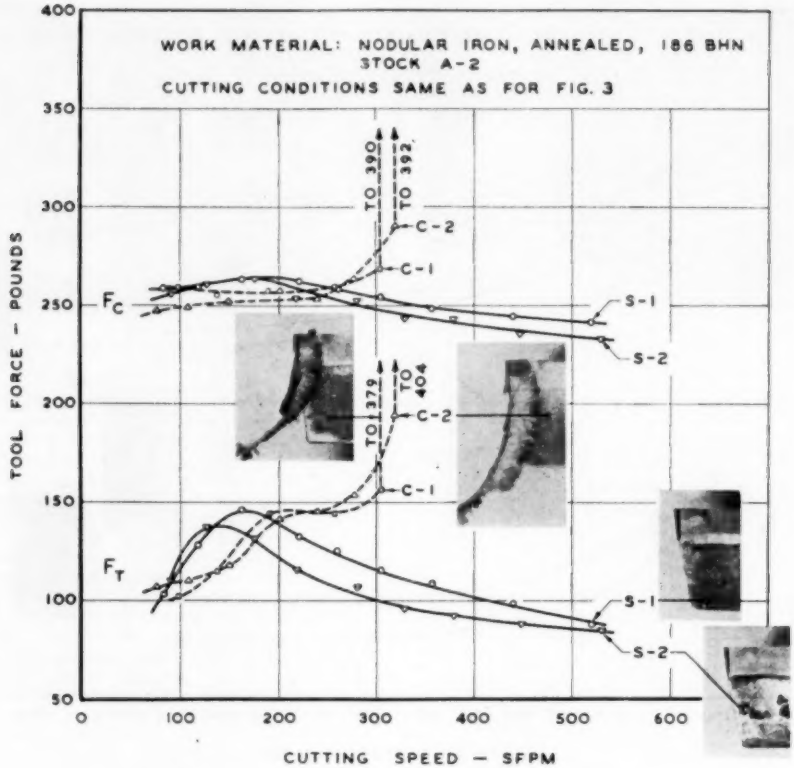

FIG. 4 CUTTING SPEED - TOOL FORCE RELATIONSHIPS FOR STOCK A-2

about 3×. These are shown in Fig. 3. Examination of the illustrations, showing the flank build-up, reveals that the glazed-appearing portion of the build-up (that part attached solidly to the tool) extends down the tool flank about half the thickness of the carbide insert. This build-up was "welded" solidly to the tool and could not be removed without damage to the carbide by any means except grinding. It is noted that both cast-iron cutting grades show flank build-up whereas neither steel-cutting grade shows this phenomenon.

Annealed stock A-2: The results of the cutting tests on annealed nodular-iron stock A-2 (186 Bhn) are shown in Fig. 4. It is evident that annealing has a definite effect on the cutting behavior in comparison to that shown for the as-cast stock.

The cutting force is relatively independent of tool grade up to a cutting speed of about 250 sfpm. The thrust force is more sensitive to tool changes over the same speed range.

Tool C-1 reveals very little change in the cutting force up to about 300 sfpm where it suddenly rises from 268 to 390 lb. The thrust force increases abruptly from 156 to 379 lb at the same speed. The extent of the flank build-up and its effect on tool forces is much more pronounced with annealed stock than on the as-cast material. This is clearly shown in Figs. 3 and 4. The flank-build-up speed is not greatly different in the two cases. Visual inspection during the cut revealed that the flank build-up occurred rapidly (about 3 sec), and that the extension or tail on the build-up started to grow immediately at a rate of $\frac{1}{4}$ to $\frac{1}{2}$ ips. The short time available for the initial readings during build-up leaves some doubt as to their actual value.

In general, the performance of tool C-2 was very similar to tool C-1 although the flank-build-up speed is a little higher. However, the similarity in trend is clearly evident. Tests in this series were halted when the build-up had occurred and the then steady readings recorded.

Some subsequent tests conducted at speeds above those causing flank build-up revealed a decrease in forces. This will be discussed in a later section.

It is noted in Fig. 4 that the flank build-up has reduced the end-clearance angle approximately to zero. The side-clearance angle was likewise reduced to the helix angle of the feed. In further pursuit of this aspect, the end and side-clearance angles were doubled (on tool C-2), and a repeat test conducted. The flank-build-up phenomenon occurred at the same speed as before and the clearance angles were reduced to the same extent.

Tests on the steel-cutting grades, tools S-1 and S-2, revealed that they gave similar performance. Neither of these tools showed evidence of flank build-up although there was a slight built-up edge (top) at speeds below 160 sfpm. The tool forces for S-2 were slightly lower as was the case in cutting as-cast stock.

The effect of annealing upon tool forces can be observed in Figs. 3 and 4 with reference to curves for tools S-1 or S-2 (which do not show flank build-up). The thrust force is only slightly influenced by annealing. In the range of 120 to 500 sfpm the magnitude of the forces and the decrease in F_t with speed is about the same in either case (i.e., 30 to 35 per cent). The cutting forces are somewhat higher on as-cast stock, about 25 per cent at 120 sfpm, but reducing to only 3 to 4 per cent at 500 sfpm. The decrease in F_c with increase in speed is more pronounced in as-cast stock, being about 25 per cent as compared to 6–9 per cent after annealing.

One test using 18-4-1 high-speed steel ground to the same specifications as the cemented carbides was conducted on annealed stock. The tool forces closely parallel those for tool S-1. There was no evidence of flank build-up when the test was halted at 200 sfpm due to tool failure.

Annealed Stock B-2: The flank-build-up phenomenon observed for the cast-iron cutting grades of carbide on annealed nodular iron suggested the need for further study at speeds above those at which the build-up occurred. A supplementary heat of stock was obtained and annealed to 180 Bhn. Tests on the whole series of tools revealed trends similar to those shown for stock A-2. Both components of the tool force were slightly lower in accord with the slight difference in hardness.

To avoid confusion, only the force curves for a general-purpose cast-iron cutting grade C-4, and a typical general-purpose steel cutting grade S-4, are shown. These two tools were generally representative of the respective types with regard to both force- and flank-build-up effects.

The cutting speed - thrust force curves for both tools are shown in Fig. 5. There is little difference in the forces up to a surface speed of about 375 sfpm. At this speed the flank build-up occurred suddenly, and the thrust force for tool C-4 increased to 3 times its prior value with the extension of the build-up growing at a rate of about $^1/_2$ ips. Additional cuts at higher speeds were accompanied by successively lower forces with the flank build-up still present and the extension growing in length. During these cuts the chips and adhering build-up in the vicinity of the tool were visibly red. At 600 sfpm the thrust force is still over $2^1/_2$ times the value prior to flank build-up. Some tools of a similar type showed a tendency for the thrust to drop at this speed although the action was sporadic. It may be that at speeds above the range investigated here the thrust force drops more than indicated.

Tool S-4 showed the occurrence of flank build-up at the same nominal speed, i.e., 375 sfpm. The thrust force increased to about 180 per cent with the formation of flank build-up.

Examination of the build-up at the maximum-force reading showed no apparent difference between this tool and that on tool C-4 for the same conditions. However, continuation of the cut at this speed was accompanied by the disappearance of the flank build-up and a corresponding decrease in force to a value slightly lower than the initial reading at the same speed.

The tool was reground and the previous test was repeated until the flank-build-up speed was reached. In this case, however, the cut was not stopped after flank build-up occurred. The maximum force then dropped with the simultaneous disappearance of the flank build-up, in 12 sec, to a steady value slightly below the "quickly observed" initial reading. Further increases in cutting speed resulted in lower thrust force with absence of flank build-up.

The cutting-force curves for the two tools, Fig. 6, revealed the same abrupt changes although the effects were proportionately of smaller magnitude. The disappearance of the flank build-up on the S-4 tool (and others of a similar grade) suggested the possibility of a barrier oxide film affecting chip adhesion.

It was noted throughout these tests that the occurrence of flank build-up was accompanied by a deterioration in the surface finish of the work. Several spot checks indicated that the surface roughness was consistently greater, sometimes almost 3 times as high, measured in microinches rms. Likewise, the diameter of the cut stock was reduced about 0.002 in. due to the flank build-up.

Nodular Iron and Annealed Steel Compared. Comparison of the tool forces for nodular cast iron with those encountered in steel cutting (10) under the same conditions reveals that the forces are considerably lower for the nodular iron. As is seen in Figs. 4 and 7, the difference between the cutting force F_c for the annealed 9445 steel (183 Bhn) and that for the annealed nodular iron (186 Bhn) is about 200 lb at a common speed of 125 sfpm for a comparable grade (i.e., S-1) of cemented-carbide cutting tool. The force for steel at this speed is over 70 per cent higher than that for nodular iron. Cutting-force differences at other speeds are seen to diminish with increasing speed because the

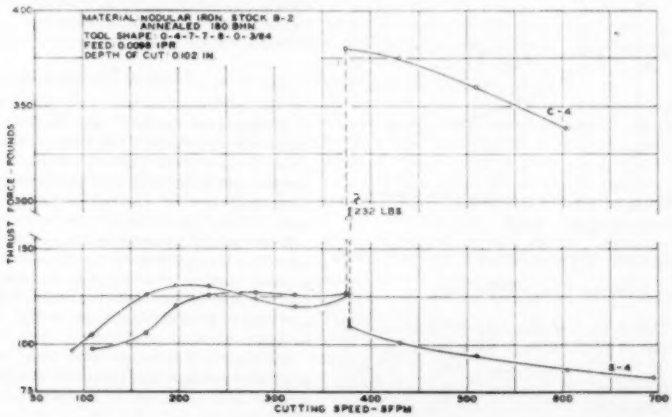

FIG. 5 CUTTING SPEED - THRUST FORCE RELATIONSHIPS FOR STOCK B-2

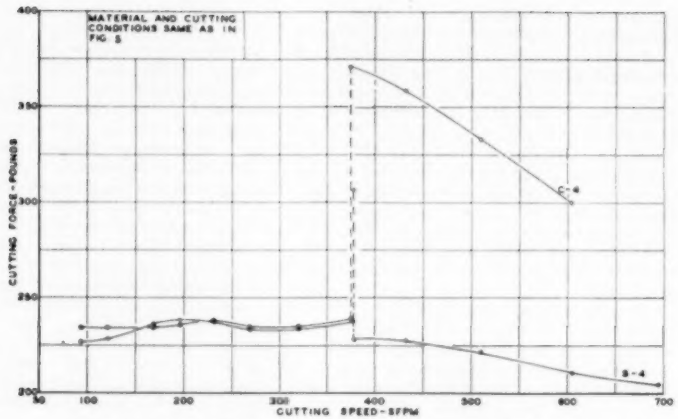

FIG. 6 CUTTING SPEED-CUTTING FORCE RELATIONSHIPS FOR STOCK B-2

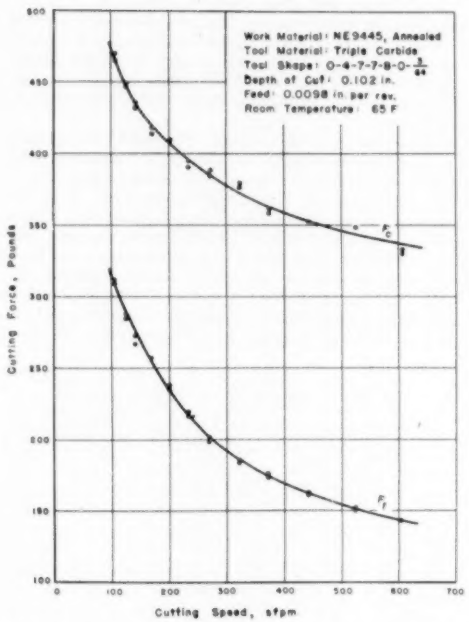

FIG. 7 EFFECT OF CUTTING SPEED ON TOOL FORCES FOR NE 9445 STEEL
(From Trigger and Chao, reference 10.)

force drop for the iron is far less than that for steel over the range of speeds tested. The difference at 500 sfpm is still about 45 per cent, however. The relatively small effect of speed on tool forces for nodular iron is held to be due to the minor change in chip thickness, about 10 per cent as compared to over 40 per cent for the steel over the same range. The lower tool forces encountered in machining nodular iron are thought to be due to the "notch effect" and lubricating qualities of the graphite nodules.

Differences of the same order of magnitude were noted in a comparison of the results of these tests with those conducted on spheroidized SAE 52100 steel at a hardness of 187 Bhn (11).

The effect of the hardness of nodular iron upon the tool forces may also be seen from the results of the tool-force tests, Figs. 3 and 4. Considering only those tools which exhibit no flank build-up it was found that the forces decrease with a decrease in hardness for all of the tools over the hardness range tested. The higher resistance to cutting this material in the as-cast condition is due, presumably, to the stronger pearlitic matrix as compared to the ferritic matrix of the completely annealed stock. Since the chip thickness was affected only slightly by speed, or change in hardness, the path of failure is nearly constant and tool forces increase with stock hardness and strength. This is different from the behavior noted for steel by Chao and Trigger (12), where it is shown that in the cutting of steel the tool forces decrease slightly with increased workpiece hardness. Their explanation for this trend is that the length of the shear path decreased in greater proportion than the shear strength increased. As a consequence, the cutting forces are lower.

CUTTING-TEMPERATURE TESTS

Cutting-temperature tests were conducted to study the effect of cutting speed on the magnitude and variation of tool-chip interface temperatures. The method used was the same as that employed in previous papers by one of the authors (13). The carbide tools in the tool-work thermocouple setups were similar in composition[6] to the C-4 and S-4 tools used in the cutting-force tests. Other cutting conditions were likewise the same.

Readings of the surface speed, potentiometer millivolts, and room temperature were taken and recorded for each cut. The millivolt readings were corrected to calibration reference-junction temperature and transposed to tool-chip interface temperature (deg F) from the calibration curves. The calibration curve for tool S-4 is shown in Fig. 8.

The cutting-temperature tests were conducted on annealed stock B-2 (180 Bhn), and the results of several duplicate tests, all in close agreement, are summarized in Fig. 9. The cutting

[6] Supplied by the same manufacturer but not necessarily identical in composition.

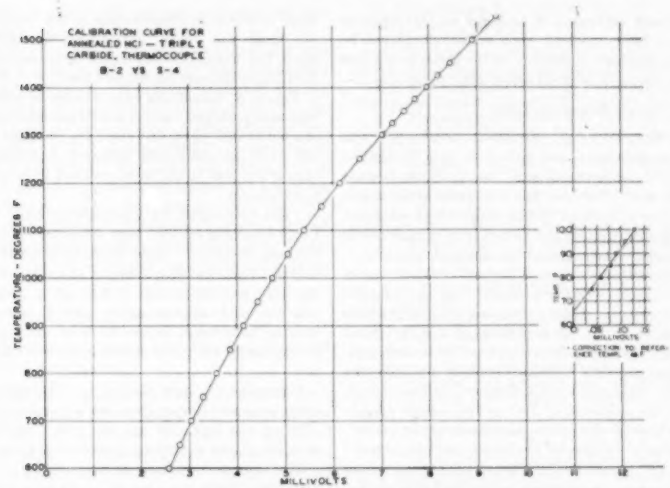

FIG. 8 CALIBRATION CURVE FOR ANNEALED NODULAR IRON-CEMENTED CARBIDE THERMOCOUPLE

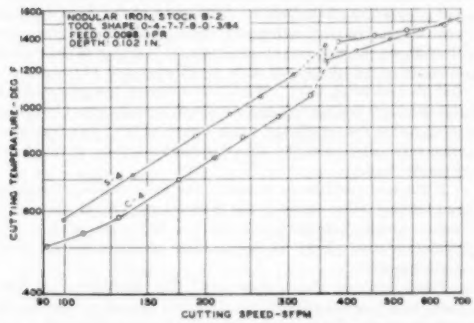

FIG. 9 CUTTING SPEED - CUTTING TEMPERATURE RELATIONSHIPS FOR STEEL-CUTTING AND CAST-IRON-CUTTING GRADES OF CEMENTED CARBIDES ON NODULAR IRON

speed - cutting temperature relationship for tool S-4 is a straight line on logarithmic co-ordinates up to the speed at which flank build-up occurred. The formation of the build-up was accompanied by an abrupt rise in the cutting temperature. The subsequent disappearance of the build-up (in about 15 sec) was coincident with the sudden decrease in temperature as shown. This test was repeated several times with freshly ground tools and the same decrease in the range of 125 to 150 F was noted. The slope of the cutting speed - cutting temperature line is much less above the flank build-up speed—an observation in accord with the effect on tool forces.

The curve for tool C-4 follows the same general pattern up to the flank build-up speed. However, the temperatures are considerably lower—a matter attributed primarily to the larger contact area with the C-4 tools. This aspect was investigated at four different speeds below that at which flank build-up occurred and the data summarized in Table 3. It is noted that the contact area decreases with increase in speed for both tools and that the area for tool C-4 is greater than that for S-4. As a consequence, the cutting temperatures for C-4 are lower since the heat is distributed over greater area.

The curve for tool C-4 reveals that the temperature rise coincident with flank build-up is greater, over 200 F, and the cutting temperature did not drop back since the build-up remained on the tool. The change in slope for the S-4 tool at the flank-build-up speed is thought to be due to the formation of a protective oxide

TABLE 3 RESULTS OF CONTACT-AREA TESTS

Work material: Nodular iron stock B-2; depth of cut: 0.100 in. annealed, 180 Bhn; feed: 0.0098 in.; tool shape: 0-4-7-7-8-0-$^3/_{64}$

Tool S-4			Tool C-4	
Cutting speed, sfpm	Contact area, $in.^2 \times 10^{-3}$	Interface temperature, deg F	Contact area, $in.^2 \times 10^{-3}$	Interface temperature, deg F
140	10.41	718	10.70	605
188	10.06	858	10.67	725
245	7.75	1015	10.42	860
285	6.57	1105	9.25	945

film on the tool, while the change for the C-4 tool is believed to be due to the flank build-up itself. The reduced slope for tool C-4 above flank build-up speed may not reveal the true picture. The toolwork thermocouple is, in effect, a number of parallel thermocouples and indicates an average temperature over the area of contact of the dissimilar metals. The presence of flank build-up adds extra parallel thermocouples which are somewhat removed from the region of maximum temperature. For this reason, comparison of the cutting temperature for tools C-4 and S-4 above flank-build-up speed should be done with caution.

At about 600 sfpm the two tools indicate equal interface temperatures, yet the cutting force F_c, for tool C-4 is nearly 50 per cent greater and the thrust is 4 times as high. Furthermore, the chips and flank adhesion were visibly red with tool C-4 whereas no such tendency was noted with the steel-cutting grade. This observation together with the higher forces may point to an impaired tool life. On the other hand, the flank build-up may protect the cutting edge sufficiently to augment the tool life.

Although it is recognized that tool forces and cutting temperatures are significant in their effect on tool life, other factors such as interface friction, abrasiveness of the work material, and tool-chip contact area are also important. While it was desira-

ble to conduct life tests on tools C-4 and S-4 at 600 sfpm to evaluate the effect of flank build-up, such studies could not be undertaken due to a shortage of stock. In the absence of these tests, no predictions are made on the basis of short-time runs.

Flank-Adhesion Tests

The occurrence of flank adhesion, or build-up, and its effect on tool forces, cutting temperatures, and surface finish is thought to be significant in a better understanding of the machining process as applied to nodular iron. The fact that the extent of the build-up varied with the type of carbide tool on a particular condition of the workpiece suggested that certain elements or compounds in the tool may be a fundamental cause of the different behavior.

Oxide-Film Theory. Skaupy (14) and Metcalfe (15) have proposed an oxide-film theory which postulates that the superior steel-cutting performance of carbides containing titanium carbide (TiC) can be accounted for by the formation of a TiO_2 film at cutting temperatures. This oxide film interposed between the tool surface and the chip prevents intimate contact between the chip and the carbide. Metcalfe further suggests, on the basis of x-ray evidence, that the oxidation of TiC to TiO_2 occurs readily because "it does not involve disruptive movement of the atoms" and that the oxide layer is "adherent, tenacious, and nonporous." Furthermore, while TiC is oxidized at a lower temperature than WC, the TiO_2 film protects the material against further oxidation at higher temperatures. This protection is not offered to the same extent by the "bulky and porous WO_2" according to Metcalfe.

Dawihl (16) concurs, in general, with the foregoing hypothesis and states that the cratering of the tool during steel cutting is caused by the alternate welding and tearing apart of the chip and tool material. He states further that there is no welding between TiO_2 itself and steel, and that the TiO_2 film inhibits contact between the carbides and the chip, thereby retarding the welding-on tendencies. Dawihl found that the oxidation of TiC raised the welding-on temperatures by several hundred degrees.

The cutting tests on nodular iron gave excellent evidence of flank adhesion whenever it occurred. Therefore a number of short-time supplementary tests were conducted on annealed iron (stock B2, 180 Bhn) in an attempt to discover the conditions under which flank adhesion would, or would not, occur. The tools consisted of two groups, one containing titanium carbide and the other no titanium carbide. Flank adhesion was indicated by the abrupt increase in tool forces and appearance of the flank build-up extension.

Tools Containing Titanium Carbide. Several representative tools (S-1, S-3, and S-4) containing titanium carbide were tested for flank adhesion, and all responded in the same general manner. Tool S-4 was typical of the group and responded as follows when subjected to the series of tests:

At a cutting speed of 350 sfpm flank build-up developed rapidly and, after the maximum tool forces were reached, the build-up was observed to disappear in 15 sec.

The tool was reground and tested at 495 sfpm. Flank build-up formed but took only 5 sec to disappear.

Immediately following this test, and without regrinding, the tool was tested at speeds ranging from 100 to 700 sfpm and at no time did the build-up reappear. The flank of the tool was then dressed lightly with a diamond hone and tested again at 350 sfpm. The flank build-up developed and disappeared as before. The flank was honed again and retested at 495 sfpm with the same results.

The tool was reground and the flank was heated with a slightly oxidizing, oxyacetylene flame to a temperature of approximately 1250 F. Following this treatment, cutting tests over the entire range of speeds from 100 to 700 sfpm failed to show any sign of flank build-up or irregularities in the tool-force pattern. When the flank was lightly honed and the tool was tested at 350 sfpm, the flank build-up again appeared and was removed by continuing the test for about 15 sec.

Tool C-3, containing only a trace of titanium, was tested at various speeds and reacted somewhat differently. Flank build-up started at 360 sfpm, and the force readings fluctuated rapidly as the build-up alternately appeared and disappeared. Continuation of the test to 685 sfpm resulted in no permanent removal of the build-up.

Tools Containing No Titanium Carbide. Tools C-4, C-5, and C-6, containing no TiC, were subjected to a series of tests similar to those described. Once flank build-up occurred it was not removed by additional cutting at any speed within the capacity of the lathe and for periods of time up to 3 min. Heating the carbide inserts to approximately 1250 F as was done for the TiC-bearing tools failed to prevent flank build-up which still occurred at nominally the same speeds observed with the freshly ground tool.

Formation of Flank Build-Up. The separating surface of the chips produced during these tests revealed evidence of a built-up edge on the tool. In general, this condition was more severe with the cast-iron cutting grades of carbide.

It is thought that some of the particles of the built-up edge are torn loose from the chip or workpiece and squeezed past the cutting edge. At high cutting speeds the particles are heated sufficiently to adhere to the flank of the tool probably by some sort of welding phenomenon. Formation of the flank build-up evidently occurs by this thermomechanical action. It was noted throughout the tests on annealed nodular iron that flank build-up occurred at practically the same speed regardless of the grade of carbide tool being used. When the adhering particles decrease the clearance enough to cause a sudden increase in tool forces the temperature rises suddenly. It is suggested that TiO_2 formation then takes place and the adhering flank build-up is swept free from the tool.

If the tool contains no titanium, the flank build-up continues and forms a tail as shown in the illustrations. It may be that at higher speeds (and temperatures) the WC tools exhibit WO_2 formation with effects similar to those observed for the steel-cutting grades.

Flank-Adhesion Tests—Summary. The flank-adhesion tests point to a "barrier effect" of a TiO_2 film caused by heating the carbide insert. No evidence of flank adhesion was observed once this oxide film was formed. Whether this condition would remain for a longer duration of cut is not known. The tests do, however, appear to support the hypothesis proposed by Skaupy and Metcalfe. The evidence may be summarized as follows for the short-time tests:

(*a*) All tools containing little or no TiC showed flank build-up on both as-cast and annealed nodular iron.

(*b*) All tools which did not display flank build-up on as-cast stock or only temporary build-up on annealed material, contained TiC.

(*c*) Tests on TiC bearing tools which showed temporary build-up on the annealed stock indicate that adhesion occurred at a temperature below that of TiO_2 formation. Presumably the additional flank friction then raised the temperature sufficiently to cause oxidation to TiO_2 after which the adhering flank build-up was swept away. The time necessary for removal of flank build-up was reduced at higher cutting speeds (and temperatures). This was probably due to the more rapid formation of TiO_2. Since these tests were all of short duration, it is quite probable that oxide-film formation would occur at somewhat lower speeds (and temperatures) on longer runs.

(*d*) Once the TiO_2 film had been formed by cutting action,

flank build-up did not occur until the tool had been reground and the oxide film removed.

(*e*) When the flank of a freshly ground tool containing TiC was oxidized at 1250 F prior to use, no flank build-up occurred over the range of 100 to 700 sfpm. The same treatment was not effective in the prevention of flank build-up in the non-TiC tools.

(*f*) An indication that the formation of an effective oxide film depends upon the amount of TiC is gleaned from a comparison of test results for tools S-2 and C-3. S-2 containing 32 per cent of TiC showed no evidence of flank build-up under any condition tested. Tool C-3 with only a little (fraction of 1 per cent) TiC formed a flank build-up which was unstable and alternately formed and disappeared at high speeds and elevated temperatures. Evidently the oxide film was not extensive enough to serve as an effective barrier.

Conclusions

The following conclusions are based upon the short-time test procedures used in this investigation:

1 Typical cast-iron cutting grades of carbide exhibit flank build-up when machining both as-cast and annealed nodular iron under the present cutting conditions. Steel-cutting grades of carbide do not show flank build-up on as-cast nodular iron but temporary build-up does appear when the iron is in the annealed condition.

2 Flank build-up occurs gradually in the cutting of as-cast nodular iron whereas with annealed stock the action takes place rather abruptly. In general, this adhesion phenomenon is much more pronounced in the case of annealed nodular iron.

3 Flank adhesion results in a large increase in tool forces. The action is a gradual one in the as-cast material but abrupt for the annealed stock.

4 For similar steel-cutting grades of carbide, the tool forces for the nodular iron, both as-cast and annealed, are lower than those encountered in steels of approximately the same hardness as the annealed iron. (NE 9445, 183 Bhn and SAE 52100, 187 Bhn.)

5 The formation of the flank build-up, if abrupt, is accompanied by a sudden rise in the cutting temperature.

6 Machining with the presence of the flank build-up on the tool has the following undesirable effects: (*a*) Higher cutting temperatures, (*b*) higher tool forces, and consequently larger power consumption, (*c*) impaired dimensional accuracy, and (*d*) inferior surface finish.

7 Formation of the flank build-up appears to be a thermo-mechanical action. The kind of welding which takes place is not unlike that which occurs in metal spraying.

8 Results of the flank-adhesion tests indicate the existence of a barrier effect of a TiO_2 film. The evidence supports the contention that the superior steel-cutting performance of carbide tools containing TiC is due to the presence of the oxide film.

Acknowledgment

The authors extend acknowledgment to Mr. H. W. Highriter of Vascoloy-Ramet Corporation; Mr. F. W. Lucht of Carboloy Company, Inc.; Mr. W. L. Kennicott of Kennametal, Inc., for the cemented-carbide tools used in the investigation, and to The International Nickel Company, Inc., for the spheroidal-graphite cast-iron stock.

BIBLIOGRAPHY

1 "Production of Nodular Graphite Structures in Gray Cast Iron," by H. Morrogh, Trans. AFS, vol. 56, May 7, 1948, pp. 72–90.

2 "Ductile Cast Iron—A New Engineering Material," by A. P. Gagnebin, K. D. Millis, and N. B. Pilling, *Iron Age*, vol. 163, February 17, 1949, pp. 79–84.

3 "Magnesium Treatment of Nodular Graphite Cast Iron," by C. K. Donoboe, Regional Foundry Conference, Birmingham, Ala., February 17, 1949.

4 "Nodular Iron Produced With Li, Ca, Ba, Sr, Na," by A. L. De Sy, *Metal Progress*, vol. 58, September, 1950, p. 357.

5 "The Industrial Status of Ductile Iron," by A. P. Gagnebin, *Mechanical Engineering*, vol. 73, February, 1951, pp. 101–108.

6 "Magnesium Additions and Desulphurization of Cast Iron," by J. E. Rehder, *American Foundryman*, vol. 16, September, 1949, pp. 33–37.

7 "Nodular Cast Irons," by J. E. Rehder, *Canadian Metals*, vol. 13, no. 3, March, 1950, pp. 65–71.

8 "An Introduction to the Annealing of Nodular Iron," by J. E. Rehder, Trans. AFS, Preprint No. 50-17, presented at the annual meeting, 1950, of the American Foundrymen's Association.

9 "United States Air Force Machinability Report, 1950," Curtis-Wright Corporation, Wood-Ridge, N. J., 1950.

10 "An Analytical Evaluation of Metal-Cutting Temperatures," by K. J. Trigger and B. T. Chao, Trans. ASME, vol. 73, January, 1951, pp. 57–68.

11 "Thermophysical Aspects of Metal Cutting," by B. T. Chao, K. J. Trigger, and L. B. Zylstra, to be presented at the Annual Meeting, Atlantic City, N. J., November 25–30, 1951, of The American Society of Mechanical Engineers.

12 "Cutting Temperatures and Metal-Cutting Phenomena," by B. T. Chao and K. J. Trigger, Trans. ASME, vol. 73, August, 1951, pp. 777–793.

13 "Progress Report No. 1 on Tool-Chip Interface Temperatures," by K. J. Trigger, Trans. ASME, vol. 70, 1948, pp. 91–98.

14 "Oxide-Film Theory of Cemented-Carbide Wear Resistance," by F. Skaupy, *Kolloid Zeitschrift*, vol. 102, 1943, pp. 269–276.

15 "The Composite Carbides in Steel-Cutting Cemented-Carbides," by A. G. Metcalfe, *Metal Treatment*, vol. 13, 1946, pp. 127–133.

16 "Investigation of the Processes in the Wear of Cemented-Carbide Tools," by Walter Dawihl, *Zeitschrift für Technische Physik*, vol. 21, 1940, pp. 337–345.

Discussion

M. Eugene Merchant.[7] The authors have prepared an interesting paper on the characteristics observed in their machining tests on nodular cast iron. They put particular emphasis on the flank build-up which they observed when machining this material. However, it should be pointed out that this particular behavior is not peculiar to nodular cast iron alone. It is observed when machining many types of cast iron, as well as some other materials, when machining conditions are similar to those used by the authors. When this flank build-up occurs in the machining of any of these materials it produces the same adverse effects as those noted by the authors.

The authors make a good case for the conclusion that the formation of a film of titanium oxide on the tool will prevent flank build-up, or adhesion. This is interesting to note, since this action is apparently another example of the chemical functioning of a cutting fluid to reduce friction and adhesion by the formation of a low-shear-strength solid film at the interface between tool and work material. In this case the cutting fluid is the oxygen of the air, and it reacts with the titanium carbide in the tool material, under the action of the high temperatures and pressures that exist at the sliding surfaces, to form a relatively low-shear-strength film of titanium oxide at that interface, thereby reducing metal-to-metal contact, adhesion, and friction. In the more common types of cutting-fluid action, the fluid is usually a liquid, and one or more of the chemical additives which it contains (for example, chlorine-containing compounds) reacts with the work material at the chip-tool interface, under the action of the high temperatures and pressures that exist there, to form a low-shear-strength solid film (for example, iron chloride) thereby reducing metal-to-metal contact, adhesion, and friction. Thus the authors' findings serve to extend the field of knowledge of the chemical action of cutting fluids in machining.

[7] Assistant Director of Research, The Cincinnati Milling Machine Company, Cincinnati, Ohio. Mem. ASME.

L. J. Nowikowski.[8] It is a well-known fact that tool-chip adhesion takes place when machining a variety of materials. In some cases, turning gray iron, for example, the flank adhesion is as exaggerated as that obtained by the authors when turning nodular iron.

The tool-chip adhesion that takes place when turning such materials as cast steel, titanium, and high-temperature alloys is not severe as that obtained when turning the gray and nodular cast irons. The interesting thing is that it takes place even when using the steel-cutting grades of carbide.

The problem of reaction between tool and chip interface is basically the same whether the adhesion takes place along the tool flank or the tool face. The theory of TiO_2 film formation suggests the possibility of more work being done on carbide tools to eliminate tool-chip adhesion when machining any material.

One is liable to gain the impression after reading this paper that the steel-cutting grade is definitely superior to that of the cast-iron grade of carbide in turning the nodular iron. The authors have been careful to point out they are making no predictions on the basis of their short-time tool-force runs. We have found in our laboratory tests that the cast-iron grades of carbide appear to provide longer tool life than the steel-cutting grades. For example, we have found that in cutting an as-cast nodular iron similar to that used by the authors, the tool life with the cast-iron grade of carbide at 300 fpm and 0.010 in. per revolution feed was 2.75 times that of the steel-cutting grade of carbide (40 min versus 14.5 min.) In cutting the as-cast nodular iron we have not observed any cases where superior tool life could be obtained by use of the steel-cutting-grade carbide. All of our tests were made at cutting speeds where a reasonable tool life was experienced. By reasonable we mean a tool life of at least 10 min.

At this point the question might arise as to how the flank wear was determined when tool-chip adhesion took place. At first the chip adhesion presented a definite problem since it covered the wear land completely. After experimenting it was found that by rotating the workpiece at extremely slow speeds, 50 to 75 fpm, and allowing the tool to come in contact with the workpiece under power feed for a few seconds, the chip removed completely with no effect on the carbide cutting tool. Applying a copious supply of water-soluble cutting fluid during the chip-removal operation aids in freeing the built-up adhering chip.

This problem of tool-chip adhesion is interesting, and the study should be continued further. We believe it is part of the old problem of tool-work compatibility. We have found that certain carbides wear excessively when cutting certain alloys that ordinarily should be easy to machine. For example, carbides wear rapidly in machining silver which is extremely soft. Likewise certain steel-cutting grades of carbide wear more rapidly when machining alloy steels annealed to a softer state than a harder state. The over-all problem of wear of carbide as a function of carbide composition and workpiece composition deserves wider attention and additional study.

It is hoped that this paper will not leave the erroneous impression that nodular iron is more difficult to machine than comparable engineering alloys. On the contrary, it has been found that for equivalent hardnesses nodular iron machines practically the same as flake-graphite cast iron. If the tool-life comparison is made on the basis of equivalent tensile strength, then it is found that the nodular iron machines in a far superior manner to that of the flake-graphite cast iron. For example, for equivalent tool life, a flake-graphite cast iron with 60,000 psi tensile strength would have to be machined at approximately 150 fpm whereas a nodular iron having a tensile strength of 70,000 psi could be machined at almost a 1000 fpm (see Fig. 10, herewith, taken from United States Air Force Machinability Report—1950).

[8] Metallurgical Engineer, Metcut Research Associates, Cincinnati, Ohio.

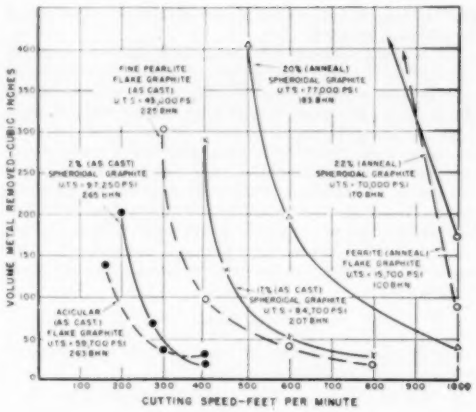

Fig. 10

In our opinion it would have been more appropriate for the authors to make this investigation of chip adhesion on flake-graphite cast irons and thus avoid what might be confusion in presenting an old problem on a new alloy.

Authors' Closure

The flank adhesion phenomena encountered in this investigation appears to be similar to the effect of cutting fluids in so far as the formation of a low-shear-strength film is concerned. The absence of flank build-up was associated with low tool forces, indicative of a reduced frictional sliding stress.

In point of further information on the oxide-film aspects a few supplementary tests were conducted after the manuscript had been submitted. These tests were performed on tool S-4 in various atmospheres. The test conditions were the same as those for Figs. 5 and 6 of the paper, except that the cutting speed was constant at 330 sfpm. The observation of prime interest was the duration of flank build-up, that is, the elapsed time between the inception of the rise in tool forces and their return to (or slightly below) the "quickly observed" initial reading. The results are summarized in the accompanying Table 4.

TABLE 4 SUMMARY OF TEST RESULTS

	Tool-forces-lb						
	Initial		Peak		End		Elapsed time to return, min
Atmosphere	F_0	F_1	F_0	F_1	F_0	F_1	
Still air	236	117	312	285	236	116	0.63
N_2 stream	236	117	315	272	235	117	0.55
O_2 stream	236	117	...	...	236	117	0.04 to 0.05

The nitrogen and oxygen-enriched atmospheres were provided by directing a stream from a welding torch upward along the tool flank. The slightly lowered elapsed time in the nitrogen-enriched atmosphere is attributed to better agitation of the oxygen from the inspirated air. The removal of the incipient flank adhesion occurred so rapidly in the oxygen-enriched atmosphere that the increase in forces could not be observed.

These supplementary tests corroborate those reported in the body of the paper and leave little doubt but that a TiO_2 film is effective as a barrier to flank adhesion. The lower tool forces may be accounted for on the basis of a low-shear-strength film as pointed out by Dr. Merchant. However, this does not necessarily

mean a longer tool life. The oxide film is not a barrier to tool wear. In fact, quite the contrary is the case as will be pointed out in a later section of this closure.

As clearly stated in the paper and referred to by Mr. Nowikowski in his remarks, no tool-life predictions were made on the basis of short-time tool-force tests. The principal objective of this investigation was a study of the tool-chip adhesion phenomena, and sufficient stock of a given composition was not available for extensive tool-life studies. However, some further work was possible, and the remainder of the stock has since been utilized in tool-life tests on the basis of flank wear. The results are summarized in Fig. 11 of this closure.

During the series of tests reported in this figure it was noted that neither tool S-1 nor S-2 showed flank build-up and the flank-wear pattern was generally uniform and easily measured. Flank adhesion occurred with the C-tools and was not readily removed by cutting at speeds of 40 to 50 fpm. The wear land could be delineated by a grinding technique in which the build-up was removed by grinding with the identical angle setting employed in the finishing of the tool flank. While this method is subject to error unless extreme care is used in grinding, it did provide a reproducible means of determining flank wear. Tool C-1 is not included in Fig. 11 since the cutting speed was 372 fpm (380 sfpm) while the other tools were tested at 270 fpm (282 sfpm). Under this difference in speed the wear relationship for C-1 was close to S-1.

It is evident from Fig. 11 that the TiC bearing tools were definitely inferior to the non-TiC tools in regard to flank wear. The wear curves illustrated in Fig. 11, taken in conjunction with the force curves in Fig. 3 of the paper, are a further indication of the complex mechanism of tool wear. Even though the tool forces for S-1 and S-2 are lower (initially) these tools wear much more rapidly than the cast-iron cutting grades C-2 and C-3. Evidently

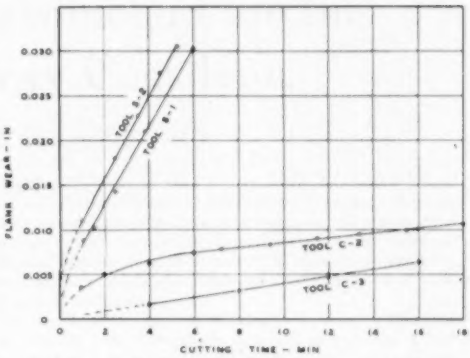

FIG. 11 CUTTING-TIME TOOL-WEAR RELATIONSHIPS FOR VARIOUS TOOLS

(Work material: Nodular iron, stock B-1, as-cast, 246 Bhn. Depth of cut: 0.101 in. feed: 0.0098 ipr. Tool shape: 0-4-7-7-8-0-$^1/_{32}$. Cutting speed: 270 fpm, mean.)

the flank build-up exerts considerable protective effect on the tool. Higher tool forces are more tolerable than rapid tool wear. The authors agree heartily with Mr. Nowikowski that the problem of tool wear deserves more study.

The authors fail to see how Mr. Nowikowski can gain "the erroneous impression that nodular iron is more difficult to machine than comparable engineering alloys." If he will refer to the fourth paragraph of the paper he will find the same machinability comparisons as those expressed in his discussion, taken from the same source.

A Comparison of Parameters for the Machining of Gray Cast Iron

By L. V. COLWELL,[1] H. J. HOLMES,[2] AND F. B. ROTE[3]

This investigation was designed to compare several types of data as parameters for predicting cutting speeds for gray iron. A series of eleven irons, representing ranges of alloys, ferrite, graphite, and mechanical properties was used in the study. Cutting forces, power, and energy were determined from drilling and milling tests, and cutting speed - tool life lines were determined for each of the irons. Finally, correlations were attempted between the cutting speed (V20) for a 20-min tool life, and all other available types of information. The net result of this approach was a comparison of the relative reliability of the different types of data. This comparison showed that combined carbon, microhardness, and the nucleation or graphitizing tendency hold the greatest promise of developing into reliable parameters, while Brinell hardness, tensile strength, drilling forces, and milling power show little promise of providing useful information. This study was preliminary in nature and was intended only as a screening process for narrowing down the field for future investigations. Consequently, the correlations between cutting speed and combined carbon, microhardness, and nucleation tendency are undeveloped, and applications should not be attempted without further investigation.

WE are still far short of the goal of being able to predict the proper cutting speed for a given tool life for the machining of cast iron, steel, and other metals. Many of the factors which determine tool life are not understood thoroughly, and it appears likely that there are others which have not even been discovered as yet. There are so many variables to be considered that the amount of work to be done seems almost limitless. This investigation was designed to permit a comparison of several types of data and parameters for the machining of cast iron. It was believed this approach would narrow down the field and limit the amount of work to be done in the future by revealing those factors which show the greatest promise of correlating with cutting speed.

The results of this study demonstrate that many of the variables correlate with cutting speed in a very general way in that they show definite trends over a broad range of the variable. However, they fail completely when used as bases for predicting change in cutting speed from one typical iron to another. Microstructure, mechanical properties, chemical composition, and metal-cutting data other than the cutting speed - tool life relationship were considered as possible parameters for predicting cutting speed. A comparison of these shows that microhardness, combined carbon, and the nucleation or graphitizing tendency give the greatest promise of developing into useful parameters for predicting the proper cutting speed to be used for machining cast iron.

The Cast Irons Prepared for This Study

A series of twelve irons, differing in composition, were prepared for this machinability study. Number four of the series could not be machined and therefore was abandoned. The chemical compositions of the remaining eleven irons as obtained by chemical analysis are shown in Table 1, along with the mechanical properties. All of the irons were of the so-called gray-iron type and did not include either malleable or the new ductile irons.

Microstructures of all the irons are shown at ×1000 in Figs. 1, 2, and 3. Irons Nos. 1, 3, 7, and 10 are shown in Fig. 1; these

TABLE 1 CHEMICAL COMPOSITION AND MECHANICAL PROPERTIES OF IRONS TESTED

Iron no.	TC	GC	CC[a]	Weight, per cent S	P	Mn	Si	Ni	Cr	Mo	Tensile[b] strength, psi	Bhn
1	3.05	2.40	0.65	0.087	0.23	0.82	2.67	[c]	..	..	..	181
2	2.88	2.08	0.80	0.141	0.28	0.70	2.01	0.62	0.87	..	19100	207
3	2.88	2.23	0.65	0.147	0.29	0.72	2.02	..	..	..	43100	241
5	2.55	2.00	0.55	0.034	0.12	1.33	2.91	1.19	..	0.35	56600	234
6	2.60	2.07	0.53	0.031	0.12	1.36	2.50	..	..	..	46600	204
7	3.07	2.95	0.12	0.089	0.25	0.79	3.65	..	..	..	19900	126
8	2.69	2.06	0.63	0.035	0.13	1.13	1.64	0.97	..	..	40400	217
10	3.07	2.64	0.43	0.095	0.23	0.76	2.81	..	..	..	20100	137
11	3.09	2.43	0.66	0.109	0.24	0.69	2.35	0.13	0.58	0.06	41700	212
12	3.04	2.28	0.76	0.104	0.41	0.65	2.44	0.13	1.10	0.05	44500	226
13	2.75	2.27	0.48	0.098	0.35	1.15	3.05	0.14	0.09	0.06	37800	209

[a] Combined carbon is obtained as the difference between total carbon and graphitic carbon (plus HNO_3 insoluble carbides, if any).
[b] Average of duplicate test specimens machined from 1.2-in. bars.
[c] No analysis.

irons might be called either a plain-carbon or a silicon series since the manganese, phosphorus, and sulphur are all normal except for a somewhat higher sulphur in iron No. 3. Irons Nos. 1 and 3 are almost identical in composition and the microstructure shows about 5 per cent of ferrite in each of them. Iron No. 10 with higher silicon shows about 40 per cent ferrite while iron No. 7 with the highest silicon shows approximately 90 per cent ferrite.

Fig. 2 shows the structures of irons Nos. 8, 2, and 5, respectively, representing plain nickel, nickel-chrome, and nickel-molybdenum irons. Fig. 3 shows irons Nos. 6, 11, 12, and 13. The first of these, No. 6, would belong to the silicon series except for high manganese accompanied with very low sulphur and phosphorus

[1] Professor of Production Engineering, University of Michigan, Ann Arbor, Mich. Mem. ASME.
[2] Ford Motor Company, Ypsilanti, Mich.; formerly Assistant Professor of Production Engineering, University of Michigan.
[3] Albion Malleable Iron Company, Albion, Mich.; formerly Associate Professor of Production Engineering, University of Michigan.

Contributed by the Production Engineering Division and Cutting Fluids and Metal Cutting Data and Bibliography Research Committees and presented at the Annual Meeting, Atlantic City, N. J., November 25–30, 1951, of The American Society of Mechanical Engineers.

Note: Statements and opinions advanced in papers are to be understood as individual expressions of their authors and not those of the Society. Manuscript received at ASME Headquarters, August 30, 1951. Paper No. 51—A-47.

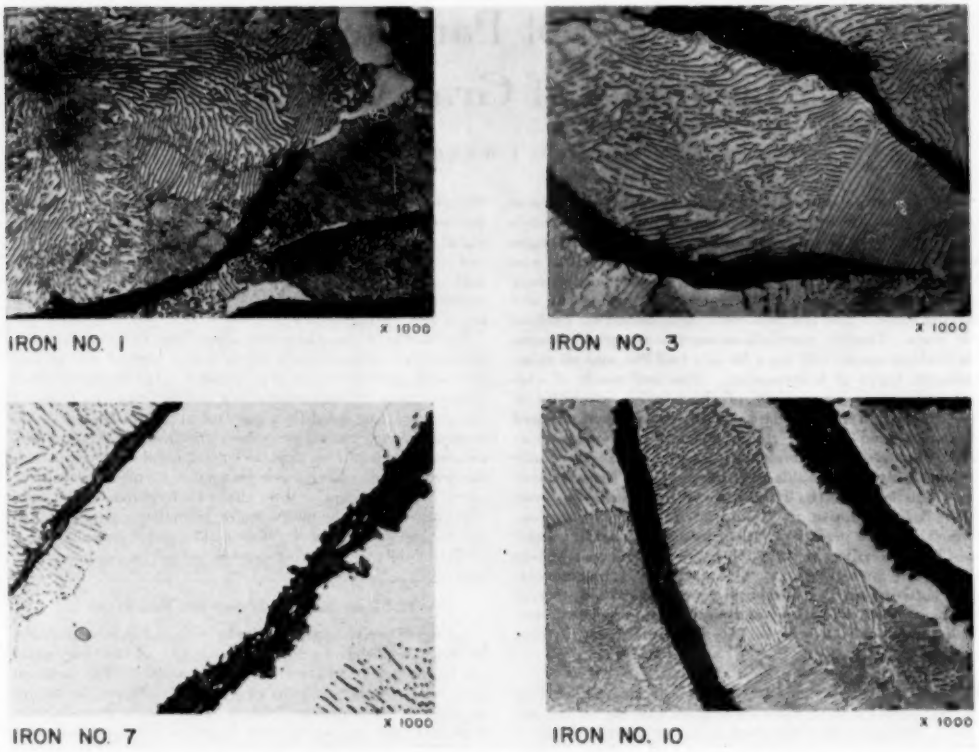

FIG. 1 A SILICO-FERRITE SERIES OF IRONS CONTAINING SILICON PERCENTAGES OF 2.67, 2.02, 3.65, AND 2.81 IN IRONS NOS. 1, 3, 7, AND 10, RESPECTIVELY
(Corresponding ferrite percentages are approximately 5, 5, 90, and 40.)

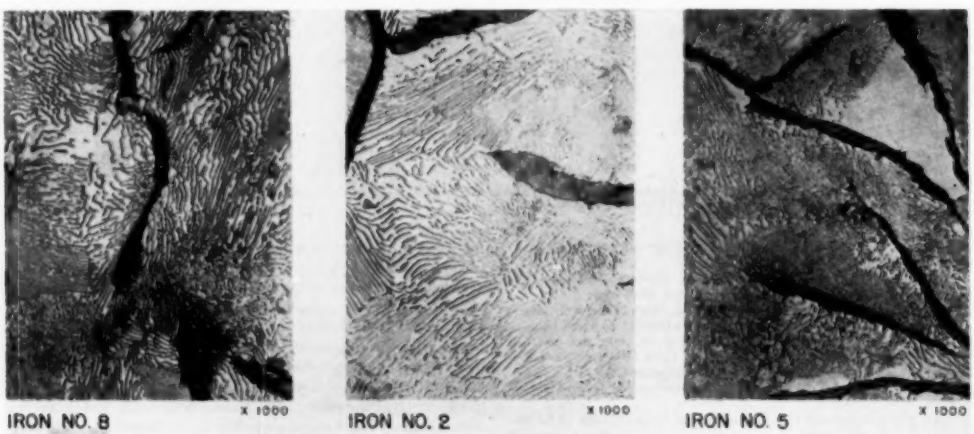

FIG. 2 IRONS NOS. 8, 2, AND 5 CONTAIN NICKEL, NICKEL-CHROMIUM, AND NICKEL MOLYBDENUM, RESPECTIVELY
(Iron No. 8 is also low in silicon, containing only 1.64 per cent.)

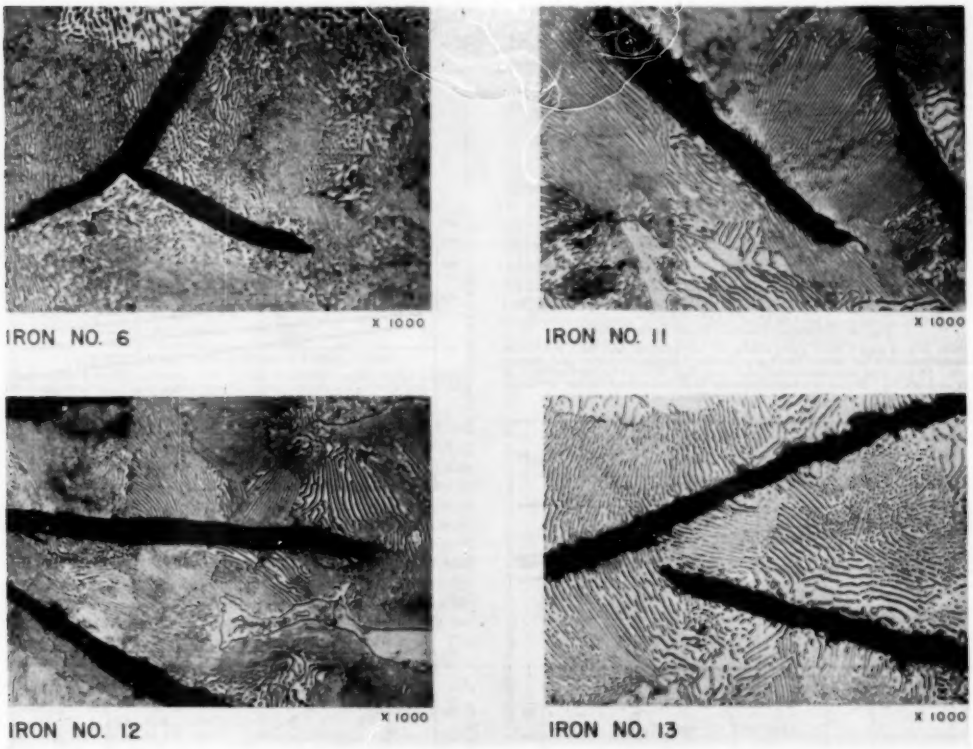

FIG. 3 IRONS ALLOYED WITH MANGANESE AND CHROMIUM
(Nos. 6 and 13 contained over 1 per cent of manganese. Nos. 11 and 12 contained 0.58 and 1.10 per cent of chromium, respectively.)

and must be considered as an alloy iron. Nos. 11 and 12 are chromium irons. No. 13 contains small amounts of nickel, chromium, and molybdenum along with high manganese and very high phosphorus. Iron No. 12 also contained very high phosphorus. With the exception of irons Nos. 7 and 10, all of the irons were substantially all pearlite.

The mechanical properties of the irons are given in Table 1. The tensile strength was obtained from the average of duplicate specimens machined from 1.2-in. rounds; there are no strength data for iron No. 1, since the test bars were lost.

MACHINING TESTS

The machining tests included turning, drilling, and milling. The turning tests were used to determine the cutting speed - tool life relationship while the other types of cuts were used to obtain information on cutting forces and energy consumption or power requirements.

In cutting cast iron the chips are always well broken, the force and power requirements are low, and there is little latitude in the surface finish. Consequently, the cutting speed - tool life relationship remains as the most important factor or criterion of machinability for gray irons. Therefore cutting speed for a given tool life was treated as the only important dependent machining property, and all other types of metal-cutting data obtained were considered along with the structure, mechanical properties, and composition as possible criteria for predicting change in cutting speed.

CUTTING SPEED - TOOL LIFE TESTS

The cutting speed - tool life equation was determined for each of the eleven irons with the same tools and the same size of cut. The tools were $^1/_2$-in-square bits of 18-4-2 high-speed steel as made by Braeburn. They were ground to the shape 0, 6, 6, 6, 6, 15, $^3/_{64}$. All cuts were made dry on a 14-in. American "Pacemaker" engine lathe at a depth of cut of 0.050 in. and at a feed of 0.010 ipr. The material turned was cast in the form of 6-in-diam × 18-in-long cylinders cored to 2 in. diam. Approximately $^1/_4$ in. was removed from the outer surface in preparing for the turning tests. All tools were run to final breakdown failure.

The results of the tool-life tests are shown plotted in Figs. 4, 5, and 6 and summarized in Table 2.

The cutting speed for a 20-min tool life (V20) was selected as the single property of the tool-life curve for comparison with the other data. This relatively high speed was selected in preference to V480, for example, because the latter would have to be obtained by extrapolation, and slight errors in slope would lead to substantial errors in the extrapolated speed. The values of V20 as given in Table 2 are compared with other machining data, with

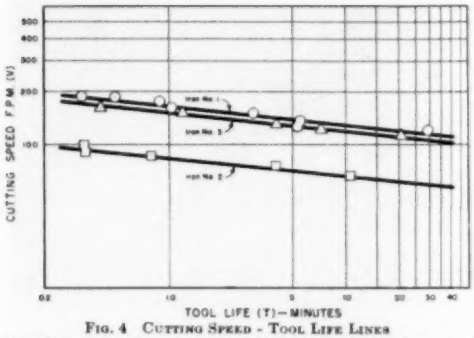

FIG. 4 CUTTING SPEED - TOOL LIFE LINES

(Irons Nos. 1 and 3 were quite similar in composition and both contained approximately 5 per cent of ferrite, while No. 2 contained nickel and chromium. 18-4-2 type high-speed-steel tools at a feed of 0.010 ipr, and a depth of cut of 0.050 in. Points represent time for final breakdown failure of tools.)

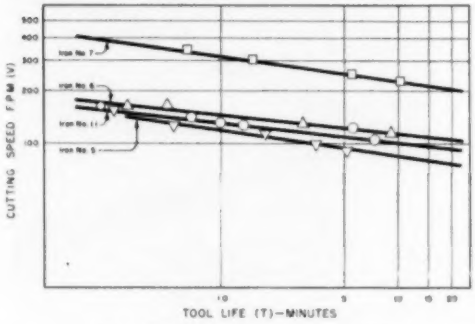

FIG. 5 CUTTING SPEED - TOOL LIFE LINES

(Same cutting conditions as in Fig. 4. Iron No. 7 with high silicon contained about 90 per cent ferrite.)

microstructure, with mechanical properties, and with chemical composition, in an effort to find a good correlation.

TABLE 2 SUMMARY OF TOOL LIFE TESTS

Depth of cut = 0.050 in.
Feed = 0.010 ipr. Tool shape: 0, 6, 6, 6, 6, 15, 1/64

$VT^n = C$

Iron no.	C	n	V20-fpm
1	162	0.100	120
2	82	0.100	61
3	150	0.103	110
5	119	0.150	79
6	145	0.107	105
7	315	0.140	208
8	170	0.125	117
10	230	0.140	152
11	130	0.100	94
12	100	0.140	66
13	127	0.100	94

CUTTING SPEED VERSUS DRILLING TORQUE AND THRUST

A standard two-flute 1/2-in-diam twist drill was used to drill the irons at a speed of 354 rpm and at feeds of 0.004, 0.006, and 0.009 ipr. An indicating dynamometer provided continuous readings of torque and thrust. These readings were plotted on log-log co-ordinates and extrapolated to a feed of 0.010 ipr. The values of both torque and thrust at this feed are shown in Table 3.

The cutting speeds (V20) are shown plotted against the corresponding drill-torque values in Fig. 7. The numbers opposite each point identify the corresponding iron as given in Table 1.

TABLE 3 DRILLING TORQUE AND THRUST

Drill diameter = 1/2 in. Feed = 0.010 ipr

Iron no.	Torque, lb-ft	Thrust, lb
1		
2	13.0	590
3	13.6	710
5	14.1	710
6	14.2	630
7	10.5	370
8	14.1	640
10	10.5	440
11	15.3	400
12	14.3	660
13	14.0	600

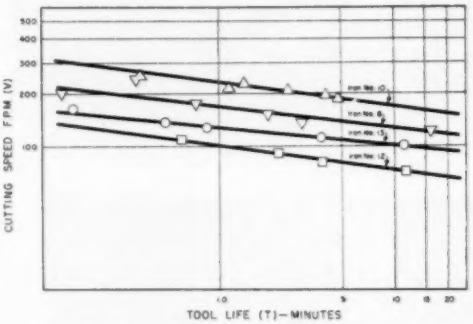

FIG. 6 CUTTING SPEED - TOOL LIFE LINES

(Same conditions as in Figs. 5 and 6. Iron No. 10 contained about 40 per cent ferrite.)

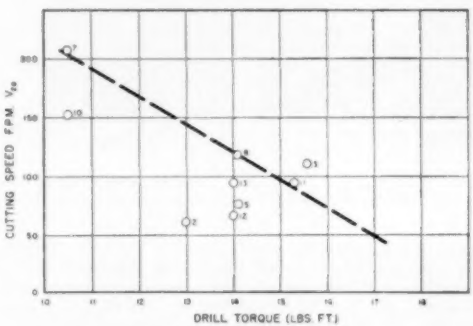

FIG. 7 CUTTING SPEED VERSUS DRILL TORQUE

(Dashed line represents expected variation of cutting speed with drill torque. Tests were made with 1/2-in-diam, two-flute twist drill. Drill was reground between successive tests. Correlation is very poor.)

The dashed line in Fig. 7 indicates the expected trend of decreasing cutting speed with increasing drill torque. It is obvious that drill torque cannot be relied upon to give an accurate indication of change in those properties which determine the cutting speed.

Fig. 8 is a plot of the cutting speed (V20) against the corresponding drill-thrust values. Again, a dashed line has been used to indicate the expected general trend. The distribution of points is substantially different from the torque values, and the relative positions of the irons are radically different. It is obvious that drill thrust also is not a useful parameter for predicting cutting speed for a given tool life.

CUTTING SPEED VERSUS MILLING POWER

A No. 2 vertical-spindle milling machine was set up with a 10-tooth, 2 7/8-in-diam high-speed-steel cutter with 0 deg radial rake,

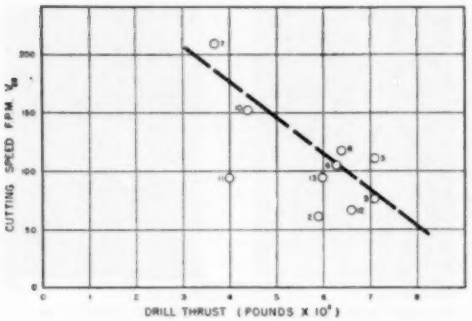

FIG. 8 CUTTING SPEED VERSUS DRILL THRUST
(Correlation with drill thrust is poor. Dashed line represents expected trend. Feed rate was 0.010 ipr; speed was 354 rpm, and drill diameter was 1/2 in.)

—5 deg axial rake, a 1/16-in. × 45-deg chamfer, and 6-deg relief angles. A series of tests was run on 2-in. × 6-in. × 18-in-long cast bars for which the feed, depth of cut, width of cut, and cutting speed were varied, and the input horsepower was recorded on a wattmeter. The data thus obtained were orderly and consistent for all irons. The indicated horsepower was reduced to horsepower per cubic inch per minute and the average for a feed of 0.010 in. per tooth, a width of 0.500 in., and depths of 0.200, 0.300, 0.400, and 0.500 in. was determined for the purpose of this study. The effect of depth of cut was almost negligible for the test range, thus making it possible to use 40 test points in obtaining the power values. The cutting speed was 61 rpm or 46 fpm. The horsepower per cubic inch per minute values are summarized in Table 4.

TABLE 4 MILLING-POWER VALUES

Iron no.	Hp/cu in/min	Iron no.	Hp/cu in/min
1	0.71	8	0.72
2	0.73	10	0.57
3	0.80	11	0.75
5	0.76	12	0.69
6	0.71	13	0.82
7	0.51		

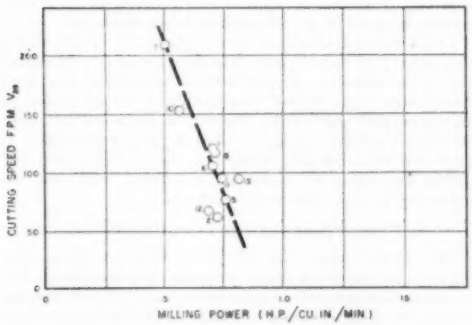

FIG. 9 CUTTING SPEED VERSUS MILLING POWER
(Milling-power data were obtained with a 2 1/2-in-diam, 10-tooth shell-end mill with 0 deg radial rake and negative 5-deg helix angle. Feed = 0.010 ipt; 61 rpm; 1/2 in. width of cut. Data are average for 0.200, 0.300, 0.400, and 0.500 in. depth of cut.)

The dashed line in Fig. 9 shows the expected trend in cutting speed with increasing power requirements. Although the correlation is better than with drilling, it is still far short of the precision necessary to provide a useful parameter for predicting cutting speed and tool life. In order to predict tool life within plus or minus 30 per cent, it is necessary to predict cutting speed accurately within plus or minus 3 to 5 per cent depending upon the slope of the tool-life curve.

CUTTING SPEED VERSUS MILLING ENERGY

In a different series of milling tests a pendulum-type dynamometer was used to obtain direct readings of the number of foot-pounds of energy required to cut one chip of a given size. The cutting tool was a single-point high-speed-steel tool, ground and mounted so as to provide 5 deg radial rake, 0 deg axial rake, and 6 deg relief. The cutter was used to cut a groove 1/4 inch wide. The tests were made at a constant depth of 0.100 in. and over a range of feeds so as to obtain accurate values at a particular feed. Table 5 gives the energy per chip, and the corresponding values of horsepower per cubic inch per minute for a cut 0.100 in. deep and 0.250 in. wide at a feed of 0.010 in. per tooth.

TABLE 5 MILLING-ENERGY VALUES

Iron no.	Energy per chip, ft-lb	Hp/cu in/min	Iron no.	Energy per chip, ft-lb	Hp/cu in/min
1			8	7.7	.93
2	8.5	1.03	10	7.1	.86
3	9.9	1.19	11	7.8	.94
5	8.7	1.05	12	7.7	.93
6	8.2	.99	13	9.3	1.12
7	7.0	.85			

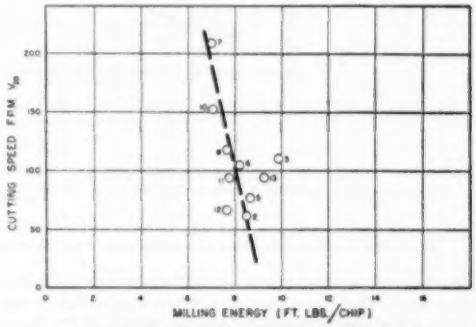

FIG. 10 CUTTING SPEED VERSUS MILLING ENERGY
(Data obtained with a pendulum-type dynamometer. Feed = 0.010 ipt; depth = 0.100 in.; width of cut = 0.250 in.)

The milling-energy values are shown plotted with the corresponding cutting speeds in Fig. 10. The dashed line again shows the expected trend, but individual points deviate considerably from any central tendency. Lack of good correlation is not surprising in view of the complexity of the metal-cutting process. The relatively poor correlations shown in Figs. 7 to 10, inclusive, for drilling and milling forces and energy simply indicate that at least some of the factors determining cutting speed are different from those determining the cutting forces and energy consumption.

CUTTING SPEED VERSUS MICROSTRUCTURE (FERRITE)

Fig. 11 shows the photomicrographs of irons Nos. 1, 3, 10, and 7, respectively. It will be recalled that these four irons all contained normal phosphorus and manganese and that the silicon was varied so that both Nos. 1 and 3 developed about 5 per cent free ferrite, while Nos. 10 and 7, respectively, developed approximately 40 and 90 per cent ferrite. The cutting speeds (V20) for

IRON NO. 1 X 100
PERCENT FERRITE - 5

IRON NO. 3 X 100
PERCENT FERRITE - 5

IRON NO. 10 X 100
PERCENT FERRITE - 40

IRON NO. 7 X 100
PERCENT FERRITE - 90

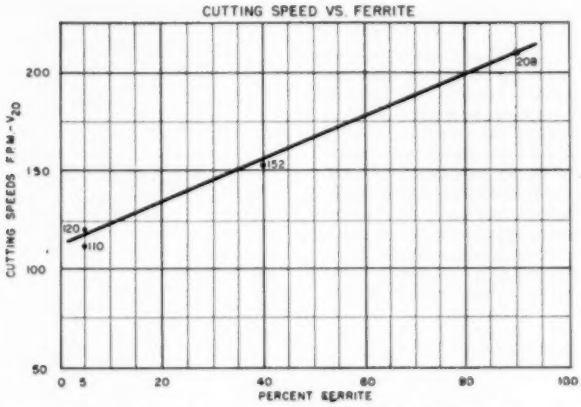

FIG. 11 CUTTING SPEED CORRELATES WELL WITH PER CENT FERRITE
(Precise determination of percentage of constituents is a lengthy process and is subject to human equation when timesaving estimates are made.)

these irons are shown plotted versus the estimated percentages of free ferrite. There are too few points to provide a precise correlation and furthermore the estimates of the amounts of free ferrite are of questionable accuracy. However, there can be little doubt about the potency of increased silicon content in providing higher cutting speeds. Whether the higher speeds are due to the increased free ferrite, or the reduced amount of combined carbon or some combination of the two is not evident from these tests. A good argument can be made in favor of the smaller quantity of carbides since the zero elongation of the gray irons makes it difficult for the ferrite to exert a beneficial effect on the mechanism of cutting.

CUTTING SPEED VERSUS MICROSTRUCTURE (GRAPHITE)

Fig. 12 contains photomicrographs of irons Nos. 10, 12, 5, 3, and 8, which represent a descending series of graphite size. The first four are all type A while the last one is type E with the familiar dendritic pattern. The graph below the micrographs shows the corresponding cutting speeds for each of the graphite conditions. There appears to be an inverse relationship between graphite-flake size and cutting speed, excepting the first point. However, almost any desired shape of curve could be obtained by selection, since there are either two or three speed selections for every flake size with the exception of the type E. Consequently, it may be assumed that there is no correlation between cutting speed and the graphite part of the microstructure.

Graphite is undoubtedly a potent factor in the cutting of cast iron, but this appears to come about through the zero elongation; that is, the discontinuity contributed by the graphite flake gives rise to zero elongation and thus establishes the mechanism of cutting peculiar to gray iron. Its effect seems to end there since all shapes and sizes of graphite flakes in the quantities found in gray iron result in zero elongation. In malleable iron and ductile iron where the elongation is different from zero, the influence of graphite may be quite different.

CUTTING SPEED VERSUS TENSILE STRENGTH

The tensile strengths for these irons were determined from duplicate specimens machined from the transverse bars. The as-cast specimens were less consistent and gave values only about 40 per cent of the machined specimens. All of the materials for iron No. 1 were lost along with the transverse bar, so there is no tensile-strength data for this iron.

The cutting speeds (V20) are plotted against the corresponding tensile strengths in Fig. 13. The attempted correlation is obviously poor, since the two highest and the lowest cutting speeds all occur at substantially the same strength, while the remainder of the points are distributed over a substantial area. Tensile

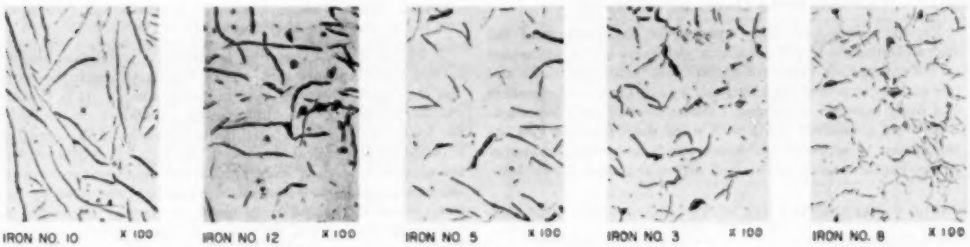

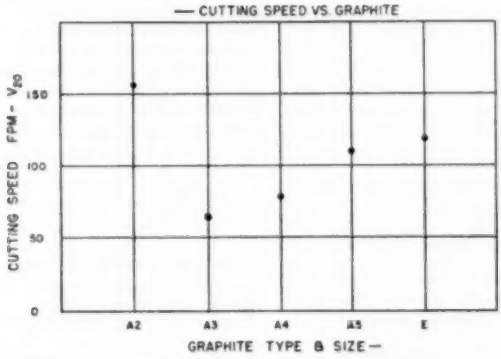

FIG. 12 THERE IS NO CONSISTENT CORRELATION BETWEEN CUTTING SPEED AND GRAPHITE TYPE AND SIZE
(There are two or three alternative selections of cutting speed for each type and size of graphite with the exception of the last one, type E.)

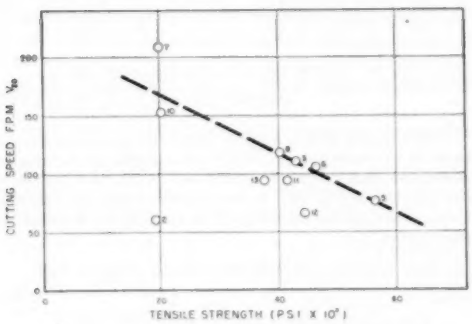

FIG. 13 CUTTING SPEED VERSUS TENSILE STRENGTH
(Tensile specimens machined from transverse bars and duplicate tests made. Correlation with cutting speed is very poor.)

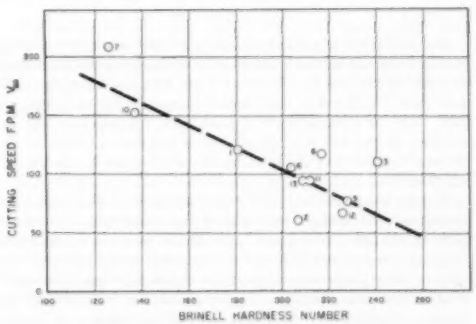

FIG. 14 CUTTING SPEED VERSUS BRINELL HARDNESS
(Average of three hardness impressions on tool-life specimens. General correlation is fair, but specific correlation is poor, since both cutting speed and Bhn are relatively precise quantities.)

strength gives the poorest correlation of all the data considered in this investigation. The dashed line in Fig. 12 is not intended to indicate any central tendency, but rather the expected trend of cutting speed as affected by tensile strength.

CUTTING SPEED VERSUS BRINELL HARDNESS

Fig. 14 is a plot of the cutting speeds against the corresponding Brinell hardness numbers. The correlation is not good although it is somewhat better than that shown in Fig. 13 for tensile strength. It is significant that the distribution of points in Fig. 14 is substantially different from that in Fig. 13. This indicates that there is not a precise correlation between tensile strength and Brinell hardness.

Cutting Speed Versus Microhardness

Various values have been reported for the hardness of the microconstituents of ferrous alloys, and there is fair agreement on the appropriate values for simple constituents like ferrite and free carbide; however, some latitude may be expected for pearlite and other complex structures. The results of other investigations were considered along with some work done on this investigation to arrive at the approximate or average values of Knoop hardness numbers obtained with a 50-gram load (Table 6).

TABLE 6 REPRESENTATIVE KNOOP HARDNESS NUMBERS; 50-GRAM LOAD

Constituent	Hardness number
Free ferrite	240
Coarse pearlite	350
Medium pearlite	400
Fine pearlite	450
Steadite	900
Free carbide	1500

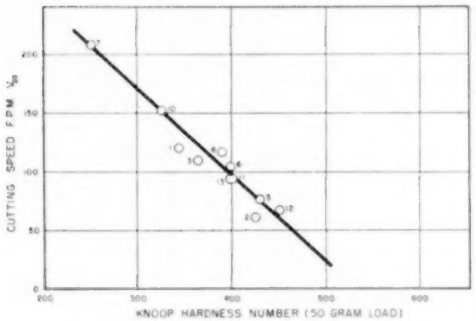

Fig. 15 Cutting Speed Versus Microhardness

(Hardness numbers are a linear weighted average applied to visual estimates of constituent percentages. A high sensitivity of average to percentage of constituents shows some promise for a good correlation. Proper treatment of this approach may require nonlinear weighting and may produce a nonlinear correlation.)

Fig. 15 shows the cutting speeds (V20) plotted against average Knoop hardness numbers obtained by multiplying the percentage of each constituent by the appropriate hardness from the table and then dividing the sum of such products for each iron by 100. The correlation is very good and, furthermore, the individual points not now on the curve can be corrected to the curve and yield completely reasonable percentages for the various constituents.

It must be emphasized, however, that there is a fair amount of fortuitous circumstance surrounding the visual estimates of the percentages of constituents, and there remains considerable doubt as to the validity of the hardness values given in the table. Also, there is no reason for believing that a properly weighted average hardness or the correlation itself should be linear. Nevertheless, the idea is rational and shows considerable promise of developing into a useful and reliable parameter for predicting cutting speeds.

For the method to be come practicable, it would be necessary to develop a rapid and reliable method for determining the percentages of effective constituents. It is possible that a pattern of successive microhardness tests could be designed to produce an average which would correlate with cutting speeds without any knowledge of the percentages of constituents. Much work remains to be done, but the results of this preliminary study seem to indicate that such effort may be profitable.

Cutting Speed Versus Chemical Composition (Combined Carbon)

It will be recalled that Fig. 11 showed a correlation between cutting speed and per cent of free ferrite, although the ferrite was the result of varying percentages of silicon. It is doubtful whether the changes in cutting speed are the direct result of either the ferrite or the silicon; the same doubts exist in connection with the other chemical elements in the iron. It is believed that the changes in cutting speed are a direct result primarily of the changes in the carbides or combined carbon, and possibly to a lesser extent to changes in the matrix properties. However, the latter possibility is not very probable since there is very little plastic flow associated with the mechanism of cutting gray iron.

Fig. 16 shows an attempted correlation between cutting speed and combined carbon as determined by chemical analysis. The solid straight line fits five of the eleven points very well. All of these points represent what might be called "plain-carbon" irons with the exception of No. 8, and in this case the silicon and nickel are in such proportion as to produce the graphitizing potential of about 2.1 per cent silicon; thus iron No. 8 might also be classified as a plain-carbon iron. The six remaining irons all contained significant amounts of various effective alloying elements such as chromium, manganese, molybdenum, and phosphorus as well as nickel.

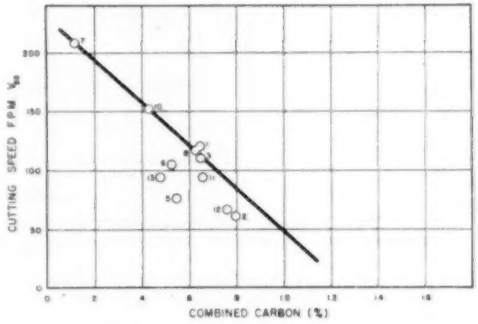

Fig. 16 Cutting Speed Versus Combined Carbon

(All plain-carbon irons lie close to curve while all alloy irons fall below curve on speed scale.)

It is reasonable that all of the so-called alloying elements could exert an influence through either the carbides or the matrix material to cause the points representing these irons to fall below the solid line in Fig. 16. A determinant was set up from the chemical analysis shown in Table 1 to solve for the constants in the equation

$$ECC = CC + K_1\text{Cr} + K_2\text{Mo} + K_3\text{Mn} + K_4\text{P} + K_5\text{Ni}$$

where

ECC = equivalent combined carbon
CC = combined carbon (by analysis)
K_1, K_2, K_3 = appropriate constants
Cr, Mo = percentages of elements shown by chemical analysis except for manganese, which was included only in excess of 55/32 of sulphur content

Solution of the determinant gives the following equation

$$ECC = CC + \text{Cr}/6 + 3\,\text{Mo}/4 + \text{Mn}^*/4 + \text{P}/3 - \text{Ni}/10 \quad [1]$$

* In excess of 55/32 of the per cent of sulphur.

Equation [1] was applied to all eleven irons since all of them contained manganese and phosphorus. The resulting equivalent combined carbon values are plotted along with the corresponding cutting speeds in Fig. 17.

The correlation is very good considering the relatively few irons involved, but neither the curve nor Equation [1] should be accepted as the final solution to the problem, since there are some rather important questions remaining to be answered.

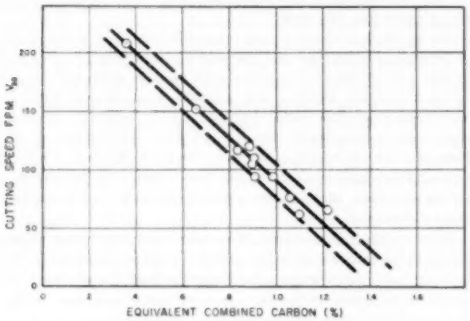

FIG. 17 CUTTING SPEED VERSUS EQUIVALENT CARBON

(Application of a determinant solution to all points of Fig. 16 produces sharp correlation. "Equivalent combined carbon" may imply some change in matrix properties as well as in carbides.)

It must be recognized that the upper half of the curve is determined by the same irons which were used to establish the correlation with free ferrite. Consequently, the determining factor in this region could be ferrite rather than combined carbon. If this were true there would be a discontinuity just below the points for irons Nos. 1, 3, and 8, and the lower region would be determined by free carbides. Thus the line might be expected to curve either way. On the other hand, if the upper region of the line in Fig. 17 is determined by combined carbon, then the curve might very well be a straight line as it is shown. Obviously, considerable work needs to be done before these questions can be answered, but the determination of the true nature of this correlation may prove a significant step forward in the solution of the complex, over-all problems of machining.

CUTTING SPEED VERSUS CHEMICAL COMPOSITION (GRAPHITIZING TENDENCY)

The chemical analysis in Table 1 was inserted in the nucleation-tendency formula to obtain a set of "NT" values for the irons. The formula used for this purpose was as follows

$$NT = TC + Si/3 + P/3 + Ni/6 + Cu/12 - Cr/2 - Mo/2 - Va - Mn^4/6 \quad [2]$$

where

NT = nucleation tendency
TC = total carbon

The nucleation-tendency values are shown plotted against cutting speeds in Fig. 18. The correlation is very good for all irons except Nos. 1, 8, and 13. However, both the correlation and the deviations may be coincidence since the actual graphitization and the associated combined carbon are subject to melting, pouring, and mold practice, as well as the graphitizing tendency. Consequently, the curve in this figure may mean only that these practices were quite uniform for all irons except Nos. 1, 8, and 13. On the other hand, the fact that this correlation is substantially better than most of the attempted correlations with

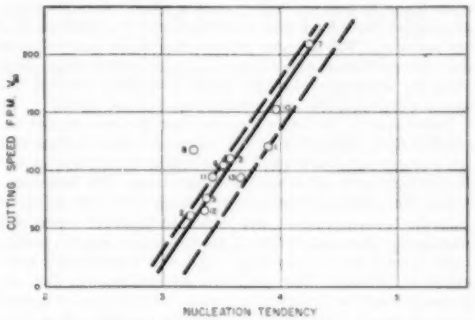

FIG. 18 CUTTING SPEED VERSUS NUCLEATION TENDENCY

(Correlation probably is as good as it is because of fair uniformity in foundry practice since varying degrees of graphitization can be achieved for a given nucleation tendency.)

other machining data and mechanical properties is further evidence of the validity of the theory that combined carbon is the principal determinant of cutting speed.

CONCLUSIONS

Since the purpose of this study was to compare possible parameters for predicting cutting speed for machining gray iron, it is appropriate to sum up by listing the several types of tests considered in order of descending degree of correlation as follows:

1 Combined carbon or equivalent.
2 Microhardness.
3 Nucleation tendency (adjusted for foundry practice).
4 Milling power and energy (fair to poor).
5 Brinell hardness number (poor).
6 Drilling torque (poor).
7 Drilling thrust (very poor).
8 Tensile strength (very poor).

The dissipation of useful tool life when machining cast iron is uniquely characterized by abrasion, and it can be expected that those tests or parameters which come closest to the determinants of abrasion will prove to be the most reliable for predicting cutting speed and the dependent tool life.

Discussion

E. A. CYROL.[4] This discussion is from the point of view of the end use of data on machining speeds for cast iron, steel, and other metals; the effective and economic use of machines, cutting tools, and manpower in the factory machine shop. Certainly the data available at the present time on machining speeds are no more than crude approximations helpful only as rough guides, and investigations such as those described in the paper are probings with the greatest potential. Undoubtedly, most of the factors which are responsible for determining tool life as yet are unrecognized, and the factory management that is striving for most efficient utilization of its machine and cutting tools is left to its own halting experimentations.

Experience indicates quite clearly that in the well-managed machine shop the machine operator must be provided with the correctly fashioned cutting tools and *the pertinent setup data, such as feeds and speeds to be used.*

Where the tool-engineering department exercises the control over the feeds and speeds used in the machine shop, the productiv-

[4] E. A. Cyrol & Company, Chicago, Ill.

ity is 25 to 50 per cent higher than in plants where the determination of the cutting speeds and feeds is left to the foreman or the operator. Will someone estimate how much more this productivity could be increased if the most economical cutting speeds could be unerringly predicted from correlations between the known physical or chemical characteristics of the metals?

Unfortunately, the study indicates that the most readily obtainable data, such as the Brinell hardness number and the tensile strength, are poor to very poor as possible parameters for predicting cutting speed for machining gray iron. The best correlations were obtained from comparisons of combined carbon or equivalent, microhardness, and nucleation tendency versus cutting speed. Appraisal of these properties cannot be made readily at our present level of knowledge; and even if trustworthy techniques of measuring these properties are forthcoming, their use probably would be limited to large-scale investigations of general types of metals. This would preclude the possibility of predicting proper speeds for specific lots of material received by machine shops for machining. Future researchers along the path indicated by the present study might take this consideration into account. The ideal situation would permit easy analysis and procurement of the significant characteristic for predicting the proper cutting speeds for lots of materials to be machined in seperate runs in the plant. This, together with universal use of variable speeds on machine-tool equipment, would yield economies pleasant to contemplate.

Authors' Closure

Mr. Cyrol has restated the reasons for vigorous prosecution of investigations of the type we have reported on here by pointing out substantial gains in productivity in shops where tool engineering exercises control over machining specifications and predicts further substantial improvement when such control can have a more precise basis. However, he warns that any tests for basing predictions of machining performance must be simpler than those for the microhardness and equivalent combined carbon parameters proposed in this paper.

We agree that simpler tests must be developed to meet the conditions of short time and low cost necessary for effective and general use; further, we predict that simpler tests will be developed once the ultimate determinants of machining performance have been positively identified. It is necessary to know what these determinants are and to know all about the mechanism of their operation. These necessary facts seem to have evaded investigators thus far and has resulted in the cut-and-try use of many more or less simple tests with widely varying degree of success.

Even if equivalent combined carbon or microhardness should prove to be generally reliable and no simpler test could be developed, substantial gains in productivity would result from the ability of foundries to control these variables and thus reduce the need for receiving inspection in the machine shop.

Thermophysical Aspects of Metal Cutting

By B. T. CHAO,[1] K. J. TRIGGER,[2] and L. B. ZYLSTRA,[3] URBANA, ILL.

Some basic issues in the theory of metal cutting are analyzed in the earlier part of this paper. Several controversial subjects are clarified by the experimental results presented. The remainder of the paper describes a further attempt to ascertain the effect of cutting speed and feed on the mechanism of chip formation in high-speed machining operations. A differential equation of the temperature field in the chip as well as that in the workpiece has been set up, and the nature of the solution studied. It has been found that the temperature distribution both in the work material and in the deformed chip in the immediate vicinity of the tool-chip interface depends upon a dimensionless number which is expressible as the ratio of the product of the cutting speed and feed to the thermal diffusivity of the metal cut. This ratio is called the thermal number, and its significance in metal cutting is illustrated and the limitations discussed.

Survey of Present Theories in Metal Cutting and Related Subjects

WHILE the subject of metal cutting has been under study for over a century, it is only in recent decades that it gradually has been undergoing a transition from an art to a science. The basic mechanics of chip formation developed independently by Merchant and Piispanen was a grand contribution in this respect. While it is best adaptable to type 2 chips, both investigators have extended the application to discontinuous chips with only slight modifications.

In his study of the plasticity conditions for a continuous chip without built-up edge, Merchant (1)[4] made use of an observed fact reported by Bridgman (2) that the flow stress by shear of some of the polycrystalline metals increases with the compressive stress. Mathematically, he suggested the following simple relationship

$$S_s = S_0 + kS_n \quad \ldots\ldots [1]$$

where

S_s = mean flow stress along shear plane
S_0 = flow stress of the material under zero compressive stress
k = slope of flow stress versus compressive-stress curve, considered as a constant for a given work material
S_n = mean compressive stress on shear plane

Such influence of the normal stress on the flow stress amounts to the same thing as the existence of an internal friction in the material. This view was held by Piispanen (3).

Both Merchant and Piispanen have applied the principles of least work to derive the plasticity conditions. From chip geometry, it can be shown readily that

$$F_c = S_s A_0 \cos(\tau - \alpha)/[\sin\phi \cos(\phi + \tau - \alpha) - k \sin\phi \sin(\phi + \tau - \alpha)] \quad \ldots\ldots [2]$$

where

F_c = cutting force
A_0 = cross-sectional area of "chip" before removal from work piece = depth of cut × feed
τ = friction angle at interface = $\tan^{-1}\mu$
α = true rake angle of tool
ϕ = shear angle

When work done in cutting reaches its minimum, F_c is also a minimum. Consequently, to apply the principle of minimum energy, both Merchant and Piispanen differentiate Equation [2] with respect to ϕ and equate it to zero. This yields the relationship

$$2\phi + \tau - \alpha = \cot^{-1}k = C \quad \ldots\ldots [3]$$

In the process of differentiation, they consider τ to be independent of ϕ, i.e., $\partial\tau/\partial\phi = 0$. It is not clear that this is justifiable.

Nevertheless, despite the assumptions involved in Merchant's formulation of the plasticity Equation [3], it has been found to agree with experimental results to within ±6 per cent for several kinds of steel and two nonferrous materials tested by the authors. Chao and Bisacre (4) have shown that the temperature rise during high-speed metal-cutting operations has no serious effect on Merchant's analysis.

The question of strain-hardening has been one of the most controversial subjects in the theory of metal cutting. Shaw (5) contends that the true stress-strain relationship of the material in the shear zone is not unlike that determined in a quasi-static test. Consequently, a linear relationship can be assumed actually to exist between the shear-plane displacement and the flow stress. On the other hand, Drucker (6) suggests that at high rates of strain the dynamic flow stress is raised and the true stress-strain curve approaches an ideally plastic horizontal line. This view is held by Chao and Bisacre (4).

When a single crystal is subjected to stress, slip will start when the resolved shear stress has reached a certain constant value, irrespective of the normal stress on the slip plane. This is referred to as the law of critical resolved shear stress (7). For pure metals, it is of the order of magnitude of 200 psi and was found unaltered by hydrostatic pressures up to 600 psi. Conditions governing the beginning of flow under stress in ductile polycrystalline aggregates are more complicated. However, the fact that the yield stress for ordinary low-carbon steel does not differ to a perceptible extent in tension and in compression suggests the independence of flow stress on normal stress.

Bridgman (2) reported the increase of flow stress with normal stress in the case of a drill rod (1.25 C steel) but he failed to observe any significant change in the flow stress of SAE 1045 steel when the compressive load changed from zero to 5700 kg per sq cm or 81,000 psi. However, his experiments did show that under high compressive stress a ductile material can sustain a

[1] Assistant Professor, Department of Mechanical Engineering, University of Illinois.
[2] Professor, Department of Mechanical Engineering, University of Illinois. Mem. ASME.
[3] Instructor, Department of Mechanical Engineering, University of Washington. Formerly Graduate Student, Department of Mechanical Engineering, University of Illinois.
[4] Numbers in parentheses refer to Bibliography at end of paper.

Contributed by the Production Engineering Division and Metal Cutting Data and Bibliography and Cutting Fluids Research Committees and presented at the Annual Meeting, Atlantic City, N. J., November 25–30, 1951, of The American Society of Mechanical Engineers.
Note: Statements and opinions advanced in papers are to be understood as individual expressions of their authors and not those of the Society. Manuscript received at ASME Headquarters, August 6, 1951. Paper No. 51—A-41.

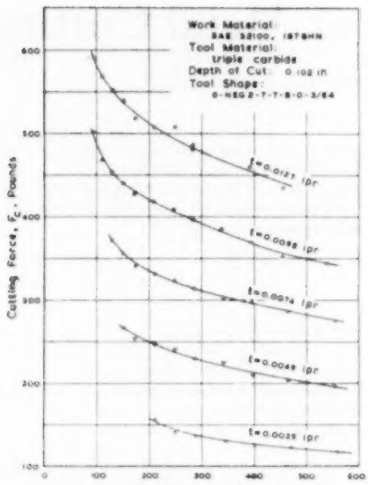

FIG. 1(a) CUTTING SPEED - CUTTING FORCE RELATIONSHIP AT VARIOUS FEEDS

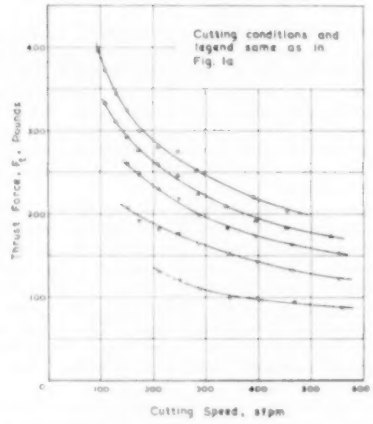

FIG. 1(b) CUTTING SPEED - THRUST FORCE RELATIONSHIP AT VARIOUS FEEDS

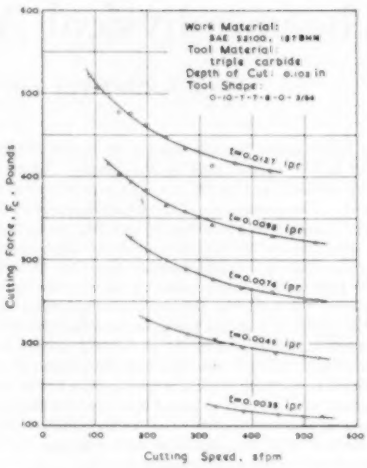

FIG. 2(a) CUTTING SPEED - CUTTING FORCE RELATIONSHIP AT VARIOUS FEEDS

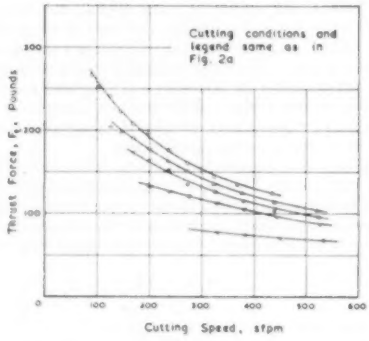

FIG. 2(b) CUTTING SPEED - THRUST FORCE RELATIONSHIP AT VARIOUS FEEDS

shear strain without rupture many times greater than it can in the absence of such compressive stress. A strain of over 300 per cent was reported by Bridgman. It is interesting to note that the compressive stress and the resulting large shear strains recorded by Bridgman are not unlike those obtained in metal-cutting operations. However, he reported no data obtained at high rates of strain.

One of the purposes of this investigation is to clarify some of these important issues.

Test Procedure. In order to investigate the validity of Equation [1] and the resulting expression for the plasticity condition formulated by Merchant, tests were conducted on spheroidized SAE 52100 steel (187 Bhn) using wide ranges of speeds and feeds and side rake angles of 10 deg, 4 deg, and negative 2 deg.

The test logs consisted of $5^1/_2$-in-OD tubing having a wall thickness of $^5/_8$ in., and approximately 30 in. long. They were all taken from a single 12-ft stock length to insure minimum variation in physical properties. Microexamination of specimens prepared from samples cut from the extreme ends of the stock showed negligible variation in structure and hardness. The general method of measuring tool forces, chip thicknesses, and tool-chip contact areas was the same as that reported in an earlier paper (8). One improvement in procedure was employed in the measurement of contact areas. The tool photograph was projected on a screen, and the enlarged outline was sketched for area determinations.

All tools used were of identical "triple-carbide" composition of ASA Specification O-Var-7-7-8-0-3/64. The setting angle was

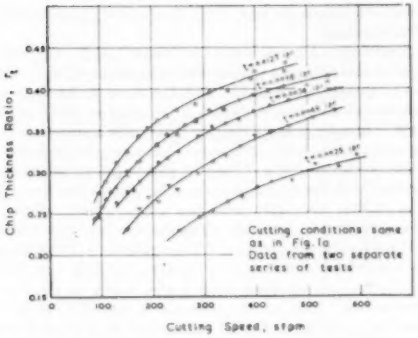

FIG. 3 CUTTING SPEED - CHIP THICKNESS RATIO RELATIONSHIP AT VARIOUS FEEDS

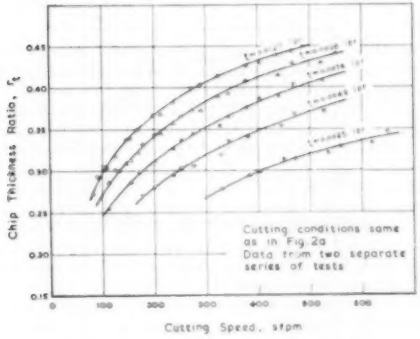

FIG. 4 CUTTING SPEED - CHIP THICKNESS RATIO RELATIONSHIP AT VARIOUS FEEDS

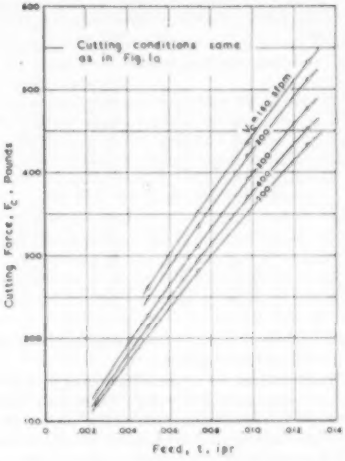

FIG. 5(a) EFFECT OF FEED ON CUTTING FORCE AT VARIOUS CUTTING SPEEDS

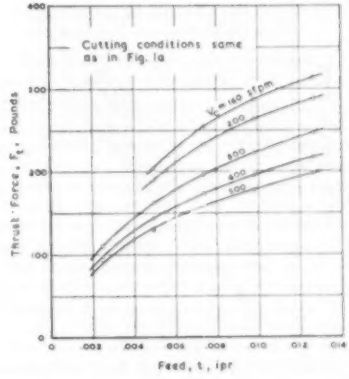

FIG. 5(b) EFFECT OF FEED ON THRUST FORCE AT VARIOUS CUTTING SPEEDS

90 deg in all tests. Conventional turning was used throughout the experiment and all tests were done dry. During the tests the separating surface of the chips was inspected for each run, and only those cutting conditions which produced type-2 chips were recorded.

Test Results. Results for both components of tool force and for chip-thickness ratio at various cutting speeds, feeds, and tool rake angles are summarized in Figs. 1(*a*, *b*), 2(*a*, *b*), 3, and 4.

Inasmuch as the various values for the 4-deg side-rake angle fell between those of the negative 2- and positive 10-deg tools, only the latter two are reported in this paper. The general trend of the curves is the same as that obtained in cutting mill-annealed NE9445 steel. It might be noted that when the feed was 0.0025 ipr, no readings were recorded for speeds below 280 sfpm since, under this condition, the chips produced showed evidence of excessive built-up edge during cutting.

The effect of feed on tool forces is shown in Figs. 5(*a*, *b*) and 6(*a*, *b*). Within the range of the present investigation, the cutting force at a given speed varies nearly linearly with feed. This linearity deteriorates very rapidly for feeds finer than the smallest employed, since all the curves should meet at the origin. However, at these finer feeds a type-2 chip might not be obtained even at higher speeds than in the range investigated.

Unlike the cutting force, the relationship between the thrust force and the feed is more or less parabolic. At a given cutting speed, it increases with feed, but the rate of increase diminishes as feed increases.

These trends also were found to be true when the mill-annealed NE9445 steel was cut with the same triple-carbide tool.

Values of shear angle ϕ, friction angle τ, and the so-called machining constant C were calculated for all combinations of speeds, feeds, and tool-rake angles. The pertinent data were obtained from the experimental curves for tool forces and chip-thickness ratio. Table 1 lists the values of C calculated from Equation [3].

It is seen that there is a systematic, though small, variation of C with cutting speed. The effect of changing feed is rather erratic, and somewhat smaller. An increase of tool-rake angle from negative 2 deg to positive 10 deg decreases the "machining

TABLE 1 SUMMARY OF CALCULATED VALUES OF MACHINING CONSTANT, C DEG, FOR SPHEROIDIZED SAE 52100 STEEL

Cutting speed, sfpm	Feed, ipr				
	0.0025	0.0049	0.0074	0.0098	0.0127
	(*A*) For Tool Rake, $\alpha = -2$ Deg				
120	..	..	..	65.3	65.8
160	..	64.6	66.7	66.9	66.9
200	..	66.6	68.2	68.0	68.0
240	..	67.8	69.2	68.7	68.8
280	66.1	68.9	69.8	69.1	69.5
320	66.9	69.6	70.3	69.6	69.9
400	68.2	71.0	70.8	70.2	70.2
480	69.8	72.1	71.4	70.8	70.8
540	70.8	72.7	71.8	71.1	..
	(*B*) For Tool Rake, $\alpha = +10$ Deg				
120	..	..	..	60.5	62.5
160	..	..	61.7	62.8	64.0
200	..	62.7	63.3	64.2	64.9
240	..	64.2	64.4	65.1	65.6
280	..	65.6	65.2	65.8	66.1
320	63.7	66.7	66.0	66.3	66.5
400	66.4	67.8	67.0	66.9	67.0
480	68.4	68.5	67.6	67.5	67.4
540	69.0	69.1	67.9	67.7	..

constant" by about $2^1/_2$ deg. The reasons for these changes are unknown to the authors at present.

The over-all average for all combinations of speeds, feeds, and two different rake angles is 67.4 deg. More than 95 per cent of the individual values calculated fell within ±5 deg of this average. Previous cutting data obtained by the authors on NE9445 steel and annealed 0.27C steel reveal similar results. It is concluded, therefore, that as a first degree of approximation the experimental results do agree with Merchant's plasticity equation for type 2 chips.

According to Piispanen and Merchant's theory, this work material should exhibit a pronounced "Bridgman effect." Since C has an average value of 67.4 deg, the slope of the shear stress-compressive stress curve (which is the same as cot C) should be 0.416. In order to check this, the shear stress and the corresponding compressive stress at the shear plan were calculated for all the conditions tested. Fig. 7 shows a plot of the stress values thus obtained with the exception of those for the smallest feed. These were omitted since they introduce a "size effect" which is another complicating variable. The smallest feed is not included in Fig. 8 for the same reason. The significance of this size effect has recently been discussed by Backer, Marshall, and Shaw (9) and its influence on shear stress is also shown in Fig. 9 at the smallest feed. It is apparent that the normal stress at the shear plane has a negligible effect on the dynamic flow stress of the material. The dash-dot line in the figure illustrates the hypothetical relationship as postulated by Equation [1].

Bridgman's experiments were recently repeated by Bisacre

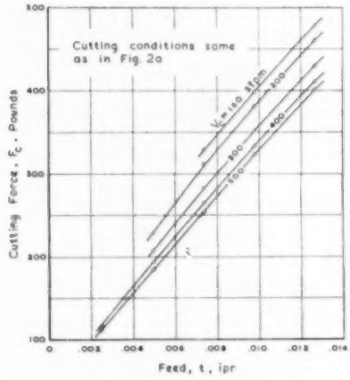

Fig. 6(a) Effect of Feed on Cutting Force at Various Cutting Speeds

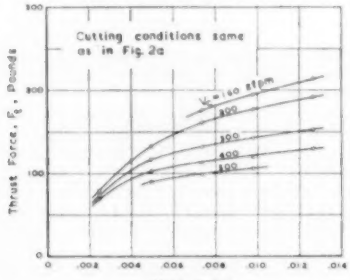

Fig. 6(b) Effect of Feed on Thrust Force at Various Cutting Speeds

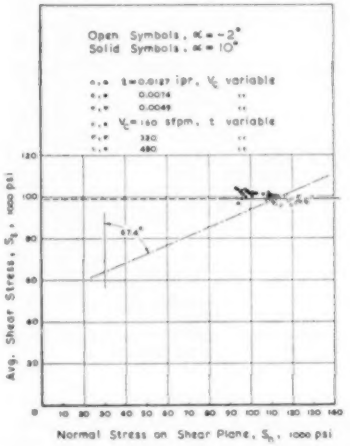

Fig. 7 Effect of Normal Stress on Dynamic Shear Stress in Chip Formation

(Work material: SAE 52100, 187 Bhn; tool material, triple carbide.)

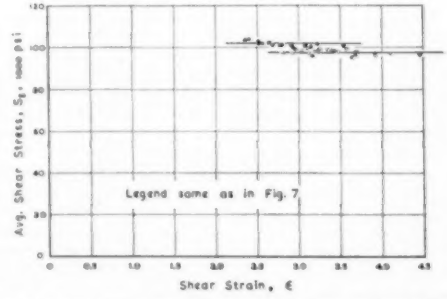

Fig. 8 Shear Stress - Shear Strain Relationship in Type 2 Chips

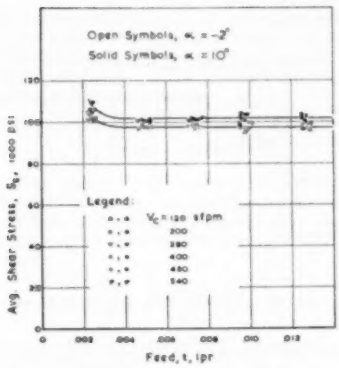

FIG. 9 EFFECT OF FEED ON AVERAGE SHEAR STRESS

(10) on α-brass. The change in shear stress as the compressive stress increased from zero to 33,000 psi was found to be practically nil. However, calculated results from cutting tests on the same material show a mean value of C to be about 65 deg. The evidence is, therefore, that there is little justification to regard this constant to be the same as $\cot^{-1} k$, where k is the slope of the shear stress versus compressive stress curve.

Shaw (5) has recently introduced a theory of strain-hardening which takes into consideration the effect of the inhomogeneity of the material being cut Such a theory is indeed plausible if the true stress-strain relationship of the material at the shear zone were of a shape similar to that determined in quasi-static tests. As mentioned earlier, there are at present conflicting opinions in regard to this point. A wide range of shear strains and the corresponding stresses can be calculated readily from the data available in this investigation. This is illustrated in Fig. 8. It is interesting to note that within the range of shear strains encountered in most high-speed metal-cutting operations on steel, the stress-strain curve can be approximated by a horizontal line—a conclusion reached by one of the authors (4) several years ago. Careful examination of the data plotted in Fig. 8 reveals that there is a slight tendency for the shear stress to drop at larger strains. The course of the stress-strain relationship is uncertain for values of strain smaller than those available for the plot. In so far as the mechanism of chip formation is concerned, the shear stress at the shear zone is substantially constant, and is independent of the different temperatures caused by changes in speed, feed, and tool rakes provided no size effect is introduced.

The heating effect due to shear occurs only after shear has taken place. The dynamic shear characteristics of the metal during high-speed machining operations appear to be unaffected by the temperature rise due to deformation, since the latter does not occur until after the shear energy has been imparted to cause shearing deformation. This is reflected in the constancy of the shear stress in spite of the large rise in temperature (600 to 1100 F) caused by deformation at the shear zone under different cutting conditions.

It is recognized that preceding deformation, the uncut chip (i.e., work material) is heated owing to the existence of a temperature gradient at the junction of the deformed-nondeformed material. Since the temperature gradient is very steep and the time for heating the nondeformed material is very short prior to its entry into the shear zone, it is believed that such heating has no effect on the dynamic shear properties.

This flat characteristic of the stress-strain relationship does not imply that the material is not hardened by severe deformation. The hardness of the chip has been found to be several times that of the undeformed material.

According to the dislocation theory for the plastic deformation of crystalline solids, time is required for the metal to exhibit an increase in hardness and strength after deformation has taken place. The time necessary depends upon the magnitude of deformation, the temperature of the material, and the length of the path to be traversed by the dislocation. At the high temperatures caused by shearing deformation, diffusion of the dislocation is very rapid involving time of the order of 10^{-6} sec or less. Static hardness measurement of the chip, necessarily conducted long after chip formation, may give little clue as to the physical properties of the metal during shear at the shear zone. Such hardness tests, however, give a good idea of the result of this deformation. Merchant, in a discussion of a paper (11) by one of the authors, points out that the increase in chip hardness due to shearing strain bears a linear relationship to the amount of strain provided no annealing takes place in the chip.

The inconsequential effect of temperature rise at the shear zone upon the shear stress during cutting is not to be confused with the effects encountered in hot-machining metals. In the latter case the uncut stock is heated externally prior to its entry into the shear zone. As a consequence, the shear resistance has been lowered prior to any deformation, and a reduction in cutting forces results from this weakened condition. It is, therefore, necessary to distinguish the heating effect due to any external source from that caused by chip deformation per se.

EFFECT OF CUTTING SPEED AND FEED ON TEMPERATURE DISTRIBUTION—ITS ROLE IN MECHANISM OF CHIP FORMATION

There are two distinct regions of heat generation during machining operations which produce a type 2 chip. They are the shear zone and the tool-chip interface. In the former, shearing of the metal results in a temperature rise of several hundred degrees in the bulk of the chip. The resulting temperature will be referred to as the chip bulk temperature. Such a temperature rise has little influence on the shearing stress of the work material during the shearing deformation. The capacity of the work material to withstand dynamic shearing stress during high-speed machining operations is that which it has at the time of entry into the shear zone.

However, as it leaves the shear zone the metal has been deformed severely and heated to a high temperature. Under such conditions the dislocation theory postulates very rapid strain-hardening and other temperature-dependent effects on the properties. It is estimated, from the data in Table 3, that the time required for the chip to traverse the tool-contact is of the order of 10^{-3} to 10^{-4} sec. Consequently, at the chip bulk temperatures involved, this traverse time is long as compared with that required for diffusion of the dislocations. It is believed, therefore, that a strain-hardened chip will exhibit its influence at the tool-chip interface.

An extremely steep temperature gradient exists in the chip at this interface owing to the high relative velocity of the tool and the chip. This steep temperature gradient is thought to have an effect on the variability of interface friction with temperature.

Differential Equation of Heat Flow in Metal Cutting. The problem of determining the temperature distribution in the work material and in the chip is one of heat conduction in a moving medium. For orthogonal cutting, it is simplified to a two-dimensional problem. The reference axes are chosen as indicated in Figs. 10 (*a* and *b*).

Consider the flow of heat through an elementary volume with edges dx, dy, and a unit length in the direction perpendicular

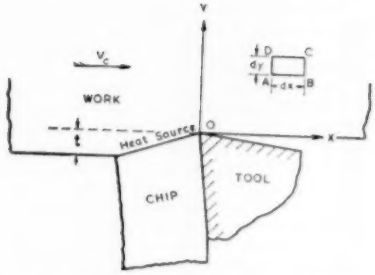

FIG. 10(a) HEAT FLOW IN THE UNCUT WORK MATERIAL

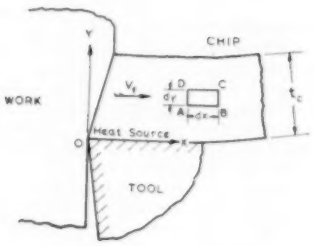

FIG. 10(b) HEAT FLOW IN THE DEFORMED CHIP MATERIAL

to the XY-plane. The heat entering along the x-axis in a unit time by conduction is

$$-K\,dy\,\frac{\partial\theta}{\partial x}$$

where K is the thermal conductivity and θ the temperature at the mid-point of face AD. In Fig. 10(a), K should be denoted as K_w, the thermal conductivity of the work material while in Fig. 10(b), it should be denoted as K_c, the thermal conductivity of the deformed chip at higher temperatures.

The amount of heat leaving per unit time along the same axis, is

$$-dy\left[K\frac{\partial\theta}{\partial x}+\frac{\partial}{\partial x}\left(K\frac{\partial\theta}{\partial x}\right)dx\right]$$

The difference between the heat entering and leaving is the net rate of heat storage in the elementary volume due to conduction along the x-axis.

It is

$$\frac{\partial}{\partial x}\left(K\frac{\partial\theta}{\partial x}\right)dx\,dy$$

Similarly, for the y-direction, this difference is

$$\frac{\partial}{\partial y}\left(K\frac{\partial\theta}{\partial y}\right)dx\,dy$$

Owing to the motion of the medium (the uncut work material or the deformed chip material) parallel to the x-axis along which there exists a temperature gradient, there is also a change of heat storage in the elementary volume. This is virtually a body convection and may be evaluated as follows:

The heat carried into this volume per unit time through face AD due to body convection is

$$C\rho V\theta\,dy$$

where C, ρ, and V are the specific heat, density, and the speed of motion, respectively. In the work material they should be referred to as C_w, ρ_w, and V_c (cutting speed), while in the chip they should be referred to as C_c, ρ_c, and V_f, the chip-flow velocity.

The heat carried away is

$$\left(C+\frac{\partial C}{\partial x}dx\right)\rho V dy\left(\theta+\frac{\partial\theta}{\partial x}dx\right)$$

since ρ and V are constants. (The slight variation in ρ with temperature is neglected.)

The difference, therefore, is the net rate of heat storage in the elementary volume due to motion parallel to the x-axis. Neglecting small quantities of the second order, it becomes

$$-\rho V\frac{\partial}{\partial x}(C\theta)\,dx\,dy$$

In most metal-cutting operations, the process of heat flow can be looked upon as being quasi-stationary in nature. In other words, an observer stationed at the source fails to notice any change in temperature with time in the medium around him. Under such conditions, and neglecting all heat losses, the general differential equation of heat flow in metal cutting is as follows

$$\frac{\partial}{\partial x}\left(K\frac{\partial\theta}{\partial x}\right)+\frac{\partial}{\partial y}\left(K\frac{\partial\theta}{\partial y}\right)-\rho V\frac{\partial}{\partial x}(C\theta)=0 \quad\ldots\ldots [4]$$

This equation is valid for the temperature distribution in the work material as well as that in the chip, provided suitable subscripts are attached to the properties of matter in their respective case.

Equation [4] can be simplified by ignoring the variation of the specific heat and thermal conductivity of the material from point to point in the uncut stock and in the chip. In the latter case the values corresponding to the chip bulk temperature are used. To what extent this simplification may affect the accuracy of the analysis cannot be foreseen at present.

Following this simplification, the equation becomes:

For the workpiece

$$\frac{\partial^2\theta}{\partial x^2}+\frac{\partial^2\theta}{\partial y^2}-\frac{V_c}{k_w}\frac{\partial\theta}{\partial x}=0 \quad\ldots\ldots [4a]$$

For the deformed chip

$$\frac{\partial^2\theta}{\partial x^2}+\frac{\partial^2\theta}{\partial y^2}-\frac{V_f}{k_c}\frac{\partial\theta}{\partial x}=0 \quad\ldots\ldots [4b]$$

where

$$k_w=\frac{K_w}{C_w\rho_w},\quad\text{and}\quad k_c=\frac{K_c}{C_c\rho_c}$$

are the thermal diffusivities of the work and chip material, respectively.

Dimensional Analysis of Heat Flow in Metal Cutting. Exact solutions for the foregoing set of equations with the boundary conditions shown in Figs. 10(a) and 10(b) are difficult if not impossible. Numerous approximate solutions have been found (4), but it is possible to generalize the results by dimensional

analysis. This theory teaches that all physical processes depend upon certain dimensionless values. It is possible to obtain these values from the differential equations without actually solving them.[8] For this purpose it is necessary to write these equations in the dimensionless form. If the subscripts are dropped from Equations [4a] and [4b], they become

$$\frac{\partial^2\theta}{\partial x^2} + \frac{\partial^2\theta}{\partial y^2} - \frac{V}{k}\frac{\partial\theta}{\partial x} = 0 \quad \ldots\ldots\ldots\ldots [4c]$$

θ is made dimensionless, by dividing it by θ_0, a known constant temperature. It will be the room temperature in Equation [4a] or the chip bulk temperature in Equation [4b]. In the same way, a length can be selected to make x and y dimensionless. In other words, let

$$\theta' = \frac{\theta}{\theta_0}, \quad x' = \frac{x}{L}, \quad y' = \frac{y}{L},$$

where L has the dimension of a length. Substitute these values into Equation [4c] and obtain

$$\frac{\partial^2\theta'}{\partial x'^2} + \frac{\partial^2\theta'}{\partial y'^2} - \frac{VL}{k}\frac{\partial\theta'}{\partial x'} = 0 \quad \ldots\ldots\ldots\ldots [4d]$$

A reasonable choice of L will be the feed t in Fig. 10(a), and the chip thickness t_c in Fig. 10(b). In the latter case, the average length of contact between the tool and the chip is another possibility.

The quantity VL/k is dimensionless, and is here referred to as the thermal number R_t. It is apparent that the solution for Equation [4d] can be written as

$$\theta' = f(R_t, x', y') \quad \ldots\ldots\ldots\ldots [5]$$

For given values of x' and y', θ' is a function of R_t only. In particular, it should be replaced by $(R_t)_w$, which is $V_s t/k_w$, for the temperature distribution in the work material and by $(R_t)_c$, which is $V_f t_c/k_c$, for the chip.

Changes in $(R_t)_w$ will alter the relative division of heat generated by the main chip shear between the chip and the work material. Changes in $(R_t)_c$ not only will affect the division of interface heat between the tool and the chip but also the temperature gradient at the interface. It is seen that for a given combination of tool and work material and for fixed tool angles, both $(R_t)_w$ and $(R_t)_c$ are important factors governing temperature conditions in metal-cutting operations. Tool-chip contact area plays an important role in affecting the interface temperature (12). Unfortunately, owing to the lack of knowledge of the nature of the contact, any quantitative relationship is difficult at the present time.

In orthogonal cutting, $V_f = V_s r_t$, and $t_c = t/r_t$ where r_t is the chip-thickness ratio. Consequently

$$(R_t)_c = (R_t)_w \frac{k_w}{k_c} \quad \ldots\ldots\ldots\ldots [6]$$

Since the thermal diffusivity of a material depends primarily upon the temperature which, in turn, is a function of $(R_t)_w$ and $(R_t)_c$, it follows that

$$\frac{k_w}{k_c} = \psi\,[(R_t)_c\ (R_t)_w]$$

This indicates that, in so far as the temperature-dependent properties which affect the mechanism of chip formation are concerned, there is no necessity to differentiate between $(R_t)_c$ and $(R_t)_w$. Accordingly, $V_s t/k_w$ shall be designated by R_t without subscripts.

This thermal number also can be derived from pure dimensional reasoning. It represents the ratio of two times—the transit time and the relaxation time of the material (13). In metal-cutting problems, it governs essentially the following:

(a) The ratio of the heat conducted from the shear zone into the workpiece to the heat convected by the moving chip. The larger the number, the smaller this ratio.

(b) The ratio of the heat conducted from the interface into the tool to the heat convected by the moving chip. With a larger thermal number, this heat ratio becomes smaller.

Like any other applications of the dimensional analysis, the theory needs experimental verification. This is particularly true for the present case in which numerous assumptions and approximations have been made.

Experimental Results. (a) *Dependence of shear zone temperature rise on thermal number:* From the cutting data presented in the first part of the paper it is possible to estimate the temperature rise at the shear zone due to main chip shear. Details have been given previously (8). Among other factors the method takes into consideration the variation of the specific heat with temperature. This latter relationship may be obtained from the ASM "Metals Handbook" (1948) for a steel having a composition similar to that used in this investigation.

The thermal diffusivity of SAE 52100 steel at room temperature has been found to be 1.03 in.^{2} per min. Fig. 11 illustrates

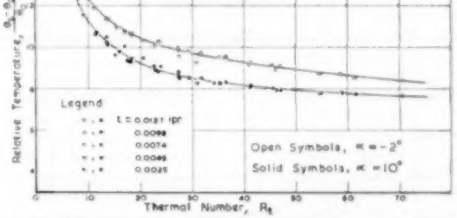

FIG. 11 DEPENDENCE OF RELATIVE TEMPERATURE ON THERMAL NUMBER
(Tool shape: O-Var-7-7-8-0-3/64.)

the results obtained by plotting the ratio of the average temperature rise at the shear zone to the initial temperature $(\theta_s - \theta_0)/\theta_0$ against the thermal number. This temperature ratio may be called the relative temperature. The scatter of the points in the plot is not great considering the wide range of cutting speeds and feeds employed in the investigation. Within the realm of continuous chips without built-up edge, it is seen that a decrease in feed and/or speed results in an increase in the chip bulk temperature. At high speeds and heavy feeds, however, this change is relatively small.

(b) *Dependence of chip-thickness ratio and shear strain on thermal number:* Chip-thickness ratio and unit shear strain are two important geometrical quantities (dimensionless) involved in metal-cutting operations. Figs. 12(a), 12(b), and 13 illustrate that they are, in general, unique functions of the thermal number and the tool-rake angle for a given combination of tool and work material. The trend of the strain-thermal number curves bears a striking resemblance to that of the relationship

[8] This method is widely used in the rational analysis of the mechanism of boundary-layer convection heat transfer.

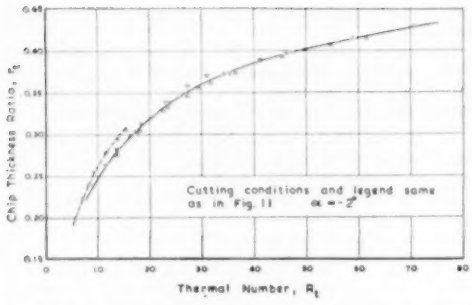

FIG. 12(*a*) DEPENDENCE OF CHIP-THICKNESS RATIO ON THERMAL NUMBER

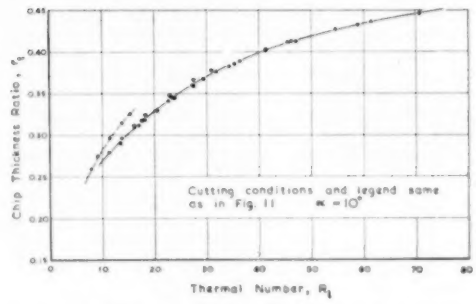

FIG. 12(*b*) DEPENDENCE OF CHIP-THICKNESS RATIO ON THERMAL NUMBER

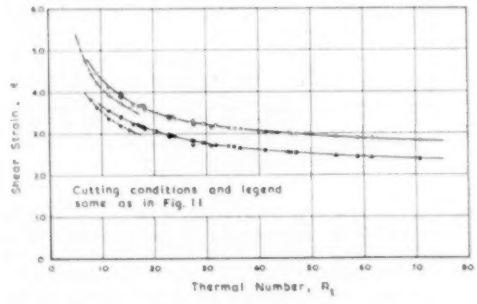

FIG. 13 DEPENDENCE OF UNIT SHEAR STRAIN ON THERMAL NUMBER

between the relative temperature and the thermal number. The dynamic flow stress S_s of the material is practically constant in nearly all cutting conditions reported in this paper. Since the work of shearing deformation, $S_s\epsilon$, is solely responsible for the heating at the shear zone it is evident that the similarity should exist.

However, critical examination of Figs. 12 and 13 reveals that at the smallest feed employed deviations worthy of consideration are apparent. A possible explanation for the deviation may be the size effect as noted in Fig. 9.

(*c*) *Coefficient of friction at tool-chip interface:* Previous reports (4) on a 0.27 C steel disclosed the existence of a functional relationship between the coefficient of friction at the interface and the thermal number for a given rake angle of the tool. However, the results of the present investigation show considerable scattering in such relationships as illustrated in Fig. 14. Feed has a definite, though relatively slight effect.

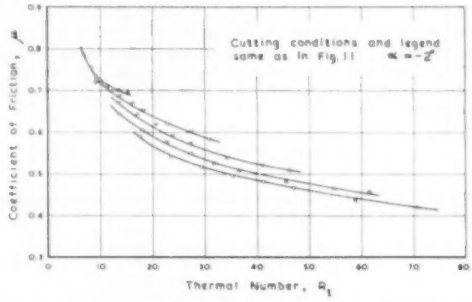

FIG. 14 RELATIONSHIP BETWEEN COEFFICIENT OF FRICTION AND THERMAL NUMBER, ILLUSTRATING THE SEPARATE EFFECT OF FEEDS

The nature of the frictional behavior at the interface can be studied best by breaking it down into its components, namely, the apparent sliding stress and the apparent contact stress. This was first suggested by Hahn in his discussion of a recent paper by two of the authors (12). Both of these stresses depend not only on the tool-chip contact area[4] but also on the temperature involved. To study this rather complex mechanism, cutting temperatures and tool-chip contact areas were determined at various speeds, feeds, and two different side-rake angles. The results are illustrated in Figs. 15(*a*), 15(*b*), and 16. The relationship of the cutting temperatures to cutting speeds is a system of approximately parallel lines on logarithmic co-ordinates.

At a chosen speed the cutting temperature increases with an increase in feed. It is noted, however, that this effect becomes smaller as the feeds are further increased. The relationship of cutting temperature to feed at constant speed is substantially a logarithmic one in the usual range of feeds (14). When compared at the same speed and feed, the difference in the interface temperature observed for the negative 2-deg and positive 10-deg side-rake tools is very slight—an antithesis of the commonly expected trend. This is thought to be due to the following two reasons:

(*a*) While the tool forces are lower for the positive 10-deg tool, the product of the frictional force at the interface and the chip flow velocity, FV_f, is practically identical for the two tools. This is shown by the calculated results in Table 2. The quantity FV_f

TABLE 2 RATE OF FRICTIONAL WORK LIBERATED AT INTERFACE AS AFFECTED BY TOOL RAKE

		FV_f, ft-lb/min	
		$\alpha = -2$ deg	$\alpha = +10$ deg
$V_c = 160$ sfpm	$t = 0.0074$ ipr	10800	10700
	$t = 0.0098$	13210	13250
	$t = 0.0127$	15750	16210
$V_c = 280$ sfpm	$t = 0.0025$	7330	7480
	$t = 0.0049$	13340	13520
	$t = 0.0098$	21700	21850
$V_c = 480$ sfpm	$t = 0.0049$	21520	21640
	$t = 0.0074$	28160	27700
	$t = 0.0127$	38380	39940

[4] All the tool-chip contact-area values reported here are apparent contact areas.

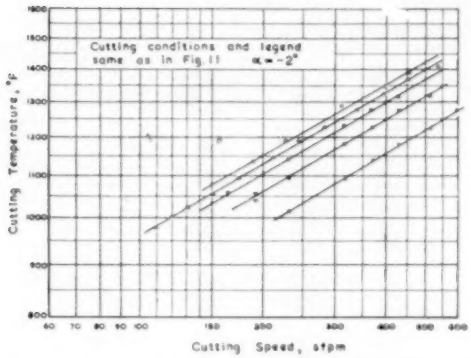

FIG. 15(*a*) CUTTING SPEED - CUTTING TEMPERATURE RELATIONSHIP AT VARIOUS FEEDS

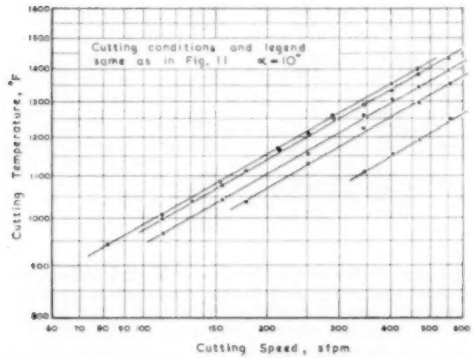

FIG. 15(*b*) CUTTING SPEED - CUTTING TEMPERATURE RELATIONSHIP AT VARIOUS FEEDS

represents the rate of heat generation at the interface and has a direct bearing on the interface temperature.

(*b*) The negative 2-deg-rake tool results in a slightly larger tool-chip contact area at a given speed and feed. The chip bulk temperature is higher due to the higher shearing strain involved, but the rise in temperature due to interface rubbing is less since the heat is distributed over a greater area. Evidently the increase in chip bulk temperature for the negative 2-deg side-rake angle is offset by the fact that the interface heat is distributed over a larger contact area. While not included in this paper, the cutting temperature - cutting speed relationship for the positive 4-deg side-rake angle is approximated by either Fig. 15(*a*) or 15(*b*). Within the range of tool angles investigated, it appears as if the side-rake angle has little effect on the average tool-chip-interface temperature. Some years ago one of the authors (15) reported a slight (3 per cent) increase in interface temperature for a negative 2° 20′ back-rake angle. Inasmuch as the latter change has a more pronounced effect in "jamming" at the nose radius and consequent change in chip formation, the two are not thought to be in conflict.

As pointed out in a previous paper (12), the steep temperature gradient existing at the interface is perhaps responsible for the

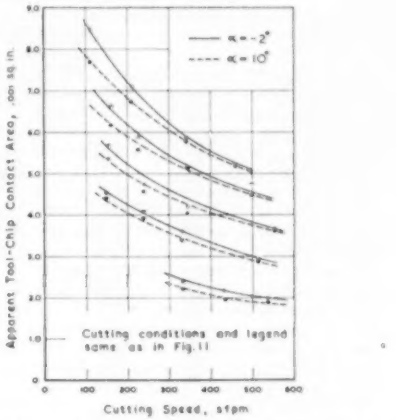

FIG. 16 RELATIONSHIP BETWEEN APPARENT TOOL-CHIP CONTACT AREA AND CUTTING SPEED AT VARIOUS FEEDS AND TWO TOOL RAKE ANGLES

variation of the coefficient of friction with speed and feed. Attempts to correlate the effect of temperature on friction behavior studied under isothermal conditions with that at the tool-chip interface are liable to be misleading. The coefficient of static friction between clean metallic surfaces has been shown by several investigators to be expressible as the ratio S/H, S being the flow stress of the material at contact, and H the mean pressure hardness of the softer of two contacting solids (which is the compressive force per unit area of the actual contact). While theories for the coefficient of kinetic friction are still lacking, it is not unreasonable to assume from the nature of frictional behavior between solids that it can be expressed by the same ratio, provided S refers to the flow stress at the interface temperature, and H refers to the compressive stress at the bulk temperature of the softer metal, i.e., chip bulk temperature. Since both S and H refer to the same contact area, it is immaterial whether the true or the apparent contact areas are used in so far as the coefficient of friction is concerned. In the foregoing discussion no account has been taken of the effect of state of stress (due, for instance, to the change in tool rake or feed). That the change in interface friction can be explained on the basis of the preceding postulate under various cutting conditions may be seen from Table 3.

It is seen that in all cases an increase in the chip bulk temperature (due to a reduction in the cutting speed and/or feed) results in a decrease in the apparent contact stress. This is due to the softening which takes place as a consequence of the heating to a higher temperature. However, when compared at equal chip bulk temperatures the contact stresses are not the same if the tool-rake angle is altered. It is thought that the higher strain associated with the negative side-rake angle is responsible for the higher apparent contact stress. Evidently temperature is not the sole factor which influences the contact stress.

The apparent frictional sliding stress decreases as the interface temperature is increased. However, an effect due to feed and tool-rake angle is also present.

Examination of the nature of contact under a magnification of 30× to 50× reveals that the stress distribution is not at all uniform. The intensity of the contact stress varies rather abruptly from zero at the point of departure of the chip from the tool face to a maximum covering only a portion of the total area. It starts

TABLE 3 EFFECT OF CHIP BULK TEMPERATURE AND INTERFACE TEMPERATURE ON TOOL-CHIP FRICTION

Room temperature = (initial workpiece temperature) = 74 F
Work material: SAE 52100 spheroidized, 187 Bhn
Tool material: Triple-carbide
Depth of cut: 0.102 in.

Cutting speed, V_c, sfpm	Coef. of friction, μ	Apparent tool-chip contact area, in.$^2 \times 10^{-2}$	Chip bulk temperature deg F	Apparent contact stress, psi (H)	Interface temp, deg F	Apparent frictional sliding stress, psi (S)
			For Tool Rake α = −2 Deg			
Feed, t = 0.0049 ipr						
200	0.71	4.23	956	60300	1062	42600
280	0.67	3.81	887	62200	1150	41700
400	0.62	3.32	818	65800	1250	40800
540	0.59	2.89	760	69600	1343	40800
Feed t = 0.0074 ipr						
160	0.67	5.54	913	55000	1051	43600
240	0.62	4.94	858	67000	1155	41600
320	0.58	4.50	804	69600	1232	40000
480	0.53	3.86	753	74800	1358	39200
Feed t = 0.0098 ipr						
160	0.61	6.57	885	7960	1075	41200
240	0.55	5.85	814	1300	1180	39300
320	0.51	5.32	780	74400	1262	37800
480	0.47	4.59	721	78500	1387	36500
Feed t = 0.0127 ipr						
160	0.54	7.72	83-	70400	1093	38300
240	0.50	6.79	782	74700	1201	37000
320	0.47	6.05	74[illegible]	79400	1282	37100
480	0.42	5.15	69[illegible]	85900	1410	36100
			For Tool Rake α = +10 Deg			
Feed t = 0.0049 ipr						
200	0.85	4.04	873	49900	1072	42200
280	0.83	3.61	800	51600	1158	42800
400	0.77	3.17	735	54600	1255	42300
540	0.72	2.85	688	57300	1346	41100
Feed t = 0.0074 ipr						
160	0.79	5.26	852	55800	1050	43800
240	0.74	4.77	777	56200	1153	41400
320	0.69	4.35	714	57900	1230	39800
480	0.61	3.84	674	70900	1352	37500
Feed t = 0.0098 ipr						
160	0.73	6.18	781	67900	1095	42100
240	0.67	5.65	731	58900	1200	39400
320	0.61	5.23	691	60800	1280	37300
480	0.54	4.56	634	65900	1406	35900
Feed t = 0.0127 ipr						
160	0.68	7.19	73[illegible]	60200	1098	40800
240	0.61	6.49	687	62800	1202	38300
320	0.56	5.94	663	66200	1285	37000
480	0.50	5.09	6[illegible]	73700	1411	36500

to decrease at an appreciable distance from the cutting edge of the tool. This nonuniformity of stress distribution may indicate the necessity of future refinement in stress calculations. It has certainly a direct bearing on tool-life problems.

Conclusions

The following conclusions are based upon conditions within the scope of this investigation; however, the authors believe that they are generally applicable.

1 Merchant's plasticity equation $2\phi + \tau - \alpha = C$ agrees with experimental results to a first degree of approximation. There is a systematic, though small, variation in C with cutting speed.

2 No correlation exists between the machining constant C and the slope of the shear stress versus normal stress curve for SAE 52100 steel. In general, the influence of the normal stress on the flow stress at the shear plane is of secondary significance.

3 In commercial high-speed metal-cutting operations, the true stress-strain relationship can be regarded as a horizontal line. The large strain involved in chip formation is possible because of the high compressive stress on the shear plane.

4 Properties of the metal at the shear zone are essentially the same as those of the uncut stock. The temperature rise at the shear zone due to chip shear has negligible effect on the dynamic flow stress of the metal. With a given tool-work combination, this flow stress can be taken as a constant, except as modified by the size effect at very small feeds.

5 For a given tool rake, the chip-thickness ratio, the shear strain, and the relative temperature rise due to main chip shear are unique functions of the thermal number $V_c t/k$, an important dimensionless quantity governing the temperature distribution as well as the division of heat among the workpiece, tool, and chip.

6 The variation in interface friction due to changes in cutting conditions can be explained in terms of temperature changes. Although it is recognized that there are other contributing factors, the frictional sliding stress calculated on the basis of apparent contact area is governed mainly by the interface temperature, while the apparent contact stress depends on the chip bulk temperature and the degree of shearing strain.

7 At a given speed and feed, the rate of frictional work expended in metal cutting is practically unaffected by changing the side rake from negative 2 deg to positive 10 deg. The cutting temperature is also practically unaffected by the same change in tool rake.

8 The cutting speed - cutting temperature relationship at various feeds forms a family of approximately parallel straight lines on logarithmic co-ordinates. At a given speed, the cutting temperatures increase with an increase in feed. This effect becomes smaller as the feed is further increased.

Acknowledgment

The authors herewith express their appreciation to The Timken Roller Bearing Company, Canton, Ohio, for the SAE 52100 steel tubing used in this investigation. Grateful acknowledgment is made to Drs. F. Seitz and J. S. Koehler, Department of Physics at the University of Illinois, for the valuable discussions pertinent to this paper. Acknowledgment is also made to Miss Irene Cunningham for the typing of this manuscript.

BIBLIOGRAPHY

1 "Mechanics of the Metal Cutting Process, II. Plasticity Conditions in Orthogonal Cutting," by M. Eugene Merchant, *Journal of Applied Physics*, vol. 16, 1945, pp. 318–324.

2 "On Torsion Combined With Compression," by P. W. Bridgman, *Journal of Applied Physics*, vol. 14, 1943, pp. 273–283.

3 "Theory of Formation of Metal Chips," by V. Piispanen, *Journal of Applied Physics*, vol. 19, 1948, pp. 876–881.

4 "The Effect of Speed and Feed on the Mechanics of Metal Cutting," by B. T. Chao and G. H. Bisacre, advance copy, The Institution of Mechanical Engineers, London, England, 1951.

5 "A Quantized Theory of Strain Hardening as Applied to the Cutting of Metals," by M. C. Shaw, *Journal of Applied Physics*, vol. 21, 1950, pp. 599–606.

6 "An Analysis of the Mechanics of Metal Cutting," by D. C. Drucker, *Journal of Applied Physics*, vol. 20, 1949, pp. 1013–1021.

7 "Structure of Metals," by C. S. Barrett, McGraw-Hill Book Company, Inc., New York, N. Y., 1943, pp. 294–298.

8 "An Analytical Evaluation of Metal-Cutting Temperatures," by K. J. Trigger and B. T. Chao, Trans. ASME, vol. 73, 1951, pp. 57–68.

9 "The Size Effect in Metal Cutting," by W. R. Backer, E. R. Marshall, and M. C. Shaw, Trans. ASME, vol. 74, 1952, pp. 61–72.

10 "Report MF/MS 37 (1950) to the Mechanical Engineering Research Board of the Department of Scientific and Industrial Research," by G. H. Bisacre, Manchester, England.

11 "Discussion of 'Progress Report No. 2 on Tool-Chip Interface Temperatures,'" by K. J. Trigger, Trans. ASME, vol. 71, 1949, pp. 171–172, by M. E. Merchant.

12 "Cutting Temperatures and Metal-Cutting Phenomena," by B. T. Chao and K. J. Trigger, Trans. ASME, vol. 73, 1951, pp. 777–793.

13 "The Life of Carbide-Tipped Turning Tools," by F. F. P. Bisacre and G. H. Bisacre, Proceedings of The Institution of Mechanical Engineers, London, England, vol. 157, 1947, pp. 452–469.

14 "Discussion of 'Distribution of Heat Generated in Drilling'" by A. O. Schmidt and J. R. Roubik, Trans. ASME, vol. 71, 1949, pp. 249–250, by K. J. Trigger.

15 "Progress Report No. 1 on Tool-Chip Interface Temperatures," by K. J. Trigger, Trans. ASME, vol. 70, 1948, pp. 91–98.

Discussion

E. J. Krabacher[7] and M. E. Merchant.[8] In the paper the authors expound some basic facts about tool-chip friction which heretofore have been unexplained. Table 3 of the paper presents data which show basic reasons for variation in the coefficient of friction μ for given changes in cutting conditions. It has been known that an increase in cutting speed results in a slight decrease in μ, and that an increase in feed results in a substantial decrease in the coefficient of friction. The data presented by the authors in Table 3 show that these changes in μ due to changes in cutting conditions are related, at least to a great extent, to temperature changes in the cutting process. Also it has been known that an increase in rake angle results in an increase in μ. From Table 3 it may be seen that an increase in rake angle gives lower values of chip bulk temperature and higher values of interface temperature, resulting in an increase in the ratio S/H or coefficient of friction μ. Here, however, the large increase in μ is due mainly to a substantial decrease in the apparent contact stress H. This leads one to believe that in this case the increase in the coefficient of friction may be due largely to a lesser degree of shearing strain (and thus to less strain hardening) which would be expected at the high rake angle under similar cutting conditions.

What the authors have done is to establish a much needed relationship between chip friction and cutting temperatures. There is at present great need for additional similar work relating cutting temperatures, tool-chip contact area, and coefficient of friction so that we may better understand this phase of the metal-cutting process. The authors are to be heartily commended for their fine work along these lines.

Early in the paper it is stated that Equation [3] is arrived at by differentiating Equation [2] with respect to ϕ and setting it equal to zero. In so doing τ was considered to be independent of ϕ. The authors question whether this is justifiable. Since they show later in the paper that τ is influenced by the chip-bulk temperature and the interface temperature, and since both of these are functions of ϕ, it is obvious that an approximation is being made when τ is considered independent of ϕ in the differentiation. The situation is quite analogous to that involved in the interdependence of S_s and ϕ, where a better approximation to experiment is obtained when S_s is expressed as an empirical function of ϕ, as by the use of Equation [1] of the paper, than when it is considered to be independent of ϕ. Thus it may be expected that a still better approximation of theory to experiment will be obtained if τ can be expressed in terms of a realistic empirical function of ϕ and introduced into Equation [2] before differentiation. It is hoped that the authors will develop such a realistic function in the course of their research and improve the theory accordingly.

The authors conclude as a result of their investigation that no correlation exists between the machining constant C and the slope of the shear stress versus normal stress curve in the case of SAE 52100 steel. This conclusion they support with Fig. 7 of the paper. The authors also point out that Bridgman's experiments, repeated by Bisacre on brass, also indicate no correlation between C and the slope of the shear stress versus normal stress curve. As a result of these findings the authors believe that there is little justification to regard this constant C to be the same as are cot k, where k is the slope of the shear-stress versus compressive-stress curve. It is with this belief that we must take issue.

The data plotted in Fig. 7 cover a wide range of shearing strain as shown in Fig. 8, values ranging from approximately 2.3 to 4.5. It is possible that, owing to the wide range of strain, the plotted data actually correspond to a series of parallel lines, each associated with a given value of strain, of some slope more in line with the computed value of C. Metal-cutting data obtained in the writers' laboratory for SAE 52100 steel over a narrower range of strain show a definite increase in shear stress with compressive stress. Data were obtained for three different treatments of this steel. The data obtained from the cutting tests made on annealed material are given in Fig. 17 of this discussion. It can be seen that the agreement obtained between the average computed value of $2\phi + \tau - \alpha$ and the value as measured from the curve relating shear stress and compressive stress agrees well within the limits of a first approximation. It may also be seen that this value of

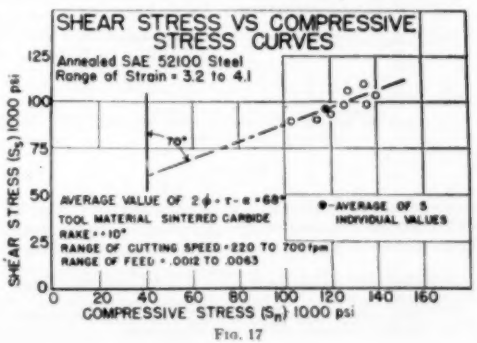

Fig. 17

[7] Research Engineer, Cincinnati Milling Machine Company, Cincinnati, Ohio. Jun. ASME.

[8] Assistant Director of Research, Cincinnati Milling Machine Company. Mem. ASME.

$2\phi + \tau - \alpha$ for the annealed SAE 52100 steel agrees closely with the value obtained by the authors for their spheroidized SAE 52100 steel. Data obtained for annealed and then cold-drawn SAE 52100 steel give a value of $2\phi + \tau - \alpha$ of 72 deg and a value of the complement of the slope angle of the curve relating shear stress and compressive stress of 66 deg, while "rocked" (severely cold drawn) SAE 52100 steel gave values of 81 and 76 deg, respectively. Therefore these data also show relatively good agreement compared to that obtained by the authors.

Tests paralleling those of Bridgman have been conducted in the writers' laboratory.[9,10] These included tests on brass. These tests, as did Bisacre's, indicated no change in shear stress for values of compressive stress up to 33,000 psi. However, this was true only for values of strain below 0.75. As the values of strain increased to values of 1 or greater, approaching those of metal cutting, a definite increase in shear stress with compressive stress was found. These higher values of strain were obtained only at values of compressive stress in excess of 40,000 psi, approaching values expected in metal cutting. An analysis of Bisacre's metal-cutting data indicates values of compressive stress S_n in the range of 50,000 to 75,000 psi, and values of strain in the range of 2 to 3. This would indicate that in Bisacre's Bridgman tests the maximum value of 33,000 psi compressive stress was not high enough to be within the range of compressive stress obtained in his metal-cutting tests. It may be concluded then that the values of strain and compressive stress obtained by Bisacre in his Bridgman tests are not comparable to those obtained in his metal-cutting tests. For this reason it is not reasonable to expect correlation between the two test methods in view of the results obtained in our own laboratory for brass.

Typical torsion-compression test data (Bridgman test) obtained in this laboratory for several steels are given in Fig. 18 and Table 4 of this discussion. The shear-stress versus compressive-stress curves in Fig. 18 show the degree of correlation obtained

TABLE 4 COMPARATIVE RESULTS OF METAL-CUTTING AND TORSION-COMPRESSION TEST DATA

		Machining constant C	
Material	Strain	Metal cutting	Torsion-compression
SAE 3115	2.9	76	79
AISI C1117	2.5	72	87
SAE 3150, spheroidized	3.1	76	85
SAE 3150, pearlitic	3.2	71	74
SAE 3450	3.0	78	83

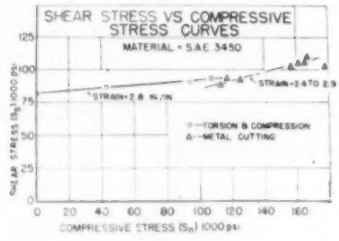

FIG. 18

between torsion-compression and metal-cutting test data for SAE 3450 steel at approximately equal values of shearing strain. These curves are typical of the correlation obtained for each of the materials presented in Table 4. It may be seen that, considering the vast differences in rate of strain, temperature, and test conditions, the agreement found may be considered good. Also, it may be seen that an increase in shear stress does occur with increasing compressive stress and that C does equal arc cot k to a first degree of approximation, which is all that the theory claims. Although these data all show support of Merchant's[11] theory of the relation between C and arc cot k, it should be borne in mind that this theory only claims to be a first approximation, and as such there obviously must be times when it will be in poor agreement with experiment, as was the case in the authors' tests. This will happen when conditions do not agree with the simple assumptions and approximations made in deriving the theoretical relationships. However, as can be seen from the data presented in this discussion, the theory as it stands does give a good approximation to experiment in many cases.

M. C. SHAW[12] AND N. H. COOK.[13] It is gratifying to note that the authors' analysis of their data leads them to the observation that normal stress on a plane of shear has negligible influence upon subrupture flow stress. This observation is in agreement with our thoughts on the matter.[14,15,16,17]

The one test of Bridgman on a high-carbon-steel specimen is the only set of data that has been uncovered in support of Equation [1] of the paper, while there are many compelling arguments that can be presented which indicate the lack of such a relationship. However, unlike the authors, we have not found Equation [3] to be in agreement with experiments. While the quantity C usually varies less than 10 per cent when the rake angle is varied from +10 to −10 deg, a more critical test of the relationship is to use values of rake angle that cover the wider range from +45 to −10 deg. When this is done the deviation between Equation [3] and experimental data is so very wide as to make it apparent that some of the reasoning leading to Equation [3] is seriously in error. The fact that the coefficient of friction is really strongly dependent upon the rake angle and, hence upon the shear angle, is one of the chief reasons for the failure of Equation [3]. The coefficient of friction is observed to vary from a value of about 0.5 for a −10-deg rake tool to a value of about 3.0 for a +45-deg-rake-angle tool when cutting dry under identical conditions. This represents a relatively enormous variation in the coefficient of friction. If there were no connection between the coefficient of friction and the rake angle, the observed coefficient of friction should remain essentially constant.

The authors have observed in Fig. 8 that the shear stress for a number of cuts does not vary significantly while the shear strain does, and from this they conclude that strain-hardening is not important in the shearing process. However, the increased hardness of chips is acknowledged, and an attempt is made to explain this inconsistency in terms of the dislocation theory. According to dislocation theory, a strain of 1 atom spacing results when a single dislocation travels across a crystallite and becomes stuck.

Strain hardening is thought to result from the "back stress"

[9] "Torsion and Compression Testing," by J. Kemeny, University of Cincinnati thesis, 1947.

[10] "Torsion and Compression Testing," by E. J. Krabacher and K. W. Whisler, University of Cincinnati thesis, 1949.

[11] Refers to authors' Bibliography (1).

[12] Head, Machine Tool Division, Department of Mechanical Engineering, Massachusetts Institute of Technology, Cambridge, Mass. Mem. ASME.

[13] Instructor, Department of Mechanical Engineering, Massachusetts Institute of Technology.

[14] Discussion of "Correlation of Plastic Deformation During Metal Cutting With Tensile Properties of the Work Materials," by J. T. Lapsley, Jr., R. C. Grassi, and E. G. Thomsen, Trans. ASME, vol. 72, 1950, p. 979.

[15] Discussion of "Basic Factors in Hot-Machining of Metals," by E. J. Krabacher and M. E. Merchant, Trans. ASME, vol. 73, 1951, p. 761, by M. C. Shaw.

[16] See discussion to authors' Bibliography (4).

[17] See authors' Bibliography (5).

that progressively increases as the number of stuck dislocations increase with strain. Thus strain hardening obviously is associated with the straining process itself and so intimately so that the two cannot be separated. This conclusion also follows from the other current explanation of strain hardening—the crystallite theory of Bragg. According to this point of view, strain hardening results from the fragmentation of larger grains into smaller crystallites of very slightly varying crystal orientation when slip occurs. Again according to this point of view, strain hardening must accompany slip. It cannot occur after slip has ceased.

We have observed cutting shear-stress values to decrease with increased chip strain to an even greater extent than that indicated in Fig. 8, and have been disturbed by this anomalous result. However, close study of many motion pictures of the cutting operation taken through the microscope have revealed the shear zone actually to increase in thickness whenever conditions are changed to provide a thicker chip, i.e., for a greater shear strain. This increase of the thickness of the shear zone provides a lower shear stress for a given shear strain as a result of a size effect and a decrease in the rate of strain. The details of this mechanism have been presented elsewhere.[18,19] From this work it would appear that the data points in Fig. 8 are not points on a single stress-strain curve, but are rather points located on a multiplicity of stress-strain curves, each one showing pronounced strain hardening. It is just as though the material were different and had a different stress-strain relationship for each of the cuts, corresponding to each data point. Thus nothing can be said regarding the tendency for a metal to strain-harden from consideration of Fig. 8.

As the authors have mentioned, Drucker and others have claimed that metals tend to behave as ideal plastics when deformed at high rates of strain. Careful examination of the literature reveals that these observations are all based upon high-speed tensile tests of the engineering type. It is well known that ordinary materials actually exhibit negative strain hardening when stress-strain data are plotted on the engineering basis, even though the corresponding true stress-true strain data will always reveal a positive strain-hardening characteristic for such metals. The only data of which the writers have knowledge that may be consulted in attempting to establish the influence of rate of strain on the strain-hardening tendency are some true stress-true strain results obtained in the Materials Laboratories at M.I.T.[20,21] These tests show a significant increase in the strain-hardening tendency when the strain rate is increased from 10^{-3} to 10^{3} sec^{-1}.

Unfortunately, the authors' differential Equations [4], [4*a*], and [4*b*] are not capable of yielding the temperature at any point in the chip or workpiece as stated. An important term has been omitted without which the boundary conditions at the tool face and shear plane could not be satisfied. The missing term is that due to the heat source at either the tool face or shear plane. Equation [4] should correctly read

$$\frac{\partial}{\partial x}\left(K\frac{\partial\theta}{\partial x}\right)+\frac{\partial}{\partial y}\left(K\frac{\partial\theta}{\partial y}\right)-V\frac{\partial}{\partial x}(\rho C\theta)+q=0 \quad \ldots [7]$$

where q is the rate at which heat is added per unit volume at the source, and all other quantities are as defined in the paper. The quantity q will be $\dot{\gamma}_s$, the specific shear energy rate for the shear plane, and $\dot{u}_f$ the specific friction energy rate (in lb per cu in. per sec) for the tool face. The temperature at any point in the workpiece or chip will depend upon both $\dot{\gamma}_s$ and $\dot{u}_f$.

Since the dimensional analysis presented was based upon the incomplete differential equation, it too is incorrect since important quantities have been omitted. The variable θ_0 (the ambient temperature) is a trivial one and should not be included in the dimensional analysis, since this quantity will be practically constant compared with the values of θ that obtain in the chip and workpiece. When this is realized, it is evident that Equation [5] is incorrect, for none of the three quantities in the function f contains the dimension temperature.

Equation [7] of this discussion, combined with physical reasoning, shows that the following variables must be included in the dimensional analysis for temperature:

- θ = temperature at any point (x, y)
- K_1 = thermal conductivity of workpiece
- K_2 = thermal conductivity of tool
- ρC = volumetric specific heat of work material (Btu per cu in. per deg)

} to fix thermal properties of system

- t = depth of cut
- a = length of chip-tool contact in direction of chip flow
- b = width of cut
- ϕ = shear angle
- α = rake angle

} to fix size and geometry of system

- V = a characteristic velocity which we will take as cutting speed
- $\dot{u}_f$ = rate of shear energy dissipated per unit volume
- $\dot{u}_s$ = rate of friction energy dissipated per unit volume

In taking the latter two quantities as measures of the source strength q, it is assumed that all of the friction and shear work appears in the form of thermal energy. This has been shown to be the case for the large strains involved in metal cutting.[22]

A total of twelve variables is required in this problem. However, we need not use these particular quantities, but may substitute others whenever a functional relationship connects the new and the old variables in a fixed way. For example, we may use the quantities u_s and u_f in the analysis in place of $\dot{u}_s$ and $\dot{u}_f$, since a characteristic velocity V already has been included.

Thus it is evident that the temperature at any point (x, y) will be

$$\theta=\psi(K_1, K_2, \rho C, t, a, b, \phi, \alpha, V, u_f, u_s) \quad \ldots [8]$$

By following the usual procedures of dimensional analysis[23] we may write

$$\frac{\theta\rho C}{u_s}=\psi_1\left(\frac{Vt}{k_1}, \phi, \alpha, \frac{a}{t}, \frac{b}{t}, \frac{u_f}{u_s}, \frac{K_2}{K_1}\right) \quad \ldots [9]$$

where

[18] "The Rotary Cutting Tool," by M. C. Shaw, P. A. Smith, and N. H. Cook, published in this issue, pp. 1065–1078.

[19] "Visual Metal-Cutting Study," by N. H. Cook and M. C. Shaw, *Mechanical Engineering*, vol. 73, 1951, pp. 922-923.

[20] "Rapid Tension Tests Using the Two Load Method," by A. V. de Forest, Technical Publication No. 1393C AIME; *Metal Technology*, December, 1941.

[21] "The True Stress-Strain Tension Test—Its Role in Modern Materials Testing," by C. W. MacGregor, *Journal of The Franklin Institute*, vol. 238, 1944, p. 130.

[22] "Surface Temperatures in Grinding," by J. O. Outwater and M. C. Shaw, Trans. ASME, vol. 74, 1952, pp. 73–86.

[23] "Analysis and Lubrication of Bearings," by M. C. Shaw and E. F. Macks, McGraw-Hill Book Company, Inc., New York, N. Y., 1949, chapt. 3.

$$k_1 = \frac{K_1}{\rho C}$$

It is thus evident that the nondimensional temperature quantity is a function not only of the nondimensional group the authors call the "thermal number," but also of several other quantities.

In Fig. 11 the authors consider the temperature along the shear plane θ_s. Now, this particular temperature will be influenced a negligible amount by the last five quantities in Equation [9] of this discussion. We could have omitted these quantities from the foregoing dimensional analysis if we had been interested in the shear-plane temperature θ_s only. In this case Equation [9] would become

$$\frac{\theta_s(\rho C)}{u_s} = \psi_2\left(\frac{V_t}{k_1}, \phi\right) \quad [10]$$

While Equation [10] will give good results for shear-plane temperatures, the more general Equation [9] must be used for a general chip or workpiece temperature. The authors have emphasized the importance of the thermal number VL/k. It should not be overlooked that there are seven other equally important nondimensional numbers in the general case

$$\left(\frac{\theta\rho C}{u_s}, \phi, \alpha, \frac{a}{t}, \frac{b}{t}, \frac{u_f}{u_s}, \text{ and } \frac{K_2}{K_1}\right)$$

The complete physical equation corresponding to Equation [10] has been derived in a recent paper.[12]
Here it was found that

$$\frac{\theta_s(\rho C)}{u_s} = \frac{1}{1 + 1.33\sqrt{\frac{k_1 \cot \phi}{Vt}}} \left(\text{for } \frac{Vt}{k_1} > 20 \tan \phi\right) \quad [11]$$

a result which obviously is in agreement with Equation [10] from dimensional analysis. Equation [11] is shown plotted in Fig. 19 of this discussion, with shear angle as parameter. It may be seen

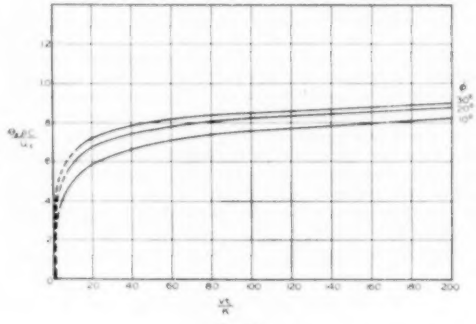

FIG. 19

that the shear-plane temperature is not altered significantly by slight changes in shear angle ϕ. The quantity on the right side of Equation [11] must always be less than 1, since it is equal to the percentage of the total thermal energy which goes to the chip. For values of $\frac{Vt}{k_1} < 20 \tan \phi$, an equation other than Equation [11] must be used, and obviously θ_s must go to zero when Vt/k_1 is zero.

In view of the authors' conclusion that the temperatures developed during cutting have negligible influence upon the shear process, the question might be asked why it was considered significant to plot shear strain against the thermal number (Fig. 13 of the paper). Actually, the temperatures associated with cutting do play a significant role in the amount of strain (and hence stress) that is present in the process. Reasons for this fact may be had by applying the concepts of this discussion.

Since this paper discusses a number of the most controversial subjects in the field of metal cutting, it is not surprising that some disagreement in interpretation should exist. The foregoing discussion should in no way detract from the credit that is due the authors for making available such a complete set of carefully obtained data and their efforts to elucidate some of the more stubborn problems of cutting.

AUTHORS' CLOSURE

The authors wish to thank all the discussers for their efforts in putting forward many valuable comments and experimental data concerning some of the fundamental yet highly controversial subjects in the theory of metal cutting. The divergence of opinion among the individual discussers on such basic issues as the effect of normal stress on the dynamic shear stress of the material, and the significance of strain-hardening during high rates of straining, clearly manifests the further need of more work along similar lines.

The torsion-compression test data furnished by Mr. Krabacher and Dr. Merchant on several constructional steels are welcome additions. It is gratifying to note that such basic studies are being carried out in Dr. Merchant's laboratory. Of more significance is the fact that, in the case of α-brass, the increase in shear stress with compressive stress is observed only when the value of strain reaches unity or greater. Nevertheless, in correlating any result obtained under quasi-static test conditions with that observed in high-speed chip formation, one should not lose sight of the strong adiabatic effect associated with the latter.

Mr. Krabacher and Dr. Merchant indicate that the true shape of the S_s versus S_n curve can be obscured by using a wide range of shearing strains as was done in Fig. 7 of the paper. They concede that if data corresponding to a narrower range of strain were plotted, the result would be a family of parallel lines, each of identical slope equal to cot C. With the wide range of cutting variables employed in this investigation, it is possible to obtain by calculation various compressive stress on the shear zone and the accompanying dynamic shear stress within very narrow ranges of strain. The results of such calculation are given in Fig. 20 and Table 5 of this closure.

It is apparent, therefore, that for the spheroidized SAE 52100 steel tested, no increase of S_s with S_n takes place for any strain below 3.6. On the contrary, for the three strain values of 2.5, 3.0, and 3.3, a slight decrease can be observed.

TABLE 5 RELATIONSHIP BETWEEN NORMAL STRESS (COMPRESSIVE) AND DYNAMIC SHEAR STRESS OF SAE 52100 STEEL AT VARIOUS STRAINS

Shear strain ϵ	Dynamic shear stress, S_s	Normal stress (compressive), S_n
2.53 ± (.01)	102000	99900
(+10° rake)	102700	95400
	103400	97500
$3.00\left(\begin{matrix}+.06\\-.03\end{matrix}\right)$	99900	115000
	100900	99500
(+10° rake)	101400	103000
$3.00\left(\begin{matrix}+.04\\-.03\end{matrix}\right)$	98700	119000
	99900	112500
(−2° rake)	99600	113000
$3.30\left(\begin{matrix}-.05\\-.08\end{matrix}\right)$	100500	110000
(+10° rake)	101400	103000
$3.30\left(\begin{matrix}+.06\\-.0\end{matrix}\right)$	98700	123000
	99500	129000
(−2° rake)	99800	118000
$3.60\left(\begin{matrix}+.08\\-.02\end{matrix}\right)$	95900	114700
	97000	121900
(−2° rake)	99500	129000
$3.90\left(\begin{matrix}+.06\\-.01\end{matrix}\right)$	94900	113500
	93800	119800
(−2° rake)	97800	125700

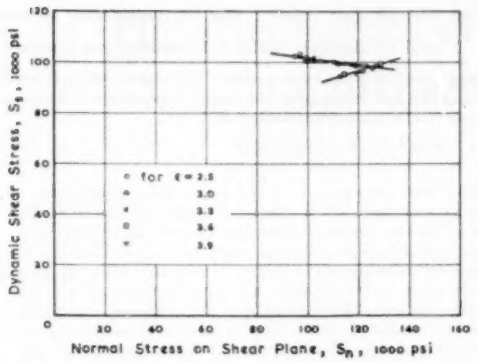

FIG. 20 EFFECT OF NORMAL STRESS ON DYNAMIC SHEAR STRESS AT VARIOUS STRAINS

(Work material: SAE 52100, 187 Bhn. Tool material: triple carbide. Depth of cut: 0.102 in. Cutting-speed range: 160 sfpm to 480 sfpm Feed range: 0.0049 ipr to 0.0127 ipr.)

A minor error has been made by Mr. Krabacher and Dr. Merchant when they use the angle between the inclined straight line and the vertical, Fig. 17, as obtained by measurement with a protractor for "direct" comparison with the value of C in Equation [3] of the paper, inasmuch as the scales used for the abscissa and the ordinate in Fig. 17 are not identical. Had equal scales been adopted, the angle would have been 65.2 deg instead of 70 deg.

Professor Shaw and Mr. Cook put great emphasis on the dependence of the tool-chip friction upon the rake angle per se, but have apparently ignored the basic cause for the existence of such a relationship. As correctly pointed out by Mr. Krabacher and Dr. Merchant, the large increase in μ is due mainly to the decrease in the apparent contact stress as a result of the lesser degree of shear strain associated with a high rake tool under otherwise identical conditions.

The dislocation theory has not yet reached the stage where we can predict the shape of the stress-strain curve of a polycrystalline metal under extremely high rates of loading. However, it is undoubtedly true today that this theory constitutes a very powerful and versatile approach to problems involving permanent deformation. When load is applied to a single crystal, permanent strain will result when the stress is large enough to cause the dislocation to move. It may be either of the Taylor-Orowan type or of the Burgers type. According to Taylor's original theory of work-hardening,[24] it is the interaction among the dislocations and the increase in the density of dislocation lines which call for an increase of stress for further deformation. Nevertheless, the speed at which a dislocation can travel and that at which the multiplication of dislocations can take place are definitely less than that of sound in the same material. This is concluded directly from energy considerations.[25] Under typical conditions, it may be less than 1/10 of the acoustic velocity.[26] Thus, if the strain rate is high enough, it is possible that the slip planes adjacent to the one on which movement already has taken place will start its movement before the dislocation can cluster and block its motion. As a result, the usual strain-hardening effect might disappear during the extremely short interval when deformation takes place.

Professor Shaw and Mr. Cook have stated that Equation [4] of the paper is not correct and formulated Equation [7] in its stead. The fallacy of this statement can be readily seen if one considers the "heat balance" of the elementary rectangular volume $ABCD$ in Fig. 10(a) or 10(b), which is at any arbitrarily chosen point (x, y) in the "interior" of the solid. The differential equation of heat conduction as given by Equation [4] was precisely derived on this basis, and is therefore valid for any interior point either in the work material or in the chip, provided suitable values of K, C, ρ, and V are assigned to the respective case as explained in the paper. For the work material, the main heat source is the shear zone which is at the "boundary" in so far as the workpiece is concerned. The tool-chip interface forms an additional source for the chip and it is also located at the boundary. The importance of segregating the general differential equation which should be satisfied by the temperature field at any interior point from the conditions at the boundary cannot be overemphasized. In fact, this forms the basic theme of the so-called "boundary-value" problems in the solution of partial differential equations. Since q does not exist in the interior of the solid, Equation [7] is thus incorrect and should be discarded.

Equation [4a] or [4b], as it stands, will yield an infinite number of possible solutions, all containing the dimensionless number R_t. However, if one were to seek the temperature distribution in the workpiece, a particular solution is required which should satisfy not only the differential equation itself but also the conditions at the boundary. This is where u_1, ϕ ... and so on, will come into the mathematical expression for temperature under given cutting conditions. Exact solutions are not known. The confusion which Professor Shaw and Mr. Cook introduce apparently results from their failure to differentiate the boundary condition from the differential equation proper.

A more complete dimensional analysis of metal-cutting problems was given by Bisacre and Bisacre.[27] While Equation [10] as derived by Professor Shaw and Mr. Cook is correct, they apparently are unaware of the fact that the shear angle ϕ itself is dependent on the thermal number R_t for a given rake angle in orthogonal cutting operations. This was first pointed out by Chao and Bisacre.[28] To see if this were also true for the spheroidized SAE 52100 steel, values of ϕ are calculated from the cutting

[24] "The Mechanism of Plastic Deformation of Crystals. Part I," by G. I. Taylor, *Proceedings of Royal Society*, London, England, series A, vol. 145, 1934, pp. 362–387.

[25] "The Theory of Plastic Flow in Single Crystals," by F. Seitz, *A Symposium on the Plastic Deformation of Crystalline Solids*, Mellon Institute, Pittsburgh, Pa., 1950.

[26] "Multiplication Processes for Slow-Moving Dislocations," by F. C. Frank and W. T. Read, Jr., ibid.

[27] Authors' Bibliography (13).

[28] Authors' Bibliography (4).

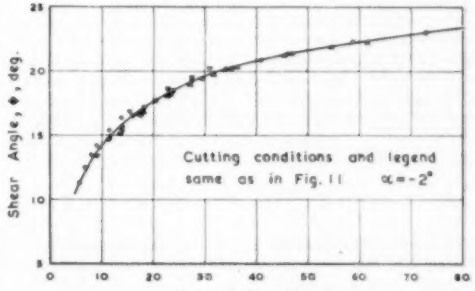

FIG. 21 RELATIONSHIP BETWEEN SHEAR ANGLE AND THERMAL NUMBER AT A FIXED TOOL RAKE IN ORTHOGONAL CUTTING; TYPE 2 CHIP

data at various R_t and results are plotted in Fig. 21 of this closure, for the negative 2-deg-rake tool. Similar results have been obtained for the positive 10-deg tool.

It is due to the existence of such a unique relationship between the shear angle and the thermal number and the fact that temperatures developed during cutting have negligible influence on the dynamic shear property, that this dimensionless product $\frac{V_c t}{k}$ plays an important role in the thermophysical aspects of high-speed chip-formation process. For a given tool and work material, and with a given tool rake, the specific shear energy u_s is evidently solely determined by R_t.

The Mechanics of Three-Dimensional Cutting Operations

By M. C. SHAW,[1] N. H. COOK,[2] and P. A. SMITH,[3] CAMBRIDGE, MASS.

The oblique tool, which has a cutting edge that is inclined to the direction of motion of the workpiece at an angle other than 90 deg, represents the most general type of cutting tool. The more complex three-dimensional tools of production may be related to an equivalent oblique tool having a given inclination angle and a corresponding effective rake angle. In this investigation the chip-flow direction and the velocity and force relations for an oblique cutting tool were compared with experimental results. The angle between the direction of chip flow and a normal to the cutting edge was found to be approximately equal to the inclination angle for ordinary friction conditions, but to be progressively larger than the inclination angle as the friction decreased. The effective rake angle for an oblique tool is found to increase without a corresponding decrease in the included tool angle. The direction of the force component in the tool face was found to deviate considerably from the chip-flow direction, particularly for larger values of inclination angle. However, the directions of maximum shear stress and shear strain on the shear plane were found to be nearly colinear for values of inclination up to 30 deg. The analytical consequences of these observations are discussed. The method of applying the oblique-tool results to three-dimensional tools is illustrated by three examples involving a lathe tool, a face-milling cutter, and a drill point. The drill-point discussion is extended to illustrate the value to be derived from a qualitative application of basic oblique-tool mechanics to the interpretation of drill test data.

Introduction

THE mechanics of a two-dimensional cutting tool in which the cutting edge is perpendicular to the cutting-velocity vector have been established independently by Merchant (1)[4] and Piispanen (2), and the results of these investigations are in good agreement with experimental data. Such cutting operations are sometimes referred to as "orthogonal." While most commercial tools are three-dimensional, there are some practical orthogonal cases. These include some finishing-planer operations, some surface-broaching operations, the lathe cut-off operation, and some plain-milling operations. Representative three-dimensional cutting tools are single-point tools with inclination or helix angle, the conventional lathe tool, the face-milling cutter, and the drill. These three-dimensional cases are not nearly as well understood as the simple orthogonal process. Noteworthy attempts to extend the orthogonal cutting mechanics to three-dimensional processes have been made by Merchant (3), Stabler (4), and Kronenberg (5). In this paper we shall re-examine the three-dimensional tool problem and attempt to correct some of the errors and misconceptions of the previous investigators. In so doing, it is hoped that a greater number of discrepancies will not have been introduced.

Cutting With Inclination

The simplest three-dimensional cutting tool is a straight cutting edge that is inclined to the velocity vector, Fig. 1(*b*). Inclination *i* is the distinguishing feature of all three-dimensional cutting operations and represents the point of departure from the orthogonal case. Inclination significantly alters chip flow and hence the performance of a tool. We shall first direct our attention to the oblique cutting tool with inclination.

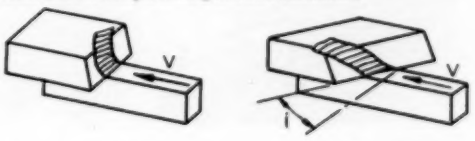

Fig. 1 Comparison of Orthogonal and Oblique Cutting Operations
(a, Orthogonal cut. b, Oblique cut.)

Two distinct rake angles are frequently employed in discussing a tool, and these may be defined as follows:

1 The "normal" rake angle α_n (sometimes called the oblique rake angle) is the angle measured from a normal to the finished surface in a plane perpendicular to the cutting edge (plane *OA* in Fig. 2). This is the angle most frequently specified and most easily measured, but is not the rake angle of greatest significance.

2 The velocity rake angle α_v (unfortunately sometimes referred to as the true rake angle[5]) is the angle measured from a normal to the finished surface in a plane containing the cutting-velocity vector (plane *OB* in Fig. 2). This particular rake angle is insignificant and is mentioned here only because it has received so much attention from previous investigators.

We may readily express α_v in terms of α_n as follows

$$\tan \alpha_v = \frac{\tan \alpha_n}{\cos i} \quad \ldots\ldots [1]$$

While the normal and velocity rake angles are easily measured, they are not of fundamental significance in the cutting process.

[1] Associate Professor of Mechanical Engineering, Massachusetts Institute of Technology. Mem. ASME.

[2] Instructor in Mechanical Engineering, Massachusetts Institute of Technology.

[3] Associate Professor of Mechanical Engineering, Massachusetts Institute of Technology. Mem. ASME.

[4] Numbers in parentheses refer to Bibliography at end of paper.

Contributed by the Production Engineering Division and Metal Cutting Data and Bibliography and Cutting Fluids Research Committees and presented at the Annual Meeting, Atlantic City, N. J., November 25-30, 1951, of The American Society of Mechanical Engineers.

Note: Statements and opinions advanced in papers are to be understood as individual expressions of their authors and not those of the Society. Manuscript received at ASME Headquarters, August 22, 1951. Paper No. 51—A-61.

[5] Not all investigators agree on a single definition. Kronenberg (5) has assigned the term true rake to the angle defined above as the velocity rake, while the American Standards Association (6) defines the rake angle we shall later define as the effective rake angle, as the true rake angle.

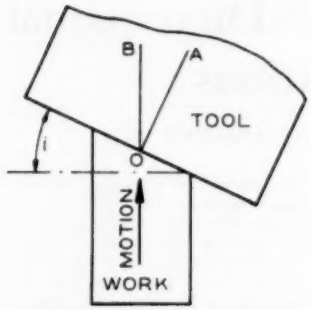

FIG. 2 PLAN VIEW OF CUTTING TOOL WITH INCLINATION

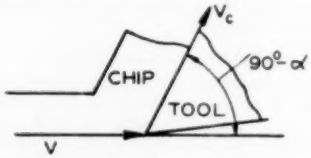

FIG. 3 ANGLE THROUGH WHICH METAL IS DEFLECTED IN ORTHOGONAL CUTTING

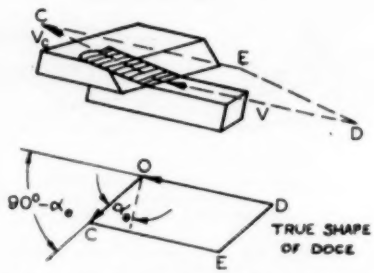

FIG. 4 EFFECTIVE RAKE ANGLE FOR OBLIQUE CUTTING TOOL

In Fig. 3 the complement to the rake angle in orthogonal cutting ($90-\alpha$) is seen to measure the angle through which the metal is deflected by the tool. In general, the greater this angle ($90-\alpha$), the greater will be the cutting work required. It is truly unfortunate that the importance of this more natural angle was not originally recognized and the rake angle so defined. In comparing three-dimensional cutting data with orthogonal data, we should adopt an effective rake angle that is comparable to that used in the two-dimensional case. Thus the effective rake angle for the oblique tool in Fig. 4 should be related to the cutting-velocity vector *DO* and the chip-flow direction *OC*, and therefore should be measured in the plane of *DO* and *OC*. The effective rake angle is labeled α_e, and it is evident in Fig. 4 that the metal is deflected through an angle ($90-\alpha_e$) as it passes across the oblique tool face. Hence α_e should play the same role in oblique cutting as α does in orthogonal cutting.

CHIP-FLOW DIRECTION

In order to determine the effective rake angle α_e for any tool with inclination, it is necessary to know the direction the chip takes as it crosses the tool face. This is most effectively specified by the angle η_c between the chip-flow direction and the normal to the cutting edge, as measured in the plane of the tool face, Fig. 5. Stabler (4) has shown that when angle η_c is known, the effective rake angle α_e may be determined readily as follows

$$\sin \alpha_e = \sin \eta_c \sin i + \cos \eta_c \cos i \sin \alpha_n \quad [2]$$

Now η_c may be directly measured in a number of ways, including:

1 Directly with a protractor as the chip flows across the tool face.

2 From chip-width measurements.

The second method has been found the most precise, particularly at the higher cutting speeds and hence will be described in detail. In Fig. 6 it is evident that for any arbitrary chip-flow direction η_c

$$\cos \eta_c = \frac{b_c}{b/\cos i} \quad [3]$$

where b_c is the width of the chip (*FC* in Fig. 6); b is the width of the work (*OG* in Fig. 6). Thus chip flow direction η_c may be determined simply from measurements of chip and work width. In making the chip-width measurement b_c, it is preferable to use a measuring microscope to measure distance *OF* on the face of the chip, Fig. 7, rather than a micrometer, which will measure horizontally.

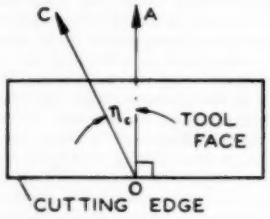

FIG. 5 VIEW OF TOOL NORMAL TO TOOL FACE, SHOWING MANNER OF SPECIFYING CHIP FLOW DIRECTION *OC*

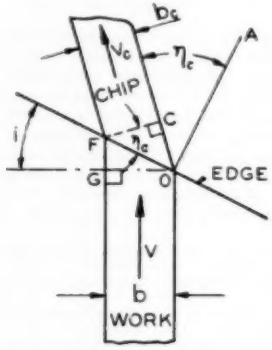

FIG. 6 PLAN VIEW OF OBLIQUE CUTTING TOOL

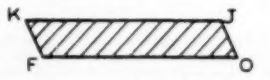

FIG. 7 TRAPEZOIDAL SHAPE OF CROSS SECTION OF CHIP IN FIG. 6

zontal distance OK. It is difficult to measure distance OF with satisfactory precision when cutting conditions are poor and there is an appreciable built-up edge. For this reason, experiments to determine η_c were conducted using an effective fluid (carbon tetrachloride) and at speeds low enough for the fluid to have ample opportunity to function. The tool used was wider than the workpiece and could be given any inclination up to 45 deg. The planing operation was used as shown in Fig. 8.

The results of these slow-speed planing tests are given in Table 1. Here the values labeled η_c were obtained by use of Equation [3], while those designated η_c' were obtained by direct measurement. The agreement is seen to be very good in most cases, but where a difference is indicated, the η_c-values are thought to be more precise than the η_c'-values. A study of Table 1 will reveal that angle η_c decreases when a cutting variable is changed that normally decreases the coefficient of friction.

Thus it is found that:

1 η_c decreases as rake angle (α_n) is increased.

2 η_c increases when a more efficient cutting fluid is used.

3 η_c increases as the friction characteristics of the metal cut improve (cold-drawn steel as opposed to soft aluminum which usually exhibits inferior friction characteristics to those of harder steel).

The angle η_c is evidently sensitive to changes in cutting conditions that normally give rise to a significant change in the coefficient of friction. At the same time η_c is seen to be little affected by changes in depth of cut t, or cutting speed V.

The angle η_c is seen generally to increase with the inclination angle i, and Stabler (4) reports that experimentally the angle η_c was equal to the angle i, for all test conditions he investigated, including tool and work materials, rake angles, and speeds. In the following discussion we will refer to this observation as Stabler's rule of chip flow. The data of Table 1 are shown plotted in Fig. 9, together with Stabler's rule. From this it is evident that chip-flow direction is not simply a matter of geometry as proposed by Stabler, but is also influenced by other considerations, which include chip friction as already mentioned. Re-examination of the data of Table 1 shows that Stabler's rule is approached as the cutting process becomes less efficient, i.e., as the coefficient of friction increases.

FIG. 8 PLANING APPARATUS WITH TOOL CAPABLE OF BEING GIVEN ANY INCLINATION

(Three-dimensional cutting dynamometer for measuring forces will be described later.)

TABLE 1 VALUES OF CHIP-FLOW DIRECTION FOR OBLIQUE CUTTING TOOLS

Quantity varied	Rake angle, α, deg	Depth of cut, t, in.	Cutting speed, V, ipm	Fluid	i, deg	η_c', deg	b_c, in.	η_c, deg
(SAE 1015 COLD ROLLED STEEL b = 0.248 IN.)								
α	−10	0.002	20	CCl_4	30	48	...	...
↓	0	↓	↓	↓	↓	49	0.191	48
↓	10	↓	↓	↓	↓	41	0.219	40
↓	30	↓	↓	↓	↓	35	0.234	35
i	10	↓	↓	↓	0	0	0.248	0
↓	↓	↓	↓	↓	15	25	0.237	23
↓	↓	↓	↓	↓	30	41	0.222	39
↓	↓	↓	↓	↓	45	60	0.185	58
↓	↓	0.006	↓	↓	15	29	0.236	24
↓	↓	↓	↓	↓	30	45	0.209	43
↓	↓	↓	↓	↓	45	58	0.187	58
t_c	↓	0.002	↓	↓	30	41	0.222	39
↓	↓	0.004	↓	↓	↓	45	0.203	45
↓	↓	0.006	↓	↓	↓	45	0.212	43
↓	↓	0.008	↓	↓	↓	46	0.212	42
↓	↓	0.012	↓	↓	↓	45	0.218	41
V_f	↓	0.006	1.0	↓	↓	43	0.209	43
↓	↓	↓	5.5	↓	↓	43	0.201	46
↓	↓	↓	20	↓	↓	45	0.212	42
Fluid	↓	0.008	↓	CCl_4	↓	46	0.212	42
↓	↓	↓	↓	ethanol	↓	36	0.243	34
↓	↓	↓	↓	benzene	↓	32	0.248	30
↓	↓	↓	↓	oil	↓	36	0.257	22
↓	↓	↓	↓	dry	↓	27	...	...
(ALUMINUM b = 0.248 IN.)								
α	−10	0.006	20	CCl_4	30	45	0.212	42
↓	0	↓	↓	↓	↓	40	0.244	32
↓	10	↓	↓	↓	↓	32	0.269	...
↓	30	↓	↓	↓	↓	27	0.258	...
i	10	↓	↓	↓	15	15	0.250	0
↓	↓	↓	↓	↓	30	32	0.253	24
↓	↓	↓	↓	↓	45	44	0.259	43
↓	30	↓	↓	↓	15	15	0.255	7
↓	↓	↓	↓	↓	30	27	0.255	27
↓	↓	↓	↓	↓	45	44	0.250	45

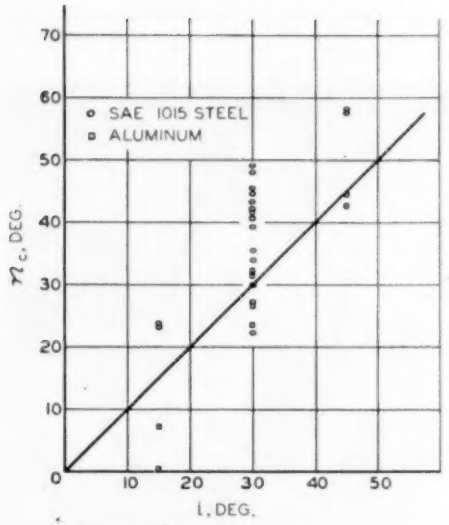

FIG. 9 RELATIONSHIP BETWEEN ANGLES η_c AND i (Stabler's rule.)

The physical significance of Stabler's rule may be recognized by reference to Equation [3]. Here it is evident that when η_c is said to be equal to i, this is the same as saying that the chip width b_c is the same as the work width b. Thus Stabler's rule merely says that the chip will take a direction relative to the cutting edge such that there is no change in width as the metal crosses the cutting edge. While this is known to be a very good approximation in orthogonal cutting, where side flow is usually negligible, it is seen to be but a first approximation for a tool having inclination.

Kronenberg (5) has assumed that the velocity rake angle α_v (which he refers to as the true rake angle) is the significant rake angle of a tool with inclination. This is equivalent to saying that chip flow will be in direction OB in Fig. 2. We may compute angle AOB in Fig. 2 readily, which will be designated γ, to obtain

$$\tan \gamma = \tan i \sin \alpha_n \quad \ldots\ldots\ldots\ldots\ldots\ldots [4]$$

Now, according to Kronenberg's assumption, the chip-flow angle η_c should be equal to this angle γ. In Fig. 10 the data of Table 1 are shown plotted with tan i as the abscissa and tan η_c as ordinate. The lines refer to Equation [4] with η_c substituted for γ—one line for each value of α_n tested. Here it is evident that Kronenberg's assumption is not at all in agreement with experiment.

This is the picture as we now see it. Stabler's rule presents a better basis for predicting the chip-flow direction than the true-rake-angle method, but still leaves something to be desired with regard to accuracy. Friction obviously plays a significant role. It should be observed, however, that the friction is not apt to be as low in practice as the values obtained at slow speed using carbon tetrachloride and hence practical deviations from Stabler's rule considerably less than the maximum observed in Table 1 should be expected in practice. At any rate, we are obliged to use Stabler's rule until a better approximation to fact is to be found.

When Equation [2] is simplified by use of Stabler's rule, we obtain

$$\sin \alpha_v = \sin^2 i + \cos^2 i \sin \alpha_n \quad \ldots\ldots\ldots\ldots\ldots\ldots [5]$$

A plot is to be found in Fig. 7 of reference (3) that is very helpful in the application of Equation [5].

VELOCITY RELATIONS

Once the chip-flow direction is established, the velocity and strain relations for oblique cutting follow directly from geometry. While most of the equations of this section previously have been stated correctly by Merchant (3), they will be reviewed here concisely as a matter of convenience. As in orthogonal cutting, there is a shear plane when cutting with an oblique tool. This shear plane will contain the cutting edge and will rise from the finished surface as we proceed into the workpiece in front of the cutting edge. The direction of the shear plane is most conveniently defined in terms of a normal shear angle ϕ_n measured in a plane normal to the cutting edge, i.e., in a vertical plane along OA in Fig. 2. In Fig. 11 a section view of a partially formed chip is shown in a plane normal to the cutting edge. The angles ϕ_n and α_n are as shown, and we obtain a relationship between these two angles and the chip and workpiece thicknesses just as in orthogonal cutting (1)

$$\tan \phi_n = \frac{\frac{t}{t_c} \cos \alpha_n}{1 - \frac{t}{t_c} \sin \alpha_n} \quad \ldots\ldots\ldots\ldots\ldots\ldots [6]$$

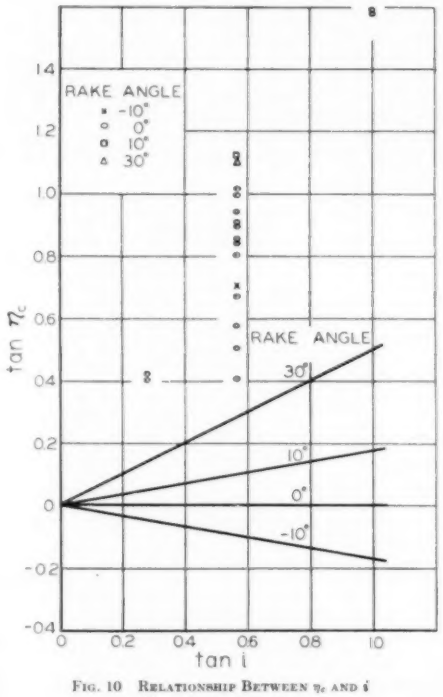

FIG. 10 RELATIONSHIP BETWEEN η_c AND i (Kronenberg's assumption.)

where t and t_c are the depth of cut and chip thickness, respectively. If the back of the chip is very rough, it is usually more precise to use a chip-length ratio rather than a chip-thickness ratio. This may be done as a consequence of the volume-continuity relationship of plasticity which expresses the fact that

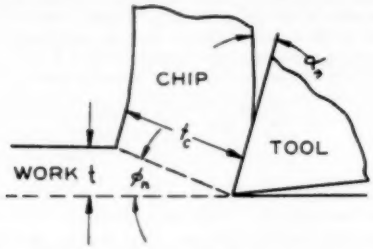

FIG. 11 SECTION OF PARTIALLY FORMED CHIP IN PLANE NORMAL TO CUTTING EDGE

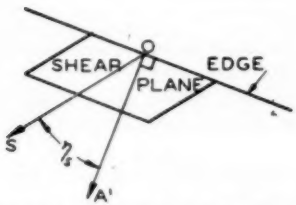

FIG. 12 VIEW OF SHEAR PLANE FROM A DIRECTION NORMAL TO SHEAR PLANE, SHOWING MANNER OF SPECIFYING SHEAR FLOW DIRECTION *OC*

the volume of the metal is unchanged in any process involving large plastic strains; hence

$$lbt = l_c b_c t_c \quad [7]$$

where l and l_c are corresponding work and chip lengths. From Equation [7]

$$\frac{t}{t_c} = \frac{l_c b_c}{lb} \quad [8]$$

The direction of shear flow is given by a line in the shear plane that makes an angle η_s with a line that lies in the shear plane and is normal to the cutting edge (see Fig. 12). This shear-flow angle η_s is found to be

$$\tan \eta_s = \frac{\tan i \cos (\phi_n - \alpha_n) - \tan \eta_c \sin \phi_n}{\cos \alpha_n} \quad [9]$$

In orthogonal cutting the shear strain γ is

$$\gamma = \cot \phi + \tan (\phi - \alpha) \quad [10]$$

while in the case of an oblique tool this obviously becomes

$$\gamma = \frac{\cot \phi_n + \tan (\phi_n - \alpha_n)}{\cos \eta_s} \quad [11]$$

In accordance with the principles of kinematics, the three velocity vectors involved in oblique cutting must form a closed velocity triangle. These three velocities shown in Fig. 13 are

1 V, the cutting velocity which is directed along *DO* in Fig. 4.
2 V_c, the chip velocity which is directed along *OC* in Fig. 4.
3 V_s, the shear velocity which must be directed from *O* toward *E* in Fig. 4 in order that the three vectors form a closed triangle.

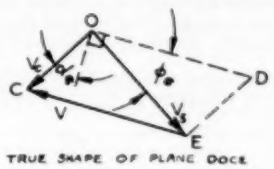

FIG. 13 VELOCITY COMPONENTS SHOWN IN PLANE *DOCE* IN FIG. 4

The relationship between these velocities may be found readily by use of a three-dimensional model of the velocity triangle to give

$$\frac{V_c}{V} = \frac{\cos i \sin \phi_n}{\cos \eta_s \cos (\phi_n - \alpha_n)} \quad [12]$$

$$\frac{V_s}{V} = \frac{\cos i \cos \alpha_n}{\cos \eta_s \cos (\phi_n - \alpha_n)} \quad [13]$$

Just as an effective rake angle α_e was defined previously for an oblique cutting tool, an effective shear angle ϕ_e may be defined similarly (see Fig. 13). This effective shear angle lies in the plane of *DOCE* in Fig. 4.

From Fig. 13 it is evident that

$$\sin \phi_e = \left(\frac{\cos \eta_s \cos \alpha_e}{\cos \eta_c \cos \alpha_n}\right) \sin \phi_n \quad [14]$$

It should be recalled that the value of α_e may be obtained from Equation [2].

FORCE RELATIONS

When considering the forces acting upon an oblique cutting tool, investigators in the past (3, 4) have assumed that the resultant force in the plane of the tool face acts in the direction of chip flow (*OC* in Fig. 4) while the resultant force in the shear plane has been assumed to be in the direction of shear flow (*OE* in Fig. 4). A little reflection will show that both of these conditions cannot generally be fulfilled physically. If the chip above the shear plane be taken as a free body, there are but two forces acting upon it—a resultant force on the tool face R, and a resultant force on the shear plane R'. To satisfy the conditions of equilibrium, the forces R and R' must be equal in magnitude, parallel to each other and oppositely directed. It can be demonstrated readily with the aid of a model that for any values of ϕ and α, there will be only one resultant force direction such that the forces in the tool face F_e and along the shear plane F_s will be in the directions V_e and V_s, respectively. Since a variety of values of R can actually exist for given values of ϕ and α, it follows that in the general case F_e and V_e, and F_s and V_s cannot be colinear simultaneously.

The foregoing observations cease to appear paradoxical when we recognize that the shear and friction processes in cutting are mutually related. Our familiarity with the behavior of such bodies as the plane slider in Fig. 14 leads us to expect a body to move in the direction of the applied force, i.e., in direction *OA* when force F_1 is acting, but *OB* when force F_2 is acting. Only by erecting a wall along *CD* can our slider be made to take path *OA* when subjected to force F_2. While there is no physical wall between the chip and tool, the restraint offered by the adjacent

shear process provides an action similar to the wall in the foregoing analogy.

The foregoing observation also may be demonstrated experimentally. To do this, a sensitive dynamometer was constructed capable of measuring forces simultaneously in three orthogonal directions without any interference between the components. This device, Fig. 8, employed wire resistance gages as the strain-measuring elements. Representative results are given in Table 2.

In making these tests, the dynamometer was oriented with its axes in the x, y, z-directions of Fig. 15. Here y extends along the work surface parallel to cutting velocity V; x is along the work surface normal to V, while z is in the vertical direction. In order to find the component of the resultant force in the plane of the tool face, it is convenient to change to the x', y', z' right-hand orthogonal set in Fig. 15, where x' is along the cutting edge, y' is normal to the tool face, and z' is normal to the cutting edge, but in the plane of the tool face. If a_1, b_1, and c_1 are the direction cosines of the x' axis relative to the x, y, z-co-ordinate system, and a_2, b_2, c_2, and a_3, b_3, c_3, the direction cosines of y' and z', respectively, then the transformation may be readily made as follows

$$\left.\begin{aligned} F_x' &= a_1F_x + b_1F_y + c_1F_z \\ F_y' &= a_2F_x + b_2F_y + c_2F_z \\ F_z' &= a_3F_x + b_3F_y + c_3F_z \end{aligned}\right\} \quad \ldots\ldots\ldots\ldots [15]$$

where

$a_1 = \cos i$;	$b_1 = -\sin i$;	$c_1 = 0$
$a_2 = \cos \alpha_n \sin i$;	$b_2 = \cos \alpha_n \cos i$;	$c_2 = \sin \alpha_n$
$a_3 = -\sin \alpha_n \sin i$;	$b_3 = -\sin \alpha_n \cos i$;	$c_3 = \cos \alpha_n$

If δ_c is the angle that the force in the plane of the tool face F_c makes with the normal to the cutting edge in this plane, i.e., the z'-axis in Fig. 15, then

$$\tan \delta_c = \frac{F_{x'}}{F_{z'}} = \frac{\cos i\, F_x - \sin i\, F_y}{-\sin \alpha_n \sin i\, F_x - \sin \alpha_n \cos i\, F_y + \cos \alpha_n F_z} \quad \ldots\ldots [16]$$

The angle the force in the shear plane F_s makes with the normal to the cutting edge in this plane may be similarly found

$$\tan \delta_s = \frac{-\cos i\, F_x + \sin i\, F_y}{\cos \phi_n \sin i\, F_x + \cos \phi_n \cos i\, F_y + \sin \phi_n F_z} \quad [17]$$

where in this case the positive z'-axis is in the direction opposite that used in the derivation of Equation [16]. The angles ζ_c and ζ_s in Table 2 are the differences between the corresponding values of η and δ.

There are several forces of interest in an oblique cutting process. These include the following:

1 The resultant force acting on the tool face R, or on the shear plane R' ($R = R'$)

$$R = (F_x'^2 + F_y'^2 + F_z'^2)^{1/2} \quad \ldots\ldots [18]$$

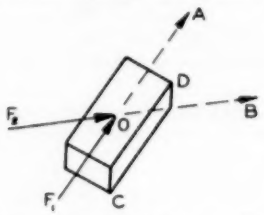

FIG. 14 PLANE SLIDER SHOWING PATH TAKEN UNDER ACTION OF DIFFERENTLY DIRECTED FORCES

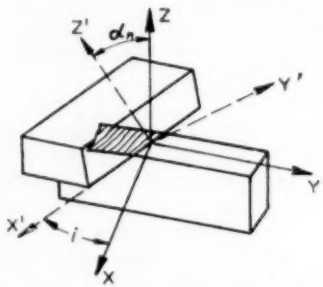

FIG. 15 SKETCH OF INCLINED CUTTING TOOL SHOWING AXES OF REFERENCE

TABLE 2 REPRESENTATIVE CUTTING DATA FOR OBLIQUE CUTTING TOOLS
(Depth of = 0.005 in.)

α_n, deg	0	10	30	10	→	→
i, deg	30	→	→	0	15	30
b, in.	0.25	→	→	→	→	→
b_c, in.	0.19	0.22	0.24	0.240	0.24	0.22
l, in.	3.93	→	→	→	→	→
l_c, in.	1.71	2.30	2.84	1.32	1.96	2.30
F_x', lb	−130	−100	−90	0	−50	−100
F_y', lb	−330	−270	−200	−300	−290	−270
F_z', lb	80	55	20	120	95	55
V, ipm	20	→	→	→	→	→
V_c, ipm	9.56	11.4	13.6	6.74	9.84	11.4
V_s, ipm	18.6	18.1	15.5	20.0	20.0	18.1
η_c, deg	48.6	40.0	33.3	0	21.2	40.0
δ_c, deg	33.3	25.6	9.9	0	10.9	25.6
ζ_c, deg	15.3	14.4	23.4	0	10.3	14.4
η_s, deg	11.0	8.6	8.2	0	4.7	8.6
δ_s, deg	9.8	12.1	8.6	0	7.1	12.1
ζ_s, deg	1.2	−3.5	−0.4	0	−2.4	−3.5
ϕ_c, deg	18.1	28.5	42.0	19.4	27.0	28.5
ϕ_s, deg	25.3	34.3	44.2	19.4	28.4	34.2
α_s, deg	22.1	25.9	39.6	10	14.5	25.9
F_c, lb	95.6	114	124	170	147	114
F_{cn}, lb	−351	−270	−179	−274	−271	−270
$F_c \sin \zeta_c$, lb	25.3	28.5	49.4	0	26.3	28.5
$F_c \cos \zeta_c$, lb	92.2	111	114	170	144	111
F_s, lb	313	236	151	244	219	236
F_{sn}, lb	185	184	180	213	218	184
μ	0.26	0.41	0.64	0.62	0.53	0.41
σ, psi × 10^{-3}	39.8	62.7	83.5	56.7	82.5	62.7
τ, psi × 10^{-3}	67.2	80.7	70.0	65	77	80.7
γ	3.44	2.20	1.33	2.98	2.28	2.20
w_f, psi × 10^{-3}	35.8	50.8	62.2	46.2	57.0	50.8
w_s, psi × 10^{-3}	233	171	94	196	176	171
w, psi × 10^{-3}	268	222	156	242	233	222
w_f/w	0.13	0.23	0.40	0.19	0.25	0.23

2 The component of force along the tool face F_c

$$\left.\begin{aligned} F_c &= [F_x'^2 + F_z'^2]^{1/2} \\ &= [(\cos i\, F_x - \sin i\, F_y)^2 \\ &+ (-\sin\alpha_n \sin i\, F_x - \sin\alpha_n \cos i\, F_y + \cos\alpha_n F_z)^2]^{1/2} \end{aligned}\right\} \quad [19]$$

3 The component of force normal to the tool face, F_{cn}

$$F_{cn} = F_y' = \cos\alpha_n \sin i\, F_x + \cos\alpha_n \cos i\, F_y + \sin\alpha_n F_z \quad [20]$$

4 The components of force in the tool face that are parallel to the chip flow direction ($F_c \cos\zeta_c$), and normal to the chip-flow direction ($F_c \sin\zeta_c$), respectively.

5 The component of force along the shear plane, F_s

$$F_s = [(-\cos i\, F_x + \sin i\, F_y)^2 + (-\cos\phi_n \sin i\, F_z - \cos\phi_n \cos i\, F_y - \sin\phi_n F_z)^2]^{1/2} \quad [21]$$

6 The component of force normal to the shear plane, F_{sn}

$$F_{sn} = -\sin\phi_n \sin i\, F_x - \sin\phi_n \cos i\, F_y + \cos\phi_n F_z \quad [22]$$

7 The components of force in the shear plane that are parallel to the shear flow direction ($F_s \cos\zeta_s$), and normal to the shear flow direction ($F_s \sin\zeta_s$), respectively.

The coefficient of friction μ, is usually defined as the tangential force divided by the normal force. We must generalize this definition here and refer to the tangential-force component in the direction of relative motion to take care of the fact that the friction force and the velocity vectors are not colinear; thus

$$\mu = \frac{F_c \cos\zeta_c}{F_{cn}} \quad [23]$$

There are two stress components associated with the shear plane that are of interest—a shear component τ and a normal component σ. These may be computed as follows

$$\tau = \frac{F_s}{bt} \sin\phi_n \cos i \quad [24]$$

$$\sigma = \frac{F_{sn}}{bt} \sin\phi_n \cos i \quad [25]$$

Finally, there are three specific energies involved in the oblique cutting process. These are as follows:

1 The friction energy per unit volume

$$u_f = \frac{F_c \cos\zeta_c V_c}{bt\, V} = \frac{F_c}{A_c} \cos\zeta_c \quad [26]$$

where A_c is the cross-sectional area of the chip.

2 The shear energy per unit volume

$$u_s = \frac{F_s \cos\zeta_s V_s}{bt\, V} = \tau\gamma \cos\zeta_s \quad [27]$$

3 The total energy per unit volume

$$u = u_f + u_s = \frac{F_y}{bt} \quad [28]$$

Experimental Observations

All of the foregoing quantities have been computed for the representative tests of Table 2, and allow the following observations to be made:

1 The quantity $(\eta_c - i)$ which is a measure of the deviation from Stabler's rule is seen to decrease with increased coefficient of friction, or to decrease with decreased shear strain as previously observed in connection with Table 1.

2 As would be expected from geometrical considerations, η_s increases whenever η_c increases, but at a lower rate.

3 The inclination angle is seen to have a very significant influence upon the effective rake angle, particularly at high values of the inclination angle. As might be expected, the effective shear angle ϕ_s is seen to increase with α_n.

4 The deviation between the chip-flow vector and the resultant-force vector in the plane of the tool face (as measured by angle ζ_c) is seen to increase with both an increase in the effective rake angle α_n and an increase in the inclination angle i.

5 The deviation between the shear-velocity vector and the resultant-force vector in the shear plane (as measured by angle ζ_s) is seen to be insignificant in all of the tests.

6 The fact that ζ_c is insignificant while ζ_s is substantial would indicate that the shear process predominates over the friction process. That this is actually so may be seen by a comparison of the two processes as indicated by the ratio u_f/u.

7 The coefficient of friction on the tool face is seen to decrease with increased inclination angle i. This is particularly significant inasmuch as the coefficient of friction will increase with increased rake angle in orthogonal cutting. However, as already mentioned, when inclination angle is increased, the effective rake angle is seen to increase. Thus the special geometry associated with an inclination angle has a greater effect upon the coefficient of friction than does the effective rake angle.

8 The shear stress on the shear plane is seen to increase with inclination angle while the shear strain decreases. An explanation for this paradox is presented in reference (7).

9 The total energy per unit volume u is seen to decrease with increased inclination. This decrease is due to a decrease in the shear strain which in turn is due to an increase in the effective rake angle with increased inclination. Obviously, the decrease in u is not due to a decrease in the friction energy per unit volume u_f with increased inclination.

Views of representative chips obtained using the three angles of inclination of the tests of Table 2 are shown in Fig. 16. All chips are for a length of cut of approximately 4 in. Here the change from the flat spiral chip of orthogonal cutting to the helical chip that is characteristic of a tool with inclination is evident.

One of the functions of inclination is to alter the chip-flow direction, and the manner in which side flow increases with the inclination of the cutting edge is evident in Fig. 16.

Stabler (4) has derived an expression relating the rake, shear, and friction angles in orthogonal cutting (his Equation [29]), based upon two assumptions:

1 That the angles i and η_c are equal in oblique cutting (Stabler's rule).

2 That the direction of maximum shear strain is in the direction of maximum shear stress on the shear plane (i.e., that $\eta_s = \delta_s$ or $\zeta_s = 0$)

The reason that such a relationship between the rake, shear, and friction angles may be obtained from purely geometrical considerations is posed by Stabler as a "knotty problem." It would appear that the difficulty here lies in the fact that, in general, neither of the above assumptions is valid. We have seen in Table 1 that when the coefficient of friction is relatively low, assumption 1 is only approximate while assumption 2 is good. It is shown in reference (7) that under less favorable friction conditions (dry cutting), assumption 1 improves, but assumption 2 ceases to be good. Thus the afore-mentioned development is based upon two assumptions that are not, in general, good approximations at the same time.

The Lathe Tool

While there are some production tools that employ simple in-

FIG. 16 REPRESENTATIVE CHIPS
(Rake angle, $\alpha_n = 10$ deg; length of cut, $l = 4$ in.; depth of cut, $t = 0.005$ in.; cutting speed, $V = 20$ ipm.; cutting fluid, carbontetrachloride.)

clined cutting edges, such as those just discussed, most tools in use appear geometrically more complex. However, when carefully studied, these tools may be reduced to equivalent inclined cutting tools. Were this not so, it is unlikely that we should be as interested in the inclined tool as the extent of the foregoing discussion would indicate.

Most practical three-dimensional tools are found to have two edges that cut simultaneously. Probably the most common tool of this type is the ordinary lathe tool, Fig. 17. Here the primary cutting edge is the side-cutting edge while the secondary edge is the end-cutting edge. Since the depth of cut is usually much greater than the feed per revolution, what happens along the secondary cutting edge is negligible compared with what happens along the primary cutting edge. Bickel (8) has demonstrated this to be the case in some ingenious experiments conducted in Zürich.

If the nose radius is small, we can consider the side-cutting edge as an oblique cutting tool such as that shown in Fig. 1(*b*). From the geometry of Fig. 17 it can be shown that the angle of inclination i, of the side-cutting edge is given by

$$\tan i = \tan \alpha_b \cos c_s - \tan \alpha_s \sin c_s \quad \ldots\ldots [29]$$

while the normal rake angle α_n is given by

$$\tan \alpha_n = (\tan \alpha_s \cos c_s + \tan \alpha_b \sin c_s) \cos i \quad \ldots\ldots [30]$$

For the tool in Fig. 17, Equations [29] and [30] yield the following results

$$i = 4.1 \text{ deg}$$
$$\alpha_n = 15.5 \text{ deg}$$

Assuming Stabler's rule to hold, Equation [5] then gives

$$\alpha_s = 15.7 \text{ deg}$$

Thus to a first approximation we may consider the relatively complex tool in Fig. 17 equivalent to a simple oblique cutting tool having a 4-deg angle of inclination and an effective rake angle of about 16 deg.

THE FACE-MILLING CUTTER

The foregoing analysis of tool geometry may also be readily applied to a face-milling cutter. Fig. 18 shows the manner in

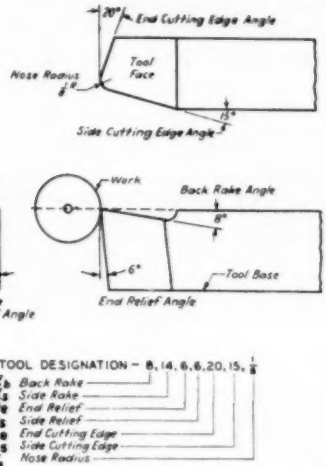

FIG. 17 REPRESENTATIVE LATHE TOOL SHOWING AMERICAN STANDARDS ASSOCIATION NOMENCLATURE

which a single tooth of a face-milling cutter operates, while Fig. 19 shows the principal angles of such a cutter. These angles are shown in Table 3 together with their lathe-tool counterparts.

In order to illustrate the use of the foregoing procedure in finding the effective rake angle α_s and inclination i of a face-milling cutter, consider the following example:

$$\text{Axial rake angle, } \alpha_a = 10 \text{ deg}$$
$$\text{Radial rake angle, } \alpha_r = -10 \text{ deg}$$
$$\text{Corner angle, } c = 30 \text{ deg}$$

For this case the inclination and effective rake angles are found to have the following values by the following steps similar to those employed in the lathe-tool example:

$$i = 13 \text{ deg}$$
$$\alpha_s = -2 \text{ deg}$$

THE DRILL POINT

As a final example, we might apply the foregoing methods to the analysis of a drill point. The principal drill nomenclature is shown in Fig. 20, and the lathe-tool equivalents of the more important drill angles are given in Table 4.

The analysis of the drill point is somewhat more involved than that for other tools inasmuch as the values of the first two items in Table 4 vary with the radius to the point in question on the inclined cutting edge. The helix angle is the angle whose tangent

TABLE 3 EQUIVALENT ANGLES FOR FACE-MILLING CUTTER AND LATHE TOOL

Lathe tool	Face-milling cutter
Side-rake angle, α_b	Radial-rake angle, α_r
Back-rake angle, α_b	Axial-rake angle, α_a
Side-cutting edge angle, c_s	Corner angle, c

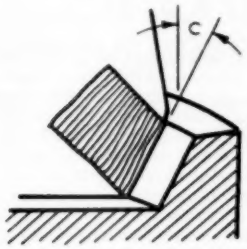

FIG. 18 ACTION OF FACE-MILLING CUTTER SHOWING MANNER IN WHICH INCLINED PERIPHERAL CUTTING EDGE PRODUCES CHIP

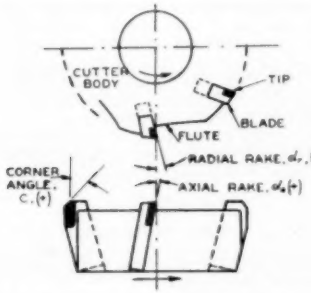

FIG. 19 FACE-MILLING CUTTER WITH INSERTED BLADES, SHOWING PRINCIPAL ANGLES

is the ratio of the circumferential length at the radius of interest to the pitch length of the helix, that is

$$\text{Helix angle} = \tan^{-1}\frac{2\pi r}{\text{pitch}}$$

TABLE 4 EQUIVALENT ANGLES FOR DRILL AND LATHE TOOL

Lathe tool	Drill
Side-rake angle, α_b	$\sin^{-1}\left(\frac{w}{2r}\right)^a$
Back-rake angle, α_b	Helix angle
Side-cutting edge angle, c_s	$^1/_2$ point angle

[a] Where w is web thickness and r is radius to point in question.

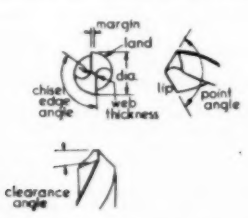

FIG. 20 DRILL NOMENCLATURE

The drill angle that corresponds to the side-rake angle of a lathe tool (i.e., $\sin^{-1} w/2r$) is also observed to vary across the cutting edge.

It is instructive to apply the foregoing reasoning to an actual drill point of the following dimensions:

Diameter	3.5 in.
Helix angle	28 deg
Point angle	122 deg
Chisel-edge angle	135 deg
Web thickness	0.4 in.

An end view of the point of this drill is shown in Fig. 21. The characteristics of the three points along the cutting edge labeled 1, 2, and 3 in Fig. 21, are summarized in Table 5.

TABLE 5 DRILL-POINT CHARACTERISTICS

Point	r, in.	α_s, deg	α_b, deg	c_s, deg	i, deg	α_n, deg	α_r, deg
1	1.750	−6.5	28.0	61	19	21.4	25
2	1.000	−11.5	16.0	61	17	7.6	12
3	0.256	−51.5	4.1	61	49	−19.9	25

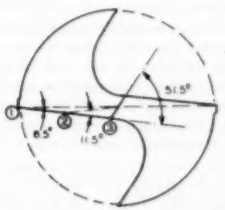

FIG. 21 END VIEW OF DRILL POINT

The inclination is seen to increase as the center of the drill is approached. As a consequence of the relatively high inclination near the center of the drill, the effective rake angle is seen to be reasonably large (25 deg), even though the normal rake angle α_n at this point is but −19.9 deg. The cutting that occurs near the center of a drill might be described as a slicing action. The metal at the very center of the drill ($r = {}^1/_4$ in.), and under the chisel edge is not cut in the normal sense, but is removed by a process that resembles extrusion. This is not a very efficient process and tends to limit the extent to which the web thickness of a drill may be increased.

From the foregoing drill analysis it is evident that the web thickness, helix angle, and point angle are the three dimensions of greatest significance in determining drill performance. In order to demonstrate one method in which an analytical approach may be used to advantage, we will now consider the influence that each of these three variables has upon i, α_n, and α_s. If but one of the dimensions of the drill of Table 5 is allowed to change at a time, the values of Table 6 are obtained. Here it is seen that certain of the basic drill dimensions primarily influence the outer portions of the drill while others influence the drill predominantly at the point.

Table 7 shows the influence of increases of point angle, helix angle, and web thickness upon the quantities (90-α_n) and α_s. The quantity (90-α_n) is important with regard to the mechanical strength and heat capacity of the cuttipg edge, while α_s is of importance with regard to the energy involved in the cutting operation (the energy required to cut a given volume of metal decreases as α_s increases). It is evident that large values of both (90-α_n) and α_s are desirable, but usually this cannot be arranged. However, this situation can be approached in the case of the drill.

Let us suppose that a given drill is failing at its periphery due to overheating. We should like, therefore, to increase (90-α_n) at

TABLE 6 CHANGES IN EFFECTIVE DRILL DIMENSIONS WHEN ONE DRILL DIMENSION IS VARIED AT A TIME

(Drill-point angle = 140 deg; helix angle = 32 deg; web thickness = 0.2 in.)

		Standard of Table 5											
Point	r, in.	i	α_n	α_e	i'	α_n	α_e	i'	α_n	α_e	i'	α_n	α_e
1	1.750	19	21.4	25	16	24.2	27	21	23.5	31	17	22.1	25
2	1.000	17	7.6	12	16	10.6	14	18	10.5	15	12	10.8	13
3	0.256	49	−19.9	25	52	−12.6	33	49	−19.9	25	22	−8.3	1

the periphery and at the same time decrease α_e. By increasing the helix angle, α_e will be increased but (90-α_n) will be decreased (see Table 7). The decrease in (90-α_n) may be offset, however, by decreasing the point angle without an appreciable change in α_e. In this instance drill life might be improved by a simultaneous increase in helix angle and decrease in point angle. Little would be gained by adjusting the web thickness in this case since web thickness only alters the geometry near the point of the drill. Of course we have considered only the geometrical aspects of the problem in the foregoing discussion. Actually, improvement also may frequently be derived by changes in such operating variables as feeds and speeds.

If in another case a drill were failing due to overheating near the point, little would be gained by adjusting the helix angle. If the web thickness were increased, less heat would be developed due to cutting near the point (α_e less) and (90-α_n) would increase (see Table 7), but a greater amount of metal would have to be extruded. Therefore an increase in web thickness could in this case improve drill performance or make it worse depending upon the metal cut and a number of other factors. The answer could be obtained only by trial. An increase in point angle in this instance would improve matters in so far as α_e and the heat generated are concerned, but at the same time there would be less metal available to conduct heat away. Again, the answer could be obtained only by test.

In the foregoing discussion, but two of the many types of drill failure have been discussed. While Table 7 may be applied similarly to other modes of failure, such discussion would lie beyond the scope of this paper.

Conclusion

The underlying motivation for all metal-cutting studies is to obtain an understanding of the three-dimensional cutting operations of production. It is only natural that the simpler two-dimensional case should have been studied first; but before the full importance of this work can be realized, it is necessary to learn how it may be applied to the three-dimensional problems of industry. The key to this procedure lies in a complete understanding of the characteristics of the inclined cutting tool. When all aspects of this type of tool are known and can be expressed analytically, it will be possible to put tool design on a rational basis.

TABLE 7 INFLUENCE OF A CHANGE OF DRILL DIMENSIONS UPON INCLUDED EDGE ANGLE (90-α_n) AND EFFECTIVE RAKE ANGLE (α_e)

	At edge of drill		At point of drill	
For an increase of:	90-α_n	α_e	90-α_n	α_e
Point angle	−	+	−	+
Helix angle	−	+	0	0
Web thickness	0	0	+	+

Notes:
− = decrease
+ = increase
0 = negligible change

The fact that an art as old as metal cutting should have progressed so little in the direction of a science is a most discouraging thought. However, some encouragement is to be found in the fact that it was less than 15 years ago that the first attempts were made to attack this problem from the standpoint of analytical mechanics. More work in this direction is sorely needed.

Acknowledgments

The authors wish to express their gratitude to Messrs. J. Leach, D. J. Spooner, and M. Hablanian, of the Machine Tool and Metal Cutting Division, for aid in this investigation.

Some of the concepts presented here are an outgrowth of a general investigation of the cutting of nonerystalline materials sponsored by the United Shoe Machinery Corporation.

BIBLIOGRAPHY

1 "Mechanics of the Metal Cutting Process," by M. E. Merchant, *Journal of Applied Physics*, vol. 16, 1945, p. 267.

2 "Lastunmuodostumisen Teorina," by V. Piispanen, *Teknillinen Aikakauslehti*, vol. 27, 1937, p. 315.

3 "Basic Mechanics of the Metal-Cutting Process," by M. E. Merchant, *Journal of Applied Mechanics*, Trans. ASME, vol. 66, 1944, p. A-168.

4 "The Fundamental Geometry of Cutting Tools," by G. V. Stabler, Preprint, The Institution of Mechanical Engineers, London, England, 1951.

5 "Cutting-Angle Relationships on Metal-Cutting Tools," by M. Kronenberg, *Mechanical Engineering*, vol. 65, 1943, p. 901; discussion, vol. 66, 1944, p. 668.

6 American Standards Association Standard "Terminology and Definitions, Single Point Tools," January, 1939.

7 "The Rotary Cutting Tool," by M. C. Shaw, P. A. Smith, and N. H. Cook, published in this issue, pp. 1065–1076.

8 "Geometrie der Schneide," by E. Bickel, Industrielle Organization, Heft 1, 2, 3, 4, 1949.

The Rotary Cutting Tool

By M. C. SHAW,[1] P. A. SMITH,[2] and N. H. COOK,[3] CAMBRIDGE, MASS.

A novel lathe-type cutting tool in the form of a disk that may be rotated about its central axis is described and analyzed. Such a rotary tool is found to correspond to an equivalent oblique tool having an angle of inclination whose tangent is equal to the ratio of the tool and work-surface velocities. In addition to the inherent feature of the oblique tool of providing a greater effective rake angle without a corresponding decrease in the actual included angle of the tool, the rotary tool (1) provides a rest period for the cutting edge, thus enabling the edge to be cooled and the adsorbed film on the tool surface to be replenished between cuts; (2) enables the relative chip velocity to be increased to provide a lower coefficient of friction without necessitating a corresponding increase in the rate of metal removal. A rotary tool of 10-deg rake angle is capable of reducing total power required to make a given cut by about 30 per cent and at the same time to operate with a temperature about 400 F lower than that for the equivalent stationary tool. Representative test data for both rotary and stationary tools are analyzed and discussed. The shear stress on the shear plane is found to decrease with increased shear strain in the case of either a rotary tool or an oblique tool. This anomalous result is explained in terms of a size effect associated with the change in thickness of the shear plane that accompanies a change in the angle of inclination.

Introduction

EXPERIENCE with conventional single-point cutting tools of the type used for rough-turning operations indicates that the following items are of primary interest with regard to the design of tools of long life.

1 The energy required to shear a unit volume of metal should be as small as possible.

2 The energy associated with the friction between chip and tool should be as small as possible.

3 The tool point should be as massive as possible.

Now, these items are not mutually independent, and a compromise solution must usually be arranged. For example, it is desirable to have as large a rake angle as possible from the standpoint of the energy required to shear the metal, but as small a rake angle as possible from the standpoint of the strength and thermal capacity of the tool point. It is well known that the coefficient of friction between chip and tool, when cutting in air, decreases with an increase in chip velocity. However, in single-point cutting, we are limited as to the maximum allowable chip velocity inasmuch as the metal must be cut at a faster rate in order to achieve a greater chip velocity; and this involves a continuously increasing rate of energy dissipation at the tool point. While a cutting fluid represents one of the most effective methods of decreasing the coefficient of friction, it is necessary for the fluid to reach the tool point against the adverse work and chip velocities in order to be effective. Thus the speed at which a given cutting fluid ceases to be useful in decreasing chip-tool friction is usually influenced by its ability to penetrate to the tool point. From the foregoing brief discussion of single-point tools, it is evident that the following items of tool performance would be highly desirable when attempting to cut metal at a high rate of speed with long tool life:

1 A large effective rake angle in so far as the shear process is concerned, but a small actual rake angle from the standpoint of strength and heat flow.

2 Positive means for carrying the fluid to the tool point at high cutting speeds as in the case of a journal bearing.

3 The possibility of increasing chip velocity without necessitating a corresponding increase in cutting speed.

The ordinary inclined cutting edge, Fig. 1(*b*), as used in a helical milling cutter or the teeth of a broach, offers a means of accomplishing the first objective. In this case the effective rake angle, in so far as the shear process is concerned, is greater than the actual geometrical rake angle that is of importance with regard to the strength of the tool point. However, a tool of this type does not satisfy the other two objectives. If the tool were to be moved in a direction parallel to the cutting edge as the workpiece advanced on the tool [slicing action, see Fig. 1(*c*)] we have a very simple means for accomplishing objectives 2 and 3. Fluid could then be absorbed on the cutting edge and be carried to the chip-tool interface as the tool advanced in a direction parallel to the edge. Also, it would be possible to increase the chip velocity largely independently of the work or cutting velocity.

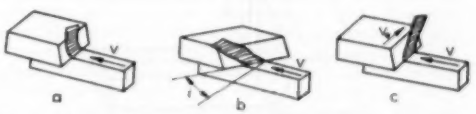

FIG. 1 COMPARISON OF THREE BASIC TYPES OF CUTTING TOOLS (*a*, Orthogonal tool. *b*, Oblique tool. *c*, Tool with moving edge—slicing action.)

The practical way of providing the sidewise motion of the tool is to use a continuous cutting edge in the form of the rotary tool shown in Fig. 2. Here, a particular portion of the cutting edge is in operation for a very brief period, which is followed by a much longer rest period during which the thermal energy associated with cutting has ample opportunity to be dissipated to the bulk of the cutter. In this respect the rotary tool resembles a multitoothed tool such as a milling cutter.

By following a line of reasoning similar to that just outlined we were led to investigate the rotary tool to be described. However, since undertaking this work, it has been learned that the idea of a rotary tool is not new, but that such devices have been used on occasion for many years, in both positively driven and

[1] Associate Professor of Mechanical Engineering, Massachusetts Institute of Technology. Mem. ASME.

[2] Associate Professor of Mechanical Engineering, Massachusetts Institute of Technology. Mem. ASME.

[3] Instructor in Mechanical Engineering, Massachusetts Institute of Technology.

Contributed by the Production Engineering Division and Metal Cutting Data and Bibliography and the Cutting Fluids Research Committees and presented at the Annual Meeting, Atlantic City, N. J., November 25-30, 1951, of THE AMERICAN SOCIETY OF MECHANICAL ENGINEERING.

NOTE: Statements and opinions advanced in papers are to be understood as individual expressions of their authors and not those of the Society. Manuscript received at ASME Headquarters, August 22, 1951. Paper No. 51—A-62.

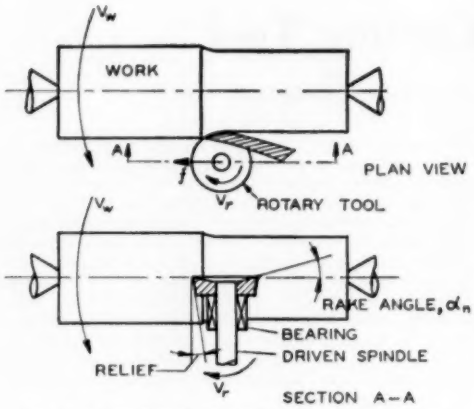

FIG. 2 ROTARY TOOL SHOWN IN USE IN A ROUGH-TURNING OPERATION

self-propelled types. In this paper we will present an analysis of the rotary tool and indicate its relation to other more common tool types. Representative performance data for both rotary and conventional tools will then be presented and discussed.

ANALYSIS OF ROTARY TOOL

If the diameter of a rotary tool is large compared with the depth of cut, which is usually the case, curvature of the cutting edge may be ignored. Therefore we may consider the linearized process in Fig. 3(*a*) for purposes of analysis. Here the cutting edge is normal to the work velocity V_w and moves in a direction normal to V_w with a velocity V_r. The chip will be observed to flow off to the side as shown in the figure, with a velocity V_c. This rather unfamiliar cutting process may be reduced to a much more common type by applying the kinematical device of re-examining the problem from a different vantage point.

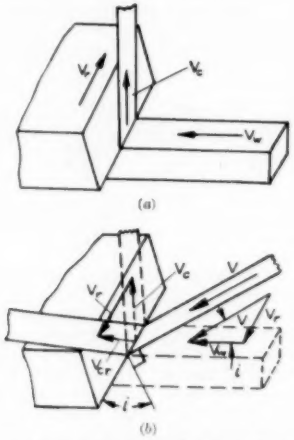

FIG. 3 ROTARY CUTTING PROCESS AS OBSERVED FROM FIXED POINT IN SPACE AND FROM FIXED POINT ON TOOL

(*a*, Rotary cutting process as observed from a fixed point in space. *b*, Solid lines show kinematically equivalent cutting process as seen from a fixed point on tool.)

Instead of observing the operation from a fixed point in space as in Fig. 3(*a*), let us observe the process from a fixed point on the cutting tool. Such a picture may be obtained by simply translating everything in Fig. 3(*a*) to the left with a velocity V_r. This will bring the tool to rest, will cause the workpiece to move in an inclined direction with a velocity V, and will cause the chip to appear to flow off to the left rather than to the right, see Fig. 3(*b*).

The velocity of the chip across the tool face will be equal to V_w, which is the vector sum of velocities V_c and V_r. The solid lines in Fig. 3(*b*) represent the cutting process that is kinematically equivalent to that in Fig. 3(*a*). This equivalent process is seen to be that of Fig. 1(*b*)—cutting with a simple inclined cutting tool. Thus one of the significant features of a rotary tool is to provide what is equivalent to an inclined cutting edge, the effective inclination angle i being given by

$$\tan i = \frac{V_r}{V_w} \quad \ldots\ldots [1]$$

The inclined cutting tool shown in Fig. 1(*b*) has already been considered in detail in a previous paper.[4] In the discussion of the rotary tool that follows, the same notation will be used and it will be assumed that the reader is familiar with the reference cited.[4]

CHIP-FLOW DIRECTION

Just as in the case of an inclined cutting edge, knowledge of the chip-flow direction is very important. A view of a tool normal to the tool face is shown in Fig. 4. Here vector OC represents the absolute velocity of the chip, while vectors DC and OD are the rotational velocity V_r, and the velocity of the chip relative to the tool V_{cr}, respectively. The absolute chip-flow direction is

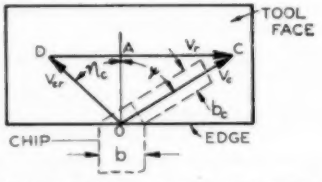

FIG. 4 VIEW NORMAL TO TOOL FACE, SHOWING VELOCITY VECTORS THAT LIE IN FACE OF TOOL

measured by the angle ψ to normal OA, while the direction of the relative velocity vector is measured by angle η_c. This latter angle is the more important one for it corresponds to the chip-flow angle of the equivalent oblique tool, and when η_c is known, then

$$\sin \alpha_s = \sin \eta_c \sin i + \cos \eta_c \cos i \sin \alpha_n \quad \ldots\ldots [2]$$

where α_n is the effective rake angle measured in the plane of V_w and V_{cr}, Fig. 3(*b*).

Of the several methods of determining η_c that were considered, that which proved most satisfactory was one involving measurements of the width b_c and thickness t_c of the chip, the width of

[4] "The Mechanics of Three-Dimensional Cutting Operations," by M. C. Shaw, N. H. Cook, and P. A. Smith, published in this issue, pp. 1055-1064.

the workpiece b, and depth of cut t. From Fig. 4 it is evident that

$$\tan \eta_c = \frac{DA}{AO} = \frac{V_c - V_c \sin \psi}{V_c \cos \psi} \quad \ldots\ldots [3]$$

and that

$$\cos \psi = \frac{b_c}{b} \quad \ldots\ldots [4]$$

By virtue of the incompressibility of metal during plastic deformation processes, we have

$$V_w bt = V_c b_c t_c \quad \ldots\ldots [5]$$

Combining Equations [1], [3], [4], and [5] we have

$$\tan \eta_c = \frac{t_c}{t} \tan i = \left[\left(\frac{b}{b_c}\right)^2 - 1\right]^{1/2} \quad \ldots\ldots [6]$$

Thus determination of the angle η_c requires the chip thickness ratio (t_c/t), the chip width ratio (b/b_c) and the angle of inclination i. Values of b_c may be determined by means of a measuring microscope while t_c may be obtained with a point micrometer.

In order to study the manner in which the angle η_c varies with inclination angle i, the arrangement shown in Fig. 5 was used. The workpiece was in the form of a tube, the relative arrangement of tool and workpiece being as shown in Fig. 6. The tool could be driven in either direction by means of a drill press. Several tool speeds could be obtained by means of a number of step pulleys. The workpiece was mounted in a chuck attached to the horizontal milling-machine spindle, while the tool and its accessory-drive equipment were attached to a special tool dynamometer mounted on the milling-machine table. The dynamometer used was capable of measuring accurately the three components of force shown in Fig. 6, with no mutual interference.

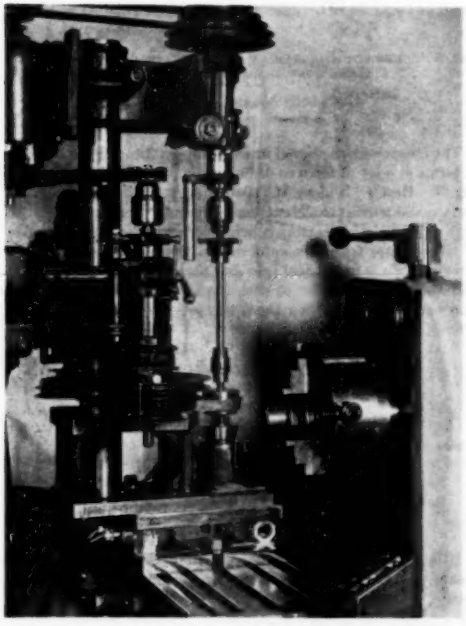

FIG. 5 TEST APPARATUS FOR STUDYING CUTTING CHARACTERISTICS OF ROTARY TOOL

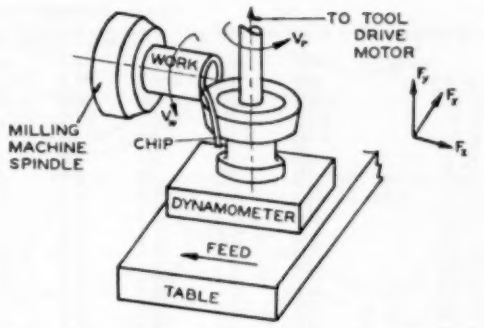

FIG. 6 SCHEMATIC DIAGRAM SHOWING RELATIVE ARRANGEMENT OF WORKPIECE AND TOOL IN FIG. 5

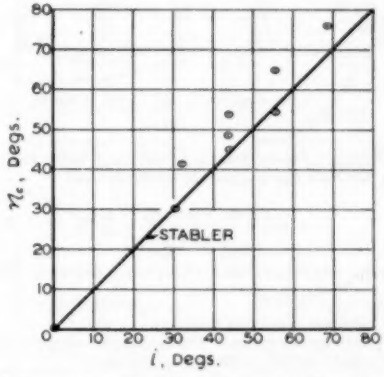

FIG. 7 VARIATION OF CHIP FLOW ANGLE (η_c) WITH ANGLE OF INCLINATION i

Representative results are given in Table 1. Here, the chip-flow angle η_c was computed by means of Equation [6], while the angle of inclination i was obtained from Equation [1]. The chip-flow angle η_c is shown plotted against inclination angle i in Fig. 7. It is evident that Stabler's rule, Equation [1] which states that $\eta_c = i$, is in fairly good agreement with the experimental points.

VELOCITY RELATIONS

As in the case of an oblique cutting tool, the normal shear angle is measured in a plane perpendicular to the cutting edge and

$$\tan \phi = \frac{\frac{t}{t_c} \cos \alpha_n}{1 - \frac{t}{t_c} \sin \alpha_n} \quad \ldots\ldots [7]$$

where α_n is the rake angle measured in the same normal plane.

The direction of shear flow will be along a line in the shear plane that makes an angle η_c with a normal to the cutting edge

TABLE 1 REPRESENTATIVE ROTARY-TOOL DATA

(Clearance angle, δ_n = 10 deg; rake angle, α_n = 10 deg; tool diameter = 2.5 in.; tool material = 18-4-1 high-speed steel; mean work diameter (tube) = 1.81 in.; work material, SAE 1015 steel.)

Fluid	Air	Air	Air	Air	Air	Air	Air	CCl_4	Oil	Air	Air
V_w, fpm	44.2	44.2	44.2	44.2	119	119	119	44.2	44.2	44.2	119
V_r, fpm	26.2	42.5	65.4	108	75.4	118	174	42.2	42.2	0	0
t, in.	0.0054	0.0054	0.0054	0.0054	0.0055	0.0055	0.0055	0.0054	0.0054	0.0054	0.0055
b, in.	0.193	0.192	0.191	0.191	0.191	0.191	0.191	0.191	0.191	0.191	0.191
t_c, in.	0.020	0.017	0.014	0.012	0.020	0.016	0.011	0.017	0.020	0.027	0.036
b_c, in.	0.102	0.090	0.086	0.118	0.110	0.095	0.103	0.083	0.080	0.213	0.204
F_x, lb	136	180	200	200	125	170	195	145	175	0	0
F_y, lb	−412	−280	−215	−185	−355	−280	−210	−280	−300	−562	−625
F_z, lb	340	260	190	200	355	250	195	210	250	562	725
i, deg	30.7	43.9	55.9	68.7	32.2	44.7	55.8	43.9	43.9	0	0
V_c, fpm	22.6	29.9	37.8	32.0	56.8	82.3	110	32.2	28.4	8.85	18.2
V_{cr}, fpm	13.8	21.9	40.2	79.5	43.5	58.4	100	20	20.4	8.85	18.2
V_s, fpm	46.5	30.3	49.8	46.3	124	135	137	51.3	50.3	43.4	117
V, fpm	51.3	62.2	79.0	117	141	167	209	62.2	62.2	44.2	119
ϕ_c, deg	30.5	49.0	64.9	75.8	41.1	45.2	55.5	45.0	54.2	0	0
δ_c, deg	18.5	30.6	41.7	41.1	16.8	29.9	40.4	29.8	30.4	0	0
ϵ_c, deg	12.0	18.4	23.2	34.7	24.3	15.3	13.1	15.2	23.8	0	0
η_c, deg	23.6	30.9	32.8	30.9	21.3	32.7	37.2	32.9	30.6	0	0
δ_s, deg	24.0	44.4	60.6	71.0	27.1	43.5	64.8	38.7	38.2	0	0
ϵ_s, deg	−0.4	−13.5	−27.8	−40.1	−5.8	−10.8	−27.6	−5.8	−7.6	0	0
ϕ_n, deg	15.6	18.3	22.3	28.0	16.0	19.8	28.4	18.2	15.6	11.6	8.9
ϕ_s, deg	14.7	19.3	28.0	40.5	17.9	19.3	26.5	17.9	18.0	11.6	8.9
α_n, deg	29.2	37.2	52.0	67.1	27.4	36.4	46.4	35.4	39.4	10	10
n	1.21	1.45	1.55	1.70	1.36	1.33	1.70	1.27	1.26	1.42	1.68
σ, psi × 10^{-3}	109.2	102.5	95.0	121.0	115.5	106.5	123.0	85.7	84.0	129.0	120.0
τ, psi × 10^{-3}	83.2	73.6	84.6	96.8	72.1	79.7	97.5	70.6	73.5	85.3	74.3
γ	3.97	3.69	3.15	2.37	3.85	3.51	2.74	3.79	4.22	4.90	6.35
u, psi × 10^{-3}	473	436	496	656	415	417	471	387	453	544	596
u_c, psi × 10^{-3}	331	282	262	189	276	276	237	267	309	419	472
u_f, psi × 10^{-3}	142	154	234	467	139	141	234	130	144	125	124
u_f/u	0.30	0.35	0.47	0.71	0.34	0.34	0.50	0.34	0.32	0.23	0.21
R, %	16	38	58	74	18	38	58	35	36	0	0

$$\tan \eta_r = \frac{\tan i \cos (\phi_n - \alpha_n) - \tan \eta_c \sin \phi_n}{\cos \alpha_n} \quad \ldots\ldots [8]$$

The expression for shear strain in a chip from a rotary tool is the same as that for a chip produced by an oblique tool.

$$\gamma = \frac{\cot \phi_n + \tan (\phi_n - \alpha_n)}{\cos \eta_r} \quad \ldots\ldots [9]$$

The several velocities involved with a rotary tool are as follows, Fig. 3(*b*)

1 V_w, absolute velocity of workpiece

2 V_r, velocity of rotation. This is absolute velocity of tool

3 V, relative velocity between work and tool

$$V = \sqrt{V_w^2 + V_r^2} \quad \ldots\ldots [10]$$

4 V_c, absolute velocity of chip; from Equation [5]

$$V_c = \frac{bd}{b_c t_c} V_w$$

5 V_{cr}, relative velocity between chip and tool

From Fig. 4 and Equations [3], [4], and [5] it is evident that

$$V_{cr} = \frac{t}{t_c \cos \eta_c} V_w \quad \ldots\ldots [11]$$

6 V_s, relative velocity between chip and workpiece. This vector lies in shear plane at an angle η_s (Equation [8]) with a normal to cutting edge, and has a magnitude that is given by

$$V_s = \frac{\cos i \cos \alpha_n}{\cos \eta_r \cos (\phi_n - \alpha_n)} V \quad V = \frac{t \cos \alpha_n}{t_c \sin \phi_n \cos \eta_r} V_w \quad \ldots [12]$$

The effective shear angle ϕ_s, measured in the plane of the velocity vectors V and V_{cr}, may be obtained from

$$\sin \phi_s = \frac{\cos \eta_c \cos \alpha_s}{\cos \eta_r \cos \alpha_n} \sin \phi_n \quad \ldots\ldots [13]$$

where α_s may be obtained from Equation [2].

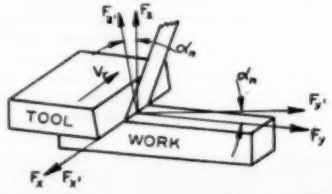

FIG. 8 SCHEMATIC DIAGRAM OF ROTARY TOOL SHOWING POSITIVE DIRECTIONS OF FORCE CO-ORDINATES

FORCE RELATIONS

The forces were measured using the apparatus of Figs. 5 and 6, in terms of a set of force co-ordinates F_x, F_y, and F_z as shown in Fig. 8. Here F_z is along the cutting edge, F_y is along the work surface and normal to the cutting edge, and F_x is perpendicular to both F_z and F_y. It is more convenient to use the $F_{x'}$, $F_{y'}$, $F_{z'}$ set of co-ordinates for purposes of analysis, where $F_{x'}$ is in the F_x direction, $F_{z'}$ is in the tool face and normal to the cutting edge, and $F_{y'}$ is perpendicular to both $F_{x'}$ and $F_{z'}$. The transformation equations connecting these two sets of co-ordinates are as follows

$$\left.\begin{aligned} F_{x'} &= a_1 F_x + b_1 F_y + c_1 F_z \\ F_{y'} &= a_2 F_x + b_2 F_y + c_2 F_z \\ F_{z'} &= a_3 F_x + b_3 F_y + c_3 F_z \end{aligned}\right\} \quad \ldots\ldots [14]$$

where the direction cosines are

$$\begin{aligned} a_1 &= 1 & b_1 &= 0 & c_1 &= 0 \\ a_2 &= 0 & b_2 &= \cos \alpha_n & c_2 &= \sin \alpha_n \\ a_3 &= 0 & b_3 &= -\sin \alpha_n & c_3 &= \cos \alpha_n \end{aligned}$$

If δ_s is the angle that the force in the plane of the tool face makes with the normal to the cutting edge in this plane (z'-axis) then

$$\tan \delta_s = \frac{F_{x'}}{F_{z'}} = \frac{F_x}{-\sin \alpha_n F_y + \cos \alpha_n F_z} \quad \ldots\ldots [15]$$

Likewise, the angle the force in the shear plane F_s makes with the normal to the cutting edge is similarly found to be

$$\tan \delta_s = \frac{F_v}{-\sin \phi_n F_y - \cos \phi_n F_x} \quad [16]$$

Angles ζ_c and ζ_s in Table 1 are the differences between the corresponding values of η and δ. The forces of interest are as follows:

1 The resultant force on the tool face R or on the shear plane R'

$$R = R' = [(F_{x'})^2 + (F_{y'})^2 + (F_{z'})^2]^{1/2} \quad [17]$$

2 The component of force along the tool face F_c

$$F_c = (F_{x'}^2 + F_{z'}^2)^{1/2} = [F_x^2 + (-\sin \alpha_n F_y + \cos \alpha_n F_z)^2]^{1/2} \quad [18]$$

3 The component of force normal to the tool face F_{cn}

$$F_{cn} = F_{y'} = \cos \alpha_n F_y + \sin \alpha_n F_z \quad [19]$$

4 The component of force along the shear plane F_s

$$F_s = [F_x^2 + (\sin \phi_n F_y + \cos \phi_n F_z)^2]^{1/2} \quad [20]$$

5 The component of force normal to the shear plane F_{sn}

$$F_{sn} = -\sin \phi_n F_y + \cos \phi_n F_z \quad [21]$$

The coefficient of friction on the tool face will be

$$\mu = \frac{F_c \cos \zeta_c}{F_{cn}} \quad [22]$$

as in the case of the oblique cutting tool. The shear and normal stress on the shear plane may be obtained as follows

$$\tau = \frac{F_s}{bt} \sin \phi_n \quad [23]$$

$$\sigma = \frac{F_{sn}}{bt} \sin \phi_n \quad [24]$$

The specific energies are as follows:

1 Friction energy per unit volume

$$u_f = \frac{F_c \cos \zeta_c V_{cr}}{btV_w} = \frac{\cos \zeta_c F_c}{\cos \eta_c bt_c} \quad [25]$$

2 Shear energy per unit volume

$$u_s = \frac{F_s \cos \zeta_s V_s}{btV_w} = \tau\gamma \cos \zeta_s \quad [26]$$

3 Total energy per unit volume

$$u = u_f + u_s = \frac{F_y}{bt} + \frac{F_x}{bt} \tan i \quad [27]$$

The ratio of the power required to drive the tool to the total power is

$$R = \frac{F_x \tan i}{btu} = \frac{1}{1 + \frac{F_y}{F_x} \cot i} \quad [28]$$

Discussion of Experimental Results

The principal observed and computed values for a number of rotary-tool tests are given in Table 1 and Fig. 9. Some of the scatter in the curves of Fig. 9 is due to the fact that all tests are not conducted at the same speed V_w, and in two of the tests a fluid was used. However, it is evident that the angle of inclination i is the predominant variable that controls the performance of this tool. In two of the tests the tool was stationary. The following general observations may be made regarding the performance of the rotary tool tested:

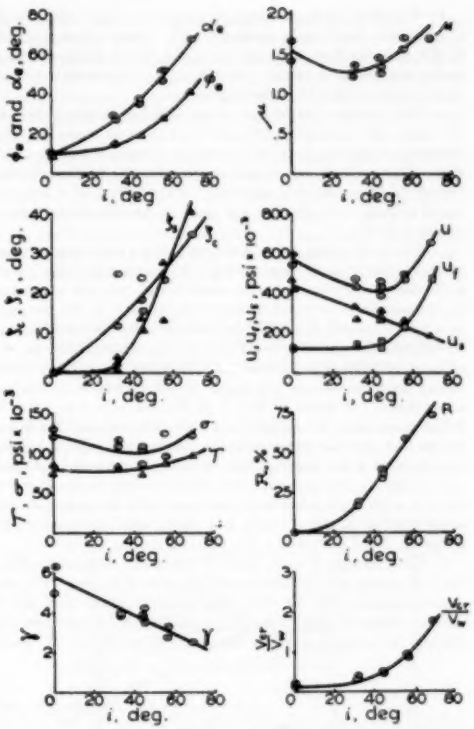

Fig. 9 Variation of Principal Cutting Variables With Angle of Inclination for Rotary Tool With 10-Deg Rake Angle

1 The effective rake angle α_e is seen to increase as the angle of inclination is increased by increasing the tool velocity V_r. It is evident that effective rake angles of over 60 deg may be obtained with a rotary tool having an actual normal rake angle of but 10 deg.

2 The effective shear angle ϕ_e is seen to increase as the effective rake angle increases, from a value of about 10 deg for the stationary tool to a value of over 40 deg when the angle of inclination was about 70 deg.

3 The resultant force in the shear plane F_s is seen to be practically colinear with the shear velocity vector V_s for small values of inclination. However, the angle ζ_s, which measures the angle between F_s and V_s, is seen to increase rapidly for values of i greater than about 30 deg. This observation is consistent with the results of a previous analysis[4] on an oblique cutting tool, where it was found that ζ_s was insignificant for inclination angles up to 30 deg. The angle ζ_c between F_c and V_c was observed to vary more nearly linearly with inclination i, both in this and the previous investigation.[4]

4 The shear stress on the shear plane is seen to increase with i, while the shear strain decreases. This same paradoxical behavior also has been observed for conventional oblique cutting tools,[4] and deserves further investigation. This matter will be discussed in detail in the following section.

5 The coefficient of friction on the tool face is seen at first to decrease with increased inclination and then to increase. The minimum value of μ appears to occur at a value of i of about 30 deg. This result is also in agreement with the friction characteristic of the previously mentioned investigation of a conventional oblique tool,[4] where μ was observed to decrease for values of i up to 30 deg.

6 The total energy per unit volume u has a minimum value at an inclination angle of about 45 deg. This minimum value is seen to be due to a tendency for the shear energy per unit volume u_s to decrease with increased i (due predominantly to the decrease in γ with increased α_n), while the friction energy per unit volume u_f exhibits the opposite trend (due to the tendency for the coefficient of friction to increase with increased α_n). The friction energy begins to increase at a rapid rate with increased inclination at a value of i of about 30 deg. It is at about this same value of i that ζ_s ceases to be negligible, and it is believed that this is due to the fact that for higher values of inclination angle the shear process plays a less dominant role in the cutting process and gives way to the friction process. The steep increase in the ζ_s-curve above $i = 40$ deg appears to be associated with the corresponding steep increase in the u_f-curve and the gradual decrease in the u_s-curve.

7 The quantity R is the ratio of the power required to drive the tool to the total power in the rotary-tool process. For the tool investigated here ($\alpha_n = 10$ deg) about $^1/_3$ of the total power goes to drive the tool, while the remaining $^2/_3$ is consumed in driving the workpiece, when the angle of inclination is about 45 deg. From the afore-mentioned minimum points in the curves of u and μ, it would appear that the optimum angle of inclination is somewhat under 45 deg. Therefore a rotary tool should be operated with a surface speed V_r just under that of the work speed V_w, and the capacity of the tool-drive motor should then be about one half that of the main spindle motor used to drive the workpiece.

8 In the introduction it was suggested that one of the advantages of the rotary tool might be a reduction in the coefficient of friction due to the increase in the velocity of the chip relative to the tool V_{cr}, without at the same time making it necessary to increase correspondingly the work speed V_w. The quantity V_{cr}/V_w is a measure of this relative increase in chip speed, and it is evident in Fig. 9 that V_{cr}/V_w increases with an increase in the inclination angle. However, the coefficient of friction does not decrease continuously with an increase in V_{cr}/V_w. The reason for this lies in the fact that large rake angles inherently give large coefficients of friction.

As i increases above about 30 deg, the effective rake angle begins to increase rapidly, and neutralizes the beneficial effect associated with the increase in V_{cr}/V_w. Consequently, the coefficient of friction reaches a minimum at a value in the neighborhood of 30 deg. Thus the advantage with regard to coefficient of friction associated with increased chip speed is tempered by a simultaneous increase in the effective rake angle. As soon as the coefficient of friction begins to increase with increased V_r or i, the larger values of V_{cr} cease to be advantageous and actually represent a liability. The friction energy involves the product of V_{cr} and the coefficient of friction and will rise rapidly when both of these quantities begin to rise with increased i. The relatively flat portion of the u_f-curve up to an inclination of about 40 deg is due to the tendency for the decrease in μ with increased i to offset the corresponding increase in V_{cr}.

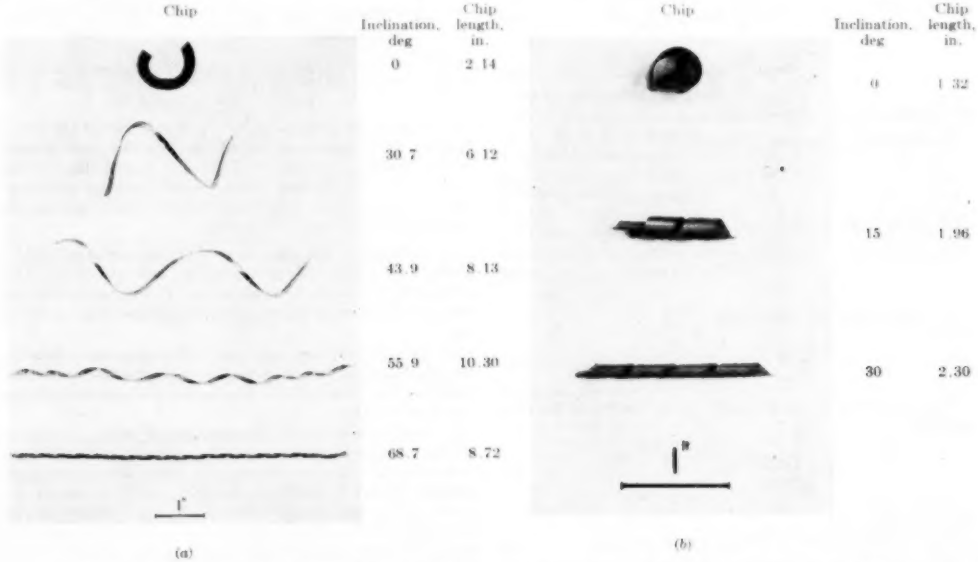

FIG. 10 CHIPS PRODUCED BY A ROTARY TOOL AND BY A CONVENTIONAL OBLIQUE TOOL; RAKE ANGLE $\alpha_n = 10$ DEG

(*a*, Chips from rotary tool; length of cut, 12 in.; cutting speed, $V_w = 44$ fpm; depth of cut, 0.0054 in.; cutting fluid, none. *b*, Chips from oblique tool; length of cut, 4 in.; cutting speed, 20 ipm; depth of cut, 0.005 in.; cutting fluid, carbontetrachloride.)

Representative chips produced with a rotary tool and with a conventional oblique tool are shown together in Fig. 10 to facilitate comparison. The similarity between the helical forms of both sets of chips is evident. The chip produced with a stationary tool ($i = 0$) is seen to be very inferior to those produced with tool rotation. The lengths of all chips in Fig. 10(*a*) correspond to a 12-in-length of cut, and it may be observed that the chip length increases with inclination to a point somewhat above 45 deg. The chip-length ratio of the longest chip is seen to approach unity.

Shear Stress - Shear Strain Paradox

As already mentioned, it has been found for both the conventional oblique tool and the rotary tool that the shear stress on the shear plane increases with increased inclination, while the corresponding shear strain decreases. From this we might infer that the material cut has a strange true stress - true strain curve with negative slope. This is most unlikely and other explanations must be sought.

While strain is the variable that normally has the greatest influence upon stress in a given test, there are numerous other items that normally influence the subfracture flow stress of a piece of metal.[5] These include (1) temperature; (2) rate of strain; (3) size of specimen. It can be shown that in metal cutting the effect of the shear-induced temperature on the shear plane is largely neutralized by the very large rate of strain that obtains. The higher the cutting speed (and hence the higher the rate of strain) the greater will be the temperature on the shear plane. The fact that these two variables have opposing effects upon flow stress tends to minimize the influence of temperature and rate of strain in metal cutting. Therefore it appears unlikely that either of these two variables could be responsible for the afore-mentioned anomaly.

The size effect involved in variation of the depth of cut has been shown to be of primary importance in metal cutting.[6,7] In the present problem, however, the depth of cut is constant, and it would appear that a size effect is not operative. However, we may consider a new type of size effect, in metal cutting—a size effect associated with the thickness of the shear plane as opposed to the depth of cut. Motion pictures taken through the microscope clearly reveal that when a relatively hard metal is cut with a good fluid, the shear plane is sharp and at the same time the shear angle is large. Conversely, when a relatively soft metal is cut, the region of shear is irregular and thick and the shear angle is of course low. In general, it is observed that the zone of shear along the shear plane decreases in thickness whenever ϕ increases. It is, therefore, conceivable that the shear flow stress associated with a metal cut with a high shear angle will be greater than that cut with a low shear angle since in the first case the shear zone will be small whereas in the second case it is large. We might refer to this as a shear-volume type of size effect.

Let us apply this idea to the stress-strain data of Table 1 and Fig. 9. In Fig. 11 points from the τ and γ-curves in Fig. 9 have been plotted for each 10 deg of inclination from 0 deg to 60 deg. The numbers beside each of these points refer to the corresponding values of ϕ_s. It may be seen that the points corresponding to the largest values of τ were obtained at large values of ϕ_s. This is in agreement with the previously proposed shear-volume size effect. A number of true stress-strain curves have been drawn in Fig. 11, each one corresponding to a different specimen size (or value of shear angle ϕ_s). The dotted curve is what might be expected from a conventional true stress-strain specimen of 0.505 in. diam.

In our previous work on size effect, the rake angle was maintained essentially constant, and hence there was only a small variation in ϕ for the several test points. In this way the shear-volume type of effect was about constant, and the effect of depth of cut could be studied independently. It would now appear that the flow stress in metal cutting is not related to the shear strain on a single curve for two reasons in place of one. These are as follows:

1 A size effect associated with depth of cut.

2 A size effect associated with the thickness of the shear plane, which is largely controlled by the effective shear angle ϕ_s.

Surface Effects

Two of the tests of Table 1 were performed in the presence of fluids. In the first case carbon tetrachloride was applied to the tool just before it reached the cutting zone. The total energy

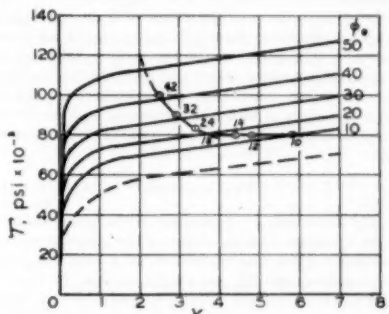

Fig. 11 Stress-Strain Curves for Specimens of Different Size, and Relation of These Curves to Metal-Cutting Data Obtained With Different Shear Angles

per unit volume in this case was less than that for the corresponding dry case as was the coefficient of friction. However, the results were not very spectacular. A thin amber-colored film was evident on the chips when using carbon tetrachloride, which appeared to result from a chemical reaction between fluid and chip. It would thus appear that the fluid was getting to the cutting zone and reacting. The failure of the results with carbon tetrachloride to approach those obtained in very low-speed tests could be due to the failure of the chloride film to prevent the surfaces from coming into contact at the high temperatures obtaining at the speed of these tests. Ferric chloride has a relatively low melting point (600 F at atmospheric pressure) and hence should not be expected to be very effective at speeds that will give surface temperatures much in excess of this value.

The second fluid used was a straight mineral oil. A large cloud of smoke resulted when this material was applied to the cutting edge. The total energy per unit volume was actually observed to be greater in this case than when a similar cut was taken in air. This might be explained by the fact that the oil itself was an ineffective cutting fluid, and the large smoke cloud that resulted

[5] The presence of normal stress on a shear plane has sometimes been considered to influence flow stress. While there is ample evidence in support of an increase in fracture strength with normal stress on a shear plane, the most reliable data available support the view that subfracture-flow stresses are independent of normal stress.

[6] "A Quantized Theory of Strain Hardening as Applied to the Cutting of Metals," by M. C. Shaw, *Journal of Applied Physics*, vol. 21, 1950, p. 599.

[7] "The Size Effect in Metal Cutting," by W. R. Backer, E. R. Marshall, and M. C. Shaw, Trans. ASME, vol. 74, 1952, pp. 61–72.

from its thermal decomposition could have tended to exclude air from reaching the tool.

An interesting observation was made concerning the importance of air in cutting with a rotary tool. When the tool was operated with $V_r << V_w$ and with a relatively large depth of cut, a wedge-shaped chip was produced such as that shown in Fig. 12. One side of the chip was thin with a high shear angle ϕ_1, while the other side of the chip was much thicker and the shear angle ϕ_2 correspondingly lower. Numerous cracks were evident along the thick edge of the chip, while the thin edge was completely continuous. All observations indicated a lower coefficient of friction at the thin region A than in the thick region B.

It would appear that oxygen carried in by the tool reacts with the chip in the vicinity of A and produces a low-friction oxide film in this area. If the width of cut AB is sufficient, the available oxygen may be consumed by the time the tool reaches point B and high friction (and hence low ϕ) will result in this area. If the foregoing explanation of this wedge formation were correct, the direction of the wedge should reverse when the direction of the tool is reversed. This was found to be the case.

The degree of wedging was pronounced only at low values of inclination. At the higher relative tool speeds and smaller depths of cut the chip was relatively uniform in cross section. In those instances where a wedge-shaped chip was obtained, the mean chip thickness was measured using a point micrometer.

The foregoing rotary-tool experience with air emphasizes the possibilities of the rotary principle as a means for introducing a cutting fluid. The failure of the two tests to substantiate the expected advantage of the rotary tool in conducting fluids to the cutting area is not conclusive. More work with other fluids capable of operating at higher temperatures, such as the heavy-duty sulphur-bearing oils, is required before a firm statement can be made.

Temperatures

The chip-tool interface temperatures of stationary and rotating tools were determined by the chip-tool thermocouple technique. The workpiece which was in the form of a tube was insulated from the machine, and the connections made in the manner described in a previous paper.[8] This work was done on a lathe, and the experimental setup is shown in Fig. 13. A recording self-balancing potentiometer was used to record the emf generated. The equilibrium temperatures were the values recorded, and in most cases quite a long cut had to be taken before the values became constant.

The results of this study are given in Fig. 14. Here it is seen that the temperature is a minimum at an angle of inclination of about 40 deg. This value corresponds approximately to those for minimum coefficient of friction and specific energy, Fig. 9. It may also be seen in Fig. 14 that a rotary tool operating at optimum speed may have a temperature that is as much as 400 F lower than that for an equivalent stationary tool. This is a very significant decrease in temperature.

Concluding Remarks

The rotary tool described herein is seen to be equivalent to an oblique cutting tool in many respects. In the case of the oblique tool, inclination is supplied to the tool geometrically, while in the case of the rotary tool it is introduced kinematically. The mechanics of the two tools are practically identical. There are, however, certain significant differences between these two tools, the following items being peculiar to the rotary tool:

1 A rest period during which time the cutting edge has an opportunity to cool and the adsorbed film of air or fluid has a chance to be replenished.

2 The rotary tool provides a means of increasing the relative velocity between chip and tool without necessitating a corresponding increase in the rate at which metal is cut.

Both the rotary tool and an oblique tool provide a greater effective rake angle without weakening the tool by requiring a corresponding increase in the normal rake angle. Both tools also provide means of controlling the direction of chip flow, which in some instances is of practical importance.

From the tests that have been made using a high-speed-steel rotary tool having a 10-deg normal rake angle, it would appear that the inclination angle should be about 40 deg in order to operate under conditions of minimum friction, total energy, and chip-tool interface temperature. This means that the surface velocity of the tool should be about 80 per cent of that of the work. Under this condition the power to drive the tool will be about one half of that required to drive the workpiece. Under optimum conditions the total power required for a given rate of cutting might be expected to be about 30 per cent less with a rotary tool than with the corresponding stationary tool, and at the same time the rotary-tool temperature might be expected to be some 400 F lower than that obtained at the point of a conventional tool. In the case of machine tools that are underpowered for use

[8] "The Effect of the Cutting Fluid Upon Chip-Tool Interface Temperature," by M. C. Shaw, J. D. Pigott, and L. P. Richardson, Trans. ASME, vol. 73, 1951, pp. 45–56.

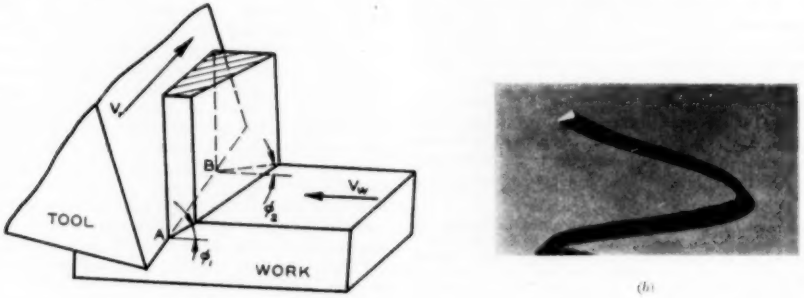

(a) (b)

Fig. 12 Wedge-Shaped Chip Produced by Rotary Tool When Depth of Cut Is Large and V_r Is Considerably Less Than V_w

(a, Schematic diagram. b, Photograph of chip.)

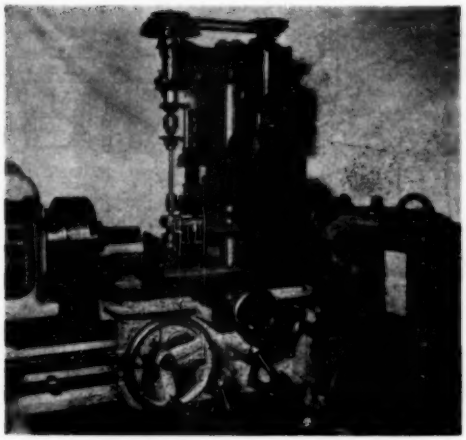

FIG. 13 ROTARY TOOL SETUP ON A LATHE TO MEASURE CHIP-TOOL INTERFACE TEMPERATURES

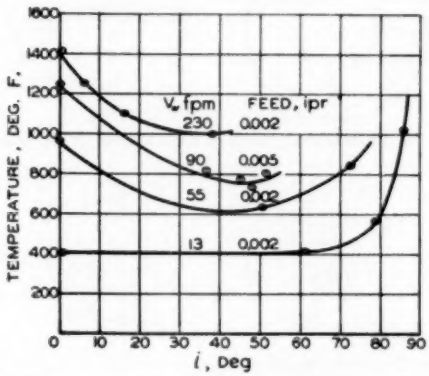

FIG. 14 REPRESENTATIVE CUTTING TEMPERATURE FOR ROTARY TOOL

(Work material SAE 1015 steel; tool material, 18-4-1 high-speed steel; tool diameter, 2.5 in.; rake angle, α_n = 10 deg.)

with present-day tool materials, the rotary tool may provide a means of overcoming this difficulty by requiring less total power for a given cut, and at the same time providing a convenient means for increasing the total power available to the machine by about 50 per cent.

The rotary cutting operation might be of practical interest in those cases where a large volume of metal must be removed in the shortest possible time. It would seem adaptable to large planers and shapers as well as to rough-turning operations. In the latter application, it would be advisable to make the tool of carbide and reduce the diameter to a minimum in order to avoid chatter that might arise when the cutting edge is long. The $2^1/_2$-in-diam tool investigated here did not chatter, however, even when the width of cut was $^1/_4$ in.

We have not had an opportunity to determine the relative life of a rotary tool, but the tests that have been run would lead us to expect it to be at least two orders of magnitude higher than that for an equivalent stationary tool. On one occasion, when machining a tube of $^3/_{16}$-in. wall thickness at 950 fpm and a feed rate of 0.005 ipr, a conventional high-speed-steel cutting edge was destroyed completely in about 5 sec, while a rotary tool made from identical tool steel exhibited no signs of distress after cutting for several minutes.

It is realized that more test work needs to be carried out on rotary cutting tools before their performance characteristics can be appreciated fully. It is hoped that others also will become interested in this device to the point of studying the life and efficiency characteristics of such tools with different rake angles using various cutting fluids.

ACKNOWLEDGMENTS

The authors wish to express their gratitude to Messrs. J. Leach, C. W. Christiansen, F. Anderson, D. J. Spooner, and M. Hablanian of the M.I.T. Machine Tool and Metal Cutting Division, for aid in this investigation. A grant from The Shell Oil Company that was used in connection with this work is gratefully acknowledged.

Discussion

R. S. HAHN.[9] Some time ago the writer independently carried out some tests on this type of metal cutting.[10] It may be of some interest to compare the writer's results with those of the authors.

The writer has found it more convenient to measure the chip-length ratio instead of the thickness ratio as the authors have done, because the chips are not always smooth on the back side. The chip-length ratio is given by

$$\frac{l_c}{l_0} = \frac{\sin \phi}{\cos (\phi - \alpha) \cos \psi}$$

Then, too, it is unnecessary to compute the angle η_c from Equation [6] of the paper, since this angle can be obtained directly from the chip. As shown in Fig. 15, herewith, the direction of the fine scratches on the burnished surface of the chip make an angle of $(\eta_c + \psi)$ in the authors' notation or $(\delta + \theta)$ in Fig. 15. By measuring these scratches with a microscope having a rotatable reticule in the ocular, it is a simple matter to obtain η_c.

The writer's results also indicate the existence of force components on the tool face and shear plane as evidenced by the angles ζ_c and ζ_s. The authors are to be congratulated on their recognition of forces acting at right angles to the direction of relative motion on the shear and tool-face planes—a fact not generally appreciated.

Although the writer used tungsten-carbide cutters with —10 deg rake, the minimum in friction coefficient at i = 30 deg, and the rise in shear stress were observed likewise.

It may be of some practical interest, in rounding out this excellent paper, to present some tool-life data accumulated on this type of tool. It can be said safely that tool life is many times that of conventional tools, even at high cutting speeds. Fig. 16 herewith shows the distance traveled to failure plotted against cutting speed. These data pertain to $^3/_8$-in-diam tungsten-carbide right circular cylinders where the end of the cylinder was used as the rake surface. These cylinders, when mounted in suitable holders, were used to cut on an 8-in. log in a lathe, the traction of the chip itself across the end of the cylinder, causing the tool to rotate. The outstanding life will be seen easily by comparing the solid curves (wherein the cylinders were

[9] Research Engineer, The Heald Machine Company, Worcester, Mass. Mem. ASME.

[10] "On Napier's Metal Cutting Process," by R. S. Hahn (to be published).

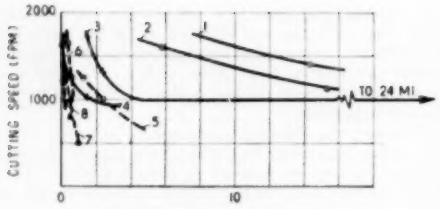

(Material SAE 4150, Rockwell hardness 16 C.)

Curve no.	Carbide grade	Lead	Depth of cut	Type of cutting
1	Carboloy 831	0.0044	0.005	Rotary
2	Carboloy 831	0.0076	0.015	Rotary
3	Carboloy 883	0.0044	0.005	Rotary
4	Carboloy 883	0.0076	0.015	Rotary
5	Carboloy 831	0.0044	0.005	Stationary
6	Carboloy 831	0.0076	0.015	Stationary
7	Carboloy 883	0.0044	0.005	Stationary
8	Carboloy 883	0.0076	0.015	Stationary

FIG. 15 COMPARATIVE LIFE TESTS BETWEEN ROTARY CUTTER AND STATIONARY CUTTER

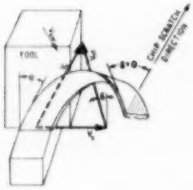

FIG. 16 ILLUSTRATION OF CHIP IN ORTHO-OBLIQUE CUTTING PROCESS SHOWING CHIP-FLOW ANGLE θ AND CHIP-SCRATCH ANGLE δ

permitted to rotate) with the dashed curves (where the cylinders are held stationary).

Although James Napier in 1868 did not have the materials and equipment we have today, he foresaw the great advantage and important commercial possibilities of this type of tool.

The authors, in analyzing and presenting the features of this type of cutting, are to be commended not only for its research value but for its important possible commercial value.

E. K. HENRIKSEN.[11] In the conclusion, the authors invite others to participate in the study of the rotating tool. In a way we already have anticipated this invitation. The idea was conceived and the work was done by Mr. Wilbur H. Moore who graduated in 1951 from Cornell as a mechanical engineer and who is now an Ensign in the United States Navy. In 1949 Mr. Moore presented to the writer the idea of a rotating circular cutting tool as the subject for his "fifth-year project." A patent survey and the experimental and theoretical work were done through the period March, 1950-May, 1951, and the report was completed in June, 1951. Mr. Moore's approach and the methods employed differ somewhat from those described in the paper, and he also presented some aspects of the problem not covered there. A brief extract follows:

A STUDY OF THE APPLICATION OF A ROTATING, TOOTHLESS CUTTER TO THE CREATION OF SURFACES OF REVOLUTION AND OTHER SURFACES, BY WILBUR H. MOORE, BME

Out of a discussion of using the common friction-type band saw for the generation of various surfaces arises the possibility of replacing the flexible saw blade by a circular wheel. This, when rotated at high speed, may be used as a friction cutter, or

[11] Professor in Charge, Department of Materials Processing, Cornell University, Ithaca, N. Y. Mem. ASME.

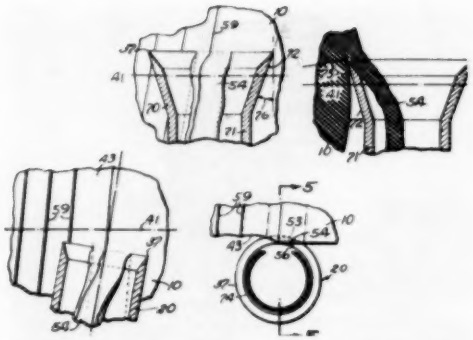

FIG. 17 TUBULAR ROTATING TOOL FOR TRIMMING TYPEWRITER PLATENS

(From patent survey, carried out in connection with W. H. Moore's project, Cornell 1951.)

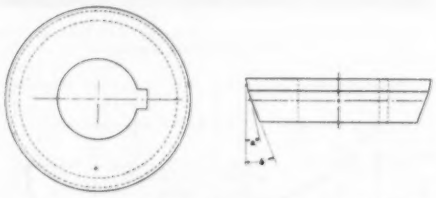

FIG. 18 EXPERIMENTAL CIRCULAR TOOL, USED BY W. H. MOORE

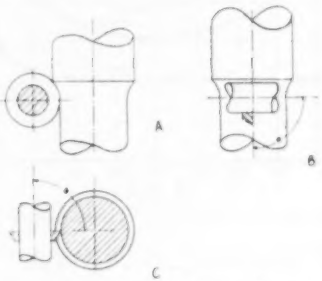

FIG. 19 CIRCULAR TOOL AS A LATHE TOOL

modified, with no teeth, as a rotating shearing cutter, or without rotation, as an ordinary cutter which may be indexed, when dull, to present a new sharp edge. If used as a rotating shearing cutter, there is the severing effect of the sawtooth edge which the cutter would have even if ground as a toothless cutter, plus the effect of rotation on the frictional forces acting on the chip.

Several variations of this idea exist. One[12] is used for the trimming of platens for typewriters and is a slightly flared tube rotating about a vertical axis, the upper edge of which is sharpened, Fig. 17 of the discussion. The experimental cutter is shown in Fig. 18. Its peripheral surface is ground to form two cones (angles a and b) in order to save grinding when resharpening (this detail is omitted in the following illustrations).

[12] U. S. Patent No. 2,061,581, W. A. Lippincott: Apparatus for rimming cylinders.

In Fig. 19 is shown the tool mounted on a lathe, an arrangement which can be modified by terminating the shaft at the face of the cutter, and by varying the angles ϕ and θ in either direction. It is evident that this tool also can be used with planers, shapers, and the like.

Fig. 20 illustrates four sections *A-B-C-D* through the work and the cutting tool, each at right angles to the cutting edge. The

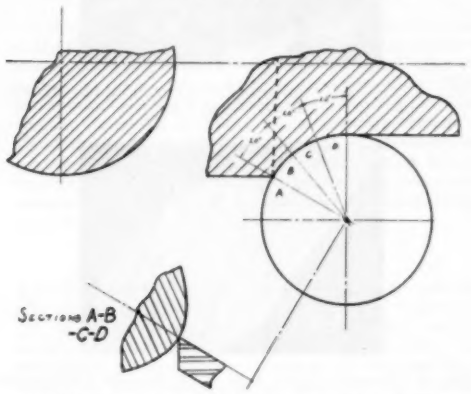

FIG. 20 CIRCULAR TOOL IN ON-CENTER POSITION, WITHOUT TILT

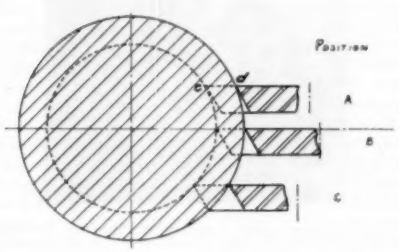

FIG. 21 CIRCULAR TOOL, SHOWN IN VARIOUS RELATIONS TO CENTER HEIGHT

characteristic angles, when measured in planes perpendicular to the cutting edge, remain the same from *A* to *D*, but the cutting speed varies along the line of contact from plane *A* to plane *D*. The maximum cutting speed, measured on the work, occurs at *A*, the minimum cutting speed occurs at *D*. The tool velocity is constant for all points along the edge, but the *relative* speed between work and tool varies, in size and direction, from *A* to *D*. It will come closest to the vertical at *A*, and it will deviate most from the vertical at *D*. Marks on the machined surface, owing to imperfections in the tool edge, will follow lines of relative velocity at *D*.

If the position of the cutter is shifted in a vertical direction, movement upward will result in a decrease in the relief angle and an increase in the rake angle; moving it downward results in changes in the opposite direction. It is obvious that vertical movement has the same effect as changing angle ϕ in Fig. 19, which may simplify the design of the tool-holding device. Various positions are shown in Fig. 21. Position *A* is selected so as to have one value of relief angle equal to zero. This is the case for point *c*, which is equivalent to section *D* in Fig. 20, in other words, that point of the cutting edge which is cutting on the smallest diameter. Position *A* is, therefore, the extreme upper position where cutting still is possible. It is evident, however, that at point *d* the relief angle has not been reduced to zero, so there is a considerable variation in relief angle along the arc from point *d* to point *c*. By tilting the tool the angles will be changed. A tool in a tilted position is shown in Fig. 22, and in Fig. 23 are shown the four sections *A*, *B*, *C*, and *D*, clearly indicating the changes in angles. For the tilted position shown the rake angles are increased and the relief angles are decreased.

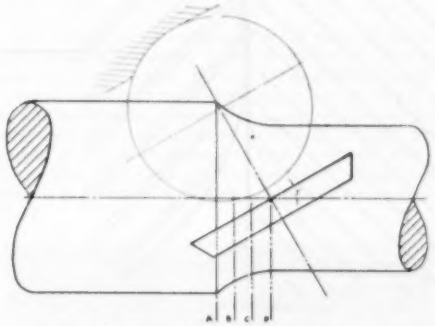

FIG. 22 CIRCULAR TOOL IN TILTED POSITION

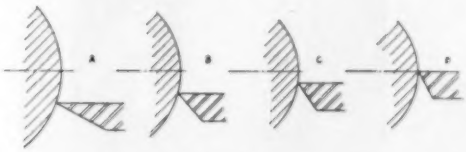

FIG. 23 EFFECT OF TILT ON RAKE AND RELIEF ANGLES

The cross section of the cut has a characteristic comma-shape, as shown in Fig. 24. Consideration of chip form and chip formation leads to the question of direction of rotation, and two different and independent viewpoints may be represented.

One way of determining the direction of rotation is derived from the chip form; for reasons of cooling the cutter should rotate from points of large chip thickness to points of small chip thickness; when applied to Fig. 24, this means counterclockwise rotation.

The other viewpoint for choosing the direction of tool rotation can be applied to a tilted cutter and consists in a consideration of chip flow. If a tilted tool is cutting without rotation, the chip will show a tendency to flow "down hill," that is, to approach (but not necessarily to coincide with) the direction of maximum slope of the tool face. In order to facilitate the chip flow in the best possible manner, it may be expected that the direction of rotation should coincide with this down-hill direction.

The chip strikes the tool with a higher velocity at section *A*, Fig. 22, then at section *D*. Consequently it will curl, and there will be a tendency to compress the thicker edge of the chip while the thinner edge will be under tension.

The experimental work was done on a gear-hobbing machine. This machine was selected because it offers, without alteration of any kind, all the feeds, angles, and directions required. The choice of speeds is somewhat restricted which, however, was of minor importance for the present project, aimed, essentially, at a

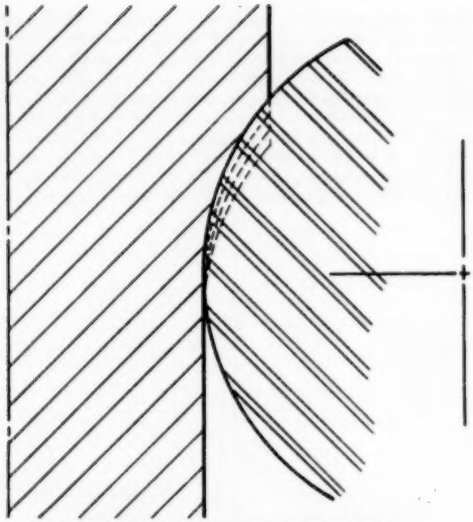

FIG. 24 CHIP CROSS SECTION FOR CIRCULAR TOOL

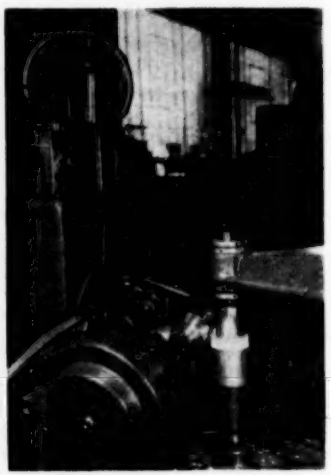

FIG. 25 EXPERIMENTAL SETUP ON GEAR-HOBBING MACHINE, USING CIRCULAR TOOL

basic study of the method. The setup is shown in Fig. 25. A characteristic sample of a chip taken in aluminum is shown in Fig. 26. The frayed edges indicate the tension in the chip, as

FIG. 26 ALUMINUM CHIPS, PRODUCED IN W. H. MOORE'S EXPERIMENTS, COARSE FEED

FIG. 27 ALUMINUM CHIPS, FROM W. H. MOORE'S EXPERIMENTS, FINE FEED

FIG. 28 CAST-IRON CHIPS FROM W. H. MOORE'S EXPERIMENTS

explained before, and chip surfaces show lines of relative velocity. A chip, from a light cut, is shown in Fig. 27; the difference between the thin edge frayed by tensile stresses (upper part of the illustration) and the thick edge, exposed to compression, is evident. Some tests were made on cast iron, and a sample of the chips is shown in Fig. 28.

The writer wishes to join in well-deserved compliments and congratulations to the three authors.

AUTHORS' CLOSURE

The authors wish to acknowledge the contributions to the art of rotary-tool design and performance contained in the discussions of Dr. Hahn and Professor Henriksen. Several interesting ideas are presented in these discussions but it does not appear that any additional comment on our part is necessary.

Measuring the Cooling Properties of Cutting Fluids

By G. M. HAIN,[1] CINCINNATI, OHIO

The ability of a cutting fluid to reduce the temperature at the chip-tool interface in the machining of metals is of utmost importance to long tool life. This ability depends, in part, on the heat-transfer properties of the fluid. This paper describes a simple technique for evaluating the heat-transfer properties of fluids. An alternating current of about 50 amp heats the walls of a length of stainless-steel hypodermic tubing while fluid is forced through it at a constant rate. Thermocouples brazed at intervals to the outside of the tube wall measure the wall temperature from which heat-transfer data are derived.

Introduction

SCHALLBROCH, Schaumann, and Wallichs (1)[2] measured tool life as a function of chip-tool interface temperature in dry cutting with high-speed steel tools and found that tool life varied inversely as approximately the 20th power of this temperature. M. E. Merchant (2) and M. C. Shaw and his coworkers (3) have reported that coolants reduce the chip-tool interface temperature partly by reducing the friction between chip and tool and partly by direct transfer of heat. Reducing chip friction against the tool not only reduces frictional heat at this point, but, by raising the angle of the shear plane, also lowers the amount of heat produced in plastic flow of metal at the shear plane. On the other hand, the heat-transfer properties of the fluid provide direct cooling of tool, chip, and workpiece. For cutting-fluid development purposes it is desirable to measure, or at least, to compare the heat-transfer properties of the fluid separately from the friction-reducing properties. The fact that tool life is so significantly influenced by small temperature differences, furthermore, makes it desirable that the apparatus used to measure heat transfer be capable of a high degree of sensitivity.

Measurements of the heat-transfer properties of cutting fluids made in the past (4) have not been very sensitive—not sensitive enough, for example, to distinguish between various water-soluble cutting fluids in recommended dilutions and at temperatures approximating workpiece temperatures in the machining of metals with coolants.

A stainless-steel tube heated by passing an alternating or direct current along it makes an excellent and easily measured source of heat flux. The temperatures of its wall are easily measured by brazing fine-wire thermocouples to it. When fluids are pumped through such a tube to remove heat, the walls are not corroded nor is the flow of fluid disturbed in an irreproducible way by wall irregularities. For these reasons, stainless-steel tubes have been used in this way in many previous investigations of heat transfer (5, 6). The tube used in the present investigation was selected to give high sensitivity.

Apparatus

Fig. 1 shows the apparatus used in this study of the cooling properties of cutting fluids. A stainless-steel tube A, enclosed in a box to shield it from air currents, is heated along a portion of its length by passing a heavy alternating current through it. The fluid to be evaluated is pumped at a constant flow rate from a small tank by a metering pump C, through a copper coil immersed in a constant-temperature bath D, through tube A to drain. The tube-heating power is controlled by a single knob B. Tube A is shown in detail with its attached thermocouples in Fig. 2.

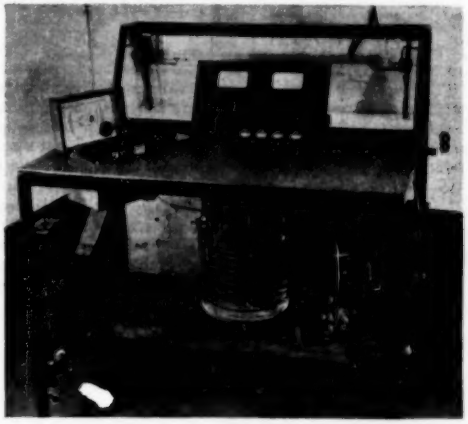

Fig. 1 Apparatus for Measuring Heat-Transfer Properties of Cutting Fluids
(A, Heat-transfer tube; B, tube heat control; C, metering pump; D, constant-temperature bath.)

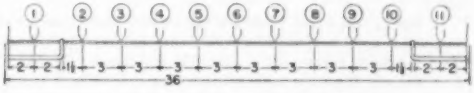

Fig. 2 Heat-Transfer Tube Detail

This heat-transfer tube is a 36-in. length of 12-gage stainless-steel hypodermic tubing (0.109 in. OD × 0.012 in. wall) with fine-wire copper-constantan thermocouples (B & S 30 gage, 0.010 in. diam) brazed to its outside wall at 3-in. intervals as shown in Fig. 2. Since the wires are large for the wall thickness, the junctions and wires are well wrapped with Fiberglas tape to minimize heat losses. The emf is measured with a portable

[1] Research Chemist, The Cincinnati Milling Machine Company.

[2] Numbers in parentheses refer to the Bibliography at the end of the paper.

Contributed by the Production Engineering Division and the Cutting Fluids Research Committee and presented at the Annual Meeting, Atlantic City, N. J., November 25–30, 1951, of The American Society of Mechanical Engineers.

Note: Statements and opinions advanced in papers are to be understood as individual expressions of their authors and not those of the Society. Manuscript received at ASME Headquarters, August 13, 1951. Paper No. 51—A-40.

potentiometer supplemented with a 12-point thermocouple switch and an ice-point junction. The leads supplying the heating current are 0.25-in. copper rod brazed to the center 27 in. of the tube. This section has an electrical resistance of approximately 0.22 ohm. In the end sections there is no heat input, and so the couples measure the input and outlet temperatures of the fluid itself. The alternating-current supply consists of a 2-kw continuously variable autotransformer feeding a stepdown transformer with a secondary winding rated at 100 amp and 18 volts. Power is measured with a large-scale voltmeter and a large-scale ammeter. Although direct current has been used by other investigators (5) for tube power, its use produces stray emf in the thermocouple circuits for which corrections are difficult to make. No insulation is used on the tube since the heat loss to the air is slight, i.e., less than 1.5 watts for aqueous cutting fluids under the conditions of the test used.

From a reservoir of 1 gal capacity, the fluid under test is metered to the constant-temperature-bath coil and then to the tube by means of a Zenith No. 5, type B, metering pump driven through lathe-change gears to give precisely 6.63 cu in. per min, 13.25 cu in. per min, or 19.85 cu in. per min. The constant-temperature bath is a conventional type designed for kinematic-viscosity measurement. Set at 90 F ± 0.1 F, it has ample capacity to maintain fluid-input temperature within a few tenths of a degree Fahrenheit.

Results of Tests

The results of a test are interpreted graphically, using the differences between input temperature and the tube-wall temperatures as ordinates and the distances along the heated section of the tube as abscissas. Since the heat input W per unit length of tube is uniform, the bulk temperature of the fluid rises almost linearly with distance along the tube. By "bulk temperature" is meant the average temperature of the fluid which would result if the fluid flowed into a mixing chamber at this point. The over-all temperature difference Δt at any point is the tube-wall temperature less the bulk temperature of the fluid at that point. The over-all heat-transfer coefficient h at any point is heat-flux density divided by temperature difference or

$$h\ (\text{Btu/hr sq ft deg F}) = \frac{\text{heat input (watts} \times 3.413)}{\text{tube-wall area (sq ft)} \times \Delta t\ (\text{deg F})}$$

$$= \frac{\text{watts} \times 3.413}{\frac{27 \times 0.0855\ \pi}{144} \times \Delta t\ (\text{deg F})} = \frac{67.6\ W}{\Delta t}$$

A setting which provides satisfactory sensitivity for a wide range of fluids is 365 watts for the tube power and 13.25 cu in. per min for the flow rate. This corresponds to a bulk velocity of 3.21 fps. Typical results are shown in Table 1 and Figs. 3, 4, 5, 6, and 7.

In Figs. 3 and 4 and Table 1 it can be seen that aqueous cutting fluids have heat-transfer coefficients significantly different from water for a given set of operating conditions. In general, heat transfer improves with dilution, but one aqueous cutting fluid may be a considerably better heat-transfer fluid than another at the same dilution. Part of the difference is due to oil content but viscosity differences are probably equally important. Fig. 5 shows two cutting oils both having viscosity of 100 SUS at 100 F, but showing differences in specific heat, as indicated by differences in the bulk temperature at the outlet, and an average over-all heat-transfer coefficient, differing by about 20 per cent, as indicated by the tube-wall temperature differences. Fig. 6 shows similar differences in two nonpetroleum heat-transfer oils, and Fig. 7 shows the characteristics of Stoddard solvent, a low-viscosity, high-boiling-point naphtha. Fig. 7 also shows the characteristics of two emulsions prepared from Stoddard solvent each containing 10 per cent Stoddard solvent and 90 per cent water, but one oil-in-water type and the other water-in-oil type. Despite the fact that the water-in-oil-type emulsion had a consistency comparable to whipped cream, its heat-transfer properties more closely resembled those of water than those of Stoddard solvent.

It is of interest to note that most of the curves of tube-wall temperatures shown in Figs 3 to 7 appear as two straight lines joined by a connecting curve. The straight-line portion at the

TABLE 1 HEAT-TRANSFER PROPERTIES
(13.25 cu in. per min and 365 watts heat input)

	h, over-all heat-transfer coefficient 9 in. from input, Btu/hr sq ft deg F	Rise in tube-wall temperature in 27 in., deg F
Water	1760	48
Water dispersion, 1:50 cutting fluid A	1370	53
Water dispersion, 1:10 cutting fluid A	948	63
Water dispersion, 1:15 cutting fluid B	632	61
Water dispersion, 1:15 cutting fluid C	1120	54
Cutting oil B (100 SUS at 100 F)	158	355
Cutting oil A (100 SUS at 100 F)	188	318
Nonpetroleum heat-transfer oil A	135	292
Nonpetroleum heat-transfer oil B	173	355
Stoddard solvent	149	216
Stoddard solvent 10 per cent, water 90 per cent (o-w)*	947	68
Stoddard solvent 10 per cent, water 90 per cent (w-o)*	547	117

* (o-w) is predominantly oil-in-water-type emulsion. (w-o) is predominantly water-in-oil-type emulsion.

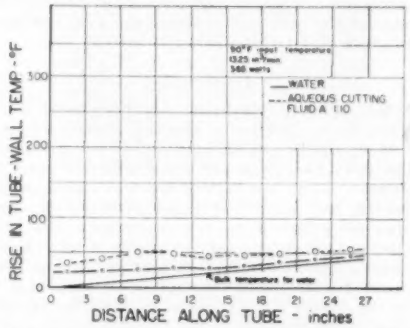

Fig. 3 Chemical-Emulsion Type of Water-Soluble Cutting Fluid at 1:10 Dilution in Comparison With Water

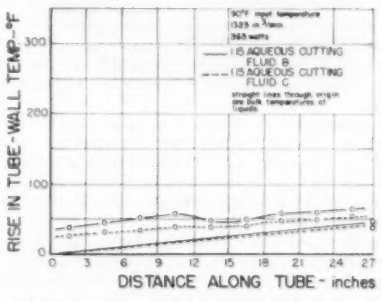

Fig. 4 Two Conventional Soluble Oils at 1:15 Dilution (Apparent advantages of C as a coolant are largely offset by its instability as an emulsion.)

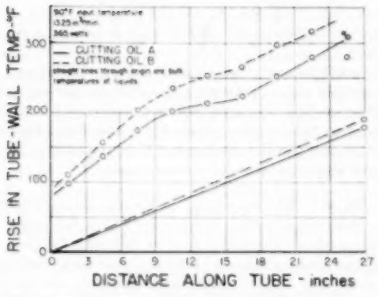

FIG. 5 TWO STRAIGHT CUTTING OILS OF SAME NOMINAL VISCOSITY—100 SUS AT 100 F—SHOWING WIDE DIVERGENCE IN HEAT-TRANSFER PROPERTIES

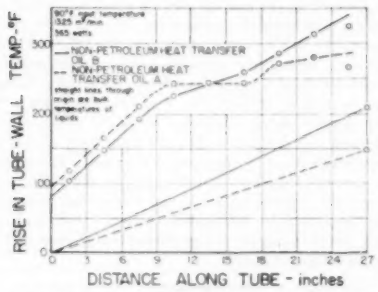

FIG. 6 TWO NONPETROLEUM HEAT-TRANSFER FLUIDS SHOWING A REVERSAL IN RELATIVE HEAT-TRANSFER ABILITIES WITH INCREASING TEMPERATURE

inlet end of the curve represents streamline flow, the final straight line, turbulent flow, and the connecting curve a transition region. The characteristic shape of these curves remains the same for all three flow rates and over a wide range of power inputs which avoid boiling conditions.

CONCLUSIONS

It is evident that with the present instrument it is possible to demonstrate and measure significant differences in the over-all heat-transfer coefficients of dilute aqueous cutting-fluid mixes as the concentration is changed. Furthermore, the instrument is able to show significant differences in the heat-transfer properties of apparently similar water-soluble cutting fluids at a given dilution.

Of particular interest to those concerned with metal cutting are the large differences in the relative cooling abilities of cutting oils in comparison with water-base cutting fluids. Although the specific heats of oils are only about one half that of water, the heat-transfer coefficients for cutting oils are only about one seventh that of water, or of cutting fluids containing larger percentages of water.

The long tube used in the present instrument makes it possible to obtain a complete picture of heat transfer in both the streamline and turbulent regions, over a wide range of temperatures.

ACKNOWLEDGMENTS

The author wishes to thank Dr. M. E. Merchant, Mr. Robert L. Henry, and other members of the research staff of the Cincinnati Milling Machine Company for their assistance on this project. Special mention should be made of the work of Mr. Edward Schloss and Mr. James Howard who constructed and tested the first working model of this apparatus as part of a University of Cincinnati Co-operative undergraduate thesis project.

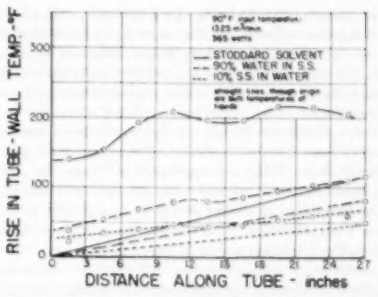

FIG. 7 STODDARD SOLVENT COMPARED WITH 10 PER CENT STODDARD SOLVENT EMULSIONS OF BOTH OIL-IN-WATER AND WATER-IN-OIL TYPES

BIBLIOGRAPHY

1 "Testing for Machinability by Measuring Cutting Temperature and Tool Wear," by H. Schallbroch, H. Schaumann, and R. Wallichs, Vortrage der Hauptversammlung der Deutsche Gesellschaft für Metallkunde, Verein deutscher Ingenieure Verlage, 1938, pp. 34–38.

2 "Fundamentals of Cutting Fluid Action," by M. Eugene Merchant, *Lubrication Engineering*, vol. 4, 1950, pp. 163–167.

3 "The Effect of the Cutting Fluid Upon Chip-Tool Interface Temperature," by M. C. Shaw, J. D. Pigott, and L. P. Richardson, Trans. ASME, vol. 73, 1951, pp. 45–52.

4 "A Physicochemical Investigation of the Cooling Ability of Liquids in Cutting Metals," by N. A. Pleteneva and P. A. Rebinder, Izvestiya Akademii Nauk SSSR (Bulletin of the Academy of Sciences of the USSR), 1946, pp. 1823–1829.

5 "Heat Transfer to Water at High Flux Densities With and Without Surface Boiling," by Frank Kreith and Martin Summerville, Trans. ASME, vol. 71, 1949, pp. 805–815.

6 "Heat Transfer at High Rates to Water With Surface Boiling," by W. H. McAdams, W. E. Kennel, C. S. Minden, R. Carl, P. M. Picornell, and J. C. Dew, *Industrial and Engineering Chemistry*, vol. 41, 1949, pp. 1945–1953.

Discussion

B. T. CHAO[3] AND K. J. TRIGGER.[4] With the arrangement of the heat-transfer tube used by the author, conduction losses due to the two end sections of the hypodermic tubing and due to the two heavy copper leads may become appreciable. In fact, this is reflected in the characteristic dip of the tube-wall temperature at a point farthest from the fluid-inlet end, Figs. 5, 6, and 7 of the paper. The rate of heat loss actually can be calculated from the Fourier equation of conduction by finding the slope of the temperature-distance curve at the two ends.

The author indicates that the "local" heat-transfer coefficient can be evaluated by the formula[5] $h = 67.6\ W/\Delta t$. From the temperature-distance plot given in Figs. 3 to 7 of the paper, it is evident that Δt varies from point to point along the length of the tube. Consequently, h also varies accordingly. Under such circumstances it is doubtful that the bulk temperature of the fluid

[3] Assistant Professor of Mechanical Engineering, University of Illinois, Urbana, Ill.

[4] Professor of Mechanical Engineering, University of Illinois, Mem. ASME.

[5] In this equation, W should be the electrical input in watts over 27 in. length of the tube, but not the heat input per unit length of the tube as the author has defined.

will vary linearly with distance along the tube. The tabulated values of h given in Table 1 of the paper are calculated at a point 9 in. from the inlet and which is just as arbitrary as any other location. It is hardly justifiable to consider these individual local values as a fair representation of the cooling property of the various cutting fluids.

There are numerous factors which contribute to such a wide variation of heat-transfer coefficients for a given fluid at a given mass rate of flow. They are, among other things, the change of viscosity and thermal conductivity of the fluid with temperature and, most important of all, the change in flow pattern as the fluid traverses along the tube. This latter factor has an important bearing on the mechanism of heat transfer.

This method of evaluating the heat-transfer coefficients by forcing the fluid through the stainless-steel tubing is useful in obtaining data for apparatus of a similar flow pattern. The writers question that it will yield really useful data for the cooling property of cutting fluids.

The bulk of the fluid applied during a cutting operation traverses the cutting orbit without much change in temperature. Some of the fluid, however, comes in contact with the high-temperature zone and it is subjected to such effects as evaporation, volatilization, viscosity changes, and so on, due to high temperatures. While the proportion of fluid being so affected may be relatively small, the occurrence of such effects may be significant. Problems of the effect of cutting-fluid temperature on cooling power, the formation of barrier films, the vapor-phase effects among others, may bear an important relationship to cutting-fluid performance.

It is the writers' opinion that such properties should be evaluated under conditions which closely simulate those existing during actual cutting operations.

R. S. Hahn.[6] This paper represents a start in the right direction to discover the important qualities involved in cutting fluids. There are several points which are not clear to the writer. For example, it appears that the temperature of the incoming and outgoing liquid is read by thermocouples on the OD of the tube at the ends which are unheated. If so, in view of the fact that the thermal diffusivity of the fluid is generally very small $\kappa = 0.001$ cm^2 per sec compared to stainless steel $\kappa = 0.05$ cm^2 per sec, it would seem that large temperature gradients might well exist between the tube and the liquid. Furthermore, what would prevent heat conduction along the tube into these unheated regions?

Another point not clear is that the heat-transfer coefficient apparently is computed for the full 27-in. length of tube (assuming a constant temperature difference Δt along the tube), but is recorded in Table 1 at 9 in. from the input end.

It is obvious how the heat-transfer properties of the coolant may be important in removing heat from the tool and workpiece (for instance, to maintain dimensional accuracy). However, it is not clear how the cooling effect of the fluid acts to reduce the chip-tool interface temperature by direct heat transfer as the author stated. Presumably the fluid bathing the top surface of the chip as it leaves the shear zone al stracts heat from the chip, but at normal cutting speeds (300 fpm) it may be shown that this cooling must occur after the chip is well past the shear zone and has passed over the tool face. Wilson[7] has shown the temperature distribution in a strip moving from a hot region into a cold region. This strip might well be considered as a chip leaving the work and being cooled by cutting fluid. He shows that the temperature falls approximately as

$$\exp\left[\frac{V}{2\kappa} - \sqrt{1 + \left(\frac{V}{2\kappa}\right)^2}\right] X$$

where V is the velocity (cm per sec) and κ is the thermal diffusivity (cm^2 per sec). If we take $V = 150$ cm per sec and $\kappa = 0.10$ cm^2 per sec it will be seen that on a microscopic basis the fall in temperature is very slow. It would be interesting if the author would show how direct heat transfer from the chip to the fluid will reduce chip-tool interface temperatures.

M. C. Shaw.[8] The importance of tool temperature upon tool life has been demonstrated in reference (1) of the paper. The temperature referred to in this work is, however, the mean chip-tool interface temperature, as opposed to the mean temperature of the entire tool, or the mean temperature of the workpiece. The temperature of the chip-tool interface will be altered a negligible amount if the fluid merely cools the tool in bulk. This is evident in Fig. 11 of reference (3) of the paper, where it is seen that when the fluid does not have time to penetrate to the zone of heat dissipation, because the cutting speed is too high or the depth of cut (and hence the contact area between chip and tool) is too great, the fluid has little effect upon the chip-tool interface temperature. To be really effective a coolant must penetrate to points that are close to the areas where heat is being dissipated, i.e., close to area A or B in Fig. 8 of this discussion. Otherwise the thermal energy dissipated along the shear zone A or along the tool face B will flow into the main body of the tool or workpiece before it can be absorbed by the fluid. The speed with which a coolant can penetrate between chip and tool C and between tool and finished surface D and form a continuous film is extremely important in cutting-fluid action. Once such a film is formed, the heat-transfer film coefficient and the specific heat of the fluid play important roles.

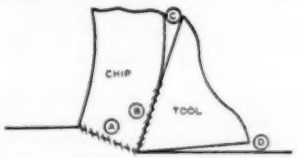

Fig. 8 Schematic View of Partially Formed Chip
(A and B are the principal areas where heat is generated, while C and D are the regions where fluid penetration must occur for effective cooling action.)

The apparatus described by the author provides a means for comparing the cooling properties of a fluid (heat capacity and heat-transfer coefficient) under conditions that provide "complete contact" between the metal surface and the fluid. Under such conditions water is found to be a better coolant than a water-base cutting fluid, and a cutting oil is found to be only one seventh as effective as water, even though the ratio of specific heats of these materials is one half. These observations suggest that both the water-base fluid and the cutting oil contain surface-active agents that are metallophilic in nature and hence cause a decrease in the heat-transfer film coefficient. The fact that the viscous water-in-oil emulsion of Fig. 7 of the paper exhibited cooling properties that were superior to those for the nonviscous oil-in-water emulsion is further evidence of the importance of a surface-active agent in a coolant, since emulsifiers that produce water-in-oil emulsions are usually metallophilic while those that are used to produce oil-in-water emulsions tend to be metallophobic.

[6] Research Engineer, The Heald Machine Company, Worcester, Mass. Mem. ASME.

[7] "On Convection of Heat," by H. A. Wilson, Proceedings of the Cambridge Philosophical Society, vol. 12, 1904, pp. 403–423.

[8] Head, Machine Tool Division, Department of Mechanical Engineering, Massachusetts Institute of Technology, Cambridge, Mass. Mem. ASME.

The important speed of film formation is not evaluated by this test. While pure water has the best cooling capacity of any fluid when it is in complete contact with a heated metal surface, its film-forming tendency is poor relative to most other materials. Since cutting oils have a tendency to spread over a metal surface more quickly and more completely than does pure water, it is not surprising to find oils providing superior cooling performance in some instances despite the adverse 1 to 7 cooling ratio of oil relative to water. The question of whether an oil or water-base fluid offers the best cooling characteristics is a popular one and frequently enters discussions involving cutting fluids. There seems to be good production experience in support of both points of view. It would appear that water-base fluids can be provided with surface-active agents that have a strong enough tendency toward film formation to render them better coolants than oils. It would appear further that all water-base fluids are not so endowed and thus, in some instances, may exhibit cooling characteristics in cutting that actually are inferior to those for oils.

The author's test conditions also differ from those in actual practice in another important way. The test heat-transfer conditions are actually quasistatic relative to the conditions found in a cutting operation. In turning, the time available for heat transfer is measured in milliseconds and in grinding in microseconds. In the present test the time required for the fluid to flow from one end of the tube to the other is close to 1 sec. This temporal difference between test and actual conditions would be important if the heat-transfer conditions were influenced by a phase change of a constituent of the cutting fluid; to be more specific, crystalline waxes which have a latent heat of fusion sometimes have been added to fluids in order to promote good cooling. The idea behind this action is that the wax particles will melt upon coming in contact with the hot surface, thus absorbing an amount of thermal energy equivalent to their latent heat of fusion. The latent heat that is thus absorbed augments the specific heat of the fluid to provide improved cooling characteristics. Now, it takes a significant time for wax to melt, and since there is a considerable difference in the time constants for the author's test and the cutting process, there is real danger in concluding that the wax will operate in the foregoing manner in practice even though it can be demonstrated that it has a real influence in promoting heat transfer in the author's apparatus.

The author attributes the change in slope of the temperature curves to a change from laminar to turbulent flow. If we compute the Reynolds numbers for the case of water flow in Fig. 3 of the paper, we find the following values at the beginning, middle, and end of the tube: 2660, 3520, and 4400 (based upon kinematic viscosities of 0.86×10^{-5}, 0.65×10^{-5}, 0.52×10^{-5} sq ft per sec at these three points, respectively). From this we might conclude that the flow in this case is turbulent all the way since the critical value of Reynolds number is usually from 1000 to 2000. If we make similar calculations for the data in Fig. 5 of the paper, we find the following values of Reynolds number at the beginning, middle, and end of the tube: 68.2, 309, and 739 (based upon the following assumed values of kinematic viscosity: 33.5×10^{-5}, 7.4×10^{-5}, and 3.1×10^{-5} sq ft per sec, which are reasonable values for a 100 sec oil at 100 F at the temperatures obtaining). These values of Reynolds number indicate laminar flow at all points. Since a discontinuity appears in both the curves for water and oil despite the values of Reynolds number pertaining, it would appear that the change in slope that is evident in the several curves is not due to a change from laminar to turbulent flow.

When a fluid enters a tube, it must flow a considerable distance down the tube before the velocity distribution across the tube is developed fully. This distance one must go downstream before the flow is fully developed is called the "transition length."[9] The fluid at the entrance to a tube has a uniform velocity distribution across the tube, which gradually changes to a parabolic velocity distribution in the case of laminar flow, or a velocity distribution that is between that for uniform flow and a parabolic distribution in case the flow is turbulent when transition is complete. The transition length-to-diameter ratio has been estimated by Langhaar to be about 0.058 (Reynolds number). From this we might estimate the transition length to be (0.0855) (0.058) (3520) for the case of water in Fig. 3 of the paper, or roughly about 17.5 in., which is in reasonable agreement with the location of the break in the curve for water in Fig. 3.

It is evident in Fig. 3 that the initial slope of the curve is less steep than the slope of the curve beyond the transition point. This may be explained by observing that the flow in the first part of the tube is more nearly uniform and less turbulent than that in the second part of the tube where turbulence is developed fully. Thus it would appear that the change of slope observed in the curves in Figs. 3 to 7 of the paper are associated with the transition length required for the flow to become fully developed and not due to a change from laminar to turbulent flow. It would appear further from the values of Reynolds number presented previously that the fully developed flow is laminar in the case of oil but turbulent in the case of water. Since heat-transfer characteristics of a fluid are known to be significantly different for laminar and turbulent flows it does not seem that the comparison made between the oil and water-base materials is on a firm basis. It would have been better to compare the heat-transfer characteristics of the fluids investigated at more nearly equal Reynolds numbers and to ignore the portion of the data in the region where the flow was not fully developed.

In conclusion it should be stated that the author has presented an interesting means for comparing the cooling properties of fluids. However, considerable care must be exercised in interpreting the data obtained by this procedure. In making comparisons between tests the Reynolds number should be considered. It must be kept in mind that the speed of film formation, which often is at least as important as the heat-transfer characteristics of the fluid in cutting-fluid cooling action, is not included in this test. Furthermore, the time constant of this test is entirely different from that in practical cutting operations. Owing to the several important differences between the conditions found in cutting and those of the author's test it would appear that the relative cooling characteristics of cutting fluids may not be predicted from this test alone.

Author's Closure

The author wishes to thank those who gave their time so generously in the preparation of discussions.

Professors Chao and Trigger have raised several questions. First, consider the problem of conduction losses at the ends of the tube. This problem was recognized by the author in Figs. 5, 6, and 7 where it can be seen that the points corresponding to location 10 of Fig. 2 are not used in drawing the curves. The tube-wall temperatures at other locations do not appear to be appreciably influenced by this heat loss, and to compensate for it by lagging the tube and by adiabatically lagging the conductors with supplementary heaters to obtain more accurate values of specific heat would greatly increase the time necessary to reach temperature equilibrium. For water-base fluids the end loss effect is not appreciable.

That the power input along the tube varies linearly with distance under the conditions shown in Fig. 5 has been verified by

[9] For a concise discussion of this topic see "Engineering Applications of Fluid Mechanics," by J. C. Hunsaker and B. G. Rightmire, McGraw-Hill Book Co., Inc., New York, N. Y., 1947.

measuring the voltage drops between thermocouple attachment points with a Hewlett-Packard model 400-A vacuum tube a-c voltmeter. No voltage varied from the assumed linear condition by more than 0.1 volt when the total drop for the tube was 10 volts. Consequently the bulk temperature, which should not be confused with the temperature at the axis of the tube, must rise very nearly linearly for water, since water's specific heat changes so little over the temperature range involved. However, the straight line drawn for the oils is a simplification of fact, since a 100 SSU oil has a specific heat of approximately 0.47 at 100 F and 0.57 at 300 F. This would result in a gently sloping curve lying above the straight line shown and intersecting it at the origin and at the end point.

The selection of a point 9 in. along the heating path in the calculation of h values was not entirely arbitrary. It was chosen as a point well away from end effects and as being in a position which avoided the anomalous center section in every case. Professors Chao and Trigger are undoubtedly right in their view that the flow conditions in practice are too complex to duplicate with such a simple apparatus, but the runs require little effort and serve as screening tests for the time-consuming tool-chip interface temperature measurements and tool-life measurements that must be the final criteria.

In answer to Dr. Hahn's question concerning the accuracy of temperature readings taken on the unheated sections of tube and used as the bulk temperatures of the incoming and outgoing fluid, the readings for *water and water-base fluids* accurately check the temperature rise calculated for the known specific heat of the fluid for the known heat input. On the other hand, in the case of *oil*, analysis of Fig. 5 readily shows that at location 11, Fig. 2, the tube-wall temperature is a poor measure of bulk temperature, since an assumed average specific heat of 0.51 for the conditions of Fig. 5 would result in a bulk temperature rise of 96 F instead of the 150 F shown. Clearly a longer and preferably lagged section of tubing is needed in this case. Continuing with Dr. Hahn's questions, the heat flux in an increment of tube length is always proportional to the product of h and Δt for that area. In many papers on heat transfer, average values of h for the whole tube are used. Here it is possible to assign local values to h because the local heat transfer per unit area is known to be a uniform 24.67×10^4 Btu/hr sq ft. and local Δt's can likewise be assigned by subtracting the calculated bulk temperature for the points along the tube from the measured tube-wall temperatures. A discussion of the reasons for selecting a point 9 in. from the input end is given earlier in this closure.

Concerning the removal of heat from the chip, Dr. Hahn might consider the steady-state picture in the plane perpendicular to the tool face in the area of contact, with the chip-tool interface as the hottest point. Since the chip-tool interface assumes that temperature necessary to drive the generated heat at a steady rate through a series of resistance paths to an ambient temperature, a decrease in any of the resistance paths, or in the ambient temperature necessarily lowers that temperature. The resistance of a solid-to-liquid boundary is inherently less than that of a solid-to-gas boundary; therefore the coolant serves to lower the boundary resistance wherever it flows over the metal. This includes the surface of the chip near the point of cut, since this surface is one of the heat paths from the chip-tool interface; therefore this fluid flow over the chip lowers the chip-tool interface temperature.

The chip after leaving the tool face takes considerable time to reach a temperature approaching the ambient temperature, as Dr. Hahn has pointed out, but this extra cooling is a welcome extra dividend for the comfort of the operator. He has chosen for his example, however, a chip flow rate of 300 fpm. If we assume a cutting ratio of 0.5, the actual cut speed is then 600 fpm, a figure well above the practical cutting speed for high-speed steel tools.

The question has been raised by all four discussers as to the ability of a fluid such as water to sensibly lower the chip-tool interface temperature under usual cutting conditions. That it does so at practical cutting speeds for high-speed steel is demonstrated in Fig. 11 of reference (3). Furthermore, lathe tests in our own laboratory[10] with high-speed steel cutting SAE 3115 steel, using a 0.100 depth of cut and 0.0127 feed (ASA Standard B5.19-1946) at 200 fpm showed a reduction in chip-tool interface temperature from 1033 F dry to 927 F with water as a coolant, but only to 983 F with a 100 SSU oil. That this is a practical reduction in chip-tool interface temperature is borne out by the corresponding tool lives of 3 min, 35 min, and 19 min, respectively. Part of the reduction in chip-tool interface temperature by the fluids in these tests was undeniably due to a reduction in the chip friction against the tool, but tool-dynamometer studies were not made for this series of tests.

The author is unable to agree with Dr. Shaw's line of reasoning in regard to the metal-wetting properties of fluids. Water has a high-contact angle against a metal surface coated with oil, and does not tend to spread by itself on such a surface, but water has a zero contact angle against all clean metals and thus completely wets them. The tool face and the freshly cut metal surface are readily wet by water. Moreover, the capillary pressure which drives fluid into the close clearances of areas C and D and on into area B of Dr. Shaw's Fig. 8, does so with twice as much force for water as for oil, since the surface tension of water is approximately twice as great. In addition, the viscous resistance for water is only about one tenth that of the usual cutting oil. The capillary driving pressure in the case of water is calculated to be of the order of 800 psi for a capillary clearance with a one microinch radius. Tests with many *stable* commercial oil-in-water emulsions show that these fluids readily wet a clean steel surface and continue to do so after the surface has had time to adsorb a polar film from the fluid.

The author's conclusion that the break shown in the center of most of the tube-wall temperature curves was due to a change from streamline flow to turbulent flow has been challenged by Dr. Shaw, but his explanation of the data in terms of a "transition length" necessary for velocity redistribution does not seem to satisfy the data any better, since the break in the curves occurs at approximately the same place for water with a viscosity at 100 F of 0.7 cp as for the more viscous heat-transfer oil of Fig. 6 with a viscosity at 100 F of 45 cp. While the anomalous break in the curves may not be due to a transition from pure streamline to turbulent flow, it still appears to be caused by a change in the flow pattern of the fluid close to the tube wall.

Dr. Shaw's analysis of the possible mechanics of heat transfer for water-base fluids containing emulsified wax does not apply to the data presented, as none of the fluids tested contained emulsified wax.

A device for sensitively measuring the cooling properties of cutting fluids under comparable conditions and with a minimum of effort is, despite its oversimplification, a useful screening tool preliminary to the running of costly, time-consuming cutting tests. That it does not compare these fluids under conditions giving the same Reynolds number seems unimportant, since the machine tool that the fluids will be used on, like the test device, maintains approximately constant flow conditions, with the Reynolds number varying widely with the fluid viscosity.

[10] "Effects of Coolants on Tool Temperature and Tool Life," by D. M. Cunningham and R. E. Phillips, University of Cincinnati, Mechanical Engineering thesis, 1951.

The Stresses in a Pressure Vessel With a Flat Head Closure[1]

By G. W. WATTS[2] and H. A. LANG,[3] CHICAGO, ILL.

This paper presents the results of computations for determining the stresses in a cylindrical pressure vessel with a flat head closure. The accurate bending theory of shells is used to evaluate the local bending stresses in the neighborhood of the junction of the flat head and the cylindrical body. Tables show the magnitudes of the shear stress, the circumferential stress, and the axial stress as multiples of $pd/2t$. For the axial and circumferential stresses, the tables show the magnitude and sense of the stress on the internal and external surfaces of the vessel. The locations where these stresses are critical are also determined. Curves are given showing the maximum stresses as functions of the diameter-thickness ratio of the shell and of the thickness ratio of head to shell body. The range of calculation includes most vessel sizes encountered in practice.

Tables of influence numbers for the cylinder and the flat head are presented. These tables can be utilized in problems in which other elastic structures are attached to either member. The paper includes a discussion of the mathematical procedure.

Nomenclature

The following nomenclature is used in the paper:

p = internal pressure, psi
M_0 = bending moment per unit length of circumference exerted by head on cylinder (positive sense is shown in Fig. 1)
Q_0 = shear force per unit length of circumference exerted by head on cylinder (positive sense is shown in Fig. 1)
N_0 = axial force per unit length of circumference acting on cylinder; positive when tension
N_1 = radial force per unit length of circumference on mid-plane of head at junction; positive when tension
M_1 = axial bending moment per unit length of circumference on head at junction (positive sense is shown in Fig. 2)
s = stress, psi
w_0 = radial displacement of cylinder at junction; positive inward
E = modulus of elasticity, psi
d = mean diameter of cylinder
t = thickness of cylinder
T = thickness of flat head closure
μ = Poisson's ratio (= 0.3 for steel)
D = flexural rigidity of cylinder = $Et^3/12(1-\mu^2)$
D_1 = flexural rigidity of head = $ET^3/12(1-\mu^2)$
δ = radial displacement of mid-plane of head; positive outward
δ_1 = radial displacement of surface of head acted upon by pressure; positive outward
w = axial displacement in head at any radius; positive outward
$\beta = \sqrt[4]{12(1-\mu^2)/(dt)^2}$
$\lambda = \beta M_0/Q_0$
I = stress ratio = stress divided by $pd/2t$ (see Table 7 for complete details)
a_1, a_3, a_5 / b_4, b_3, b_5 = influence numbers for cylinders
a_1, a_2, a_3 / b_1, b_2, b_3 = influence numbers for head
α = semiapex angle of conical head
x_s = location of maximum shear-stress ratio in cylinder
x_a = location of maximum axial-stress ratio in cylinder
x_c = location of maximum circumferential-stress ratio in cylinder

Introduction

The present paper dealing with the stresses in a pressure vessel with a flat head closure is part of a continuing program instituted by the Design Division of the Pressure Vessel Research Committee of the Welding Research Council of the Engineering Foundation. This program, which consists of both analytical and experimental investigations, is intended to benefit engineers who are engaged in the design and manufacture of pressure vessels.

The present paper is the second of a series which ultimately will cover the kinds of vessel heads in common use. A previous paper considered the pressure vessel with a conical head. A subsequent paper will consider a pressure vessel with a hemispherical head. Each design paper consists of tables and curves for determining the maximum stress in a pressure vessel under the specified end closure.

The theory of plates and shells can be found in standard reference books.[4,5] Consequently, this report is limited to a description of the computational procedure together with a discussion of the results. The problem logically consists of two parts: (*a*) The shear force Q_0 and axial bending moment M_0 at the head cylinder junction, Fig. 1, must be determined from the continuity of the radial displacement and rotation at the junction. (*b*) When these are known we may determine the shear, circumferential, and axial stresses at the junction in the cylinder and in the flat head. The maximum stresses in both bodies other than at the junction also can be found. Each stress is divided by $pd/2t$,

[1] This work is part of a continuing program instituted in 1946 by the Design Division of the Pressure Vessel Research Committee of the Welding Research Council of the Engineering Foundation, New York, N. Y.

[2] Director of Engineering, Standard Oil Company (Indiana). Fellow ASME.

[3] Formerly, Project Engineer, Engineering Research Department, Standard Oil Company (Indiana). Mem. ASME.

Contributed by the Petroleum Division and presented at the Annual Meeting, Atlantic City, N. J., November 25-30, 1951, of The American Society of Mechanical Engineers.

Note: Statements and opinions advanced in papers are to be understood as individual expressions of their authors and not those of the Society. Manuscript received at ASME Headquarters, November 1, 1951. Paper No. 51—A-146.

[4] The theory of shells is discussed in "Theory of Plates and Shells," by S. Timoshenko, McGraw-Hill Book Company, Inc., New York, N. Y., first edition, 1940.

[5] A general mathematical treatment of pressure vessels will be found in "The Basic Elastic Theory of Vessel Heads Under Internal Pressure," by G. W. Watts and W. R. Burrows, Trans. ASME, vol. 71, 1949, pp. 55–73.

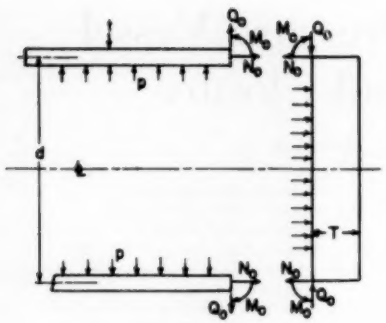

FIG. 1

the circumferential stress in a thin unrestrained cylinder under uniform pressure, to form the stress index denoted by I. The values at the junction are distinguished from the maxima in the cylinder and in the head by subscripts j and m, respectively. The subscripts, s, a, c, denote shear, axial, and circumferential, respectively. There are thus twelve stress indexes, denoted by I_{sm}, I_{am}, I_{cm} and I_{sj}, I_{aj}, I_{cj}. It will be clear from the context whether these refer to the cylinder or the flat head. It will be shown later that it is not necessary to compute all twelve indexes in order to determine which is the greatest.

The stress ratio I has two distinct advantages. It reduces the magnitude of the results and enables one to tell immediately whether a stress is greater or less than the hoop stress in a thin cylinder. It frequently is substantially linear when plotted against the diameter-thickness ratio d/t of the cylinder. By contrast, a curve of stress divided by pressure is more nearly parabolic.

Conclusions

The analysis of stress in a cylindrical pressure vessel with a flat head closure leads to the following general conclusions:

1 The axial stress at the junction is the largest stress. When the head is as thin or thinner than the cylinder, this stress is located in the head. When the head is thicker than the cylinder, this stress is located in the cylinder.

2 When the ratio of diameter to thickness of the cylinder d/t is constant, increasing the thickness of the head will reduce the magnitude of the over-all maximum stress. The limiting case corresponds physically to a cylinder rigidly connected to an unyielding wall.

3 The maximum stress increases rapidly when the head thickness is less than the cylinder. For this reason, in all practical design work the head should be thicker than the cylinder.

4 The maximum stress increases when the cylinder is made larger or thinner, i.e., whenever the ratio d/t increases.

5 A curve of maximum stress divided by the circumferential hoop stress, $pd/2t$, plotted as a function of the diameter-thickness ratio of the cylinder is, for each value of thickness of head to thickness of cylinder, very nearly a straight line. Thus, for each ratio of T/t, two calculations to determine this straight line would suffice for finding the maximum stress at any ratio of d/t.

6 When a pressure vessel has a flat head, the maximum stress is considerably greater than the maximum stress resulting from replacing the flat head by a conical head of the same thickness having an apex angle of 120 deg or less (see, for example, Fig. 5).

7 It is not practical to use a very thick flat head to obtain a stress lower than would occur for a conical head (of any apex angle not too near 180 deg). The thickness required to accomplish this is excessive and frequently the head would weigh more than the conical head. This is equivalent to saying that the stress increases quite rapidly as the angle of discontinuity between center lines of cylinder and head approaches 90 deg.

8 There is a thickness ratio between $T/t = 1.0$ and $T/t = 1.2$ for which the axial stress at the junction has the same magnitude in both cylinder and head. An estimate of its value can be made by linear interpolation between the values given for $T/t = 1.0$ and 1.2. This optimum thickness ratio is not constant but varies with the ratio d/T.

9 The equal axial and circumferential stresses at the center of the head are about 60 per cent of the over-all maximum stress when the head is not thicker than the cylinder. As the head thickness increases relative to the cylinder thickness, these stresses gradually become a much smaller fraction of the over-all maximum stress.

Analysis

Fig. 1 shows the loads acting upon a long cylindrical pressure vessel. The loading consists of a uniform pressure p which, acting alone, produces a uniform expansion of the vessel; a bending moment per unit length of circumference M_0; a shear force per unit length of circumference Q_0; and an axial force per unit length N_0. The axial force N_0 is produced by the pressure acting on the head which tends to stretch the vessel. The shear force Q_0, and bending moment M_0, are produced by the restraint exerted by the head in preventing the expansion of the vessel under pressure.

Fig. 1 also shows the loads applied to the head which is regarded as a thin elastic plate. The equilibrium of forces axially determines N_0. It is first necessary to determine the shear force Q_0, and bending moment M_0, from the required continuity of displacement and rotations at the junction.

From the theory of a cylindrical shell, the radial displacement (positive inward) w_0, and the rotation

$$-\left(\frac{dw}{dx}\right)_{x=0} = -w_0'$$

at the junction are[6]

$$w_0 = -\frac{1}{2\beta^3 D}(\beta M_0 + Q_0) - \frac{pd^2}{4Et}\left(1 - \frac{\mu}{2}\right)$$

$$-w_0' = -\frac{1}{2\beta^2 D}(2\beta M_0 + Q_0)$$

The dimensionless form of these two equations is chosen to be

$$\frac{ETw_0}{pd^2} = a_4 + \frac{M_0}{pd^2}a_5 + \frac{Q_0}{pd}a_6 \quad \ldots\ldots\ldots [1]$$

$$-\frac{ET^2w_0'}{\beta^2\, dtpd^2} = b_4 + \frac{M_0}{pd^2}b_5 + \frac{Q_0}{pd}b_6 \quad \ldots\ldots\ldots [2]$$

where

$$a_4 = -\frac{T}{t}\left(\frac{2-\mu}{8}\right) \qquad b_4 = 0$$

$$a_5 = -\frac{1}{2}\frac{T}{t}(\beta d)^2 \qquad b_5 = -\left(\frac{T}{t}\right)^2(\beta d)$$

$$a_6 = -\frac{1}{2}\frac{T}{t}(\beta d) \qquad b_6 = -\frac{1}{2}\left(\frac{T}{t}\right)^2$$

[6] Page 393 of footnote 4.

and

$$\beta d = \sqrt[4]{12(1-\mu^2)}\sqrt{\frac{d}{t}}$$

The quantities a_1, a_2, a_4, b_1, b_2, and b_4 are "influence numbers." Thus a_4 is the value of ETw_0/d when the cylinder is loaded by unit shear force $Q_0 = 1$. Similarly, a_1 is the value of ETw_0/d^2 produced by unit pressure p. The advantage of these influence numbers rests on the fact that they depend only upon ratios such as the thickness ratio T/t, and the cylinder-diameter-thickness ratio d/t, which define the geometry of the problem. These ratios characterize the vessel shape for a fixed value of Poisson's ratio μ. For the present calculations, $\mu = 0.3$, a value which applies for most steels. Small variations in μ result only in altering the numerical results by a very small amount.

The equations for w_0 and $-w_0'$ include the effect of N_0. From equilibrium of forces in an axial direction $N_0 = pd/4$. This value neglects the slight correction which arises from the fact that the pressure acts on the area of head corresponding to the inner diameter of the cylinder while the line of action of N_0 corresponds to the mean diameter of the cylinder.

The head, treated as a thin elastic plate, deflects under pressure and bending moment at the edge. Compression or extension of the head by forces in its mid-plane is regarded as independent of these deflections. This is justifiable if the deflections are small.[7]

The deflection curve for a simply supported plate under uniform pressure and edge moment M_1 is[8]

$$w = \frac{p}{64D_1}\left(\frac{5+\mu}{1+\mu}\frac{d^2}{4} - r^2\right)\left(\frac{d^2}{4} - r^2\right) + \frac{M_1}{2D_1(1+\mu)}\left(\frac{d^2}{4} - r^2\right) \quad [3]$$

The rotation at the edge, $r = d/2$ is

$$\left(\frac{dw}{dr}\right)_{r=\frac{d}{2}} = -\left[\frac{pd^2}{64D_1(1+\mu)} + \frac{M_1 d}{2D_1(1+\mu)}\right] \quad [4]$$

The effect of a uniform tension in the mid-plane of the plate of amount N_1 is to produce a radial displacement of amount

$$\delta = \frac{1}{E}(1-\mu)\frac{N_1}{T}r \quad [5]$$

This is the displacement of the center line of the head. The displacement of the edge abutting the cylinder is

$$\delta_1 = \delta + \frac{T}{2}\left(\frac{dw}{dr}\right)_{r=\frac{d}{2}} \quad [6]$$

Fig. 2 shows the details at the junction and indicates the positive sense of w_0, $-w_0'$, δ, and $(dw/dr)_{r=d/2}$. As indicated in Fig. 1, the shear force Q_0 acts at the edge of the head. This may be replaced by a compressive force Q_0 in the mid-plane of the flat head, provided the moment M_0 is decreased by $Q_0T/2$. Hence $N_1 = -Q_0$ and $M_1 = (Q_0T/2) - M_0$. The conditions to be satisfied at the junction are

$$w_0 = -\delta_1 = -\delta - \frac{T}{2}\left(\frac{dw}{dr}\right)_{r=\frac{d}{2}} \quad [7]$$

[7] "Mathematical Theory of Elasticity," by A. E. H. Love, Dover Publications, New York, N. Y., fourth edition, 1944, p. 553; also Reference 4, p. 52.

[8] Pages 59–62 of footnote 4.

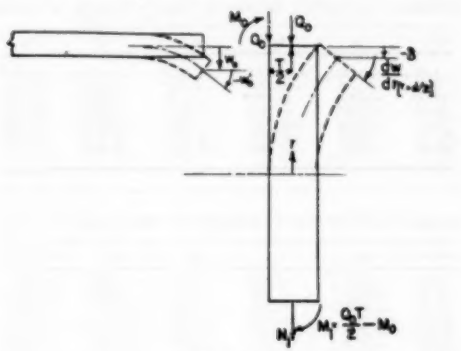

FIG. 2

$$-w_0' = \left(\frac{dw}{dr}\right)_{r=\frac{d}{2}} \quad [8]$$

In dimensionless form, these reduce, respectively, to

$$\frac{M_0}{pd^2}a_1 + \frac{Q_0}{pd}a_4 + a_4 = \frac{M_0}{pd^2}a_1 + \frac{Q_0}{pd}a_2 + a_3 \quad [9]$$

$$\frac{M_0}{pd^2}b_1 + \frac{Q_0}{pd}b_4 = \frac{M_0}{pd^2}b_1 + \frac{Q_0}{pd}b_2 + b_3 \quad [10]$$

where

$$a_1 = -3(1-\mu)\frac{d}{T} \qquad b_1 = \frac{6(1-\mu)}{(\beta d)^4}\frac{d}{t}\frac{d}{T}$$

$$a_2 = 2(1-\mu) \qquad b_2 = -\frac{3(1-\mu)}{(\beta d)^2}\frac{d}{t}$$

$$a_3 = \frac{3}{32}(1-\mu)\frac{d}{T} \qquad b_3 = -\frac{3}{16}\frac{(1-\mu)}{(\beta d)^3}\frac{d}{t}\frac{d}{T}$$

The last two equations determine the dimensionless quantities M_0/pd^2 and Q_0/pd. The influence numbers are given in Tables 1 to 6. It is to be noted that they may be used in other problems. Thus a_1, a_2, a_3, b_3, and b_4 refer only to the cylinder. Allowing for differences in notation, these were used in a previous paper for determining stresses when the pressure vessel had a conical head.

Table 6 shows the influence numbers for the flat head based upon seven values of d/T. Tables 1 to 5 are influence numbers for the cylinder assuming the head-cylinder thickness ratio T/t is 0.8, 1.0, 1.2, 1.6, and 2.0, respectively.

The stresses are represented in dimensionless form by dividing the stress by $pd/2t$ which represents the circumferential stress in a thin cylinder under internal pressure only. The resulting stress ratios are denoted by the symbol I. The shear stress, axial stress, and circumferential stress are denoted by subscripts s, a, and c, respectively. Subscript j denotes junction, and m a maximum stress ratio other than at the junction. The maximum stress of any type may occur at the junction in either the head or the cylinder. It may equally well occur at one point in the cylinder or one point in the head which does not correspond to the junction. There are then a total of twelve values of stress ratio I to be considered.

A considerable amount of computing time can be saved by considering the stresses in more detail. Imagine the head and cylinder are separated. Under pressure the cylinder expands uni-

TABLE 1 INFLUENCE NUMBERS FOR CYLINDER, $T/t = 0.8$

d/t	a_4	a_5	a_6	b_5	b_6
3.20	-0.1700	- 4.2298	- 1.3007	- 2.0812	-0.3200
8.00	-0.1700	- 10.5745	- 2.0567	- 3.2906	-0.3200
32.00	-0.1700	- 42.2981	- 4.1133	- 6.5813	-0.3200
64.00	-0.1700	- 84.5963	- 5.8171	- 9.3073	-0.3200
80.00	-0.1700	-105.7454	- 6.5037	-10.4059	-0.3200
240.00	-0.1700	-317.2361	-11.2647	-18.0236	-0.3200
400.00	-0.1700	-528.7268	-14.5427	-23.2684	-0.3200

TABLE 2 INFLUENCE NUMBERS FOR CYLINDER, $T/t = 1.0$

d/t	a_4	a_5	a_6	b_5	b_6
4.00	-0.2125	- 6.6091	- 1.8178	- 3.6357	-0.5000
10.00	-0.2125	- 16.5227	- 2.8743	- 5.7485	-0.5000
40.00	-0.2125	- 66.0908	- 5.7485	-11.4970	-0.5000
80.00	-0.2125	-132.1817	- 8.1296	-16.2592	-0.5000
100.00	-0.2125	-165.2271	- 9.0892	-18.1784	-0.5000
300.00	-0.2125	-495.6813	-15.7429	-31.4859	-0.5000
500.00	-0.2125	-826.1356	-20.3241	-40.6481	-0.5000

TABLE 3 INFLUENCE NUMBERS FOR CYLINDERS, $T/t = 1.2$

d/t	a_4	a_5	a_6	b_5	b_6
4.80	-0.2550	- 9.5171	- 2.3696	- 5.7351	-0.7200
12.00	-0.2550	- 23.7927	- 3.7783	- 9.0679	-0.7200
48.00	-0.2550	- 95.1708	- 7.5566	-18.1359	-0.7200
96.00	-0.2550	- 190.3416	-10.6867	-25.6430	-0.7200
120.00	-0.2550	- 237.9271	-11.9681	-28.6754	-0.7200
360.00	-0.2550	- 713.7812	-20.6917	-49.6672	-0.7200
600.00	-0.2550	-1189.6352	-26.7167	-64.1200	-0.7200

TABLE 4 INFLUENCE NUMBERS FOR CYLINDER, $T/t = 1.6$

d/t	a_4	a_5	a_6	b_5	b_6
6.40	-0.3400	- 16.9193	- 3.6790	- 11.7730	-1.2800
16.00	-0.3400	- 42.2981	- 5.8171	- 18.6147	-1.2800
64.00	-0.3400	- 169.1926	-11.6342	- 37.2294	-1.2800
128.00	-0.3400	- 338.3851	-16.4532	- 52.6503	-1.2800
160.00	-0.3400	- 422.9814	-18.3952	- 58.8648	-1.2800
480.00	-0.3400	-1263.9443	-31.8615	-101.9568	-1.2800
800.00	-0.3400	-2114.9071	-41.1330	-131.6257	-1.2800

TABLE 5 INFLUENCE NUMBERS FOR CYLINDER $T/t = 2.0$

d/t	a_4	a_5	a_6	b_5	b_6
8.00	-0.4250	- 26.4363	- 5.1416	- 20.5665	-2.0000
20.00	-0.4250	- 66.0908	- 8.1296	- 32.5185	-2.0000
80.00	-0.4250	- 264.3634	-16.2593	- 65.0370	-2.0000
160.00	-0.4250	- 528.7268	-22.9941	- 91.9762	-2.0000
200.00	-0.4250	- 660.9085	-25.7081	-102.8325	-2.0000
600.00	-0.4250	-1982.7254	-44.5278	-177.1112	-2.0000
1000.00	-0.4250	-3304.5424	-57.4851	-229.9406	-2.0000

TABLE 6 INFLUENCE NUMBERS FOR FLAT HEAD

d/T	a_1	a_2	a_3	b_1	b_2	b_3
4.00	- 5.4000	+1.4000	+ 0.2625	- 5.0839	-0.6355	- 0.1589
10.00	- 21.0000	+1.4000	+ 0.6563	+ 12.7098	-0.6355	- 0.3972
40.00	- 84.0000	+1.4000	+ 2.6250	+ 50.8391	-0.6355	- 1.5887
80.00	- 168.0000	+1.4000	+ 5.2500	+101.6782	-0.6355	- 3.1774
100.00	- 210.0000	+1.4000	+ 6.5625	+127.0978	-0.6355	- 3.9718
300.00	- 630.0000	+1.4000	+19.6875	+381.2933	-0.6355	-11.9154
500.00	-1050.0000	+1.4000	+32.8125	+635.4889	-0.6355	-19.8590

formly while the head rotates inward toward the center line of the cylinder. The shear force Q_0 must then be directed opposite to the sense shown in Fig. 1. The shear force produces tensile stress in the head. The shear force will rotate the cylinder toward its axis. The bending moment M_0 must be positive to diminish this rotation. In the head M_1 will have a direction opposite to that shown in Fig. 2 in order to satisfy continuity of rotation at the joint. Therefore the quantity $\lambda = \beta M_0/Q_0$ is negative. It may be anticipated that λ always lies in the range -1.0 to 0 for a value in excess of -1.0 implies that the moment produces a larger deflection on the cylinder at the junction than the shear force—a circumstance which is physically unlikely. The value $\lambda = -1.0$ corresponds, in fact, to no deflection at the cylinder junction except that resulting from the pressure. Anticipating a result which is verified by the calculations, we assume further that $-1.0 \leq \lambda \leq -0.228$. The corresponding expressions for stress ratios I are shown in Table 7. When λ lies in the range indicated, the maximum circumferential stress in the cylinder occurs at the junction. Similarly, the shear stress and the axial stress in the cylinder are a maximum at the junction.

In the head, the shear stress is a maximum at the junction. The axial and circumferential stresses are largest either at the junction or at the center of the head. At the latter point these two stresses become equal.

The equations of Table 7 for the maximum stress ratios in the cylinder away from the junction can be determined by applying the calculus of maxima and minima. The expression for the circumferential stress ratio is quite complex and is omitted from Table 7.

The stress ratios in the head can be computed directly from the general expressions below for shear force and bending moments in the head at any radius[9] r.

[9] Page 62 of footnote 4.

$$M_r = M_1 + \frac{p}{64}(3 + \mu)(d^2 - 4r^2) = \text{radial bending moment}$$

$$M_c = M_1 + \frac{p}{64}(3 + \mu)\left[d^2 - 4r^2\frac{(1 + 3\mu)}{(3 + \mu)}\right] = \text{circumferential bending moments}$$

$$Q = \frac{pr}{2} = \text{shear force}$$

The shear stress at radius r is $(3/2)(Q/T)$. The force Q_0 produces a tensile stress radially and circumferentially of amount Q_0/T. To this is added the tensile stress produced by bending, which is $6M_r/T^2$ radially and $6M_c/T^2$ circumferentially.

Limitations of the Analysis

The shear force Q_0 not only produces stretching of the midplane of the head but diminishes the bending moments and deflections. The latter effect is not considered in the present analysis. The omission of this effect is justified when the maximum deflection of the head does not exceed about one half the thickness of the head. For larger deflections, the actual bending stresses in the head would always be less than the computed values of bending stress because of the strengthening effect of the shear force Q_0.

It must be kept in mind that the stress ratios at the junction are nominal values only. The assumptions common to the elastic theory of a cylinder and of a flat plate are violated at and near the junction where a local state of stress, dependent upon the method of attachment, exists. The present analysis makes no attempt to consider this local state of stress.

Whenever d/T or d/t is less than 10, it is unlikely that the theories used in this paper are applicable. They are limited to thin plates and shells. For thin plates a common requirement is that the deflections nowhere exceed half the plate thickness.

TABLE 7 EQUATIONS FOR STRESS RATIOS

Stress ratios in cylinder at junction:

Shear

$$I_{sj} = 3\left|\frac{Q_0}{pd}\right|$$

Axial

$$I_{aj} = \frac{1}{2} + 12\,\frac{d}{t}\left|\frac{M_0}{pd^2}\right|$$

Circumferential

$$I_{cj} = \left|1 + 2\beta d\left(\frac{Q_0}{pd}\right)(1+\lambda)\right| + 12\mu\,\frac{d}{t}\left|\frac{M_0}{pd^2}\right|$$

Maximum stress ratios in cylinder (other than at junction):
Shear

$$I_{sm} = \frac{I_{sj}\sqrt{1+2\lambda+2\lambda^2}}{e^{\beta x_s}} \qquad \frac{x_s}{d} = \frac{\tan^{-1}\left(\frac{1+\lambda}{\lambda}\right)}{\beta d}$$

Axial

$$I_{am} = \frac{1}{2} + 3.4126\sqrt{\frac{d}{t}}\,I_{cm} \qquad \frac{x_a}{d} = \frac{x_s}{d} - \frac{\pi}{4}\,\frac{1}{\beta d}$$

Stress ratios in the head at junction:
Shear

$$I_{sj} = \frac{3}{4}\,\frac{t}{T}$$

Axial

$$I_{aj} = \frac{2t}{T}\left|\frac{Q_0}{pd}\right| + 12\,\frac{d}{t}\left(\frac{t}{T}\right)^2\left|\frac{M_0}{pd^2} - \frac{Q_0}{pd}\left(\frac{T}{2d}\right)\right|$$

Circumferential

$$I_{cj} = \frac{2t}{T}\left|\frac{Q_0}{pd}\right| + 12\,\frac{d}{t}\left(\frac{t}{T}\right)^2\left|\frac{M_0}{pd^2} - \frac{Q_0}{pd}\left(\frac{T}{2d}\right) - \left(\frac{1-\mu}{32}\right)\right|$$

Stress ratios at the center of the head, ($r = 0$):
Axial and circumferential

$$I_{a_0} = I_{c_0} = \frac{2t}{T}\left|\frac{Q_0}{pd}\right| + 12\,\frac{d}{t}\left(\frac{t}{T}\right)^2\left|\frac{M_0}{pd^2} - \frac{Q_0}{pd}\left(\frac{T}{2d}\right)\right| - \frac{1}{64}(3+\mu)$$

The results contained in the tables and curves were computed by two separate persons. Agreement to four decimal places or better was obtained for all stress ratios listed in Tables 9 to 13.

Convention Used in Tables 9 Through 13

In this paper the problem of determining the magnitude of the maximum stress has been primarily emphasized. A few additional calculations make it possible to indicate not only the stress magnitude but its sense (whether tension or compression) and its location (whether on the internal or external surface of the vessel). In Tables 9 through 13 the following convention is adhered to:

1 For every circumferential or axial-stress ratio, two figures are listed for each diameter-thickness ratio. The upper figure represents the value of the stress ratio at the external surface of the vessel. The lower figure represents the value of the stress ratio at the internal surface of the vessel. A plus sign denotes tension and a minus sign denotes compression.

2 Every shear-stress ratio refers to a shear stress at the middle surface of the vessel. The following sign convention, consistent with Fig. 1, is adhered to:

(*a*) The positive sign of I_{sj} in the head denotes that the stress has the direction of N_0 in Fig. 1.

(*b*) The positive sign of I_{sj} in the cylinder denotes that the stress is directed radially inward opposite to the sense of Q_0 in Fig. 1.

(*c*) The negative sign of I_{sm} in the cylinder denotes that the stress is directed radially outward when the shell wall is located to the left of the stress in Fig. 1.

TABLE 8 BENDING MOMENT RATIO, M_0/pd^2, AT JUNCTION SHEAR FORCE RATIO, Q_0/pd, AT JUNCTION

d/t \ T/t	0.8	1.0	1.2	1.6	2.0
4.00	0.0162	0.0161	0.0158	0.0149	0.0138
10.00	0.0214	0.0202	0.0189	0.0165	0.0142
40.00	0.0260	0.0248	0.0235	0.0207	0.0179
30.00	0.0274	0.0264	0.0253	0.0228	0.0201
100.00	0.0275	0.0268	0.0258	0.0234	0.0209
300.00	0.0282	0.0286	0.0278	0.0261	0.0241
500.00	0.0296	0.0291	0.0285	0.0271	0.0254

d/t \ T/t	0.8	1.0	1.2	1.6	2.0
4.00	−0.1351	−0.1337	−0.1412	−0.1436	−0.1432
10.00	−0.1745	−0.1821	−0.1862	−0.1868	−0.1808
40.00	−0.3106	−0.3169	−0.3508	−0.3627	−0.3555
30.00	−0.4346	−0.4740	−0.5022	−0.5303	−0.5305
100.00	−0.4855	−0.5313	−0.5647	−0.6059	−0.6048
300.00	−0.3176	−0.9371	−1.0002	−1.1041	−1.1177
500.00	−1.1004	−1.2221	−1.3179	−1.4533	−1.5357

TABLE 9* STRESS INDEXES IN A CYLINDRICAL PRESSURE VESSEL WITH FLAT HEAD, $T/t = 0.8$

d/t	d/T	Cylinder at Junction: Shear I_{sj}	Cylinder at Junction: Axial I_{aj}	Cylinder at Junction: Circum. I_{cj}	Head at Junction: Shear I_{sj}	Head at Junction: Axial I_{aj}	Head at Junction: Circum. I_{cj}
3.20	4.00	+0.4053	− 0.1230 + 1.1230	+ 0.2777 + 0.6515	+0.9375	− 1.6459 + 2.3244	− 0.1364 + 1.0019
8.00	10.00	+0.5236	− 1.5526 + 2.5526	+ 0.2802 + 0.9514	+0.9375	− 4.0800 + 4.8927	− 0.7967 + 1.6714
32.00	40.00	+0.9318	− 9.4693 + 10.4693	− 7.8878 + 1.0938	+0.9375	− 17.1300 + 18.6629	− 4.0080 + 5.5579
64.00	80.00	+1.3032	− 20.5390 + 21.5390	− 6.3591 + 6.2640	+0.9375	− 35.0455 + 37.2176	− 8.7955 +10.9676
80.00	100.00	+1.5565	− 26.1604 + 27.1604	− 6.1021 + 7.5938	+0.9375	− 44.0843 + 46.5118	−11.2718 +13.6993
240.00	300.00	+2.5127	− 83.5093 + 84.5093	−25.6722 +24.7333	+0.9375	−135.5023 +139.7402	−37.0668 +41.3027
400.00	500.00	+3.3011	−141.6722 +142.6722	−43.3606 +41.9427	+0.9375	−227.6461 +233.1479	−63.5816 +69.0834

d/t	d/T	Maxima in Cylinder: Shear I_{sm}	Maxima in Cylinder: Axial I_{am}	Maxima in Cylinder: Circum. I_{cm}	Location of Maxima in Cylinder: Shear x_s/d	Location of Maxima in Cylinder: Axial x_a/d	Location of Maxima in Cylinder: Circum. x_c/d	Head at Center I_{c_0} = I_{a_0}
3.20	4.00	−0.0345	+ 0.7105 + 0.2695	+1.0452 +0.9865	0.6583	0.4168	0.7465	+ 1.0008 + 0.7694
8.00	10.00	−0.0281	+ 0.7715 + 0.2286	+1.0583 +0.9826	0.5077	0.3549	0.5634	+ 3.8514 + 2.7817
32.00	40.00	−0.0612	+ 1.2960 + 0.2960	+1.1709 +0.9691	0.2898	0.2134	0.3176	+ 13.8075 + 12.2546
64.00	80.00	−0.0568	+ 2.0494 + 1.0494	+1.3326 +0.9010	0.2095	0.1558	0.2295	+ 26.8295 + 24.6574
80.00	100.00	−0.0632	+ 2.4315 + 1.4315	+1.4117 +0.8766	0.1886	0.1403	0.2062	+ 33.2594 + 30.8320
240.00	300.00	−0.1100	+ 6.3158 + 5.3158	+2.7484 +0.6282	0.1106	0.0825	0.1206	+ 96.5289 + 92.2911
400.00	500.00	−0.1427	+10.2609 + 9.2609	+3.0912 +0.3773	0.0858	0.0642	0.0937	+159.0727 +153.5708

* Correction to Table 9. Under Head at Junction, at d/t of 3.20, the lower value of I_{cj} should be 1.0119.

TABLE 10 STRESS INDEXES IN A CYLINDRICAL PRESSURE VESSEL WITH FLAT HEAD, $T/t = 1.0$

		Cylinder at Junction			Head at Junction		
d/t	d/T	Shear I_{sj}	Axial I_{aj}	Circum. I_{cj}	Shear I_{sj}	Axial I_{aj}	Circum. I_{cj}
4.00	4.00	+0.4160	− 0.2711	+ 0.1850	+0.7500	− 1.3258	− 0.2758
			+ 1.2711	+ 0.6477		+ 1.8305	+ 0.8305
10.00	10.00	+0.5163	− 1.9217	− 0.4865	+0.7500	− 3.1502	− 0.5253
			+ 2.9217	+ 0.9665		+ 3.5796	+ 1.2536
40.00	40.00	+1.0047	− 11.3840	− 3.7209	+0.7500	− 13.2237	− 2.7237
			+ 12.3840	+ 3.4095		+ 14.5633	+ 4.0633
80.00	80.00	+1.1280	− 24.8413	− 8.0591	+0.7500	− 27.2373	− 6.2373
			+ 25.8413	+ 7.1457		+ 29.1333	+ 9.1333
100.00	100.00	+1.5960	− 31.7130	−10.2394	+0.7500	− 34.3383	− 8.0883
			+ 32.7130	+ 9.0884		+ 36.4636	+10.2136
300.00	300.00	+2.8111	−102.3113	−32.2278	+0.7500	−106.5596	−27.8097
			+103.3113	+29.4590		+110.3079	+31.5579
500.00	500.00	+3.6602	−174.2607	−54.3632	+0.7500	−179.6413	−48.3913
			+175.2607	+50.4733		+184.5215	+53.2715

		Maxima in Cylinder			Location of Maxima in Cylinder			Head at Center
d/t	d/T	Shear I_{sm}	Axial I_{am}	Circum. I_{cm}	Shear x_1/d	Axial x_2/d	Circum. x_3/d	$I_{co} = I_{ao}$
4.00	4.00	−0.0330	+ 0.7252	+1.0434	0.6051	0.1891	0.6839	+ 1.1132
			+ 0.2748	+0.9356				− 0.5945
10.00	10.00	−0.0291	+ 0.8135	+1.0673	0.4564	0.3198	0.5063	+ 3.0173
			+ 0.1865	+0.9798				− 2.3309
40.00	40.00	−0.0446	+ 1.4432	+1.2068	0.2531	0.1597	0.2530	+ 11.5263
			− 0.4432	+0.9384				− 10.1867
80.00	80.00	−0.0621	+ 2.3947	+1.4068	0.1968	0.1385	0.2045	+ 22.2627
			− 1.3947	+0.5788				− 20.3667
100.00	100.00	−0.0694	+ 2.8681	+1.5084	0.1679	0.1247	0.1837	+ 27.5367
			− 1.8681	+0.8436				− 25.4114
300.00	300.00	−0.1217	+ 7.6929	+2.5412	0.0984	0.0795	0.1275	+ 79.0653
			− 6.6929	+0.5402				− 75.3171
500.00	500.00	−0.1593	+12.5306	+3.5935	0.0765	0.0572	0.0836	+129.7919
			−11.5306	+0.2277				−124.3535

TABLE 11 STRESS INDEXES IN A CYLINDRICAL PRESSURE VESSEL WITH FLAT HEAD, $T/t = 1.2$

		Cylinder at Junction			Head at Junction		
d/t	d/T	Shear I_{sj}	Axial I_{aj}	Circum. I_{cj}	Shear I_{sj}	Axial I_{aj}	Circum. I_{cj}
4.80	4.00	+0.4236	− 0.1094	+ 0.1032	+0.6250	− 1.1303	− 0.2272
			+ 1.1094	+ 0.6438		+ 1.5729	+ 0.6979
12.00	10.00	+0.5556	− 2.2303	− 0.6604	+0.6250	− 2.5167	− 0.3292
			+ 3.2303	+ 0.9778		+ 3.1174	+ 0.9699
48.00	40.00	+1.0524	− 13.0147	− 4.1476	+0.6250	− 10.5516	− 1.8066
			+ 14.0147	+ 3.6612		+ 11.7340	+ 2.9740
96.00	80.00	+1.5066	− 28.6321	− 9.5845	+0.6250	− 21.9048	− 4.4048
			+ 29.6321	+ 7.5949		+ 23.5788	+ 6.0788
120.00	100.00	+1.6912	− 36.0575	−12.1742	+0.6250	− 27.6863	− 5.9113
			+ 37.0575	+10.1203		+ 29.5587	+ 7.6937
360.00	300.00	+3.0246	−119.7956	−38.3617	+0.6250	− 86.3992	−21.2742
			+120.7956	+33.7957		+ 90.2598	+24.6348
600.00	500.00	+3.9535	−205.0247	−64.3249	+0.6250	−147.1182	−37.7431
			+206.0247	+58.4399		+151.5179	+42.1359

		Maxima in Cylinder			Location of Maxima in Cylinder			Head at Center
d/t	d/T	Shear I_{sm}	Axial I_{am}	Circum. I_{cm}	Shear x_1/d	Axial x_2/d	Circum. x_3/d	$I_{co} = I_{ao}$
4.80	4.00	−0.0319	+ 0.7381	+1.0511	0.5662	0.3670	0.5162	+ 0.9603
			+ 0.2619	+0.9848				− 0.4896
12.00	10.00	−0.0295	+ 0.8492	+1.0750	0.4179	0.2932	0.4634	+ 2.6195
			+ 0.1508	+0.9777				− 2.0189
48.00	40.00	−0.0469	+ 1.6888	+1.2380	0.2345	0.1724	0.2575	+ 10.0704
			− 0.6888	+0.9291				− 8.9010
96.00	80.00	−0.0659	+ 2.7037	+1.4731	0.1700	0.1259	0.1960	+ 19.3452
			− 1.7037	+0.8591				− 17.6712
120.00	100.00	−0.0739	+ 3.2621	+1.5930	0.1528	0.1134	0.1672	+ 23.8762
			− 2.2621	+0.8234				− 21.9938
360.00	300.00	−0.1310	+ 8.9931	+2.8212	0.0896	0.0669	0.0980	+ 87.7881
			− 7.9931	+0.4577				− 84.4277
600.00	500.00	−0.1711	+14.8002	+4.0701	0.0697	0.0521	0.0762	+140.6941
			−13.8002	+0.0858				−136.3016

TABLE 12 STRESS INDEXES IN A CYLINDRICAL PRESSURE VESSEL WITH FLAT HEAD, $T/t = 1.6$.

		Cylinder at Junction			Head at Junction		
d/t	d/T	Shear I_{sj}	Axial I_{aj}	Circum. I_{cj}	Shear I_{sj}	Axial I_{aj}	Circum. I_{cj}
6.40	4.00	+0.4309	− 0.6456	− 0.0339	+0.4688	− 0.9066	− 0.1504
			+ 1.6456	+ 0.6535		+ 1.1667	+ 0.5095
16.00	10.00	+0.5604	− 2.5721	− 0.9211	+0.4688	− 1.7062	− 0.2656
			+ 3.5721	+ 0.9324		+ 2.1732	+ 0.9326
64.00	40.00	+1.0882	− 15.3932	− 5.5651	+0.4688	− 7.1171	− 0.9526
			+ 16.3932	+ 3.9709		+ 8.0232	+ 1.1695
128.00	80.00	+1.5923	− 34.5291	−12.0173	+0.4688	− 15.7101	− 1.8351
			+ 35.5291	+ 8.9697		+ 16.3370	+ 3.2120
160.00	100.00	+1.8027	− 44.5061	−15.3430	+0.4688	− 19.0328	− 2.6795
			+ 45.5061	+11.6951		+ 20.5350	+ 4.1733
480.00	300.00	+3.3122	−150.0018	−49.2227	+0.4688	− 61.5511	−12.3123
			+151.0018	+41.1006		+ 64.3112	+15.0925
800.00	500.00	+4.3749	−259.7367	−83.6914	+0.4688	−105.3203	−23.2390
			+260.7367	+72.4306		+108.9560	+26.9347

		Maxima in Cylinder			Location of Maxima in Cylinder			Head at Center
d/t	d/T	Shear I_{sm}	Axial I_{am}	Circum. I_{cm}	Shear x_1/d	Axial x_2/d	Circum. x_3/d	$I_{co} = I_{ao}$
6.40	4.00	−0.0302	+ 0.7010	+1.0560	0.5026	0.3318	0.5069	+ 0.7503
			+ 0.2990	+0.9833				− 0.3011
16.00	10.00	−0.0296	+ 0.9035	+1.0866	0.3624	0.2564	0.4015	+ 2.1669
			+ 0.0965	+0.9782				− 1.6939
64.00	40.00	−0.0483	+ 1.8314	+1.2253	0.2021	0.1421	0.2213	+ 8.3536
			− 0.8314	+0.9349				− 7.1468
128.00	80.00	−0.0699	+ 3.1939	+1.5795	0.1464	0.1082	0.1693	+15.9275
			− 2.1939	+0.8277				−14.6005
160.00	100.00	−0.0759	+ 3.7039	+1.7108	0.1317	0.0975	0.1551	+19.8191
			− 2.7039	+0.7324				−18.2869
480.00	300.00	−0.1436	+11.2196	+3.1066	0.0771	0.0578	0.0916	+54.6645
			−10.2196	+0.3135				−51.7044
800.00	500.00	−0.1894	+18.7957	+4.9257	0.0602	0.0449	0.0693	+88.0191
			−17.7957	−0.1689				−84.3994

TABLE 13* STRESS INDEXES IN A CYLINDRICAL PRESSURE VESSEL WITH FLAT HEAD, $T/t = 2.0$

		Cylinder at Junction			Head at Junction		
d/t	d/T	Shear I_{sj}	Axial I_{aj}	Circum. I_{cj}	Shear I_{sj}	Axial I_{aj}	Circum. I_{cj}
8.00	4.00	+0.4295	− 0.8203	− 0.1198	+0.3750	− 0.6173	− 0.0928
			+ 1.8258	+ 0.6656		+ 0.9041	+ 0.3791
20.00	10.00	+0.5425	− 2.9169	− 1.0833	+0.3750	− 1.2159	− 0.0966
			+ 3.9169	+ 0.9669		+ 1.5775	+ 0.2650
80.00	40.00	+1.0665	− 16.6809	− 6.2522	+0.3750	− 5.0062	− 0.2438
			+ 17.6809	+ 4.0566		+ 5.7172	+ 0.4472
160.00	80.00	+1.5916	− 38.1305	−13.6995	+0.3750	−10.7312	− 0.2312
			+ 39.1305	+ 9.5088		+11.7923	+ 1.2923
200.00	100.00	+1.8161	− 49.5714	−17.5805	+0.3750	−13.7295	− 0.6025
			+ 50.5714	+12.5081		+14.9371	+ 1.8121
600.00	300.00	+3.1432	−173.0186	−57.7312	+0.3750	−45.6751	− 6.3001
			+174.0186	+46.4099		+47.9706	+ 8.5956
1000.00	500.00	+4.6072	−300.9208	−89.2275	+0.3750	−79.1766	−13.3516
			+301.9208	+83.4219		+82.8480	+16.6230

		Maxima in Cylinder			Location of Maxima in Cylinder			Head at Center
d/t	d/T	Shear I_{sm}	Axial I_{am}	Circum. I_{cm}	Shear x_1/d	Axial x_2/d	Circum. x_3/d	$I_{co} = I_{ao}$
8.00	4.00	−0.0290	+ 0.7301	+1.0601	0.4587	0.3039	0.5124	+ 0.6107
			+ 0.2119	+0.9821				− 0.3334
20.00	10.00	−0.0287	+ 0.9385	+1.0941	0.3234	0.2263	0.3587	+ 1.8779
			+ 0.0615	+0.9720				− 1.5162
80.00	40.00	−0.0431	+ 1.9670	+1.3149	0.1795	0.1315	0.1974	+ 7.3683
			− 0.9670	+0.9262				− 6.6575
160.00	80.00	−0.0701	+ 3.5262	+1.6497	0.1304	0.0962	0.1429	+14.0183
			− 2.5262	+0.8065				−12.9577
200.00	100.00	−0.0796	+ 4.3408	+1.8216	0.1173	0.0867	0.1284	+17.2100
			− 3.3408	+0.7545				−16.0004
600.00	300.00	−0.1495	+12.9953	+3.6826	0.0690	0.0514	0.0754	+47.1374
			−11.9953	+0.2012				−44.8429
1000.00	500.00	−0.1996	+22.0138	+5.6252	0.0537	0.0401	0.0587	+75.5109
			−21.0138	−0.3772				−72.4395

* Correction to Table 13. Under Head at Junction, at $d/t = 20$, the upper value of I_{sj} should be positive. At $d/t = 1000$, the upper value of I_{cj} should be -13.5516. Under Maxima in Cylinder, at $d/t = 8$, the lower value of I_{am} should be $+0.2199$.

Discussion of Results

(*a*) *Variation of M_0/pd^2 and Q_0/pd.* Examination of Tables 1 to 5 shows that the cylinder influence numbers a_4, a_5, a_6, b_5, and b_6 all increase or remain constant with increasing d/t. This simply means that unit loads (p, M_0, Q_0) produce increased deflection and rotation as the cylinder becomes more flexible. An identical conclusion applies to the head-influence numbers of Table 6.

Again, increasing T/t results in increases in the influence numbers of the cylinder. Imagine a head of fixed diameter and thickness. Increasing T/t is equivalent to making the cylinder thinner. Thus, increasing either d/t or T/t means increased cylinder flexibility as a consequence of having less wall thickness.

As any shell becomes thinner, we approach the membrane solution which implies no bending moment. This is consistent with the results of Table 8 which show that M_0/pd^2 decreases as T/t increases. However, the decrease is slight. In fact, the bending moment at the junction in the cylinder is scarcely affected by changes in cylinder thickness. If the head thickness is decreased (d/T increasing) the head becomes more flexible and the greater curvature implies larger bending moments. The increase is again slight. For example, a hundredfold increase in d/T doubles M_0/pd^2.

Similar conclusions do not apply to the shear force Q_0/pd. This is because it induces not only bending but radial tension in the head. As the cylinder becomes thinner (T/t increasing) Q_0/pd must increase but does so slightly. Under these circumstances the pressure produces larger radial deformations and the increase in Q_0/pd is required to maintain continuity of deflections. The same effect contributes to continuity of rotation.

For thinner heads (d/T increasing), Q_0/pd increases for the same reasons. A thinner head deflects and rotates more under pressure. The shear force stretches the head more and cancels some of the rotation induced by the pressure. A hundredfold increase in d/T increases Q_0/pd by 10 times.

(*b*) *Discussion of Stresses.* Tables 9 to 13 show the three types of stress ratios in the cylinder and in the head at the junction. The tables also list the equal axial- and circumferential-stress ratios at the center of the head and the magnitude and location of the maximum shear-stress and axial-stress ratios in the cylinder.

1 When the head-cylinder thickness ratio T/t is 0.8 or 1.0, the axial-stress ratio in the head at the junction is a maximum for all computed values of d/t (Tables 9 and 10). When T/t = 1.2, 1.6, or 2.0, the maximum stress ratio is the axial junction-stress ratio in the cylinder (Tables 9, 12, and 13), with the exception of the first reading of Table 11 corresponding to d/T = 4. For thin vessels (large d/t), the maximum stress may be 100 to 200 times greater than the circumferential hoop stress.

2 In general, when the ratio d/t (or d/T) increases, all stress ratios increase. This simply means that the ratio of the stress (of any type) to the circumferential hoop stress $pd/2t$ becomes larger for progressively thinner vessels.

3 In general, when the thickness ratio T/t increases, the stress ratios in the head decrease. The head is becoming stiffer and deflects less so that the bending stress is reduced. The shear stress in the head is also reduced since the shear force is distributed over a greater thickness.

4 For any fixed ratio d/T, the stress ratios in the cylinder I_{zj}, $I_{\theta j}$, I_{sm} increase with T/t while the remaining stress ratios, I_{zm} and $I_{\theta j}$, decrease. The shear force Q_0 increases relative to pd. This accounts for the stress ratios which increase. I_{zj} decreases because the effect of decreasing M_0/pd^2 outweighs the effect of increasing Q_0/pd. The decrease in I_{zm} is associated with the change in its location, x_z/d.

5 The foregoing conclusions are not always correct for values of d/T less than 10 where departures from the theory occur.

6 Fig. 3 shows that the maximum stress ratio I_{max}, as a function of d/t, is nearly a straight line for any of the computed thickness ratios T/t. The lowest stress occurs when the head is twice the thickness of the cylinder. It is to be noted that the increase in stress when T/t is reduced from 1.0 to 0.8 is very much greater than the decrease in stress when T/t is increased from 1.0 to 1.2.

Fig. 4 exhibits the same conclusion except that the ratio of maximum stress to pressure is plotted instead of I_{max}. A curve of this type is recommended as the most advantageous for design purposes.

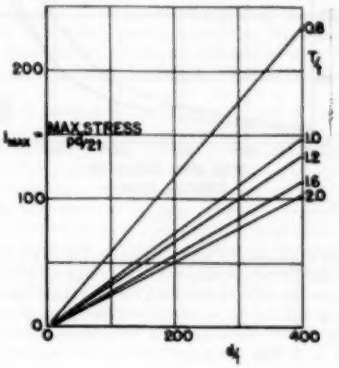

Fig. 3

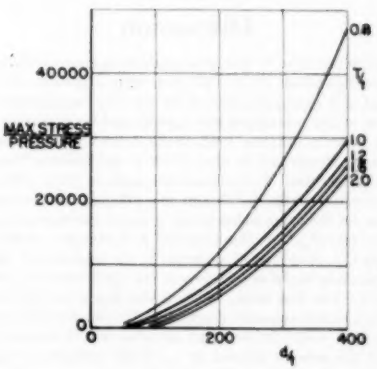

Fig. 4

7 It is of interest to compare the differences between the present results and those found for a conical head, especially when the apex angle is 120 deg. The limiting case of a cone with apex angle approaching 180 deg would correspond physically to a flat head but the equations connecting the deflection and rotation at the junction would differ from those used here. In the former case the middle surface of the conical head and the cylinder meet at the junction. In the present paper it is that surface of the head which is exposed to pressure whose deflection and rotation are equated to the deflection and equal rotation of the middle surface of the cylinder. The stress ratios tend to increase as the

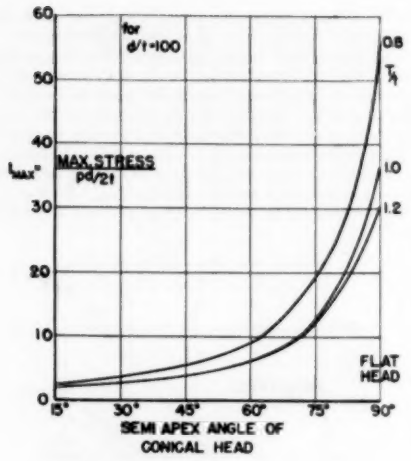

FIG. 5

apex angle of the conical head increases. The stress ratios in the flat head should then be larger than the ratios for a conical head. Fig. 5 shows the effect of increasing the cone angle upon the maximum stress ratio for $d/t = 100$ and various values of T/t. In this figure the present results are used to correspond to the limiting value, $\alpha = 90$ deg. It is evident that the maximum stress is severest in a flat head, since the discontinuity of the center line of the head and the cylinder is greatest in this case.

Discussion

D. B. WESSTROM.[10] The same analysis as given by the authors in their Equations [1] to [10], but with Equations [5] to [7] omitted, and a complete solution for the longitudinal stress in the cylinder at the junction of the cylinder and head, was presented by the writer in October, 1945, to the Boiler Code Subcommittee on Special Design and in May, 1946, to the Pressure Vessel Research Committee. It was presented again in May, 1950, to the Subcommittee on Special Design, in a different form, with a final solution for the stress index in the cylinder, corresponding to the authors' ratio I_{a_j}. At that time Mr. J. J. Murphy, of the M. W. Kellogg Company, called attention to the omission of the term corresponding to the second term in the right-hand side of Equation [6]. The first term, which is also Equation [5], was purposely omitted because the magnitude of the tension Q_b in the plane of the head would be such that its effect would be quite small. In fact, the writer's solution for I_{a_j} of the cylinder, as corrected by Mr. Murphy, and with Equation [5] omitted, checks the values given by the authors in Tables 9 to 13 within 3.3 per cent in the most extreme case, and within less than 1 per cent in all cases where the shell diameter-to-thickness ratio d/t is over 35.

Another reason for the omission of Equation [5] by the writer was the fact that it balanced the neglect of another factor neglected also by the authors, which is that, if the head is to have a deflection curve, the edge of the head must be drawn inward to satisfy the geometrical requirement that the length of the curve be constant. As this inward movement takes place, however, a resistance to it is set up by circumferential compressive stresses in the head at and near its periphery. It was believed that the net effect, combined with the stretching of the head by the tension Q_b, would be so negligible as to justify omission of Equation [5].

Deviations of from 1 to 3.3 per cent for cases in the lower values of d/t are not of great significance, however, inasmuch as the authors themselves state that for d/t less than 10, it is unlikely that the theories used are applicable. This is also true of the first term given in Table 7 for I_{a_j} of the cylinder. When $d/t = 10$, this term is 0.405 instead of 0.50, and for lower values of d/t, the error in this term is progressively greater.

The writer is of the opinion that the stress index I_{a_j} for the cylinder is the only index of any practical significance. In any practicable pressure-vessel design, the head thickness will be considerably greater than the shell thickness and therefore the highest stress will be in the cylinder. Also, since Q_b is relatively small, and is actually in a direction opposite to that shown in Fig. 1 of the paper, the so-called maximum longitudinal stress in the cylinder (stress index I_{a_m}) could not possibly be greater than the peak longitudinal stress at the junction. All this is confirmed by the results in Tables 11 to 13 for d/t of 10 or higher.

Lest the designer be confused by the extremely high values of I_{a_j} for the cylinder reported by the authors, it should be stated that these do not represent practical engineering designs, inasmuch as I_{a_j} is a measure of the stress in terms of the hoop stress in the cylinder. If the designer makes the cylinder as thin as the Code will permit, by using the maximum permissible stress, and limits the longitudinal stress at the junction to the same value, I_{a_j} must not exceed unity, and if he elects to tolerate a stress twice as great, I_{a_j} can be as great as 2. Further, if he is willing to make the cylinder twice as thick as otherwise necessary, I_{a_j} can be as large as 4, and so on. Therefore only the extreme lower left-hand corner of Fig. 3 of the paper would be of any engineering usefulness. It will be found also that in most cases the ratio of head thickness to shell thickness T/t will be greater than the value of 2 at which the authors' tables stop. What is needed is a chart for I_{a_j} for values perhaps as high as 10, and T/t values from 1 to 10, of which the range 2 to 8 will cover most designs.

The writer has developed the complete solution for I_{a_j} of the cylinder. It can be expressed in nondimensional form by placing $T/t = a$ and $d/t = b$. It also takes into account the location of the joint between the head and shell, nT being the distance from the mid-plane of the head thickness to the joint; positive when the joint is on the same side of the mid-plane as the cylinder. With a, b, and n thus defined, we have for the cylinder

$$I_{a_j} = \frac{1}{2} + \frac{C_1a^3 - 2C_2na + C_3b^{1/2} + 2C_4nab + C_5b/a}{C_6a^3 + 2C_7na + C_8/a + C_9b^{1/2} + 4C_{10}n^2a^2/b^{1/2} + C_{11}a^3/b^{1/2}}$$

in which

$C_1 = 2.94317$	$C_6 = 1.90702$
$C_2 = 3.74071$	$C_7 = 4.84761$
$C_3 = 1.00000$	$C_8 = 1.026862$
$C_4 = 0.908912$	$C_9 = 2.66667$
$C_5 = 0.385077$	$C_{10} = 4.40610$

$$C_{11} = 1.46869$$

For the case covered by the authors' paper, in which $n = 0.50$, the foregoing formula becomes

$$I_{a_j} = \frac{1}{2} + \frac{C_1a^3 - C_2a + C_3b^{1/2} + C_4ab + C_5b/a}{C_6a^3 + C_7a + C_8/a + C_9b^{1/2} + (C_{10} + C_{11})a^3/b^{1/2}}$$

With this formula and a table of five-place logarithms, the authors' values of I_{a_j} for the cylinder in Tables 9 to 13 can be

[10] Mechanical Engineer, E. I. du Pont de Nemours & Company, Engineering Department, Wilmington, Del. Mem. ASME.

checked to four or five significant figures. Therefore it should be possible with this formula to construct a chart for any range of T/t and d/t desired.

If the stretching of the head plate, per Equation [5] of the paper, is neglected, the coefficients C_5, C_8, and C_{11} become zero.

The authors' very searching investigation thus confirms the results of a less elaborate analysis, which without much difficulty can be expressed in a form immediately useful to the designer.

Authors' Closure

The authors wish to thank Mr. Wesstrom for his thorough study of the paper, and his working out of a single formula giving the axial stress index in the cylinder at the junction for any values of d/t and T/t. It is reassuring to have such close checks on the numerical values.

In deriving his formula, Mr. Wesstrom introduces a factor which permits moving the head-shell junction point up or down throughout the thickness of the head. The authors' case is represented by $n = 0.5$ (junction at inner surface of head). If the junction is located at any other point, it will be necessary either to modify certain dimensions so that, for instance, the head can be fitted inside the shell, or else to overlook interferences between the parts in computing stresses and deflections.

Mr. Wesstrom also points out that since internal pressure acts at the inside rather than at the mean diameter of the shell, the average axial stress will be 0.405 rather than 0.50 for a cylinder with $d/t = 10$. Although the authors agree, it should not be thought that changes of this kind would permit a truly accurate stress analysis of thick-walled vessels. The presentation of stress-index numbers to several significant figures is convenient for checking purposes, but no claim is made that actual stresses are known to such accuracy. As noted above, it is impossible for a simple cylinder and disk to fully represent the actual geometry at the junction. Also, although bending stresses are assumed to vary linearly through the thickness of a plate, it is well known from photoelastic studies that at a projecting corner the stresses are zero, while at a re-entrant corner they are nonlinear and extremely high.

In spite of these imperfections, it is believed that the results in the paper represent stress conditions in thin-walled vessels with fair accuracy. Although the development of more realistic analyses for thick-walled vessels is desirable, the high stresses computed from present results are sufficient to show that flat heads are not a suitable or efficient closure for high-pressure vessels.

The authors agree with Mr. Wesstrom that a problem is created by the discrepancy between the high values computed for "secondary stresses" (usually not specifically mentioned in the Codes) and the much lower values which the Codes allow for primary or membrane stresses. If secondary stresses were required to be held down to the present working stresses (which contain large "safety factors"), the resulting vessel designs would be most uneconomical. Perhaps the next developmental step should be a study to determine what secondary stress values are actually being permitted by the present Codes.

Low-Temperature Separation for High-Pressure Gas-Distillate Wells

By C. O. GLASGOW,[1] TULSA, OKLA.

The process for extracting hydrocarbons from high-pressure gas at low temperatures is not new. As early as 1936 experimental work was done in cycling plants to increase hydrocarbon recovery by low-temperature separation at elevated pressures which resulted in increased revenue from the sale of liquid fractions and reduced the horsepower requirement for injecting the gas back to formation. Low-temperature separation is now finding wide application in small compact-type low-temperature units for individual gas-distillate wells in order to increase stock-tank liquid for a rapid payout investment, and at the same time reduce the water content of the gas to meet pipe-line specifications. Performance tests, calculated studies, and a description of this last-mentioned low-temperature unit are presented to show the advantages of more efficient equipment for high-pressure gas-distillate production.

Introduction

WITH the increased demand for natural gas and distillate values ranging from $2.50 to $3.00 per bbl, producers are giving more serious consideration to better methods of gas production—methods that not only increase income by more efficient utilization of high pressures but also methods that eliminate the many troubles encountered in producing high-pressure gas such as hydrate formation, corrosion, and high hydrocarbon dew points of the gas in long transmission lines.

Since the recent trend has been toward higher gas-transmission-line pressures, which increases the temperature at which hydrates form, the pipe-line companies have found it necessary to purchase gas with a water and hydrocarbon dew point below the minimum temperature encountered from the well to the point of consumption. Many of the gas-transmission companies require a water content of 7 lb or less per million cu ft and a hydrocarbon content not to exceed 0.2 gal per thousand cu ft.

These factors naturally have brought about the installation of many high-pressure gas-processing plants and packaged gas-dehydration units where central processing is feasible. However, there are many areas where high-pressure gas cannot be processed economically in a central plant and, therefore, for the producer to have a market for his product, he must process his gas at the well head. This is where low-temperature extraction units are rapidly becoming standard production equipment, as by using the high-pressure gas and expanding to a lower pressure, a resulting lower temperature is obtained for separation. The net result is a salable gas with a low water-vapor and hydrocarbon dew point and an increase of 5 to 15 bbl per million cu ft of stock-tank liquid over and above regular heater, separator production methods. The limitation of this process is governed only by the pressure drop available between the well head and the gas-transmission line.

Mechanical Process

There are many different types of small unitized low-temperature extraction plants, each designed to accomplish a given result depending on the well-stream composition, pressure, temperature, and operation limitations. Basically, any low-temperature separation process utilizing the Joule-Thompson effect of expanding high-pressure gas to a lower pressure to obtain refrigeration must have its component parts so designed for efficient removal of hydrates and liquid hydrocarbons from the gaseous stream and at the same time provide trouble-free operation under all weather conditions.

In order to eliminate confusion and permit more detailed discussion of this process it will be desirable to confine this paper to only one standard unit which has the greatest application and flexibility for most high-pressure gas-distillate wells.

For a more comprehensive understanding of this type of low-temperature unit refer to the illustrated schematic flow diagram shown in Fig. 1.

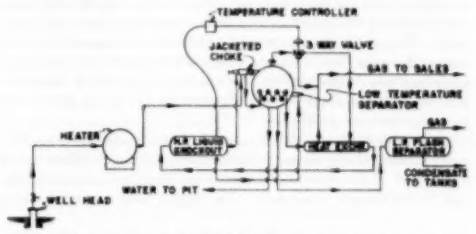

FIG. 1 FLOW DIAGRAM OF LOW-TEMPERATURE CONDENSATE-RECOVERY SYSTEM

The high-pressure gas from the well is first taken through a heater to insure trouble-free operation due to changes in flow rates and weather conditions. However, the heater may not be necessary on high-temperature wells in warm climates where the unit is installed close to the well and a fairly high rate of flow can be maintained. Heaters generally used for this type of service have a high-pressure gas coil submerged in a body of water which in turn is heated by a direct-fired gas furnace thermostatically controlled by either having the thermostat bulb in the water or in the gas-outlet line. When the thermostat bulb is used in the gas-outlet line, a second thermostat is generally used on the water bath and set at a temperature of 180 to 190 F to prevent boiling of the water.

The high-pressure gas from the heater then enters the jacket around the choke to prevent hydrate formation ahead of the point of expansion, and then is conducted into the heating coil placed in the lower part of the low-temperature separator. This heating coil is submerged in the liquid section of the low-temperature separator for the purpose of melting the hydrates formed as a result of expansion of the gas so that they can be removed as liquid water and also to heat the hydrocarbons removed so as to

[1] Chief Engineer, National Tank Company. Jun. ASME.

Contributed by the Petroleum Division and presented at the Petroleum Mechanical Engineering Conference, Tulsa, Okla., September 24–26, 1951, of THE AMERICAN SOCIETY OF MECHANICAL ENGINEERS.

NOTE: Statements and opinions advanced in papers are to be understood as individual expressions of their authors and not those of the Society. Manuscript received at ASME Headquarters, March 20, 1951.

effect some stabilization, or in other words, selective stripping of the propane and lighter fractions from the mixture to produce a stable liquid that will retain most of the pentanes and heavier, when flashed to the low-pressure separator.

After the gas leaves the heating coil it is piped to the heat exchanger where it is cooled by the cold gas leaving the low-temperature separator. The gas then enters the high-pressure liquid knockout which removes all water and condensate that can be separated at the corresponding temperature and pressure on the knockout. The liquids removed are then discharged to the lower part of the low-temperature separator.

Since the gas leaving the high-pressure knockout enters the expansion choke it is important to have very accurate regulation of the temperature at this point. This is accomplished by a temperature controller with the control bulb located either in the knockout or in the high-pressure line entering the choke which in turn controls the position of the diaphragm-operated three-way valve. This valve splits the flow of cold gas from the low-temperature separator to send only that part of the gas through the shell side of the exchanger as demanded by the temperature controller. For the most economical operation this temperature should be maintained as close to the hydrate-forming temperature as possible to obtain the maximum temperature drop through the expansion choke; yet at the same time it should not be permitted to go so low as to cause freezing in the knockout or choke.

The liquid-free high-pressure gas then enters the jacketed choke and is expanded into the upper part of the low-temperature separator. The reduction of pressure and temperature changes many of the hydrocarbons from the vapor phase to the liquid phase and causes the formation of hydrates. These are separated from the gas stream and the gas passes out the top of the separator as a dry gas at its corresponding temperature and pressure. This gas is then warmed by the heat exchanger before entering the sales line. The hydrates formed and the condensed hydrocarbons removed from the gas are deposited in the lower heated section of the separator where the hydrates are melted and the hydrocarbons stabilized.

The water from the high-pressure knockout plus that obtained from melting the hydrates is separated from the distillate in the lower part of the low-temperature separator by means of baffles and is discharged separately. The liquid hydrocarbons leaving all free water removed are then staged through at least one intermediate flash separator before being released to the storage tanks.

Fig. 2 shows a field installation of one of these units as previously described.

Low-Temperature Dehydration

The importance of water removal by the low-temperature process cannot be overlooked because of the increased demand for high-pressure dehydrated gas. As previously mentioned, most gas-transmission companies demand a water-vapor content not to exceed 7 lb per million cu ft. Referring to Fig. 3 which shows the water content of natural gas at various pressures and corresponding dew points, one can readily see that this specification can be met by low-temperature separation where flowing pressures are high enough to give sufficient refrigeration. Thus, if the delivery pressure is 800 psi, a water-vapor dew point of 28 deg will be required to produce gas with a water content of 7 lb per million cu ft.

Actual field experiences have shown the water-vapor content to range from 8 to 18 deg below equilibrium temperature conditions. Fig. 4 shows actual field tests of observed dew points at various

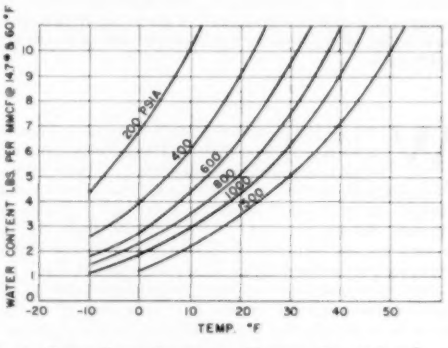

Fig. 3 Water-Vapor Content of Natural Gas at Saturation

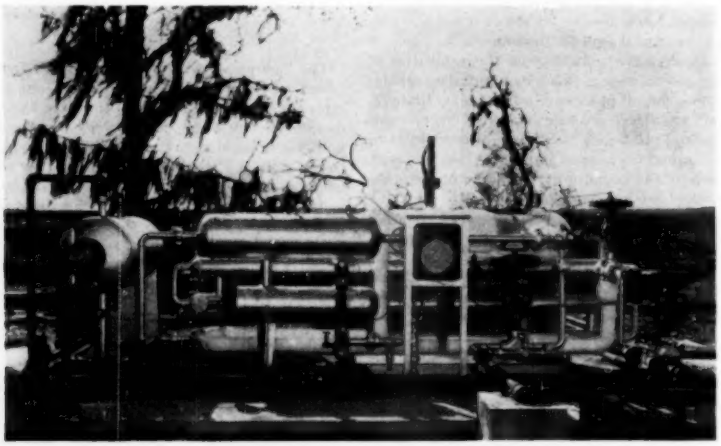

Fig. 2 Low-Temperature Extraction Unit Near Orange, Texas

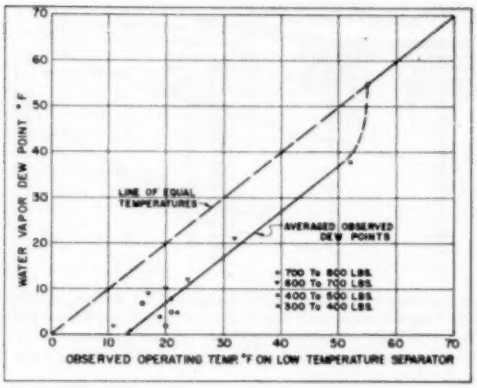

FIG. 4 WATER-VAPOR DEW POINTS COMPARED TO OBSERVED OPERATING TEMPERATURES

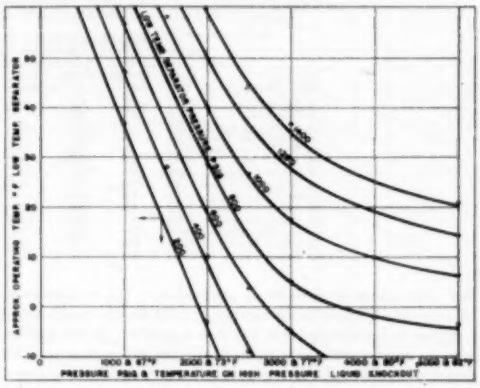

FIG. 5 CURVES FOR PREDICTION OF APPROXIMATE OPERATING TEMPERATURE OF LOW-TEMPERATURE SEPARATOR

pressures and temperatures. The average dew-point depression below operating temperatures is 13 to 14 deg. For estimating purposes one can assume safely a 10-deg depression for average conditions.

Mr. E. G. Hammerschmidt[2] has reported in his findings in dealing with hydrates that this condition does exist and has been able to produce in a chiller, after hydrates were formed, a water-vapor dew point 13 deg below the actual temperature of the gas. The conditions existing in a low-temperature separator are similar to the chiller and actual field observations have substantiated this dew-point depression. It must be remembered, however, that this dew-point depression is obtained only when the low-temperature separator is operating at a pressure and temperature conducive to the formation of hydrates.

Since the application of a low-temperature unit for the purpose of dehydrating gas is dependent on the available pressure drop between the well head and transmission line, it is important to have some means to predict whether such a process can be used. In order to make an approximation Fig. 5 has been developed from a number of actual field tests to show the degree of cooling that can be expected from the expansion of the gas in a low-temperature unit.

Since all the liquids are removed ahead of expansion by the knockout, one should expect a fairly constant degree of cooling that could be applied to all gases; however, owing to the wide variation of well-stream compositions this one set of curves can be used only as an approximation.

For example, it is desired to deliver gas at 1000 psi with a water content not to exceed 7 lb per million cu ft. Referring to Fig. 3, we find the water-vapor dew point at 7 lb of water and 1000 psi operating pressure to be 32 deg, assuming a 10-deg dew-point depression would mean an operating temperature on the unit of 42 deg. Referring to Fig. 5, we find the intersection of the 42-deg operating temperature line and 1000-psi separator-pressure curve shows a minimum high-pressure knockout pressure of 1900 lb. Therefore to meet these conditions one must have a well with a flowing pressure in excess of 2000 lb to make such an installation practical. Flowing temperatures also must be considered in order to properly size the heater if needed and also to make sure of ample heat-exchanger capacity.

[2] "Formation of Gas Hydrates in Natural Gas Transmission Lines," by E. G. Hammerschmidt, *Industrial Engineering and Chemistry*, vol. 26, 1934, pp. 851–855.

Low-temperature dehydration is also being used on off-shore gas-distillate wells to permit the transportation of the high-pressure gas to shore without hydrate formation. Fig. 6 shows four units located on one central platform in the Gulf of Mexico. The gas is processed at low temperature and the water removed from both the gas and distillate at approximately 1000 psi. The distillate is then metered and recombined with the gas and transported approximately 27 miles through the pipe line to shore. The water-vapor content of the gas at the platform before recombination with the distillate averages 3 to 3.5 lb per million cu ft. The water content at shore which is the combined stream averages 3.8 to 4 lb per million cu ft. Thus, with a water content of 4 lb and a pressure of 1000 psi, the line is protected down to a temperature of approximately 18 F.

Therefore it can be safely said that low-temperature separation if properly applied does have a place in the dehydration of high-pressure natural gas.

INCREASED HYDROCARBON RECOVERY

From an operating standpoint the producer not only obtains a water-vapor dew-point depression from low-temperature separation but also a hydrocarbon dew-point depression of the gas. This is important especially in long transmission lines as it eliminates liquid accumulation and thereby increases the transmission efficiency.

Removing these hydrocarbons at the well is actually where the producer realizes his greatest benefit as far as investment in equipment is concerned. Many installations pay out the total investment in a matter of a few months by increased distillate production over standard separation methods. To show the value of this increase in production Table 1 has been prepared from actual field data where a direct comparison could be made between conventional and low-temperature operation. The fourteen installations were taken over a wide area where high-pressure gas is produced with wellhead flowing pressures ranging from 1680 to 3150 psi and condensate production from 13 to 223 bbl per million cu ft of gas. These data indicate an increase of a minimum of 4 bbl per million to a maximum of 17 bbl per million cu ft of sales gas. The last column in this table shows the value of this increase on a yearly basis per million cu ft of gas produced. Thus, for example, a well producing an average of 5MMCF of gas per day with an increase of 5 bbl per million cu ft and selling for $2.65 per barrel amounts to $24,181.25 per year additional reve-

TABLE 1 FIELD DATA SHOWING INCREASED LIQUID-HYDROCARBON RECOVERY WITH LOW-TEMPERATURE SEPARATION COMPARED TO CONVENTIONAL METHODS

Unit no.	Location	Operating conditions: Wellhead b-p separator Press, psi	Wellhead b-p separator Temp, deg F	Low-temperature separator Press, psi	Low-temperature separator Temp, deg F	Condensate recovery, low-temp separator, bbl/MMCF	Increase in condensate by separation, low-temperature, bbl/MMCF	Additional yearly revenue per MMCF gas value of condensate $2.65/bbl
1	Oklahoma	2625	82	450	−8	17	6	$ 5803.50
2	Oklahoma	3150	85	380	0	44	7	6770.75
3	West Texas	2500	78	875	32	15	4	3869.00
4	Southwest Texas	1800	75	365	22	24	5	4836.25
5	North Louisiana	2670	90	950	50	105	15	14508.75
6	East Texas	2350	94	830	42	14	4	3869.00
7	South Texas	2800	82	840	14	16	5	4836.25
8	North Louisiana	1680	80	500	42	223	12	11607.00
9	South Louisiana	2750	86	600	16	48	15	14508.75
10	South Louisiana	2900	85	600	10	52	17	16443.25
11	South Louisiana	2830	82	805	20	50	13	12574.25
12	So. Mississippi	2960	85	465	10	90	14	13541.50
13	South Louisiana	2350	80	650	24	21	5	4836.25
14	South Texas	2750	82	530	0	13	5	4836.25

nue over standard methods of production. The producer realizes seven-eighths of this amount, or $21,158.59, which represents a payout on his investment in less than 6 months. In those areas where a greater increase is realized, one can well understand the magnitude of the value of low-temperature separation to increase hydrocarbon recovery.

Leaving the practical application and results obtained from low-temperature separation and delving lightly into the theory of increased recovery, Fig. 7 has been prepared to illustrate the source of additional hydrocarbons. This chart shows the calculated per cent recovery of each well-stream component at a constant pressure of 500 psi and a temperature range of 10 to 70 F. These calculations are based on a final flash in the storage tank at atmospheric pressure 14.7 psia and a temperature of 80 F.

The percentage increase from 70 to 10 F shows hexanes 52 to 85 per cent, normal pentanes 27 to 62.5 per cent, and isopentanes 21 to 55 per cent. This explains why with the marked increase of the lower vapor-pressure components that an increase in butanes and propanes can be realized without affecting the stability of the stock-tank liquid. In other words, the greater the percentage of pentanes and hexanes recovered the greater the percentage of the light ends can be held in equilibrium in the stock-tank liquid.

Weathering tests run on stock tanks indicate that the stability of the distillate produced by low-temperature separation compares favorably with that recovered by conventional stage separation even though the API gravity is several degrees higher. Some tests have even shown a greater degree of stability which may be contributed to the stabilization of the liquid hydrocarbons in the low-temperature separator as previously mentioned.

Fig. 8 shows the calculated condensate recovery as a function of pressure and temperature for a well having a distillate content of approximately 50 bbl per million cu ft.

These same calculations have been made on well-stream compositions ranging from 10 bbl per million to 100 bbl per million cu ft and the relationship to recovery was found to be very uni-

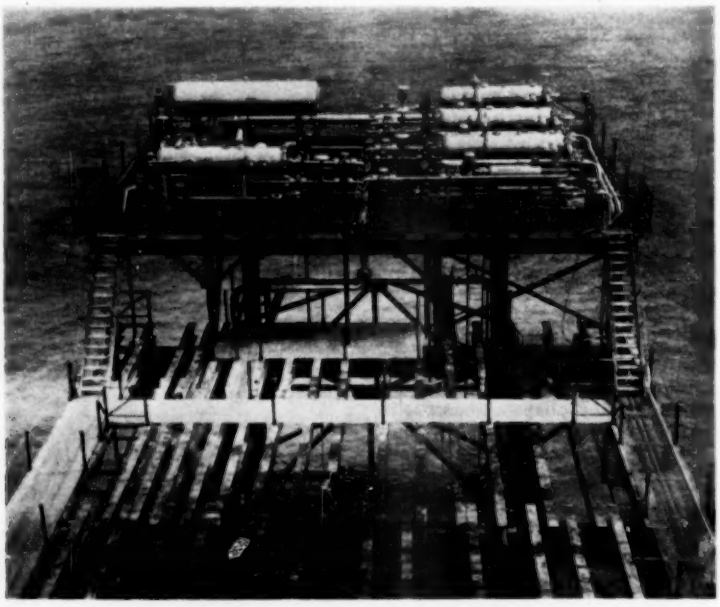

FIG. 6 FOUR LOW-TEMPERATURE EXTRACTION UNITS ON OFFSHORE LOCATION

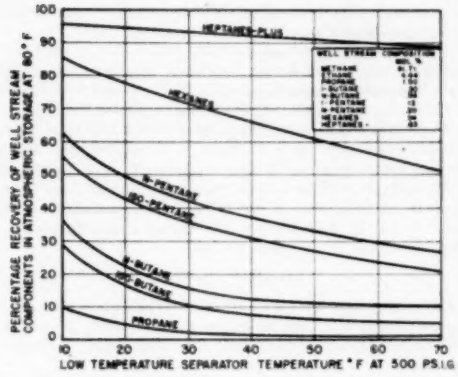

FIG. 7 PER CENT RECOVERY OF WELL-STREAM HYDROCARBON COMPONENTS

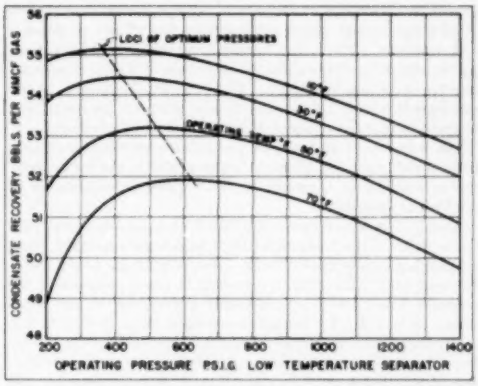

FIG. 8 CONDENSATE RECOVERY AS A FUNCTION OF PRESSURE AND TEMPERATURE

form. The important characteristic of this chart outside of being an aid in predicting additional recovery is the fact that as the separator temperature is decreased the operating pressure also must be decreased to obtain maximum stock-tank liquid. As shown, the optimum pressure at 10 F is 350 to 400 psi as compared to 600 to 700 psi at 70 F.

Actual field experiences have shown these curves to be conservative. However, one contributing factor to this is the inability of the producer always to maintain a minimum separator temperature on conventional equipment where most low-temperature units are supplied with very accurate temperature-control devices.

In those cases where it is possible to collect in one central location the liquid hydrocarbons from several low-temperature units, the use of a stabilizer may be employed to effect a reduction in the vaporization losses normally encountered in the flash from the low-pressure separator to the storage tanks.

In all cases where low-temperature separation has been applied properly, the ability of these units to operate trouble-free at temperatures well below that possible in conventional separators has resulted in a substantial increase in stock-tank liquid.

CONCLUSION

In conclusion it can be said that low-temperature separation properly utilized on high-pressure gas-distillate wells will effect a greater degree of conservation of our natural resources, make available sales gas with a low water-vapor and low hydrocarbon content, and a profitable increase in stable stock-tank liquid.

ACKNOWLEDGMENT

The author wishes to express his appreciation for the able assistance of the field personnel and members of our engineering staff for the operating data and calculated studies as presented in this paper. Also our appreciation is extended to the numerous oil companies for their co-operation in making available the operating and field test data.

Discussion

J. A. NEWSOME, JR.[2] Discussion of the subject of low-temperature separation reflects the interest of engineers in the problems of conservation and, incidentally, increasing the revenue of their respective operations. This group has a broader interest in engineering than in discussion of purely mechanical subjects. Its objective is to further the science of engineering and to encourage new and more efficient equipment for practical application. In this regard, it is indeed surprising that the author does not cover more fully the novelty of the process he is describing and give credit to the operating engineers whose ingenious approach to the problem of producing high-pressure gas-distillate wells led to our wealth of information concerning the practical application of this equipment.

The statement has been made that this process for extracting hydrocarbons is not new. This is true only to the extent that the basic physical characteristics of hydrocarbon liquefaction were fully understood, even prior to the year 1936 mentioned in the paper. It was only some 2 years ago that a commercial method and means of applying this knowledge to field conditions was proposed and reduced to practice. Since that time some 200 producing gas-distillate wells have been equipped with this type of apparatus. It is indeed regrettable that this process was not practiced during the past war period when the demand for condensate to be used in aviation gasoline stock was so great.

When low-temperature separation was attempted, it was found that means must be provided to prevent the formation of gas hydrates in the mechanical device used to reduce the pressure from a producing well to the pressure of the field separator and a means provided for handling hydrate formation in the field equipment and transportation lines themselves. The first problem was overcome when it was shown that the prior removal of liquid water would prevent the formation of hydrates within the mechanical means used to lower the pressure to the desired level. It was not until Mr. A. S. Parks, consulting engineer of Houston, Texas, designed a workable high-pressure water knockout for removing liquid water from the high-pressure stream that the potential use of cold separation became a possibility. The problem of handling hydrate formation in the equipment downstream of the pressure-reduction point was overcome by the ingenious thinking of Mr. A. F. Barry, formerly with the Superior Oil Company, but presently with the Natural Gas & Oil Corporation in Lafayette, La.

The writer does not think that sufficient credit has been given to Mr. Parks and to Mr. Barry by the industry which they have helped immeasurably. The novelty of this method and means has been fully recognized by the U. S. Patent Office which issued

[2] Parkersburg Rig & Reel Company, Houston, Texas.

Patent No. 2,528,028 on October 31, 1950, after an examination of all prior patents issued relating to earlier efforts to develop such a process. The author has done an excellent job of presenting the advantages to be obtained by the use of the Barry process, together with the economics. However, in all fairness to the engineers involved, it is felt that proper acknowledgment should be given to the men who gave this equipment to the industry.

The writer can disagree with the author's contentions in only minor detail, such disagreement being mostly in the particularly chosen mechanical approach of the various manufacturers of this type of equipment.

As in any new endeavor, a multitude of unknown factors face the engineer. We have found from field experience that there are problems of equipment design inherently unique in the Barry process. One of the more interesting of these problems is the excessive water dew-point depression achieved in the cold separator. A wealth of information obtained from field data has been presented to the industry by L. R. Records and D. W. Seely, Jr.[4] This information leads us to believe that the superdepression of water dew point is a function of both temperature and pressure in the cold separator and disappears at the predicted hydrate-forming conditions as published by Katz.[5] Various explanations of this phenomenon have been proposed, but as stated in the paper, the observations of Hammerschmidt seem to more closely fit field records. It is recommended that the operator more closely consider his pressure and temperature conditions in predicting the excessive water dew-point depression rather than accept a fixed 10 F depression as proposed by the author.

Another interesting problem in the operations of cold-separation units is the stabilizing action of the dual-temperature vessel. Each manufacturer of this equipment has his own ideas of how best to accomplish this desirable result. Basically, it is a problem of preventing the recombination of heavy hydrocarbon vapors and water vapors which rise from the reheated liquefied fractions to the zone occupied by the cold gas. This, inherently, is a design problem to minimize the contact area between the warm section of the vessel and the cold section.

Any type of equipment has its limitations and cannot be expected to be applied readily to each and every producing well. Therefore it is the problem of the engineer to make his equipment as flexible as possible in order to be able to apply the basic method to a wide variety of operating conditions. The removal of liquid water from the high-pressure stage and recombination of liquefied hydrocarbons in that stage with the gas, both to be passed into the cold separator simultaneously, results in a higher efficiency of liquid recovery in most cases. This procedure has been found to be at a disadvantage under certain abnormal conditions such as the production of a very rich mixture. Hence it is advantageous to have available a method of choosing the form of operations best suited for the particular circumstances without additions or alterations to the basic equipment.

In order more fully to acquaint those interested with pertinent operating data, the following additional references are given: "Low Temperature Separation," by A. F. Barry and A. S. Parks, in *World Oil*, June, 1950; "Dehydration of Gas at Well Head," by H. S. Reid; "Mechanical Removal of Free Water From High Pressure Gas Lines," by A. F. Barry, in *World Oil*, May, 1949; "High Pressure Free Liquid Knockouts," by L. R. Records and D. W. Seely, Jr., *Oil Gas Journal*, September 13, 1951, and "Low Temperature Separation as Applied to Gas-Condensate Production," by A. W. Francis, Jr., API Rocky Mountain District Meeting, Casper, Wyo., April 20, 1951.

Author's Closure

The writer herewith wishes to acknowledge the written discussion presented by Mr. Newsome and very briefly to delimit any misunderstanding which might have been conveyed by this discussion.

In so doing it is believed appropriate to say that no discussion of the merits of one manufacturer's unit over that of others was anticipated nor required. Neither was the paper delivered by the writer expected to pass credit for or against artisans, inventors, or manufacturers.

Neither time nor space permit more than a few brief statements concerning this matter, and division of credit of discovery is not believed to be important in this paper in view of its controversial nature.

It is not believed that the work of Drs. Lacey and Sage on Retrograde Condensation in papers delivered in the early 1930's was in vain. Also, one should not ignore the work of A. J. Paris, Jr., who obtained several patents, and one in particular in 1919, No. 1,320,168, covering the art of low-temperature separation of liquid hydrocarbons from gas at elevated pressures by first removing water, then precooling the incoming gas with the expanded gas from the system, adding glycerin to lower the dew point to prevent hydrates, and separating the resultant liquids from the gas stream.

Numerous uses, papers, and patents on low-temperature hydrocarbon recovery from natural gas at high and low pressures, including water removal, use of desiccants, and/or forming and removing hydrates with heat or heated gas indicate little novelty in the art after the nineteen-thirties.

Among the foregoing are patents to Wheeless, No. 2,193,309, Farris, No. 2,245,028, Foran, No. 2,284,112, and the use of high-pressure water knockouts ahead of high-pressure oil and gas separation or high-pressure distillate and gas separation; also the use of heat in such separators to melt hydrates was practiced generally in the late 1920's and early 1930's, as well as the use of low temperatures more effectively to recover the hydrocarbons.

It should be stated further that much more efficient and complete separation of hydrocarbons from natural gas may be accomplished at higher pressures and temperatures with old and well-known absorption methods, unless resort is had to economically produce low temperatures of the order of minus 50 to 100 F.

[4] "Low Temperature Dehydration of Natural Gas," by L. R. Records and D. W. Seely, Jr., AIME T.P. 3022, *Petroleum Technology*, vol. 192, February, 1951, pp. 61–66.

[5] "Prediction of Conditions for Hydrate Formation in Natural Gases," by D. L. Katz, Trans. AIME, *Petroleum Development Technology*, vol. 160, 1945, pp. 140–149.

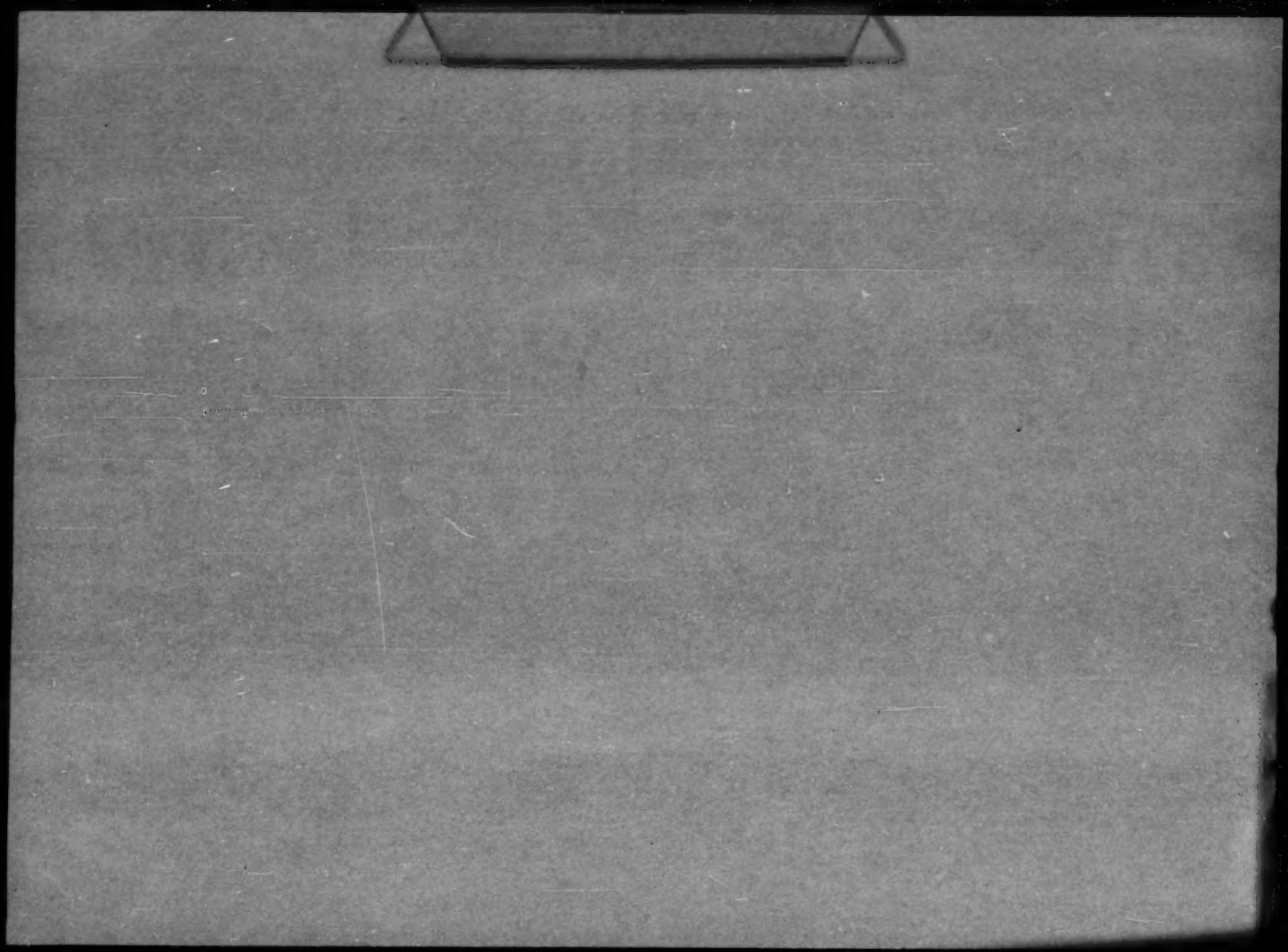

AN ASME PAPER

Its Preparation, Submission and Publication, and Presentation

To a large degree the papers prepared and presented under the ASME sponsorship are evidence by which its professional standing and leadership are judged. It follows, therefore, that to qualify for ASME sponsorship, a paper must not only present suitable subject matter, but it must be well written and conform to recognized standards of good English and literary style.

The pamphlet on "AN ASME PAPER" is designed to aid authors in meeting these requirements and to acquaint them with rules of the Society relating to the preparation and submission of manuscripts and accompanying illustrations. It also includes suggestions for the presentation of papers before Society meetings.

CONTENTS

Price 40¢. No discount allowed. *A remittance must accompany all orders for $5.00 or less. U. S. Postage Stamps are acceptable.*

THE AMERICAN SOCIETY OF MECHANICAL ENGINEERS

29 West 39th Street, New York 18, N. Y.